Distribution Agreement

In presenting this thesis or dissertation as a partial fulfillment of the requirements for an advanced degree from Emory University, I hereby grant to Emory University and its agents the non-exclusive license to archive, make accessible, and display my thesis or dissertation in whole or in part in all forms of media, now or hereafter known, including display on the world wide web. I understand that I may select some access restrictions as part of the online submission of this thesis or dissertation. I retain all ownership rights to the copyright of the thesis or dissertation. I also retain the right to use in future works (such as articles or books) all or part of this thesis or dissertation.

Signature:

_____ _____

Taylor A. F. Nelson Date

The Development and Mechanistic Studies of Group(IX)Cp*-Catalyzed Allylic C–H Functionalization Reactions Proceeding via a π-allyl Intermediate

By

Taylor A. F. Nelson
Doctor of Philosophy

Chemistry

Simon B. Blakey, Ph. D.
Advisor

Nathan T. Jui, Ph. D.
Committee Member

William M. Wuest, Ph. D.
Committee Member

Accepted:

Lisa A. Tedesco, Ph. D.
Dean of the James T. Laney School of Graduate Studies

Date

The Development and Mechanistic Studies of Group(IX)Cp*-Catalyzed Allylic C–H Functionalization Reactions Proceeding via a π-allyl Intermediate

By

Taylor A. F. Nelson
B. S., Auburn University, 2016

Advisor: Simon B. Blakey, Ph. D.

An Abstract of
A dissertation submitted to the Faculty of the
James T. Laney School of Graduate Studies of Emory University
In partial fulfillment of the requirements for the degree of
Doctor of Philosophy
In Chemistry
2020

Abstract

The Development and Mechanistic Studies of Group(IX)Cp*-Catalyzed Allylic C–H Functionalization Reactions Proceeding via a π-allyl Intermediate

By: Taylor A. F. Nelson

Allylic C–H functionalization has proven to be a simple method to form complex allylic products from their olefin counterparts. However, the traditional palladium-catalyzed allylic C–H functionalization reactions are largely limited to terminal olefins with stabilized nucleophiles. In order to fully realize the potential of allylic C–H functionalization to include a wider olefin and nucleophile scope, a novel catalyst system was deemed necessary. Herein is reported the development and mechanistic studies of novel group(IX)Cp*-catalyzed allylic C–H functionalization reactions that aim to address this problem. First, an intermolecular allylic C–H oxygenation reaction was developed utilizing internal olefins and alcohols or carboxylates as the oxygen nucleophile. Following this study, a full mechanistic investigation of a corresponding allylic C–H amination was performed revealing a novel Rh(III)/(IV)/(II) catalytic cycle followed by a Lewis-acid catalyzed allylic substitution to form the corresponding C–N bond. The mechanism described above precludes the use of an asymmetric metal-catalyst to induce enantioselectivity from direct reductive elimination. For this reason, a second-generation allylic C–H sulfamidation reaction was developed proceeding through an Ir(V) nitrenoid complex providing branched products selectively. In order to develop a regiodivergent protocol based on reagent choice, optimization of the first-generation linear-selective allylic C–H amination was also performed. Following this investigation, we sought to develop novel C–C bond forming methods. Therefore, we set out to determine the mechanism of a previously disclosed allylic C–H arylation reaction. Stoichiometric synthesis and reactivity of putative group(IX)Cp*-π-allyl intermediates afforded a more complete picture confirming a novel Rh(III)/(IV)/(II) catalytic cycle refuting the development of a corresponding allylic C–H alkylation reaction. Development of an enantioselective C–H arylation is currently ongoing.

The Development and Mechanistic Studies of Group(IX)Cp*-Catalyzed Allylic C–H Functionalization Reactions Proceeding via a π-allyl Intermediate

By

Taylor A. F. Nelson
B. S., Auburn University, 2016

Advisor: Simon B. Blakey, Ph. D.

A dissertation submitted to the Faculty of the
James T. Laney School of Graduate Studies of Emory University
In partial fulfillment of the requirements for the degree of
Doctor of Philosophy
In Chemistry
2020

Acknowledgements:

Where to begin…. I have not gotten this far without the help and guidance of many people. First and foremost, I want to thank my academic teachers, advisors, and mentors. Dr. Simon Blakey, thank you for being such a great advisor, without you I would not have succeeded this well in my studies. You encouraged me to be an independent thinker and pushed me to be more confident in my skills and gave me so many opportunities to perform amazing research. I could tell you were taking extra time for "teaching moments" to make sure I was gaining skills and can honestly say that whatever writing skills I do have I gotten from you. I will always cap my methyls, judge proposed catalytic cycles, and count my electrons. I would also like to thank my committee members Dr. Bill Wuest and Dr. Nate Jui. Dr. Nate Jui, you might not remember this, but I received the call I was accepted to Emory from you. You taught me chemistry from a new perspective and pushed me to think in a creative way. Dr. Bill Wuest, I thank you for your continued interest in my career development and overall advice, I can tell it comes from a sincere place. I also have benefited greatly from taking your chemical biology course and have garnered much respect for the intersect biology has with organic chemistry. Next, I would like to thank my mentors Dr. Cora MacBeth and Dr. Frank McDonald. You both have offered so much advice and help while I have been here and with my career development, I always felt like you both cared and I appreciate that so much. Dr. MacBeth, as a woman in science I thank you for being someone to look up to, and for continuing awesome research and being patient with me learning about inorganic chemistry and electrochemistry. Dr. Frank McDonald, you were a great professor to help with teaching, and while I do not plan to pursue teaching as a career, the skills I gained

will be helpful anywhere I go. To Dr. Huw Davies and every professor and student in the CCHF, thank you for providing me the best opportunities to not only share my research but also to learn so much more. To Dan (Dr. Morton), Rachael (Dr. Hall), Rio (Dr. Febrian), Steve, Claire, Ann, Ana, Kira (Dr. Walsh), Jan, Tim, Patrick, and Todd and everyone else who helped behind-the-scenes at Emory and the CCHF. You all are not appreciated enough, and I thank you for all the time you have put into your work. To Dr. Wu, Dr. Wang, Dr. Strobel, and Dr. Bacsa I thank you for maintaining the best facilities I may ever use. I would also like to thank all of my professors at Auburn University for providing my foundational education. Thank you, Dr. Peter Livant, for not only teaching me organic chemistry, but also dealing with me as an undergraduate researcher for three years and teaching me how to be an organic chemist. I would definitely not be here if it weren't for you. Dr. Holly Ellis, you were so very inspirational to me as a woman in science, I still remember you telling me to "pack my bags" when you realized my calling for chemistry. Dr. Anne E. Gorden, thank you for your never-ending support and advice, I especially appreciated the invitation to come speak at Auburn last year it meant so much to me. Also, you helped teach Joe how to be a chemist and while he chose a different path it's nice to have someone who can speak my language at the end of the day. And thank you Dr. Yngard, Dr. Goodwin, Dr. Mills, Dr. Zhan, Dr. Ortiz, Dr. Merner, Dr. Gorden, Dr. Goldsmith, Dr. Easley, Dr. Duin, and Mr. Swann for either teaching me chemistry, helping me with research, or offering me advice. To the future Dr.'s Theresa, Chase, Rachel, Rachel, Evan and everybody else in the group, thank you for hanging in there with me while we learned chemistry together, I had a wonderful time. And to my first chemistry teacher, Mr. Bolton, I wouldn't have gotten this far if you hadn't taught chemistry well and made it

just a little fun too. And of course, thank you to Northside Methodist Academy for 15 years of education that started me on this journey (of 9 more years of education).

To every member of the Blakey group past, present, and future; thank you for being awesome you made a great decision and, of course, be better. Dr. Robert “ROBERT” Harris, you taught me so much about organometallic chemistry and provided me with a similar mind in an imperfect world. Dr. Eric Andreansky, you started out as a senior lab member I would go to for chemistry help, you then became my cat work friend, and I am happy to say you have become one of my dear friends (Adam too). Dr. Caitlin “Caiti-Mac” Farr, you obviously helped me with my chemistry, but you were also there for me in one of my most difficult times, thank you. Soon-to-be Dr. Amaan Kazerouni, I would have never guessed how much our relationship would have grown, you listen to me talk about chemistry and life, thanks dude. Dr. Dan Liu, you are one of the nicest people ever, who always made me smile and listened to my questions about e-chem, thanks for being so great and for the hot pot. To Daniel, thanks for being the first wondergrad, I wish you the best of luck in grad school. To Ashley, Tom, Sophia, and Steven, thank you all for being great undergraduate researchers, I wish you well as you begin your careers. To Kim, thanks for being my wondergrad. I hope I have taught you well and I thank you for our wonderful friendship. Good luck as you begin your graduate school career! I would also like to thank Sam, Amber, Ana, Peipei, Robert, Sid, Brooke, and so many more for being someone to talk to. Elaine…. I could not have done this without you. You helped me with inorganic chemistry, but more importantly you were the person I went to when things got bad and they sure did. I can’t wait to continue our friendship as you start your career.

So, there's a tradition my high school had for graduating seniors that I have told a few of you about so here it goes… I, Taylor, being of unsound body and mind do hereby leave the following to members of the Blakey Lab. To Chris I leave the position of the most senior member of the lab, use your power wisely. To Michael, I leave the most superior memes, may you keep everyone smiling. To David, I leave you the title of lab artist and "nerdy things", your singing, and dancing always made me smile, keep it up. To Quincy, I leave the title of coolest lab member. How dare you be nice, fashionable, and a good chemist! To Patrick I leave more indene catalysts and being a great bay mate, even if it wasn't for long. To Christina, I leave being the most senior female lab member, you are going to do great things and don't let anything, or anyone tell you otherwise. To Eleda, Ethan, Keili, and Tiffany I leave a wonderful lab full of wonderful people, look after and support each other, grad school is a fun but also an exhausting endeavor.

And lastly, I would like to thank my friends and family. Mom, I know you might not have planned for me to get a Ph. D. but you have always been so supportive and there for me when I needed you. Dad, thank you for all the sound advice and encouragement to me as a scientist, I didn't think we would all get degrees in Chemistry but here I am. Nana and Mr. E, thank you so much for everything you do, I couldn't have asked for better grandparents. Megan, thank you for being my best friend for almost 20 years, and for all that that has entailed both good and bad. I really don't tell you how appreciative I am to have you in my life enough. To Marshall, thank you for being my best friend for almost 15 years, I have always enjoyed our discussions and your horrible jokes. And to you both, the Halo helped so much. And Joe, what can I say, you picked up your life and followed me to Atlanta so I could spend way too much time doing chemistry and not with you. You kept me sane, you kept me

safe, even during the worst of it all. It was awesome to have a chemist to come home to everyday. Everyone always says how amazing you are because it's true, I am so very lucky to have you as my person. Who knows where I would be without you? Thanks again to everyone that has touched my life, I am here today because of you.

Table of Contents

Chapter 3: The Mechanism of Rhodium-Catalyzed Allylic C–H Amination Proceeding via a Rh(IV)-π-allyl Intermediate

Chapter 5: Reactivity of Group (IX)Cp*-π-allyl Complexes as Putative Intermediates in Allylic C–H Arylation and Alkylation Reactions

Table of Figures

Table of Tables

Abbreviations:

2,5-DMBQ	2,5-dimethylbenzoquinone
Ac	acetyl
AcOH	acetic acid
Ar	aryl
b	broad
BAr^F_4	tetrakis[3,5-bis(trifluoromethyl)phenyl]borate
Bn	benzyl
Boc	*tert*-butyloxylcarbonyl
BQ	benzoquinone
Bu	butyl
Cbz	carboxybenzyl
Cp	cyclopentadiene
Cp*	1,2,3,4,5-pentamethylcyclopentadiene
Cp^E	1,3-diethylester-2,4,5-trimethylcyclopentadiene
CV	cyclic voltammetry
d	doublet
dba	dibenzylideneacetone
DCE	1,2-dichloroethane
DCM	dichloromethane
DDQ	2,3-Dichloro-5,6-dicyano-1,4-benzoquinone
DFT	density functional theory
DG	directing group

DME	dimethoxyethane
DMF	dimethylformamide
DMSO	dimethyl sulfoxide
DPP	1,3-diphenylpropene
Et	ethyl
Et_2O	diethyl ether
EtOAc	ethylacetate
EWG	electron withdrawing group
Fc	ferrocene
Fc^+	ferrocenium
FG	functional group
FT	Fourier transform
GC	gas chromatography
Hept	heptet
HFIP	hexafluoro-2-propanol
HRMS	high-resolution mass spectrometry
IR	infrared
KIE	kinetic isotope effect
L	ligand
LG	leaving group
M	metal
m	metal
Me	methyl

MeCN	acetonitrile
MRI	magnetic resonance imaging
M.S.	molecular sieves
Naph	naphthyl
NMR	nuclear magnetic resonance
NPMoV	molybdovanadophosphate
Ns	4-nitrobenzenesulfonyl
Nu	nucleophile
ORE	oxidatively-induced reductive elimination
Ph	phenyl
Piv	pivalic
Ppm	parts per million
Pr	propyl
p-tol	*para*-tolyl
PTSA	*p*-toluenesulfonic acid
q	quartet
qn	quintet
rpm	rotations per minute
s	singlet
SC-XRD	single-crystal x-ray diffractometry
Ser	serine
t	triplet
TBDPS	*tert*-butyldiphenylsilyl

TBME	tert-butyl methyl ether
t-BuOOH	pivalic acid
TCE	1,1,1-trichloroethanol
Tf	triflyl
TFA	trifluoroacetate
TFE	1,1,1-trifluoroethanol
TFT	α,α,α-trifluorotoluene
THF	tetrahydrofuran
TLC	thin-layer chromatography
TMS	tetramethylsilane
TON	turn over number
Ts	4-toluenesulfonyl
TS	transition state
UV	ultra-violet
V	voltage

Chapter 1: Introduction and Background: Allylic C–H Functionalization via π-allyl Intermediates Prior to 2018

I. Palladium-Catalyzed Reactions:

I.1. Introduction and Seminal Work:

Reaction methods for C–O, C–N, and C–C bond formation have proven crucial for the synthesis of important molecules in the pharmaceutical, agrochemical, and materials industries.[1] Unfortunately, standard methods to form these bonds require excessive functional group manipulations.[2] Standard methods have provided powerful tools for complex molecule synthesis, but the by-products of these transformation have negative environmental and monetary impacts.[3] C–H functionalization stands as one solution to this problem by obviating the need for installation and disposal of functional groups. While C–H bonds were once thought to be inert, many methods have since been developed for their direct functionalization. In many cases, a transition-metal, typically positioned by a directing group, can insert into the desired C–H bond.[4] Allylic C–H bonds are especially reactive to these transition-metal catalysts compared to other C(sp^3)–H bonds, and therefore have been of particular interest to the synthetic community.[5] One particular mode of reactivity of allylic C–H bonds proceeds via a π-allyl metal intermediate (**Figure 1-1**).[6] Activation of the allylic C–H bond of **1-1** forms an η^1-allyl intermediate (**1-2** or **1-4**) in equilibrium with the corresponding η^3-π-allyl metal complex (**1-3**). Analogous methodology utilizing an allylic leaving group, rather than a C–H bond, has provided key insight into this process (**1-5**).[7]

Terminal π-allyl complexes (**1-3**) typically react at the C1 or C3 carbons of the π-allyl moiety forming the linear (**1-6**) or branched product (**1-7**), respectively.

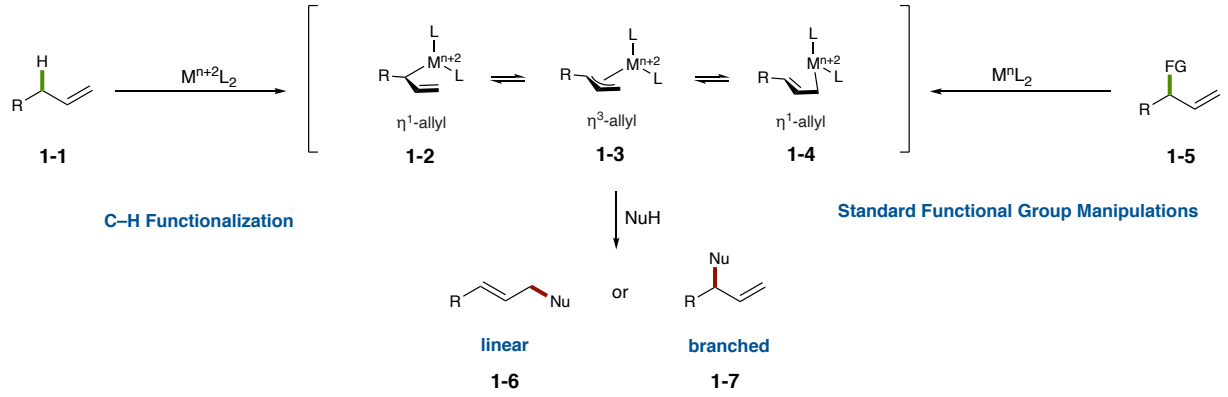

Figure 1-1. Formation of π-allyl Complexes and Equilibrium of Coordination Modes

Allylic substitution, originally disclosed by Tsuji and Trost, stands as the most well-established reaction proceeding via a π-allyl intermediate.[8] Since its discovery in 1965, transition-metal-catalyzed allylic substitution of an allylic leaving group (**1-8**), has had significant utility in synthetic chemistry (**Figure 1-2**).[9-11] More recently, alkynes (**1-9**), dienes (**1-10**), and allenes (**1-11**) have also been used as precursors in reactions proceeding via a π-allyl complex (**1-12**).[12, 13] While these methods do not require an allylic leaving group, the substrates are preoxidized, lowering the overall redox economy. For this reason, oxidative allylic C–H functionalization has become an attractive complementary method to form allylic products from the parent olefin.

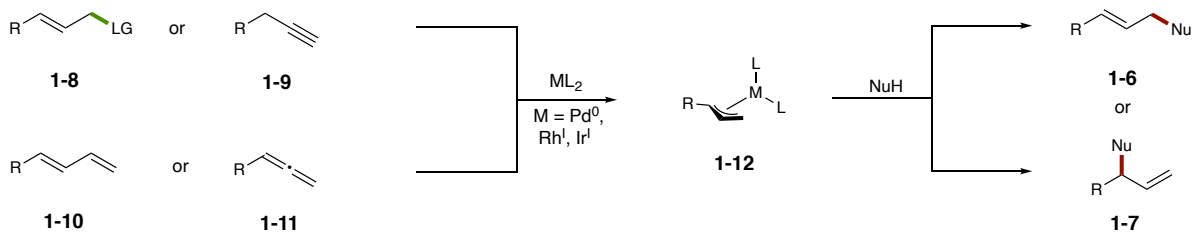

Figure 1-2. Preoxidized Allylic Precursors for π-allyl Complex Formation

The first stoichiometric allylic C–H functionalization reaction was disclosed by Hüttel in 1959 (**Figure 1-3A**).[14, 15] The authors report the isolation of palladium-π-allyl complex **1-14**, which was later shown to reductively eliminate allyl chloride **1-15**. Further stoichiometric exploration by Rappoport (1966) and co-workers showed that using DMSO as a sulfur ligand was crucial in forming allyl acetate **1-17** from 1-butene (**1-16**, **Figure 1-3B**).[16] Prior to this work, a competitive Wacker-type oxidation product (**1-18**) would have been expected and was deleterious to this reaction. Use of acetic acid as the solvent afforded allylic acetate **1-17** in 9% yield and **1-18** in 80% yield, but a 7:3 DMSO:AcOH solvent mixture provided **1-17** in 73% yield. Furthermore, in 1973, Trost developed a stoichiometric allylic C–H alkylation procedure (**Figure 1-3C**).[17] In the presence of a suitable base, palladium π-allyl chloride dimer **1-20** was isolated in 100% yield from **1-19**. This dimer could then be subjected to an alkyl nucleophile (**1-21**), providing allylic alkyl product **1-22** in 80% yield. It wasn't until 1982 that a catalytic system was developed by Uemara using relatively harsh conditions (**Figure 1-3D**).[18] This work focused on cyclic systems and allylbenzene derivatives, as other olefins produced Wacker-type products. The key to this advance was the oxidation of the Pd(0) to Pd(II) after reductive elimination to complete the catalytic cycle. When cyclopentene (**1-23**) was used as the olefin, 39% of allylic acetate **1-24** was observed,

with a 7.8 TON. While the yield was low, this example was the first catalytic method and provides a foundation for further development of allylic C–H functionalization reactions proceeding via π-allyl intermediates.

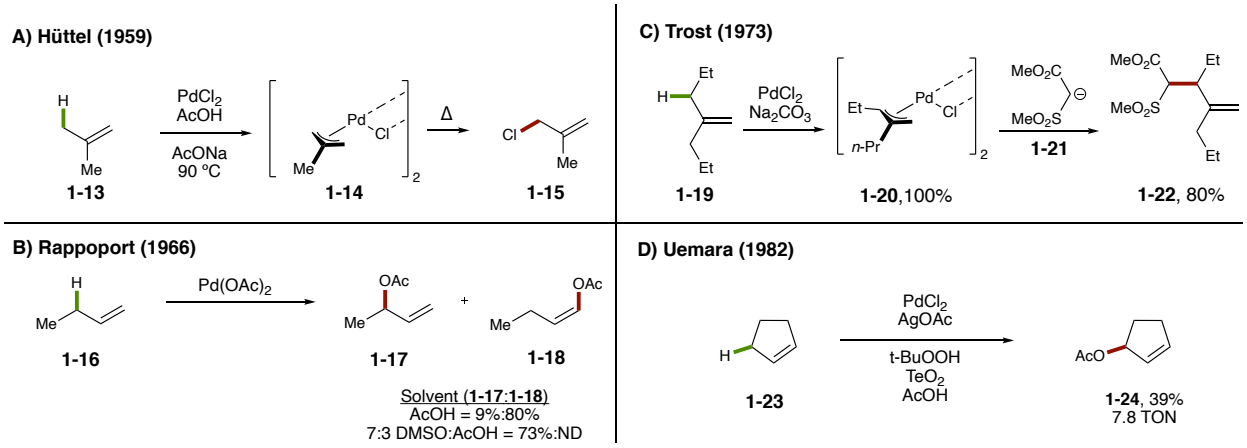

Figure 1-3. Seminal Work of Palladium π-allyl Complexes

I.2. C–O bond forming reactions

Allylic C–H oxygenation has garnered the most focus for further development since the seminal disclosures previously discussed. In 1990, Åakermark advanced the field with a palladium-catalyzed allylic C–H acetoxylation of cyclic (**1-25**) and linear olefins utilizing a benzoquinone (BQ) and manganese dioxide oxidation system (**Figure 1-4A**).[19] This work was later confirmed to proceed via a π-allyl metal complex by Bäckvall via isotope-labeling and computational studies in 1994.[20] It was not until 1998 that an etherification procedure was corroborated to also proceed via a Pd-π-allyl complex by Mortreux *et. al*. (**Figure 1-4B**).[21] This etherification focused on methoxylation of limonene (**27**) regiocontrolled by the palladium catalyst choice. If $Pd(OAc)_2$ was utilized, ether **1-28** was formed in 6% yield while ether **1-29** was isolated in 79% yield. On the other hand, when Li_2PdCl_4 was used as

the catalyst, complete regioselectivity for ether **1-28** (78%) was observed. It was confirmed that internal olefin reactivity for palladium catalysis was only observed when a second olefin could act as a directing group.

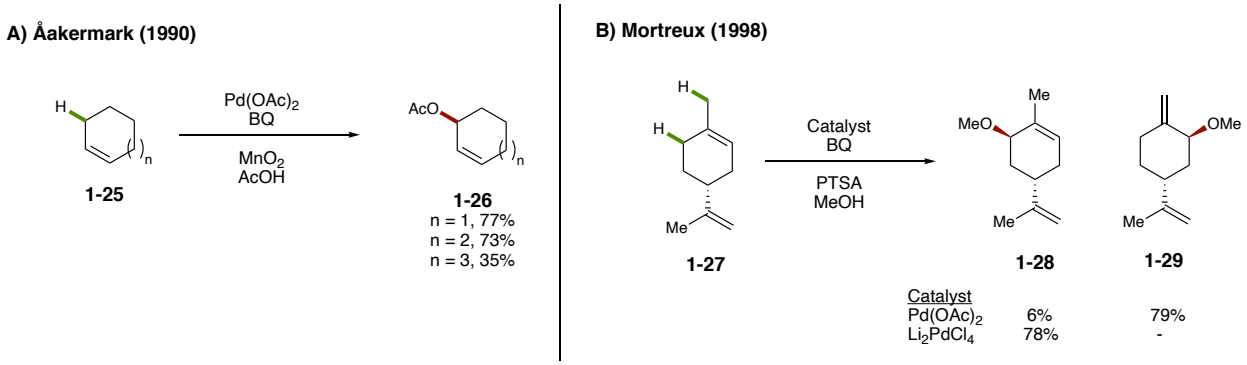

Figure 1-4. Palladium-Catalyzed Allylic C–H Oxygenation Reactions

In 2004, White and co-workers developed a regioselective acetoxylation. This disclosure expanded the utility of allylic C–H functionalization reactions to include complex molecule synthesis (**Figure 1-5**).[22] As was first seen by Rappoport and co-workers, the key to suppress Wacker oxidation was the introduction of sulfur-containing additives.[23] To selectively produce the linear product (**1-31**), DMSO was utilized as the solvent. To generate the branched product (**1-32**), a bis-sulfoxide ligand (**1-33**) could be employed, providing regioselectivity based on additive choice. An enantioselective method was later developed using a chromium salen complex.[24] As more emphasis moves towards sustainability, aerobic conditions have also been developed by Stahl and others, albeit providing racemic products.[25, 26]

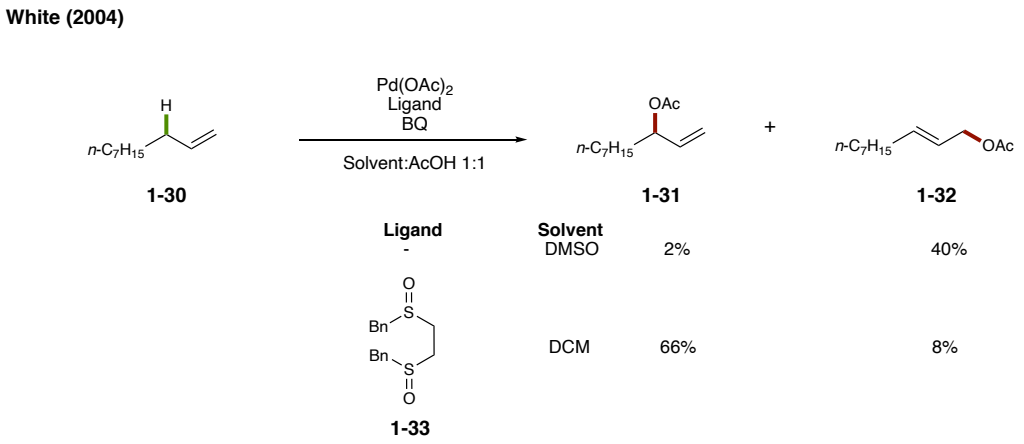

Figure 1-5. Palladium-Catalyzed Regioselective Allylic C–H Acetoxylation

Etherification procedures have had more limitations than other oxygenation reactions. For intermolecular reactions the alcohol coupling partners are simple and are typically required at solvent quantities. On the other hand, intramolecular reactions have been developed but were reliant on steric bias for reactivity. In 2014, White and co-workers developed an intramolecular allylic C–H etherification to form chroman, isochroman, and pyran derivatives, greatly expanding the scope of allylic C–H etherification (**Figure 1-6A**).[27] Prior to this disclosure, substrates required steric or electronic bias to afford appreciable yields of the cyclized product. In this example, alcohol **1-34** could be cyclized to form ether **1-35** in 41% yield under standard reaction conditions. Enantioselective methods to form chromans have since been disclosed by Gong and White, using phosphoramidite and sulfoxide-oxazoline ligands, respectively.[28, 29] In 2017, the Jiang group disclosed an intermolecular allylic C–H etherification for simple alcohols and phenol-type alcohols (**Figure 1-6B**).[30] When DMSO was utilized as the solvent and dioxygen as the oxidant, aliphatic alcohols formed ethers (**1-38**) in good to excellent yield. This was not the case for

phenolic alcohols, which required PPh_3 as the ligand and toluene as the solvent. Overall, this procedure was the first general intermolecular allylic C–H etherification reaction and provided products in good to excellent yield. Furthermore, that same year the Liu group disclosed an intermolecular trifluoromethoxylation reaction (**Figure 1-6C**).[31] Slow leaching of the alkoxide source was crucial for reactivity with olefin **1-39**, as trifluoromethoxylations are particularly challenging due to prompt decomposition of the alkoxide. In both of these intermolecular allylic C–H etherification reactions, linear cinnamyl-type products were formed.

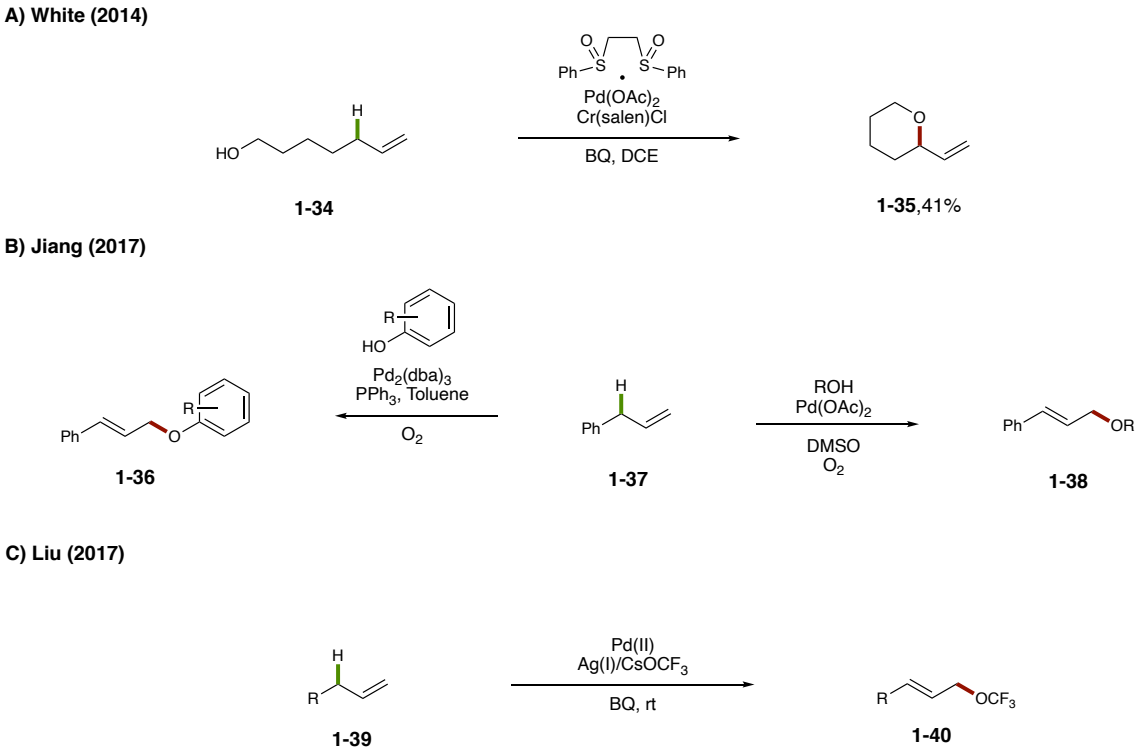

Figure 1-6. Palladium-Catalyzed Allylic C–H Etherification Reactions

I.3. C–N Bond forming reactions

While seminal allylic C–H functionalization reactions focused on C–O bond formation, allylic C–H aminations have also developed at a rapid pace.[32] In 2008, Liu and White concomitantly reported the first intermolecular allylic C–H amination reactions proceeding via a π-allyl complex intermediate (**Figure 1-7A**).[33, 34] The conditions for both disclosures were similar, but Liu's work utilized aerobic oxidation as an attractive alternative to stoichiometric oxidants. In later work, White and co-workers were able to leverage their system to utilize dioxygen as the terminal oxidant by introducing an electron transfer cocatalyst.[35] Unfortunately, the amine nucleophiles (**1-42**) required two electron-withdrawing protecting groups in each of these cases. Even though these protecting groups can be cleaved, their necessity limits the utility of these methods. In 2010, Obora and Ishii developed a system which utilized a molybdovanadophosphate salt as the electron transfer mediator to expand the nucleophile scope to diarylamines (**1-44**), but this system was specific for diarylamines (**Figure 1-7B**).[36] White and co-workers expanded the nucleophile scope further by leveraging one stronger electron-withdrawing group (Tf) rather than the usual two (**Figure 1-7C**).[37] The utilization of triflourosulfonamides (**1-46**) afforded allylic amines (**1-47**) with a wide variety of functionality in good yield. Unfortunately, the triflyl group could not be easily cleaved. Substitution for a nosyl group allowed for easier deprotection but provided decreased yields. Despite these limitations, the transformations described above were a great advance to previous methods and have been used to form complex natural products.

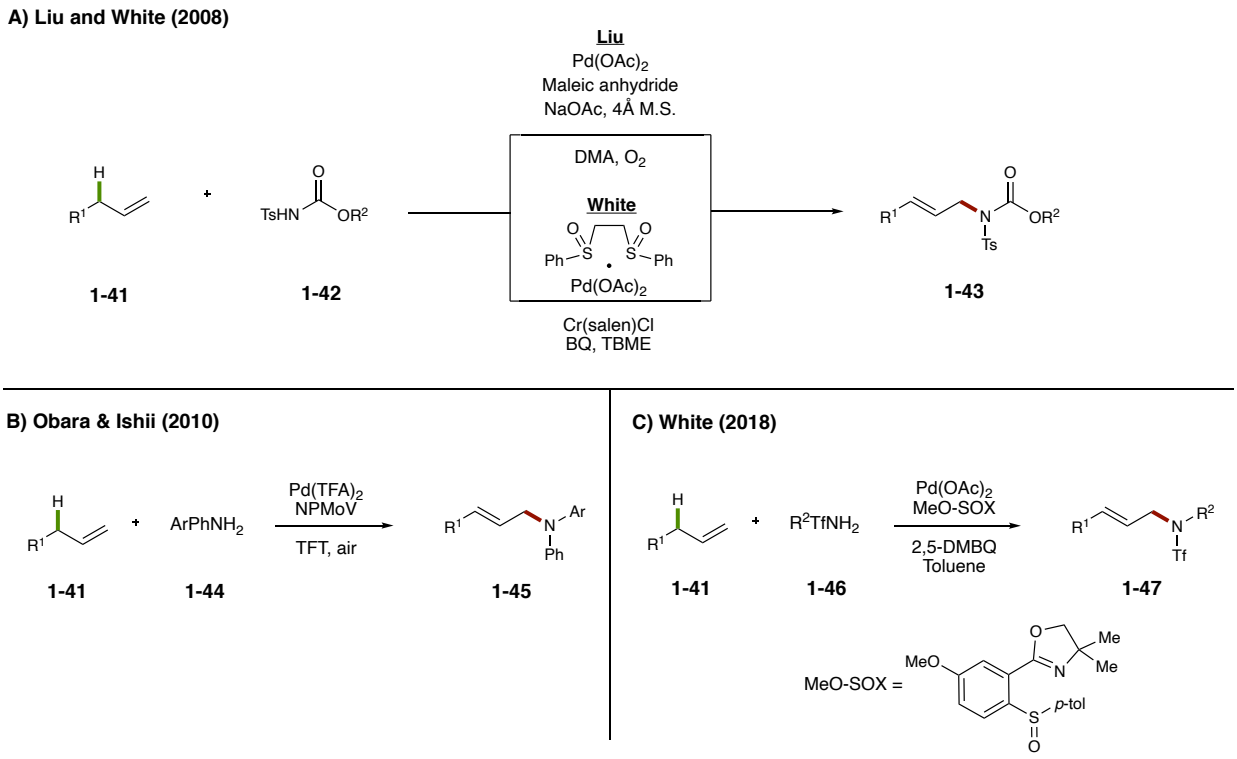

Figure 1-7. Palladium-Catalyzed Allylic C–H Amination Reactions

I.4. C–C bond forming reactions

Allylic C–H alkylations and arylations have not been developed as well as their oxygen and nitrogen counterparts.[6, 32, 38] While one of the first stoichiometric allylic C–H functionalization reactions disclosed by Trost in 1973 provided alkylated products, catalytic reactions were not studied until much later.[11] In 2008, White and co-workers reported an allylic C–H alkylation procedure leveraging White's palladium catalyst system with malonate derivatives (**Figure 1-8A**).[39] While the olefins (**1-41**) were more general, the carbon nucleophile (**1-48**) required two electron-withdrawing groups, much like the amine systems. Furthermore, few arylation procedures have been disclosed. In 2009, Bao and co-workers developed a rare example of an internal olefin (**1-50**) coupling with indoles (**1-51**,

Figure 1-8B).[40] The olefin coupling partner (**1-50**) was required to be activated by two arenes, and a modest variety of indoles were tolerated. Furthermore, in 2014, Jiang and co-workers reported another arylation procedure with fluorinated arenes (**1-53**) as the coupling partner (**Figure 1-8C**).[41] This report notes competitive Wacker-type products (**1-55**) and is limited to activated aryl nucleophiles. More specific examples have been disclosed that expand this relatively small scope; however, a general alkylation or arylation procedure has not been reported, greatly limiting the utility of these reactions in complex molecule synthesis.[42, 43]

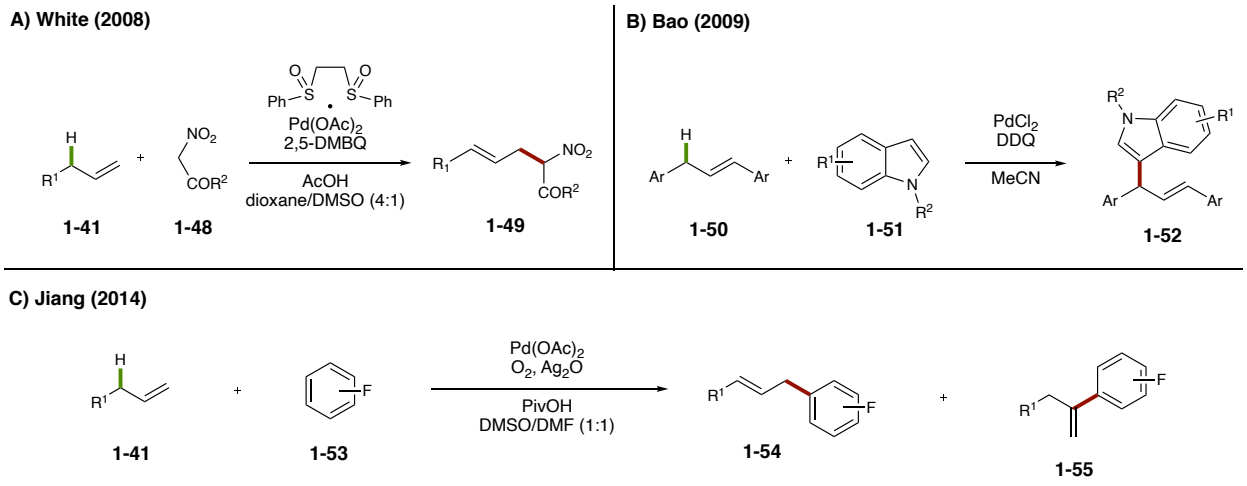

Figure 1-8. Palladium-Catalyzed Allylic C–H Alkylation and Arylation Reactions

I.5. Conclusions and Outlook

Overall, allylic C–H functionalization reactions proceeding via π-allyl intermediates has been dominated by palladium catalysis. In this case, simple C–O, C–N, and C–C bonds can be formed to provide complex allylic products.[6, 32, 38] Although allylic C–H acetoxylation reactions were the first disclosed in this class of reactions, there is a lack of breadth for

alcohol nucleophiles. This is likely due to the competitive oxidation of the alcohol coupling partner or overoxidation of the ether product. For this reason, much work is still needed for allylic C–H oxygenation procedures for general synthetic utility to be realized.

Allylic C–H amination protocols are arguably the most well-developed in this class of reactions. This being said, the nitrogen coupling partners are still limited to amines with strong electron-withdrawing groups. If only one electron-withdrawing group was utilized, deprotection was difficult, requiring a balance of reactivity and further utility of the products. This theme is also present for alkylation procedures, as almost all alkyl nucleophiles require two strong deactivating groups to provide sufficient reactivity. Arylation protocols are even further limited to indoles or fluorinated arenes.

With this in mind, it became clear that the palladium-catalyzed systems may have limitations that cannot be overcome at this time. For most cases, only terminal olefins engage in reactivity, preferentially forming the linear product. Furthermore, the nucleophiles required for reactivity must be activated to afford sufficient yields. One means of expanding the scope of allylic C–H functionalization reactions may be through the development of novel catalyst systems. While palladium has proven to be a very powerful metal in C–H functionalization, there is a vast library of metal-catalyst systems with which these transformations could be envisioned.

II. Group(IX) catalyzed systems:

The most well-studied class of C–H functionalization reactions utilizes a directing group.[44, 45] In this case, the metal catalyst ligates to the substrate (**1-56**), poising the metal for C–H activation, typically forming a metallacycle intermediate (**1-57**) followed by

reductive elimination of **1-58**. While many of these protocols have utilized palladium catalysts, group(IX)Cp* catalysts have proven to be very powerful for selective C–H functionalization.[46-51] It follows that one of the first allylic C–H functionalization reactions of internal olefins utilized a RhCp* precatalyst and a directing group. In this case, Glorius and co-workers developed a directed allylic C–H functionalization reactions to form pyrroles (**1-61**).[52] Although complete mechanistic studies have not been performed, an η^1-allyl species is likely. While not proceeding via a π-allyl intermediate, this work suggested that more methods could be developed in this area.

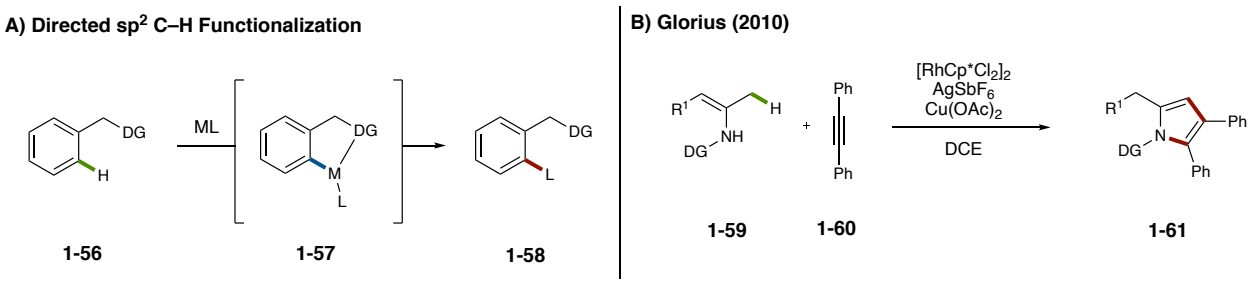

Figure 1-9. Precedent for Group(IX) Cp*-Catalyzed Allylic C–H Functionalization

II.1. Intramolecular Allylic C–H Aminations

In 2011, Li and co-workers developed a RhCp*-catalyzed oxidative olefination of *N*-(1-naphthyl)sulfonamides (**1-62, Figure 1-10A**).[53] When activated alkenes (**1-63**) were utilized, formal oxidative olefination followed by hydroamination was observed. In the case of unactivated olefins (**1-65**), only directed olefination was observed to form **1-66**. Inspired by the work described by Glorius[52] and other palladium-catalyzed work by Falck,[54] the authors also report further allylic C–H amination of the olefinated product (**1-70, Figure**

1-10B). When 4-methylpentene (**1-68**) was utilized with an excess of $Cu(OAc)_2$ oxidant, allylic C–H amination was observed in 52% yield (**1-70**), with 18% yield of olefinated product (**1-69, Figure 1-10B**). When olefin **1-69** was resubjected to reaction conditions, amine product **1-70** was also isolated, although the yield was never reported. Further studies support π-allyl complex formation. Unfortunately, complete studies were not performed on the optimization of the allylic cyclization or the mechanism.

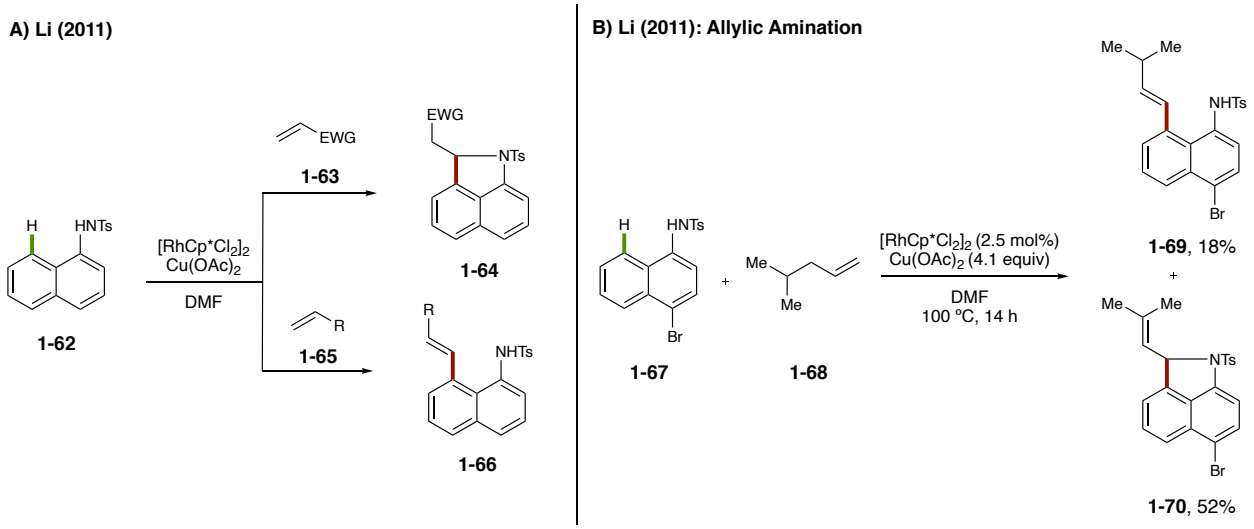

Figure 1-10. First Example of RhCp*-Catalyzed Allylic C–H Amination via a π-allyl Intermediate

In 2012, Cossy and co-workers developed an allylic C–H cycloamination of a variety of alkyl olefins (**Figure 1-11**).[55] The authors were able to react olefin **1-71** to produce 77% isolated yield of **1-72** and **1-73** (5:1) with DCE as the solvent, $[RhCp^*(MeCN)_3](SbF_6)_2$ as the precatalyst, and $Cu(OAc)_2$ as the terminal oxidant. $[RhCp^*(MeCN)_3](SbF_6)_2$ is another RhCp* precatalyst that does not require halide abstraction, obviating the need for $AgSbF_6$ which is air and light-sensitive. A variety of common amine protecting groups were utilized, resulting

in yields ranging from 14-61%, even at complete conversion. In most cases pyrrolidine and piperidine products were observed, favoring the pyrrolidine product. In another example, internal olefin **1-74** was shown to result in 50% combined yield of the cyclic products **1-75** and **1-76** in a 1:1 ratio, illustrating rare internal olefin reactivity.

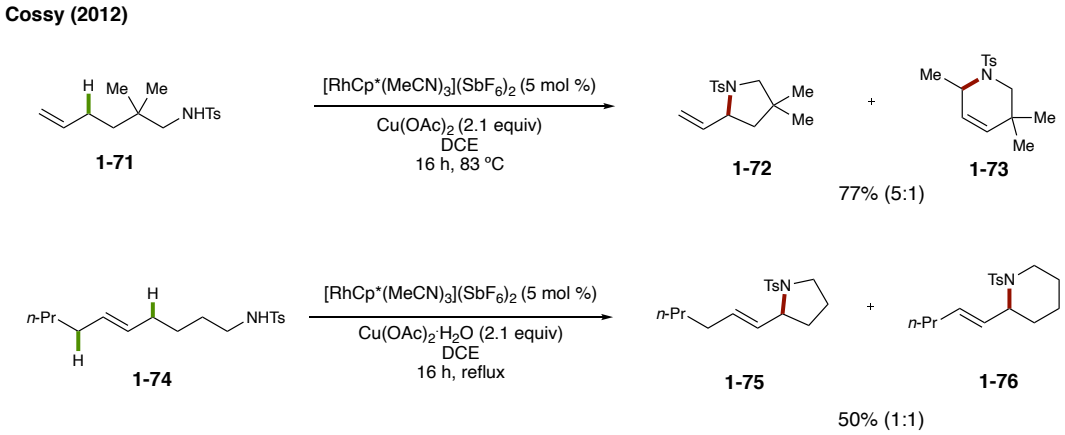

Figure 1-11. RhCp*-Catalyzed Intramolecular Allylic C–H Amination

The authors propose a catalytic cycle which proceeds via a RhCp*-π-allyl complex acting through a Rh(III/I) pathway (**Figure 1-12**). To form the piperidine products, π-allyl migration to the internal position was proposed. First ligand exchange of **1-77** provides Rh(III) complex **1-78.** For the formation of **1-72**, olefin **1-71** and $^{-}$OAc coordinate to form complex **1-79**. Concerted-metalation deprotonation to activate the C–H bond releases acetic acid, forming complex **1-80**. Deprotonation of the amine moiety is then followed by amine coordination to form Rh(III) complex **1-81**. Reductive elimination of Rh(III) complex **1-81** results in Rh(I) complex **1-82**. Ligand exchange and a 2e^{-} oxidation completes the catalytic

cycle, releasing product **1-72**. This Rh(III)/Rh(I) cycle, while not confirmed, agreed with previous directed C–H functionalization methods and allylic substitution protocols.

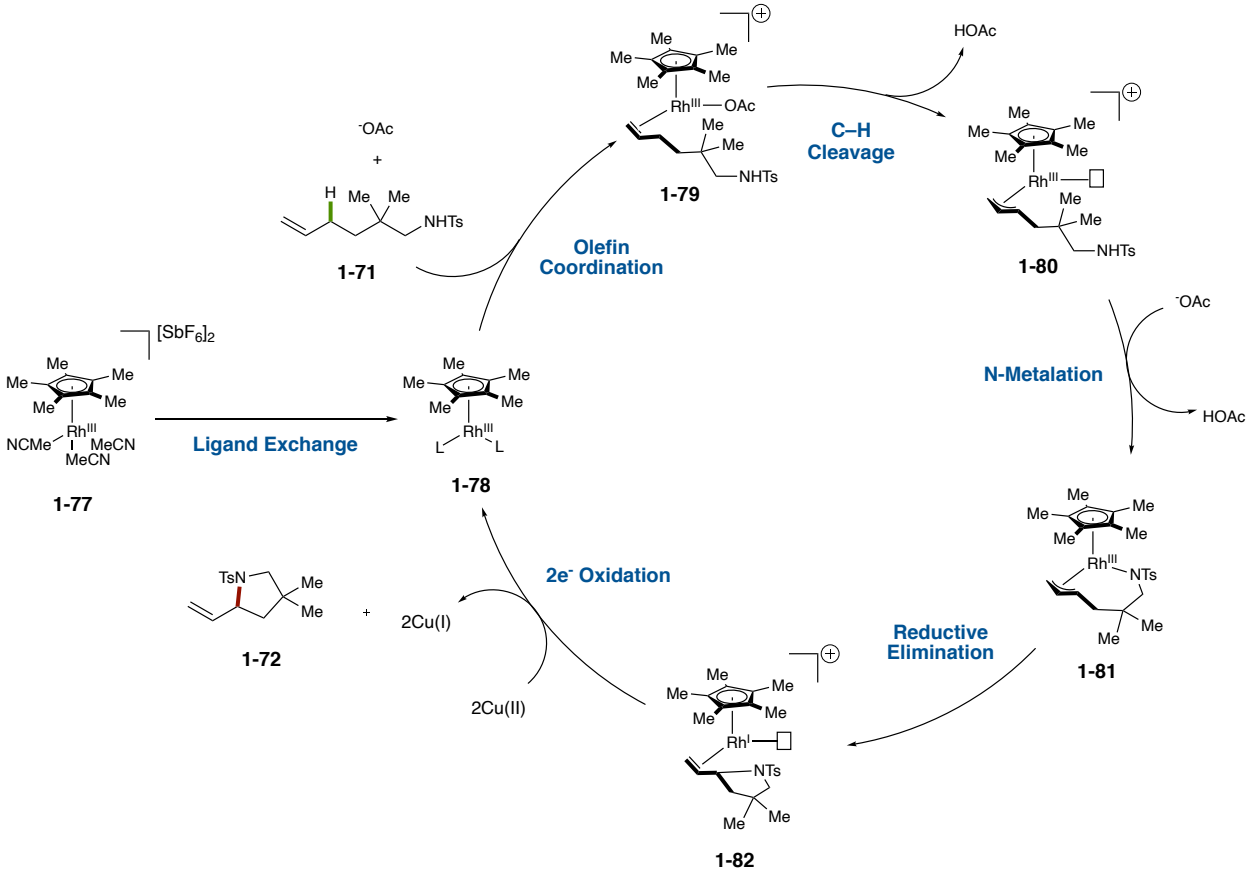

Figure 1-12. Catalytic Cycle of the Allylic Amination for the Pyrrolidine Isomer (Expanded and Corrected from Cossy et. al.)

II.2. Allylic C–H Electrocyclization to form Heterocycles

Electrocyclization reactions have also become quite popular in the C–H functionalization literature. In 2015, Rovis and co-workers developed an allylic C–H cyclization, which is initiated at an analogous π-allyl complex proposed by Cossy (**Figure 1-13**).[56] In this case, π-allyl complex formation of **1-84** would be followed by migratory

insertion of alkyne **1-60,** which could then proceed through an electrocylization to form product **1-85**. The reaction conditions were similar to those disclosed by Cossy,[55] but the $[RhCp^*Cl_2]_2$ precatalyst, in conjunction with $AgSbF_6$, as the halide scavenger, was used at a higher reaction temperature. The reaction was not limited to forming five-membered heterocycles and could, in fact, form the 6- and 7-membered cyclic amines in modest to good yield. While not yielding allylic products, this investigation illustrates that further reactivity of the π-allyl complex is not limited to intermolecular cross-coupling reactions.

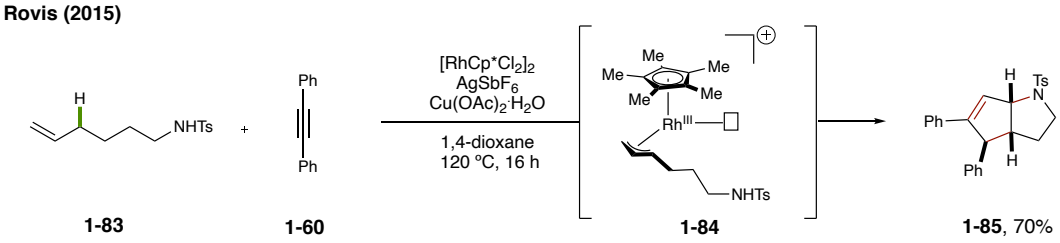

Figure 1-13. Allylic C–H Electrocyclization to form Azabicycles

II.3.<u>Stoichiometric RhCp^E-π-allyl Complex Studies</u>

In 2016, Tanaka discovered that RhCp^E-π-allyl complexes (Cp^E, 1,3-diethylester-2,4,5-trimethylcyclopentadiene) could be synthesized using C–H functionalization.[57] Optimization of the reaction conditions resulted in a heavy reliance on the silver salt counterion, as has been noted in the literature. Interestingly, in the absence of a carboxylate source, $AgBF_4$ yielded the internal regioisomer selectively (**1-87** = 22%, **1-88** = 78%). On the other hand, when 2 equivalents of CsOAc, and $AgBF_4$ were used, almost complete selectivity for the terminal isomer was observed (**1-87** = 95%, **1-88** = 1%). Furthermore, complex **1-87** was further characterized by ^1H NMR, ^{13}C NMR, and single-crystal x-ray diffractometry,

thus confirming the π-allyl complex structure. Since Cossy had proposed a π-allyl intermediate for her cyclization chemistry, the authors utilized alkylamine **1-83** as the olefin starting material, isolating complex **1-89** in 47 % yield. Further subjection of complex **1-89** to a halide scavenger, $AgSbF_6$, and an oxidant, $Cu(OAc)_2$, resulted in 51% yield of the predicted pyrrolidine product (**1-90**). Furthermore, when 2-octene (**1-91**) was utilized as the olefin source, three π-allyl complexes (**1-92, 1-93,** and **1-94**) were observed by crude ^1H NMR assay. Terminal complex **1-92** was observed in 8% yield, while internal complex (**1-93**) was observed in 42% yield. Complex **1-94** was also observed in 3% yield, likely resulting from migration of the olefin, which the authors propose proceeds intermolecularly. This work provided an excellent means to produce $RhCp^E$-π-allyl complexes as well as much needed mechanistic insight into Cossy's and others' work.

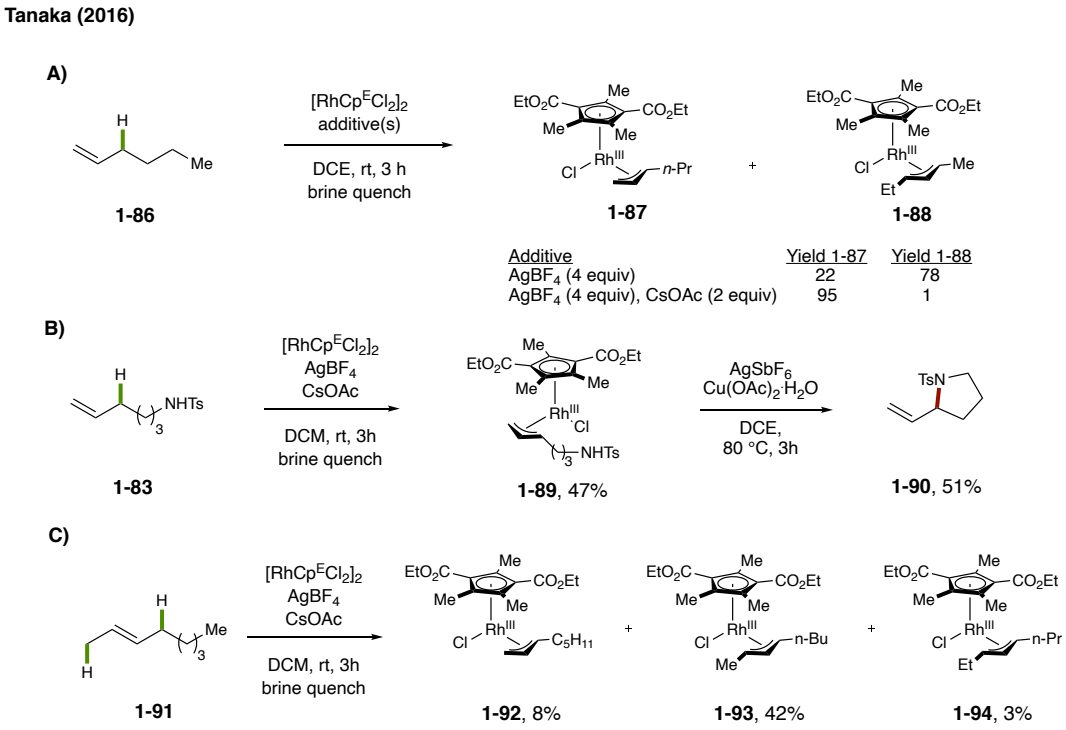

Figure 1-14. Stoichiometric Studies of π-allyl Complex Formation via C–H Functionalization

II.4. Intermolecular Allylic C–H Amination

Considering the previously disclosed information, it became clear that an allylic C–H amination of internal olefins could be realized. Jacob Burman from our lab then began an investigation towards the development of a rhodium-catalyzed allylic C–H amination of disubstituted olefins.[58] Optimization of the reaction revealed that AgOAc gave better results compared to $Cu(OAc)_2$, providing amine **1-95** in 88% yield. Furthermore, amines with only one electron-withdrawing activating group were well-tolerated allowing for alkyl and aryl amine reactivity (**Figure 1-15**). Notably, when *N*-Cbz-OMe alanine was utilized as the amine nucleophile, product **1-98** was observed in 26% yield. Likewise, a wide variety of styrenyl olefins (**1-95**) were utilized, resulting in modest to good yield. When thiophene or *N*-tosylindole derivatives were used, the corresponding products were observed in 42% (**1-100**) and 52% (**1-101**) yield, respectively. To further extend the scope of the olefin coupling partner, allylbenzene was then used, providing cinnamyl amine **1-102** in 40% yield. A trisubstituted olefin was also employed, providing **1-103** in 39% yield. Furthermore, deuterium exchange studies showed no deuterium scrambling, supporting irreversible C–H cleavage. This work was a foundation on which to develop novel methodologies and was the first intermolecular allylic C–H amination in this class of reactions.

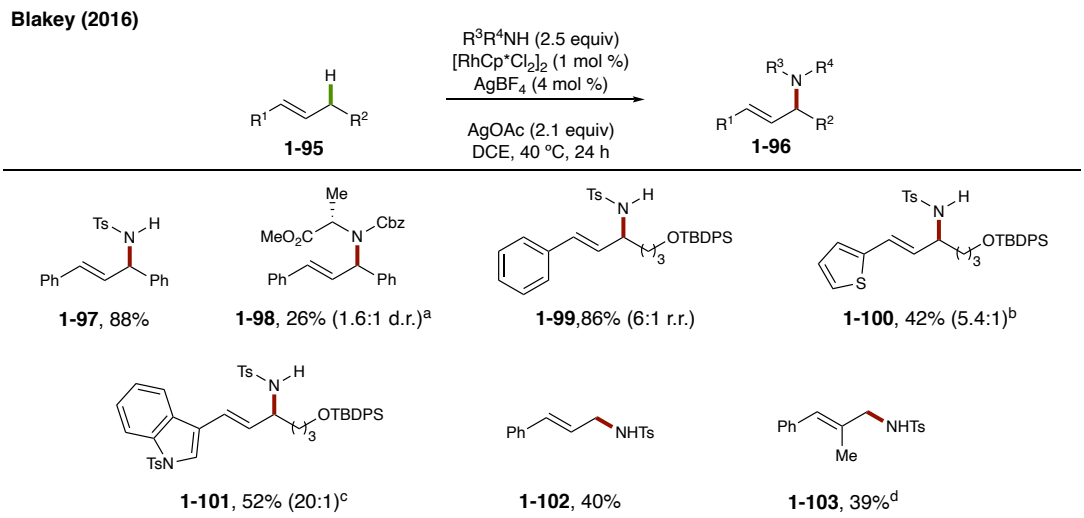

[a] Reaction was performed at 60 °C for 48 h. [b] Reaction was performed at 60 °C for 24 h. [c] Reaction was performed at 80 °C for 48 h. [d] Reaction was performed at 80 °C for 24 h.

Figure 1-15. Intermolecular RhCp*-Catalyzed Allylic C–H Amination

II.5. Conclusions and Outlook:

The work described herein provides key historical insight into palladium and group(IX)Cp*-catalyzed allylic C–H functionalization reactions prior to 2018.[6, 32, 38, 59, 60] This work has mainly focused on C–N bond formation as well as cyclization reactions. While both of these reaction types are key to forming biologically relevant molecules, there is still a lack of generality for these transformations. Furthermore, the amines are stabilized by one electron-withdrawing group, with intermolecular reactivity only observed for styrenyl variants. To fully realize the potential of allylic C–H functionalization, a variety of C–O, C–N, and C–C bond forming reactions must be developed. Likewise, catalyst controlled regioselectivity would be ideal, regardless of the electronic or steric nature of the starting substrate. Even further expansion of the nucleophile and olefin coupling partners to those seen in complex natural products would provide a system that could be widely adopted. This

dissertation describes the development of novel C–O, C–N, and C–C bond-forming allylic C–H functionalization reactions that aim to address these limitations.

III. References

1. Nicolaou, K. C., Organic synthesis: the art and science of replicating the molecules of living nature and creating others like them in the laboratory. *Proc. R. Soc. A.* **2014,** *470*, 20130690.

2. Doerksen, R. S.; Meyer, C. C.; Krische, M. J., Feedstock Reagents in Metal-Catalyzed Carbonyl Reductive Coupling: Minimizing Preactivation for Efficiency in Target-Oriented Synthesis. *Angew. Chem. Int. Ed.* **2019,** *58*, 14055-14064.

3. Santhoshkumar, R.; Cheng, C. H., Reaching Green: Heterocycle Synthesis by Transition Metal-Catalyzed C−H Functionalization in Sustainable Medium. *Chem. – Eur. J.* **2019,** *25*, 9366-9384.

4. Chu, J. C. K.; Rovis, T., Complementary Strategies for Directed C(sp^3)−H Functionalization: A Comparison of Transition-Metal-Catalyzed Activation, Hydrogen Atom Transfer, and Carbene/Nitrene Transfer. *Angew. Chem. Int. Ed.* **2018,** *57*, 62-101.

5. Yu, J.-Q.; Shi, Z., *C–H activation*. Springer: 2010; Vol. 292.

6. Fernandes, R. A.; Nallasivam, J. L., Catalytic allylic functionalization via π-allyl palladium chemistry. *Org. Biomol. Chem.* **2019,** *17*, 8647-8672.

7. Guibé, F., Allylic protecting groups and their use in a complex environment part II: allylic protecting groups and their removal through catalytic palladium π-allyl methodology. *Tetrahedron* **1998,** *54*, 2967-3042.

8. Tsuji, J., The Tsuji–Trost Reaction and Related Carbon–Carbon Bond Formation Reactions: Overview of the Palladium–Catalyzed Carbon–Carbon Bond Formation via π-Allylpalladium and Propargylpalladium Intermediates. *Handb. Organopalladium Chem. Org. Synth.* **2002**, 1669-1687.

9. Tsuji, J.; Takahashi, H.; Morikawa, M., Organic syntheses by means of noble metal compounds XVII. Reaction of π-allylpalladium chloride with nucleophiles. *Tetrahedron Lett.* **1965,** *6*, 4387-4388.

10. Trost, B. M.; Van Vranken, D. L., Asymmetric Transition Metal-Catalyzed Allylic Alkylations. *Chem. Rev.* **1996,** *96*, 395-422.

11. Trost, B. M.; Fullerton, T. J., New synthetic reactions. Allylic alkylation. *J. Am. Chem. Soc.* **1973,** *95*, 292-294.

12. Koschker, P.; Breit, B., Branching Out: Rhodium-Catalyzed Allylation with Alkynes and Allenes. *Acc. Chem. Res.* **2016,** *49*, 1524-1536.

13. Li, G.; Huo, X.; Jiang, X.; Zhang, W., Asymmetric synthesis of allylic compounds via hydrofunctionalisation and difunctionalisation of dienes, allenes, and alkynes. *Chem. Soc. Rev.* **2020,** *49*, 2060-2118.

14. Hüttel, R.; Kratzer, J., Über Olefin-Palladiumchlorid-Komplexe 1. Mitteilung. *Angew. Chem.* **1959,** *71*, 456-456.

15. Hüttel, R.; Bechter, M., Dehydrierende Dimerisierung von Phenyläthylen-Derivaten 2. Mitteilung über Olefin-Palladiumchlorid-Komplexe. *Angew. Chem.* **1959,** *71*, 456-456.

16. Kitching, W.; Rappoport, Z.; Winstein, S.; Young, W. G., Allylic Oxidation of Olefins by Palladium Acetate 1. *J. Am. Chem. Soc.* **1966,** *88*, 2054-2055.

17. Trost, B. M.; Fullerton, T. J., New synthetic reactions. Allylic alkylation. *J. Am. Chem. Soc.* **1973,** *95*, 292-294.

18. Uemura, S.; Fukuzawa, S.-I.; Toshimitsu, A.; Okano, M., Palladium-catalyzed allylic oxidation of olefins by t-butyl hydroperoxide and tellurium(IV) oxide. *Tetrahedron Lett.* **1982,** *23*, 87-90.

19. Hansson, S.; Heumann, A.; Rein, T.; Aakermark, B., Preparation of allylic acetates from simple alkenes by palladium (II)-catalyzed acetoxylation. *J. Org. Chem.* **1990,** *55*, 975-984.

20. Grennberg, H.; Bäckvall, J. E., Mechanism of palladium-catalyzed allylic acetoxylation of cyclohexene. *Chem. – Eur. J.* **1998,** *4*, 1083-1089.

21. El Firdoussi, L.; Baqqa, A.; Allaoud, S.; Allal, B. A.; Karim, A.; Castanet, Y.; Mortreux, A., Selective palladium-catalysed functionalization of limonene: synthetic and mechanistic aspects. *J. Mol. Catal. A: Chem.* **1998,** *135*, 11-22.

22. Chen, M. S.; White, M. C., A Sulfoxide-Promoted, Catalytic Method for the Regioselective Synthesis of Allylic Acetates from Monosubstituted Olefins via C−H Oxidation. *J. Am. Chem. Soc.* **2004,** *126*, 1346-1347.

23. Kitching, W.; Rappoport, Z.; Winstein, S.; Young, W. G., Allylic Oxidation of Olefins by Palladium Acetate 1. *J. Am. Chem. Soc.***1966,** *88*, 2054-2055.

24. Covell, D. J.; White, M. C., A Chiral Lewis Acid Strategy for Enantioselective Allylic C–H Oxidation. *Angew. Chem. Int. Ed.* **2008,** *47*, 6448-6451.

25. Diao, T.; Stahl, S. S., O_2-promoted allylic acetoxylation of alkenes: Assessment of "push" versus "pull" mechanisms and comparison between O_2 and benzoquinone. *Polyhedron* **2014,** *84*, 96-102.

26. Zhang, Z.; Wu, Q.; Hashiguchi, T.; Ishida, T.; Murayama, H.; Tokunaga, M., Allylic C–H acetoxylation of terminal alkenes over TiO_2 supported palladium nanoparticles using molecular oxygen as the oxidant. *Catal. Comm.* **2016,** *87*, 18-22.

27. Ammann, S. E.; Rice, G. T.; White, M. C., Terminal Olefins to Chromans, Isochromans, and Pyrans via Allylic C–H Oxidation. *J. Am. Chem. Soc.* **2014,** *136*, 10834-10837.

28. Wang, P.-S.; Liu, P.; Zhai, Y.-J.; Lin, H.-C.; Han, Z.-Y.; Gong, L.-Z., Asymmetric Allylic C–H Oxidation for the Synthesis of Chromans. *J. Am. Chem. Soc.* **2015,** *137*, 12732-12735.

29. Ammann, S. E.; Liu, W.; White, M. C., Enantioselective allylic C− H oxidation of terminal olefins to isochromans by palladium (II)/chiral sulfoxide catalysis. *Angew. Chem. Int. Ed.* **2016,** *55*, 9571-9575.

30. Li, C.; Li, M.; Li, J.; Liao, J.; Wu, W.; Jiang, H., Palladium-Catalyzed Aerobic Oxygenation of Allylarenes. *J. Org. Chem.* **2017,** *82*, 10912-10919.

31. Qi, X.; Chen, P.; Liu, G., Catalytic oxidative trifluoromethoxylation of allylic C− H bonds using a palladium catalyst. *Angew. Chem. Int. Ed.* **2017,** *56*, 9517-9521.

32. Wang, R.; Luan, Y.; Ye, M., Transition Metal–Catalyzed Allylic C(sp^3)–H Functionalization via η^3 -Allylmetal Intermediate. *Chin. J. Chem.* **2019,** *37*, 720-743.

33. Liu, G.; Yin, G.; Wu, L., Palladium-Catalyzed Intermolecular Aerobic Oxidative Amination of Terminal Alkenes: Efficient Synthesis of Linear Allylamine Derivatives. *Angew. Chem. Int. Ed.* **2008,** *47*, 4733-4736.

34. Reed, S. A.; White, M. C., Catalytic intermolecular linear allylic C–H amination via heterobimetallic catalysis. *J. Am. Chem. Soc.* **2008,** *130*, 3316-3318.

35. Pattillo, C. C.; Strambeanu, I. I.; Calleja, P.; Vermeulen, N. A.; Mizuno, T.; White, M. C., Aerobic linear allylic C–H amination: overcoming benzoquinone inhibition. *J. Am. Chem. Soc.* **2016,** *138*, 1265-1272.

36. Shimizu, Y.; Obora, Y.; Ishii, Y., Intermolecular Aerobic oxidative allylic amination of simple alkenes with diarylamines catalyzed by the $Pd(OCOCF_3)_2$/NPMoV/O_2 system. *Org. Lett.* **2010,** *12*, 1372-1374.

37. Ma, R.; White, M. C., C–H to C–N Cross-Coupling of Sulfonamides with Olefins. *J. Am. Chem. Soc.* **2018,** *140*, 3202-3205.

38. Liron, F.; Oble, J.; Lorion, M. M.; Poli, G., Direct Allylic Functionalization Through Pd-Catalyzed C–H Activation. *Eur. J. Org. Chem.* **2014,** *2014*, 5863-5883.

39. Young, A. J.; White, M. C., Catalytic Intermolecular Allylic C–H Alkylation. *J. Am. Chem. Soc.* **2008,** *130*, 14090-14091.

40. Mo, H.; Bao, W., Efficient Palladium-Catalyzed Oxidative Indolation of Allylic Compounds with DDQ via sp^3 C–H Bond Activation and Carbon-Carbon Bond Formation Under Mild Conditions. *Adv. Synth. Catal.* **2009,** *351*, 2845-2849.

41. Jiang, H.; Yang, W.; Chen, H.; Li, J.; Wu, W., Palladium-catalyzed aerobic oxidative allylic C–H arylation of alkenes with polyfluorobenzenes. *Chem. Commun.* **2014,** *50*, 7202-7204.

42. Zhang, H.; Hu, R.-B.; Liu, N.; Li, S.-X.; Yang, S.-D., Dearomatization of Indoles via Palladium-Catalyzed Allylic C–H Activation. *Org. Lett.* **2016,** *18*, 28-31.

43. Jin, M.; Ren, W.; Qian, D.-W.; Yang, S.-D., Direct Allylic C (sp^3)-H Alkylation with 2-Naphthols via Cooperative Palladium and Copper Catalysis: Construction of Cyclohexadienones with Quaternary Carbon Centers. *Org. Lett.* **2018,** *20*, 7015-7019.

44. Sambiagio, C.; Schönbauer, D.; Blieck, R.; Dao-Huy, T.; Pototschnig, G.; Schaaf, P.; Wiesinger, T.; Zia, M. F.; Wencel-Delord, J.; Besset, T.; Maes, B. U. W.; Schnürch, M., A comprehensive overview of directing groups applied in metal-catalysed C–H functionalisation chemistry. *Chem. Soc. Rev.* **2018,** *47*, 6603-6743.

45. Zhang, M.; Zhang, Y.; Jie, X.; Zhao, H.; Li, G.; Su, W., Recent advances in directed C–H functionalizations using monodentate nitrogen-based directing groups. *Org. Chem. Front.* **2014,** *1*, 843-895.

46. Lyons, T. W.; Sanford, M. S., Palladium-catalyzed ligand-directed C−H functionalization reactions. *Chem. Rev.* **2010,** *110*, 1147-1169.

47. He, J.; Wasa, M.; Chan, K. S.; Shao, Q.; Yu, J.-Q., Palladium-catalyzed transformations of alkyl C–H bonds. *Chem. Rev.* **2017,** *117*, 8754-8786.

48. Giri, R.; Thapa, S.; Kafle, A., Palladium-Catalysed, Directed C–H Coupling with Organometallics. *Adv. Synth. Catal.* **2014,** *356*, 1395-1411.

49. Peneau, A.; Guillou, C.; Chabaud, L., Recent Advances in [Cp*M^{III}] (M = Co, Rh, Ir)-Catalyzed Intramolecular Annulation Through C-H Activation. *Eur. J. Org. Chem.* **2018**, *42,* 5777-5794

50. Park, J.; Chang, S., Comparison of the Reactivities and Selectivities of Group 9 [Cp* M^{III}] Catalysts in C−H Functionalization Reactions. *Chem. Asian J.l* **2018,** *13*, 1089-1102.

51. Colby, D. A.; Tsai, A. S.; Bergman, R. G.; Ellman, J. A., Rhodium Catalyzed Chelation-Assisted C–H Bond Functionalization Reactions. *Acc. Chem. Res.* **2012,** *45*, 814-825.

52. Rakshit, S.; Patureau, F. W.; Glorius, F., Pyrrole synthesis via allylic sp^3 C– H activation of enamines followed by intermolecular coupling with unactivated alkynes. *J. Am. Chem. Soc.* **2010,** *132*, 9585-9587.

53. Li, X.; Gong, X.; Zhao, M.; Song, G.; Deng, J.; Li, X., Rh (III)-catalyzed oxidative olefination of N-(1-naphthyl) sulfonamides using activated and unactivated alkenes. *Org. Lett.* **2011,** *13*, 5808-5811.

54. Zhu, C.; Falck, J. R., N-Acylsulfonamide Assisted Tandem C–H Olefination/Annulation: Synthesis of Isoindolinones. *Org. Lett.* **2011,** *13*, 1214-1217.

55. Cochet, T.; Bellosta, V.; Roche, D.; Ortholand, J.-Y.; Greiner, A.; Cossy, J., Rhodium (III)-catalyzed allylic C–H bond amination. Synthesis of cyclic amines from ω-unsaturated N-sulfonylamines. *Chem. Commun.* **2012,** *48*, 10745-10747.

56. Archambeau, A.; Rovis, T., Rhodium(III)-Catalyzed Allylic C(sp^3)-H Activation of Alkenyl Sulfonamides: Unexpected Formation of Azabicycles. *Angew. Chem., Int. Ed.* **2015,** *127*, 13535-13538.

57. Shibata, Y.; Kudo, E.; Sugiyama, H.; Uekusa, H.; Tanaka, K., Facile Generation and Isolation of π-Allyl Complexes from Aliphatic Alkenes and an Electron-Deficient Rh(III) Complex: Key Intermediates of Allylic C–H Functionalization. *Organometallics* **2016,** *35*, 1547-1552.

58. Burman, J. S.; Blakey, S. B., Regioselective Intermolecular Allylic C–H Amination of Disubstituted Olefins via Rhodium/π-Allyl Intermediates. *Angew. Chem. Int. Ed.* **2017,** *56*, 13666-13669.

59. Nelson, T. A. F.; Hollerbach, M. R.; Blakey, S. B., Allylic C–H functionalization via group 9 π-allyl intermediates. *Dalton Trans.* **2020,** *49*, 13928-13935.

60. Kazerouni, A.; McKoy, Q.; Blakey, S. B., Recent advances in oxidative allylic C–H functionalization via group IX-metal catalysis. *Chem. Commun.* **2020**. *56*, 13287-13300

Chapter 2: Rhodium-Catalyzed C–O Bond Formation via Allylic C–H Functionalization of Internal Olefins

I. Introduction: Allylic Ethers

I.1. Synthesis

Allylic ethers and esters are important functional motifs that have been found broadly in complex synthetic intermediates and natural products.[1-3] Notable examples of allylic ethers and carboxylates in pharmaceuticals include Eribulin (**2-1**, Halaven),[4] Oseltamivir (**2-2,** Tamiflu),[5-9] and Paclitaxel (**2-3,** Taxol),[10-12]. Taxol and Halaven have had historically challenging syntheses and, for this reason, have been a focus of the synthetic community for some time. While Taxol's synthesis was eventually shortened using semi-synthetic methods,[12] Halaven still requires a lengthy 62-step synthesis. The allylic ethers in Halaven were installed using nucleophilic substitution reactions, requiring excessive functional group manipulations.[4] For oseltamivir and paclitaxel, the ethers are formed by protecting an allylic alcohol precursor. In each of these cases, the allylic alcohol is present in the natural product starting material but must be protected early on in the synthesis to induce specific reactivity. It is unsurprising that much effort has been placed on shortening the total syntheses of these complex molecules. Shortening the synthetic routes would reduce the waste produced, having monetary and environmental benefits.

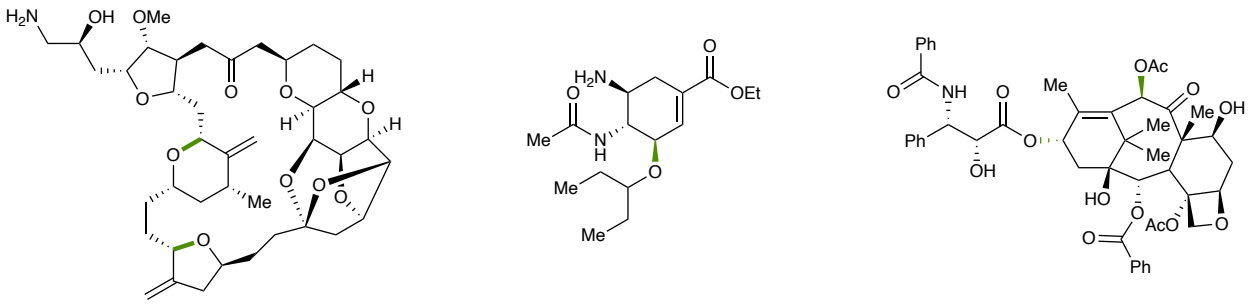

2-1

eribulin (Halaven)

anticancer

2-2

oseltamivir (Tamiflu)

antiviral influenza

2-3

paclitaxel (Taxol)

chemotherapy

Figure 2-1. Allylic Ethers and Esters Found in Complex Pharmaceutical Molecules

As was mentioned previously, allylic compounds can be accessed utilizing, functionalized olefins, allenes, alkynes, and dienes proceeding via a transition metal π-allyl complex.[13] In all these cases allylic ethers have been more synthetically challenging than their ester counterparts. Transition-metal-catalyzed allylic substitution has been used to form complex allylic ethers enantio- and regioselectivity from (**2-4**) and remains the most broadly used method described. [14, 15] Furthermore, simple S_N1' substitution chemistry can also be implemented on allylic compounds with a leaving group (**2-4**) to form the corresponding ether or ester, albeit less selectively than the transition-metal catalyzed work (**Figure 2-2A**).[16] This synthetic technique was seen in the total synthesis of halaven to form both allylic ethers. Another method to form allylic ethers includes the simple protection of allylic alcohols (**2-6**). Typically this occurs via a substitution reaction (S_N1 or S_N2) of the alcohol with an alkyl halide, which can be seen in the syntheses of paclitaxel and oseltamivir (**Figure 2-2B**).[9, 17] Analogously, nucleophilic attack of an α,β-unsaturated ketone (**2-7**) with

an alkyl Grignard (**2-8**) or lithium reagent (**2-9**) followed by substitution of an alkyl halide can be utilized as a one-pot method starting from a ketone rather than an alcohol to form ether **2-5** (**Figure 2-2C**).[18] Likewise, formal hydroetherification of a diene (**2-10**) is another method by which to form allylic ethers, although this technique has not been widely developed or adopted for synthesis (**Figure 2-2D**).[19] While these methods have proven useful, they all rely on preoxidized substrates. Arguably, a more direct means to make allylic ethers would be through the activation of an allylic C–H bond.

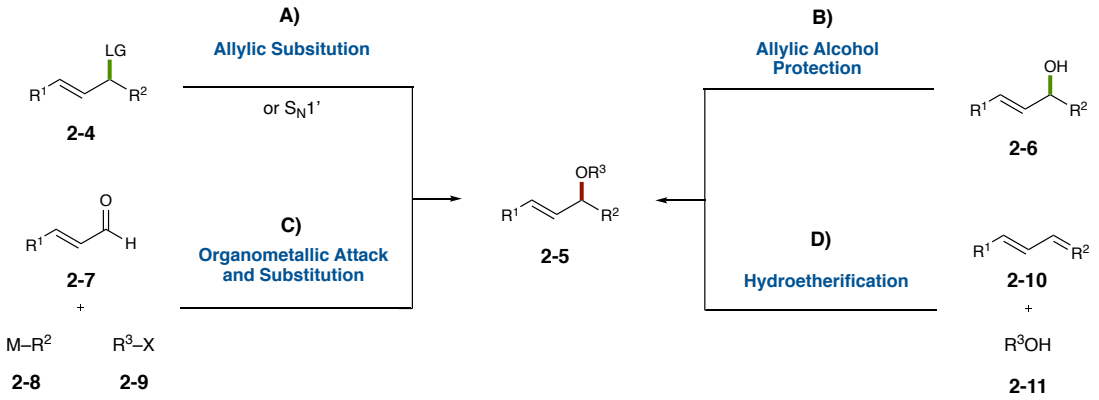

Figure 2-2. Synthetic Routes to form Allylic Ethers

I.2. Allylic C–H Functionalization

As was mentioned previously, allylic C–H functionalization has proven to be a useful method to form complex allylic products (Chapter 1, Figure 1-2). Allylic C–H acetoxylation reactions have been well studied, but the corresponding allylic C–H etherification reactions have not, limiting utility. Overall, palladium-catalyzed allylic C–H functionalization reactions

are limited to terminal olefins and the alcohol coupling partners typically lack further functionality and are required in solvent quantities.[20] Furthermore, allylic C–H etherification reactions were dominated by intramolecular, not intermolecular, reports to form pyran and furans prior to 2017. In 2017, two very important intermolecular allylic C–H etherification procedures were disclosed. The first, by Jiang *et. al.,* was a palladium-catalyzed etherification reaction proceeding via a π-allyl intermediate (**Figure 2-3A**).[21] This protocol was the first intermolecular allylic C–H etherification reaction with broad applications and was tolerant of many alcohols including phenols. Phenols are particularly challenging as nucleophilic coupling partners as they are prone to oxidation. Ligand choice was crucial for the reactivity for each alcohol class. For aliphatic alcohols, $Pd(OAc)_2$ with DMSO as the solvent was found to provide the optimal results. In the case of phenols, $Pd_2(dba)_3$ with PPh_3 as the ligand additive and toluene as the solvent provided the best yields of **2-12**. Furthermore, in both cases, dioxygen was used as the terminal oxidant. With oxidative C–H coupling reactions, having a sustainable and clean oxidant like dioxygen is ideal for the scalability and sustainability of these reactions. That same year, Liu and co-workers developed a trifluoromethoxylation of terminal olefins (**Figure 2-3B**).[22] The trifluoromethoxide anion adds complications as rapid decomposition to the corresponding ketone hinders reactivity. Also, trifluoromethoxide anions are far less nucleophilic than typical alcohols which hinders the generality of these conditions. The authors found that the slow leaching of $AgOCF_3$ from AgF and $CsOCF_3$ provided reactivity without excessive decomposition. Trifluoromethoxylation procedures are of particular importance in the pharmaceutical industry due to the drastic effect on lipophilicity that trifluoromethoxy groups provide for drug candidates.[23, 24] Likewise, fluorinated drugs are used as a contrast reagents for MRI

studies.[25, 26] While these protocols were a great advance, it became clear that the use of olefins beyond allylbenzene derivatives and alcohols with important functional motifs would be necessary for the adoption of these methods in a broader sense.

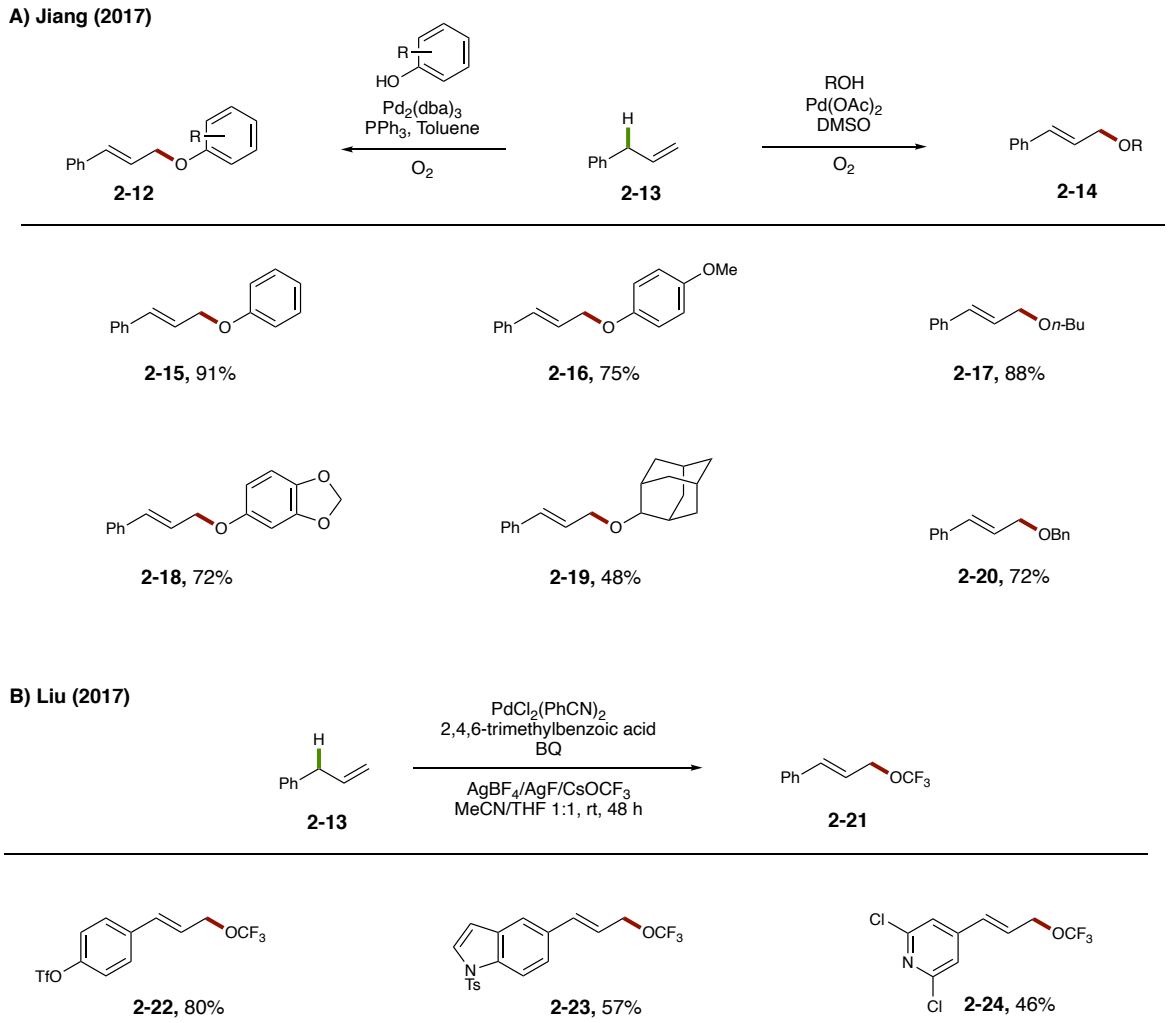

Figure 2-3. Examples of Intermolecular Allylic C–H Etherification

II. Optimization Studies

After the seminal work disclosed by Cossy,[27] Tanaka,[28] and our group on allylic C–H amination,[29] discussed in Chapter 1 (Figure 1-11, 1-12, 1-14, 1-15), an allylic C–H etherification procedure was proposed using a RhCp* catalyst system. Preliminary studies suggested that benzyl alcohol could be utilized as the alcohol nucleophile in a corresponding method. With this knowledge, optimization studies were initiated with similar conditions to those previously disclosed by our group with (**2-25**), resulting in only 27% yield of **2-26** (**Table 2-1**, **Entry 1**). We noted that silver halide scavenger counterions have been shown to have significant impact on a variety of C–H functionalization reactions.[30, 31] For this reason, another common silver(I) halide scavenger with a less coordinating counterion, $AgSbF_6$, was utilized at 60 °C for 5 hours with 5 equivalents of benzyl alcohol, resulting in a drastic increase in yield to 97% of **2-26** and 2% of acetate **2-27** (**Table 2-1, Entry 2**). This allylic acetate (**2-27**) was observed in our amination disclosure and was originally believed to be a competitive side-product resulting from nucleophilic attack of the acetate present from the AgOAc. In order to provide milder reaction conditions, the reaction temperature was lowered to 40 °C for an extended 24 h reaction time providing ether **2-26** in 95 % yield (**Table 2-1, Entry 3**). Lowering the reaction time to 4 hours at 60 °C only provided **2-26** in 68% yield (**Table 2-1, Entry 4**). In order to absolve the need for a silver(I) halide scavenger, $[RhCp^*(MeCN)_3](SbF_6)_2$ was utilized as the precatalyst providing **2-26** in only 29% yield (**Table 2-1, Entry 5**). Extending the reaction time to 24 hours did not increase the yield but resulted in 0% yield of **2-26** and a substantial 17% yield of acetate **2-27** (**Table 2-1, Entry 6**). Since the lack of silver in entries 5 and 6 resulted in low yields, a control experiment with no $[RhCp^*Cl_2]_2$ was performed. This resulted in no conversion, confirming the role of

rhodium as the precatalyst (**Table 2-1, Entry 7**). Furthermore, while benzyl alcohol is an inexpensive coupling partner, we realize that in more complex systems one would want to conserve material. For this reason, we proceeded with only 2.5 equivalents of benzyl alcohol as the nucleophile for further testing. When $AgSbF_6$ was utilized with 2.5 equivalents of benzyl alcohol for 5 hours at 60 °C, **2-26** was observed in 25% yield (**Table 2-1, Entry 8**) but extending the reaction time to 24 hours did provide an increase in yield to 91% (**Table 2-1, Entry 9**). Since the counterion had such a drastic effect on the yield earlier in this study, a small scope of non-coordinating silver salts was performed. To provide a clear comparison, the reactions were performed with 2.5 equivalents of alcohol for 5 hours. In the case of $AgNO_3$ (0%, **Entry 10**), and AgOTs (0%, **Entry 11**) no conversion was observed. On the other hand, $AgNTf_2$ (76%, **Entry 12**), AgOTf (34%, **Entry 13**), $AgPF_6$ (87%, **Entry 14**), and $AgBAr_4^F$ (91%, **Entry 15**) all provided an increase in conversion compared to $AgSbF_6$ (25%, **Entry 8**). Furthermore, since $AgBAr_4^F$ was costly and not commercially available, we chose to use $NaBAr_4^F$ (76%, **Entry 16**) as the halide scavenger, providing promising results. Due to the increased yield of acetate **2-22** observed, Ag_2O was utilized as the silver oxidant in place of AgOAc with 10 mol% acetic acid as a carboxylate source, affording ether **2-26** (71%) in moderate yield (**Table 2-1, Entry 17**). While $AgBAr_4^F$ did perform the best at lower nucleophile loading, the cost and time required to make the salt precluded $AgBAr_4^F$ for further studies. With cost and time in mind we chose to continue these studies with the conditions described in Entry 2.

Table 2-1. Optimization of RhCp*-Catalyzed Allylic C–H Etherification

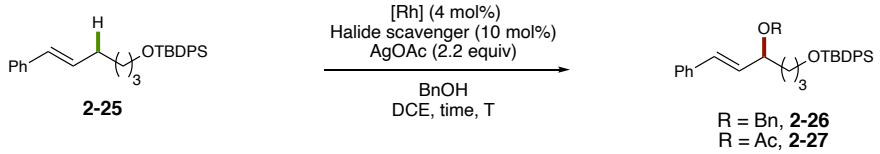

2-25

R = Bn, **2-26**
R = Ac, **2-27**

Entry	[Rh]	T(°C)	time(h)	BnOH (equiv)	halide scavenger	% yield **2-26**	% yield **2-27**
1	$[RhCp^*Cl_2]_2$	60	5	5	$AgBF_4$	27	0
2	$[RhCp^*Cl_2]_2$	60	5	5	$AgSbF_6$	97	2
3	$[RhCp^*Cl_2]_2$	40	24	5	$AgSbF_6$	95	2
4	$[RhCp^*Cl_2]_2$	60	4	5	$AgSbF_6$	68	1
5	$[RhCp^*(MeCN)_3](SbF_6)_2$	60	5	5	-	29	0
6	$[RhCp^*(MeCN)_3](SbF_6)_2$	60	24	5	-	0	17
7	-	60	5	5	$AgSbF_6$	0	0
8	$[RhCp^*Cl_2]_2$	60	5	2.5	$AgSbF_6$	25	0
9	$[RhCp^*Cl_2]_2$	60	24	2.5	$AgSbF_6$	91	4
10	$[RhCp^*Cl_2]_2$	60	5	2.5	$AgNO_3$	0	0
11	$[RhCp^*Cl_2]_2$	60	5	2.5	AgOTs	0	0
12	$[RhCp^*Cl_2]_2$	60	5	2.5	$AgNTf_2$	76	14
13	$[RhCp^*Cl_2]_2$	60	5	2.5	AgOTf	34	12
14	$[RhCp^*Cl_2]_2$	60	5	2.5	$AgPF_6$	87	6
15	$[RhCp^*Cl_2]_2$	60	5	2.5	$AgBAr^F_4$	91	11
16	$[RhCp^*Cl_2]_2$	60	5	2.5	$NaBAr^F_4$	76	7
17[a]	$[RhCp^*Cl_2]_2$	60	24	2.5	$AgPF_6$	71	1

All reactions run at 0.2 M concentration. All yields were determined by crude ^{1}H NMR analysis against 1,3,5-trimethoxybenzene as internal standard.[a] 1.1 equivalents of Ag_2O and 10 mol % acetic acid used.

III. Scope Studies of Allylic C–H Etherification

III.1. Alcohol Coupling Partner

With optimized conditions in hand, I sought to determine the steric, electronic, and functional group tolerance of the alcohol coupling partner (**Figure 2-4**). As a starting point, methanol provided moderate yield of **2-29** when 5 equivalents (47%) or 10 equivalents (51%) of alcohol was used. Ethanol provided the corresponding ether **2-30** in 70% yield under standard conditions. Isopropanol (47%, **2-31**) resulted in lowered conversion compared to ethanol even with 3.0 equiv of AgOAc, suggesting that steric hindrance may be deleterious to the reaction. Unsurprisingly, *tert*-butanol provided no desired product **2-32**.

The electronic nature of the alcohol was also explored when 2,2,2-trichloroethanol (TCE, 44%, **2-33**) and 2,2,2-trifluoroethanol (TFE, 39%, **2-34**) were utilized under standard conditions resulting in modest yields. A significant amount of acetate **2-27** was observed in the crude ^{1}H NMR spectrum when TFE was used as the alcohol, likely due to the less nucleophilic nature of the alcohol. To allow for greater competition of TFE, 10 equiv of the nucleophile was used resulting 59% yield of **2-34**. Allyl alcohol was not tolerated in the reaction, with no C–H functionalization products observed by crude ^{1}H NMR analysis. While the cause is unknown, it is feasible for allyl alcohol to competitively bind the catalyst, shutting down reactivity. It became clear that the steric nature of the alcohol was important for reactivity, and so we utilized *iso*-butyl alcohol (59%, **2-36**) and neopentyl alcohol (45%, 2-37) to test the effect of steric bulk one carbon removed from the oxygen. While not drastic, a minor decrease in yield was observed when comparing **2-36** and **2-37,** supporting our hypothesis. When phenol was utilized as the nucleophile, no product (**2-38**) was observed. Phenolic alcohols have a decreased pKa and vastly different reactivity compared to standard alcohols. Furthermore, the significant color change to black suggests that oxidation of the phenol was occurring. While *iso*-propanol did not perform well, 2-indanol provided product in good yield (65%, **2-39**) suggesting that electronics had a greater impact on yield than steric bulk of the nucleophile. When the corresponding 1-indanol was used no ether product **2-40** was observed, likely due to the inherent steric hindrance of the aryl ring. While etherification is the primary focus of this investigation, a short scope of carboxylic acids were used as the nucleophile. Acetic acid (51%, **2-27**), isobutyric acid (44%, **2-41**), and benzoic acid (26%, **2-42**) were shown to provide the corresponding allylic esters in modest to good yields. Much of the loss of yield can be attributed to competitive acetate **2-27** formation. This

issue could likely be solved by utilizing synthetic silver(I) carboxylates corresponding to the desired ester. Since benzyl alcohol provided ether **2-26** in 87% yield under standard reaction conditions, testing the electronic nature of benzyl-type alcohols may provide further insight into the effect of electronics on reaction yield. When *p*-CF_3-benzyl alcohol was used, a lower 65% yield of **2-43** was observed, likely due to the less nucleophilic nature of the alcohol. Unexpectedly, when *p*-OMe-benzyl alcohol was used, only 42% yield of **2-44** was observed even when 3 equivalents of AgOAc was used. While this alcohol was more nucleophilic, *p*-anisaldehyde was observed by crude ^{1}H NMR analysis in large quantities, suggesting competitive oxidation of the alcohol was occurring. Furthermore 2-naphthylmethanol provided ether **2-45** in 49% yield. To further probe the effect of steric bias under more ideal conditions, 1-phenylethanol was utilized providing product **2-46** in 67% yield with a modest 2.1:1 diastereomeric ratio (d.r.). While not much can be concluded from the low d.r. of this reaction, the trend of increased yield of benzyl alcohols compared to aliphatic alcohols is supported. To fully realize the potential of this transformation, important building blocks of natural products were then investigated. Small heterocycles such as 3-oxetanemethanol (33 %, **2-47**), and *N*-Boc-3-azetidinemethanol (56 %, **2-48**) provided product in modest to good yield. Furthermore, actinide protected galactose **2-49** (42%) and morpholine derivative **2-50** (75%) were isolated in good to excellent yield, albeit with no stereoinduction. Even *N*-Boc-Ser-OMe, when utilized as the nucleophile, afforded product **2-51** in 61% yield. This series shows that this allylic C–H etherification reaction could be used for the coupling of complex molecules.

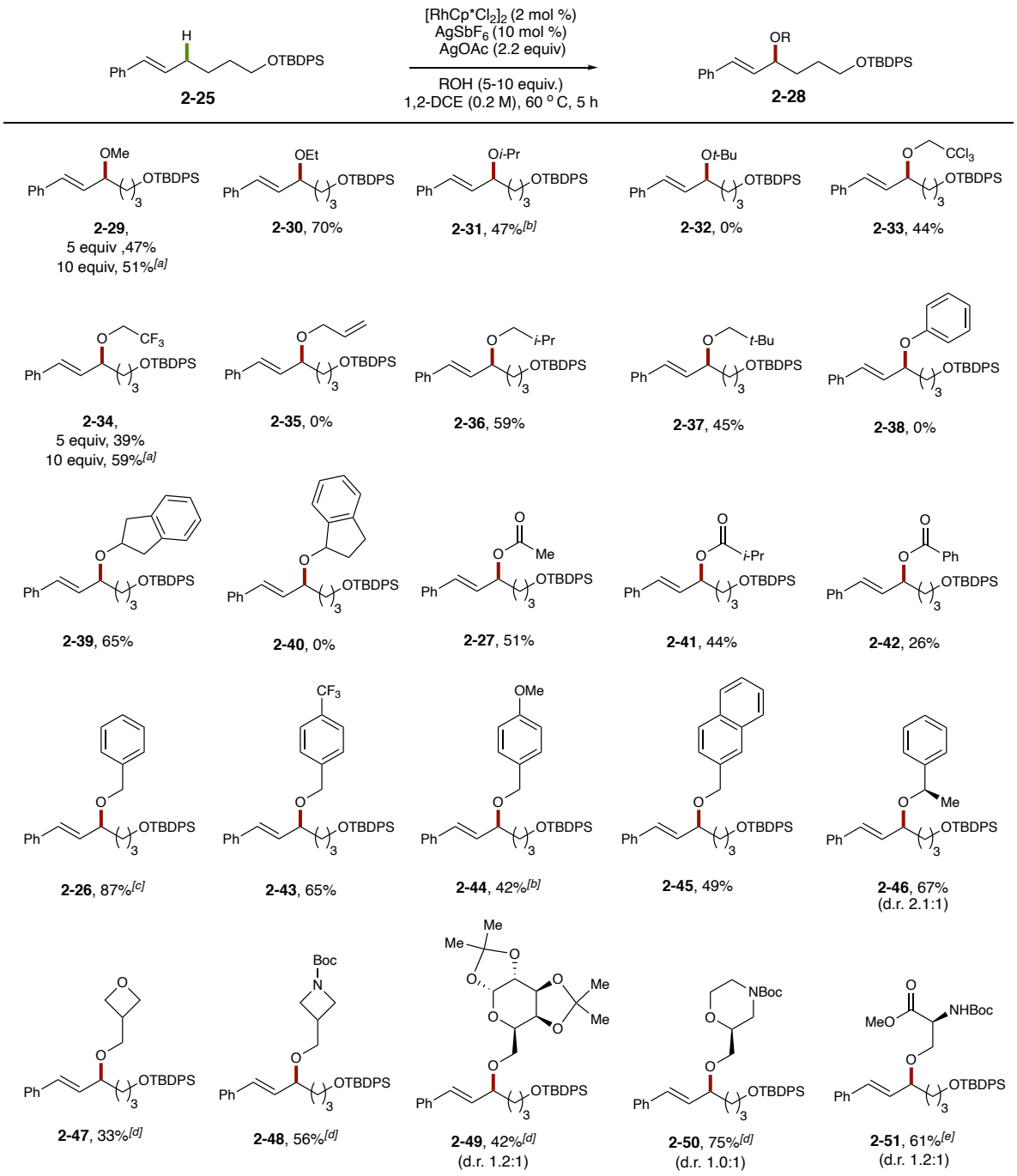

All reactions were carried out on a 0.2 mmol scale with 5 equivalents of alcohol at 60° C for 5 h unless otherwise stated. Yields are reported for isolated product. [a]10 equivalents of alcohol were used. [b]Reactions were run with 3 equivalents of AgOAc. [c]Reactions were run using 5 mol% catalyst loading.

Figure 2-4. Reaction Scope with Respect to the Alcohol Coupling Partner for Allylic C–H Etherification

III.2. Olefin Coupling Partner

After a thorough investigation of steric, electronic, and functional group tolerance of the alcohol coupling partner, my focus turned towards studying the reactivity of benzyl alcohol with a wide variety of aryl-alkyl olefin substrates. To determine the effect of steric bulk at the ortho position, both a methyl (43%, **2-52**) and an isopropyl (57%, **2-53**) group were utilized. Unsurprisingly, steric bulk did decrease the efficiency of the reaction comparatively, but the expected trend was not observed. We had expected the more sterically bulk isopropyl variant to provide lower yields, but this was not the case, likely due to the correlation of increased electron density with the increase in steric hindrance. This result suggests that the electronic nature of the ortho-substituent may have a greater effect on the reaction efficiency than the negative impact of steric hindrance. Next, we turned our focus to the understanding of the electronic nature of the aryl group by testing substituents at the para position. While no correlation with electron-density and yield could be determined as the CF_3 (45%, 48 h, **2-54**), Br (60%, 48 h, **2-55**), F (61%, 31 h, **2-56**), and OMe (58%, 4 h, **2-57**) variants gave similar yields, we could correlate reaction time with electron-density. The electron-withdrawing nature of the CF_3 group resulted in the longest reaction time (48 h) and required 5 mol% catalyst loading likely due to the less coordinating nature of the corresponding olefin. Likewise, the shortest reaction time (4 h) was observed when R = OMe was employed. The use of symmetrical 1,3-diphenylpropene with benzyl alcohol (70%, **2-58**) and methanol (53%, **2-59**) provided the corresponding ethers in good yield. Furthermore, when allylbenzene was used as the olefin coupling partner, benzyl cinnamyl ether **2-61** was provided in good yield (60%). While methods to form cinnamyl ethers from the corresponding allylbenzenes with palladium catalysts have been developed, it is

important to note that this RhCp*-catalyzed system works well with terminal and internal olefins. We then turned our focus towards the study of olefin coupling partners with complex molecule motifs. Estrone derivative **2-60** (33%), phenylalanine derivative **2-62** (41%), and tocopherol **2-63** (33%) were provided in more modest yields under standard reaction conditions. In the case of the estrone derivative, we found that the use of $AgBAr^{F}_{4}$ as the halide scavenger provided **2-60** in 75% yield, greatly increasing the yield. Unfortunately, when $AgBAr^{F}_{4}$ was used with phenylalanine derivative **2-62** (31%) or tocopherol derivative **2-63** (trace) the corresponding ethers were not provided in increased yield. So, while biologically relevant motifs were tolerated, they do appear to be deleterious to the overall reaction efficiency when benzyl alcohol is used as the alcohol coupling partner. The exchange of $AgSbF_6$ for $AgBAr^{F}_{4}$ only afforded an increase in yield for one example. While no clear trends were found for the effect of steric or electronic nature of the arene ring on yield, wide tolerance was observed including complex motifs.

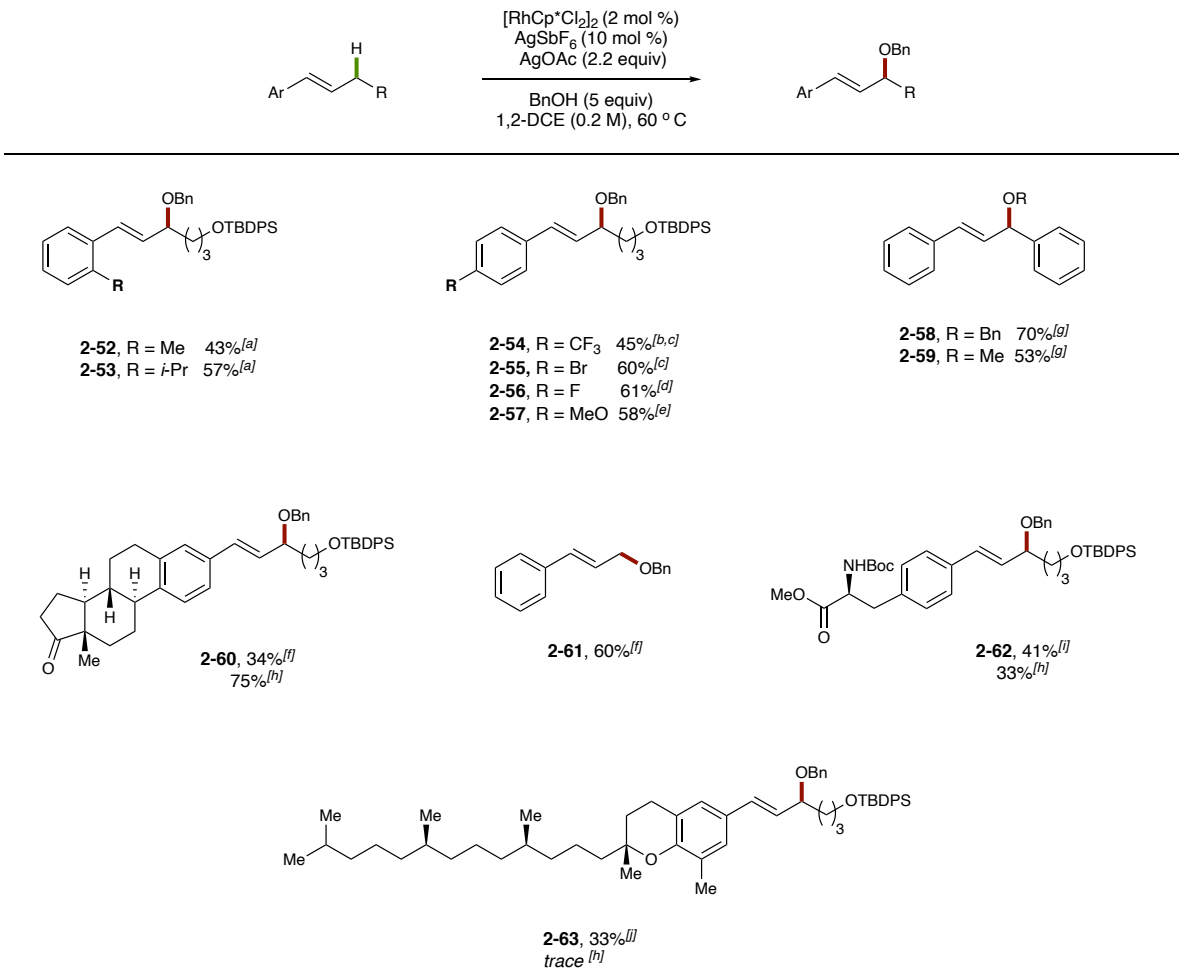

[a]Reaction time was 24 h. [b] Reactions were run using 5 mol % catalyst loading. [c] Reaction time was 48 h. [d] Reaction time was 31 h. [e] Reaction time was 4 h. [f] Reaction time was 21 h. [g] Reaction time was 6 h. [h] $AgBAr^{F}_{4}$ was utilized as the halide scavenger in place of $AgSbF_6$. [i]Reaction time was 27 h. [j] Reaction time was 26 h.

Figure 2-5. Reaction Scope with Respect to the Olefin Coupling Partner for Allylic C–H Etherification

III.3. Terminal Olefins

With the knowledge that allylbenzene could engage in this reaction, we decided to investigate the reactivity of nonactivated terminal olefins. In the case of allylcyclohexane (**2-64**) no product (**2-65**) was observed, suggesting that conjugation to the arene ring is crucial

for reactivity. On the other hand, when 4-phenyl-1-butene (**2-66**) was used as the olefin coupling partner, product **2-67** was observed in good yield (78%). Originally, etherification at the 1 or 3 position would have been expected, but only etherification at the 2 position was observed. The observed product is likely due to the migration of the π-allyl moiety to form a more stable intermediate in conjugation with the arene before the C–O bond can be formed. Similar reactivity was observed by Tanaka (Chapter 1, Figure 1-14) as three distinct π-allyl complexes were observed when 2-octene was utilized as the olefin precursor. Tanaka suggested an intermolecular mechanism for this isomerization between the π-allyl complex and starting olefin supported by experimental evidence. With this information in mind, it comes as no surprise that the thermodynamically favored product is observed as the sole product for this example. These results suggest that terminal olefins can engage in this reaction but require a product with the olefin in conjugation to an arene to form the desired product.

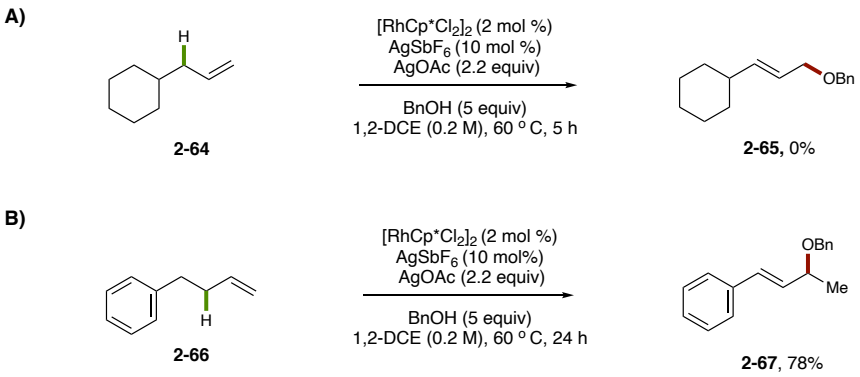

Figure 2-6. Allylic C–H Etherification of Terminal Olefins

IV. Mechanistic Investigations

As a means to understand the mechanism of this transformation, we determined that deuterium exchange and kinetic isotope effect studies should be performed. For deuterium exchange studies, deuterated 1,3-diphenylpropene (**2-68**) was used as the olefin under standard reaction conditions for 24 h. Both starting material (50%, **2-68**) and the desired ether products (30%, **2-69**) were isolated and analyzed by ^{1}H NMR assay. Since the π-allyl complex formed from olefin **2-68** is pseudosymmetrical it came as no surprise that two regioisomers were observed affording a secondary kinetic isotope effect (KIE) of 0.85. A secondary KIE of 0.85 corresponds to the rehybridization from sp^2 to sp^3 during bond formation. This proposed rehybridization would correspond to the π-allyl complex (sp^2) forming a C(sp^3)–O bond. Furthermore, all products (**2-69**) and recovered starting material (**2-68**) had 100% deuterium incorporation. No deuterium exchange in both the starting material and product suggests that C–H cleavage is irreversible. To determine a primary kinetic isotope effect, a 1:1 mixture of proteo- and deuterated 1,3-diphenylpropene (**2-68,** [D] **2-68**) was used as the starting material and the reaction stopped at 0.3 h. Analysis of the ^{1}H NMR of the isolated product showed a 3.3 (H/D) KIE. While further kinetic analysis would have to be performed for a definitive claim, a KIE of 3.3 suggests that C–H cleavage is the rate determining step.[32] Kinetic analysis of the corresponding amination protocol will be discussed in chapter 3 which supports C–H cleavage as the rate-determining step for these reactions.

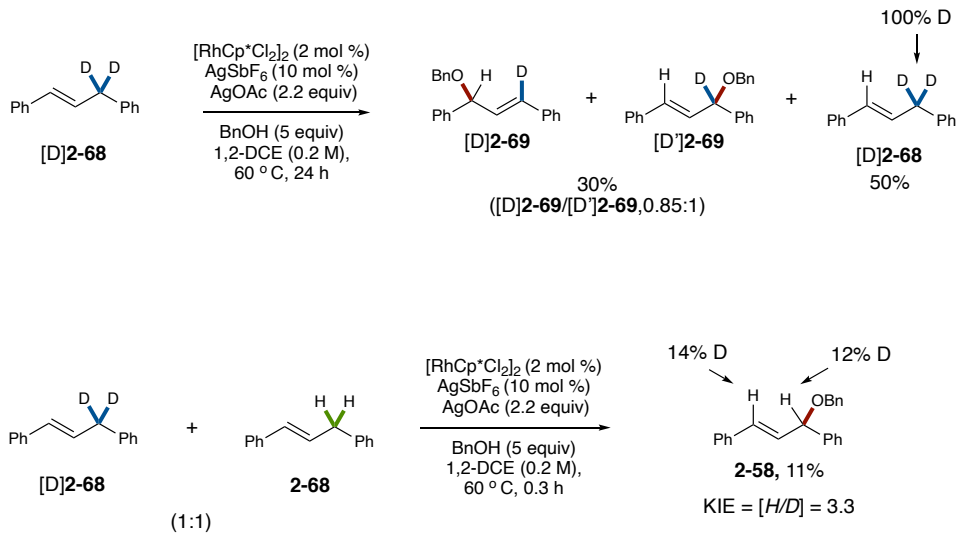

Figure 2-7. Deuterium Exchange and Kinetic Isotope Effect Studies

V. Conclusion

In conclusion, we have described the development of a regioselective allylic C–H etherification of internal olefins.[33] The key to optimization of reaction conditions was the subtle nuance in silver halide scavenger counterion. While no clear correlation can be made, counterions that are less coordinating outperformed their more coordinating counterparts. Studies of the alcohol coupling partner revealed that sterically bulky and electron-deficient alcohols had reduced yields overall. Likewise, while steric bulk decreased the overall reaction efficiency, the electronic nature of the alcohol appeared to have an overall greater effect on the yield. Alcohols with functionality present in natural products were also well tolerated, illustrating the utility of this reaction in total synthesis. Furthermore, a broad scope of olefin coupling partners was explored. While no trends in yields were observed with the variation of the electron density of the aryl group, electron deficient arenes resulted

in extended reaction times. Introduction of biologically active motifs were tolerated and for an estrone derivative, exchange of the $AgSbF_6$ additive to $AgBAr^F_4$ resulted in a drastic increase in yield. Further experiments revealed that terminal olefins were only reactive when the π-allyl complex would isomerize into conjugation with an aryl group. Deuterium exchange and primary kinetic isotope effect studies supported that C–H cleavage was irreversible and is likely the rate-determining step. This disclosure has expanded the scope of allylic C–H functionalization reactions by introducing a wider array alcohol nucleophiles and olefin coupling partners. Mechanistic investigations suggest an irreversible C–H cleavage as the rate-determining step. This work has provided a foundational for further development as this disclosure still stands as a rare example of allylic C–H etherification. A portion of the work was reported in Angewandte Chemie as a communication in 2018.[33]

VI. Experimental Procedures

VI.1. General Information:

Reactions were performed under a dry nitrogen atmosphere with anhydrous solvents using standard Schlenk techniques unless otherwise stated. Glassware was dried in an oven at 120 °C for a minimum of 6 hours or flame-dried under vacuum prior to use. Anhydrous tetrahydrofuran (THF), diethyl ether (Et_2O), 1,2-dimethoxyethane (DME) and dichloromethane (DCM) were obtained by passage through activated alumina using a *Glass Contours* solvent purification system. 1,2-dichloroethane (DCE) was distilled over CaH_2 under a nitrogen atmosphere onto activated 3Å molecular sieves in a Schlenk flask. Flash column chromatography was performed on a Biotage Isolera One flash chromatography system using Silicycle SiliaFlash® F60 silica gel (40-63 μm) as the solid phase unless

otherwise stated. Preparatory thin-layer chromatography (TLC) was performed on precoated glass backed Silicycle SiliaPure® 1.0 mm silica gel 60 plates. Analytical TLC was performed on precoated glass backed Silicycle SiliaPure® 0.25 mm silica gel 60 plates. Silver tetrakis[3,5 bis(trifluoromethyl)phenyl]borate: $AgBAr^F_4$ was prepared according to the literature.[34] (*E*)-*tert*-butyldiphenyl((6-phenylhex-5-en-1-yl)oxy)silane[29] was prepared using previously reported methods. All other reagents were obtained through major chemical suppliers and used as received unless otherwise stated. ^1H NMR was performed on a 300 MHz, 400 MHz, 500 MHz, or 600 MHz Varian Instrument using $CDCl_3$ with TMS as internal standard set to 0.00 ppm unless otherwise stated. Multiplicity (s = singlet, d = doublet, t = triplet, q = quartet, quint = quintet, m = multiplet or overlap of non-equivalent resonances, br = broad), integration. Proton-decoupled ^{13}C NMR was performed on a 150 MHz Bruker instrument using $CDCl_3$ as internal standard set to 77.16 ppm. All ^{19}F NMR were taken on a 400 MHz Varian instrument with C_6F_6 used as an external standard set to -164.9 ppm. IR spectra were collected on a Nicolet iS10 FT-IR diamond tipped spectrometer as a thin film. High resolution mass spectra were obtained using a Thermo Electron Corporation Finigan LTQFTMS (at the Mass Spectrometry Facility, Emory University).

VI.2. General Procedure A for Reaction Optimization:

Inside an N_2 atmosphere glovebox, to an oven-dried 7 mL vial equipped with a magnetic stir bar was added [Rh] (0.010 mmol, 4 mol %), halide scavenger (0.0257 mmol, 10 mol %), and AgOAc (0.56 mmol, 2.2 equiv). After all solids were weighed, the reaction vial was fitted with a septum and cap and removed from the glovebox. In a separate oven-dried 7 mL vial capped with a septum, under N_2 atmosphere a 0.20 M stock solution of (E)-tert-butyldiphenyl((6-phenylhex-5-en-1-yl)oxy)silane[29] was prepared in the appropriate solvent

(see table for details). An aliquot of this stock solution (see table for equivalents) was transferred to the vial containing the solid reagents. Benzyl alcohol (see table for equivalents) was then injected into the reaction vial via a microliter syringe. The resulting mixture was heated to temperature and stirred for the allotted amount of time (see table for details). The reaction mixture was cooled to room temperature, exposed to air, and a known amount of 1,3,5-trimethoxybenzene was added to the reaction mixture. The resulting mixture was filtered over celite and the celite was rinsed with EtOAc. The combined filtrate was concentrated under reduced pressure and analyzed by ^{1}H NMR.

VI.3. General Procedure B for Allylic Etherification:

Inside an N_2 atmosphere glovebox, to an oven-dried 7 mL vial equipped with a magnetic stir bar was added $[RhCp^*Cl_2]_2$, halide scavenger, and AgOAc. After all solids were weighed, the reaction vial was fitted with a septum and cap and removed from the glovebox. In a separate oven-dried 7 mL vial capped with a septum, under N_2 atmosphere a 0.20 M stock solution of the olefin coupling partner was prepared in DCE. An aliquot of the stock solution was transferred to the vial containing the solid reagents. The nucleophile was then added by syringe. The resulting mixture was heated to the appropriate temperature and stirred for the allotted amount of time. The reaction mixture was cooled to room temperature and exposed to air. The resulting mixture was filtered over celite and the celite was rinsed with EtOAc or Et_2O. The combined filtrate was concentrated under reduced pressure and purified by flash column chromatography on silica gel.

VI.4. General Procedure C for Suzuki Cross-Coupling:

To an oven-dried two-necked flask equipped with a stir bar with a reflux condenser was added $Pd(PPh_3)_4$ (5 mol %) followed by the placement of two septa on the reflux

condenser and remaining side-arm. The environment was exchanged with N_2 following Schlenk technique. The olefin (1.5 equiv) was weighed out and dissolved to afford a 2 M solution in 1,2-dimethoxyethane (DME). The alkene solution was then added to the reaction flask, followed by injection of the aryliodide or aryltriflate (1 equiv). This injection was followed by injection of a 2 M K_2CO_3 aqueous solution (2.8 equiv). The reaction vessel was heated to 85 °C overnight. The reaction was then allowed to cool to room temperature and was quenched with saturated aqueous sodium chloride solution followed by extraction with EtOAc (3x). The resulting solution was dried over anhydrous sodium sulfate, decanted, and concentrated under reduced pressure. The resulting residue was purified by silica gel flash column chromatography.

VI.5. Procedures and Characterization:

(E)-((4-(benzyloxy)-6-phenylhex-5-en-1-yl)oxy)(tert-butyl)diphenylsilane (2-26)

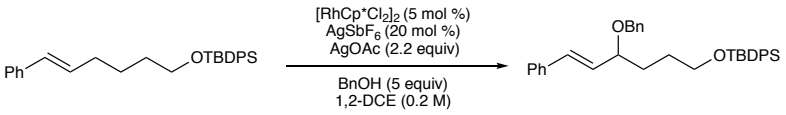

Following the general procedure B, $[RhCp^*Cl_2]_2$ (10.5 mg, 0.017 mmol, 6 mol %), $AgSbF_6$ (17.6 mg, 0.05 mmol, 20 mol %), AgOAc (100.4 mg, 0.56 mmol, 2.2 equiv), benzyl alcohol (133 µL, 1.3 mmol, 5 equiv), (*E*)-*tert*-butyldiphenyl((6-phenylhex-5-en-1-yl)oxy)silane[29] (106 mg, 0.26 mmol, 1 equiv) were used for 5 h at 60 °C. The filtration eluent was EtOAc. Purification by flash column chromatography on silica gel (48:1 Hexanes/Et_2O to 24:1 Hexanes/Et_2O) afforded allylic ether **2-26** as a clear, colorless oil (125.2 mg, 87%).

^{1}H NMR (400 MHz, $CDCl_3$): δ 7.72– 7.66 (m, 4H), 7.48 – 7.25 (m, 11H), 6.55 (d, *J* = 16.0 Hz, 1H), 6.15 (dd, *J* = 16.0, 8.0 Hz, 1H), 4.65 (d, *J* = 11.9 Hz, 1H), 4.42 (d, *J* = 11.9 Hz, 1H), 3.95 (q, *J* = 7.6, 6.7 Hz, 1H), 3.71 (t, *J* = 6.1 Hz, 2H), 1.95 – 1.61 (m, 4 H), 1.08 (s, 9H)

^{13}C NMR (150 MHz, $CDCl_3$): δ 138.90, 136.76, 135.70, 134.13, 132.49, 130.68, 129.64, 128.73, 128.70, 128.47, 127.84, 127.72, 127.55, 126. 64, 80.07, 70.23, 63.88, 32.27, 28.64, 27.02, 19.37.

IR (neat, cm^{-1}): 3026.86, 2929.77, 2856.46, 1494.04, 1471.38, 1451.91, 1427.38, 1388.75, 1359.99, 1189.51, 1109.08, 1027.99, 968.08, 822.94, 739.72, 699.92, 613.16.

HRMS (+NSI): calculated for $C_{33}H_{40}O_2NaSi$ $[M+Na]^+$ 543.2687, found 543.2690.

R_f = 0.66 (9:1 Hexanes/Et_2O).

(E)-6-((tert-butyldiphenylsilyl)oxy)-1-phenylhex-1-en-3-yl acetate (2-27)

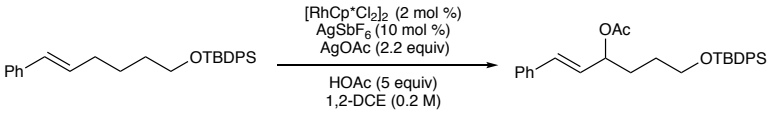

Following the general procedure B, $[RhCp^*Cl_2]_2$ (3.4 mg, 0.006 mmol, 2 mol %), $AgSbF_6$ (8.6 mg, 0.025 mmol, 10 mol %), AgOAc (94.6 mg, 0.57 mmol, 2.2 equiv), glacial acetic acid (75 µL, 1.3 mmol, 5 equiv), (*E*)-*tert*-butyldiphenyl((6-phenylhex-5-en-1-yl)oxy)silane (106 mg, 0.26 mmol, 1 equiv) were used for 5 h at 60 °C. The filtration eluent was EtOAc. Purification by flash column chromatography on silica gel (48:1 Hexanes/Et_2O to 24:1 Hexanes/Et_2O) afforded allylic ether **2-27** as a clear, colorless oil (62.5 mg, 51%).

^{1}H NMR (400 MHz, $CDCl_3$): δ 7.66 – 7.64 (m, 4H), 7.44 – 7.23 (m, 11H), 6.58 (d, *J* = 16.0 Hz, 1H), 6.11 (dd, *J* = 16.0, 8.0 Hz, 1H), 5.41 (q , *J* = 6.8 Hz, 1H), 3.68 (t, *J* = 6.2 Hz, 2H), 2.06 (s, 3H), 1.81 (m, 2H), 1.66-1.55 (m, 2H) 1.05 (s, 9H)

^{13}C NMR (150 MHz, $CDCl_3$): δ 170.48, 136.47, 135.69, 134.00, 132.70, 129.71, 128.69, 128.04, 127.78, 127.76, 126.72, 74.74, 63.60, 31.08, 28.38, 27.01, 21.49, 19.35.

IR (neat, cm^{-1}): 3070.06, 2930.42, 2856.89, 1735.18, 1589.02, 1494.64, 1472.03, 1448.84, 1427.55, 1369.70, 1234.88, 1106.22, 1016.76, 965.10, 938.05, 822.78, 742.08

HRMS (+NSI): calculated for $C_{30}H_{36}O_3NaSi$ $[M+Na]^+$ 495.2326, found 495.2320.

R_f = 0.40 (9:1 Hexanes/Et_2O)

(*E*)-*tert*-butyl((4-methoxy-6-phenylhex-5-en-1-yl)oxy)diphenylsilane. (2-29)

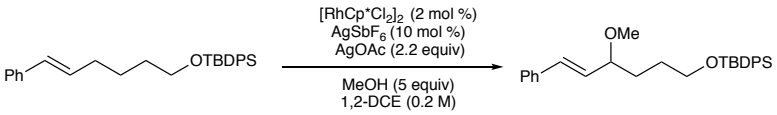

5 equiv:

Following the general procedure B, $[RhCp^*Cl_2]_2$ (3.1 mg, 0.005 mmol, 2 mol %), $AgSbF_6$ (12.4 mg, 0.036 mmol, 14 mol %), AgOAc (112.4mg, 0.67 mmol, 2.5 equiv), methanol (52 μL, 1.5 mmol, 5 equiv), (*E*)-*tert*-butyldiphenyl((6-phenylhex-5-en-1-yl)oxy)silane (106 mg, 0.26 mmol, 1 equiv) were used for 5 h at 60 °C. The filtration eluent was EtOAc. Purification by flash column chromatography on silica gel (9:1 Hexanes: Et_2O) afforded allylic ether **2-29** as a clear colorless oil (54.2 mg, 12.1mmol, 47%).

10 equiv:

Following the general procedure B, $[RhCp^*Cl_2]_2$ (3.0 mg, 0.005 mmol, 2 mol %), $AgSbF_6$ (8.8 mg, 0.026 mmol, 10 mol %), AgOAc (108.6 mg, 0.65 mmol, 2.5 equiv), methanol (104 μL, 2.57 mmol, 10 equiv), (*E*)-*tert*-butyldiphenyl((6-phenylhex-5-en-1-yl)oxy)silane (106 mg, 0.26 mmol, 1 equiv) were used for 5 h at 60 °C. The filtration eluent was EtOAc. Purification by

flash column chromatography on silica gel (9:1 Hexanes: Et_2O) afforded allylic ether **2-29** as a clear colorless oil (58.5mg, 13.2mmol, 51%).

^{1}H NMR (400 MHz, $CDCl_3$): δ 7.63 – 7.65 (m, 4H), 7.25 – 7.41 (m, 11H), 6.50 (d, *J* = 16.0 Hz, 1H), 6.03 (dd, *J* = 15.9, 8.0 Hz, 1H), 3.65 – 3.71 (m, 3H), 3.29 (s, 3H), 1.56 – 1.82 (m, 4H), 1.04 (s, 9H)

^{13}C NMR (150 MHz, $CDCl_3$): δ 136.79, 135.72, 134.15, 132.49, 130.46, 129.65, 128.72, 127.80, 127.73, 126.62, 82.47, 63.92, 56.36, 32.12, 28.55, 27.03, 19.37.

IR (neat, cm^{-1}):3070.02, 2929.98, 2856.94, 1494.53, 1487.96, 1471.94, 1462.72, 1448.30, 1427.71, 1110.36, 1090.11, 692.96

HRMS (+NSI) calculated for $C_{29}H_{36}O_2NaSi$ $[M+Na]^+$ 467.2377, found 467.2374.

R_f = 0.55 (9:1 Hexanes/Et_2O)

(*E*)-*tert*-butyl((4-ethoxy-6-phenylhex-5-en-1-yl)oxy)diphenylsilane. (2-30)

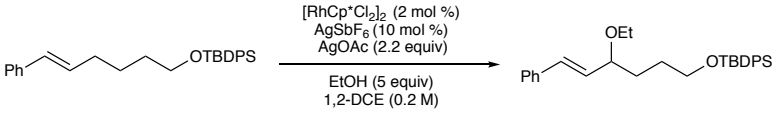

Following the general procedure B, $[RhCp^*Cl_2]_2$ (3.1 mg, 0.005 mmol, 2 mol %), $AgSbF_6$ (8.8 mg, 0.026 mmol, 10 mol %), AgOAc (93.4 mg, 0.56 mmol, 2.2 equiv), ethanol (75 μL, 1.28 mmol, 5 equiv), (*E*)-*tert*-butyldiphenyl((6-phenylhex-5-en-1-yl)oxy)silane (106 mg, 0.26 mmol, 1 equiv) were used for 5 h at 60 °C. The filtration eluent was EtOAc. Purification by flash column chromatography on silica gel (9:1 Hexanes: Et_2O) afforded allylic ether **2-30** as a clear, colorless oil (81.6mg, 17.8 mmol, 70%).

^{1}H NMR (400 MHz, $CDCl_3$): δ7.65 (m, 4H), 7.39 – 7.21 (m, 11H), 6.46 (d, *J* = 16.0 Hz, 1H), 6.04 (dd, *J* = 15.9, 7.8 Hz, 1H), 3.78 (q, *J* = 7.2, 6.4 Hz, 1H), 3.72 – 3.61 (m, 2H), 3.56 (dq, *J* = 8.9, 7.0 Hz, 1H), 3.32 (dq, *J* = 8.9, 7.0 Hz, 1H), 1.83 – 1.56 (m, 4H), 1.17 (t, *J* = 7.0 Hz , 3H), 1.04 (s, 9H)

^{13}C NMR (150 MHz, $CDCl_3$): δ 136.89, 135.71, 134.17, 131.78, 131.20, 129.64, 128.69, 127.72, 127.70, 126.59, 80.63, 63.97, 63.90, 32.26, 28.68, 27.03, 19.37, 15.53 ppm.

IR (neat, cm^{-1}):3069.93, 2929.49, 2857.01, 1494.85, 1486.77, 1471.99, 1462.23, 1448.07, 1427.59, 1105.32, 1085.08, 692.27 cm^{-1}

HRMS: (+NSI) calculated for $C_{30}H_{38}O_2NaSi$ $[M+Na]^+$ 481.2533, found 481.2527.

R_f = 0.49 (9:1 Hexanes/Et_2O)

(E)-tert-butyl((4-isopropoxy-6-phenylhex-5-en-1-yl)oxy)diphenylsilane. (2-31)

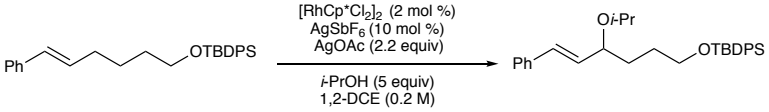

Following the general procedure B, $[RhCp^*Cl_2]_2$ (3.1 mg, 0.005 mmol, 2 mol %), $AgSbF_6$ (8.9 mg, 0.026 mmol, 10 mol %), AgOAc (104.0 mg, 0.62 mmol, 2.4 equiv), 2-propanol (98 μL, 1.28 mmol, 5 equiv), (*E*)-*tert*-butyldiphenyl((6-phenylhex-5-en-1-yl)oxy)silane (106 mg, 0.26 mmol, 1 equiv) were used for 5 h at 60 °C. The filtration eluent was EtOAc. Purification by flash column chromatography on silica gel (48:1 Hexanes/Et_2O to 24:1 Hexanes/Et_2O) afforded allylic ether **2-31** as a clear, colorless oil (50.0 mg, 10.6 mmol, 41%).

^{1}H NMR (400 MHz, $CDCl_3$): δ 7.67 – 7.65 (m, 4H), 7.42 – 7.30 (m, 11H), 6.47 (d, *J* = 16.0 Hz, 1H), 6.08 (dd, *J* = 15.7, 7.4 Hz, 1H), 3.92 – 3.87 (m, 1H), 3.75 – 3.60 (m, 3H), 1.72 – 1.60 (m, 4H), 1.11 (d, *J* = 6.1 Hz, 3H), 1.14 (d, *J* = 6.1 Hz, 3H), 1.04 (s, 9H)

^{13}C NMR (150 MHz, $CDCl_3$): δ 137.03, 135.72, 134.19, 131.99, 131.00, 129.64, 128.69, 127.72, 127.62, 126.56, 77.95, 68.79, 63.99, 32.64, 28.78, 27.03, 23.63, 21.79, 19.37.

IR (neat, cm^{-1}): 3070.13, 2963.54, 2930.15, 2857.31, 1589.34, 1494.76, 1472.04, 1427.67, 1378.78, 1328.67, 1110.21, 967.32, 822.80, 741.76

HRMS (+NSI): calculated for $C_{31}H_{40}O_2NaSi$ $[M+Na]^+$ 495.2690, found 495.2696.

$\mathbf{R}_f$ = 0.48 (9:1 Hexanes/Et_2O)

(*E*)-*tert*-butyldiphenyl((6-phenyl-4-(2,2,2-trichloroethoxy)hex-5-en-1-yl)oxy)silane. (2-33)

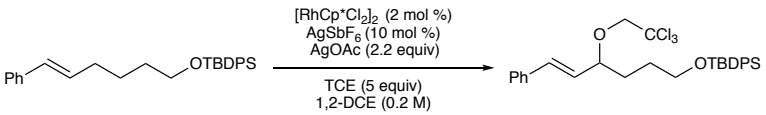

Following the general procedure B, $[RhCp^*Cl_2]_2$ (3.6 mg, 0.006 mmol, 2 mol %), $AgSbF_6$ (9.1 mg, 0.026 mmol, 10 mol %), AgOAc (99.3 mg, 0.59 mmol, 2.3 equiv), 2,2,2-trichlorethanol (124 μL, 1.3mmol, 5 equiv), (*E*)-*tert*-butyldiphenyl((6-phenylhex-5-en-1-yl)oxy)silane (106 mg, 0.26 mmol, 1 equiv) were used for 5 h at 60 °C. The filtration eluent was EtOAc. Purification by flash column chromatography on silica gel (48:1 Hexanes/Et_2O to 24:1 Hexanes/Et_2O) afforded allylic ether **2-33** as a clear, colorless oil (63.1 mg, 11.2 mmol, 44%).

^{1}H NMR (400 MHz, $CDCl_3$): δ 7.66 (dd, J = 7.9, 1.5 Hz, 4H), 7.43 – 7.25 (m, 11H), 6.56 (d, J = 16.0 Hz, 1H), 6.10 (dd, J = 16.0, 8.0 Hz, 1H), 4.17 (m, 1H), 4.11 (d, J = 11.5 Hz, 1H), 3.93 (d, J = 11.5 Hz, 1H), 3.76 – 3.66 (m, 2H), 1.92 – 1.65 (m, 4H), 1.05 (s, 9H)

^{13}C NMR (150 MHz, $CDCl_3$): δ 136.29, 135.72, 135.69, 134.11, 134.10, 133.17, 129.70, 129.26, 128.80, 128.20, 127.76, 126.76, 97.63, 82.99, 80.76, 63.75, 32.23, 28.52, 27.05, 27.03, 19.38.

IR (neat, cm^{-1}): 3069.82, 2929.61, 2856.88, 1589.09, 1471.73, 1427.41, 1389.10, 1360.70, 1188.16, 1106.56, 997.89, 968.17, 822.56, 803.88, 741.40

HRMS (+ NSI) calculated for $C_{30}H_{35}O_2Cl_3NaSi$ $[M+Na]^+$ 583.1364, found 583.1376

R_f = 0.63 (9:1 Hexanes/Et_2O)

(*E*)-*tert*-butyldiphenyl((6-phenyl-4-(2,2,2-trifluoroethoxy)hex-5-en-1-yl)oxy)silane (2-34)

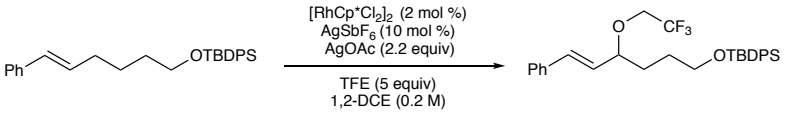

10 equiv:

Following the general procedure B, $[RhCp^*Cl_2]_2$ (3.1 mg, 0.005 mmol, 2 mol %), $AgSbF_6$ (9.2 mg, 0.027 mmol, 10 mol %), AgOAc (100.6 mg, 0.60 mmol, 2.3 equiv), 2,2,2-trifluoroethanol (194 μL, 2.6 mmol, 10 equiv), (*E*)-*tert*-butyldiphenyl((6-phenylhex-5-en-1-yl)oxy)silane (106 mg, 0.26 mmol, 1 equiv) were used for 5 h at 60 °C. The filtration eluent was EtOAc. Purification by flash column chromatography on silica gel (48:1 Hexanes: Et_2O) afforded allylic ether **2-34** as a clear, colorless oil (77.4 mg, 15.1 mmol, 59%).

5 equiv:

Following the general procedure B, $[RhCp^*Cl_2]_2$ (3.2 mg, 0.005 mmol, 2 mol %), $AgSbF_6$ (10.3 mg, 0.027 mmol, 10 mol %), AgOAc (94.3 mg, 0.57 mmol, 2.2 equiv), 2,2,2-trifluoroethanol (96 μL, 1.3 mmol, 5 equiv), (*E*)-*tert*-butyldiphenyl((6-phenylhex-5-en-1-yl)oxy)silane (106 mg, 0.26 mmol, 1 equiv) were used for 5 h at 60 °C. The filtration eluent was EtOAc.

Purification by flash column chromatography on silica gel (48:1 Hexanes: Et_2O) afforded allylic ether **2-34** as a clear, colorless oil (50.9 mg, 9.9 mmol, 39%).

^{1}H NMR (400 MHz, $CDCl_3$): δ 7.66 (d, J = 7.9 Hz, 4H), 7.43-7.28 (m, 11H), 6.52 (d, J = 16.0 Hz, 1H), 6.02 (dd, J = 16.0, 8.2 Hz, 1H), 3.96 (q, J = 7.8, 7.3 Hz, 1H), 3.85 (dq, J = 12.3, 9.1 Hz, 1H), 3.76 – 3.63 (m, 3H), 1.87 – 1.59 (m, 4H), 1.09 (s, 9H)

^{13}C NMR (150 MHz, $CDCl_3$): δ 136.18, 135.76, 135.72, 135.69, 134.08, 133.80, 129.70, 128.81, 128.71, 128.27, 127.76, 127.72, 127.13, 126.76, 124.24 (q, J = 278.8 Hz), 82.61, 65.47 (q, J = 33.8 Hz), 63.69, 32.10, 28.36, 27.03, 27.00, 19.38.

^{19}F NMR (282 MHz, $CDCl_3$): -77.14 (t, J = 8.9 Hz)

IR (neat, cm^{-1}): 3070.63, 2931.07, 2857.68, 1589.34, 1472.34, 1427.72, 1389.67, 1361.38, 1275.83, 1158.46, 1105.19, 997.91, 968.49, 909.99, 822.74, 741.00, 700.21, 667.42.

HRMS (+NSI): calculated for $C_{30}H_{35}O_2F_3NaSi$ $[M+Na]^+$ 535.2251, found 535.2252.

R_f = 0.54 (9:1 Hexanes/Et_2O)

(E)-tert-butyl((4-isobutoxy-6-phenylhex-5-en-1-yl)oxy)diphenylsilane (2-36)

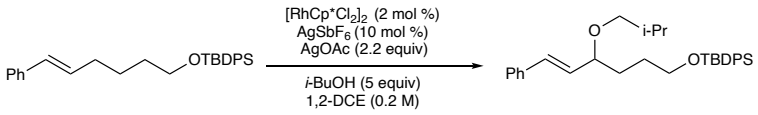

Following the general procedure B, $[RhCp^*Cl_2]_2$ (3.7 mg, 0.006 mmol, 2 mol %), $AgSbF_6$ (9.3 mg, 0.027 mmol, 10 mol %), AgOAc (100.1 mg, 0.60 mmol, 2.3 equiv), *i*-butylalcohol (95 µL, 1.3 mmol, 5 equiv), (*E*)-*tert*-butyldiphenyl((6-phenylhex-5-en-1-yl)oxy)silane (106 mg, 0.26 mmol, 1 equiv) were used for 5 h at 60 °C. The filtration eluent was EtOAc. Purification by flash column chromatography on silica gel (Pentane) afforded allylic ether **2-36** as a clear, colorless oil (73.8 mg, 59%).

^{1}H NMR (400 MHz, $CDCl_3$): δ 7.67– 7.65 (m, 4H), 7.43 – 7.22 (m, 11 H), 6.47 (d, *J* = 15.9 Hz, 1H), 6.06 (dd, *J* = 16.0 , 7.7 Hz, 1H), 3.90 – 3.71 (m, 1H), 3.68 (td, *J* = 5.8, 1.3 Hz, 2H), 3.28 (dd, *J* = 9.1, 6.6 Hz, 1H), 3.01 (dd, *J* = 9.1, 6.9 Hz, 1H), 1.83 – 1.65 (m, 5H), 1.04 (s, 9H), 0.89 (d, *J* = 6.6 Hz, 3H), 0.88 (d, *J* = 6.6 Hz, 3H).

^{13}C NMR (150 MHz, $CDCl_3$): δ 136.94, 135.71, 134.16, 131.53, 131.38, 129.64, 128.73, 128.68, 127.72, 127.65, 127.57, 80.82, 75.71, 63.97, 32.28, 28.67, 27.03, 27.01, 19.73, 19.69, 19.37

IR (neat, cm^{-1}): 3070.14, 2953.25, 2929.41, 2856.73, 1589.33, 1471.82, 1427.52, 1389.13, 1362.48, 1187.53, 1105.25, 1085.28, 997.98, 966.16, 822.57, 797.66, 741.02

HRMS (+NSI): calculated for $C_{32}H_{42}O_2NaSi$ $[M+Na]^+$ 509.2842, found 509.2846.

R_f = 0.79 (9:1 Hexanes/Et_2O)

(E)-tert-butyl((4-(neopentyloxy)-6-phenylhex-5-en-1-yl)oxy)diphenylsilane (2-37)

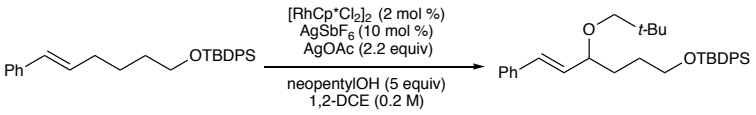

Following the general procedure B, $[RhCp^*Cl_2]_2$ (3.8 mg, 0.006 mmol, 2 mol %), $AgSbF_6$ (8.9 mg, 0.026 mmol, 10 mol %), AgOAc (103.4 mg, 0.62 mmol, 2.4 equiv), neopentyl alcohol (114 mg, 1.3 mmol, 5 equiv), (*E*)-*tert*-butyldiphenyl((6-phenylhex-5-en-1-yl)oxy)silane (106 mg, 0.26 mmol, 1 equiv) were used for 5 h at 60 °C. The filtration eluent was EtOAc. Purification by preparatory layer chromatography on silica gel (Pentane) afforded allylic ether **2-37** as a clear, colorless oil (55.6 mg, 45%).

^{1}H NMR (400 MHz, $CDCl_3$): δ 7.68– 7.64 (m, 4H), 7.44 – 7.20 (m, 11 H), 6.47 (d, *J* = 16.0 Hz, 1H), 6.06 (dd, *J* = 15.9, 7.5 Hz, 1H), 3.78 – 3.62 (m, 3H), 3.17 (d, *J* = 8.7 Hz, 1H), 2.88 (d, *J* = 8.7 Hz, 1H), 1.72-1.65 (m, 4H), 1.04 (s, 9H), 0.89 (s, 9H)

^{13}C NMR (150 MHz, $CDCl_3$): δ 137.03, 135.73, 134.23, 134.22, 131.71, 131.14, 129.64, 128.69, 127.72, 127.59, 126.56, 81.05, 79.31, 64.06, 32.33, 28.67, 27.04, 26.99, 26.96, 19.38

IR (neat, cm^{-1}): 3070.43, 2952.42, 2858.47, 1589.48, 1472.86, 1427.80, 1389.17, 1361.41, 1188.78, 1089.22, 1030.82, 1007.42, 966.85, 938.02, 823.07, 799.99, 741.72, 701.00

HRMS (+NSI): calculated for $C_{33}H_{44}O_2NaSi$ $[M+Na]^+$ 523.3003, found 523.3003.

R_f = 0.82 (9:1 Hexanes/Et_2O)

(*E*)-*tert*-butyl((4-((2,3-dihydro-1*H*-inden-2-yl)oxy)-6-phenylhex-5-en-1-yl)oxy)diphenylsilane (2-39)

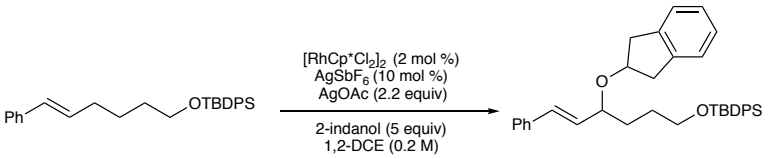

Following the general procedure B, $[RhCp^*Cl_2]_2$ (3.7 mg, 0.006 mmol, 2 mol %), $AgSbF_6$ (9.5 mg, 0.028 mmol, 11 mol %), AgOAc (104.5 mg, 0.63 mmol, 2.4 equiv), 2-indanol (174.9 mg, 1.3 mmol, 5 equiv), (*E*)-*tert*-butyldiphenyl((6-phenylhex-5-en-1-yl)oxy)silane (106 mg, 0.26 mmol, 1 equiv) were used for 5 h at 60 °C. The filtration eluent was EtOAc. Purification by flash column chromatography on silica gel (48:1 Hexanes: Et_2O) afforded allylic ether **2-39** as a clear, colorless oil (91.2 mg, 16.7 mmol, 65%).

^{1}H NMR (400 MHz, $CDCl_3$): δ 7.65 (m, 4H), 7.41 – 7.31 (m, 11H), 7.18 – 7.12 (m, 4H), 6.51 (d, *J* = 15.9 Hz, 1H), 6.11 (dd, *J* = 15.9, 7.8 Hz, 1H), 4.44 (qn, *J* = 5.8 Hz, 1H), 4.08 – 3.86 (m, 1H),

3.71 – 3.64 (m, 2H), 3.12 (dd, *J* = 16.0, 6.7 Hz, 2H), 2.98-2.87 (m, 2H), 1.76-1.59 (m, 4H), 1.04 (s, 9H).

^{13}C NMR (150 MHz, $CDCl_3$): δ 141.25, 140.94, 136.86, 135.72, 134.15, 134.14, 131.65, 131.36, 129.66, 128.72, 127.76, 127.73, 126.62, 126.58, 126.53, 124.77, 124.74, 79.38, 78.08, 63.93, 40.36, 39.27, 32.50, 28.73, 27.04, 19.37.

IR (neat, cm^{-1}): 3069.71, 3024.29, 2930.36, 2856.79, 1588.92, 1483.24, 1471.00, 1460.48, 1448.12, 1427.65, 13888.98, 1360.68, 1192.31, 1089.57, 1025.26, 968.01, 823.13, 741.30

HRMS: (+ NSI) calculated for $C_{37}H_{42}O_2NaSi$ $[M+Na]^+$ 569.2846, found 569.2846.

R_f = 0.47 (9:1 Hexanes: Et_2O)

(*E*)-6-((*tert*-butyldiphenylsilyl)oxy)-1-phenylhex-1-en-3-yl isobutyrate (2-41)

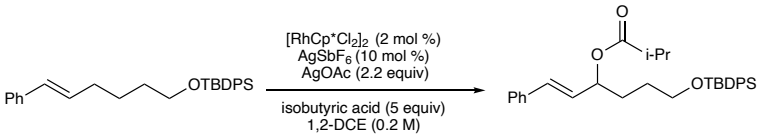

Following the general procedure B, $[RhCp^*Cl_2]_2$ (3.9 mg, 0.006 mmol, 2 mol %), $AgSbF_6$ (8.6 mg, 0.025 mmol, 10 mol %), AgOAc (100.3 mg, 0.60 mmol, 2.3 equiv), isobutyric acid (125 µL, 1.3 mmol, 5 equiv), (*E*)-*tert*-butyldiphenyl((6-phenylhex-5-en-1-yl)oxy)silane (106 mg, 0.26 mmol, 1 equiv) were used for 6 h at 60 °C. The filtration eluent was EtOAc. Purification by flash column chromatography on silica gel (48:1 Hexanes: Et_2O) afforded allylic ester **2-41** as a clear, colorless oil (56.2 mg, 11.3mmol, 44%) and allylic ester **2-27** as a clear colorless oil (25.7 mg, 5.1 mmol, 20%).

^{1}H NMR (300 MHz, $CDCl_3$) δ 7.83 – 7.57 (m, 4H), 7.49 – 7.09 (m, 11H), 6.57 (d, *J* = 16.0 Hz, 1H), 6.11 (dd, *J* = 15.9, 7.1 Hz, 1H), 5.41 (d, *J* = 7.0 Hz, 1H), 3.68 (t, *J* = 6.3 Hz, 2H), 2.55 (dt, *J* =

13.9, 7.0 Hz, 1H), 1.80 (q, *J* = 7.2 Hz, 2H), -1.58-1.53 (m, 2H), 1.17 (ddd, *J* = 7.0, 3.0, 1.5 Hz, 6H), 1.04 (s, 9H).

^{13}C NMR (151 MHz, $CDCl_3$) δ 176.49, 136.57, 135.68, 134.01, 132.37, 129.71, 128.67, 127.97, 127.76, 126.71, 74.19, 63.61, 34.37, 31.15, 28.37, 27.00, 19.35, 19.21, 19.08.

(*E*)-6-((*tert*-butyldiphenylsilyl)oxy)-1-phenylhex-1-en-3-yl benzoate (2-42)

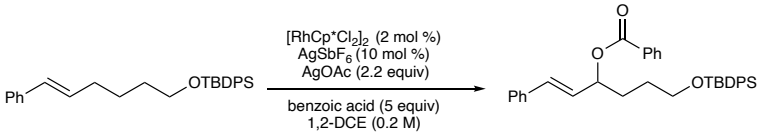

Following the general procedure B, $[RhCp^*Cl_2]_2$ (3.6 mg, 0.006 mmol, 2 mol %), $AgSbF_6$ (11.0 mg, 0.032 mmol, 12 mol %), AgOAc (96.5 mg, 0.58 mmol, 2.2 equiv), benzoic acid (158.2 mg, 1.3 mmol, 5 equiv), (*E*)-*tert*-butyldiphenyl((6-phenylhex-5-en-1-yl)oxy)silane (106 mg, 0.26 mmol, 1 equiv) were used for 5 h at 60 °C. The filtration eluent was EtOAc. Purification by flash column chromatography on silica gel (48:1 Hexanes: Et_2O) afforded allylic ester **2-42** as a clear, colorless oil (36.1 mg, 0.067mmol, 26%).

^{1}H NMR (400 MHz, $CDCl_3$) δ 8.23 – 7.83 (m, 2H), 7.66 (dd, *J* = 7.3, 1.6 Hz 5H), 7.56 – 7.16 (m, 13H), 6.68 (d, *J* = 15.9 Hz, 1H), 6.23 (dd, *J* = 16.0, 7.1 Hz 1H), 5.68 (q, *J* = 6.7 Hz, 1H), 3.72 (t, *J* = 6.3 Hz, 2H), 2.12 – 1.87 (m, 2H), 1.82 – 1.62 (m, 2H), 1.05 (s, 9H).

^{13}C NMR (151 MHz, $CDCl_3$) δ 166.01, 136.50, 135.70, 134.02, 134.01, 133.02, 132.73, 130.73, 129.77, 129.72, 128.69, 128.49, 128.05, 127.77, 126.77, 75.27, 63.63, 31.26, 28.45, 27.02, 19.36.

(E)-tert-butyldiphenyl((6-phenyl-4-((4-(trifluoromethyl)benzyl)oxy)hex-5-en-1-yl)oxy)silane (2-43)

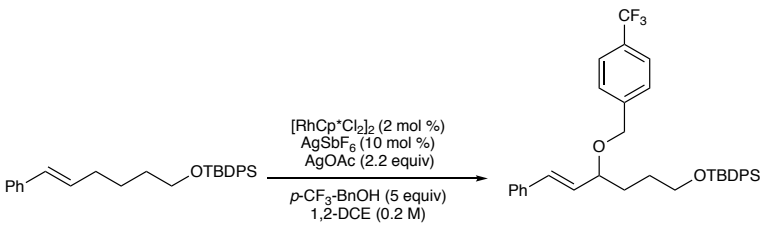

Following the general procedure B, $[RhCp^*Cl_2]_2$ (4.1 mg, 0.007 mmol, 2 mol %), $AgSbF_6$ (9.4 mg, 0.027 mmol, 11 mol %), AgOAc (108.2 mg, 0.65 mmol, 2.5 equiv), *p*-CF_3-benzyl alcohol (176 µL, 1.3 mmol, 5 equiv), (*E*)-*tert*-butyldiphenyl((6-phenylhex-5-en-1-yl)oxy)silane (106 mg, 0.26 mmol, 1 equiv) were used for 5 h at 60 °C. The filtration eluent was EtOAc. Purification by flash column chromatography on silica gel (48:1 Hexanes/Et_2O to 24:1 Hexanes/Et_2O) afforded allylic ether **2-43** as a clear, colorless oil (80.7 mg, 65%).

^{1}H NMR (400 MHz, $CDCl_3$): δ 7.65 (d, *J* = 6.5 Hz, 4H) 7.57 (d, *J* = 8.2 Hz, 2H), 7.46 – 7.24 (m, 13 H), 6.50 (d, *J* = 15.9 Hz, 1H), 6.09 (dd, *J* = 16.0, 8.1 Hz, 1H), 4.65 (d, *J* = 12.8 Hz, 1H), 4.43 (d, *J* = 12.7 Hz, 1H), 3.91 (q, *J* = 6.8 Hz, 1H), 3.76-3.57 (m, 2H), 1.95-1.58 (m, 4 H) 1.04 (s, 9H)

^{13}C NMR (150 MHz, $CDCl_3$): δ 143.12, 136.55, 135.71, 134.09, 132.87, 130.23, 129.79, 129.69, 129.57, 128.78, 128.01, 127.78, 127.74, 127.70, 126.66, 125.44, 125.41, 125.39, 125.36, 125.26, 123.46, 80.67, 69.43, 63.85, 32.26, 28.61, 27.02, 26.99, 19.37.

IR (neat, cm^{-1}): 3070.56, 2931.25, 2857.98, 1620.37, 1472.33, 1427.83, 1389.48, 1164.50, 1124.03, 1111.47, 1066.31, 1018.35, 968.66, 822.86, 742.87, 701.84

HRMS (+NSI): calculated for $C_{36}H_{39}O_2F_3NaSi$ $[M+Na]^+$ 611.2564, found 611.2569.

R_f = 0.64 (9:1 Hexanes/Et_2O)

(*E*)-*tert*-butyl((4-((4-methoxybenzyl)oxy)-6-phenylhex-5-en-1-yl)oxy)diphenylsilane (2-44)

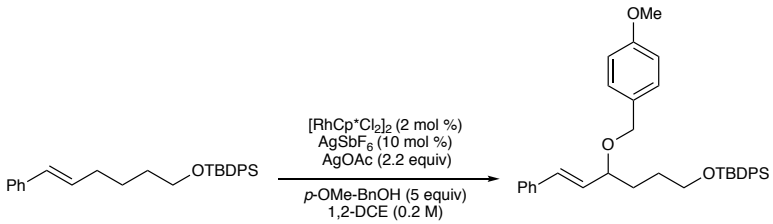

Following the general procedure B, $[RhCp^*Cl_2]_2$ (2.1 mg, 0.003 mmol, 3 mol %), $AgSbF_6$ (5.3 mg, 0.015 mmol, 12 mol %), AgOAc (65.3 mg, 0.39 mmol, 3.0 equiv), *p*-OMe-benzyl alcohol (59 µL, 0.64 mmol, 5 equiv), (*E*)-*tert*-butyldiphenyl((6-phenylhex-5-en-1-yl)oxy)silane (53 mg, 0.13 mmol, 1 equiv) were used for 5 h at 60 °C. The filtration eluent was EtOAc. Purification by flash column chromatography on silica gel (48:1 Hexanes/Et_2O to 24:1 Hexanes/Et_2O) afforded allylic ether **2-44** as a clear, colorless oil (29.9 mg, 42%).

^{1}H NMR (400 MHz, $CDCl_3$): δ 7.66-7.64 (m, 4H), 7.42-7.31 (m, 11H), 7.24-7.22 (m, 2 H), 6.87-6.85 (m, 2H), 6.50 (d, *J* = 16.0 Hz, 1H), 6.11 (dd, *J* = 16.0, 8.0 Hz, 1H), 4.54 (d, *J* = 11.5 Hz, 1H), 4.31 (d, *J* = 11.5 Hz, 1H), 3.89 (q, *J* = 7.3, 6.6 Hz, 1H), 3.80 (s, 3H), 3.66 (t, *J* = 6.1, 2H), 1.83-1.54 (m, 4 H) 1.03 (s, 9H)

^{13}C NMR (150 MHz, $CDCl_3$): δ 159.18, 136.82, 135.72, 134.16, 132.38, 130.99, 130.85, 129.65, 129.46, 128.74, 127.82, 127.77, 127.73, 126.64, 113.90, 79.72, 69.91, 63.88, 55.42, 32.26, 28.65, 27.01, 19.36.

IR (neat, cm^{-1}): 3251.55, 3070.00, 2929.74, 2856.36, 1613.22, 1512.86, 1471.66, 1427.74, 1389.06, 1324.10, 1246.71, 1171.86, 1110.17, 1089.73, 968.46, 822.31, 743.15, 701.50, 645.48, 612.75.

HRMS (+NSI): calculated for $C_{36}H_{42}O_3NaSi$ $[M+Na]^+$ 573.2794, found 573.2799.

R_f = 0.28 (9:1 Hexanes/Et_2O)

(E)-tert-butyl((4-(naphthalen-2-ylmethoxy)-6-phenylhex-5-en-1-yl)oxy)diphenylsilane (2-45)

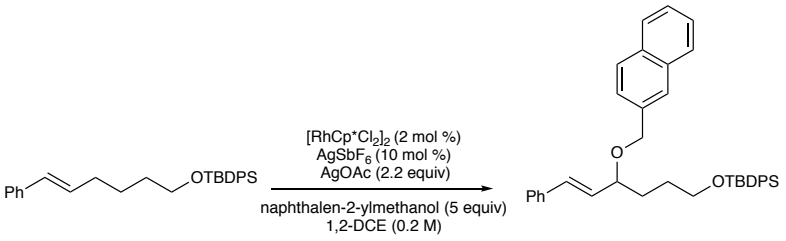

Following the general procedure B, $[RhCp^*Cl_2]_2$ (3.8 mg, 0.006 mmol, 2 mol %), $AgSbF_6$ (11.1 mg, 0.032 mmol, 12 mol %), AgOAc (98.8 mg, 0.59 mmol, 2.3 equiv), naphthalen-2-ylmethanol (203 mg, 1.3 mmol, 5 equiv), (*E*)-*tert*-butyldiphenyl((6-phenylhex-5-en-1-yl)oxy)silane (106 mg, 0.26 mmol, 1 equiv) were used for 5 h at 60 °C. The filtration eluent was EtOAc. Purification by flash column chromatography on silica gel (48:1 Hexanes/Et_2O to 24:1 Hexanes/Et_2O) afforded allylic ether **2-45** as a clear, colorless oil (71.2 mg, 49%).

^{1}H NMR (400 MHz, $CDCl_3$): δ 7.96– 7.70 (m, 4H), 7.65 – 7.63 (m, 4 H),7.47-7.20 (m, 14H), 6.53 (d, *J* = 16.0 Hz, 1H), 6.15 (dd, *J* = 15.9, 8.1 Hz, 1H), 4.66 (dd, *J* = 93.9, 12.1 Hz, 2H), 3.94 (m, 1H), 3.67 (t, *J* = 5.8 Hz, 2H), 1.87-1.56 (m, 4 H), 1.03 (s, 9H)

^{13}C NMR (150 MHz, $CDCl_3$): δ 136.75, 136.37, 135.70, 134.12, 133.44, 133.05, 132.61, 130.64, 129.64, 128.75, 128.23, 128.00, 127.87, 127.81, 127.72, 126.66, 126.48, 126.13, 126.05, 125.85, 80.04, 70.34, 63.88, 32.29, 28.67, 27.02, 19.36.

IR (neat, cm^{-1}): 3051.71, 2929.41, 2855.99, 1600.64, 1508.48, 1493.91, 1471.37, 1448.14, 1427.24, 1389.02, 1360.18, 1248.45, 1105.45, 1086.40, 997.78, 967.45, 908.66, 854.23, 819.61, 740.98

HRMS (+NSI): calculated for $C_{39}H_{42}O_2NaSi$ $[M+Na]^+$ 593.2846, found 593.2845.

R_f = 0.57 (9:1 Hexanes/Et_2O)

(*E*)-*tert*-butyldiphenyl((6-phenyl-4-(1-phenylethoxy)hex-5-en-1-yl)oxy)silane (2-46)

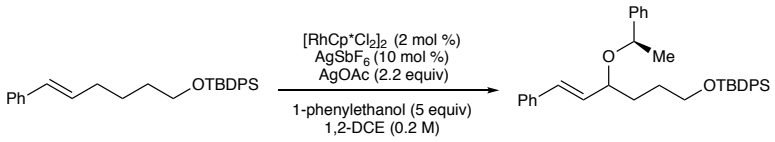

Following the general procedure B, $[RhCp^*Cl_2]_2$ (3.6 mg, 0.006 mmol, 2 mol %), $AgSbF_6$ (10.2 mg, 0.03 mmol, 12 mol %), AgOAc (104.5 mg, 0.63 mmol, 2.4 equiv), 2-phenylethanol (106.5 mg, 1.3 mmol, 5 equiv), (*E*)-*tert*-butyldiphenyl((6-phenylhex-5-en-1-yl)oxy)silane (106 mg, 0.26 mmol, 1 equiv) were used for 5 h at 60 °C. The filtration eluent was EtOAc. Purification by flash column chromatography on silica gel (48:1 Hexanes/Et_2O to 24:1 Hexanes/Et_2O) afforded allylic ether **2-46** as a clear, colorless oil (91.9 mg, 67%, 2.1:1 d.r.).

^{1}H NMR (400 MHz, $CDCl_3$): δ 7.80 – 7.72 (m, 2H), 7.75 – 7.61 (m, 4H), 7.56 – 7.23 (m, 24 H), 6.46 (d, *J* = 16.0 Hz, 0.5H), 6.44 (d, *J* = 16.0 Hz, 1H), 6.16 (dd, *J* = 15.9, 8.1 Hz, 1H), 6.09 (dd, *J* = 15.9, 7.5 Hz, 0.5H), 4.71 – 4.58 (m, 1.5H), 4.07 (q, *J* = 6.2 Hz, 0.5H), 3.79 (td, *J* = 6.2, 3.9 Hz, 1H), 3.77 – 3.72 (m, 1H), 3.67 (ddd, *J* = 7.4, 4.5, 1.6 Hz, 2H), 1.95 – 1.67 (m, 5H), 1.66 – 1.55 (m, 1H), 1.50 (t, *J* = 6.8 Hz, 4.5H), 1.14 (s, 4.5H), 1.10 (s, 9H).

^{13}C NMR (150 MHz, $CDCl_3$): δ144.79, 144.25, 137.01, 136.82, 135.71, 135.68, 134.16, 134.14, 134.13, 132.29, 131.38, 131.12, 130.92, 129.66, 129.60, 128.72, 128.57, 128.54, 128.36, 127.78, 127.74, 127.69, 127.54, 127.48, 127.23, 126.62, 126.60, 126.55, 126.35, 78.04, 74.88, 74.33, 64.01, 63.78, 32.45, 31.63, 28.68, 28.42, 27.04, 27.00, 24.82, 23.24, 19.37, 19.34.

IR (neat, cm^{-1}): 3026.19, 2929.45, 2857.21, 2160.13, 1976.96, 1588.99, 1492.31, 1471.94, 1449.10, 1427.51, 1361.37, 1207.24, 1109.67, 1087.11, 1029.01, 998.22, 967.47, 908.56, 822.57, 733.49

HRMS (+NSI): calculated for $C_{36}H_{42}O_2NaSi$ $[M+Na]^+$ 557.2846, found 557.2844.

$\mathbf{R_f}$ = 0.70 (9:1 Hexanes/Et_2O)

(*E*)-*tert*-butyl((4-(oxetan-3-ylmethoxy)-6-phenylhex-5-en-1-yl)oxy)diphenylsilane (2-47)

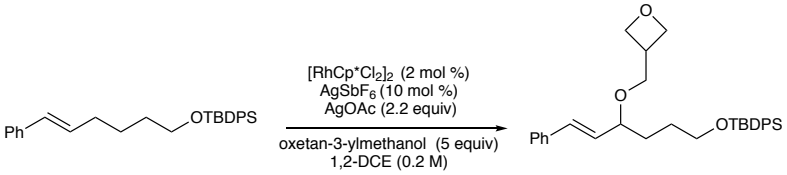

Following the general procedure B, $[RhCp^*Cl_2]_2$ (2.2 mg, 0.003 mmol, 3 mol %), $AgSbF_6$ (16.5 mg, 0.048 mmol, 37 mol %), AgOAc (47mg, 0.28 mmol, 2.2 equiv), oxetan-3-ylmethanol (50 µL, 0.64 mmol, 5 equiv), (*E*)-*tert*-butyldiphenyl((6-phenylhex-5-en-1-yl)oxy)silane (53 mg, 0.13 mmol, 1 equiv) were used for 24 h at 60 °C. The filtration eluent was Et_2O. Purification by flash column chromatography on silica gel (48:1 Hexanes/Et_2O to 24:1 Hexanes/Et_2O) afforded pure allylic ether **2-47** as a clear, colorless oil (20.7 mg, 32%).

^{1}H NMR (300 MHz, $CDCl_3$) δ 7.80 – 7.57 (m, 4H), 7.42-7.25 (m, 11H), 6.49 (d, J = 16.0 Hz, 1H), 6.04 (dd, J = 15.9, 7.9 Hz, 1H), 4.77 (ddd, J = 7.8, 6.0, 3.4 Hz, 2H), 4.42 (td, J = 6.0, 5.0 Hz, 2H), 3.79-3.66 (m, 4H), 3.51 (dd, J = 9.4, 7.1 Hz, 1H), 3.31 – 3.08 (m, 1H), 1.77-1.58 (m, 4H), 1.04 (s, 9H).

^{13}C NMR (150 MHz, $CDCl_3$): δ 136.66, 135.72, 135.69, 134.14, 134.13, 132.29, 130.59, 129.69, 128.75, 127.90, 127.75, 126.62, 81.32, 75.02, 74.96, 70.39, 63.88, 35.20, 32.19, 28.62, 27.03, 19.37.

IR (neat, cm^{-1}): 2930.33, 2857.17, 1699.40, 1588.90, 1472.29, 1427.39, 1389.07, 1363.93, 1256.06, 1110.36, 1088.04, 997.90, 968.51, 860.04, 822.81, 742.77, 701.44, 613.25, 561.09

HRMS (+NSI): calculated for $C_{32}H_{40}O_3NaSi$ $[M+Na]^+$ 523.2639, found 523.2644

R_f = 0.13 (9:1 Hexanes/Et_2O)

***tert*-butyl (*E*)-3-(((6-((*tert*-butyldiphenylsilyl)oxy)-1-phenylhex-1-en-3-yl)oxy)methyl)azetidine-1-carboxylate (2-48)**

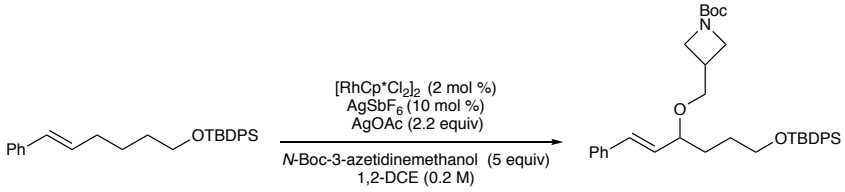

Following the general procedure B, $[RhCp^*Cl_2]_2$ (2.3 mg, 0.004 mmol, 3 mol %), $AgSbF_6$ (11.2 mg, 0.033 mmol, 25 mol %), AgOAc (50.2 mg, 0.30 mmol, 2.3 equiv), *tert*-butyl 3-(hydroxymethyl)azetidine-1-carboxylate (139 mg, 0.64 mmol, 5 equiv), (*E*)-*tert*-butyldiphenyl((6-phenylhex-5-en-1-yl)oxy)silane (53 mg, 0.13 mmol, 1 equiv) were used for 24 h at 60 °C. The filtration eluent was Et_2O. Purification by flash column chromatography on silica gel (48:1 Hexanes/Et_2O to 24:1 Hexanes/Et_2O) afforded allylic ether **2-48** as a clear, colorless oil (43.3 mg, 56%).

^{1}H NMR 1H NMR (400 MHz, $CDCl_3$) δ 7.67-7.65 (m, 4H), 7.41-7.25 (m, 11H), 6.48 (d, *J* =16.0 Hz, 1H), 6.03 (dd, *J* =16.0, 7.9 Hz, 1H), 3.97 (td, *J* = 8.4, 5.2, 2H), 3.83 -3.71 (m, 1H), 3.70-3.54 (m, 5H), 3.37 (dd, *J* = 9.5, 7.1 Hz, 1H), 2.70 - 2.75 (m, 1H), 1.80-1.53 (m, 4H), 1.42 (s, 9H), 1.04 (s, 9H).

^{13}C NMR (150 MHz, $CDCl_3$): *δ* 156.55, 136.63, 135.71, 135.68, 134.12, 132.27, 130.57, 129.68, 128.74, 127.89, 127.74, 126.63, 81.29, 79.35, 70.69, 63.87, 32.20, 28.83, 28.58, 28.55, 27.63, 27.03, 26.99, 19.36.

IR (neat, cm^{-1}): 2930.52, 2856.70, 1698.50, 1589.02, 1426.99, 1472.63, 1389.46, 1364.70, 1294.27, 1255.26, 1105.71, 1086.15, 967.66, 909.97, 860.34, 822.65, 771.68, 731.80, 700.76, 646.40, 613.17, 561.53

HRMS (+NSI): calculated for $C_{37}H_{50}O_4NSi$ $[M+H]^+$ 600.3504, found 600.3503

$\mathbf{R_f}$ = 0.11 (9:1 Hexanes/Et_2O)

tert-butyldiphenyl(((*E*)-6-phenyl-4-(((3a*R*,5*R*,5a*S*,8a*S*,8b*R*)-2,2,7,7-tetramethyltetrahydro-5*H*-bis([1,3]dioxolo)[4,5-*b*:4',5'-*d*]pyran-5-yl)methoxy)hex-5-en-1-yl)oxy)silane (2-49)

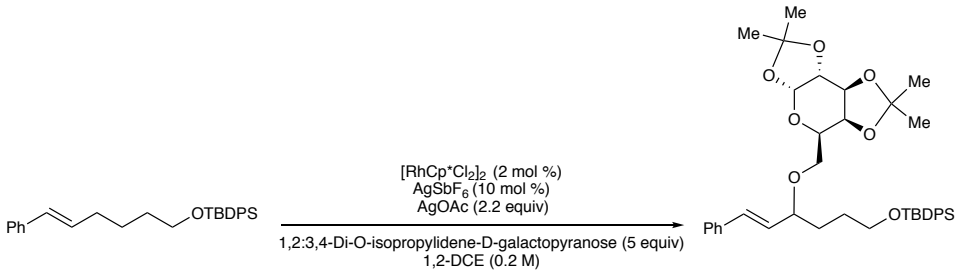

Following the general procedure B, $[RhCp^*Cl_2]_2$ (1.9 mg, 0.003 mmol, 2 mol %), $AgSbF_6$ (4.4 mg, 0.013 mmol, 9.8 mol %), AgOAc (45.2 mg, 0.27 mmol, 2.1 equiv), ((3a*R*,5*R*,5a*S*,8a*S*,8b*R*)-2,2,7,7-tetramethyltetrahydro-5*H*-bis([1,3]dioxolo)[4,5-*b*:4',5'-*d*]pyran-5-yl)methanol (156.2 mg, 0.64 mmol, 5 equiv), (*E*)-*tert*-butyldiphenyl((6-phenylhex-5-en-1-yl)oxy)silane (53 mg, 0.13 mmol, 1 equiv) were used for 24 h at 60 °C. The filtration eluent was Et_2O. Purification by flash column chromatography on silica gel (48:1 Hexanes/Et_2O to 24:1 Hexanes/Et_2O) afforded allylic ether **2-49** as a clear, colorless oil (35.7 mg, 42%).

^{1}H NMR 1H NMR (300 MHz, cdcl3) δ 7.90 – 7.53 (m, 4H),7.44-7.21 (m, 11H) 6.53 (d, *J* = 16.0, 0.46H), 6.47 (d, *J* = 16.0, 0.53H), 6.07 (dd, *J* = 16.0, 7.9, 0.53H), 6.06 (dd, *J* = 16.0, 7.7, 0.46H), 5.53 (d, *J* = 5.0, Hz, 0.5H), 5.51 (d, *J* = 5.0, Hz, 0.5H), 4.59 (d, *J* = 8.0, Hz, 0.5H), 4.58 (d, *J* = 8.0,

Hz, 0.5H), 4.31- 4.24 (m, 2H), 3.98-3.82 (m, 2H), 3.75- 3.66 (m 3H), 3.51 (dd, *J* = 11.0, 5.8 Hz, 0.5H), 3.50 (dd, *J* = 11.0, 5.8 Hz, 0.5H), 1.89- 1.19 (m, 16H), 1.04 (s, 9 H)

^{3}C NMR (150 MHz, $CDCl_3$): δ 137.04, 136.87, 135.88, 135.84, 135.72, 134.21, 132.14, 132.00, 130.80, 130.72, 129.65, 129.63, 128.75, 128.65, 128.63, 127.73, 127.67, 127.65, 126.67, 126.63, 109.28, 109.22, 108.62, 108.59, 96.50, 96.46, 81.54, 81.34, 71.37, 71.21, 70.90, 70.79, 70.76, 67.49, 67.27, 67.14, 66.70, 64.01, 63.88, 34.82, 32.23, 32.11, 31.74, 28.66, 28.65, 27.06, 27.03, 26.99, 26.25, 26.24, 26.14, 26.11, 25.43, 25.11, 25.08, 24.60, 24.52, 22.80, 19.37, 14.27.

IR (neat, cm^{-1}): 2931.25, 2857.43, 1699.73, 1472.47, 1427.82, 1381.65, 1307.03, 1255.32, 1210.88, 1168.16, 1110.43, 1071.12, 1000.40, 967.35, 918.36, 890.76, 863.90, 823.12, 743.69, 702.00, 613.47

HRMS (+NSI): calculated for $C_{40}H_{52}O_7NaSi$ $[M+Na]^+$ 695.3374, found 695.3398

R_f = 0.18 (9:1 Hexanes/EtOAc)

tert-butyl (2*S*)-2-((((*E*)-6-((*tert*-butyldiphenylsilyl)oxy)-1-phenylhex-1-en-3-yl)oxy)methyl)morpholine-4-carboxylate (2-50)

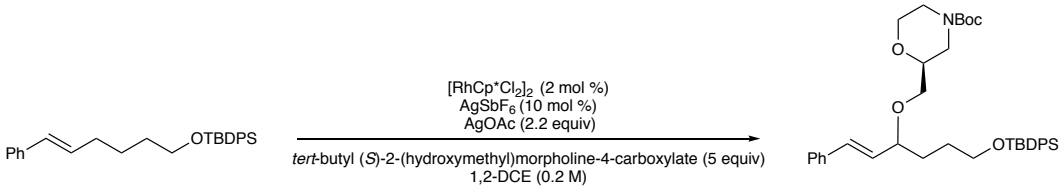

Following the general procedure B, $[RhCp^*Cl_2]_2$ (3.1 mg, 0.005 mmol, 4 mol %), $AgSbF_6$ (8.4 mg, 0.024 mmol, 19 mol %), AgOAc (46.5 mg, 0.28 mmol, 2.1 equiv), *tert*-butyl (*S*)-2-(hydroxymethyl)morpholine-4-carboxylate (144 mg, 0.64 mmol, 5 equiv), (*E*)-*tert*-butyldiphenyl((6-phenylhex-5-en-1-yl)oxy)silane (53 mg, 0.13 mmol, 1 equiv) were used for 24 h at 60 °C. The filtration eluent was EtOAc. Purification by flash column chromatography

on silica gel (48:1 Hexanes/Et_2O to 24:1 Hexanes/Et_2O) afforded allylic ether **2-50** as a clear, colorless oil (60.5 mg, 75%).

^{1}H NMR 1H NMR (600 MHz, $CDCl_3$) δ 7.71 – 7.56 (m, 4H), 7.42-7.15 (m, 11H), 6.48 (d, *J* = 15.9 Hz, 1H), 6.05 (dd, *J* = 16.0, 8.0, 0.5H), 6.04 (dd, *J* = 16.0, 8.0, 0.5H), 4.07-3.44 (m, 9H), 3.40 – 3.30 (m, 0.5H), 3.27 (dd, *J* = 10.0, 4.3 Hz, 0.5 H), 2.92 (br s, 1H), 2.71 (br s, 1H), 1.79-1.5 (m, 4H), 1.45(s, 9H), 1.04(s, 9H).

^{13}C NMR (150 MHz, $CDCl_3$): *δ* 154.89, 154.87, 136.66, 135.70, 134.12, 132.58, 132.53, 130.37, 130.35, 129.65, 128.70, 128.69, 127.85, 127.84, 127.76, 127.73, 126.64, 81.79, 80.09, 74.89, 69.47, 69.37, 66.66, 66.61, 63.87, 63.86, 32.11, 28.60, 28.52, 27.51, 27.01, 19.34.

IR (neat, cm^{-1}): 2929.85, 2857.16, 2361.54, 1695.27, 1558.89, 1472.58, 1451.27, 1426.39, 1390.93, 1365.31, 1252.04, 1238.54, 1169.02, 1105.26, 997.97, 968.02, 908.02, 865.89, 822.61, 730.36, 700.85, 646.91, 613.18

HRMS (+NSI): calculated for $C_{38}H_{51}O_5NNaSi$ $[M+Na]^+$ 652.3429, found 652.3432

R_f = 0.12 (9:1 Hexanes/EOAc)

methyl *N*-(*tert*-butoxycarbonyl)-*O*-((*E*)-6-((*tert*-butyldiphenylsilyl)oxy)-1-phenylhex-1-en-3-yl)-*L*-serinate (2-51)

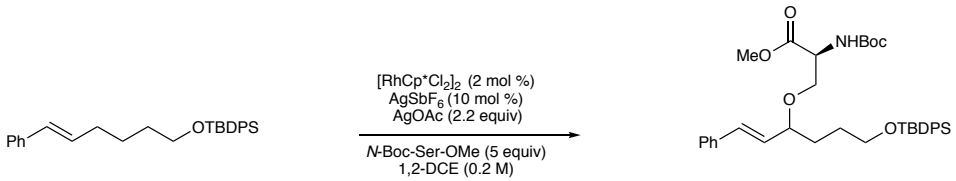

Following the general procedure B, $[RhCp^*Cl_2]_2$ (2.2 mg, 0.004 mmol, 4 mol %), $AgSbF_6$ (4.5 mg, 0.013 mmol, 13 mol %), AgOAc (50.3 mg, 0.30 mmol, 3.0 equiv), *tert*-butyl (*S*)-2-(hydroxymethyl)morpholine-4-carboxylate (266.6 mmol, 6 equiv), (*E*)-*tert*-

butyldiphenyl((6-phenylhex-5-en-1-yl)oxy)silane (43 mg, 0.10 mmol, 1 equiv) were used for 48 h at 60 °C. The filtration eluent was EtOAc. Purification by flash column chromatography on silica gel (48:1 Hexanes/Et_2O to 24:1 Hexanes/Et_2O) afforded pure allylic ether **2-51** as a clear, colorless oil (26.1 mg, 61%).

^{1}H NMR 1H NMR (400 MHz, $CDCl_3$) δ 7.71 – 7.55 (m, 4H), 7.48 – 7.11 (m, 11H), 6.45(d, *J* = 15.9,0.5H), 6.45(d, *J* = 15.9,0.5H), 5.99 (dd, *J* = 16.0, 7.9 Hz, 0.5H), 5.94 (dd, *J* = 16.0, 7.9 Hz, 0.5H), 5.34 (d, *J* = 8.9 Hz, 1H), 4.39 (d, *J* = 8.9 Hz, 1H), 3.89 (dd, *J* = 9.4, 3.3 Hz, 0.5 H), 3.77 – 3.59 (m, 7H), 3.51 (dd, *J* = 9.5, 3.5 Hz, 0.5 H), 1.86 – 1.47 (m, 4H), 1.43 (d, *J* = 8.1 Hz, 9H), 1.02 (d, *J* = 1.9 Hz, 9H).

^{13}C NMR (150 MHz, $CDCl_3$): δ 171.52, 171.44, 155.70, 155.65, 136.61, 136.58, 135.71, 134.10, 132.56, 129.89, 129.81, 129.70, 128.74, 128.72, 128.69, 127.96, 127.94, 127.76, 126.68, 126.63, 81.69, 81.37, 80.10, 80.07, 68.89, 68.39, 63.82, 63.72, 54.26, 52.50, 52.48, 32.04, 28.48, 28.45, 28.44, 27.03, 27.01, 19.36.

IR (neat, cm^{-1}): 2930.57, 2857.36, 1751.45, 1715.38, 1494.95, 1472.37, 1420.07, 1390.61, 1347.67, 1365.58, 1246.22, 1295.54, 1207.06, 1163.07, 1105.69, 1028.52, 968.97, 823.14, 743.41, 702.06, 613.50

HRMS (+NSI): calculated for $C_{37}H_{49}O_6NNaSi$ $[M+Na]^+$ 654.3223, found 654.3223

R_f = 0.04 (9:1 Hexanes/Et_2O)

(*E*)-((4-(benzyloxy)-6-(*o*-tolyl)hex-5-en-1-yl)oxy)(*tert*-butyl)diphenylsilane (2-52)

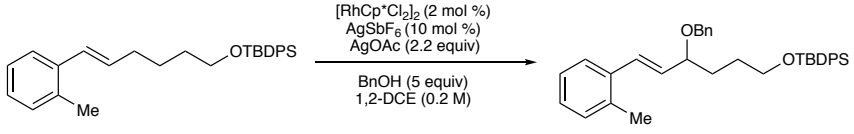

Following the general procedure B, $[RhCp^*Cl_2]_2$ (2.1 mg, 0.003 mmol, 3 mol %), $AgSbF_6$ (5.0 mg, 0.014 mmol, 11 mol %), AgOAc (50.0 mg, 0.30 mmol, 2.3 equiv), benzyl alcohol (60 µL, 5 equiv), (*E*)-*tert*-butyldiphenyl((6-(*o*-tolyl)hex-5-en-1-yl)oxy)silanesilane[29] (55 mg, 0.10 mmol, 1 equiv) were used for 24 h at 60 °C. The filtration eluent was EtOAc. Purification by flash column chromatography on silica gel (48:1 Hexanes/Et_2O to 24:1 Hexanes/Et_2O) afforded allylic ether **2-52** as a clear, colorless oil (29.5 mg, 43%).

^{1}H NMR (400 MHz, $CDCl_3$): δ 7.78 – 7.57 (m, 4H), 7.47 – 7.08 (m, 15H), 6.72 (d, *J* = 15.8 Hz, 1H), 5.99 (dd, *J* = 15.8, 8.0 Hz, 1H), 4.63 (d, *J* = 11.9 Hz, 1H), 4.40 (d, *J* = 11.9 Hz, 1H), 3.93 (q, *J* = 6.6 Hz, 1H), 3.77 – 3.57 (m, 2H), 2.35 (s, 3H), 2.03 – 1.56 (m, 4H), 1.04 (s, 9H).

^{13}C NMR (125 MHz, $CDCl_3$): δ 138.95, 136.00, 135.72, 135.53, 134.16, 132.11, 130.45, 130.39, 129.66, 128.55, 128.50, 128.44, 127.96, 127.89, 127.73, 127.58, 126.28, 125.98, 80.19, 70.21, 63.89, 32.34, 28.68, 27.02, 20.02, 19.37.

IR (neat, cm^{-1}): 2930.09, 2857.31, 1451.66, 1110.92, 968.76, 823.09, 739.69, 701.10, 613.60

HRMS (+NSI): calculated for $C_{36}H_{42}O_2NaSi$ $[M+Na]^+$ 557.2846, found 557.2846.

R_f = 0.71 (9:1 Hexanes/Et_2O)

(*E*)-((4-(benzyloxy)-6-(2-isopropylphenyl)hex-5-en-1-yl)oxy)(*tert*-butyl)diphenylsilane (2-53)

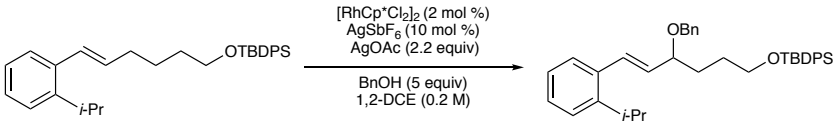

Following the general procedure B, $[RhCp^*Cl_2]_2$ (2.1 mg, 0.003 mmol, 3 mol %), $AgSbF_6$ (4.4 mg, 0.013 mmol, 9.8 mol %), AgOAc (52.3 mg, 0.31 mmol, 2.4 equiv), benzyl alcohol (66 µL,

5 equiv), (*E*)-*tert*-butyl((6-(2-isopropylphenyl)hex-5-en-1-yl)oxy)diphenylsilane (**2-S1**, 59 mg, 0.10 mmol, 1 equiv) were used for 24 h at 60 °C. The filtration eluent was EtOAc. Purification by flash column chromatography on silica gel (48:1 Hexanes/Et_2O to 24:1 Hexanes/Et_2O) afforded allylic ether **2-53** as a clear, colorless oil (46.5mg, 57%).

^{1}H NMR (400 MHz, $CDCl_3$): δ 7.68 (dd, *J* = 7.8, 1.7 Hz, 4H), 7.46-7.17 (m, 15 H), 6.89 (d, *J* = 15.7 Hz, 1H), 5.98 (dd, *J* = 15.7, 8.0 Hz, 1H), 4.66 (d, *J* = 11.9 Hz, 1H), 4.43 (d, *J* = 11.9 Hz, 1H), 3.96 (q, *J* = 7.3, 6.6 Hz, 1H), 3.70 (t, *J* = 6.0 Hz, 2H), 3.24 (hept, *J* = 7.1 Hz, 1H), 1.95- 1.65 (m , 4H) 1.36 – 1.18 (m, 6H), 1.06 (s, 9H).

^{13}C NMR (150 MHz, $CDCl_3$): δ 145.89, 138.95, 135.72, 135.20, 134.15, 132.79, 130.42, 129.66, 128.50, 128.08, 127.88, 127.73, 127.58, 126.74, 126.03, 125.05, 80.19, 77.37, 76.95, 70.25, 63.86, 32.33, 29.32, 28.69, 27.01, 23.57, 23.48, 19.37.

IR (neat, cm^{-1}): 3252.37, 3068.84, 2958.50, 2929.67, 2857.29, 1471.86, 1483.74, 1427.69, 1388.60, 1324.16, 1110.23, 1090.64, 969.38, 822.63, 737.37, 700.49, 612.99

HRMS (+NSI): calculated for $C_{38}H_{46}O_2NaSi$ $[M+Na]^+$ 585.3159, found 585.3162.

R_f = 0.71 (9:1 Hexanes/Et_2O)

(*E*)-((4-(benzyloxy)-6-(4-(trifluoromethyl)phenyl)hex-5-en-1-yl)oxy)(*tert*-butyl)diphenylsilane (2-54)

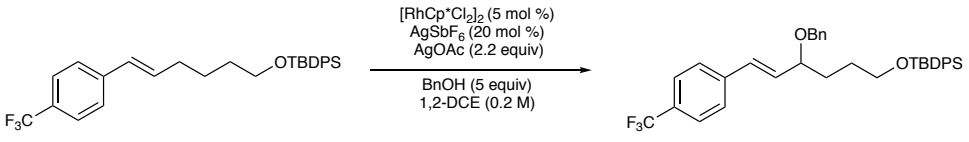

Following the general procedure B, $[RhCp^*Cl_2]_2$ (5.0 mg, 0.008 mmol, 8 mol %), $AgSbF_6$ (11.2 mg, 0.032 mmol, 32 mol %), AgOAc (47.0 mg, 0.28 mmol, 2.2 equiv), benzyl alcohol (66 µL, 5 equiv), (*E*)-*tert*-butyldiphenyl((6-(4-(trifluoromethyl)phenyl)hex-5-en-1-yl)oxy)silane[29]

(62 mg, 0.13 mmol, 1 equiv) were used for 48 h at 60 °C. The filtration eluent was EtOAc. Purification by flash column chromatography on silica gel (48:1 Hexanes/Et_2O to 24:1 Hexanes/Et_2O) afforded allylic ether **2-54** as a clear, colorless oil (33.9 mg, 45%).

^{1}H NMR (400 MHz, $CDCl_3$): δ 7.65(d, J = 7.0 Hz, 4H), 7.52 (dd, J = 43.9, 8.0 Hz, 4H), 7.43 – 6.89 (m, 11H), 6.54 (d, J = 16.0 Hz, 1H), 6.21 (dd, J = 16.0, 7.6 Hz, 1H), 4.60 (d, J = 11.9 Hz, 1H), 4.39 (d, J = 11.9 Hz, 1H), 3.95 (q, J = 6.7 Hz, 1H), 3.67 (t, J = 5.8 Hz, 2H), 2.06 -1.47 (m, 4H), 1.04 (s, 9H).

^{13}C NMR (125 MHz, $CDCl_3$): δ 140.26, 138.70, 135.71, 134.10, 133.57, 130.80, 129.69, 129.50, 128.55, 128.53, 127.96, 127.83, 127.83, 127.75, 127.68, 126.78, 125.72, 125.70, 125.67, 125.65, 125.22, 79.73, 70.54, 63.82, 32.11, 29.86, 28.52, 27.01, 26.98, 19.37.

IR (neat, cm^{-1}): 3069.97, 2930.04, 2857.04, 1615.43, 1472.07, 1435.91, 1414.23, 1426.02, 1389.73, 1322.97, 1164.87, 1107.07, 1066.32, 1028.08, 1016.48, 971.39, 863.05, 821.71, 736.20, 700.14, 613.66

HRMS (+NSI): calculated for $C_{36}H_{39}O_2F_3NaSi$ $[M+Na]^+$ 611.2564 found 611.2573.

R_f = 0.54 (85:15 Hexanes/Et_2O)

(*E*)-((4-(benzyloxy)-6-(4-bromophenyl)hex-5-en-1-yl)oxy)(*tert*-butyl)diphenylsilane (2-55)

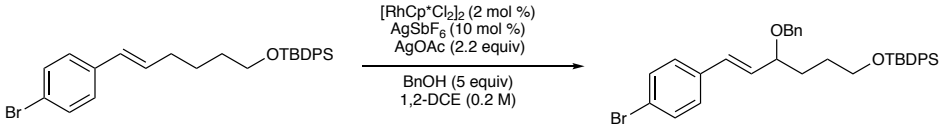

Following the general procedure B, $[RhCp^*Cl_2]_2$ (1.9 mg, 0.003 mmol, 2 mol %), $AgSbF_6$ (5.0 mg, 0.014 mmol, 11 mol %), AgOAc (48.3 mg, 0.29 mmol, 2.2 equiv), benzyl alcohol (66 μL, 5

equiv), (*E*)-*tert*-butyldiphenyl((6-(4-(bromo)phenyl)hex-5-en-1-yl)oxy)silane (**2-S2**, 63 mg, 0.13 mmol, 1 equiv) were used for 48 h at 60 °C. The filtration eluent was EtOAc. Purification by flash column chromatography on silica gel (48:1 Hexanes/Et_2O to 24:1 Hexanes/Et_2O) afforded allylic ether **2-55** as a clear, colorless oil (46.2 mg, 60%).

^{1}H NMR (400 MHz, $CDCl_3$): δ 7.66-7.63 (m, 4H), 7.46-7.21 (m, 15H), 6.44 (d, *J* = 16.0 Hz, 1H), 6.10 (dd, *J* = 16.0, 7.8 Hz, 1H), 4.59 (d, *J* = 11.9 Hz, 1H), 4.38 (d, *J* = 11.9 Hz, 1H), 3.90 (q, *J* = 6.9 Hz, 1H), 3.67 (t, *J* = 6.0 Hz, 2H), 1.88-1.55 (m. 4H), 1.04 (s, 9H).

^{13}C NMR (150 MHz, $CDCl_3$): δ 138.79, 135.71, 134.11, 131.82, 131.59, 131.11, 129.67, 128.50, 128.16, 127.82, 127.73, 127.62, 121.56, 79.89, 70.38, 63.84, 32.15, 28.56, 27.01, 19.36.

IR (neat, cm^{-1}): 3069.19, 2929.23, 2856.20, 1588.40, 1486.95, 1471.62, 1453.53, 1427.49, 1389.32, 1360.30, 1324.68, 1188.36, 1109.85, 1071.39, 1028.02, 1008.30, 969.45, 939.89, 855.08, 822.66, 805.57, 736.39,700.23, 613.60

HRMS (+NSI): calculated for $C_{35}H_{39}O_2BrSiNa$ $[M+Na]^+$ 621.1801 found 621.1792.

R_f = 0.68 (85:15 Hexanes/Et_2O)

(*E*)-((4-(benzyloxy)-6-(4-fluorophenyl)hex-5-en-1-yl)oxy)(*tert*-butyl)diphenylsilane (2-56)

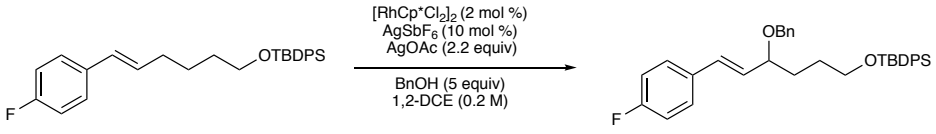

Following the general procedure B, $[RhCp^*Cl_2]_2$ (1.9 mg, 0.001 mmol, 1 mol %), $AgSbF_6$ (5.0 mg, 0.013 mmol, 10 mol %), AgOAc (49.1 mg, 0.28 mmol, 2.2 equiv), benzyl alcohol (66 µL, 5

equiv), (*E*)-*tert*-butyldiphenyl((6-(4-(fluoro)phenyl)hex-5-en-1-yl)oxy)silane[29] (55.6 mg, 0.10 mmol, 1 equiv) were used for 31 h at 60 °C. The filtration eluent was EtOAc. Purification by flash column chromatography on silica gel (48:1 Hexanes/Et_2O to 24:1 Hexanes/Et_2O) afforded pure allylic ether **2-56** as a clear, colorless oil (42.2 mg, 61%).

^{1}H NMR (400 MHz, $CDCl_3$): δ 7.65(d, *J* = 6.5 Hz, 4H), 7.41 – 7.25 (m, 13 H), 7.02 (t, *J*= 8.7 Hz, 2H), 6.47 (d, *J* = 16.0 Hz, 1H), 6.02 (dd, *J* = 16.0, 8.0 Hz, 1H), 4.60 (d, *J* = 11.9 Hz, 1H), 4.38 (d, J= 11.9 Hz, 1H), 3.90(q, *J* = 6.9 Hz, 1H), 3.67 (m, 2H), 1.83-1.60 (m, 4 H) 1.04 (s, 9H)

^{13}C NMR (150 MHz, $CDCl_3$): 163.32, 161.68, 138.87, 135.74, 135.71, 134.13, 132.95, 132.92, 131.22, 130.46, 130.45, 129.99, 129.66, 128.55, 128.49, 128.17, 128.12, 127.96, 127.82, 127.73, 127.58, 126.95, 115.70, 115.55, 79.99, 70.28, 63.87, 32.23, 28.61, 27.01, 26.98, 19.36.

^{19}F NMR (376 MHz, $CDCl_3$): -115.12 (against triflourotoluene)

IR (neat, cm^{-1}): 3069.57, 2930.60, 2857.62, 1482.98, 1461.69, 14.68.62, 1444.23, 1427.30, 1390.43, 1359.50, 1249.02, 1110.59, 822.68, 756.12, 739.75, 700.98, 613.30

HRMS (+NSI): calculated for $C_{35}H_{39}O_2FNaSi$ $[M+Na]^+$ 561.2601, found 561.2596.

R_f = 0.62 (9:1 Hexanes/Et_2O)

(*E*)-((4-(benzyloxy)-6-(4-methoxyphenyl)hex-5-en-1-yl)oxy)(*tert*-butyl)diphenylsilane (2-57)

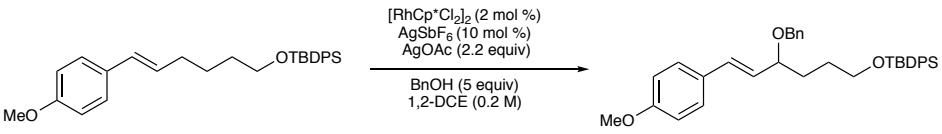

Following the general procedure B, $[RhCp^*Cl_2]_2$ (2.4 mg, 0.004 mmol, 3 mol %), $AgSbF_6$ (4.1 mg, 0.012 mmol, 12 mol %), AgOAc (46.8 mg, 0.28 mmol, 2.8 equiv), benzyl alcohol (66 µL, 5 equiv), (*E*)-*tert*-butyldiphenyl((6-(4-(methoxy)phenyl)hex-5-en-1-yl)oxy)silane[29] (57 mg,

0.10 mmol, 1 equiv) were used for 4 h at 60 °C. The filtration eluent was EtOAc. Purification by flash column chromatography on silica gel (48:1 Hexanes/Et_2O to 24:1 Hexanes/Et_2O) afforded pure allylic ether **2-57** as a clear, colorless oil (41.1 mg, 58%).

^{1}H NMR (400 MHz, $CDCl_3$): δ 7.65(d, J = 6.3 Hz, 4H), 7.44 – 7.19 (m, 13 H), 6.88 (d, J = 8.8 Hz, 2H), 6.45 (d, J = 15.9 Hz, 1H), 5.96 (dd, J = 15.9, 8.2 Hz, 1H), 4.61 (d, J = 11.9 Hz, 1H), 4.37 (d, J = 12.0 Hz, 1H), 3.88(ddd, J = 8.5, 6.5, 4.7 Hz, 1H), 3.83 (s, 3H), 3.66 (t, J = 6.0 Hz, 2H), 1.85-1.51 (m, 4 H) 1.03 (s, 9H).

^{13}C NMR (150 MHz, $CDCl_3$): δ 159.45, 139.01, 135.72, 134.16, 132.05, 129.64, 129.57, 128.46, 127.85, 127.83, 127.83, 127.73, 127.69, 127.51, 114.14, 80.26, 77.37, 76.95, 70.10, 63.92, 55.48, 32.35, 28.69, 27.02, 19.37.

IR (neat, cm^{-1}): 3069.28, 2930.20, 2856.49, 1607.21, 1511.10, 1462.02, 1452.97, 1427.36, 1390.11, 1359.63, 1302.21, 1247.57, 1173.87, 1106.59, 1035.67, 968.94, 822.14, 737.68, 700.74, 613.51.

HRMS (+NSI): calculated for $C_{36}H_{42}O_3NaSi$ $[M+Na]^+$ 573.2795, found 573.2802.

R_f = 0.45 (85:15 Hexanes/Et_2O)

(*E*)-(3-(benzyloxy)prop-1-ene-1,3-diyl)dibenzene (2-58)

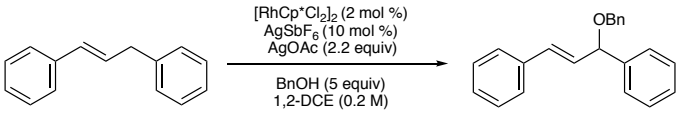

Following the general procedure B, $[RhCp^*Cl_2]_2$ (7.3 mg, 0.012 mmol, 4 mol %), $AgSbF_6$ (12.7 mg, 0.036 mmol, 14 mol %), AgOAc (121.3 mg, 0.73 mmol, 2.8 equiv), benzyl alcohol (133 µL, 5 equiv), 1,3-diphenylpropene (58.7 mg, 0.257 mmol, 1 equiv) were used for 6 h at 60 °C.

The filtration eluent was EtOAc. Purification by flash column chromatography on silica gel (200:1 Hexanes/EtOAc to 100:1 Hexanes/EtOAc) afforded allylic ether **2-58** as a clear, colorless oil (64.4 mg, 71%).[35] ^{1}H NMR spectral analysis corresponded to previous reports.

^{1}H NMR (400 MHz, $CDCl_3$): δ 7.66 – 7.13 (m, 15H), 6.63 (d, J = 15.9 Hz, 1H), 6.34 (dd, J = 15.9, 7.1 Hz, 1H), 5.01 (d, J = 7.0 Hz, 1H), 4.58 (d, J = 2.5 Hz, 2H).

(*E*)-(3-methoxyprop-1-ene-1,3-diyl)dibenzene (2-59)

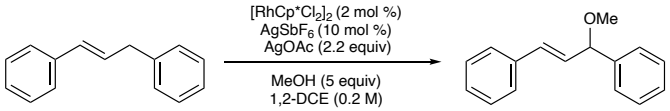

Following the general procedure B, $[RhCp^*Cl_2]_2$ (3.2 mg, 0.005 mmol, 2 mol %), $AgSbF_6$ (12.2 mg, 0.036 mmol, 14 mol %), AgOAc (101.3 mg, 0.61 mmol, 2.4 equiv), methanol (52 µL, 5 equiv), 1,3-diphenylpropene (57.4 mg, 0.295 mmol, 1 equiv) were used for 6 h at 60 °C. The filtration eluent was EtOAc. Purification by flash column chromatography on silica gel (200:1 Hexanes/EtOAc to 100:1 Hexanes/EtOAc) afforded allylic ether **2-59** as a clear, colorless oil (66.3 mg, 53%). ^{1}H NMR spectral analysis corresponded to previous reports.[36]

^{1}H NMR (400 MHz, $CDCl_3$): δ 7.40–7.22 (m, 10H), 6.63 (d, J = 15.9 Hz, 1H), 6.28 (dd, J = 15.9, 6.9 Hz, 1H), 4.80 (d, J = 6.9 Hz, 1H), 3.38 (s, 3H)

(8*S*,9*R*,13*R*,14*R*)-3-((*E*)-3-(benzyloxy)-6-((*tert*-butyldiphenylsilyl)oxy)hex-1-en-1-yl)-13-methyl-6,7,8,9,11,12,13,14,15,16-decahydro-17*H*-cyclopenta[*a*]phenanthren-17-one (2-60)

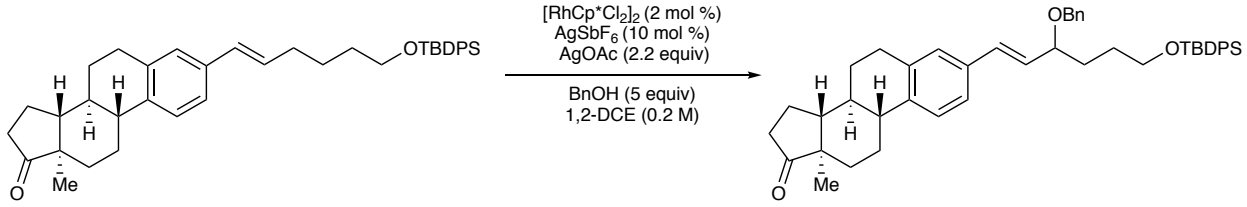

$AgSbF_6$:

Following the general procedure B, $[RhCp^*Cl_2]_2$ (3.2 mg, 0.005 mmol, 3 mol %), $AgSbF_6$ (5.6 mg, 0.013 mmol, 10 mol %), AgOAc (47.4 mg, 0.30 mmol, 2.3 equiv), benzyl alcohol (66 µL, 5 equiv), (8*S*,9*R*,13*R*,14*R*)-3-((*E*)-6-((*tert*-butyldiphenylsilyl)oxy)hex-1-en-1-yl)-13-methyl-6,7,8,9,11,12,13,14,15,16-decahydro-17*H*-cyclopenta[*a*]phenanthren-17-one **2-S5** (76 mg, 0.13 mmol, 1 equiv) were used for 21 h at 60 °C. The filtration eluent was EtOAc. Purification by flash column chromatography on silica gel (48:1 Hexanes/Et_2O to 24:1 Hexanes/Et_2O) afforded pure allylic ether **2-60** as a clear, colorless oil (mg, 34%).

$AgBAr^F_4$:

Following the general procedure B, $[RhCp^*Cl_2]_2$ (2.0 mg, 0.003 mmol, 2 mol %), $AgBAr^F_4$ (15.4 mg, 0.013 mmol, 10 mol %), AgOAc (50 mg, 0.30 mmol, 2.3 equiv), benzyl alcohol (66 µL, 5 equiv), (8*S*,9*R*,13*R*,14*R*)-3-((*E*)-6-((*tert*-butyldiphenylsilyl)oxy)hex-1-en-1-yl)-13-methyl-6,7,8,9,11,12,13,14,15,16-decahydro-17*H*-cyclopenta[*a*]phenanthren-17-one **2-S5** (76 mg, 0.13 mmol, 1 equiv) were used for 5 h at 60 °C. The filtration eluent was EtOAc. Purification by flash column chromatography on silica gel (48:1 Hexanes/Et_2O to 24:1 Hexanes/Et_2O) afforded pure allylic ether **2-60** as a clear, colorless oil (58.2 mg, 60%).

^{1}H NMR (300 MHz, $CDCl_3$) δ 7.77 – 7.52 (m, 4H), 7.55 – 7.03 (m, 14H), 6.47 (d, *J* = 15.9 Hz, 1H), 6.08 (dd, *J* = 15.9, 8.1 Hz, 1H), 4.71 (s, 1H), 4.61 (d, *J* = 11.9 Hz, 1H), 4.38 (d, *J* = 11.9 Hz, 1H), 3.90 (q, *J* = 6.9, 6.3 Hz, 1H), 3.67 (t, *J* = 5.9 Hz, 2H), 2.94 (dd, *J* = 8.7, 4.1 Hz, 2H), 2.86 – 0.54 (m, 16H).

^{13}C NMR (125 MHz, $CDCl_3$): *δ* 221.04, 139.66, 138.95, 136.85, 135.72, 134.39, 134.17, 132.31, 130.10, 129.64, 129.18, 128.73, 128.47, 128.37, 127.86, 127.83, 127.73, 127.54, 127.26, 127.21, 127.14, 125.80, 124.16, 124.11, 80.15, 70.13, 65.56, 63.89, 50.64, 48.14, 44.60, 38.33, 36.01, 32.28, 31.73, 29.54, 28.65, 27.02, 26.63, 25.90, 21.74, 19.37, 13.99, 0.14.

IR (neat, cm^{-1}): 3028.46, 2928.87, 2856.18, 1738.27, 1496.77, 1471.44, 1427.55, 1453.20, 1388.98, 1373.12, 1258.90, 1207.25, 1027.65, 1007.25, 969.39, 822.16, 737.41, 700.88, 613.78

HRMS (+APCI): calculated for $C_{47}H_{57}O_3Si$ $[M+H]^+$ 697.4072, found 697.4068.

R_f = 0.12 (9:1 Hexane/Et_2O)

(*E*)-(3-(benzyloxy)prop-1-en-1-yl)benzene (2-61)

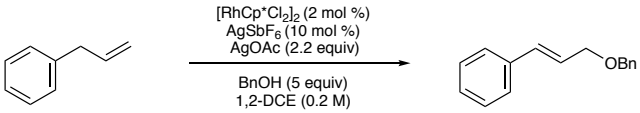

Following the general procedure B, $[RhCp^*Cl_2]_2$ (2.2 mg, 0.004 mmol, 4 mol %), $AgSbF_6$ (4.5 mg, 0.013 mmol, 13 mol %), AgOAc (52.3 mg, 0.31 mmol, 3.1 equiv), benzyl alcohol (66 µL, 5 equiv), allylbenzene (17 µL, 0.10 mmol, 1 equiv) were used for 20.5 h at 60 °C. The filtration eluent was EtOAc. Purification by flash column chromatography on silica gel (48:1 Hexanes/Et_2O to 24:1 Hexanes/Et_2O) afforded allylic ether **2-61** as a clear, colorless oil (17.4 mg, 60%).[37]

^{1}H NMR (400 MHz, $CDCl_3$): δ 7.66 – 6.93 (m, 10H), 6.63 (d, J = 16.0, 1H), 6.33 (dt, J = 15.9, 6.0 Hz, 1H), 4.57 (s, 2H), 4.20 (dd, J = 6.0, 1.5 Hz, 2H)

methyl (2*S*)-3-(4-((*E*)-3-(benzyloxy)-6-((*tert*-butyldiphenylsilyl)oxy)hex-1-en-1-yl)phenyl)-2-((*tert*-butoxycarbonyl)amino)propanoate (2-62)

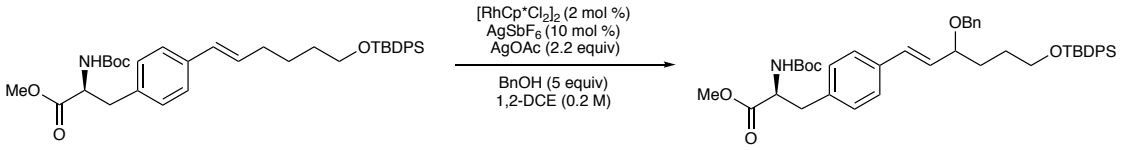

$AgSbF_6$:

Following the general procedure B, $[RhCp^*Cl_2]_2$ (3.4 mg, 0.006 mmol, 4 mol %), $AgSbF_6$ (9.1 mg, 0.026 mmol, 20 mol %), AgOAc (48 mg, 0.28 mmol, 2.2 equiv), benzyl alcohol (66 µL, 5 equiv), methyl (*S*,*E*)-2-((*tert*-butoxycarbonyl)amino)-3-(4-(6-((*tert*-butyldiphenylsilyl)oxy)hex-1-en-1-yl)phenyl)propanoate **2-S7** (79 mg, 0.13 mmol, 1 equiv) were used for 4 h at 60 °C. The filtration eluent was EtOAc. Purification by flash column chromatography on silica gel (48:1 Hexanes/Et_2O to 24:1 Hexanes/Et_2O) afforded pure allylic ether **2-62** as a clear, colorless oil (38.2 mg, 41%).

$AgBAr^F_4$:

Following the general procedure B, $[RhCp^*Cl_2]_2$ (1.6 mg, 0.003 mmol, 2 mol %), $AgBAr^F_4$ (18.2 mg, 0.013 mmol, 10 mol %), AgOAc (52.3 mg, 0.28 mmol, 2.2 equiv), benzyl alcohol (66 µL, 5 equiv), methyl (*S*,*E*)-2-((*tert*-butoxycarbonyl)amino)-3-(4-(6-((*tert*-butyldiphenylsilyl)oxy)hex-1-en-1-yl)phenyl)propanoate **2-S7** (70 mg, 0.13 mmol, 1 equiv) were used for 4 h at 60 °C. The filtration eluent was EtOAc. Purification by flash column chromatography on silica gel (48:1 Hexanes/Et_2O to 24:1 Hexanes/Et_2O) afforded pure allylic ether **2-62** as a clear, colorless oil (30.9mg, 33%).

^{1}H NMR (400 MHz, $CDCl_3$): δ 7.77 – 7.52 (m, 4H), 7.55 – 7.03 (m, 13H), 7.09 (d, *J* = 8.0 Hz, 2H), 6.47 (d, *J* = 15.9 Hz, 1H), 6.08 (dd, *J* = 15.9, 8.1 Hz, 1H), 4.98 (d, *J* = 8.3 Hz, 1H), 4.71 (m, 1H), 4.61 (m, 1H), 4.38 (d, *J* = 11.9 Hz, 1H), 3.90 (q, *J* = 6.9, 6.3 Hz, 1H), 3.74 (s, 3H), 3.67 (t, *J* = 5.9 Hz, 2H), 3.21 – 2.97 (m, 2H), 1.88 – 1.51 (m, 4H), 1.42 (s, 9H), 1.04 (s, 9H).

^{13}C NMR (150 MHz, $CDCl_3$): δ 172.42, 155.22, 138.90, 135.71, 135.66, 135.61, 134.15, 132.03, 130.62, 129.69, 129.65, 128.70, 128.47, 127.84, 127.79, 127.73, 127.55, 127.12, 126.82, 80.11, 80.04, 70.24, 65.51, 63.88, 54.52, 52.39, 38.17, 32.27, 28.62, 28.44, 27.02, 19.36.

IR (neat, cm^{-1}): 3441.52, 2930.66, 2857.37, 1746.65, 1716.44, 1653.00, 1588.90, 1558.85, 1496.66, 1472.58, 1454.87, 1428.15, 1390.42, 1365.24, 1250.39, 1212.59, 1166.69, 1110.66, 1062.50, 1027.57, 970.69, 860.04, 823.23, 738.94, 701.80, 613.64

HRMS (+NSI): calculated for $C_{44}H_{55}NO_6NaSi$ $[M+Na]^+$ 744.3691, found 744.3691.

R_f = 0.08 (85:15 Hexanes/Et_2O

(((*E*)-4-(benzyloxy)-6-((*S*)-2,5-dimethyl-2-((4*S*,8*S*)-4,8,12-trimethyltridecyl)chroman-6-yl)hex-5-en-1-yl)oxy)(*tert*-butyl)diphenylsilane (2-63)

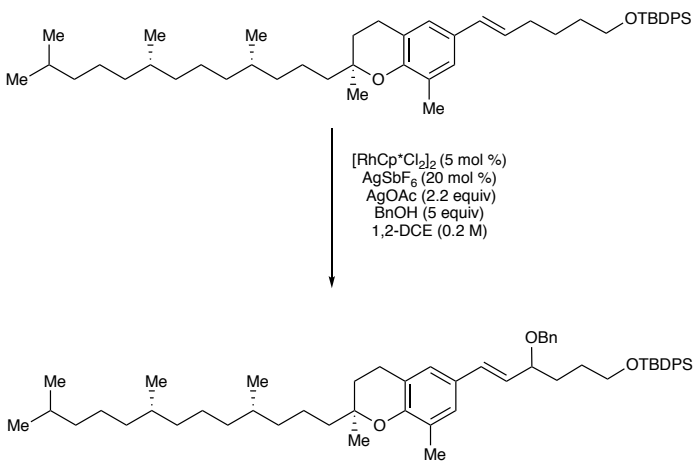

Following the general procedure B, $[RhCp^*Cl_2]_2$ (2.5 mg, 0.004 mmol, 3 mol %), $AgSbF_6$ (4.5 mg, 0.013 mmol, 10 mol %), AgOAc (48 mg, 0.29 mmol, 2.2 equiv), benzyl alcohol (66 µL, 5 equiv), *tert*-butyl(((*E*)-6-((*S*)-2,5-dimethyl-2-((4*S*,8*S*)-4,8,12-trimethyltridecyl)chroman-6-yl)hex-5-en-1-yl)oxy)diphenylsilane **2-S9** (93 mg, 0.13 mmol, 1 equiv) were used for 26 h at 60 °C. The filtration eluent was EtOAc. Purification by flash column chromatography on silica gel (48:1 Hexanes/Et_2O to 24:1 Hexanes/Et_2O) afforded allylic ether **2-63** as a clear, colorless oil (35.6 mg, 33%).

^{1}H NMR (400 MHz, $CDCl_3$): δ 7.79 – 7.50 (m, 4H), 7.54 – 7.06 (m, 11H), 7.00 (dd, J = 27.5, 2.2 Hz, 2H), 6.38 (d, J = 15.9 Hz, 1H), 5.91 (dd, J = 15.9, 8.3 Hz, 1H), 4.60 (d, J = 12.0 Hz, 1H), 4.35 (d, J = 12.0 Hz, 1H), 3.85 (d, J = 7.2 Hz, 1H), 3.66 (t, J = 6.0 Hz, 2H), 2.75 (t, J = 6.8 Hz, 2H), 2.34 – 0.54 (m, 54H).

^{13}C NMR (150 MHz, $CDCl_3$): δ 144.57, 135.72, 134.18, 132.80, 129.62, 128.44, 127.87, 127.72, 127.45, 127.33, 126.64, 125.42, 80.40, 76.47, 69.90, 63.92, 39.51, 37.57, 37.42, 32.94, 32.84, 31.37, 28.73, 28.12, 27.01, 24.95, 24.59, 24.42, 22.88, 22.78, 22.45, 21.13, 19.90, 19.79, 19.36, 14.35.

IR (neat, cm^{-1}): 2928.78, 2510.52, 2159.01, 2028.65, 1474.15, 1111.00, 910.70, 750.4

HRMS (+NSI): calculated for $C_{56}H_{80}O_3NaSi$ $[M+Na]^+$ 851.5769, found 851.5773.

R_f = 0.66 (85:15 Hexanes/Et_2O

(*E*)-(3-(benzyloxy)but-1-en-1-yl)benzene (2-67)

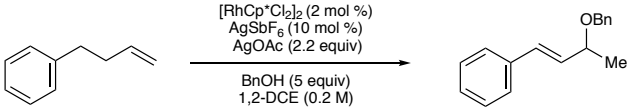

Following the general procedure B, $[RhCp^*Cl_2]_2$ (3.6 mg, 0.006 mmol, 2 mol %), $AgSbF_6$ (8.9 mg, 0.026 mmol, 10 mol %), AgOAc (94.2 mg, 0.56 mmol, 2.2 equiv), benzyl alcohol (133 µL, 5 equiv), 4-phenylbut-1ene (38 µL, 0.26 mmol, 1 equiv) were used for 17 h at 60 °C. The filtration eluent was EtOAc. Purification by flash column chromatography on silica gel (48:1 Hexanes/Et_2O to 24:1 Hexanes/Et_2O) afforded allylic ether **2-67** as a clear, colorless oil (47.3 mg, 78%).[38]

^{1}H NMR (400 MHz, $CDCl_3$): δ 7.92 – 7.54 (m, 4H), 7.45 – 7.04 (m, 6H), 6.46 (d, *J* = 16.0 Hz, 1H), 6.04 (dd, *J* = 15.9, 7.8 Hz, 1H), 3.78 (q, *J* = 7.2, 6.4 Hz, 1H), 3.67 (td, *J* = 6.0, 2.1 Hz, 1H), 3.56 (dq, *J* = 8.9, 7.0 Hz, 1H), 3.32 (dq, *J* = 8.9, 7.0 Hz, 1H), 2.06 – 1.45 (m, 1H), 1.17 (t, *J* = 7.0 Hz, 1H), 1.02 (s, 1H).

VI.6. Deuterium Exchange Experiment

(*E*)-(3-(benzyloxy)prop-1-ene-1,3-diyl)dibenzene (**2-69$_D$** and **2-69$_{D'}$**)

Following the general procedure B, $[RhCp^*Cl_2]_2$ (3.2 mg, 0.005 mmol, 4 mol %), $AgSbF_6$ (11.6 mg, 0.034 mmol, 26 mol %), AgOAc (48.3 mg, 0.29 mmol, 2.3 equiv), benzyl alcohol (133 µL, 5 equiv), deuterated-1,3-diphenylpropene (22.2 mg, 0.127 mmol, 1 equiv) were used for 24 h at 60 °C. The filtration eluent was EtOAc. Purification by preparatory layer chromatography 4% Et_2O/ Hexanes (3 sweeps) afforded pure allylic ether **2-69$_{D+D'}$** (9.8 mg, 30%) and recovered starting material **2-68$_D$** (11 mg, 50%) as a clear, colorless oil.

^{1}H NMR (400 MHz, $CDCl_3$): δ 7.56 – 6.99 (m, 15H), 6.63 (d, J = 15.9 Hz, 0.5H), 6.34 (d, J = 15.8 Hz, 1H), 5.02 (d, J = 7.1 Hz, 0.5H), 4.86 – 4.18 (m, 2H).

VI.7. Kinetic Isotope Effect

(*E*)-(3-(benzyloxy)prop-1-ene-1,3-diyl)dibenzene (**2-69$_D$** and **29$_{D'}$**)

Following the general procedure B, $[RhCp^*Cl_2]_2$ (3.2 mg, 0.005 mmol, 4 mol %), $AgSbF_6$ (10.9 mg, 0.032 mmol, 12 mol %), AgOAc (93.4 mg, 0.56 mmol, 2.2 equiv), benzyl alcohol (120 µL, 5 equiv), deuterated-1,3-diphenylpropene (48.57 mg, 0.257 mmol, 1 equiv) were used for 20 min at 60 °C. The filtration eluent was EtOAc. Purification on preparatory layer chromatography 4% Et_2O/ Hexanes (3 sweeps) afforded allylic ether without starting material which was analyzed by ^{1}H NMR with 10s relaxation delay.

^{1}H NMR (400 MHz, $CDCl_3$): δ 7.56 – 6.99 (m, 15H), 6.63 (d, *J* = 15.9 Hz, 0.5H), 6.34 (d, *J* = 15.8 Hz, 1H), 5.02 (d, *J* = 7.1 Hz, 0.5H), 4.86 – 4.18 (m, 2H).

VI.8. Starting Material Synthesis

(*E*)-*tert*-butyl((6-(2-isopropylphenyl)hex-5-en-1-yl)oxy)diphenylsilane (2-S2)

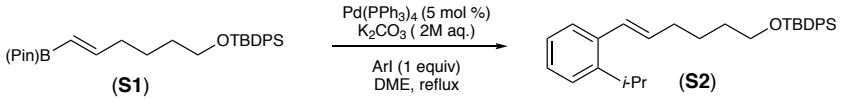

Following the general procedure C, alkene 2-S1[39] (930 mg, 2 mmol, 1.5 equiv), 1-iodo-2-isopropylbenzene (208 µL, 1.3 mmol, 1 equiv), $Pd(PPh_3)_4$ (76 mg, 0.065 mmol, 5 mol %), and K_2CO_3 (503 mg, 3.6 mmol, 2.8 equiv) were utilized. The reaction was heated at reflux in 1 mL DME overnight and was purified by flash column chromatography on silica with toluene and hexane provide pure olefin 2-S2 in (77%, 445 mg).

^{1}H NMR (400 MHz, $CDCl_3$): δ 7.69-7.66 (m 4H) 7.44- 7.11 (m, 10H) 6.68 (d, *J* = 15.5 Hz, 1H), 6.01 (dt, *J* = 15.5, 6.9 Hz, 1H), 3.69 (t, *J* = 6.2 Hz, 2H), 3.23 (hept, *J* = 6.6 Hz, 1H), 2.22 (q, *J* = 7.1 Hz, 2H), 1.66- 1.48 (m, 4H), 1.22 (d, J = 6.9 Hz, 6H), 1.05 (s, 9H).

^{13}C NMR (150 MHz, $CDCl_3$): δ 145.46, 136.41, 135.73, 134.24, 133.03, 129.66, 127.86, 127.73, 127.27, 126.51, 125.87, 124.87, 77.37, 76.95, 63.90, 33.16, 32.21, 29.17, 27.01, 25.82, 23.48, 19.38.

IR (neat, cm^{-1}): 3069.31, 2958.54, 2929.58, 2856.69, 1641.79, 1589.31, 1470.57, 1461.65, 1445.74, 1427.25, 1384.36, 1360.92, 1260.60, 1105.39, 1033.99, 997.99, 965.02, 822.47, 739.12, 755.45, 699.69, 612.96

HRMS (+NSI): calculated for $C_{31}H_{41}OSi$ $[M+H]^+$ 457.2921, found 457.2931.

R_f = 0.81 (9:1 Hexanes/Et_2O)

(*E*)-((6-(4-bromophenyl)hex-5-en-1-yl)oxy)(*tert*-butyl)diphenylsilane (2-S3)

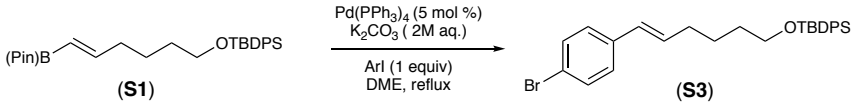

Following the general procedure C, alkene **2-S1**[39] (511mg, 1.1 mmol, 1.5 equiv), 1-iodo-4-bromobenzene (206. mg, 0.73 mmol, 1 equiv), $Pd(PPh_3)_4$ (42.6 mg, 0.036 mmol, 5 mol %), and K_2CO_3 (281.95 mg, 2.0 mmol, 2.8 equiv) were utilized. The reaction was heated at reflux in 1 mL DME overnight and was purified by flash column chromatography on silica with hexane to 30:1 toluene/hexane to afford pure olefin **2-S3** in (61%, 219.8 mg).

^{1}H NMR (400 MHz, $CDCl_3$): δ 7.65 (dd, J = 8.1, 1.7 Hz, 4H), 7.44 – 7.30 (m, 8H), 7.17 (d, J = 8.5 Hz, 2H), 6.27 (d, J = 15.9 Hz, 1H), 6.17 (ddd, J = 15.8, 6.9, 6.3 Hz, 1H), 3.81 – 3.50 (m, 2H), 2.17 (q, J = 6.9 Hz, 2H).1.63-1.48 (m, 4H) 1.04 (s, 9H)

^{13}C NMR (150 MHz, $CDCl_3$): δ 136.95, 135.72, 134.20, 131.99, 131.65, 129.67, 128.91, 127.74, 127.62, 120.53, 77.37, 76.95, 63.85, 32.84, 32.19, 27.02, 26.99, 25.58, 19.38.

IR (neat, cm^{-1}): 3070.12, 2930.08, 2856.56, 1652.13, 1588.79, 1486.78, 1471.84, 1427.48, 1389.36, 1360.72, 1110.04, 1073.13, 1008.02, 965.77, 939.19, 822.71, 739.81, 700.99, 687.58, 613.68

HRMS (+NSI): calculated for $C_{28}H_{34}OBrSi$ $[M+H]^+$ 493.1571 found 493.1557.

R_f = 0.33 (9:1 Hexanes/Toluene)

8*S*,9*R*,13*R*,14*R*)-3-((*E*)-6-((*tert*-butyldiphenylsilyl)oxy)hex-1-en-1-yl)-13-methyl-6,7,8,9,11,12,13,14,15,16-decahydro-17*H*-cyclopenta[*a*]phenanthren-17-one (2-S5)

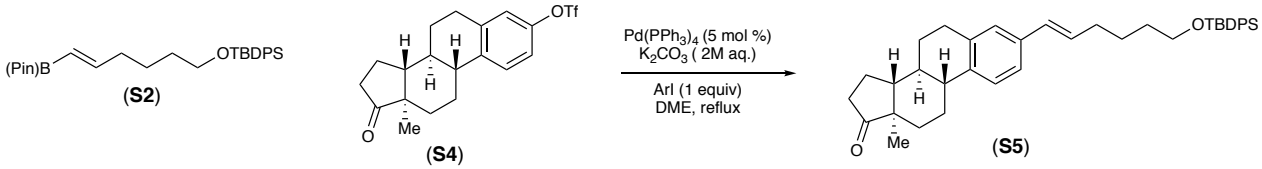

Following the general procedure C, alkene **2-S2**[39] (1.02g, 2.2 mmol, 1.5 equiv), estrone triflate **2-S4**[40] (600 mg, 1.5 mmol, 1 equiv), $Pd(PPh_3)_4$ (86.7 mg, 0.075 mmol, 5 mol %), and K_2CO_3 (580.5 mg, 4.2 mmol, 2.8 equiv, 2M aq. solution) were utilized. The reaction was heated at reflux in 2 mL DME and overnight and was purified by flash column chromatography on silica with toluene and hexane to afford pure compound **2-S5** (633.8 mg, 71% yield).

^{1}H NMR (400 MHz, $CDCl_3$): δ δ 7.76 – 7.56 (m, 4H), 7.38 (m, 6H), 7.21 (d, *J* = 8.2 Hz, 1H), 7.12 (d, *J* = 8.1 Hz, 1H), 7.06 (s, 1H), 6.28 (d, *J* = 15.5 Hz, 1H), 6.14 (dt, *J* = 16.1, 6.9 Hz, 1H), 3.75 – 3.57 (m, 2H), 2.89 (dd, *J* = 9.1, 4.2 Hz, 2H), 2.83 – 1.80 (m, 9H), 1.79 – 1.27 (m, 10H), 1.03 (s, 9H), 0.89 (s, 3H).

^{13}C NMR (100 MHz, $CDCl_3$): δ 138.53, 136.56, 135.69, 135.63, 134.19, 130.48, 129.65, 129.63, 127.71, 126.63, 125.60, 123.51, 65.98, 63.87, 50.60, 48.11, 44.52, 38.32, 35.98, 32.85, 32.17, 31.71, 29.53, 27.00, 26.66, 25.86, 25.74, 21.71, 19.35, 15.42, 13.97.

IR (neat, cm^{-1}): 2929.05, 2855.92, 1737.86, 1471.61, 1453.85, 1427.23, 1388.53, 1263.15, 1106.45, 1006.53, 965.29, 886.60, 822.31, 736.56, 700.53, 687.21, 613.24, 80.42

HRMS (+APCI): calculated for $C_{40}H_{51}O_2Si$ $[M+H]^+$591.3653, found 591.3652.

R_f = 0.20 (85:15 Hexanes/Et_2O)

methyl (*S*,*E*)-2-((*tert*-butoxycarbonyl)amino)-3-(4-(6-((*tert*-butyldiphenylsilyl)oxy)hex-1-en-1-yl)phenyl)propanoate (2-S7)

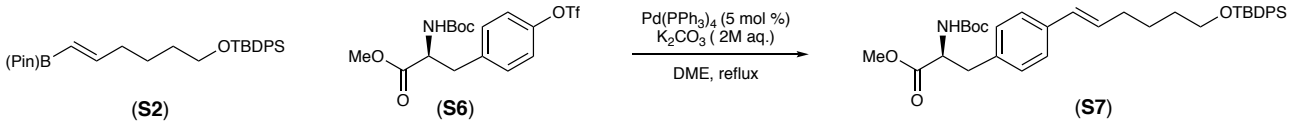

Following the general procedure C, alkene **2-S2**[39] (696 mg, 1.5 mmol, 1.5 equiv), tyrosine triflate **2-S6** (431 mg, 1 mmol, 1 equiv), $Pd(PPh_3)_4$ (57 mg, 0.05 mmol, 5 mol %), and K_2CO_3 (387 mg, 2.8 mmol, 2.8 equiv, 2M aq. solution) were utilized. The reaction was heated at reflux in 1 mL DME and overnight and was purified by flash column chromatography on silica with toluene and hexane to afford olefin **2-S7** as a pale-yellow oil (173.5 mg 28% yield).

^{1}H NMR (400 MHz, $CDCl_3$): δ ^{1}H NMR (399 MHz, Chloroform-*d*) δ 7.84 – 7.50 (m, 4H), 7.58 – 7.30 (m, 6H), 7.32 – 7.10 (m, 2H), 7.04 (d, *J* = 8.0 Hz, 2H), 6.32 (d, *J* = 15.6 Hz, 1H), 6.17 (dt, *J* = 16.0, 6.9 Hz, 1H), 4.95 (d, *J* = 8.3 Hz, 1H), 4.57 (d, *J* = 7.8 Hz, 1H), 3.90 – 3.34 (m, 5H), 3.06 (dd, *J* = 10.0, 5.9 Hz, 2H), 2.36 (s, 2H), 2.25 – 2.02 (m, 2H), 1.56 (m, 4H), 1.42 (s, 9H), 1.05 (s, 9H).

^{13}C NMR (150 MHz, $CDCl_3$): δ 172.51, 155.25, 138.02, 136.85, 135.73, 135.72, 134.59, 134.24, 131.04, 129.66, 129.60, 129.56, 129.18, 128.37, 127.74, 126.24, 125.45, 80.07, 77.37, 76.95, 63.90, 54.54, 52.35, 38.12, 32.86, 32.21, 28.45, 27.03, 27.01, 25.73, 21.60, 19.38.

IR (neat, cm^{-1}): 2930.62, 2856.73, 1746.75, 1700.11, 1588.94, 1495.04, 1472.55, 1427.48, 1389.49, 1364.55, 1252.15, 1164.54, 1109.60, 1027.93, 967.19, 935.12, 860.71, 822.72, 741.69, 701.33, 613.18, 561.01

HRMS (+NSI): calculated for $C_{37}H_{49}O_5NaSi$ $[M+Na]^+$ 638.3272, found 638.3274.

$\mathbf{R_f}$ = 0.11 (85:15 Hexanes/Et_2O)

***tert*-butyl(((*E*)-6-((*S*)-2,8-dimethyl-2-((4*S*,8*S*)-4,8,12-trimethyltridecyl)chroman-6-yl)hex-5-en-1-yl)oxy)diphenylsilane (2-S9)**

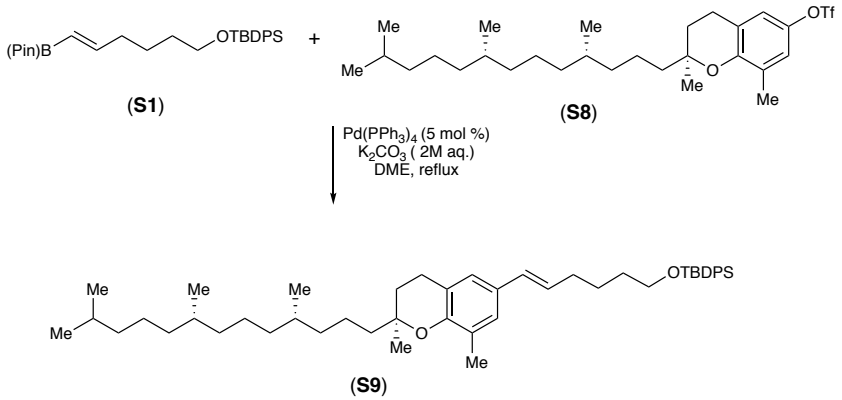

Following the general procedure C, alkene **2-S1**[39] (464mg, 1 mmol, 1.5 equiv), Tocopherol-OTf **2-S8**[41] (**S5,** 450 mg, 0.66 mmol, 1 equiv), $Pd(PPh_3)_4$ (40 mg, 0.03 mmol, 5 mol %), and K_2CO_3 (248.7 mg, 1.8 mmol, 2.8 equiv) were utilized. The reaction was heated at reflux in 1 mL DME and overnight and was purified by flash column chromatography on silica with toluene and hexane affording olefin **2-S9** as a pale-yellow oil (525 mg, 90%).

^{1}H NMR (400 MHz, $CDCl_3$): δ 7.74 – 7.61 (m, 4H), 7.49 – 7.31 (m, 6H), 7.02 – 6.80 (m, 2H), 6.23 (d, *J* = 15.7 Hz, 1H), 6.00 (dt, *J* = 15.6, 6.9 Hz, 1H), 3.67 (t, *J* = 6.2 Hz, 2H), 2.72 (t, *J* = 7.0 Hz, 2H), 2.16 (d, *J* = 11.2 Hz, 6H), 1.77 (dh, *J* = 20.0, 6.6 Hz, 2H), 1.70 – 1.40 (m, 34H), 0.98 – 0.69 (m, 14H).

^{13}C NMR (150 MHz, $CDCl_3$): δ 151.84, 141.60, 128.52, 121.85, 120.88, 119.20, 76.95, 40.29, 39.52, 37.59, 37.54, 37.52, 37.43, 32.95, 32.82, 30.80, 28.13, 24.95, 24.59, 24.30, 22.86, 22.77, 22.59, 21.07, 19.89, 19.79, 16.33,

IR (neat, cm^{-1}): 2928.23, 2857.27, 1699.95, 1652.98, 1590.11, 1558.90, 1540.03, 1506.43, 1472.60, 1427.80, 1378.20, 1363.08, 1223.34, 1149.88, 111.05, 998.25, 962.17, 878.18, 823.17, 739.71, 701.23, 613.90

HRMS (+NSI): calculated for $C_{49}H_{74}O_2NaSi$ $[M+Na]^+$ 745.5350, found 745.5350.

$\mathbf{R_f}$ = 0.77 (85:15 Hexanes/Et_2O)

VII. Characterization Data

Compound (**2-26**) ^{1}H NMR (300 MHz, $CDCl_3$)

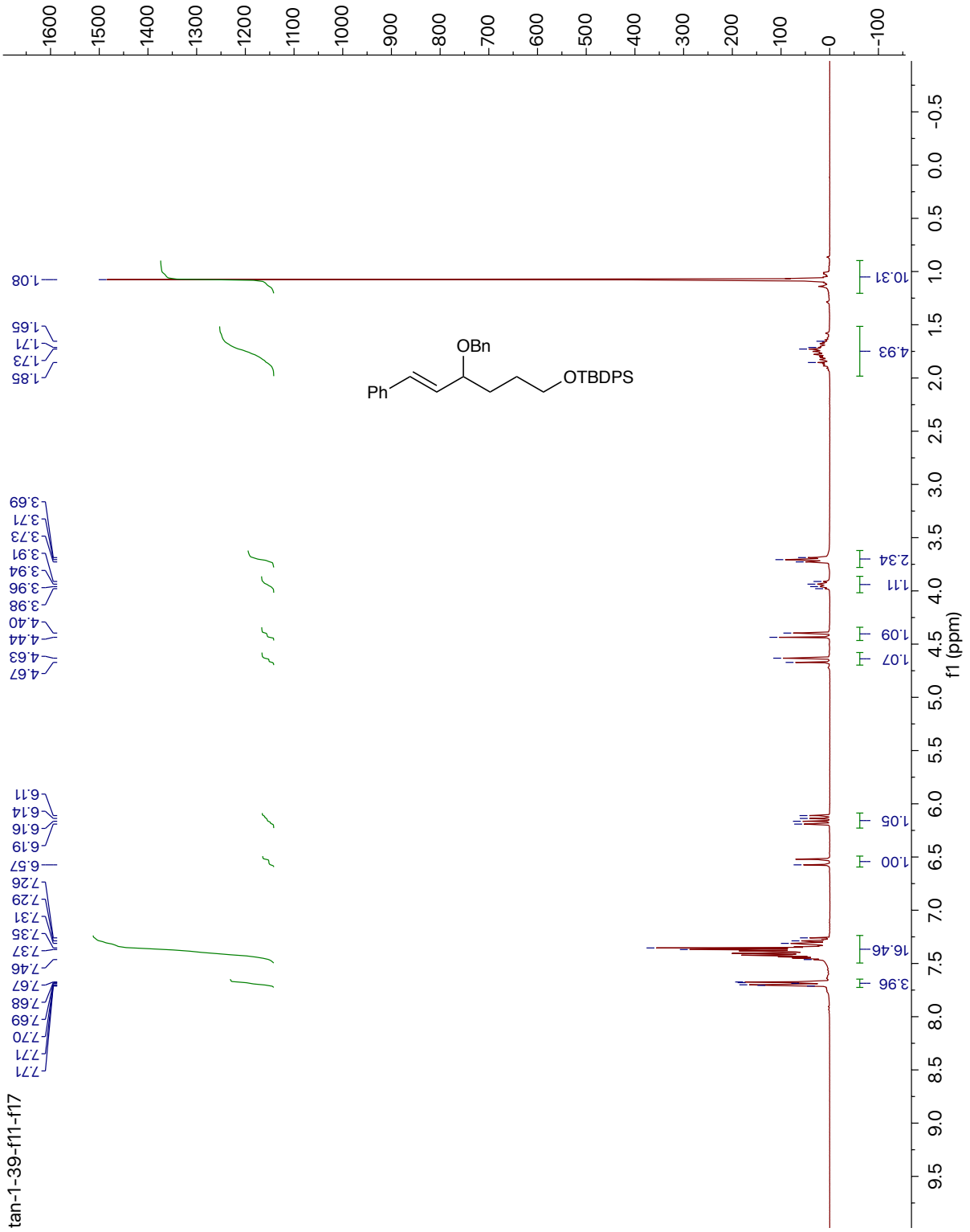

^{13}C NMR (125 MHz, $CDCl_3$)

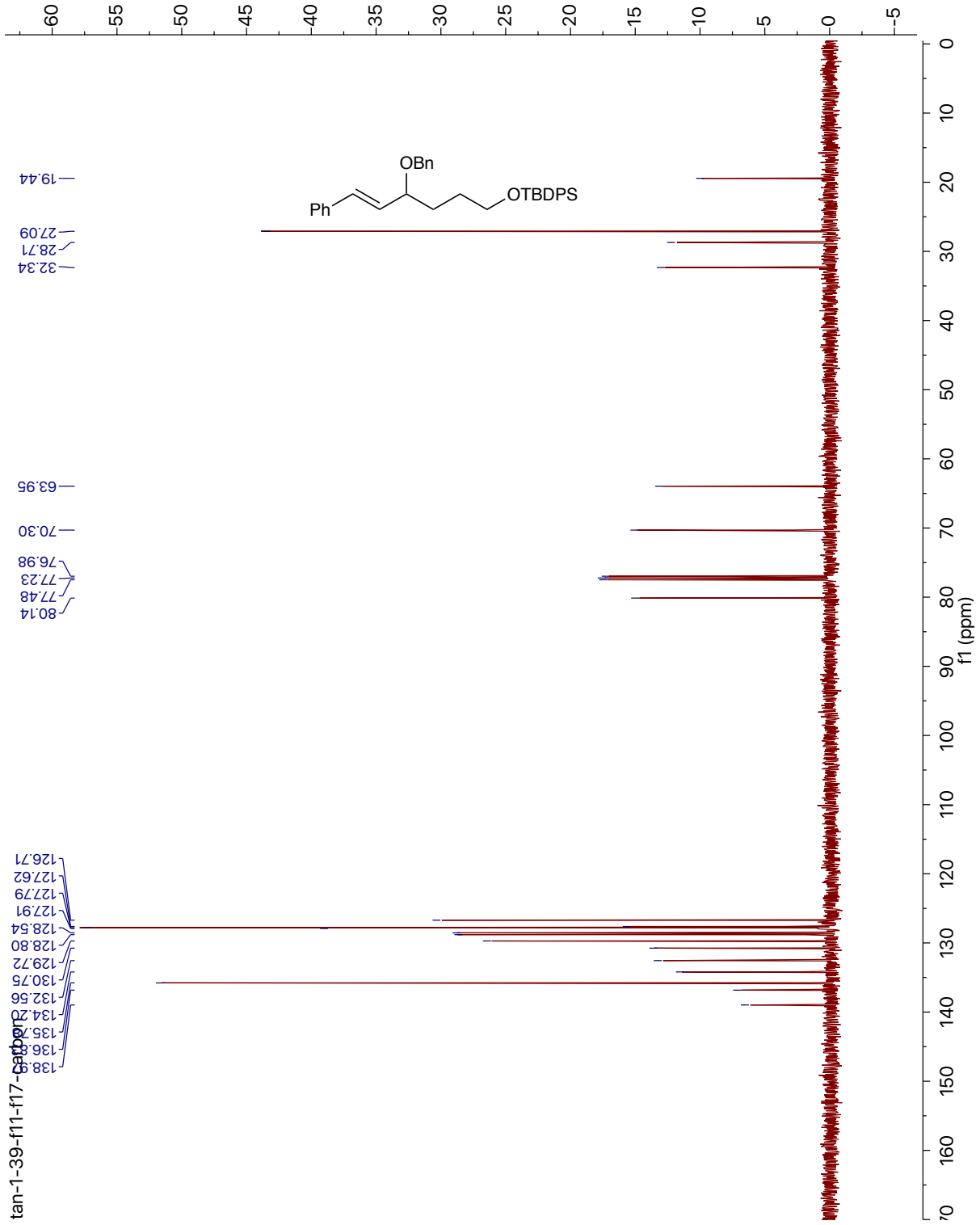

Compound (**2-27**)

^{1}H NMR (400 MHz, $CDCl_3$)

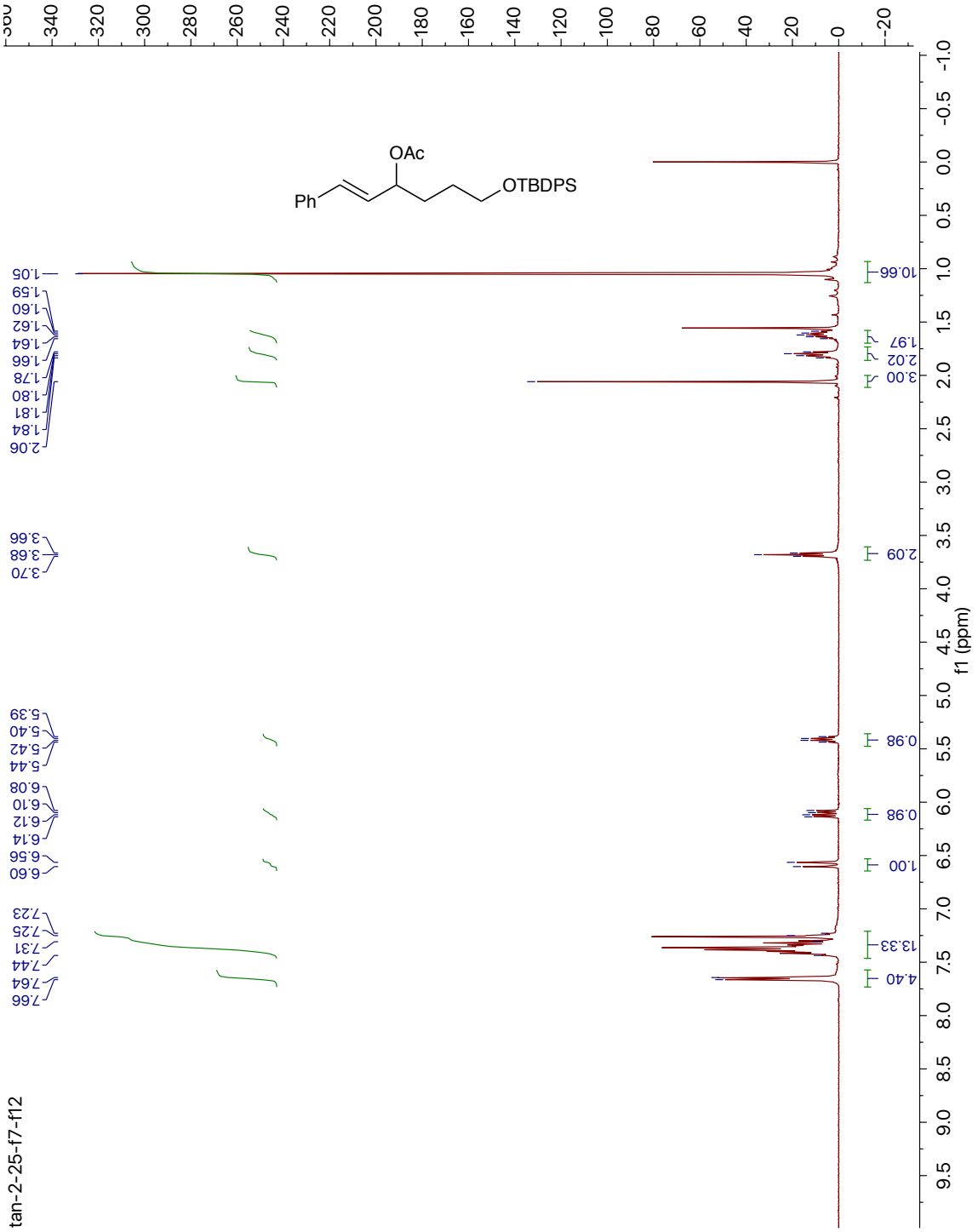

^{13}C NMR (150 MHz, $CDCl_3$)

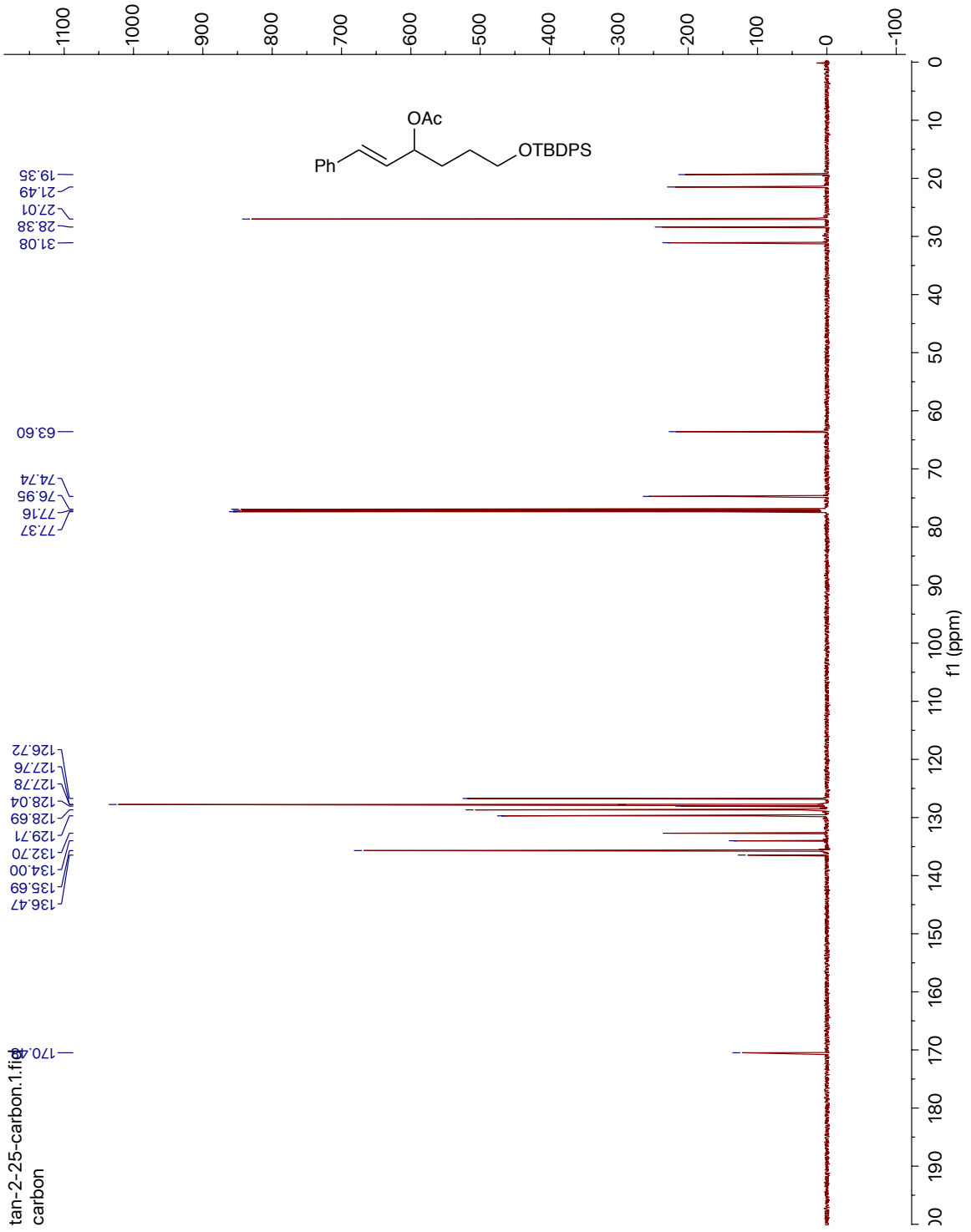

Compound (**2-29**)

^{1}H NMR (400 MHz, $CDCl_3$)

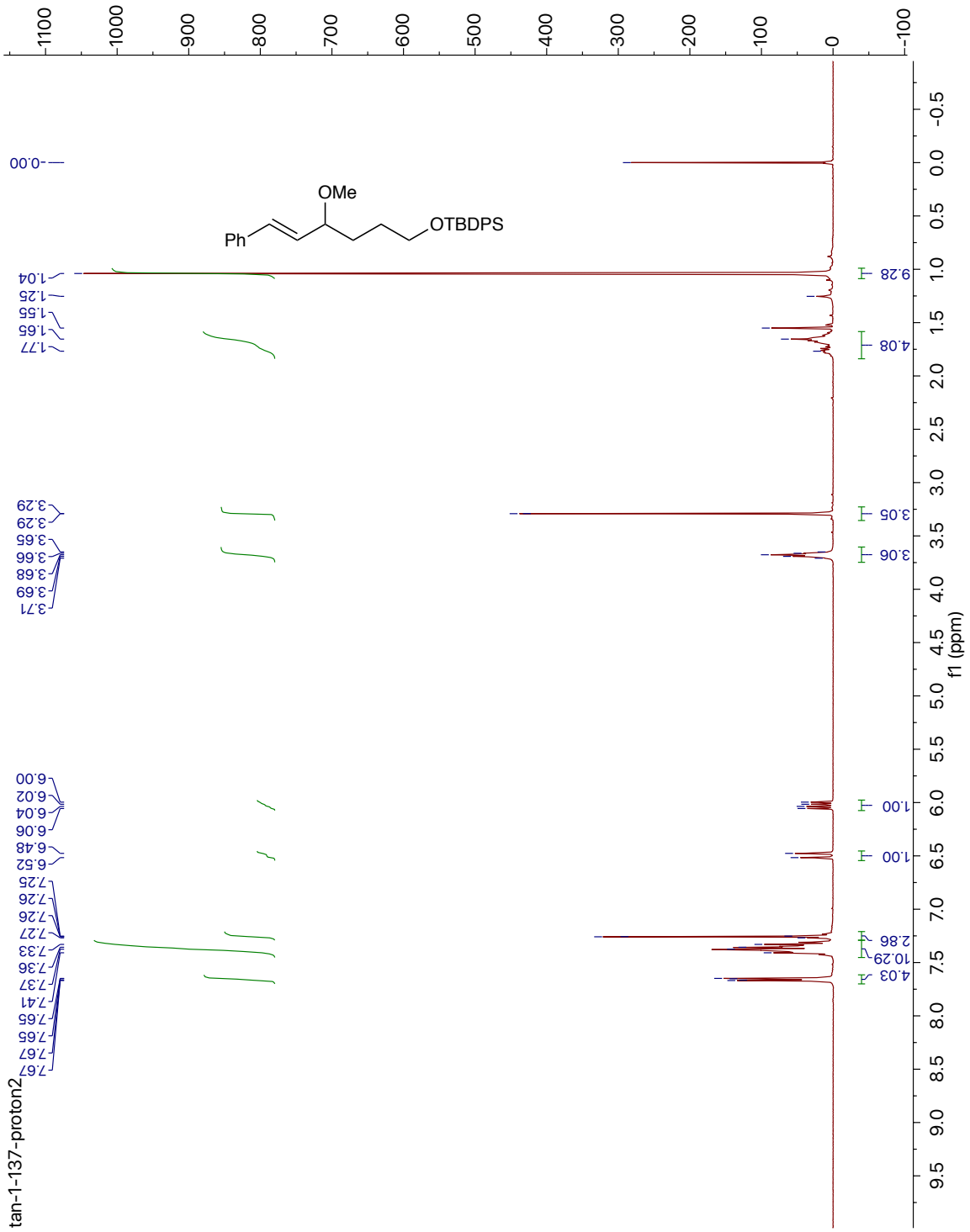

^{13}C NMR (150 MHz, $CDCl_3$)

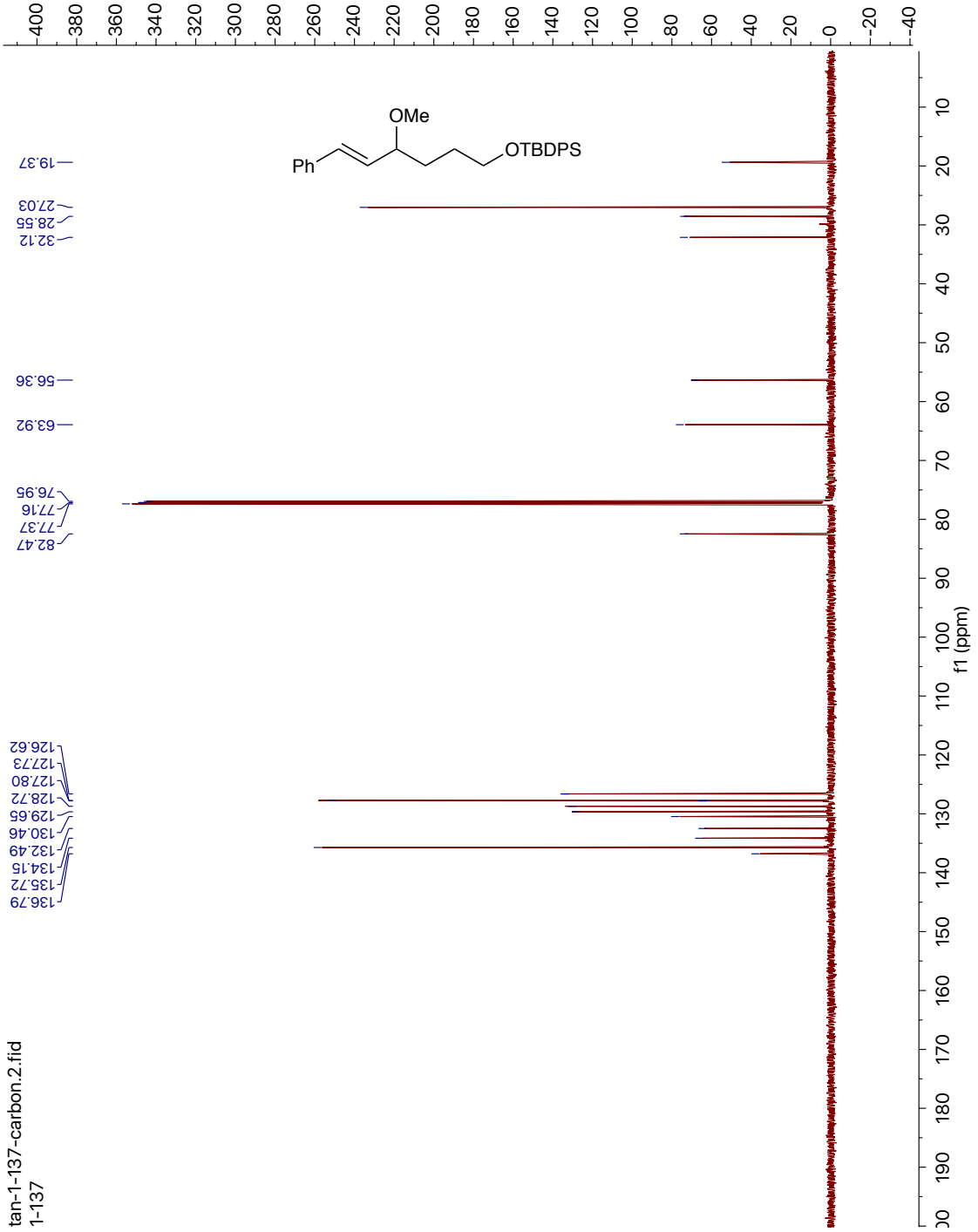

Compound (**2-30**)

^{1}H NMR (400 MHz, $CDCl_3$)

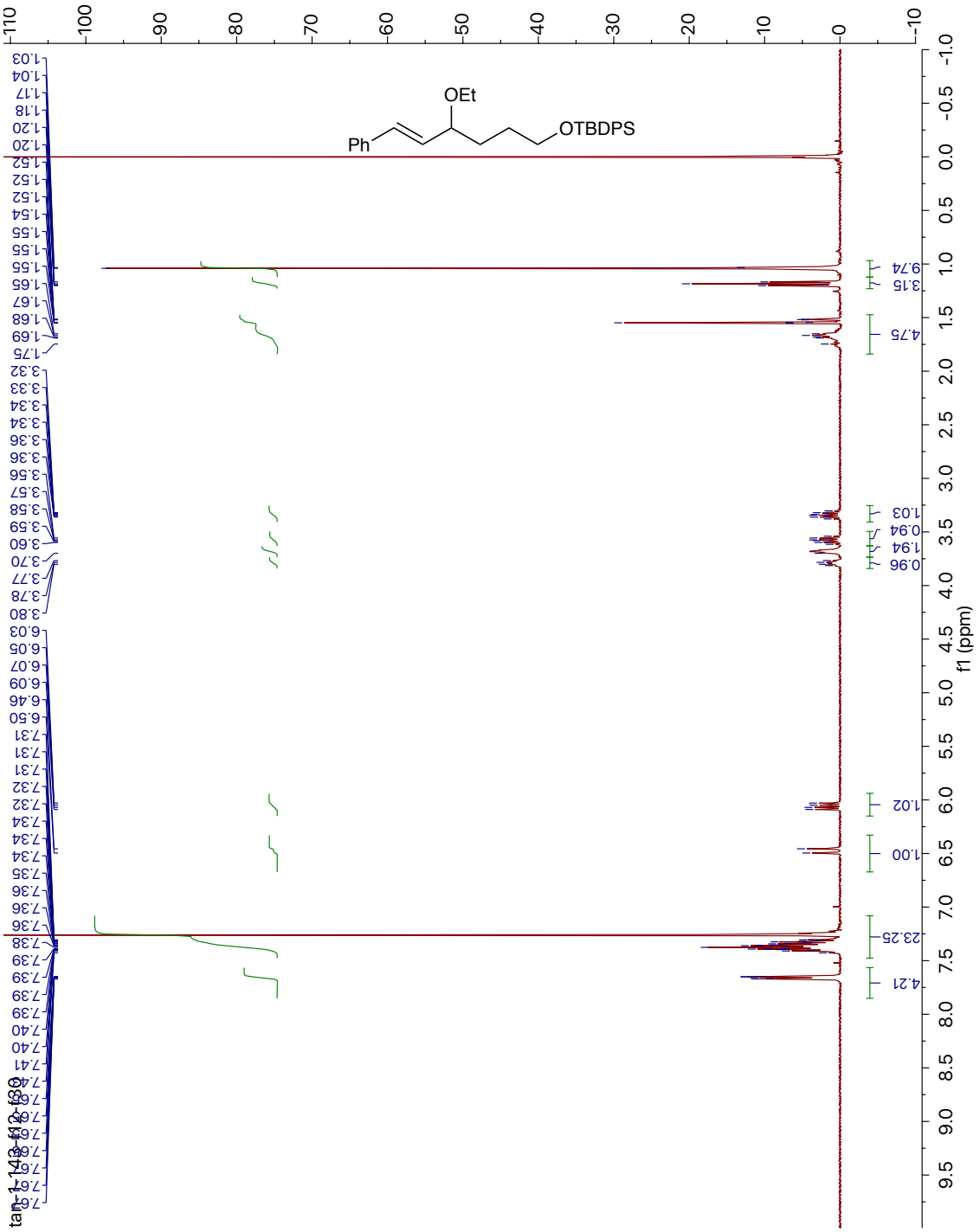

^{13}C NMR (150 MHz, $CDCl_3$)

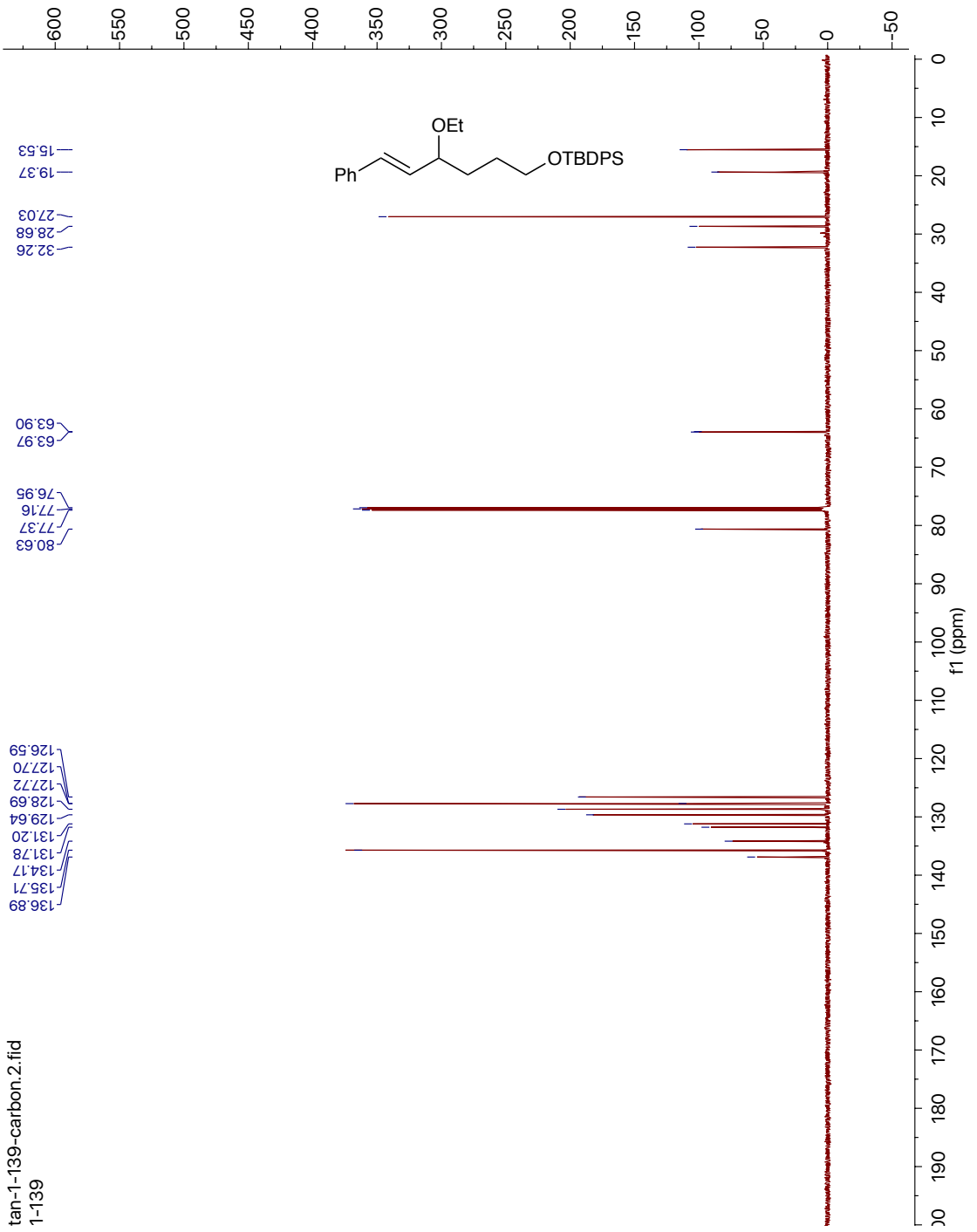

Compound (**2-31**)

^{1}H NMR (400 MHz, $CDCl_3$)

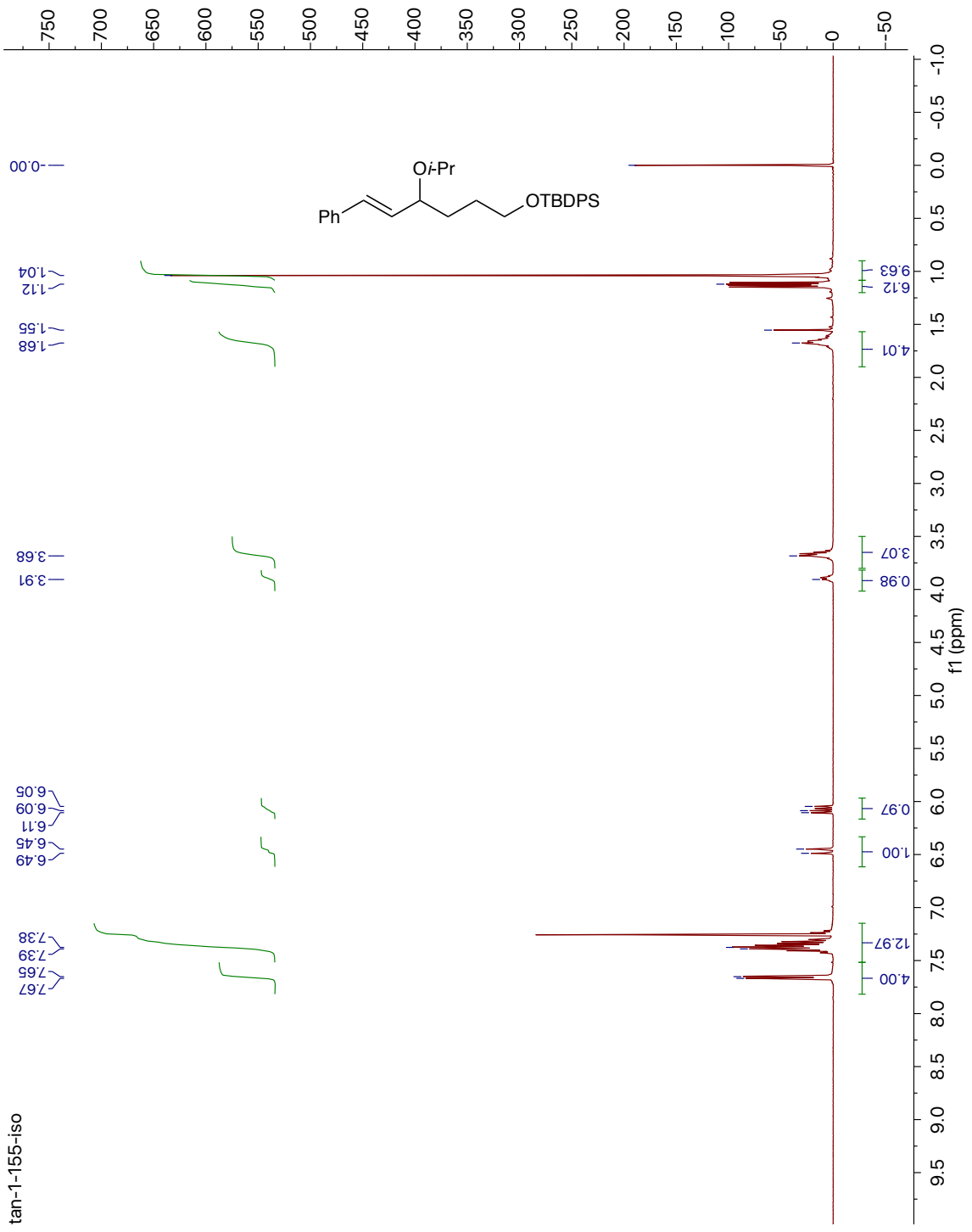

^{13}C NMR (150 MHz, $CDCl_3$)

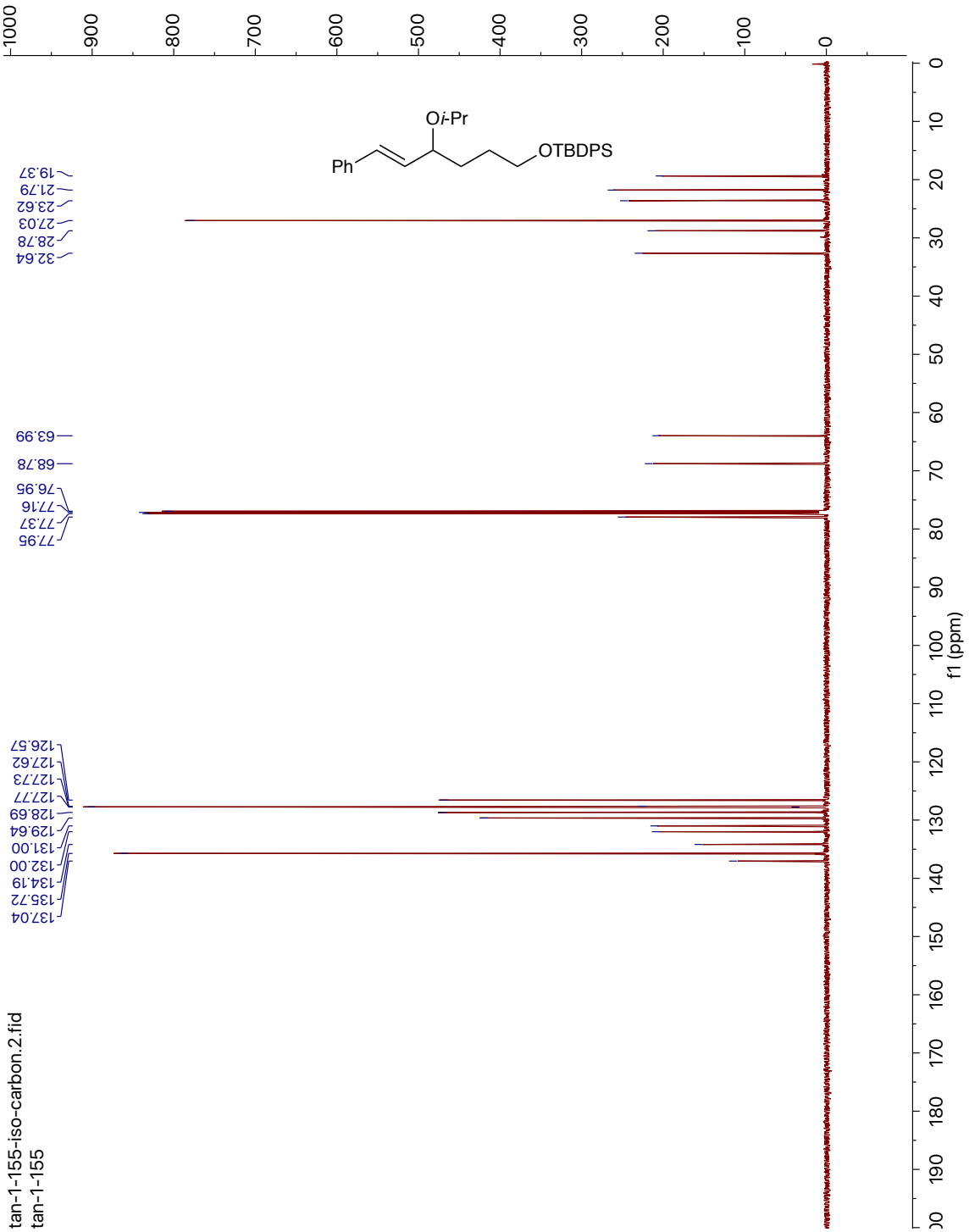

Compound (**2-33**) ^{1}H NMR (400 MHz, $CDCl_3$)

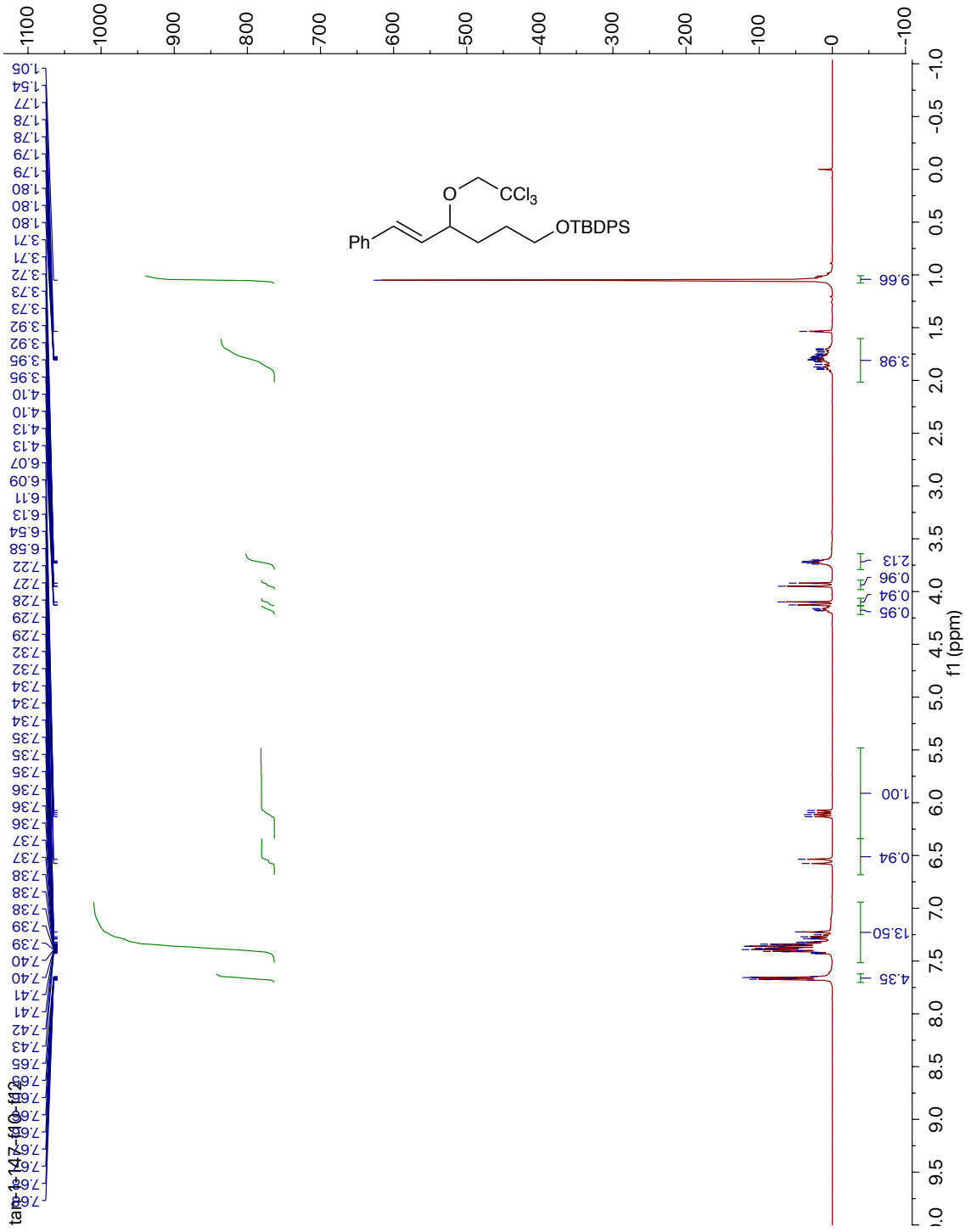

^{13}C NMR (150 MHz, $CDCl_3$)

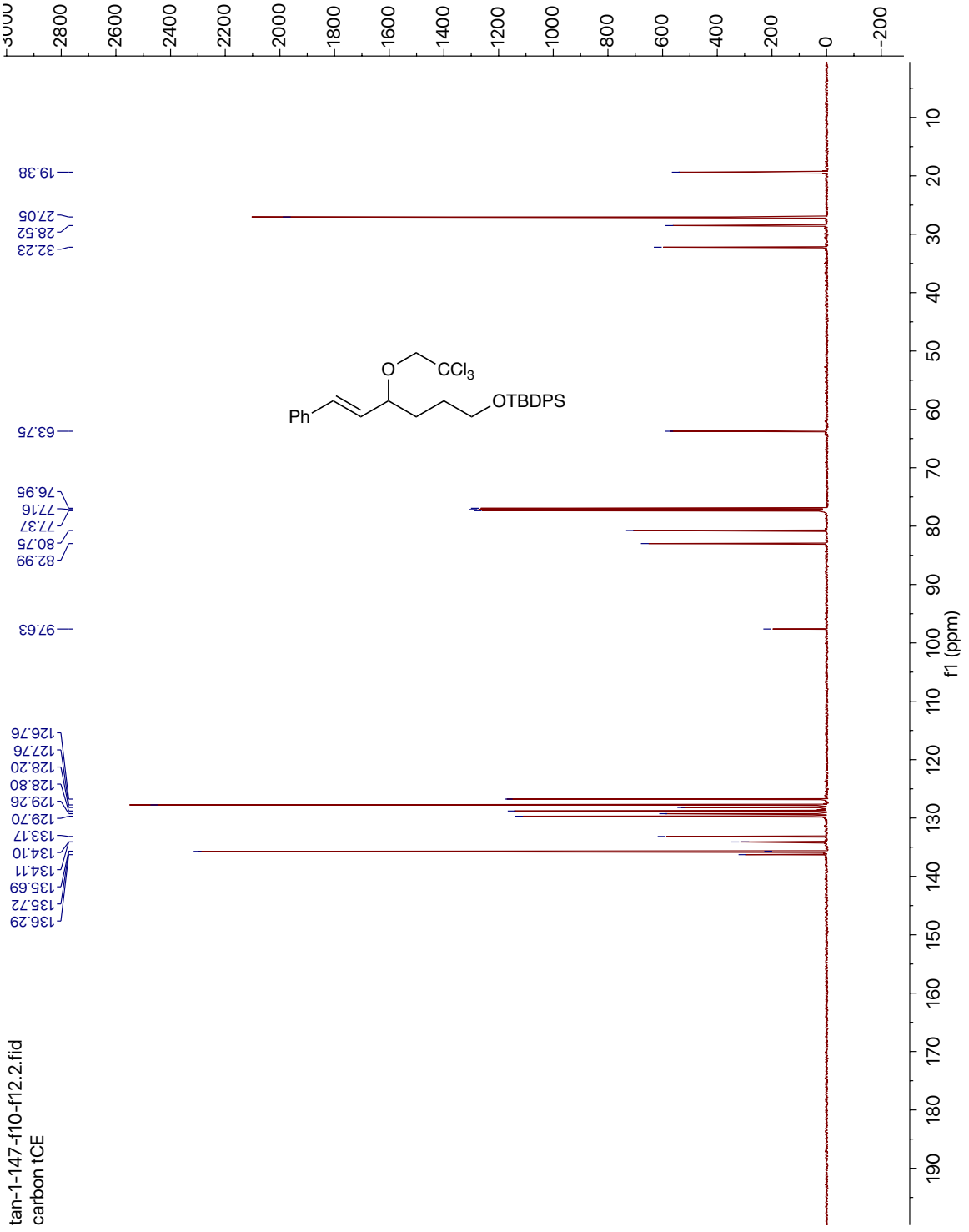

Compound (**2-34**)

^{1}H NMR (300 MHz, $CDCl_3$)

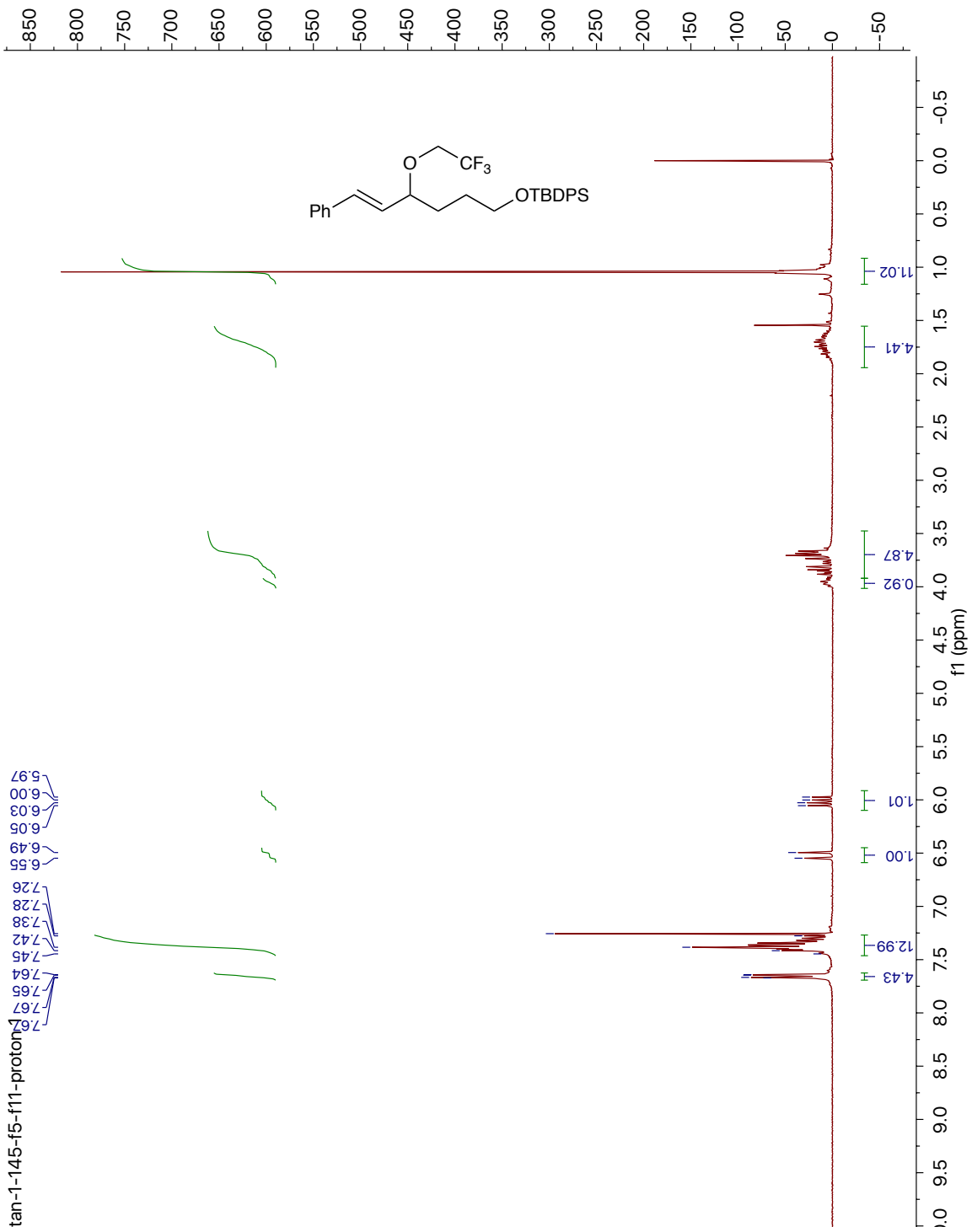

^{13}C NMR (150 MHz, $CDCl_3$)

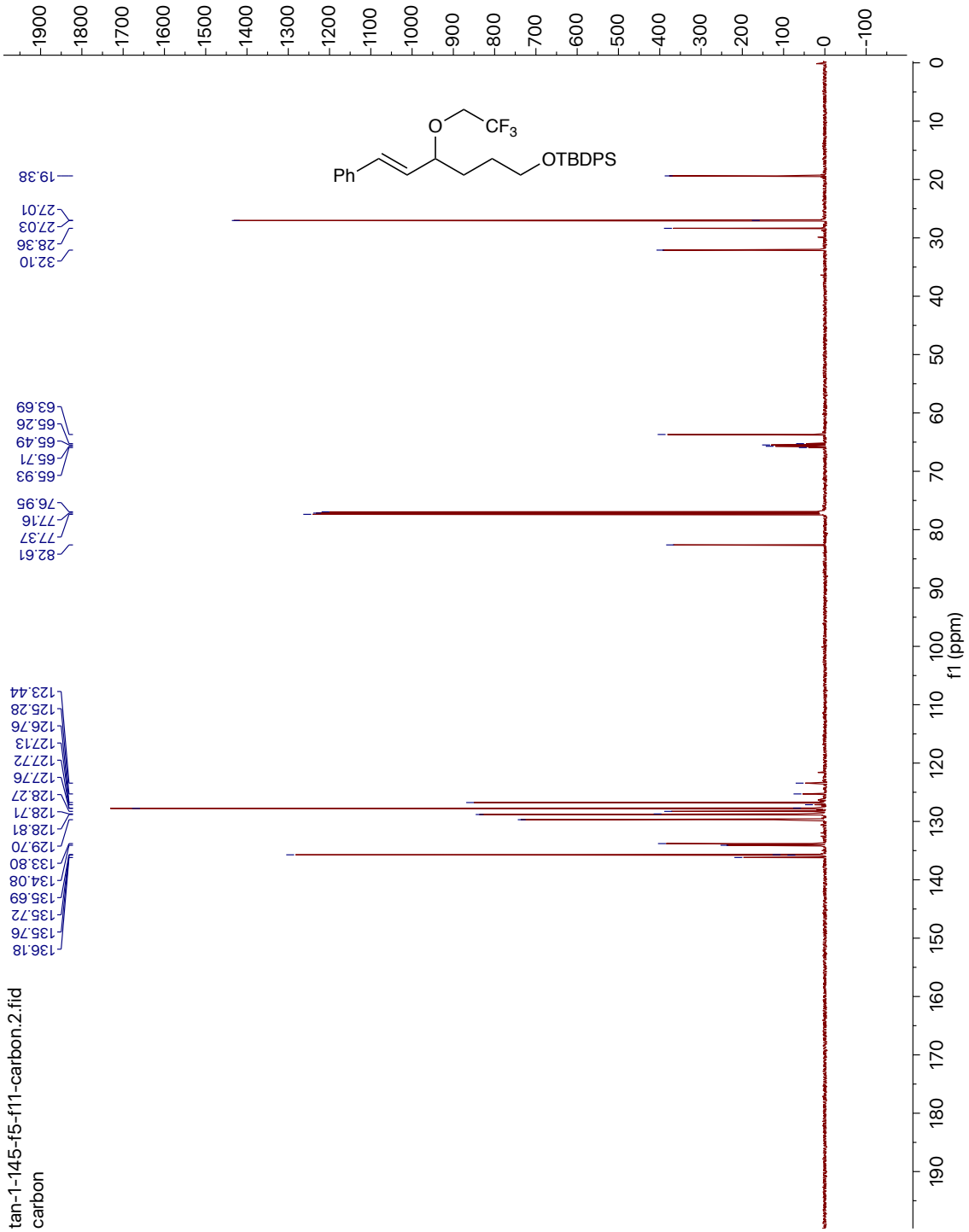

Compound (**2-36**)

^{1}H NMR (400 MHz, $CDCl_3$)

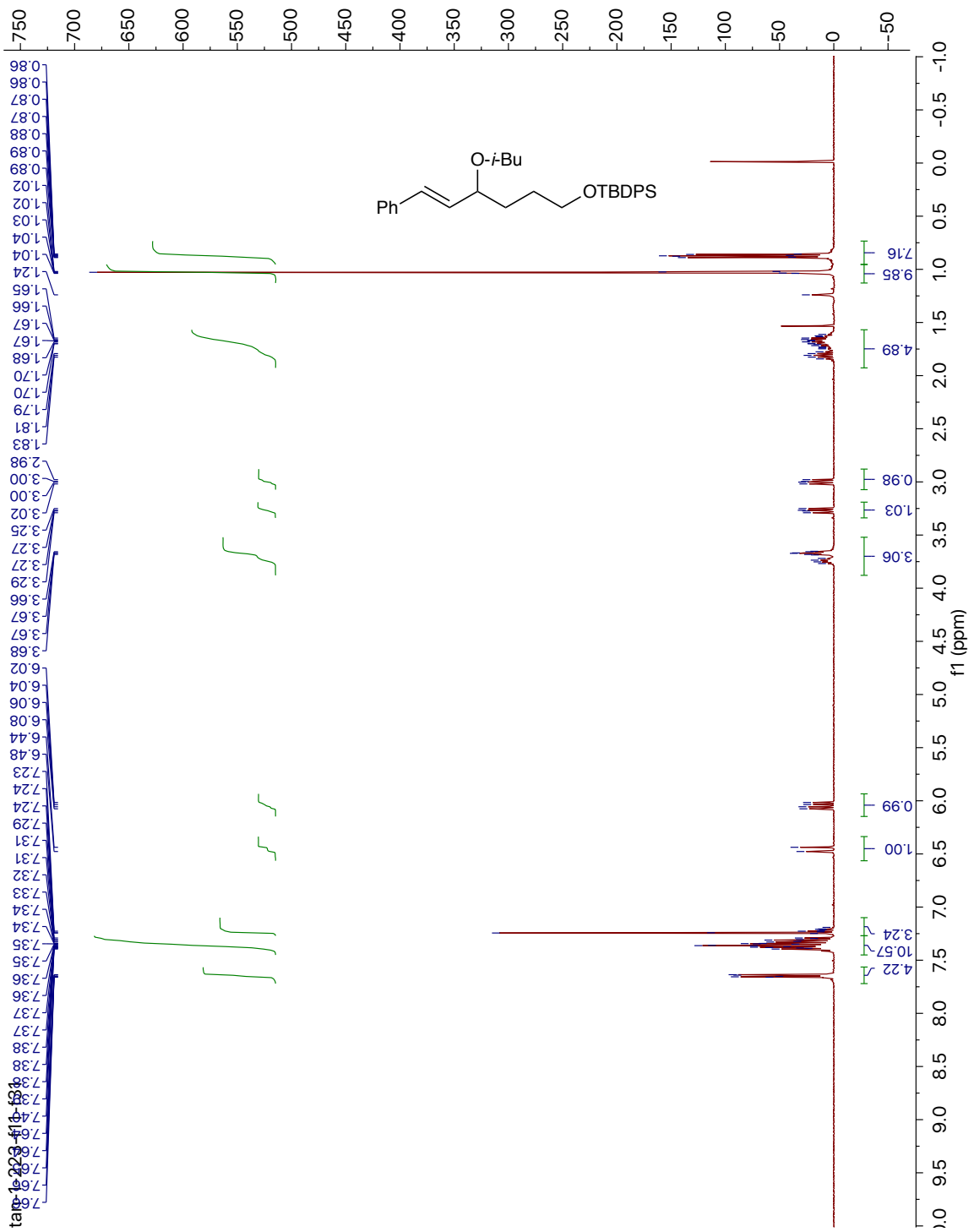

^{13}C NMR (100 MHz, $CDCl_3$)

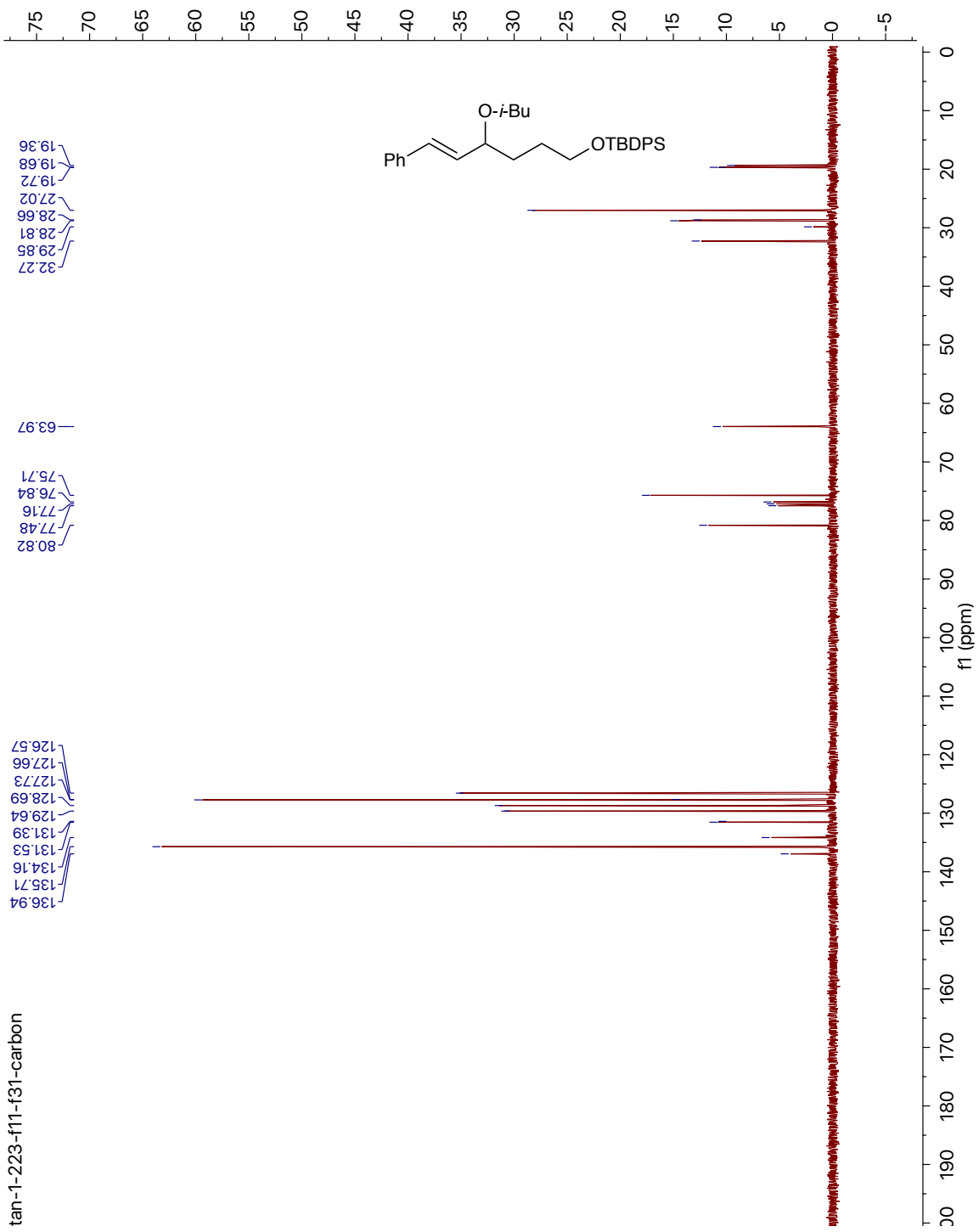

Compound (**2-37**)

^{1}H NMR (300 MHz, $CDCl_3$)

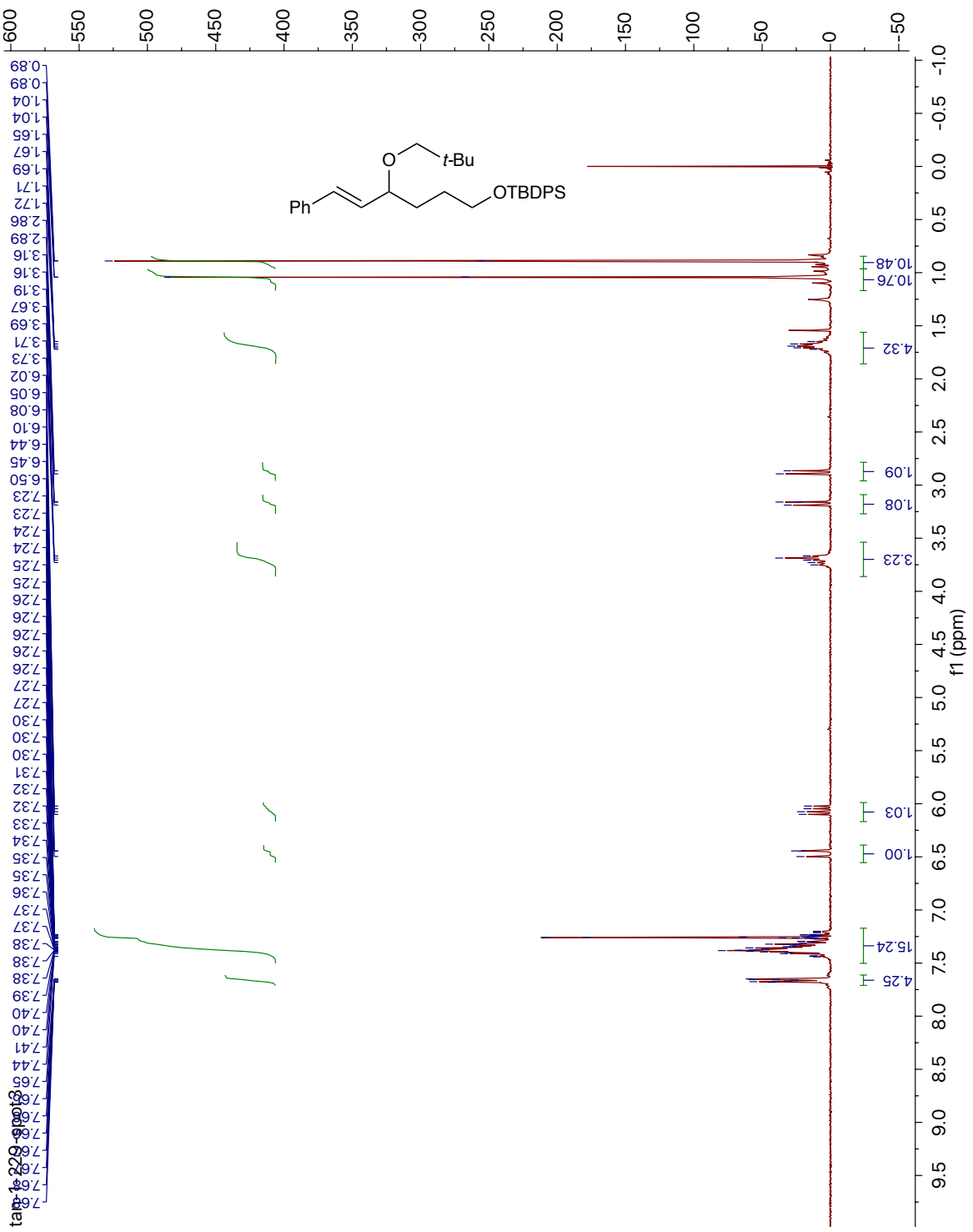

^{13}C NMR (150 MHz, $CDCl_3$)

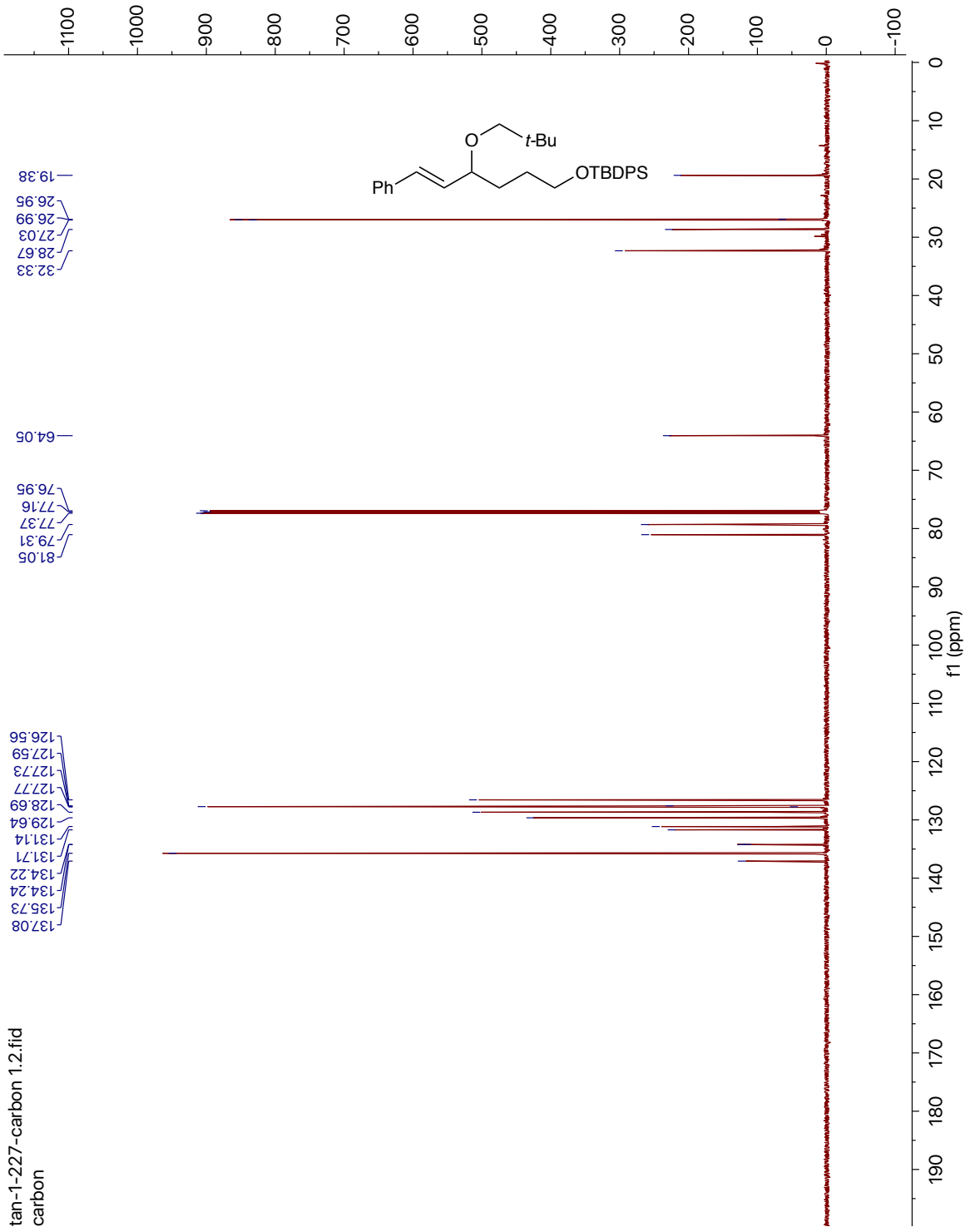

Compound (**2-39**)

^{1}H NMR (400 MHz, $CDCl_3$)

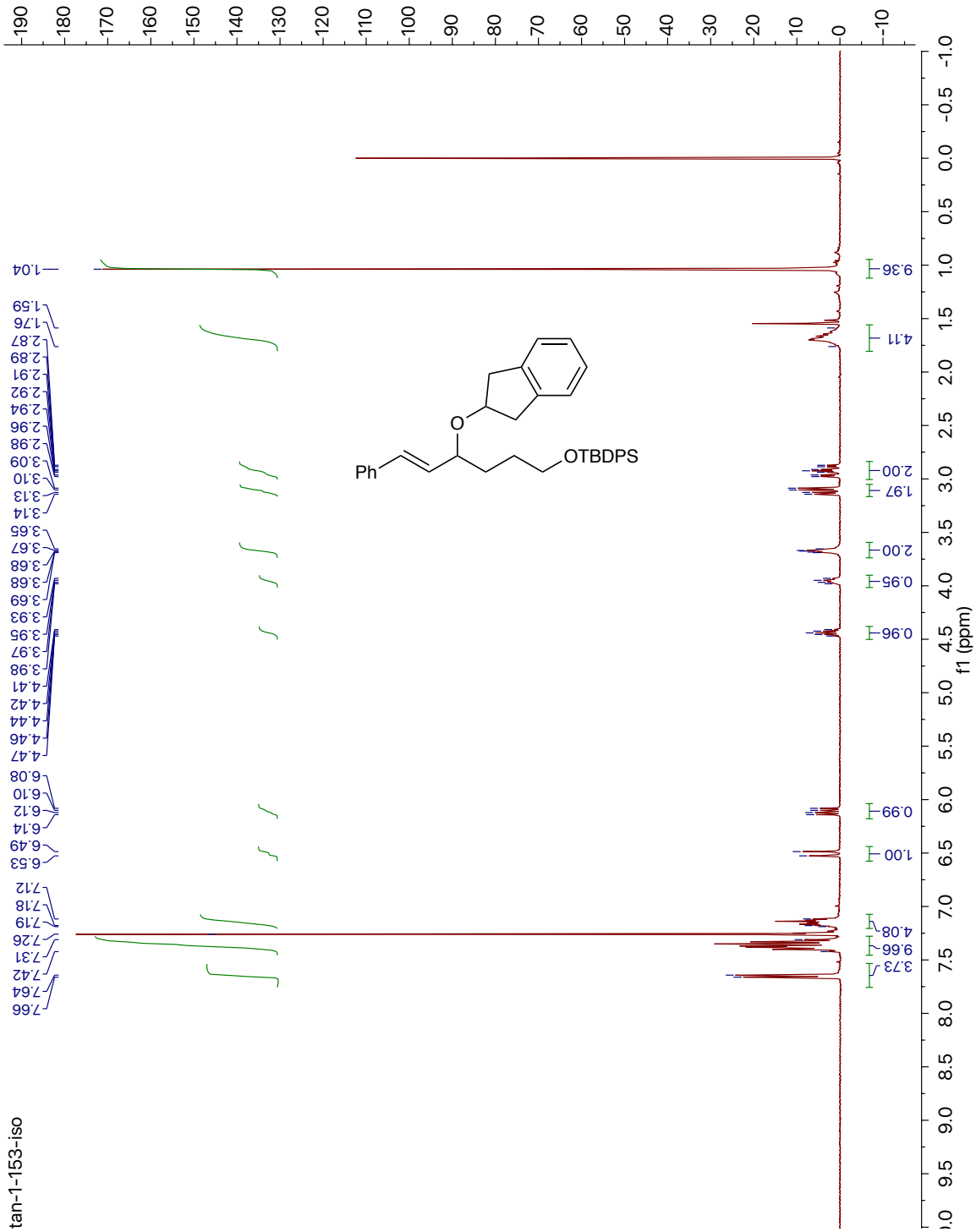

^{13}C NMR (150 MHz, $CDCl_3$)

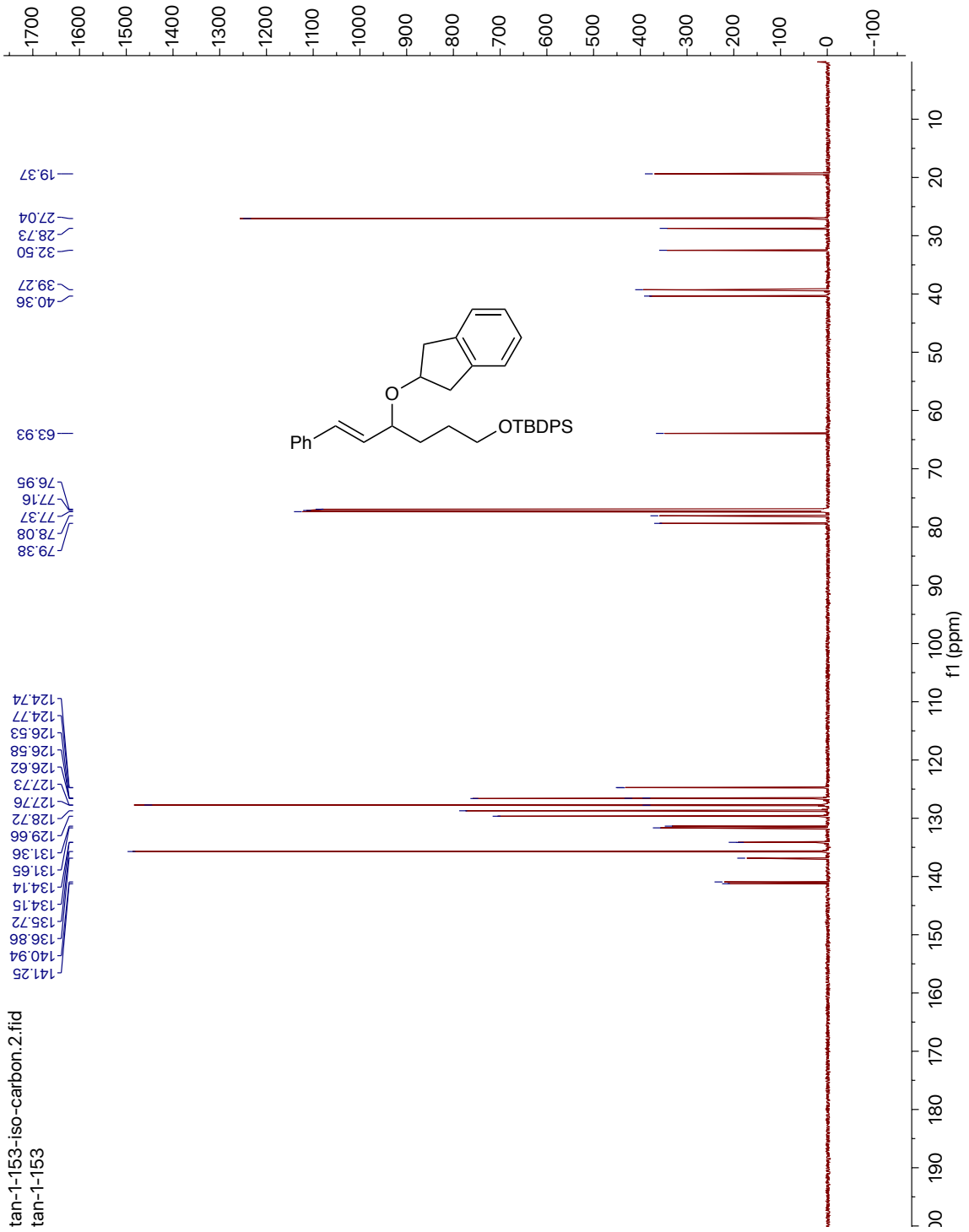

Compound (**2-41**)

^{1}H NMR (300 MHz, $CDCl_3$)

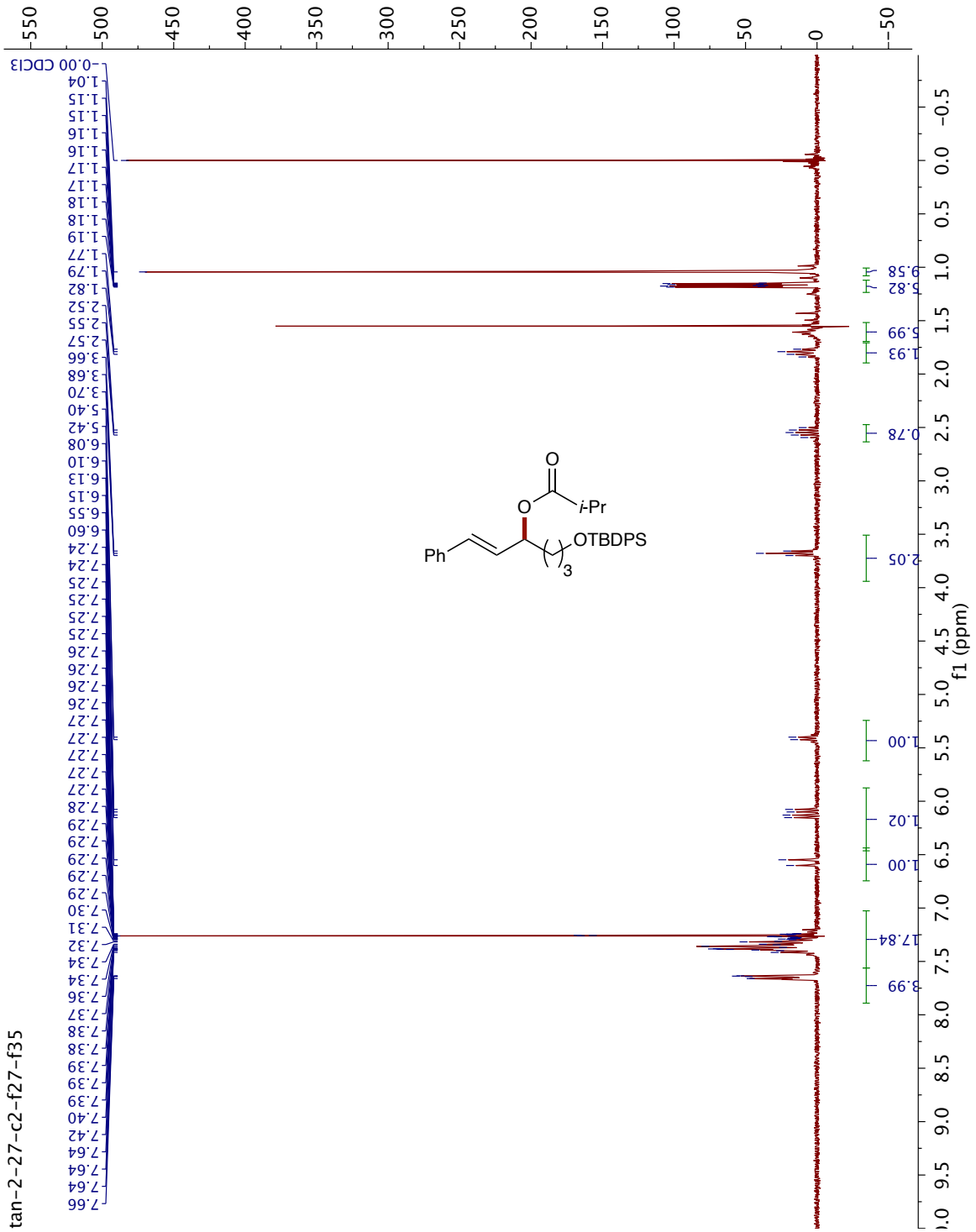

^{13}C NMR (150 MHz, $CDCl_3$)

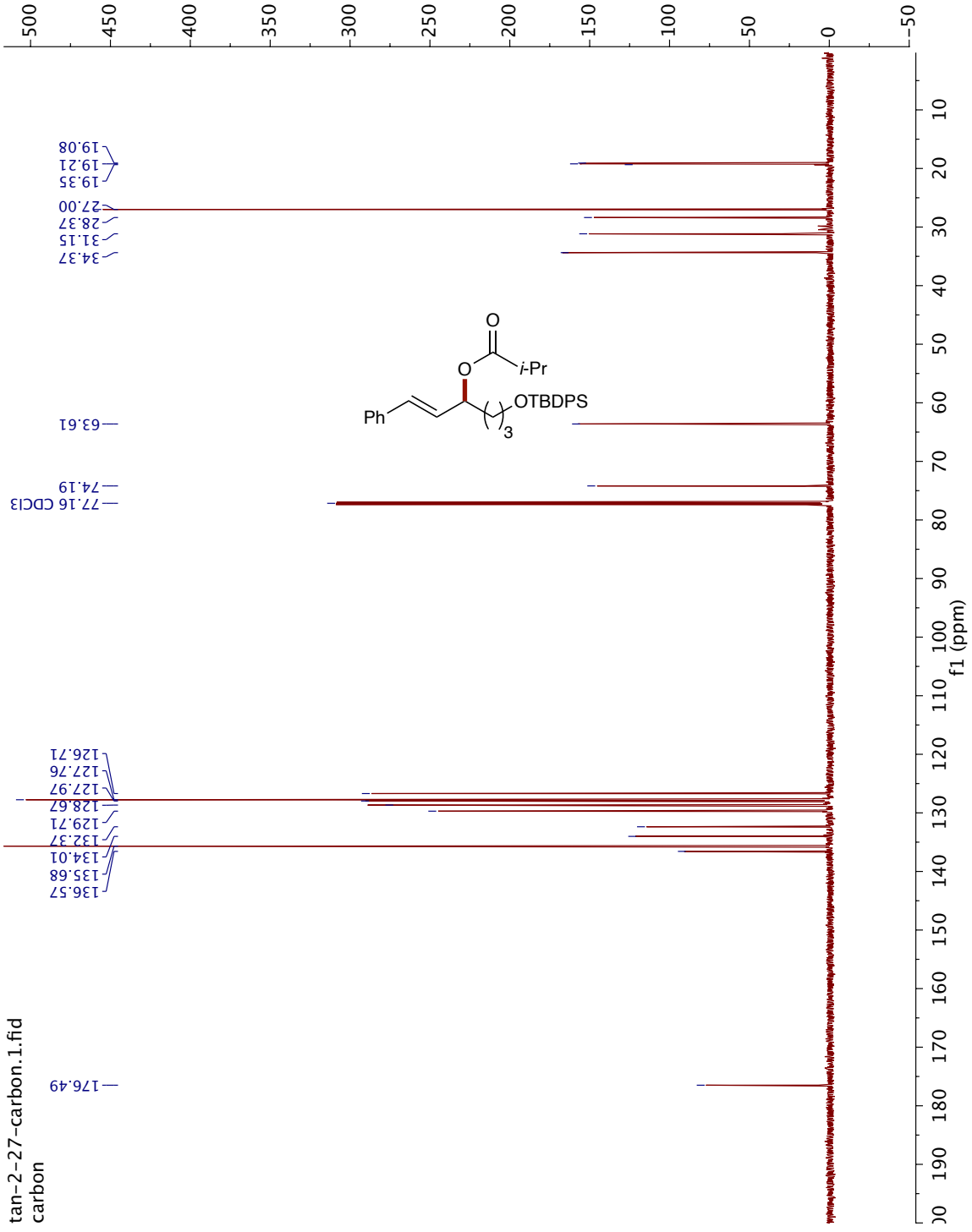

Compound (**2-42**)

^{1}H NMR (400 MHz, $CDCl_3$)

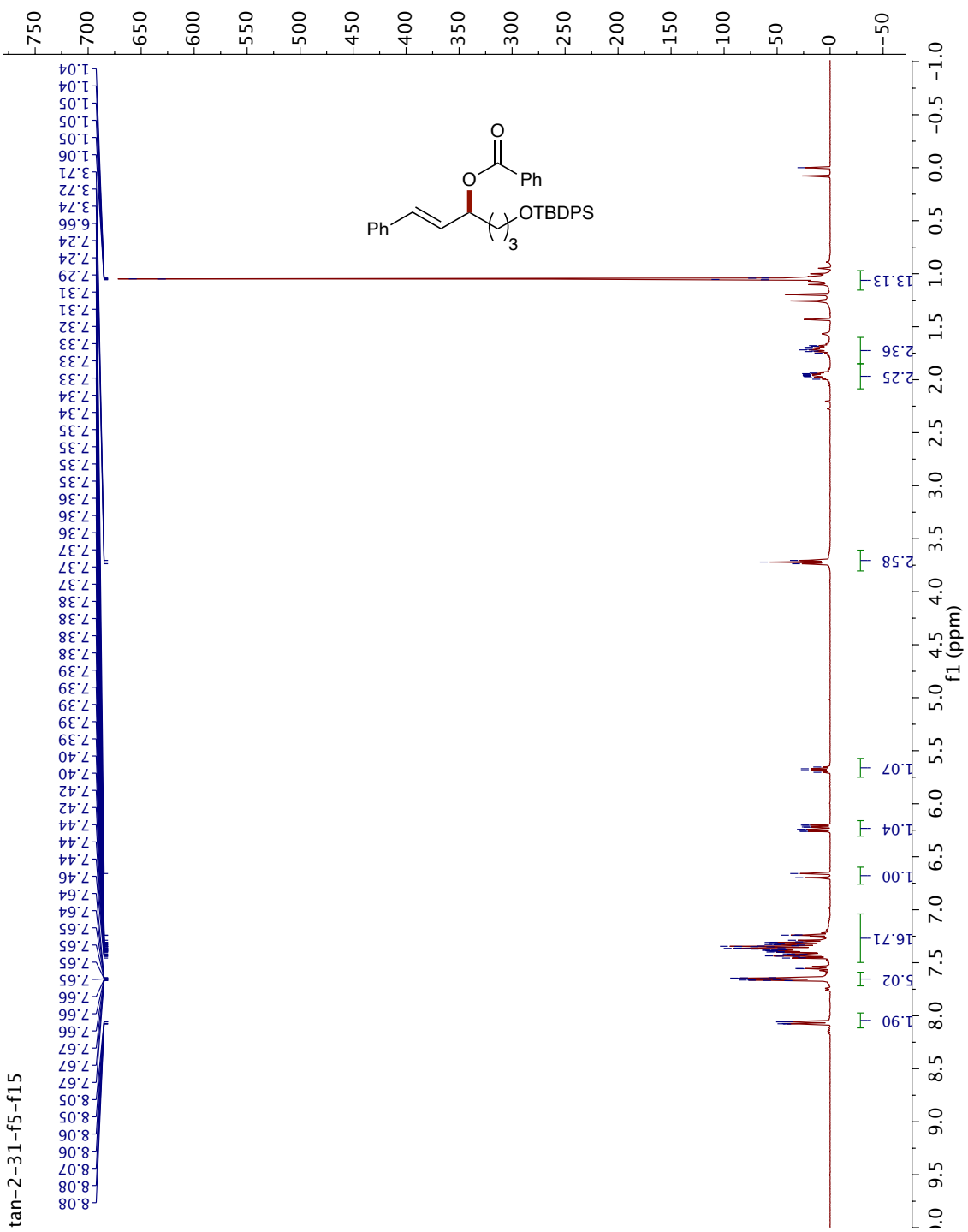

^{13}C NMR (150 MHz, $CDCl_3$)

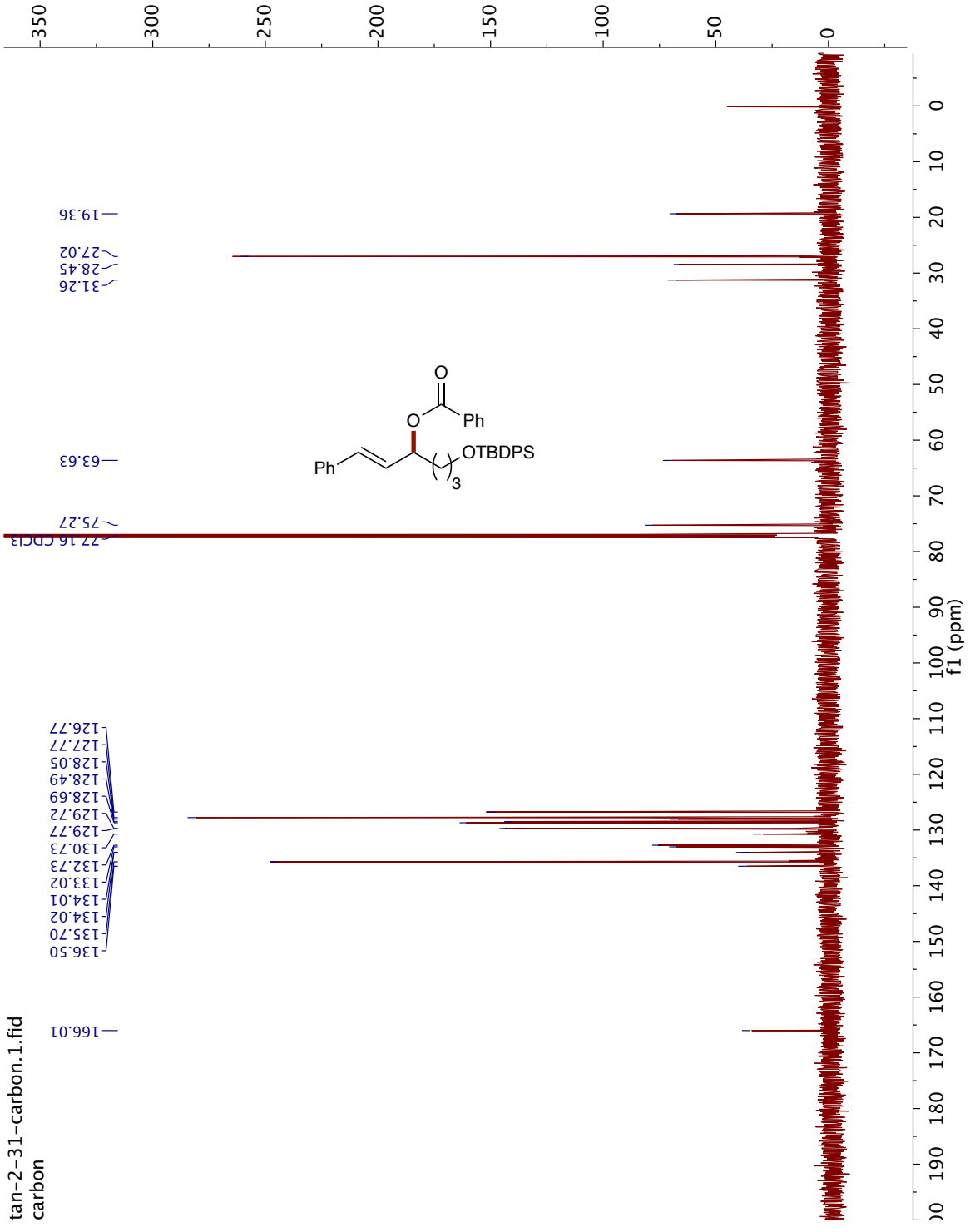

Compound (**2-43**)

^{1}H NMR (400 MHz, $CDCl_3$)

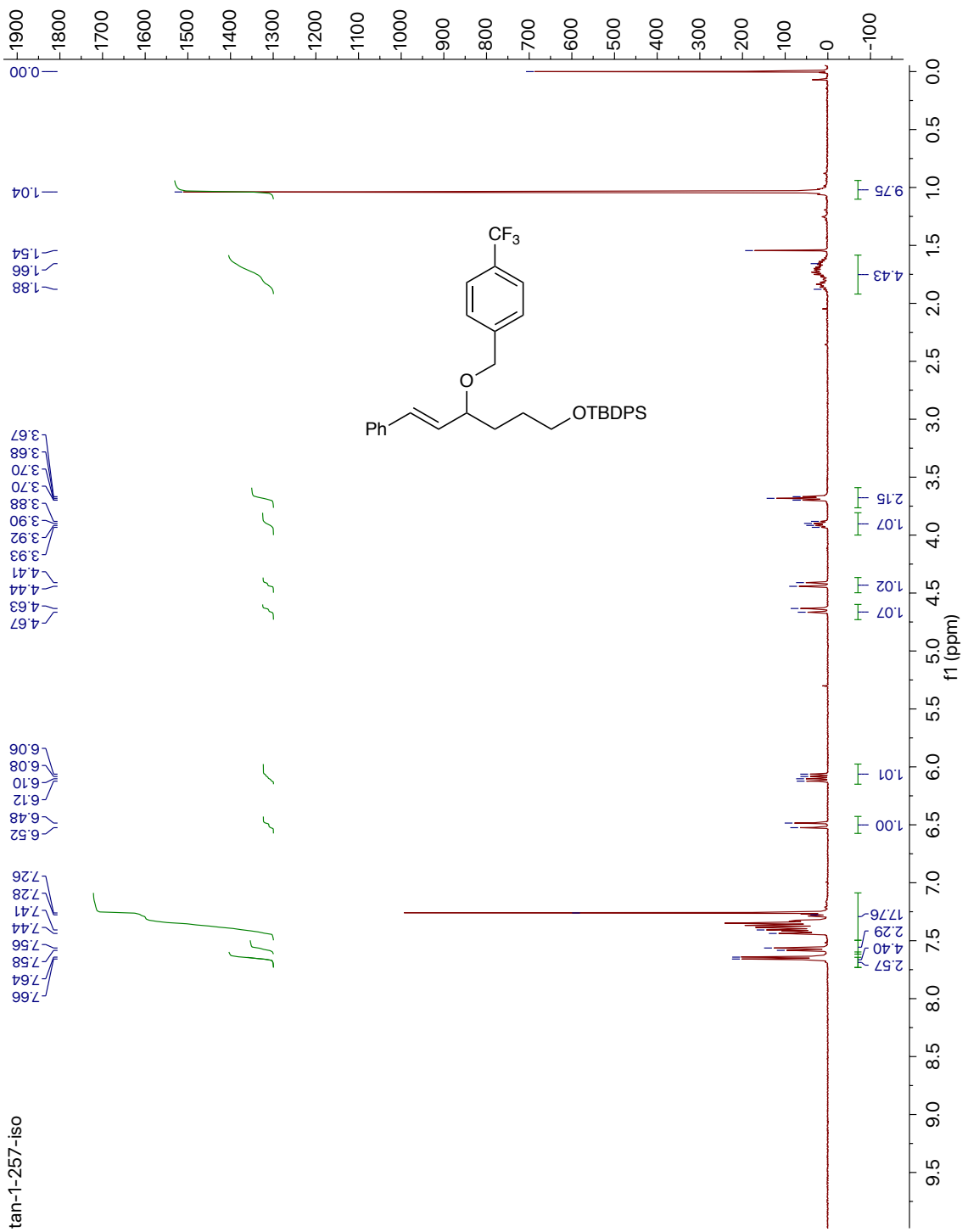

^{13}C NMR (150 MHz, $CDCl_3$)

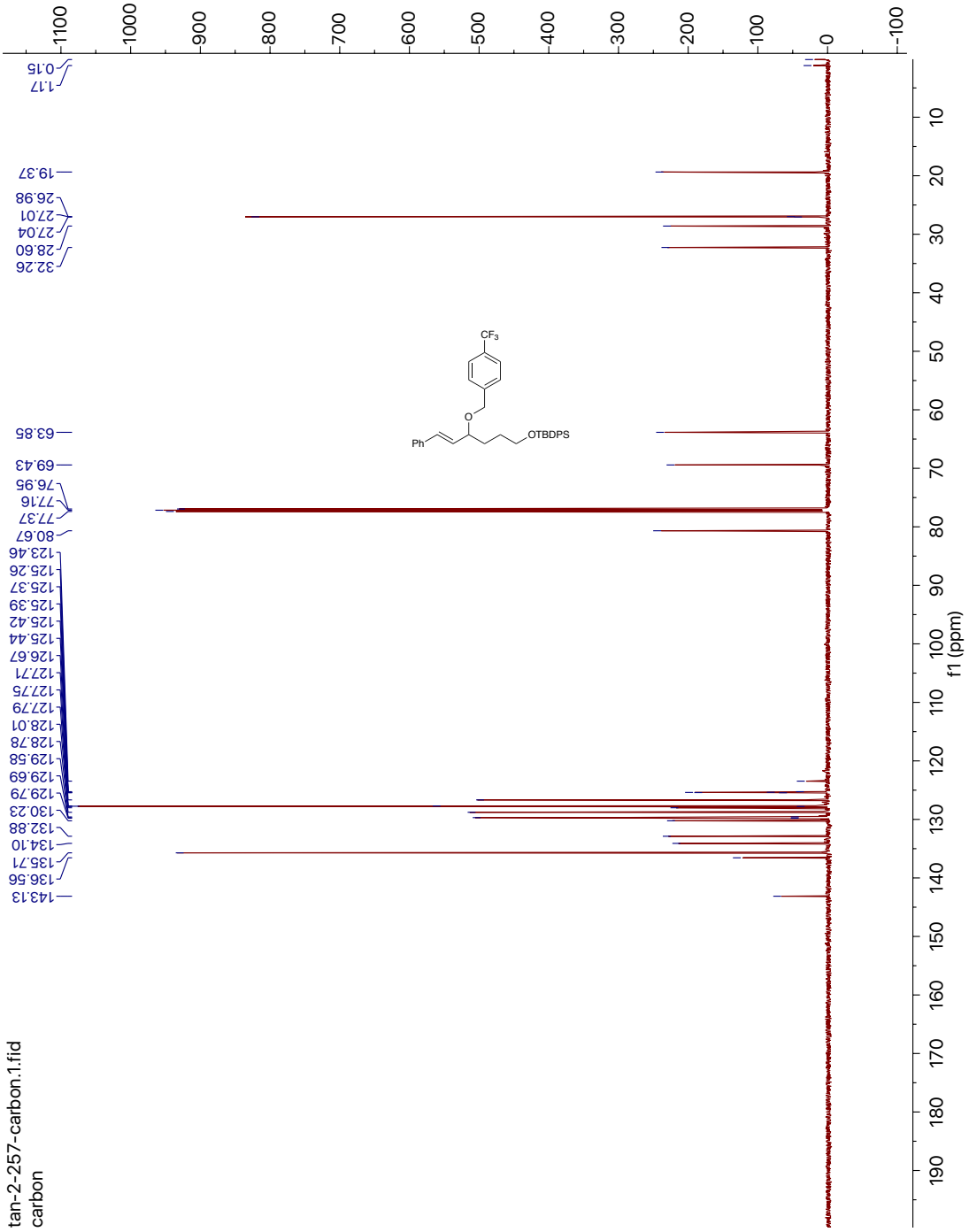

Compound (**2-44**)

^{1}H NMR (400 MHz, $CDCl_3$)

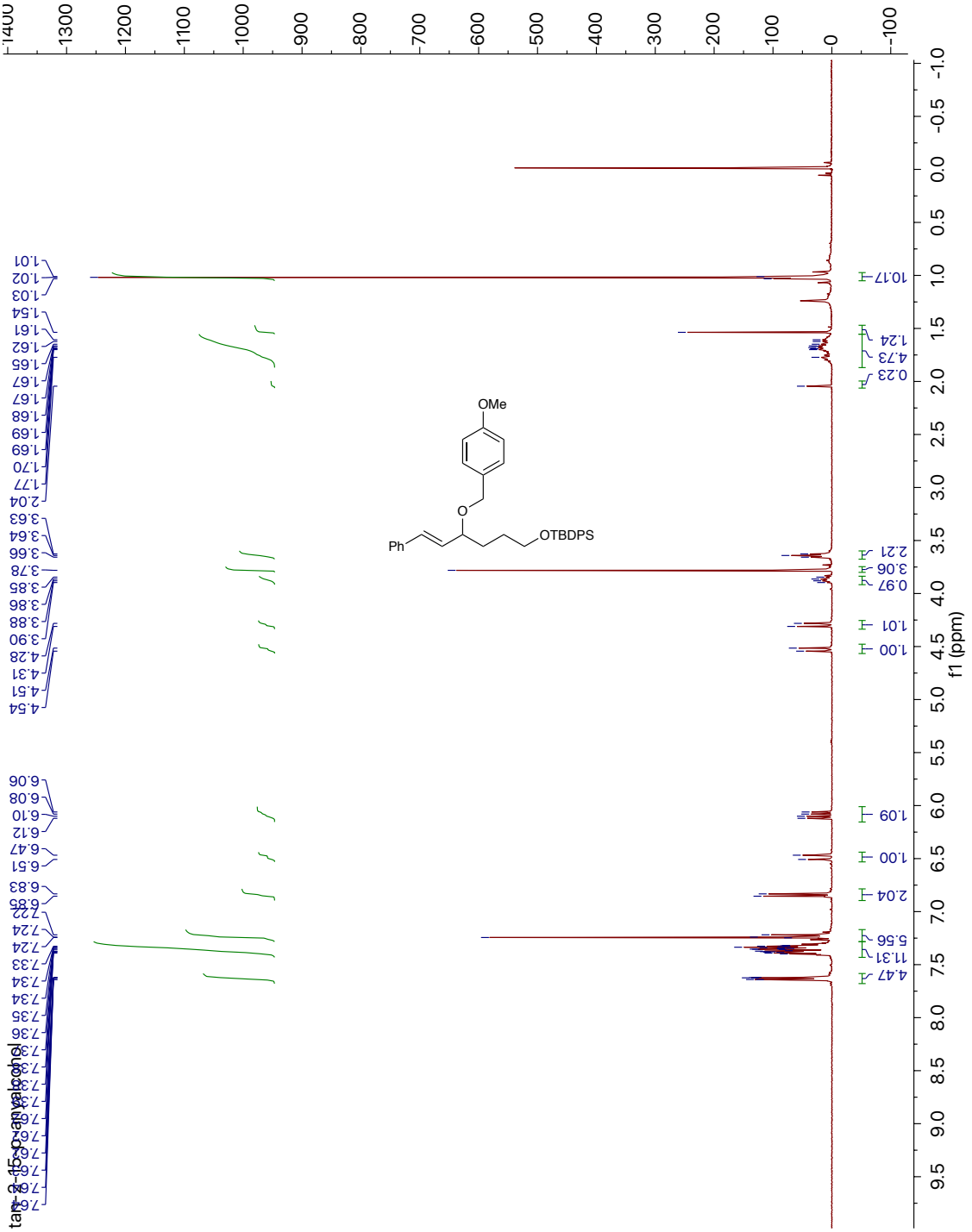

^{13}C NMR (150 MHz, $CDCl_3$)

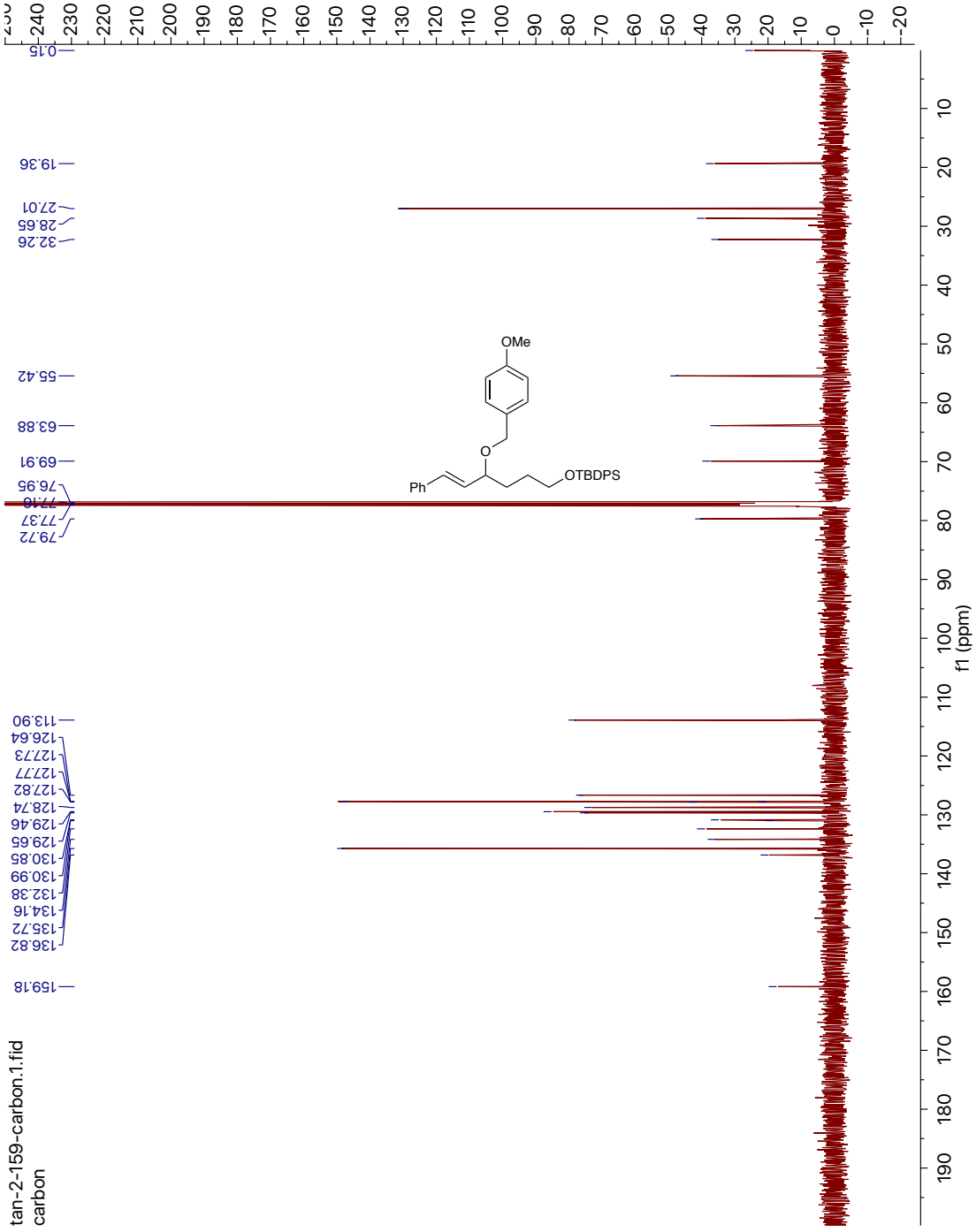

Compound (**2-45**)

^{1}H NMR (400 MHz, $CDCl_3$)

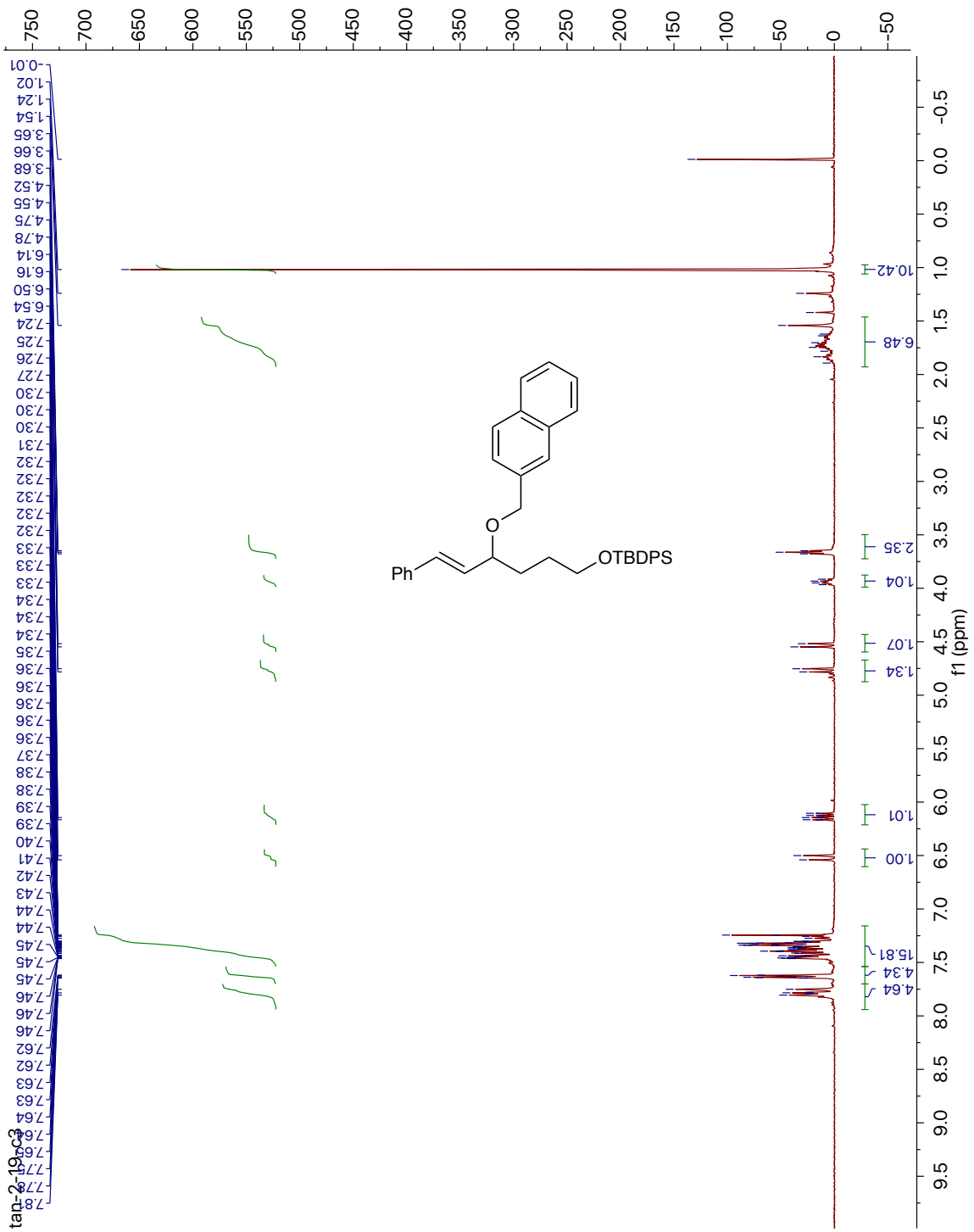

^{13}C NMR (100 MHz, $CDCl_3$)

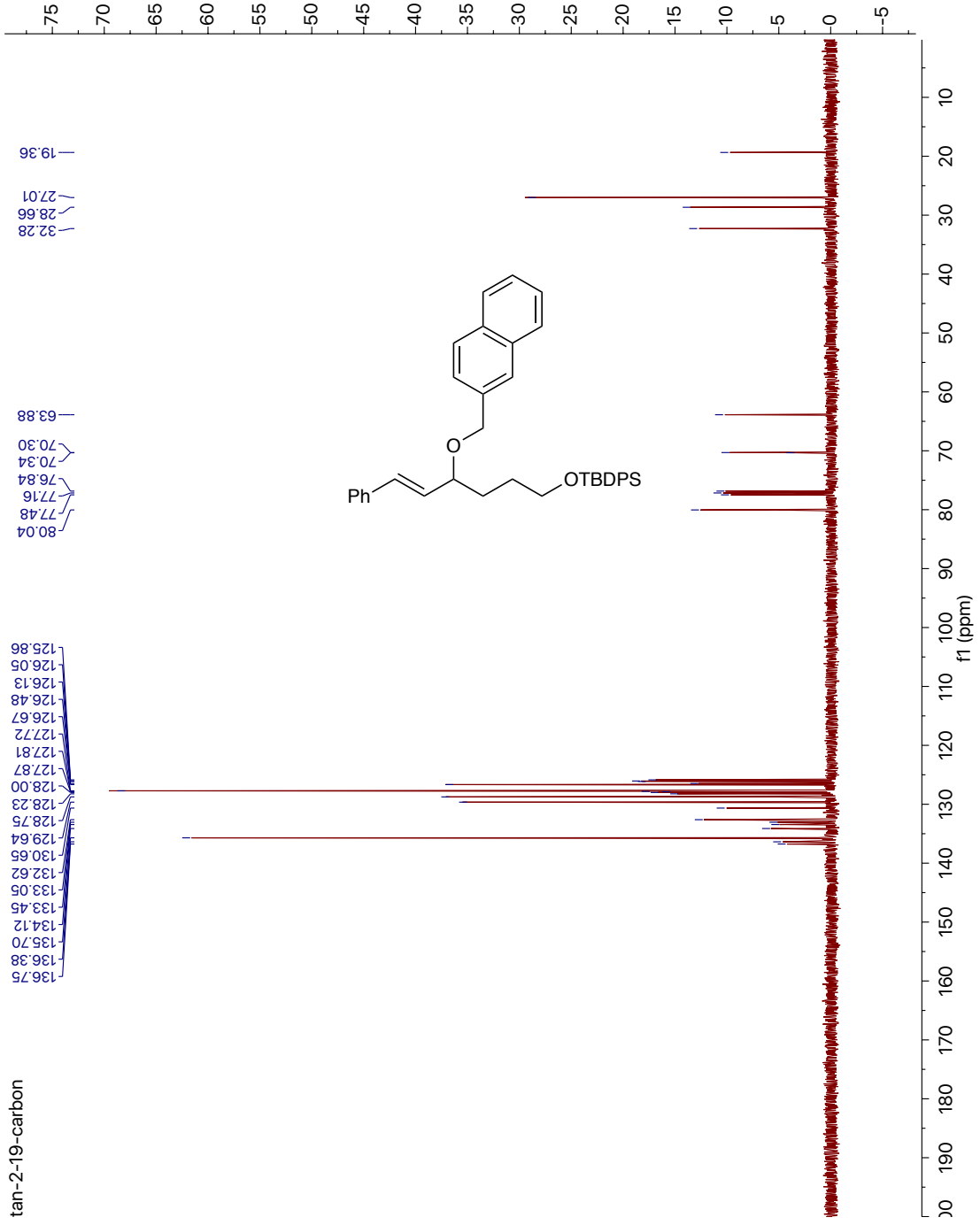

Compound (**2-46**)

^{1}H NMR (600 MHz, $CDCl_3$)

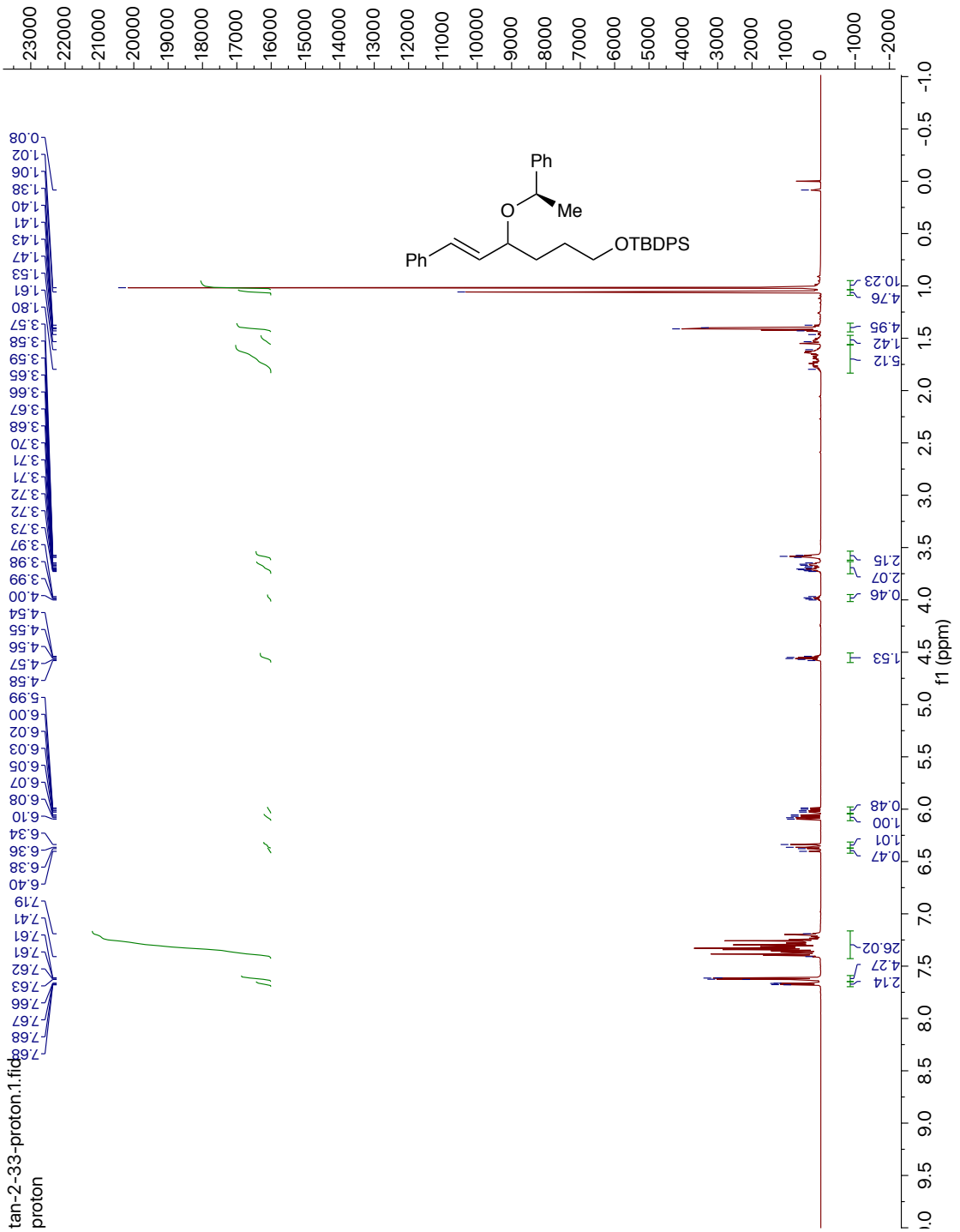

^{13}C NMR (150 MHz, $CDCl_3$)

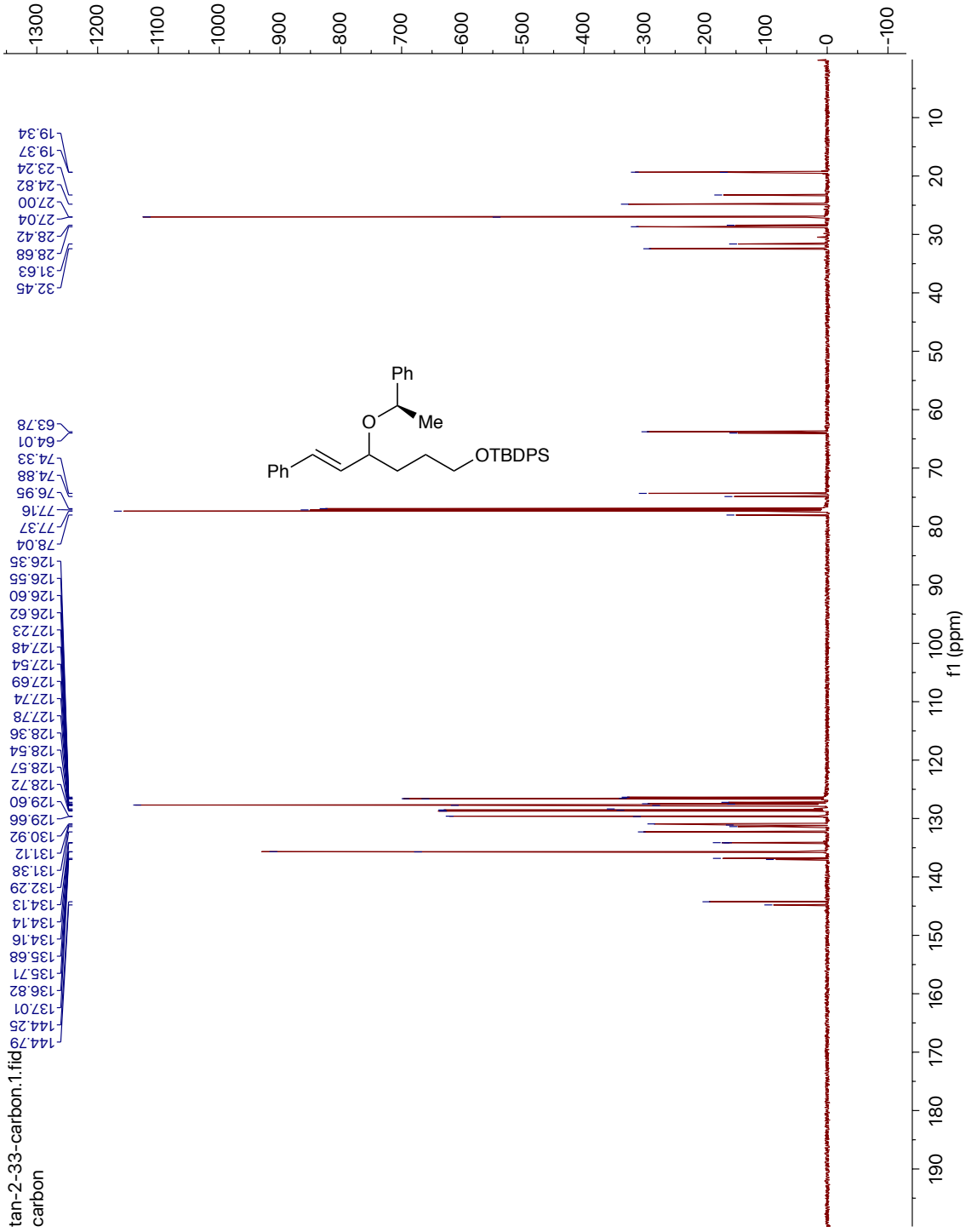

Compound (**2-47**)

^{1}H NMR (300 MHz, $CDCl_3$)

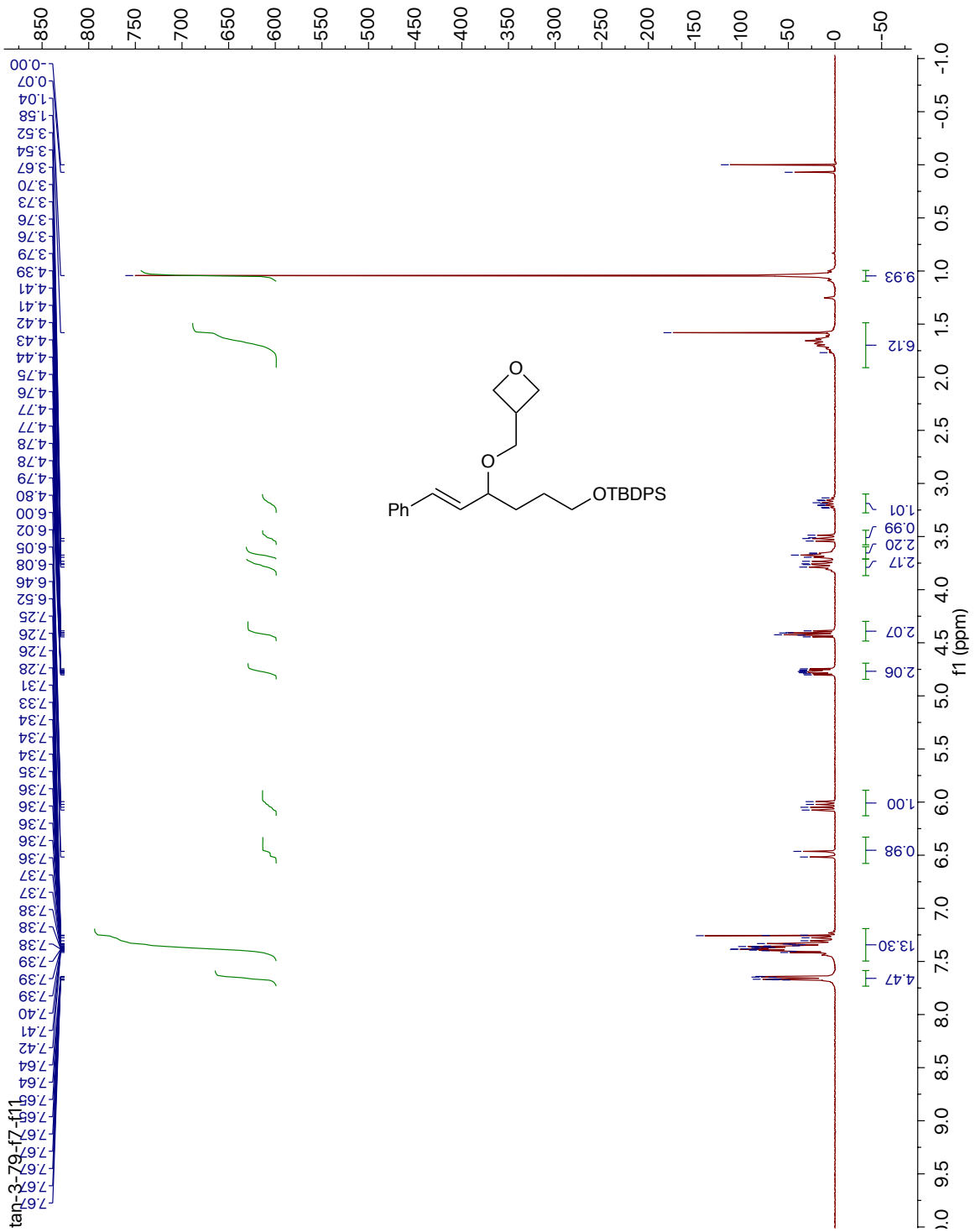

^{13}C NMR (150 MHz, $CDCl_3$)

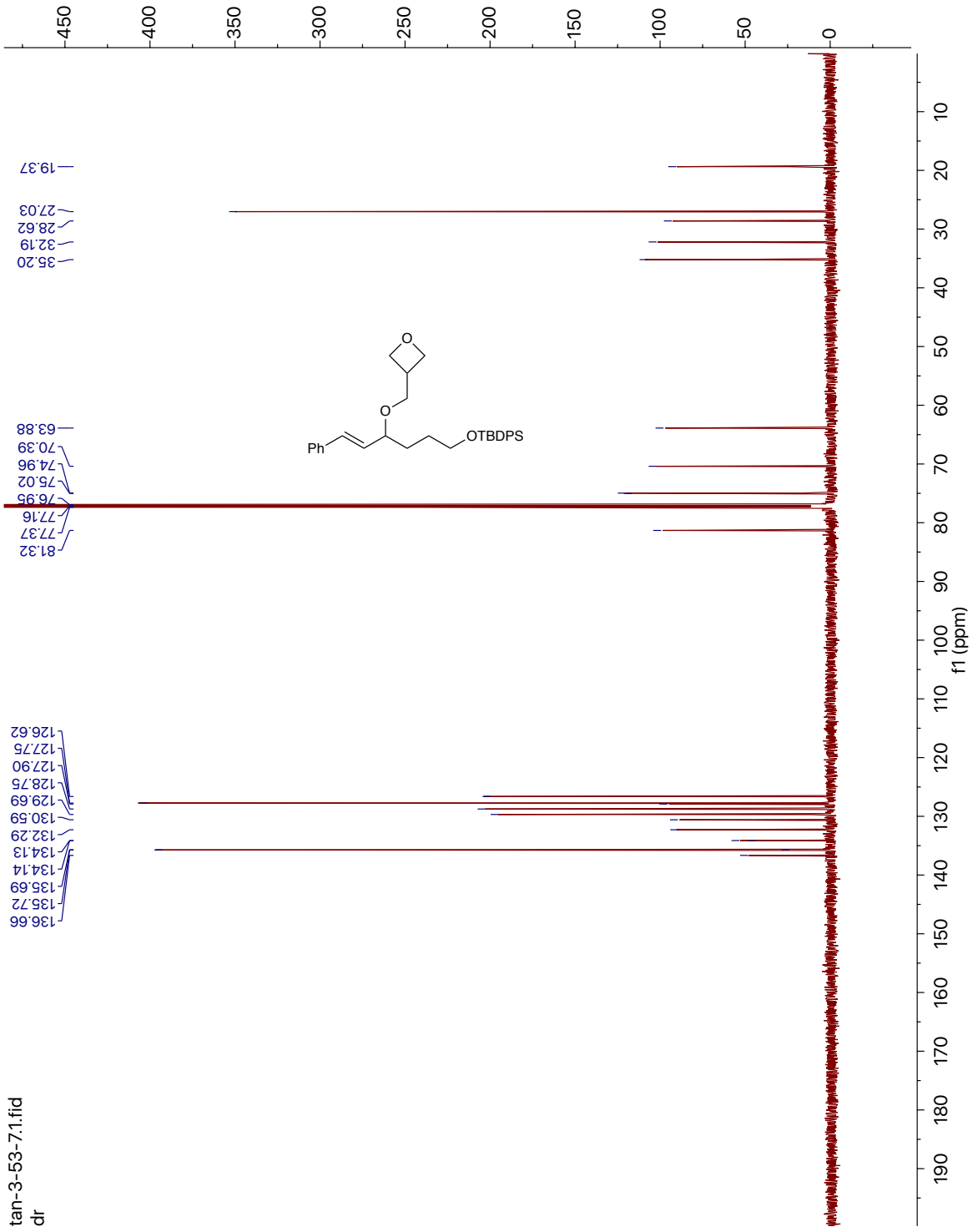

Compound (**2-48**)

^{1}H NMR (400 MHz, $CDCl_3$)

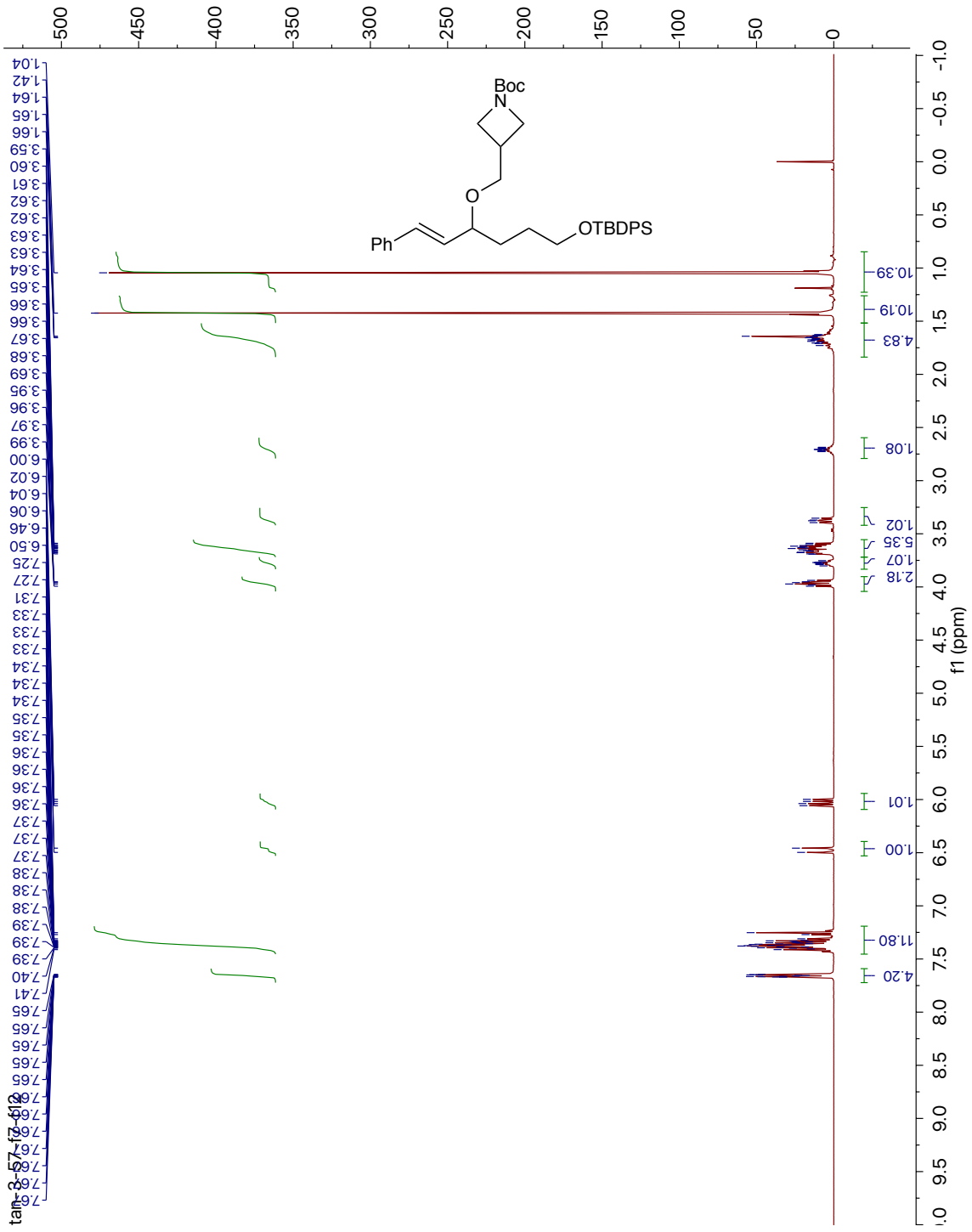

^{13}C NMR (150 MHz, $CDCl_3$)

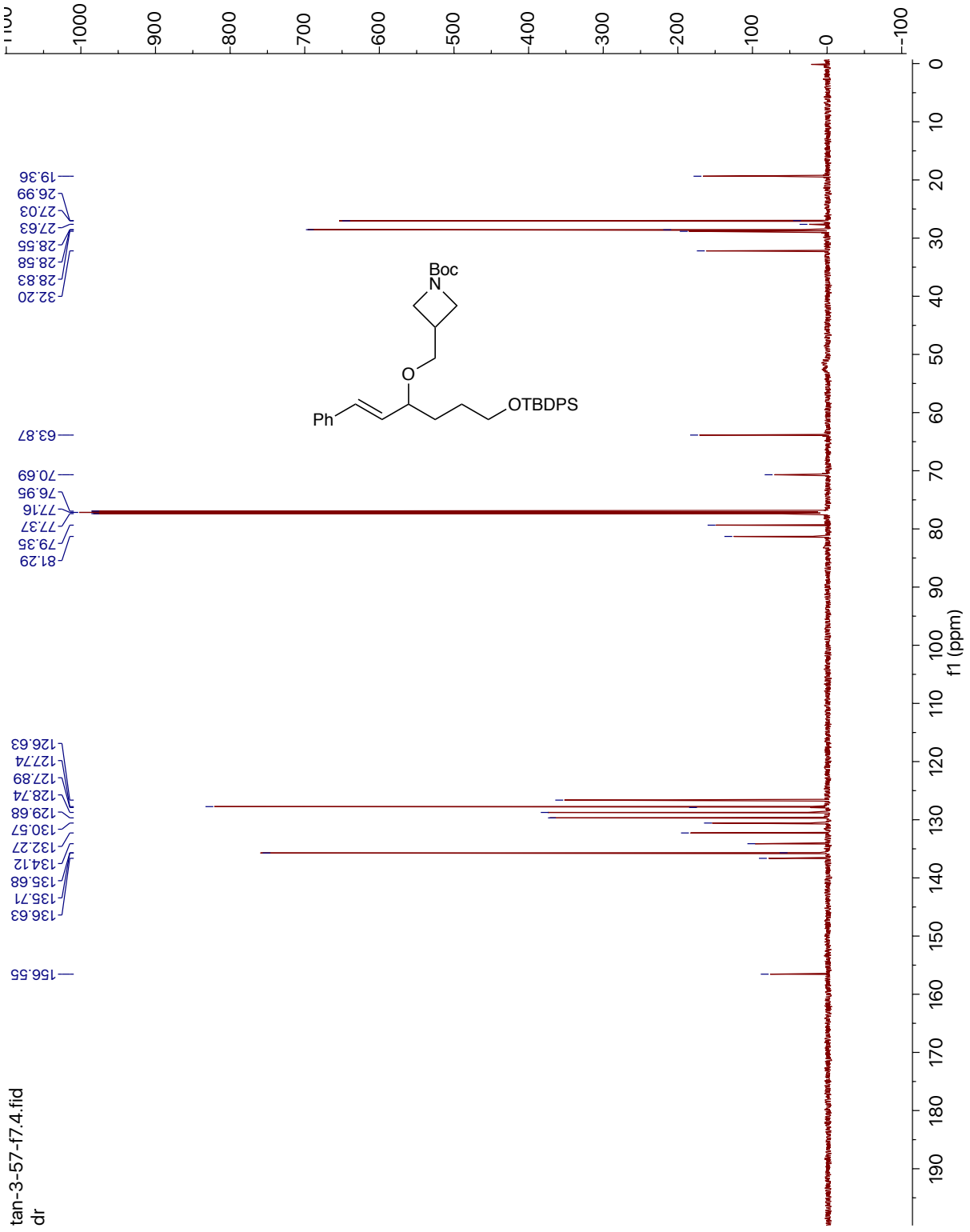

Compound (**2-49**)

^{1}H NMR (300 MHz, $CDCl_3$)

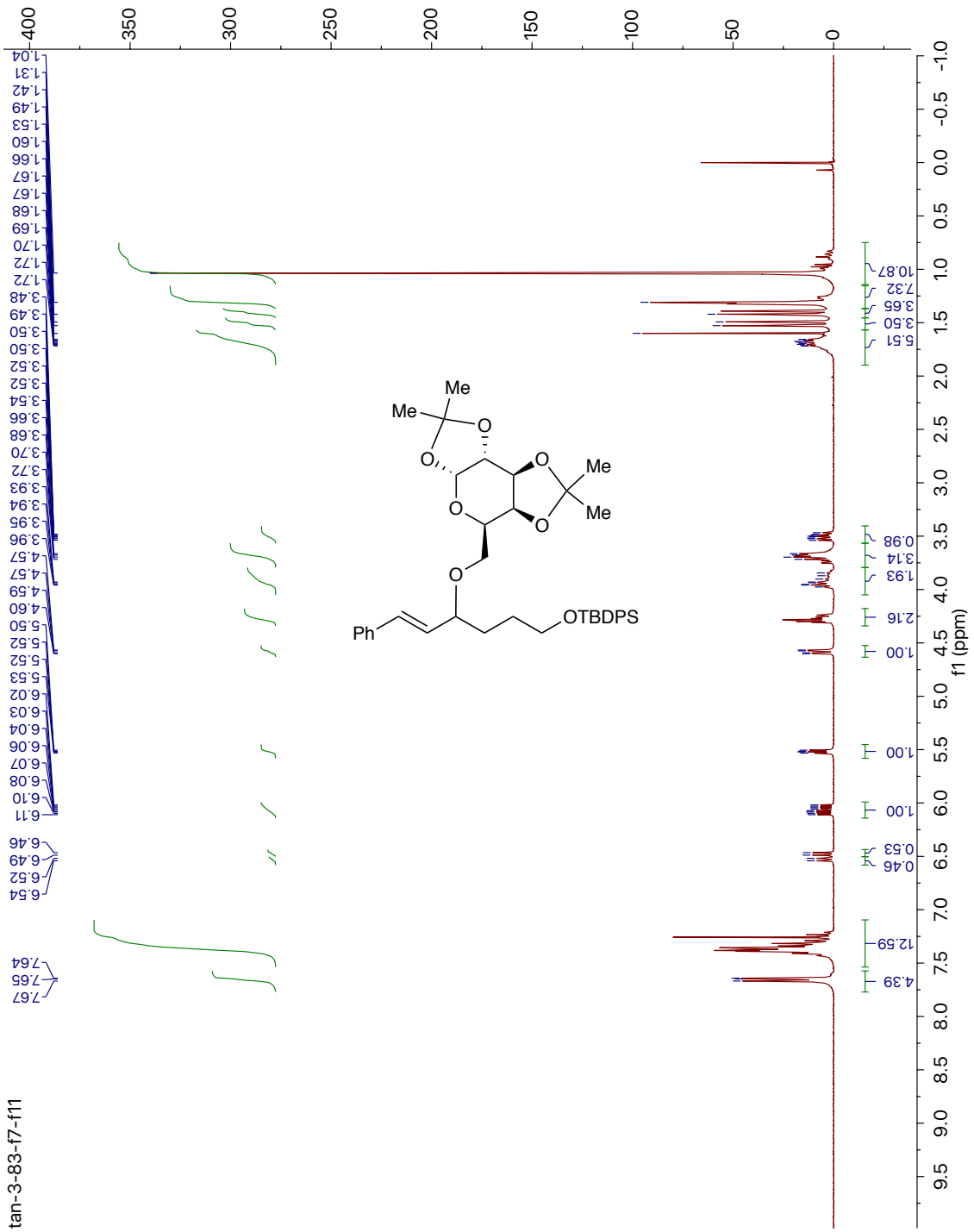

^{13}C NMR (150 MHz, $CDCl_3$)

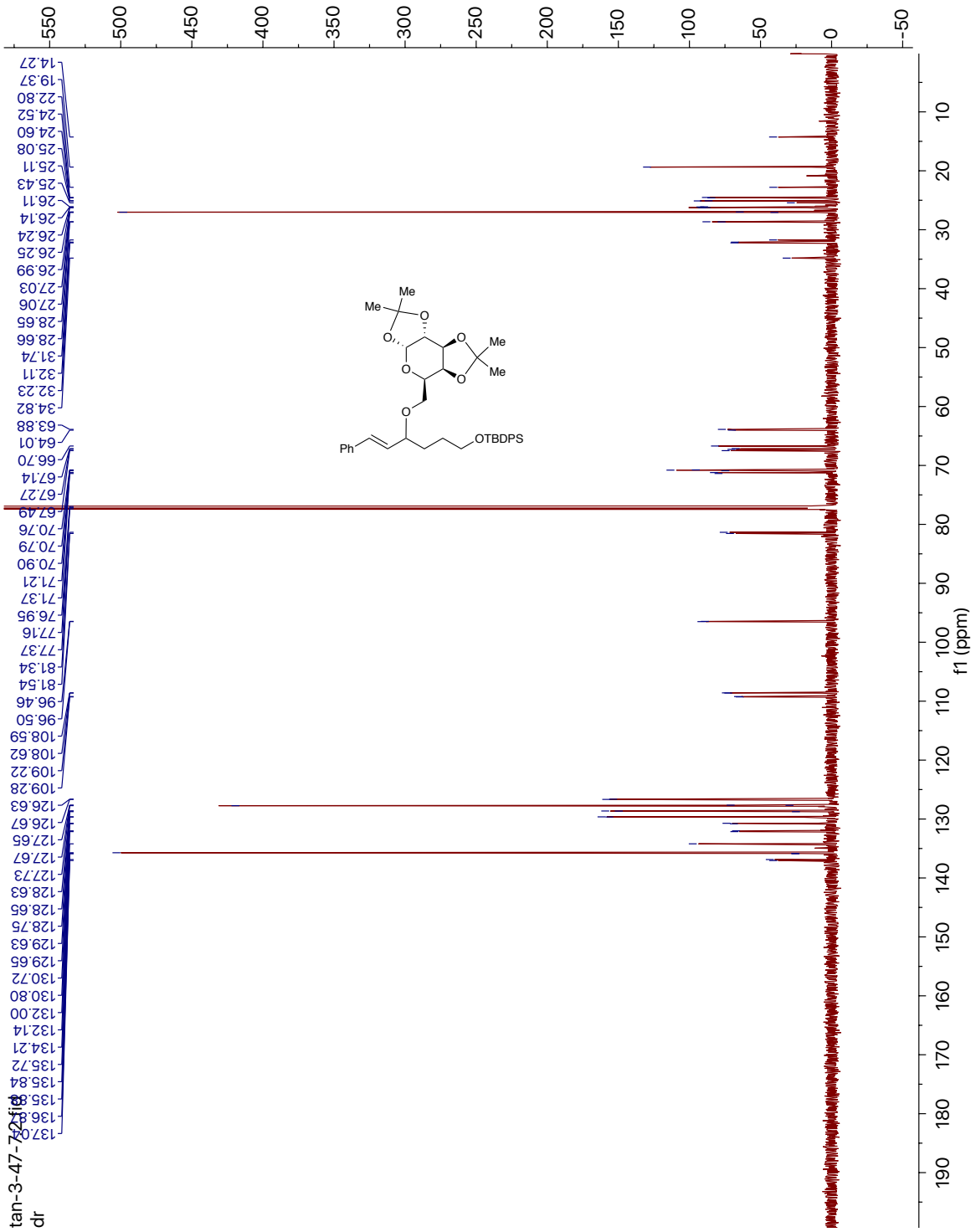

Compound (**2-50**)

^{1}H NMR (600 MHz, $CDCl_3$)

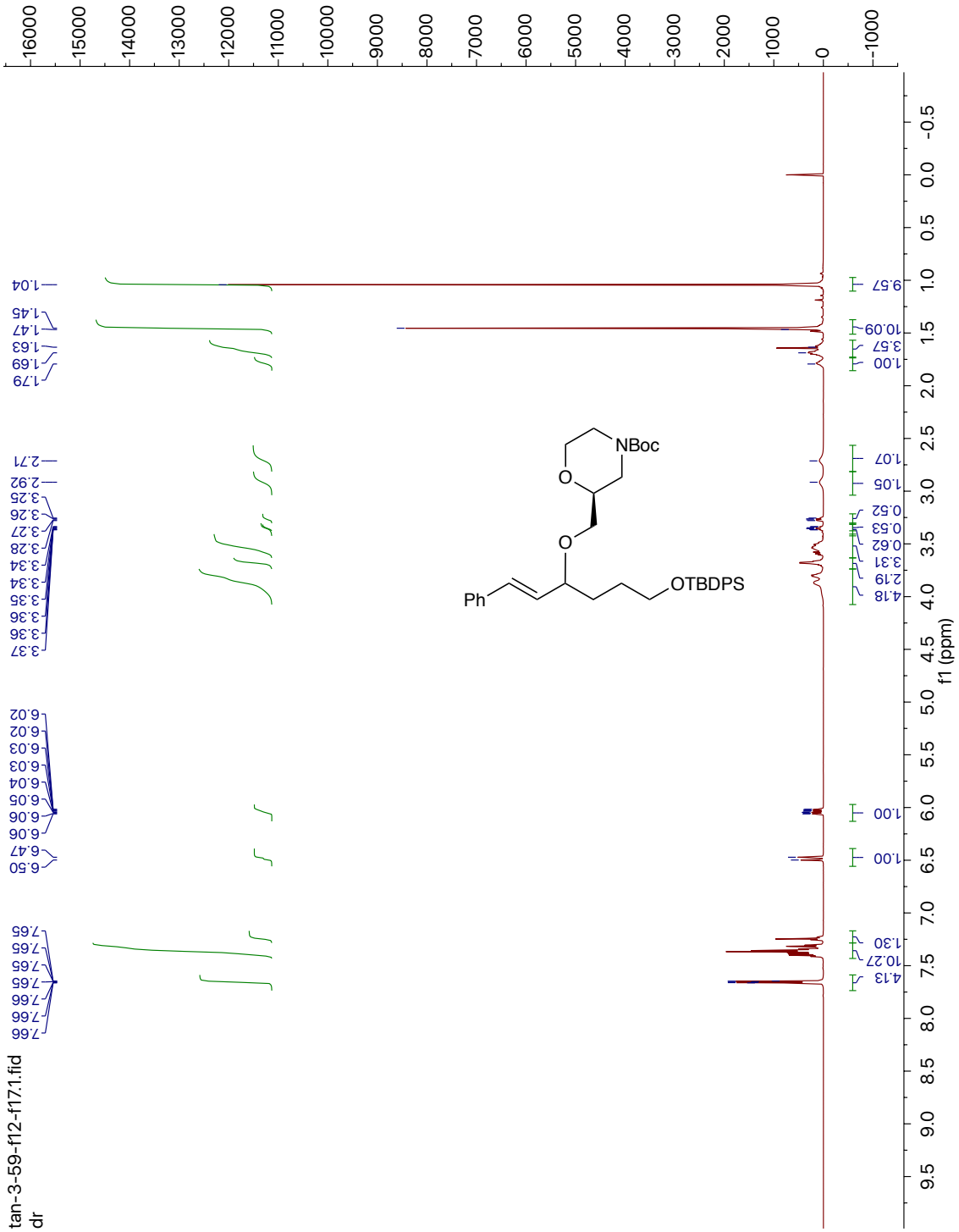

^{13}C NMR (150 MHz, $CDCl_3$)

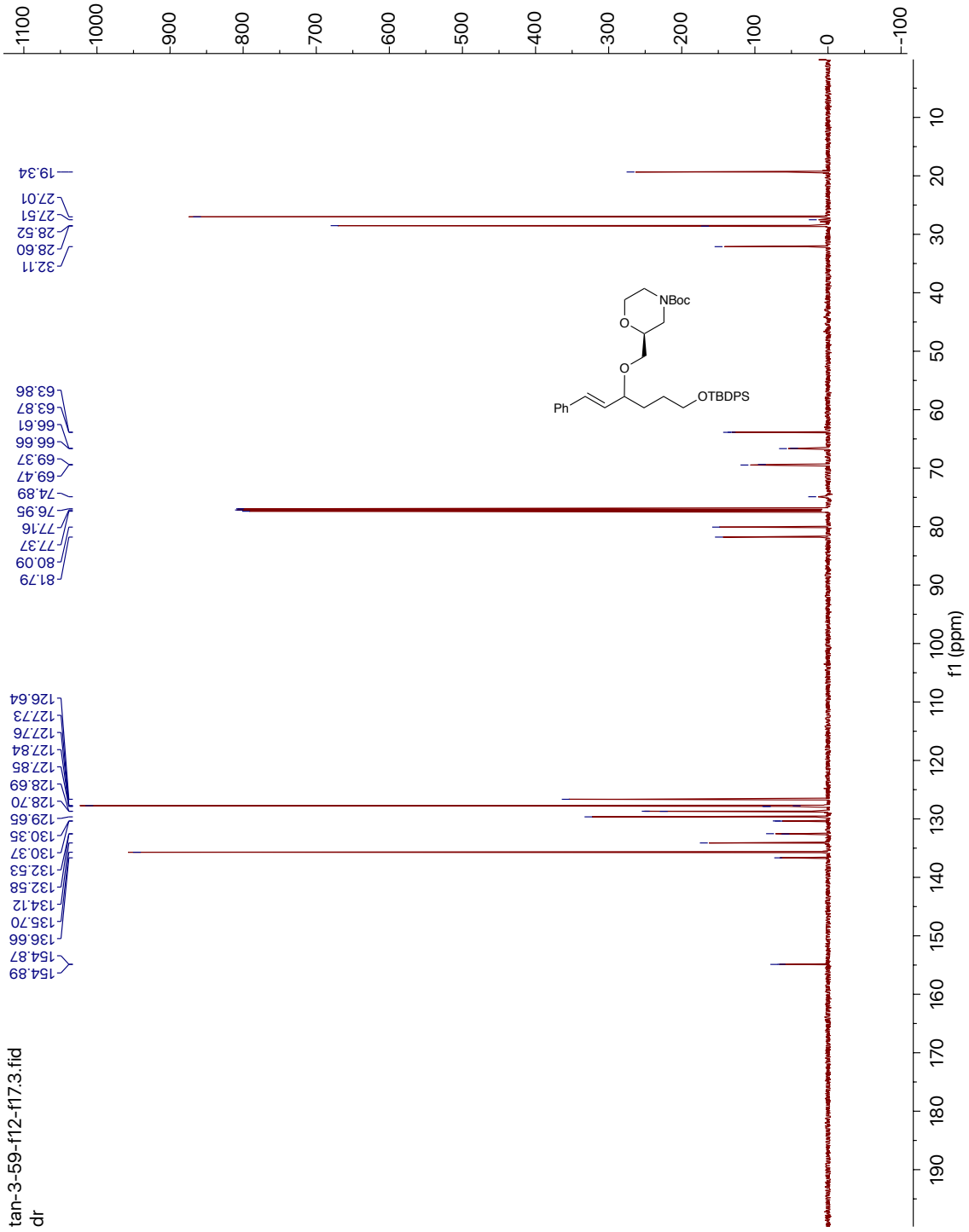

Compound (**2-51**)

^{1}H NMR (400 MHz, $CDCl_3$)

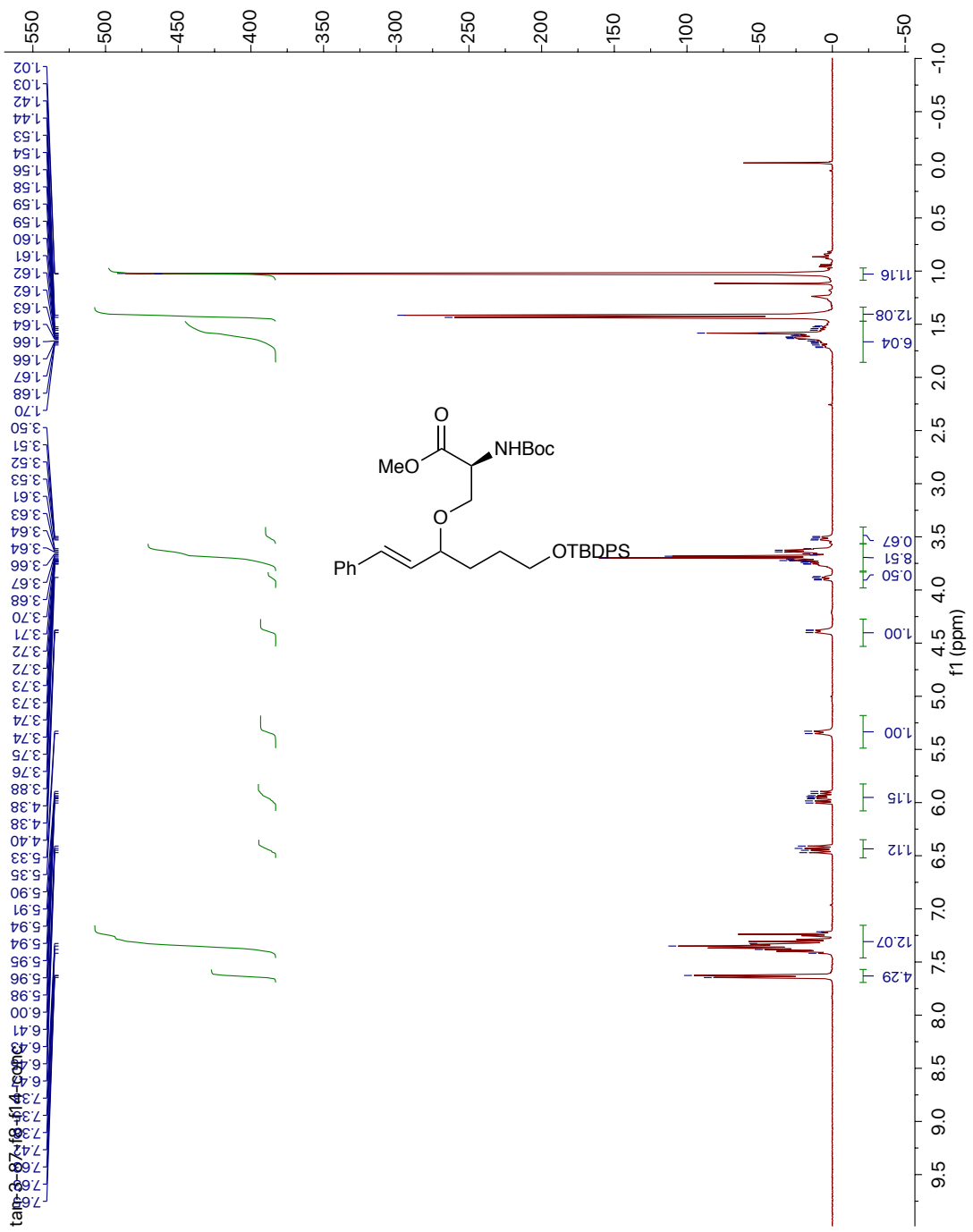

^{13}C NMR (150 MHz, $CDCl_3$)

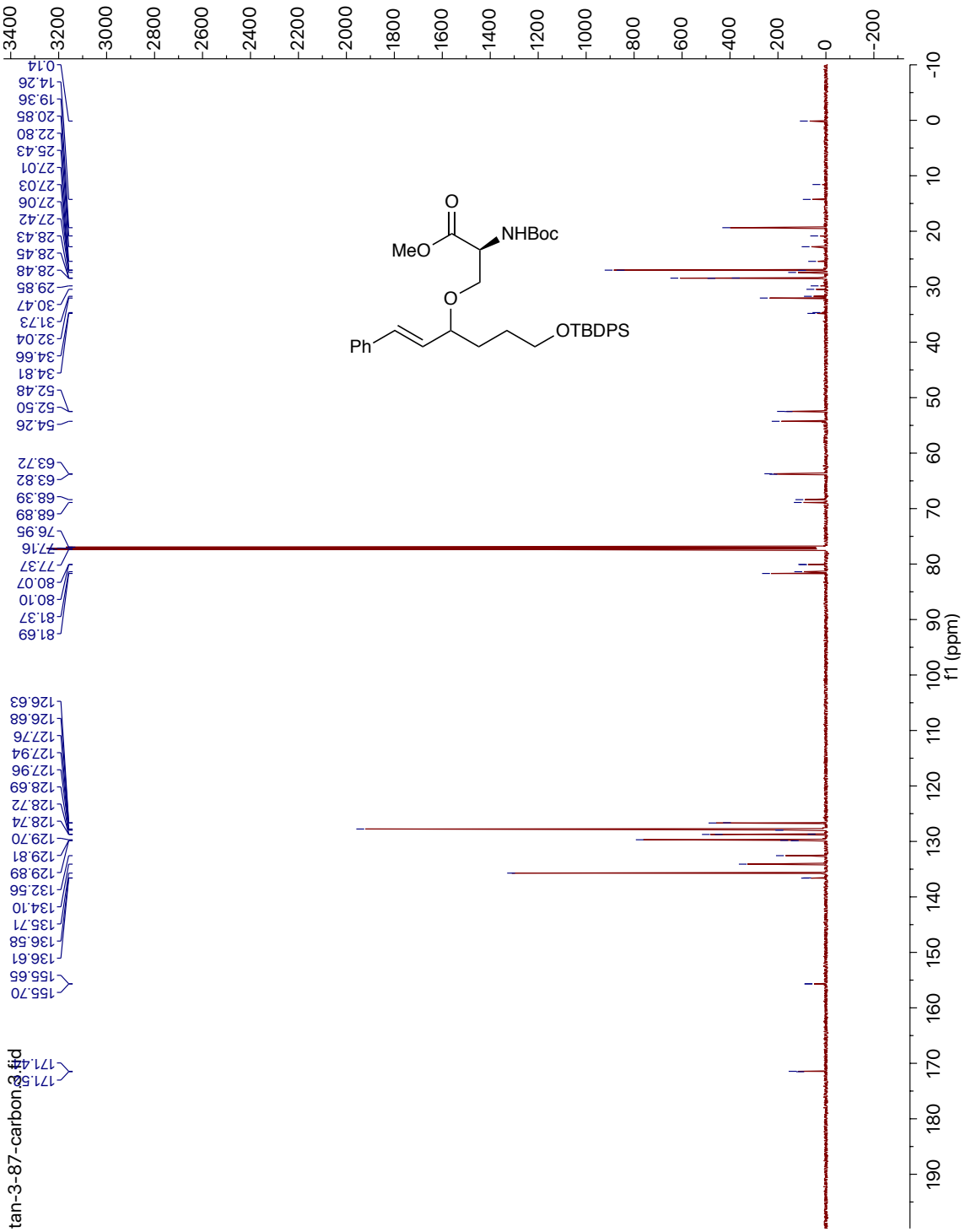

Compound (**2-52**)

^{1}H NMR (400 MHz, $CDCl_3$)

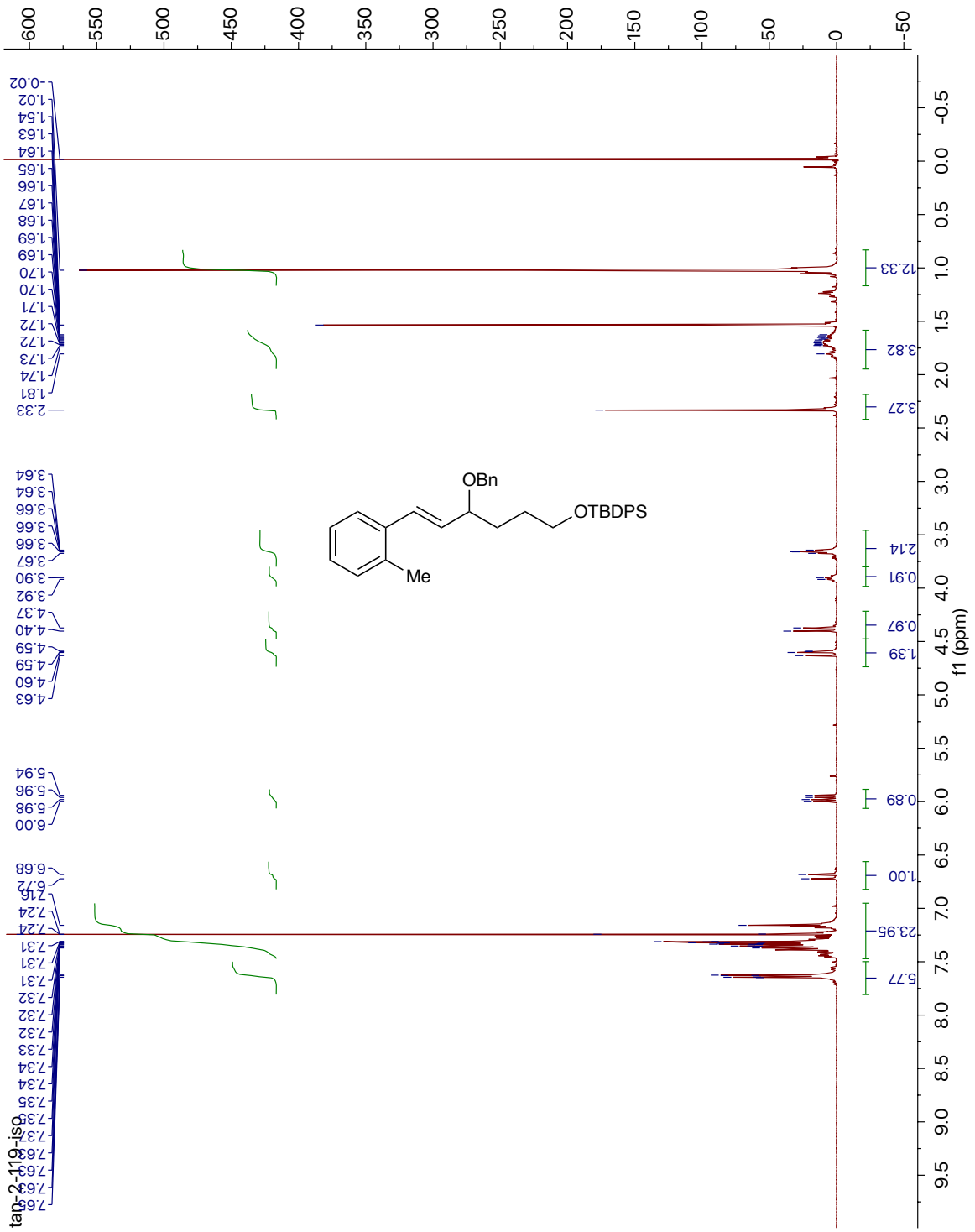

^{13}C NMR (125 MHz, $CDCl_3$)

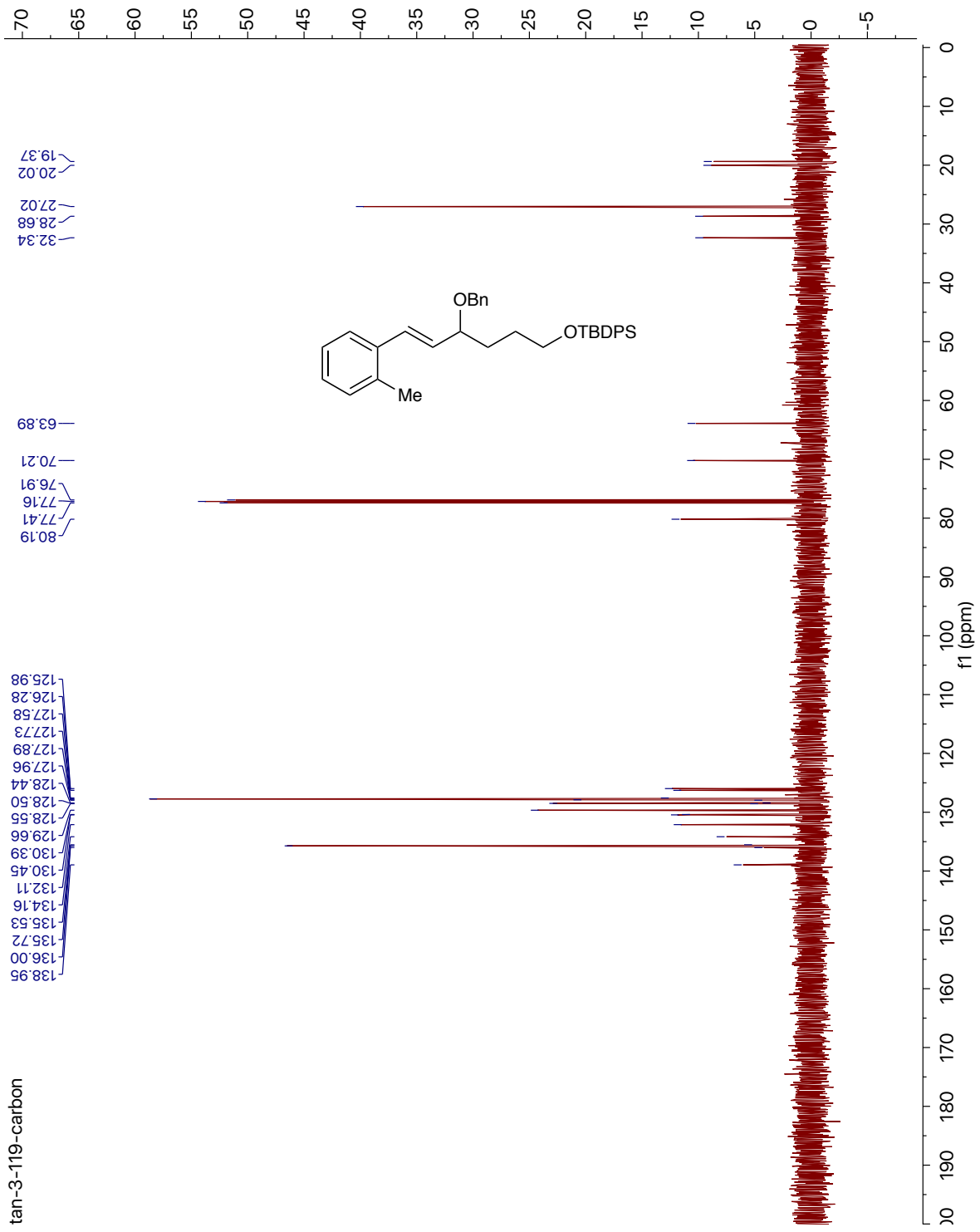

Compound (**2-53**)

^{1}H NMR (300 MHz, $CDCl_3$)

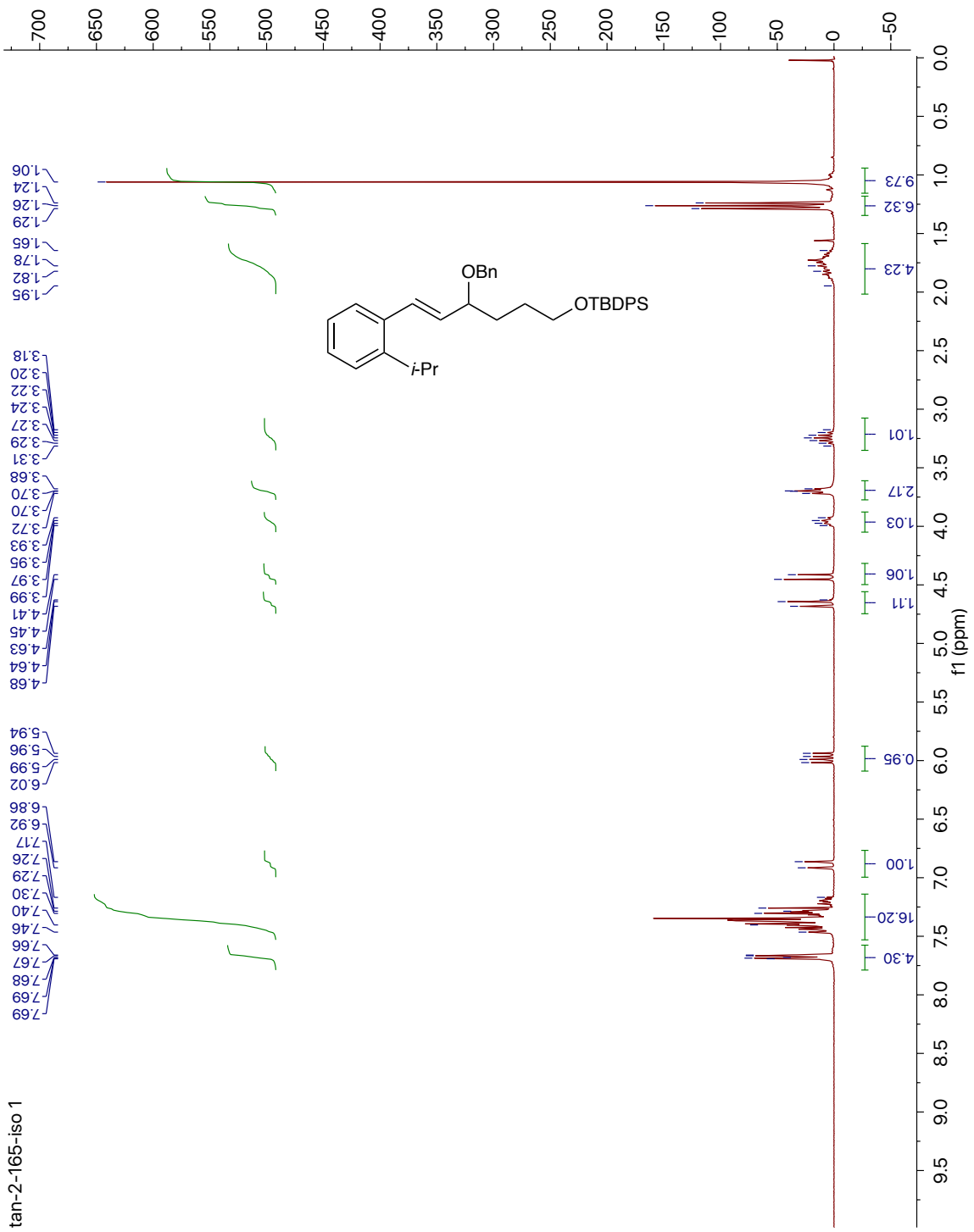

^{13}C NMR (150 MHz, $CDCl_3$)

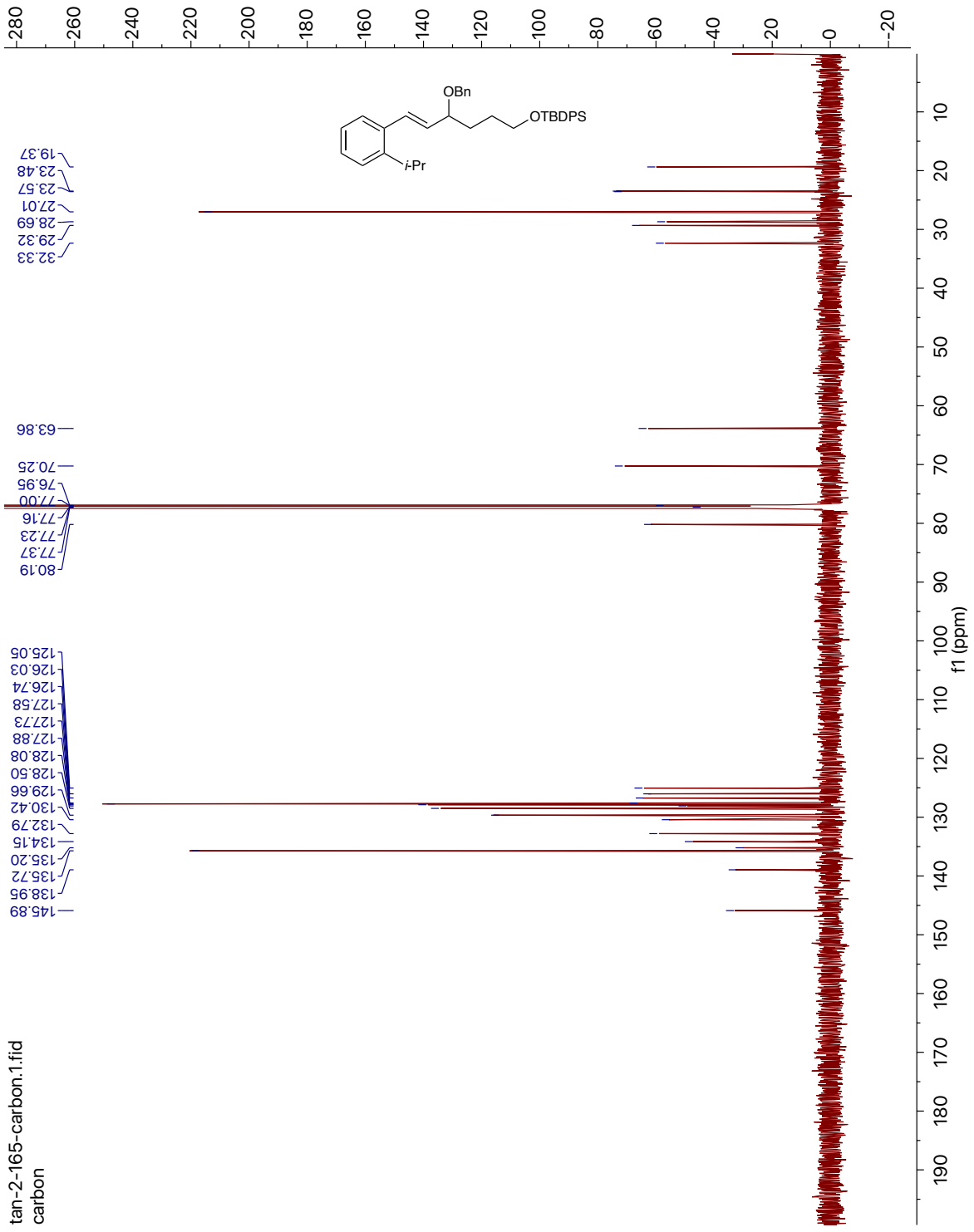

Compound (**2-54**)

^{1}H NMR (400 MHz, $CDCl_3$)

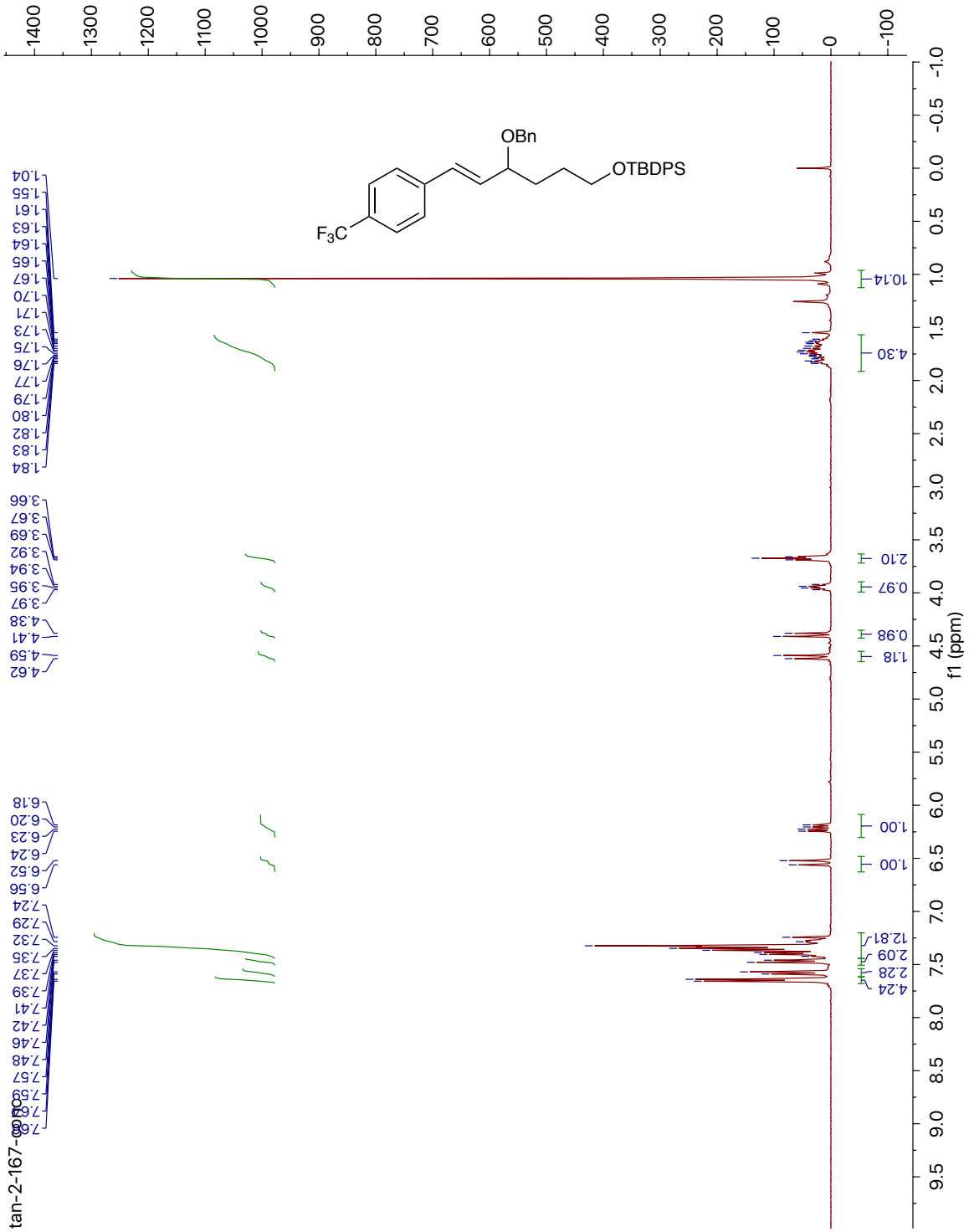

^{13}C NMR (150 MHz, $CDCl_3$)

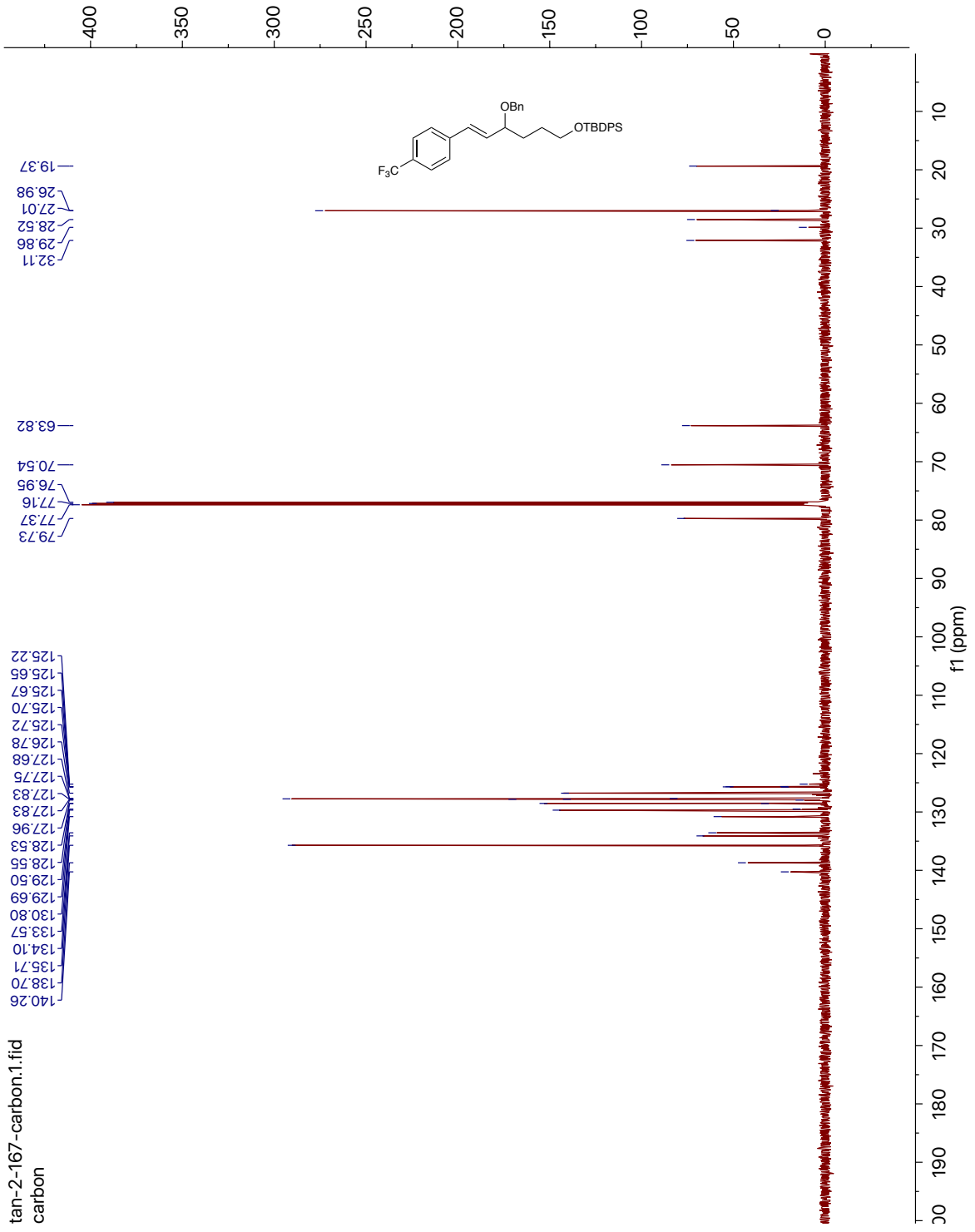

Compound (**2-55**)

^{1}H NMR (400 MHz, $CDCl_3$)

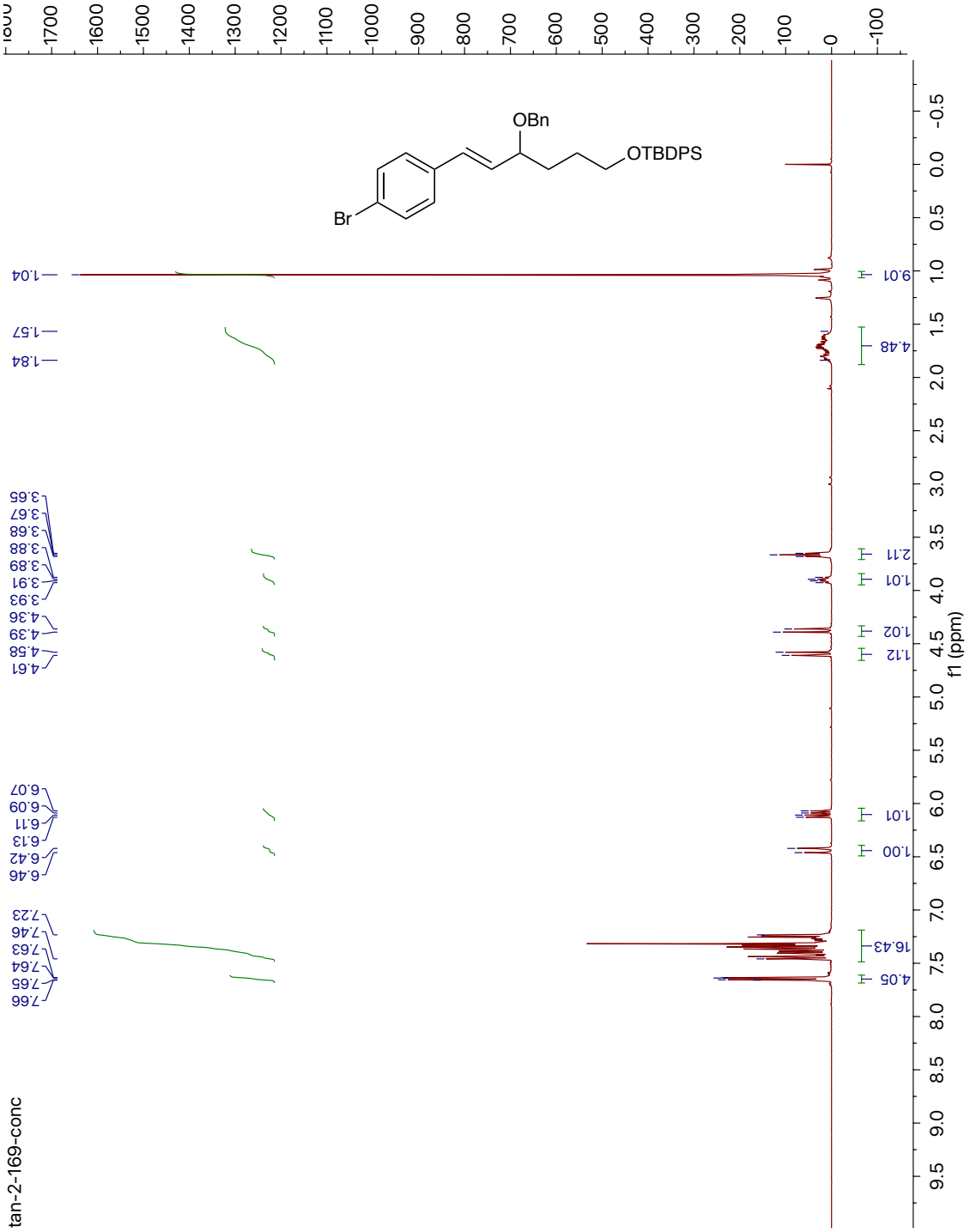

^{13}C NMR (150 MHz, $CDCl_3$)

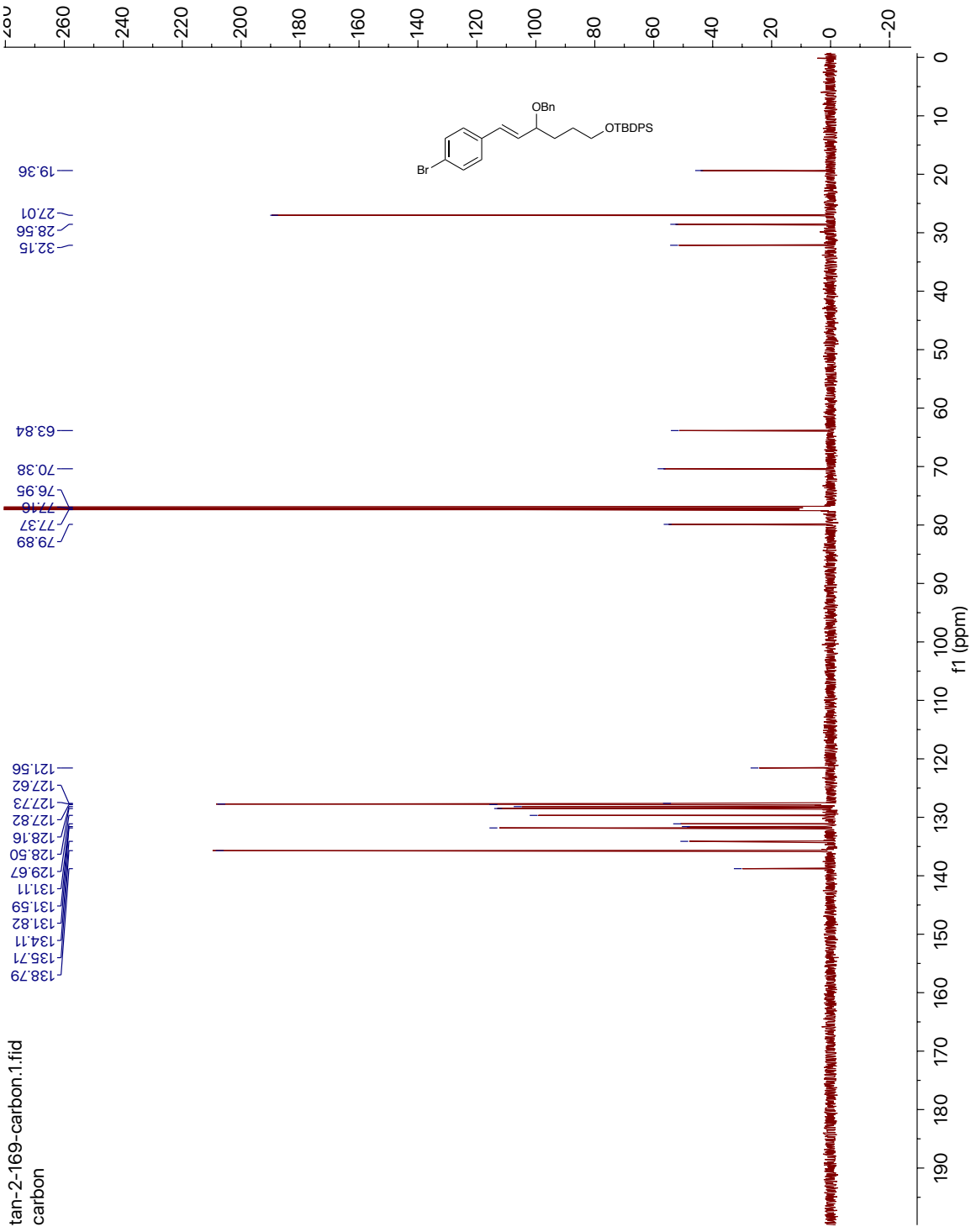

Compound (**2-56**)

^{1}H NMR (400 MHz, $CDCl_3$)

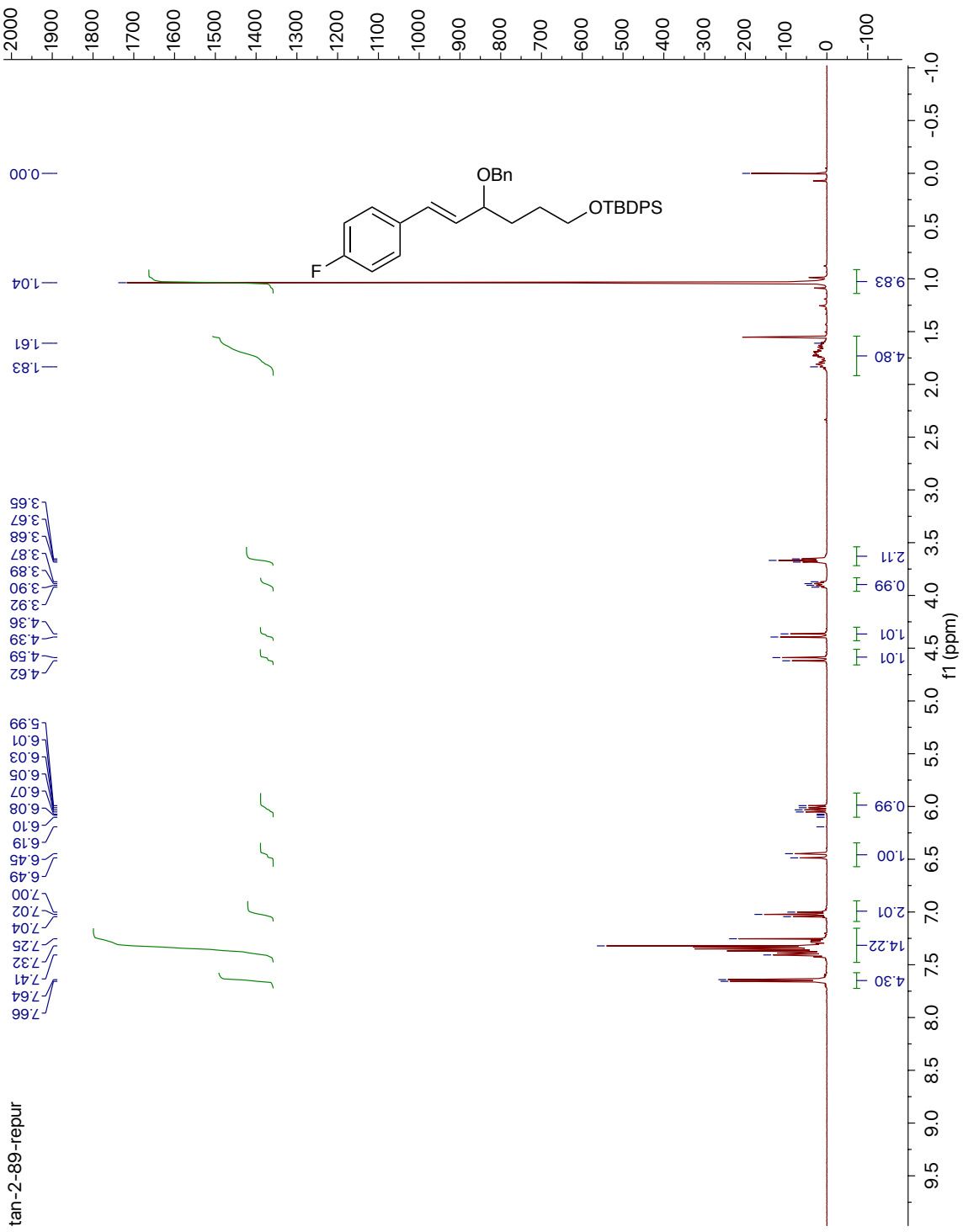

^{13}C NMR (150 MHz, $CDCl_3$)

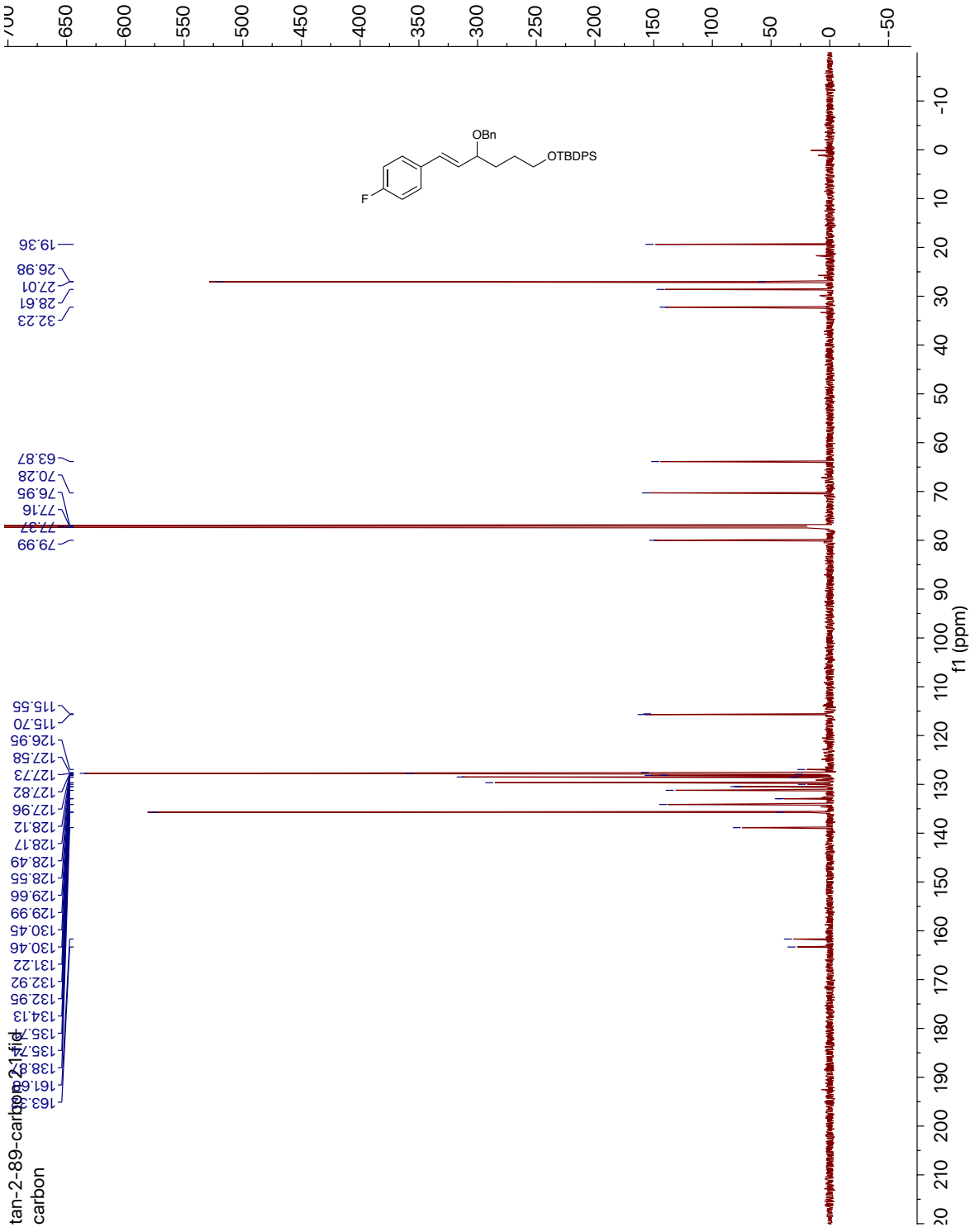

Compound (**2-57**)

^{1}H NMR (400 MHz, $CDCl_3$)

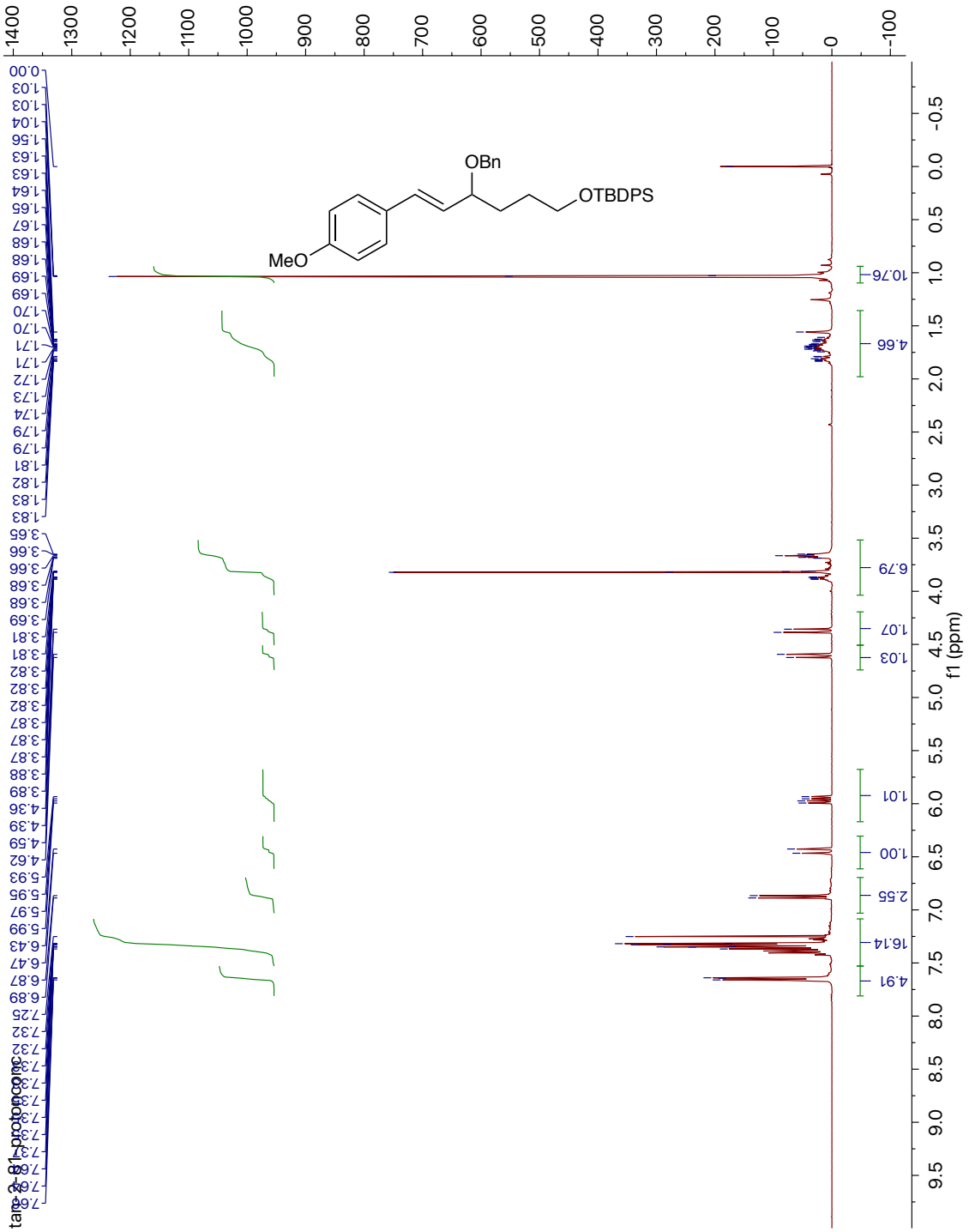

^{13}C NMR (150 MHz, $CDCl_3$)

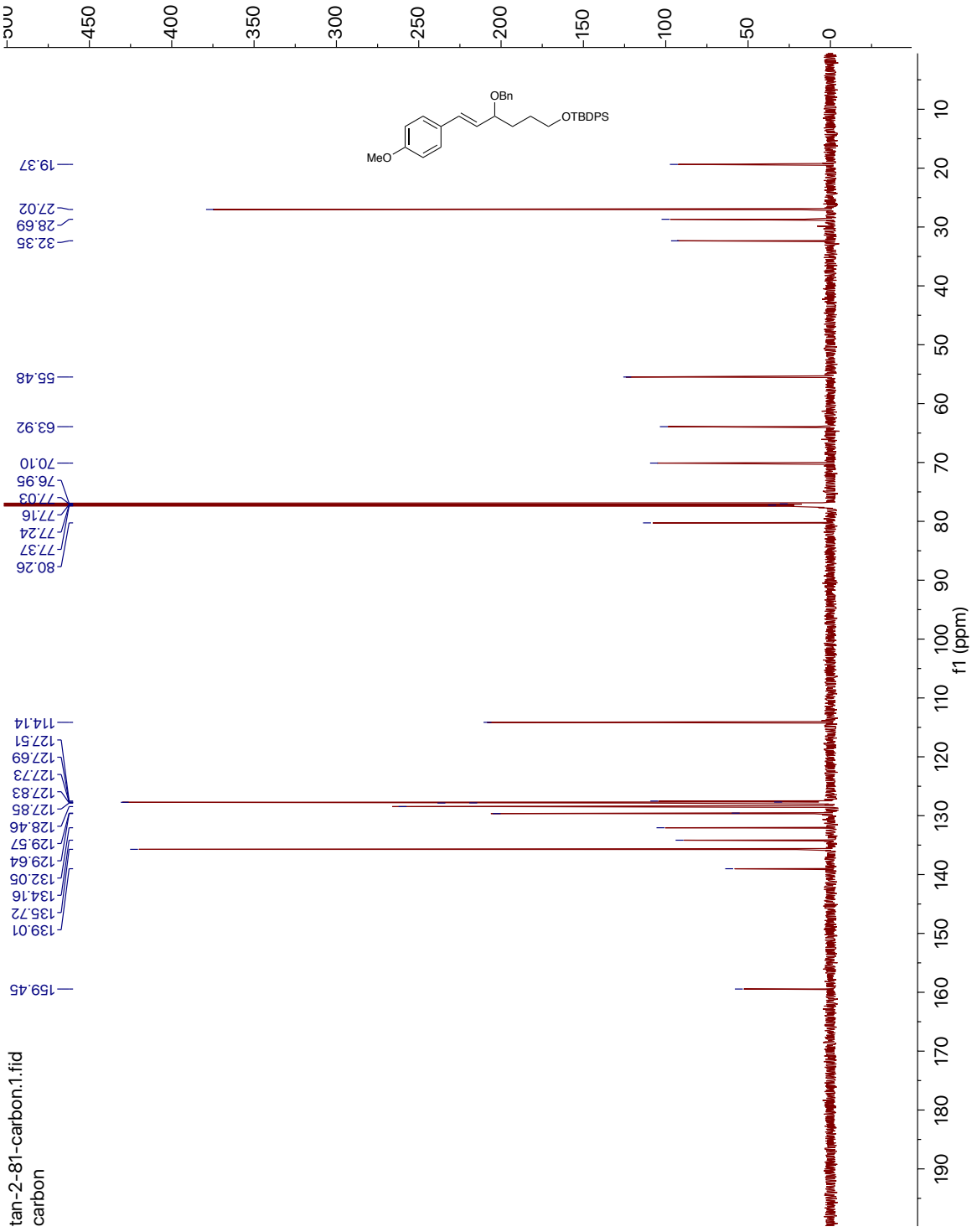

Compound(**2-60**)

^{1}H NMR (300 MHz, $CDCl_3$)

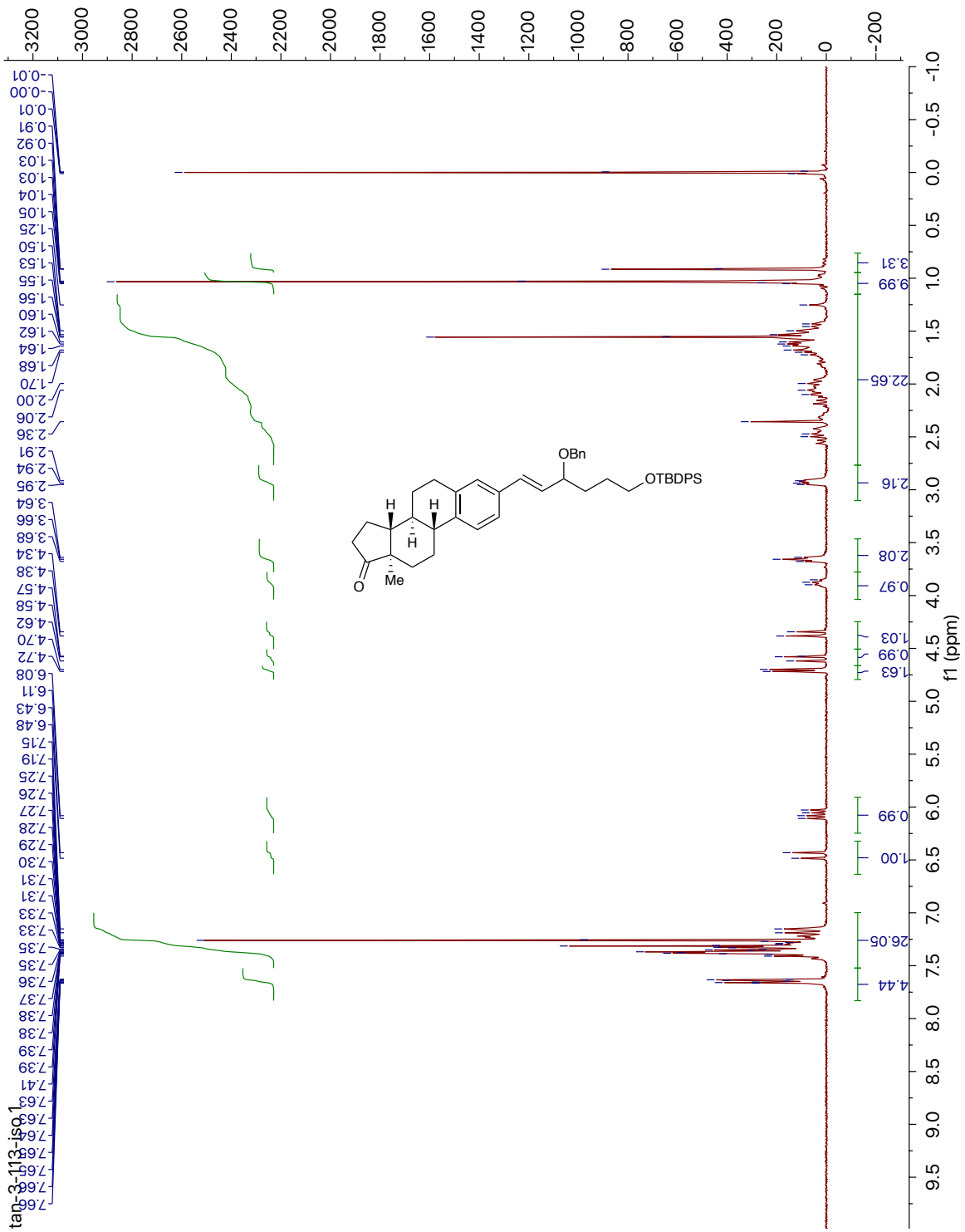

^{13}C NMR (150 MHz, $CDCl_3$)

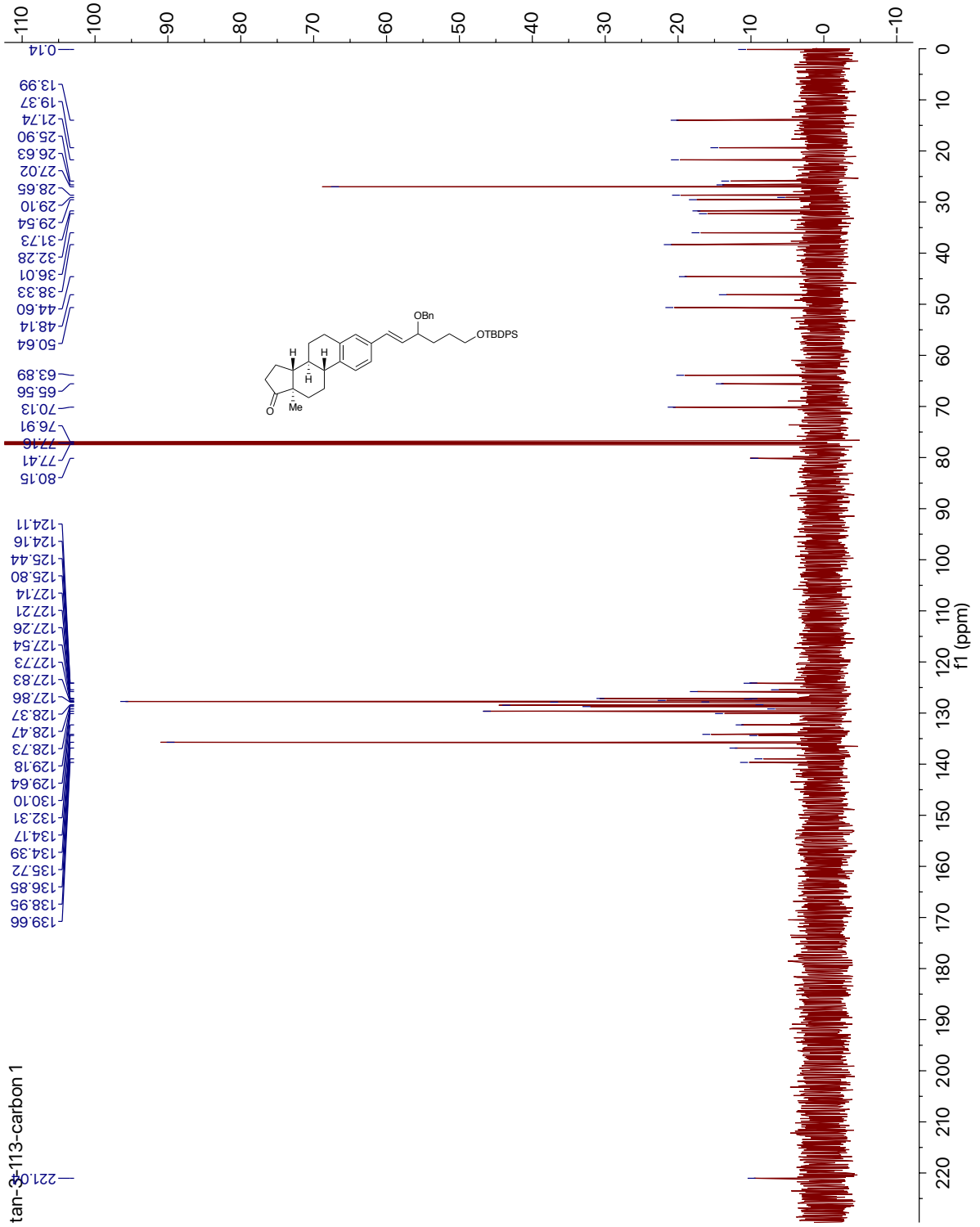

Compound (**2-62**)

^{1}H NMR (300 MHz, $CDCl_3$)

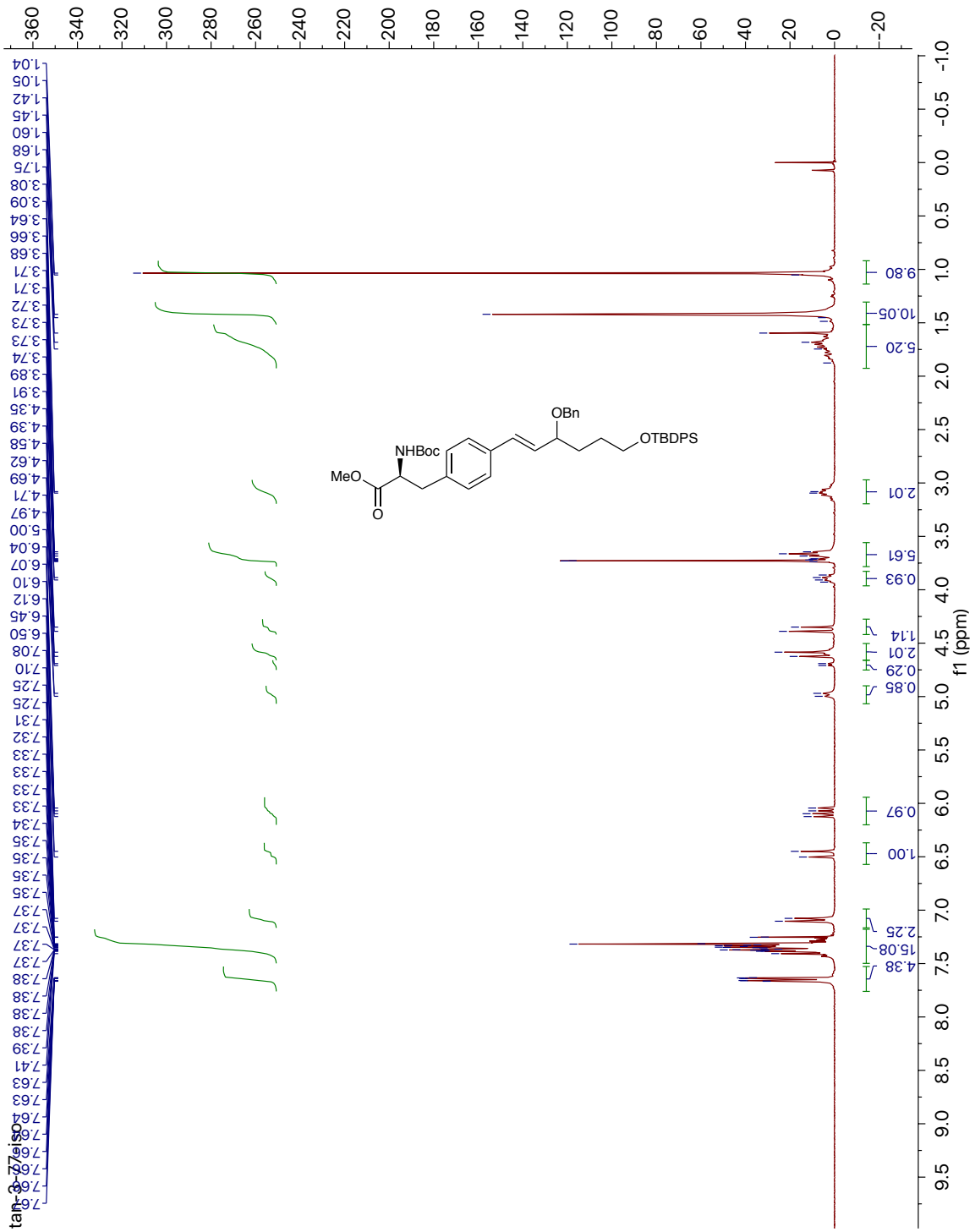

^{13}C NMR (150 MHz, $CDCl_3$)

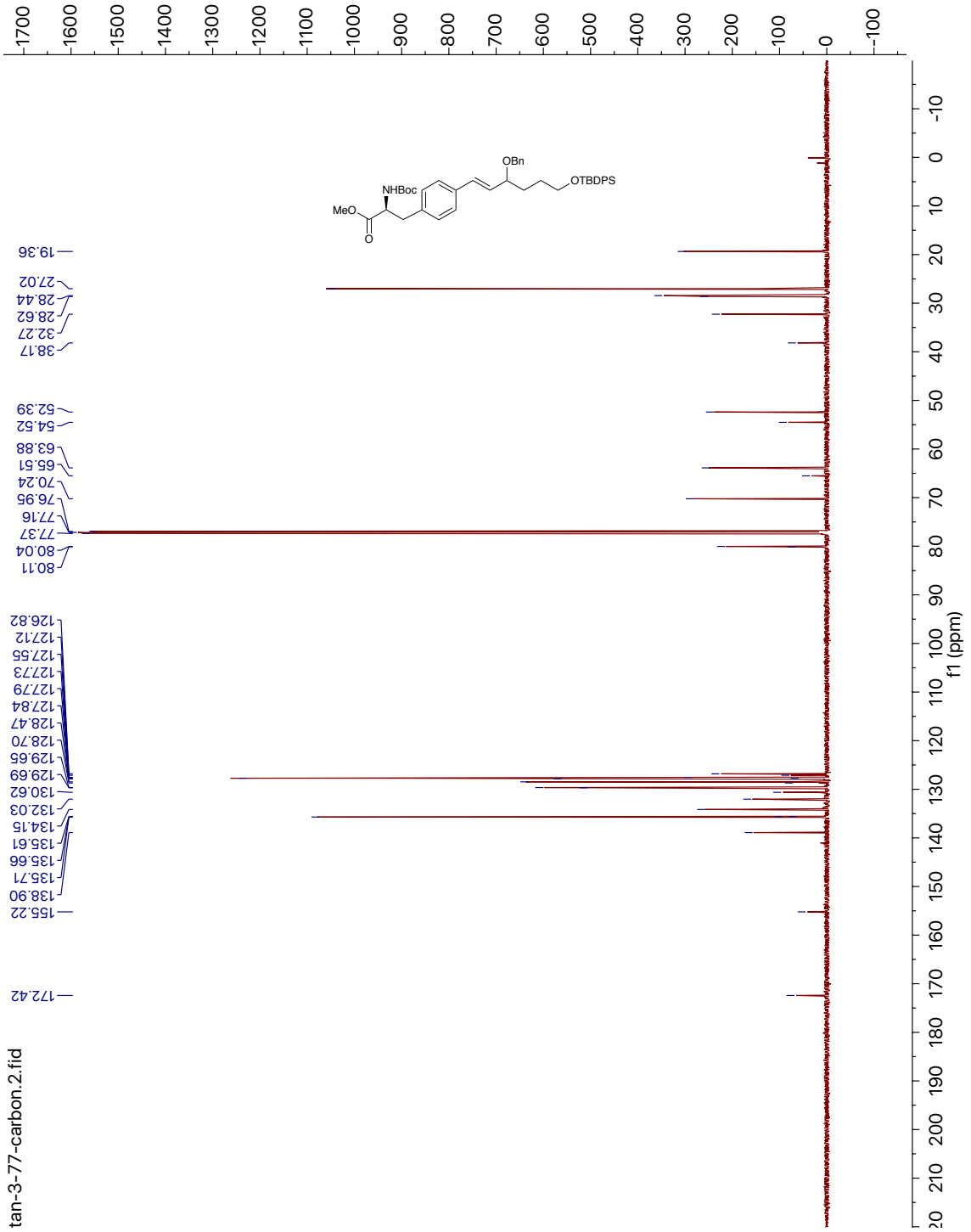

Compound (**2-63**)

^{1}H NMR (300 MHz, $CDCl_3$)

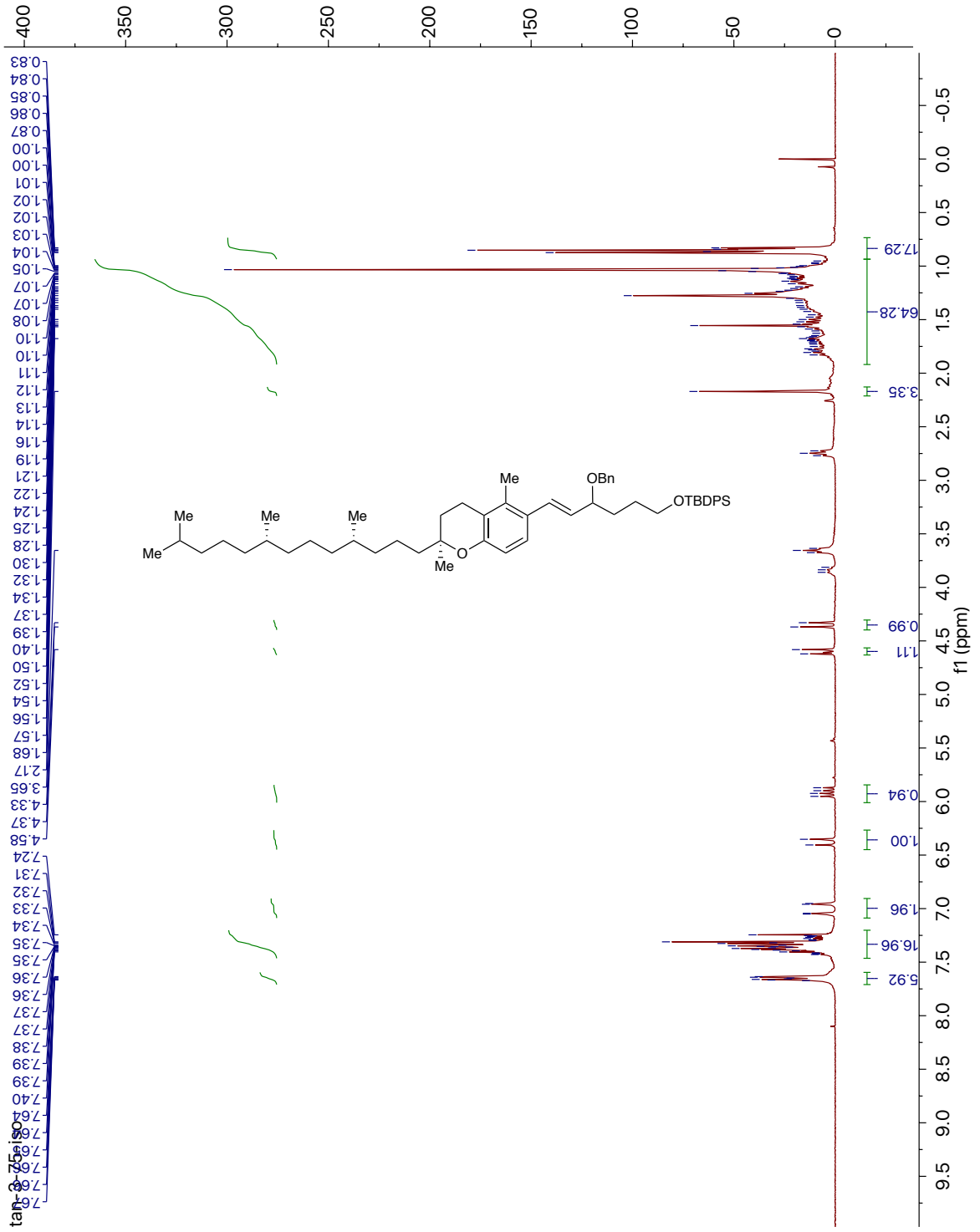

^{13}C NMR (125 MHz, $CDCl_3$)

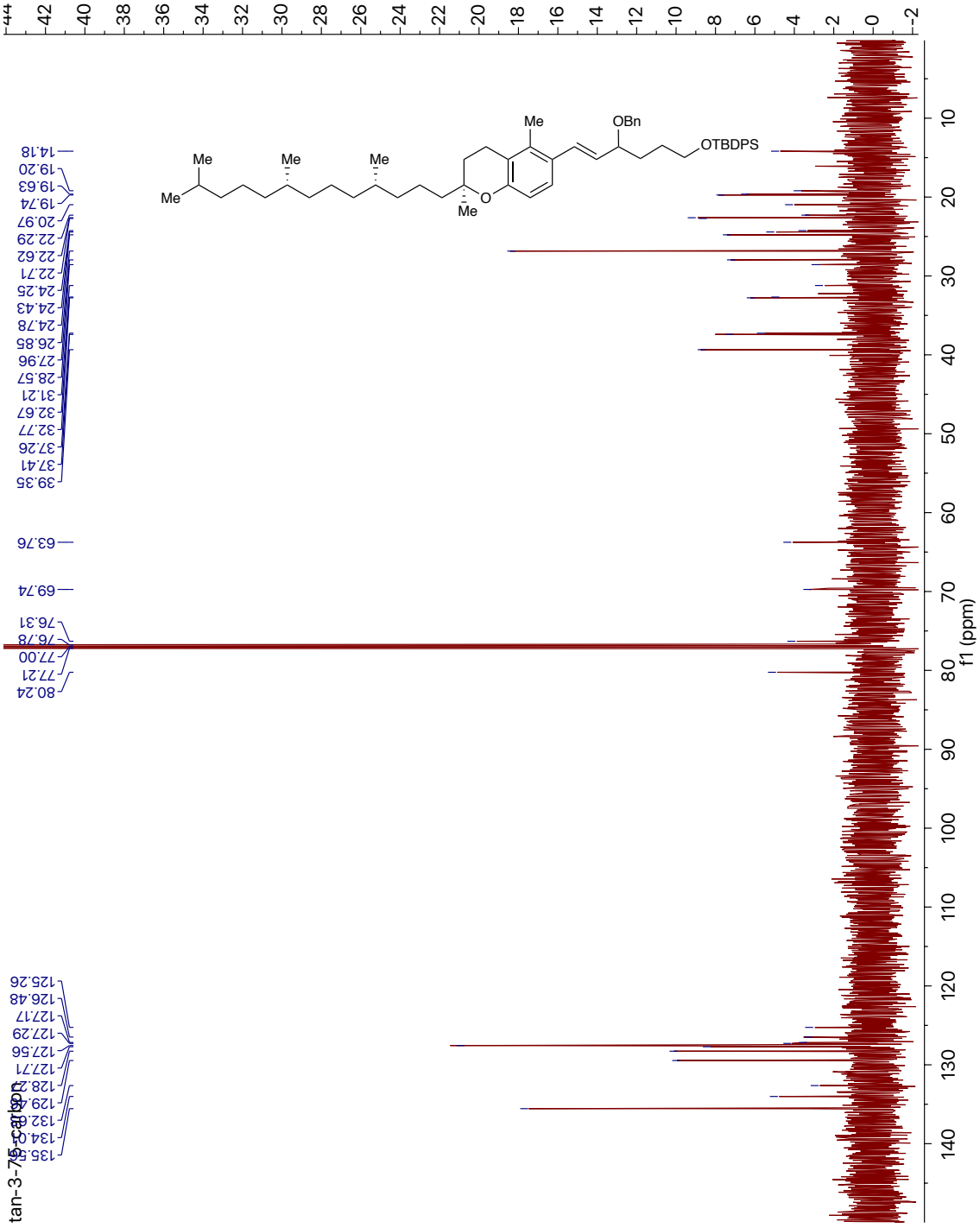

Compound (2-69$_D$/2-69$_{D'}$)

^{1}H NMR (600 MHz, $CDCl_3$)

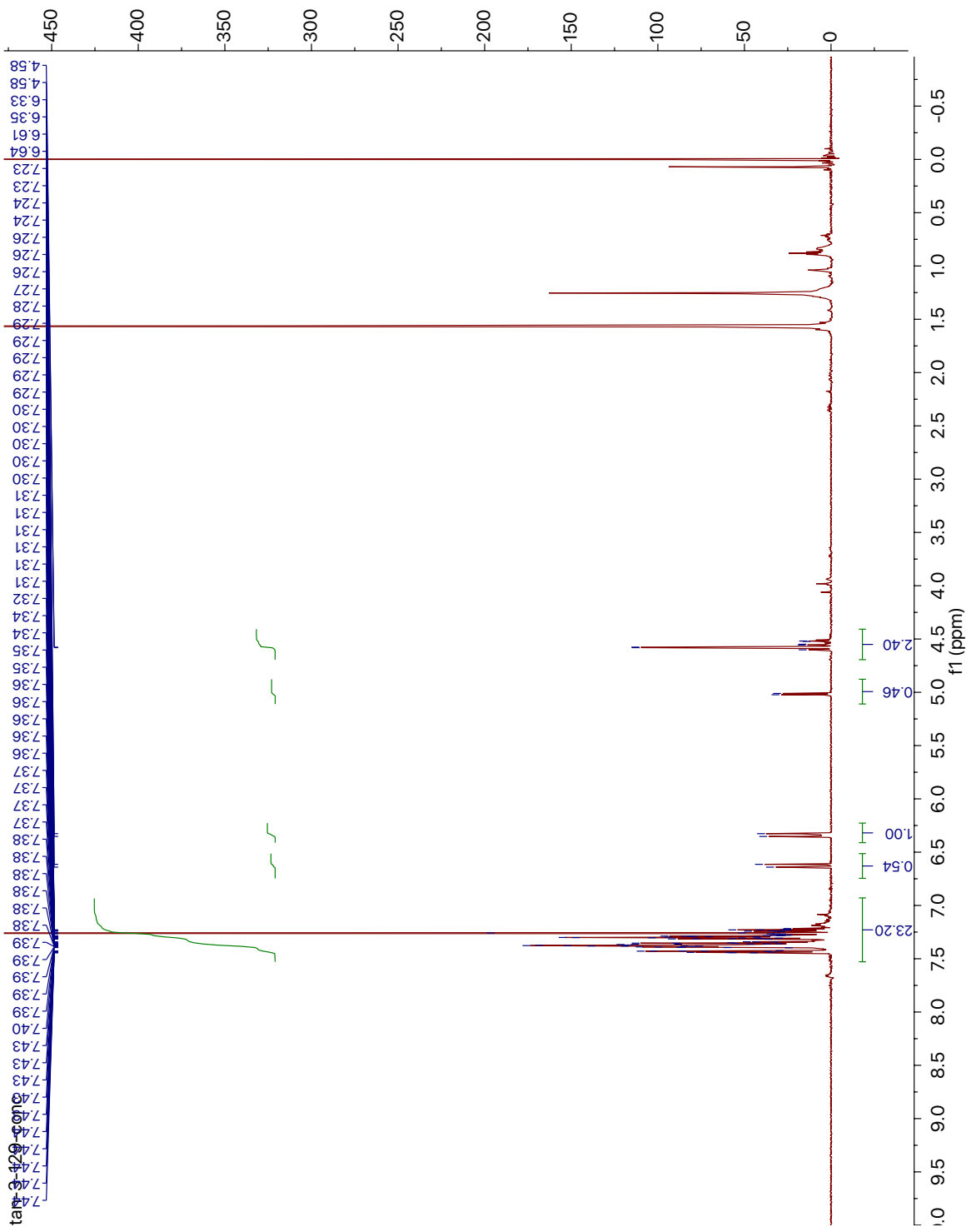

Compound (**2-69**)

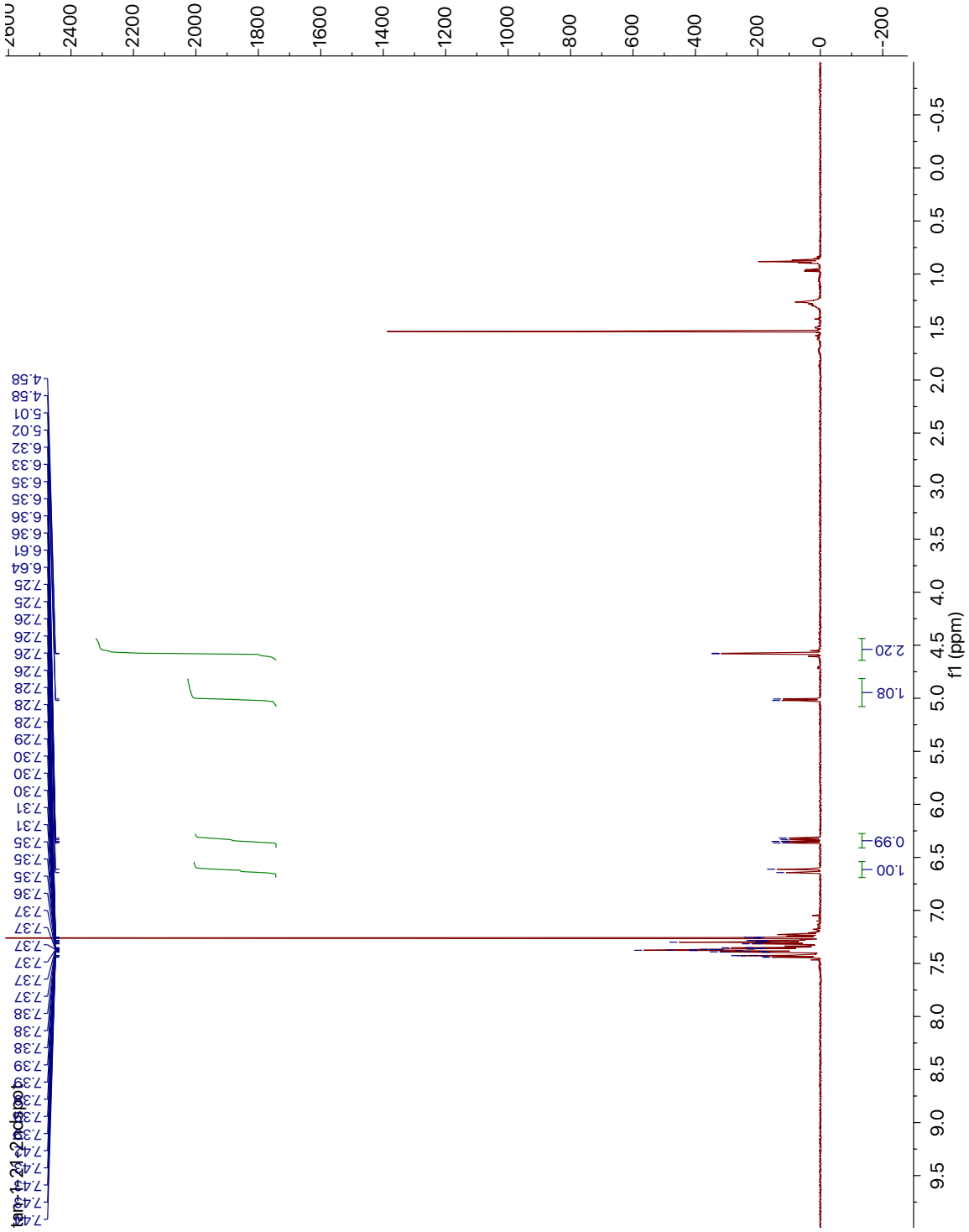

Compound (**2-68*D***)

^{1}H NMR (600 MHz, $CDCl_3$)

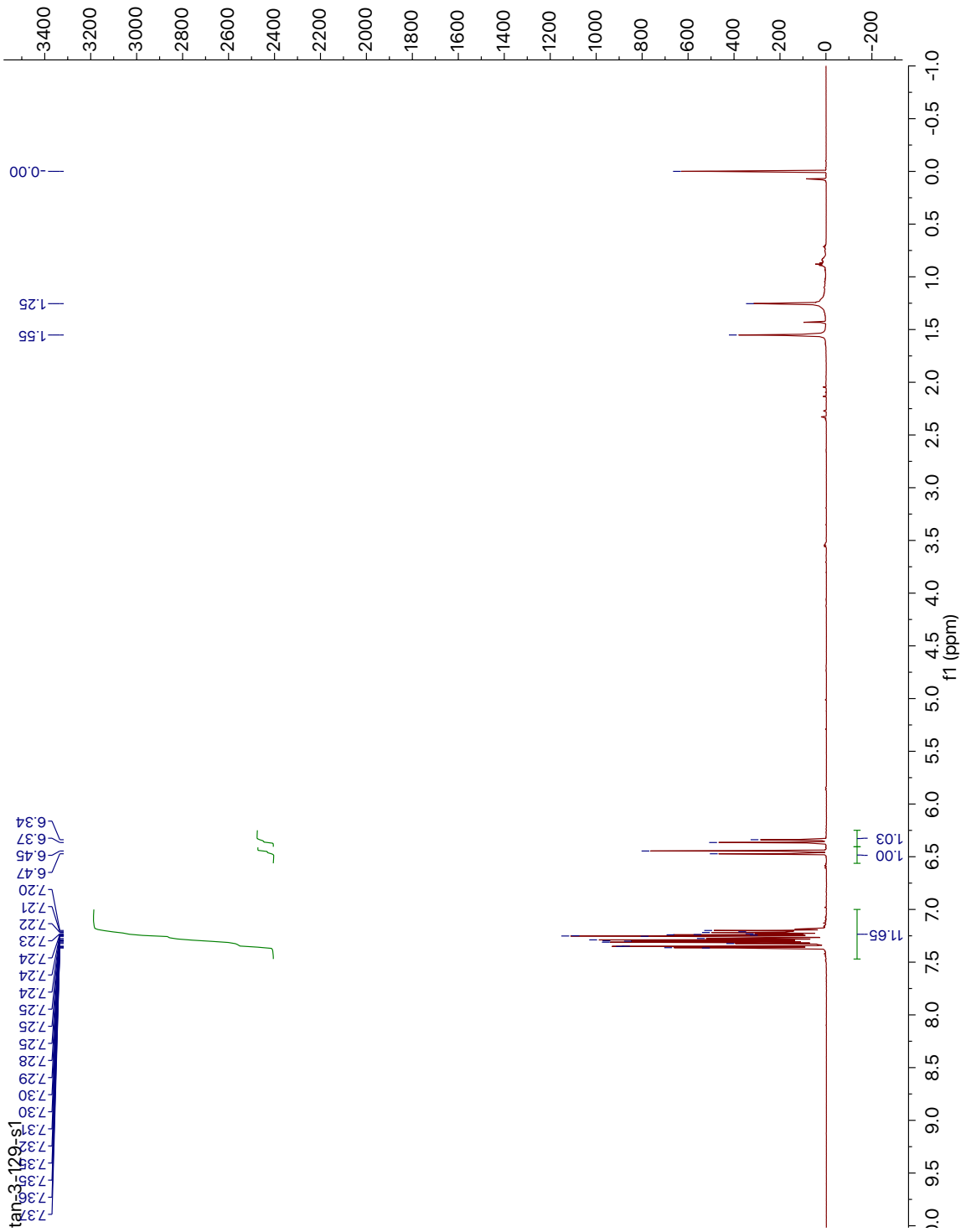

Compound (**2-S2**)

^{1}H NMR (400 MHz, $CDCl_3$)

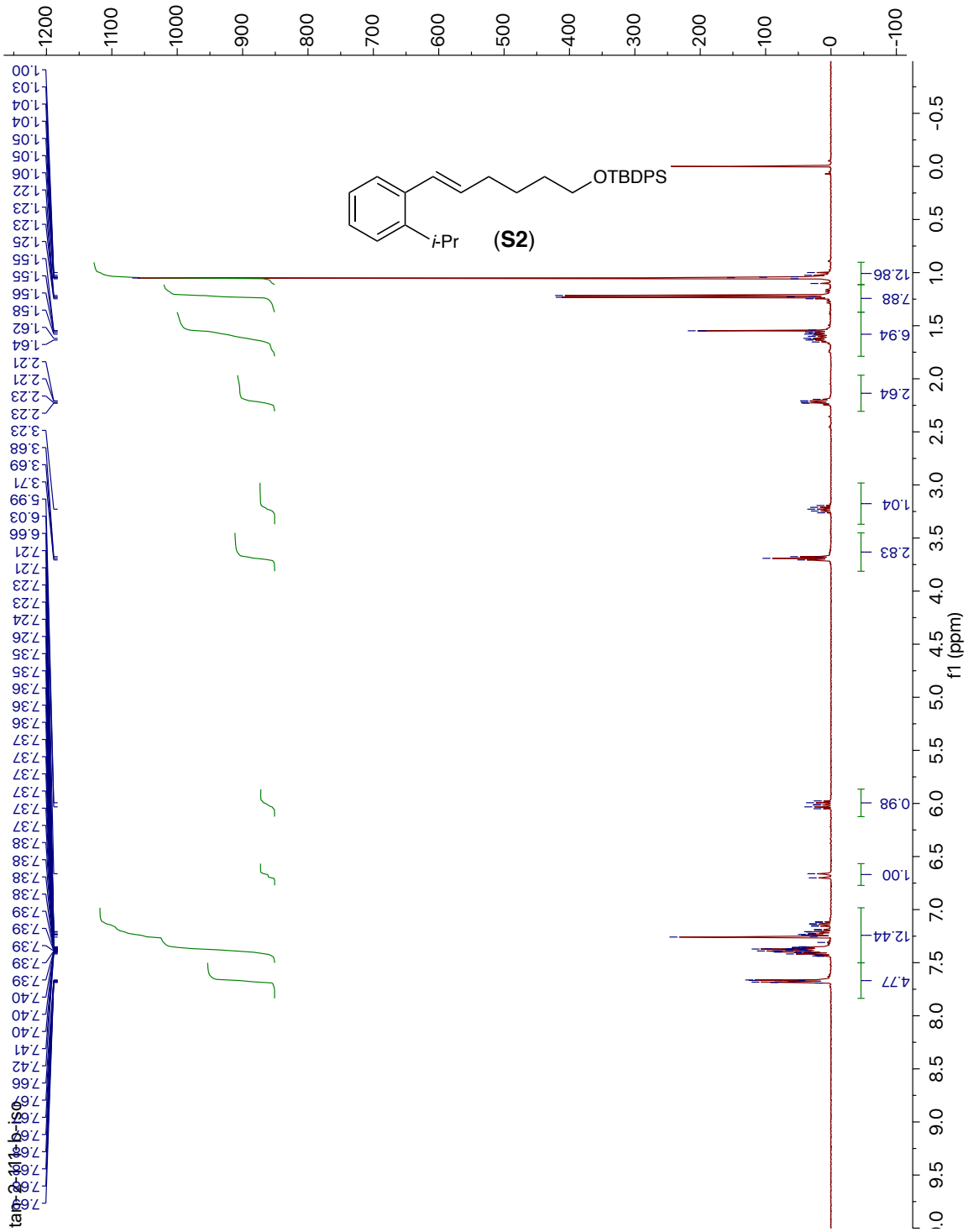

^{13}C NMR (150 MHz, $CDCl_3$)

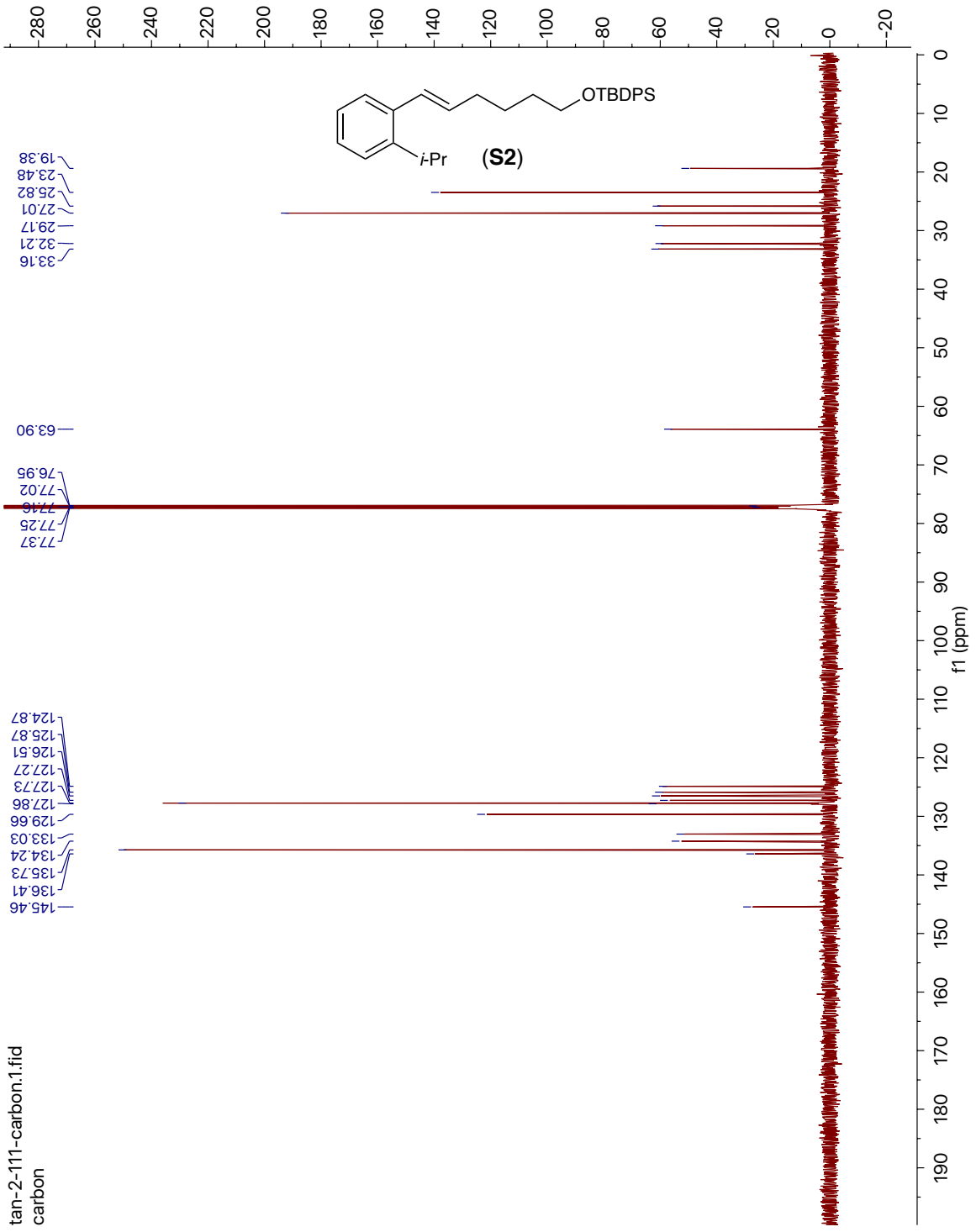

Compound (**2-S3**)

^{1}H NMR (400 MHz, $CDCl_3$)

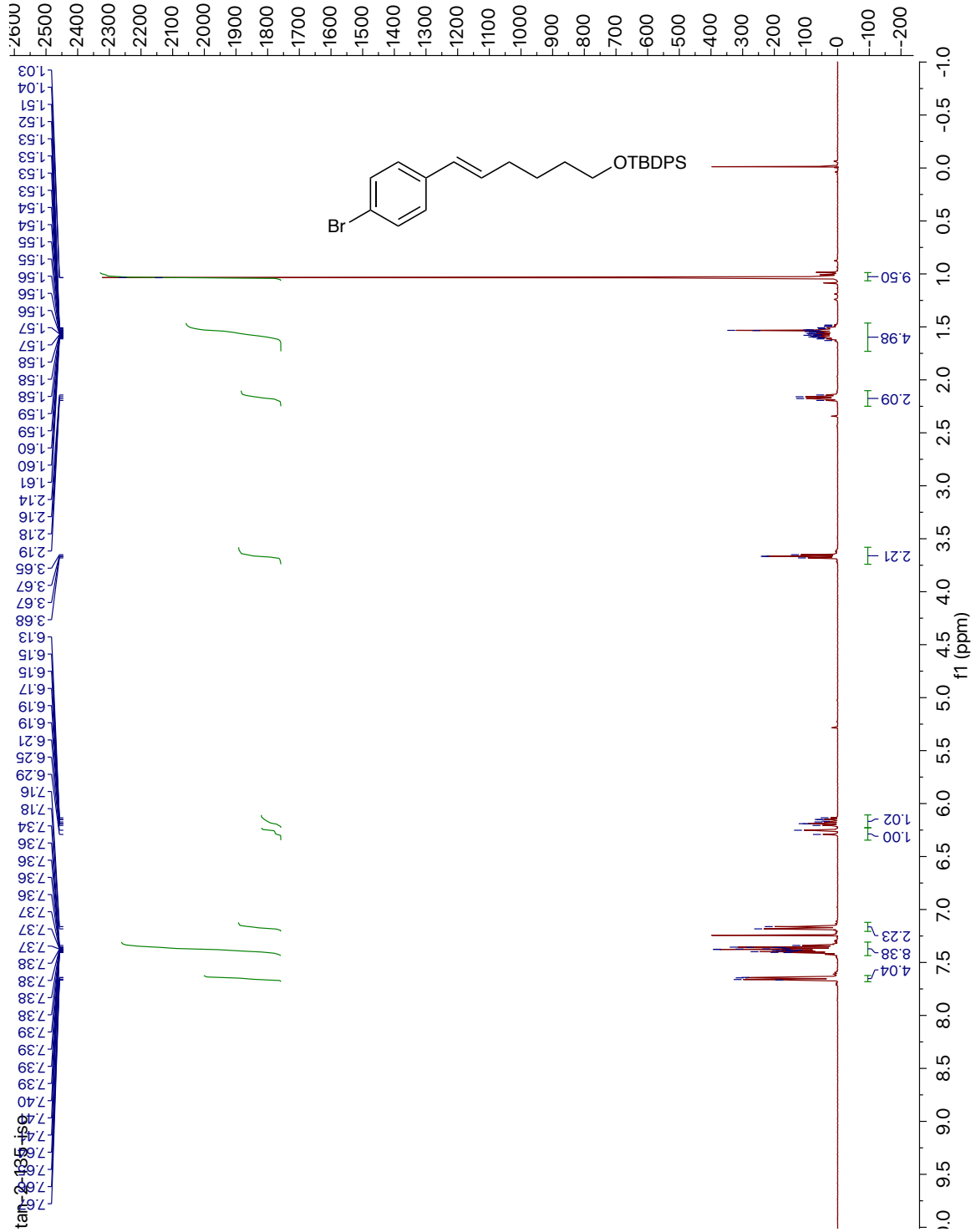

^{13}C NMR (150 MHz, $CDCl_3$)

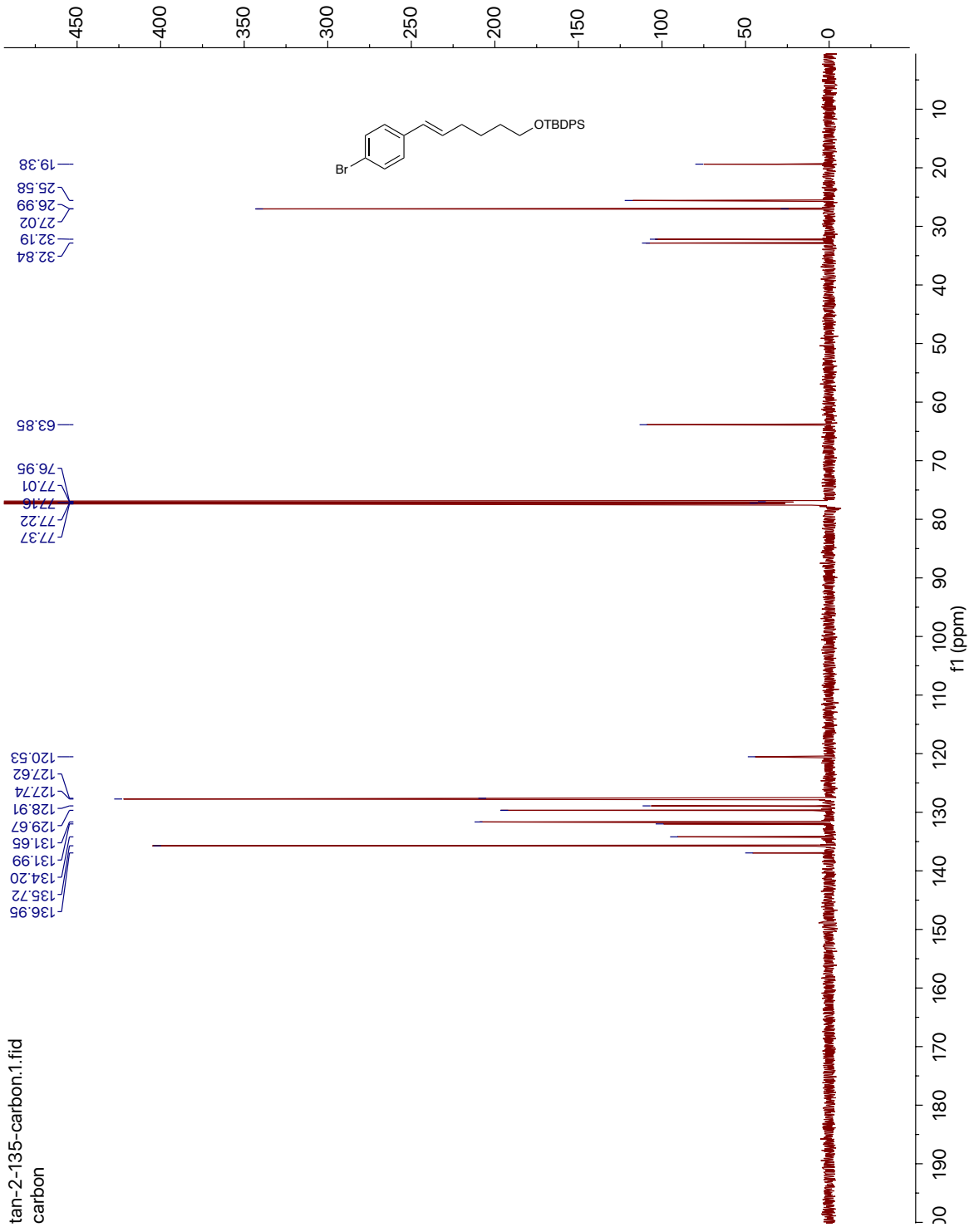

Compound (**2-S5**)

^{1}H NMR (400 MHz, $CDCl_3$)

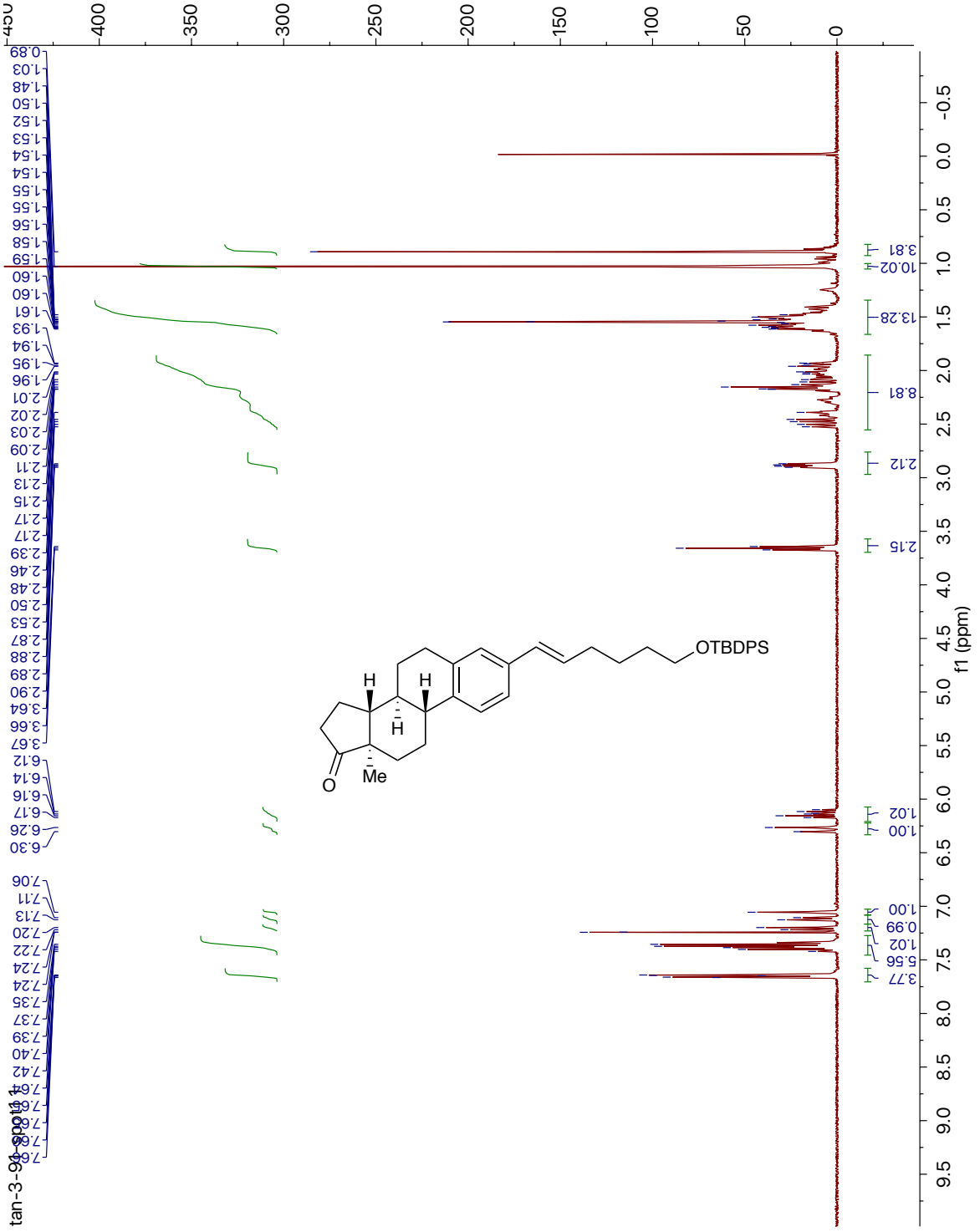

^{13}C NMR (150 MHz, $CDCl_3$)

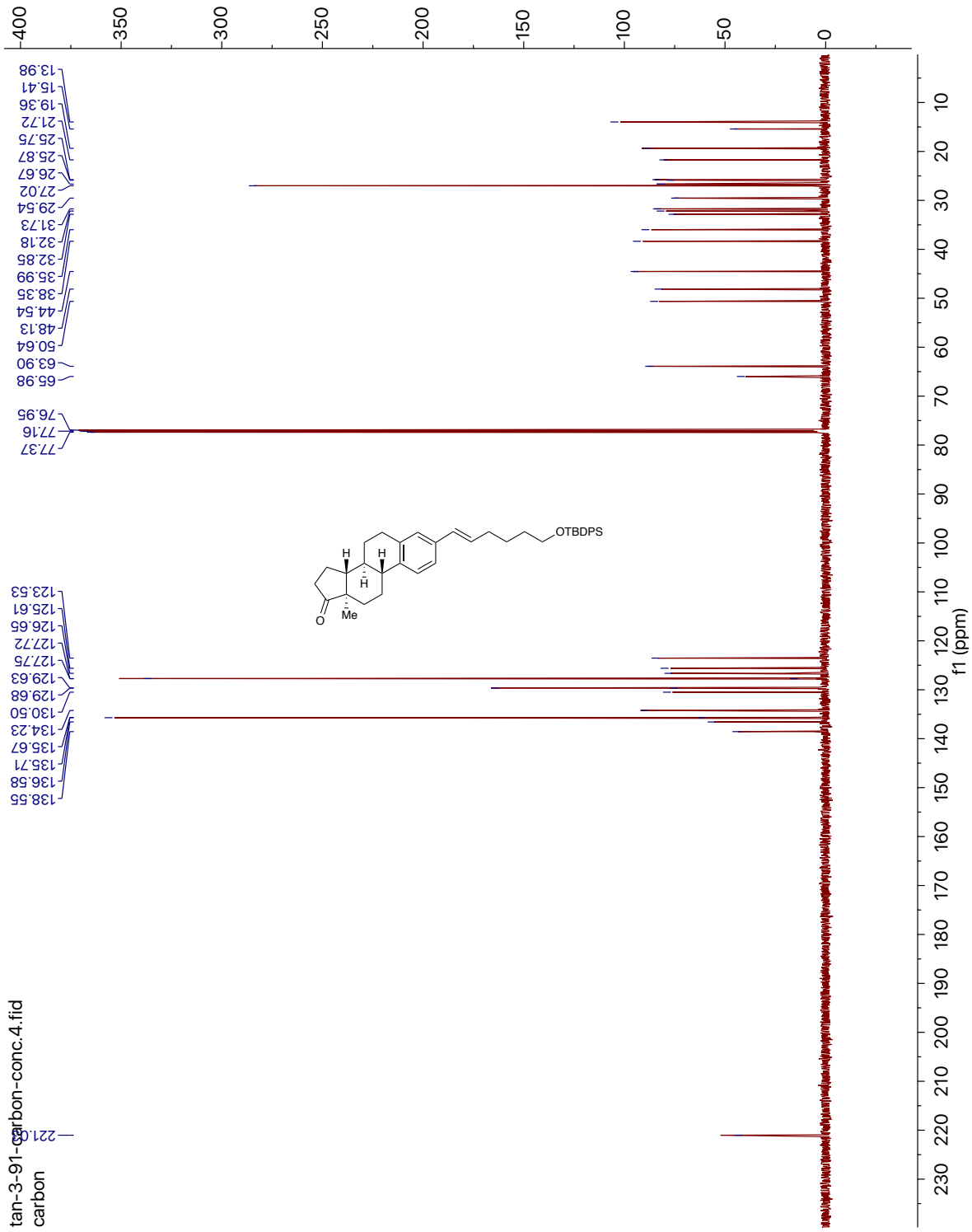

Compound (**2-S7**)

^{1}H NMR (400 MHz, $CDCl_3$)

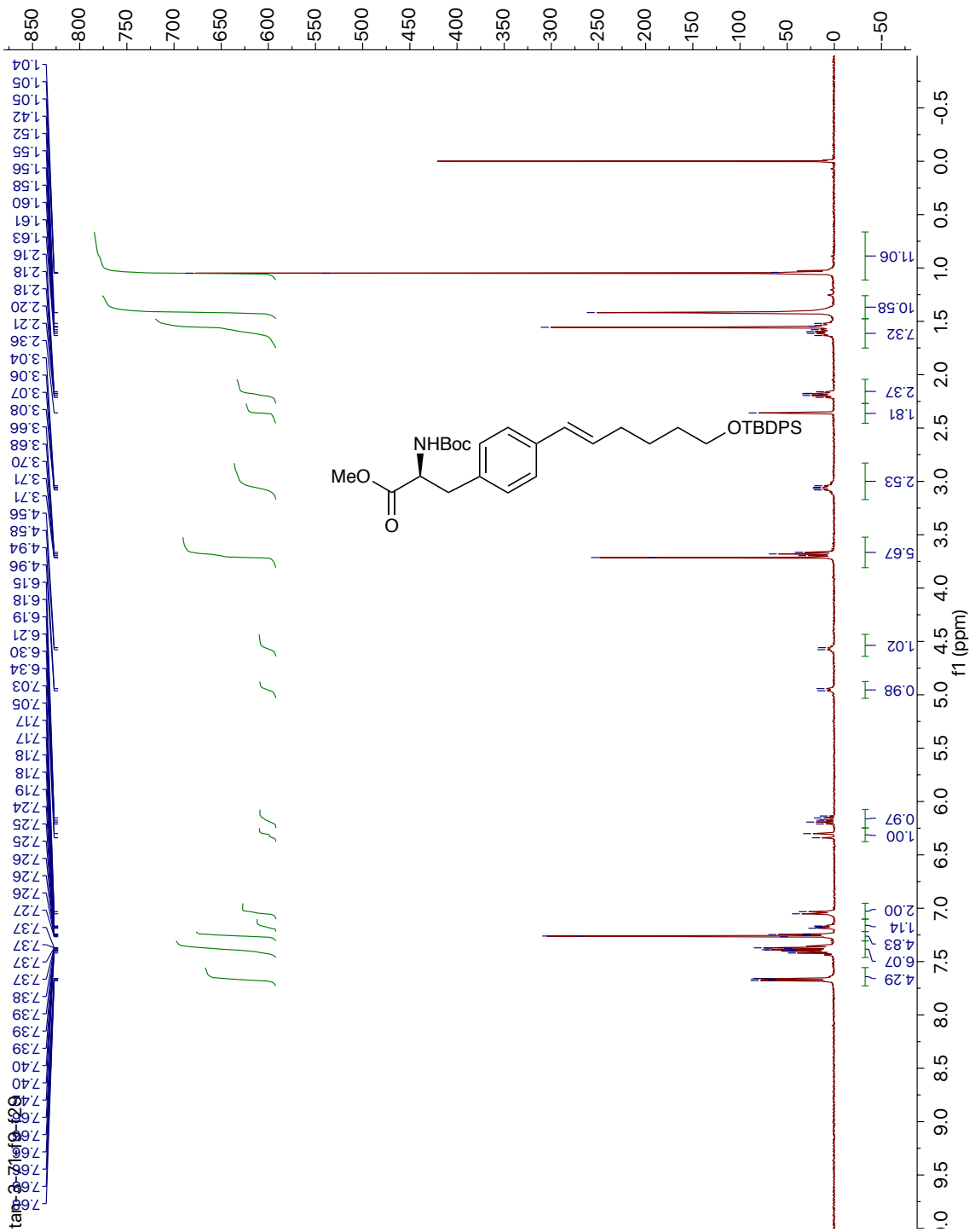

^{13}C NMR (150 MHz, $CDCl_3$)

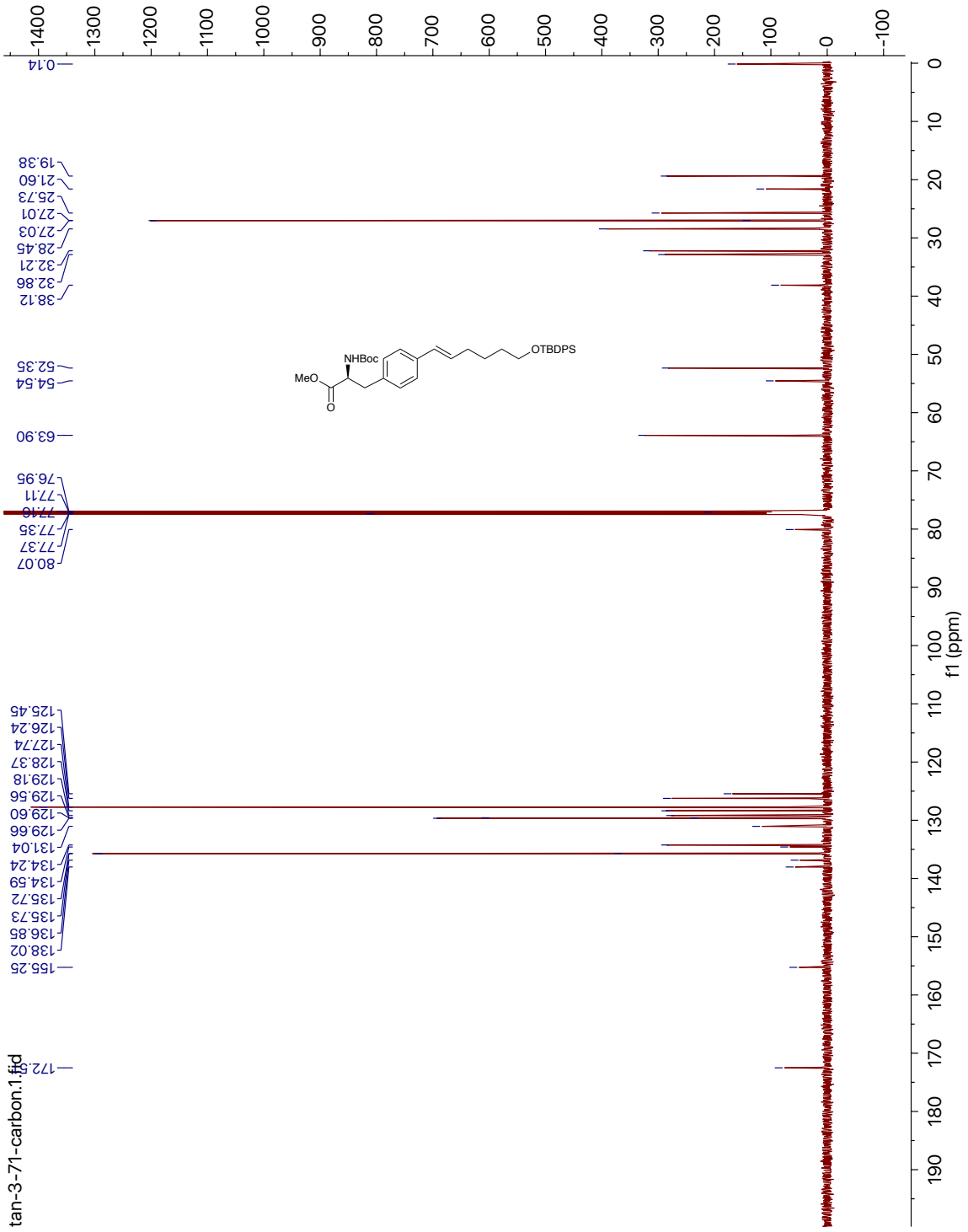

Compound (**2-S9**)

^{1}H NMR (400 MHz, $CDCl_3$)

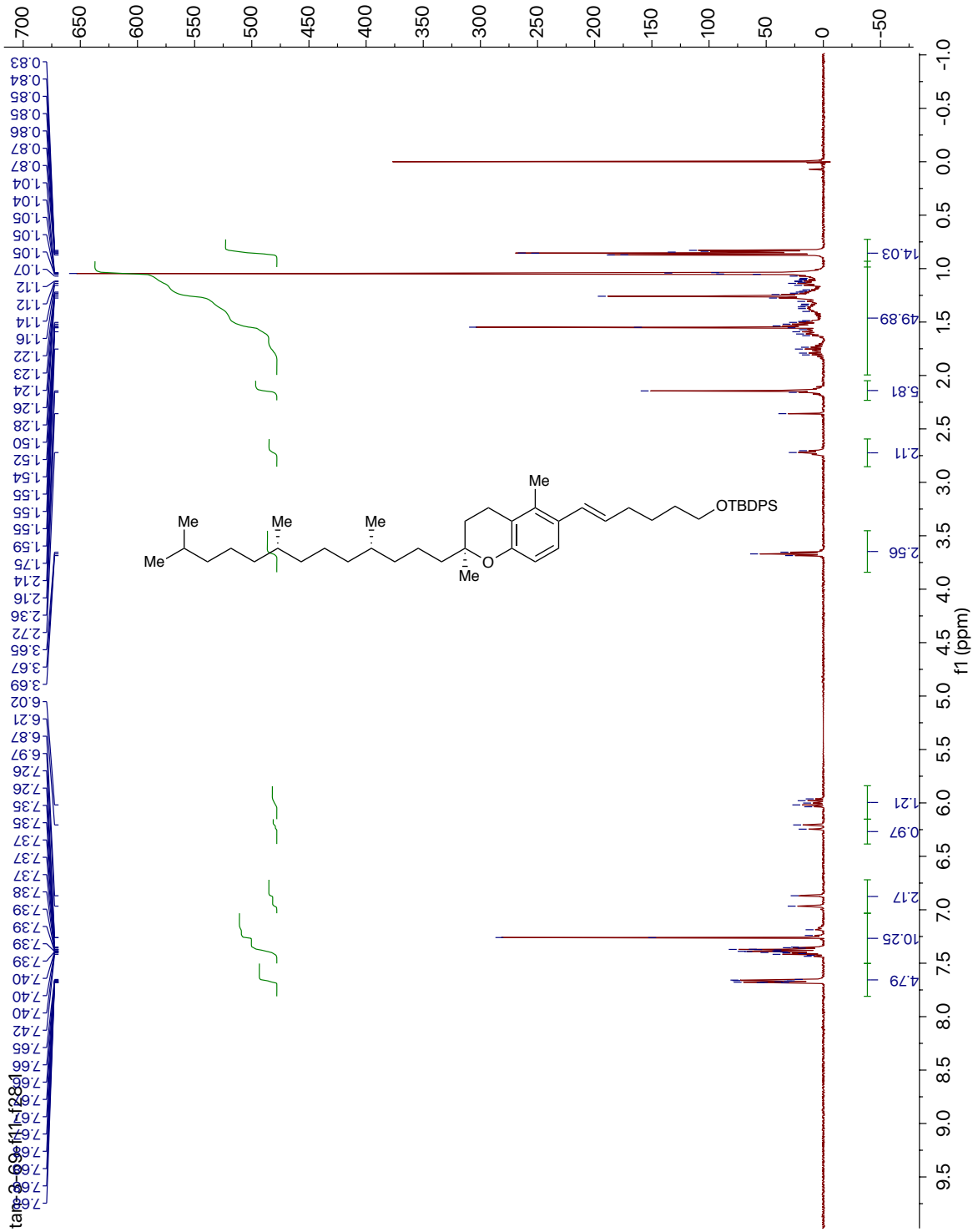

^{13}C NMR (150 MHz, $CDCl_3$)

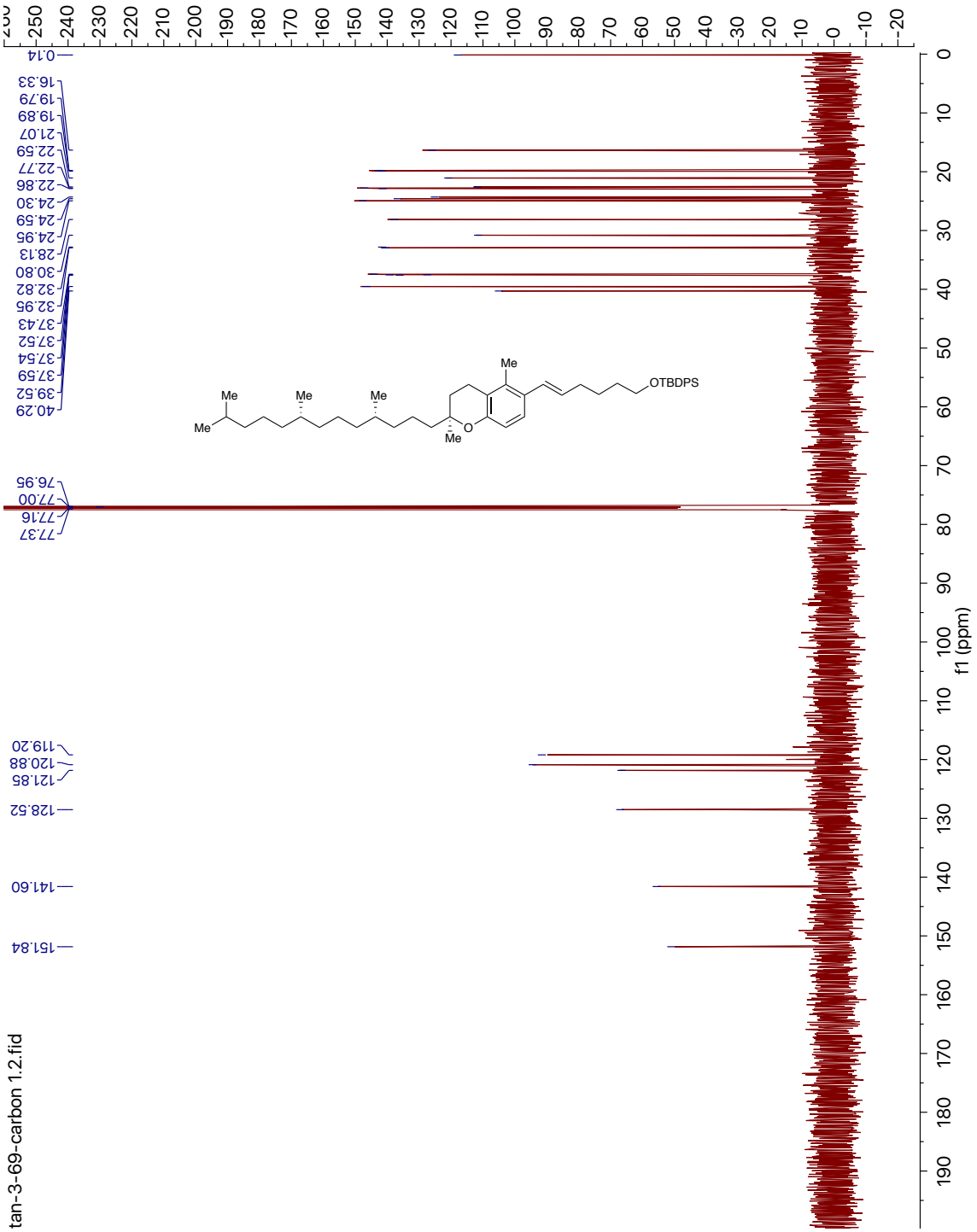

VIII. References

1. Pospíšil, J.; Markó, I. E., Efficient and stereoselective synthesis of allylic ethers and alcohols. *Org. Lett.* **2006,** *8*, 5983-5986.

2. Buckingham, J., *Dictionary of natural products, supplement 4*. CRC press: 1997; Vol. 11.

3. Butt, N. A.; Zhang, W., Transition metal-catalyzed allylic substitution reactions with unactivated allylic substrates. *Chem. Soc. Rev.* **2015,** *44*, 7929-7967.

4. Melvin, J. Y.; Zheng, W.; Seletsky, B. M., From micrograms to grams: scale-up synthesis of eribulin mesylate. *Nat. Prod. Rep.* **2013,** *30*, 1158-1164.

5. Rohloff, J. C.; Kent, K. M.; Postich, M. J.; Becker, M. W.; Chapman, H. H.; Kelly, D. E.; Lew, W.; Louie, M. S.; McGee, L. R.; Prisbe, E. J.; Schultze, L. M.; Yu, R. H.; Zhang, L., Practical Total Synthesis of the Anti-Influenza Drug GS-4104. *J. Org. Chem.* **1998,** *63*, 4545-4550.

6. Laborda, P.; Wang, S.-Y.; Voglmeir, J., Influenza Neuraminidase Inhibitors: Synthetic Approaches, Derivatives and Biological Activity. *Molecules* **2016,** *21*, 1513.

7. Hayashi, Y.; Gotoh, H.; Hayashi, T.; Shoji, M., Diphenylprolinol Silyl Ethers as Efficient Organocatalysts for the Asymmetric Michael Reaction of Aldehydes and Nitroalkenes. *Angew. Chem. Int. Ed.* **2005,** *44*, 4212-4215.

8. Karpf, M.; Trussardi, R., New, Azide-Free Transformation of Epoxides into 1,2-Diamino Compounds: Synthesis of the Anti-Influenza Neuraminidase Inhibitor Oseltamivir Phosphate (Tamiflu). *J. Org. Chem.* **2001,** *66*, 2044-2051.

9. Mita, T.; Fukuda, N.; Roca, F. X.; Kanai, M.; Shibasaki, M., Second Generation Catalytic Asymmetric Synthesis of Tamiflu: Allylic Substitution Route. *Org. Lett.* **2007,** *9*, 259-262.

10. Holton, R. A.; Somoza, C.; Kim, H. B.; Liang, F.; Biediger, R. J.; Boatman, P. D.; Shindo, M.; Smith, C. C.; Kim, S., First total synthesis of taxol. 1. Functionalization of the B ring. *J. Am. Chem. Soc.* **1994,** *116*, 1597-1598.

11. Holton, R. A.; Kim, H. B.; Somoza, C.; Liang, F.; Biediger, R. J.; Boatman, P. D.; Shindo, M.; Smith, C. C.; Kim, S., First total synthesis of taxol. 2. Completion of the C and D rings. *J. Am. Chem. Soc.* **1994,** *116*, 1599-1600.

12. Gennari, C.; Carcano, M.; Donghi, M.; Mongelli, N.; Vanotti, E.; Vulpetti, A., Taxol Semisynthesis: A Highly Enantio- and Diastereoselective Synthesis of the Side Chain and a New Method for Ester Formation at C-13 Using Thioesters. *J. Org. Chem.* **1997,** *62*, 4746-4755.

13. Koschker, P.; Breit, B., Branching Out: Rhodium-Catalyzed Allylation with Alkynes and Allenes. *Acc. Chem. Res.* **2016,** *49*, 1524-1536.

14. Olson, A. C.; Overman, L. E.; Sneddon, H. F.; Ziller, J. W., Catalytic Asymmetric Synthesis of Branched Chiral Allylic Phenyl Ethers from (E)-Allylic Alcohols. *Adv. Synth. Catal.* **2009,** *351*, 3186-3192.

15. Kirsch, S. F.; Overman, L. E.; White, N. S., Catalytic Asymmetric Synthesis of Allylic Aryl Ethers. *Org. Lett.* **2007,** *9*, 911-913.

16. Dewolfe, R. H.; Young, W. G., Substitution And Rearrangement Reactions Of Allylic Compounds. *Chem. Rev.* **1956,** *56*, 753-901.

17. Guibé, F., Allylic protecting groups and their use in a complex environment part I: Allylic protection of alcohols. *Tetrahedron* **1997,** *53*, 13509-13556.

18. Honda, M.; Takatera, T.; Ui, R.; Kunimoto, K.-K.; Segi, M., Stereoselective synthesis of allyl ethers using α,β-unsaturated acylsilanes. *Tetrahedron Lett.* **2017,** *58*, 864-869.

19. Mifleur, A.; Mérel, D. S.; Mortreux, A.; Suisse, I.; Capet, F.; Trivelli, X.; Sauthier, M.; Macgregor, S. A., Deciphering the Mechanism of the Nickel-Catalyzed Hydroalkoxylation Reaction: A Combined Experimental and Computational Study. *ACS Catal.* **2017,** *7*, 6915-6923.

20. Wang, R.; Luan, Y.; Ye, M., Transition Metal–Catalyzed Allylic C(sp^3)–H Functionalization via η^3 -Allylmetal Intermediate. *Chin. J. Chem.* **2019,** *37*, 720-743.

21. Li, C.; Li, M.; Li, J.; Liao, J.; Wu, W.; Jiang, H., Palladium-Catalyzed Aerobic Oxygenation of Allylarenes. *J. Org. Chem.* **2017,** *82*, 10912-10919.

22. Qi, X.; Chen, P.; Liu, G., Catalytic oxidative trifluoromethoxylation of allylic C− H bonds using a palladium catalyst. *Angew. Chem. Int. Ed.* **2017,** *56*, 9517-9521.

23. Zhang, X.; Tang, P., Recent advances in new trifluoromethoxylation reagents. *Science China Chemistry* **2019**.

24. Deng, Z.; Zhao, M.; Wang, F.; Tang, P., Selective C–H trifluoromethoxylation of (hetero)arenes as limiting reagent. *Nat. Commun.* **2020,** *11*, 2569.

25. Clayden, J., Fluorinated compounds present opportunities for drug discovery. *Nature* **2019,** *573*, 37-38.

26. Zhou, Y.; Wang, J.; Gu, Z.; Wang, S.; Zhu, W.; Aceña, J. L.; Soloshonok, V. A.; Izawa, K.; Liu, H., Next Generation of Fluorine-Containing Pharmaceuticals, Compounds Currently in Phase II–III Clinical Trials of Major Pharmaceutical Companies: New Structural Trends and Therapeutic Areas. *Chem. Rev.* **2016,** *116*, 422-518.

27. Cochet, T.; Bellosta, V.; Roche, D.; Ortholand, J.-Y.; Greiner, A.; Cossy, J., Rhodium (III)-catalyzed allylic C–H bond amination. Synthesis of cyclic amines from ω-unsaturated N-sulfonylamines. *Chem. Commun.* **2012,** *48*, 10745-10747.

28. Shibata, Y.; Kudo, E.; Sugiyama, H.; Uekusa, H.; Tanaka, K., Facile Generation and Isolation of π-Allyl Complexes from Aliphatic Alkenes and an Electron-Deficient Rh(III) Complex: Key Intermediates of Allylic C–H Functionalization. *Organometallics* **2016,** *35*, 1547-1552.

29. Burman, J. S.; Blakey, S. B., Regioselective Intermolecular Allylic C–H Amination of Disubstituted Olefins via Rhodium/π-Allyl Intermediates. *Angew. Chem. Int. Ed.* **2017,** *56*, 13666-13669.

30. Lotz, M. D.; Camasso, N. M.; Canty, A. J.; Sanford, M. S., Role of Silver Salts in Palladium-Catalyzed Arene and Heteroarene C–H Functionalization Reactions. *Organometallics* **2016,** *36*, 165–171.

31. Evans, P. A.; Tsuji, J., *Modern Rhodium-Catalyzed Organic Reactions*. Wiley: 2005.

32. Simmons, E. M.; Hartwig, J. F., On the Interpretation of Deuterium Kinetic Isotope Effects in C–H Bond Functionalizations by Transition-Metal Complexes. *Angew. Chem. Int. Ed.* **2012,** *51*, 3066-3072.

33. Nelson, T. A. F.; Blakey, S. B., Intermolecular Allylic C–H Etherification of Internal Olefins. *Angew. Chem. Int. Ed.* **2018,** *57*, 14911-14915.

34. Shyshov, O.; Brachvogel, R.-C.; Bachmann, T.; Srikantharajah, R.; Segets, D.; Hampel, F.; Puchta, R.; Von Delius, M., Adaptive Behavior of Dynamic Orthoester Cryptands. *Angew. Chem., Int. Ed.* **2016,** *56*, 776-781.

35. Trillo, P.; Baeza, A.; Nájera, C., Fluorinated Alcohols As Promoters for the Metal-Free Direct Substitution Reaction of Allylic Alcohols with Nitrogenated, Silylated, and Carbon Nucleophiles. *J. Org. Chem.* **2012,** *77*, 7344-7354.

36. Pati, K.; dos Passos Gomes, G.; Harris, T.; Hughes, A.; Phan, H.; Banerjee, T.; Hanson, K.; Alabugin, I. V., Traceless Directing Groups in Radical Cascades: From Oligoalkynes to Fused Helicenes without Tethered Initiators. *J. Am. Chem. Soc.* **2015,** *137*, 1165-1180.

37. Stacey, W.; R., S. D.; Ai-Lan, L., Chirality Transfer in Gold(I)-Catalysed Hydroalkoxylation of 1,3-Disubstituted Allenes. *Chem. Eur. J.* **2016,** *22*, 18593-18600.

38. Tan, J.; Zhang, Z.; Wang, Z., A novel palladium-catalyzed hydroalkoxylation of alkenes with a migration of double bond. *Org. Biomol. Chem.* **2008,** *6*, 1344-1348.

39. Tanaka, S.; Saito, Y.; Yamamoto, T.; Hattori, T., Electrophilic Borylation of Terminal Alkenes with BBr3/2,6-Disubstituted Pyridines. *Org. Lett.* **2018,** *20*, 1828-1831.

40. Horwitz, J. P.; Iyer, V. K.; Vardhan, H. B.; Corombos, J.; Brooks, S. C., In vitro inhibition of estrogen sulfoconjugation by some 2- and 4-substituted estra-1,3,5(10)-trien-17.beta.-ols. *J. Med. Chem.* **1986,** *29*, 692-698.

41. Furuya, T.; Strom, A. E.; Ritter, T., Silver-Mediated Fluorination of Functionalized Aryl Stannanes. *J. Am. Chem. Soc.* **2009,** *131*, 1662-1663.

Chapter 3: The Mechanism of Rhodium-Catalyzed Allylic C–H Amination Proceeding via a Rh(IV)-π-allyl Intermediate

I. Introduction: Mechanisms in C–H Functionalization

I.1. Rh(III)/Rh(I) Catalytic Cycles

C–H functionalization has proven to be a powerful technique to form important functional motifs and, in many cases, provides complementary reactivity to more traditional methods. While many transition-metal catalysts have been utilized for C–H functionalization, group(IX)Cp* metal catalysts are of particular interest due to their broad reactivity and use in allylic C–H functionalization.[1, 2] Unpublished work to develop an enantioselective allylic C–H amination protocol suggested that the mechanism of RhCp*-catalyzed allylic C–H amination might be more complex than originally thought. Group(IX) Cp* catalyzed directed C(sp^2)-H functionalization has been well-studied and the mechanistic understanding of these reactions may inform recent work for allylic C–H functionalization.[3,4]

In this case, directed C–H functionalization is typically initiated by the coordination of a metal catalyst by a directing group (**3-3**).[4] This coordination poises the metal center to activate the desired C–H bond via concerted-metalation deprotonation (**3-4**) with a carboxylate source (**Figure 3-1**). Activation of the C–H bond, in the case of RhCp* catalysts, forms rhodacycle **3-5.** Coordination of the coupling partner to complex **3-5** would then provide complex **3-6**. At this point, reductive elimination from complex **3-6** produces Rh(I) complex **3-7**, releasing the desired compound **3-8.** Reoxidation and ligand association then

completes the catalytic cycle. This Rh(III)/Rh(I) mechanism has been well-studied and supported experimentally and computationally.[4] The prevalence of this mechanistic paradigm for RhCp* precatalysts supported Cossy's original theory of a Rh(III)/Rh(I) allylic C–H amination discussed earlier (Chapter 1).[5]

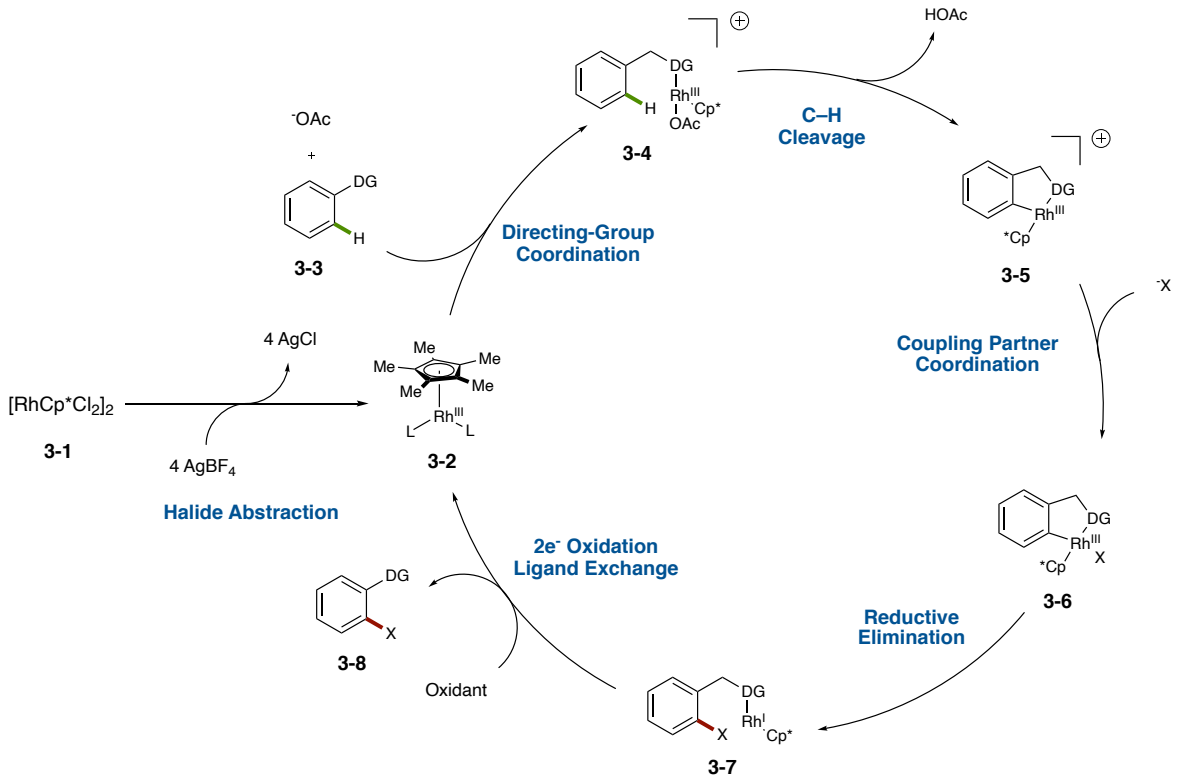

Figure 3-1. Directed C–H Functionalization via a Rh(III)/(I) Catalytic Cycle

I.2. Rh(III)/Rh(V) Catalytic Cycles

With an excess of external oxidant and other oxidizing reagents in C–H functionalization reactions, another mechanistic paradigm began to emerge.[4] In 2006 the Sanford group performed mechanistic work to supporting high-valent palladium

intermediates in C–H functionalization.[3] The use of oxidizing directing groups and other oxidizing coupling reagents lead some to consider high-valent rhodium species as intermediates as well. These oxidizing reagents typically react via carbene or nitrene intermediates and would result in a M(V) complex. Unfortunately, these M(V) oxidized species have not been isolated, likely due to their highly reactive nature. For this reason, the mechanistic data has had to rely heavily on DFT calculations. Furthermore, Glorius and co-workers published a perspective suggesting that cyclic voltammetry and ^{103}Rh NMR studies may be able to shed further light on this subject.[4] In this perspective, the authors propose a catalytic cycle that proceeds to complex **3-5** much like that of the Rh(III)/Rh(I) system described above (**Figure 3-2**). After the formation of complex **3-5**, reductive elimination does not occur, rather, oxidation to Rh(V) complex **3-9** is favored coupled with nitrene or carbene formation. Reductive elimination of complex **3-9** forms the desired product (**3-10**) as well as Rh(III) complex (**3-2**) to complete the catalytic cycle. While not fully accepted at the time of the mentioned perspective, more work has supported this novel Rh(III)/Rh(V) catalytic cycle relying on oxidative coupling reagents.[6]

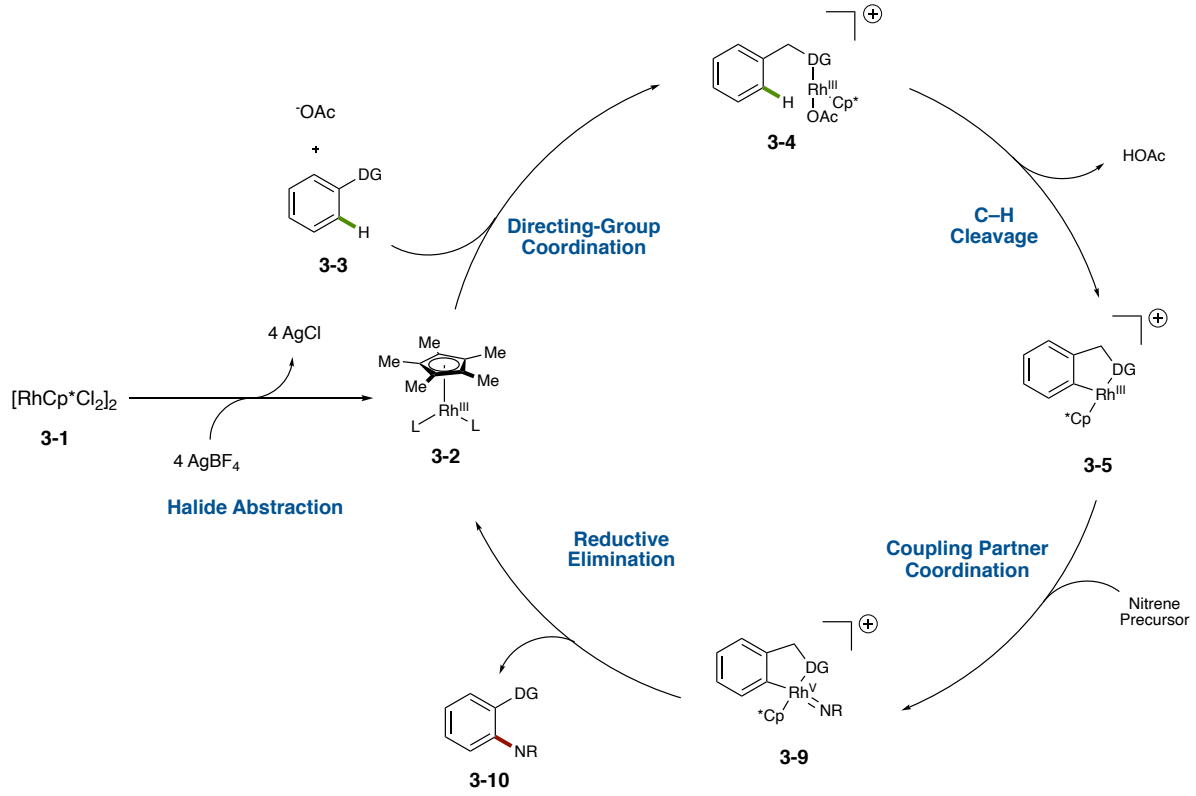

Figure 3-2. RhCp* Mechanism for C–H Functionalization using Oxidative Coupling Reagents

I.3. Ir(III)/Ir(IV)/Ir(II) Catalytic Cycles

Sukbok Chang and co-workers have performed in depth experimental analysis of various IrCp* catalyzed C–H functionalization reactions supported to proceed through a Ir(IV) or Ir(V) oxidation state.[6, 7] In these examples, directed C–H functionalization typically provides an isolable Ir(III) organometallic complex (**3-5**), which was determined to only provide reductive elimination product (**3-8**) after oxidation. For this reason, these reactions are known to proceed via an oxidatively induced reductive elimination (ORE). Much like the previous two mechanistic classes, complex **3-5** is formed through concerted-metalation deprotonation. Oxidation of complex **3-5** to the Ir(IV) oxidation state (**3-11**) is followed by

reductive elimination to form complex **3-12**. Oxidation of complex **3-12** and ligand exchange completes the catalytic cycle by providing the Ir(III) complex (**3-2**). This M(III)/M(IV)/M(II) catalytic cycle has been supported by stoichiometric oxidation and cyclic voltammetry studies and is a relatively new mechanism to be considered for C–H functionalization. There have also been similar reports proceeding through an M(V) oxidation state relying on external oxidants rather than the oxidizing coupling reagents described in (**Figure 3-3**).[8] While no mechanism can be fully proven, it became evident that higher valent species in group(IX)Cp* catalysis were feasible and should be considered for further mechanistic studies.

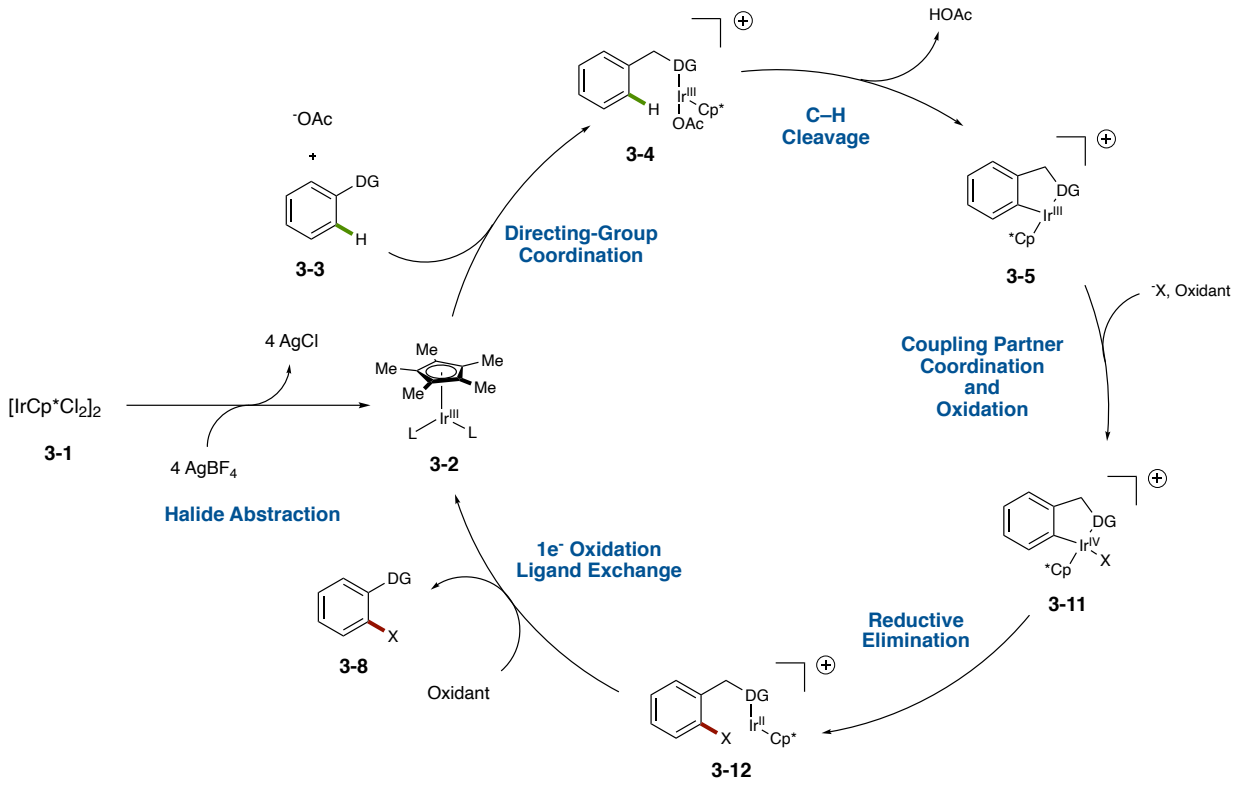

Figure 3-3. Oxidatively Induced Reductive Elimination Ir(III)/Ir(IV)/Ir(II) Catalytic Cycle

I.4. Stoichiometric π-allyl Complex Reactivity

A powerful means of understanding group(IX)Cp*-catalyzed allylic C–H functionalization reactions is through the stoichiometric isolation and reactivity of putative RhCp*-π-allyl complexes. In fact, stoichiometric reactivity of isolated π-allyl complexes has been studied with hard nucleophiles by Stryker and Bergman (**Figure 3-4**).[9, 10] In both cases, the authors observed nucleophilic attack at the C2 position of the π-allyl complex (**3-13, 3-16**) to form a metallobutane intermediate (**3-14, 3-15, 3-17**). Interestingly, Bergman's work utilized phosphine supporting ligands on rhodium while Stryker focused on ethylene complexes on iridium. In both cases, direct reductive elimination of the ligand is unfavored, relying on hard nucleophiles for reactivity. Furthermore, Tanaka and co-workers developed a method to form $RhCp^E$-π-allyl complexes through stoichiometric C–H functionalization, which was discussed in detail in Chapter 2.[11] When Tanaka reacted complex **3-18** with a halide scavenger ($AgSbF_6$), and oxidant ($Cu(OAc)_2$), nucleophilic addition at the C1/C3 position was observed (**3-19**). The difference in selectivities may be a result of inner-sphere reductive elimination or outersphere attack of the nucleophile or the relative hard or soft nature of the nucleophile, but this is unclear. These disclosures are the few examples of stoichiometric RhCp* and IrCp* π-allyl complex reactivity. It became clear that foundational work to study RhCp*-π-allyl complexes as catalytic intermediates would be needed to provide mechanistic insight for allylic C–H functionalization reactions.

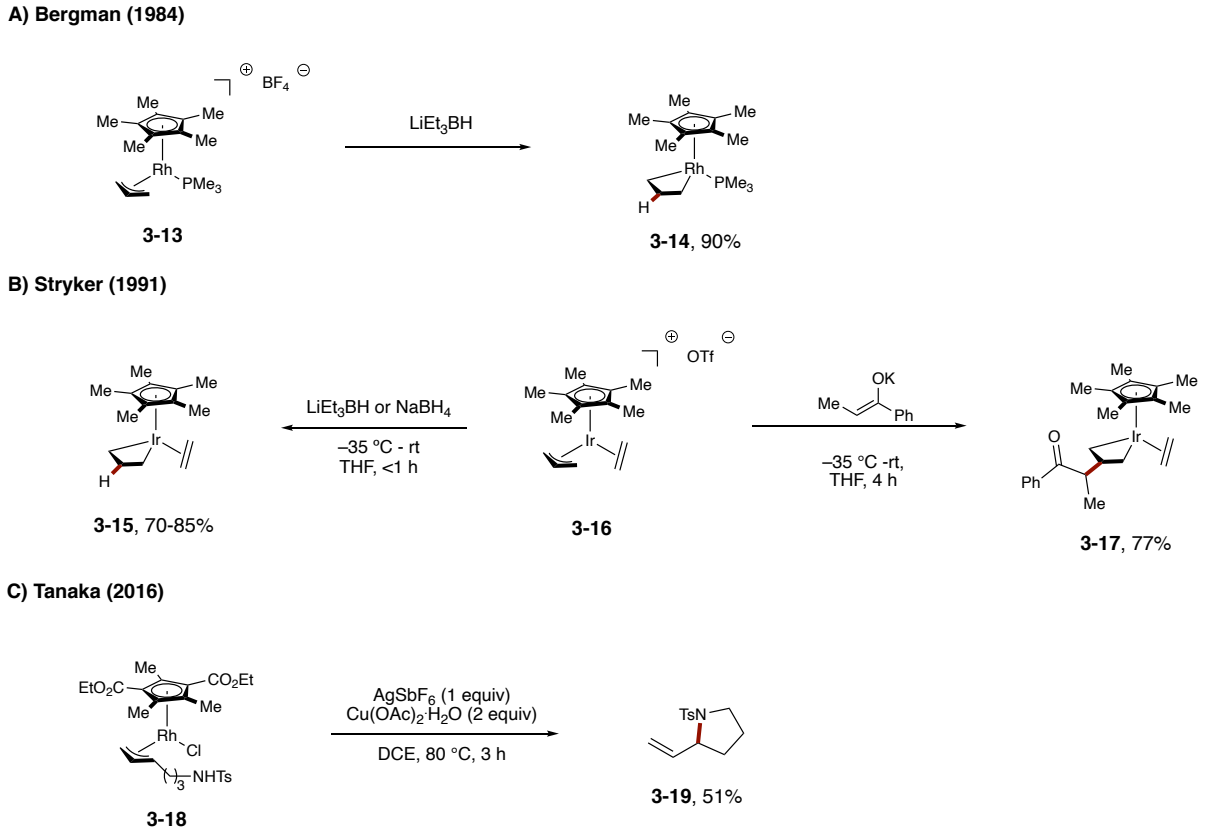

Figure 3-4. Stoichiometric Group(IX)Cp*-π-allyl Complex Reactivity

II. Results and Discussion

The First-generation amination[12] and etherification[13] procedures disclosed by our lab were originally believed to proceed through a Rh(III)/Rh(I) catalytic cycle, much like that proposed by Cossy and co-workers described in Chapter 1.[5] If this were the case, one would expect regio- and enantiocontrol to be afforded by the reductive elimination of the product from the metal-center. To test this, Jacob Burman, a previous graduate student in our lab, performed research with the Cramer group using their large library of enantioselective RhCp catalysts.[14, 15] During these studies no enantioinduction was ever

observed for C–N, C–O, or C–C bond formation. If direct reductive elimination from the metal-center was occurring, enantioselectivity should have been observed even in low quantities. Unfortunately, this was not the case. A full mechanistic study would provide insight for the development of an enantioselective method. For this reason, we began a full mechanistic investigation of the amination protocol in collaboration with Dr. Baik and Dr. MacBeth for their computational and electrochemical expertise, respectively.[16]

II.1. Kinetic Analysis and Determination of the Rate-determining Step

With the knowledge described above in hand, we knew that a novel mechanism might be facilitating this reaction. To probe the rate-law, initial-rate kinetics were performed (**Figure 3-5**). Daniel Salguiero, a previous undergraduate researcher in our lab, utilized *N*-benzylcarbamate and 1,3-diphenylpropene with $[RhCp^*Cl_2]_2$ and $AgBF_4$ under the standard reaction conditions from the original report to study the rates of this reaction. These experiments revealed that the reaction was first order in [Rh] and alkene (**3-20**), and inverse order with respect to carbamate **3-21**. The initial rates for [Rh], alkene, and 1/carbamate provided slopes of $k_1 = 2.4 \pm 0.4 \times 10^{-4}$ s^{-1}, $k_2 = 1.5 \pm 0.1 \times 10^{-5}$ s^{-1}, and $k_3 = 1.4 \pm 0.2 \times 10^{-6}$ M^2 s^{-1}, respectively. This information suggests that the *N*-benzylcarbamate may bind to the active catalyst in an off-cycle resting state. For further understanding, determination of the rate-determining step was then pursued.

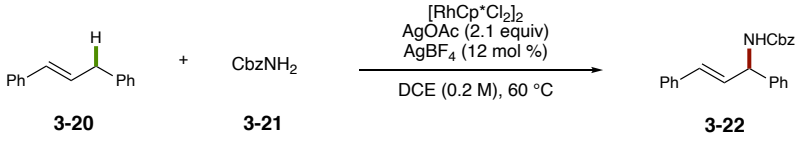

Figure 3-5. General Reaction Scheme for Initial-Rate Kinetic Analysis of Allylic C–H Amination

We then determined that kinetic isotope effect and deuterium exchange studies would provide insight into the role of C–H cleavage in the reaction. Dr. Robert Harris from our group then performed a competition experiment of a 1:1 mixture of **3-20** and **3-20^{D}** with *N*-benzylcarbamate, $[RhCp^*Cl_2]_2$, $AgBF_4$, and AgOAc. The reaction was stopped after ~10% conversion and the allylic amine products (**3-22, 3-22^{D}, 3-22$^{D'}$**) were isolated in 5% yield (**Figure 3-6**). ^{1}H NMR assay revealed 28% deuterium incorporation at the C1 and C3 positions. Due to the symmetry of the π-allyl complex that would be formed, this is expected. The 28% deuterium incorporation corresponds to a KIE of 2.6 suggesting that C–H cleavage was rate determining. Furthermore, in the seminal allylic amination publication deuterium exchange studies supported irreversible C–H cleavage.[12] The KIE studies, deuterium exchange, and first-order rate dependence of alkene confirms C–H activation as the rate-determining step.[17]

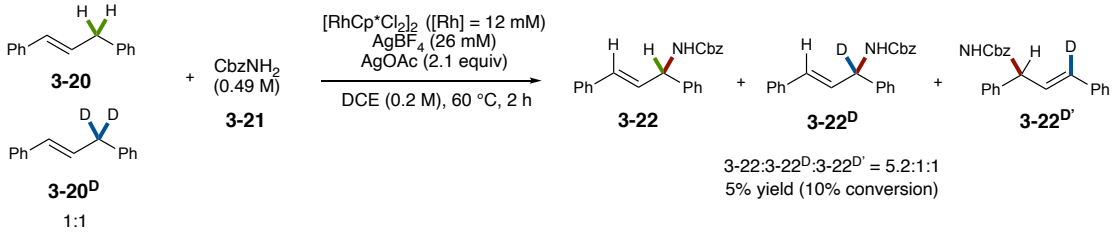

Figure 3-6. Competition Experiment for Primary Kinetic Isotope Studies

While these kinetic studies provided important insight, a full mechanistic picture could not be determined based on this information alone. For this reason, we set out to investigate the full-time course of this reaction. The standard reaction time was 24 h at 40 °C, so the temperature was raised to 80 °C to allow for full analysis in an 8 h window (**Figure 3-7**). As the reaction progressed the concentration of olefin **3-20** and amine **3-21** slowly reduced, while allylic amine **3-22** increased in concentration until plateauing at 6 h. Formation of acetate **3-22** was also observed, albeit never above 5% yield. This data confirms that, as is expected, olefin **3-20** and NH_2Cbz (**3-21**) result in the formation of allylamine **3-22**. Furthermore, acetate **3-23** was observed in small quantities during the reaction progress but was not observed after 8 h. In the seminal amination publication, resubjecting reaction products to the reaction conditions supported that acetate **3-23** may convert to amine **3-22** in situ. This full-time course study confirms the expected conversion and the likely transient nature of acetate **3-23**.

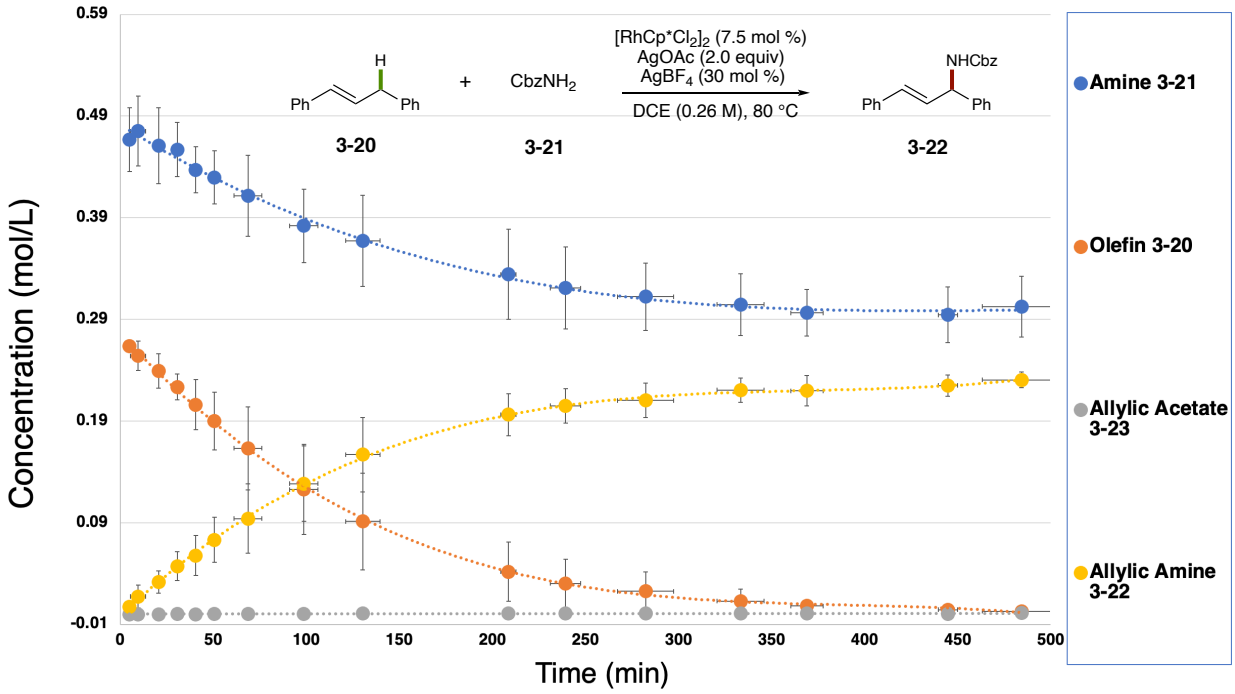

Figure 3-7. Average Reaction Time Course of Allylic C–H Amination of 1,3-diphenylpropene with Benzyl Carbamate. Standard Deviation is Reported from Triplicate Analysis

II.2.Stoichiometric π-allyl Complex Formation and Reactivity

Since this kinetic analysis supported C–H cleavage as the rate-determining step we could no longer use reaction kinetic analysis to probe the C–N bond forming step or catalyst regeneration. In order to understand this reaction better, Dr. Robert Harris set out to synthesize several putative π-allyl intermediates and test their stoichiometric reactivity. He started with the corresponding conditions of π-allyl complex formation reported by Tanaka which provided none of the desired RhCp*-π-allyl complex **3-27**. However, when $[RhCp^*(MeCN)_3][SbF_6]_2$ (**3-24**) , CsOAc (1.5 equiv), and 4-phenyl-1-butene (**3-25**) were

stirred at room temperature for 16 h, a 9:1 ratio of π-allyl complexes **3-26** and **3-27** were isolated in 53% yield. Elevating the reaction temperature to 80 °C in DCE afforded complex **3-27** in 61% yield as the sole thermodynamic product. Full characterization by ^{1}H NMR, ^{13}C NMR, and SC-XRD confirmed the structure of complex **3-27** (**Figure 3-8**, **inset**).

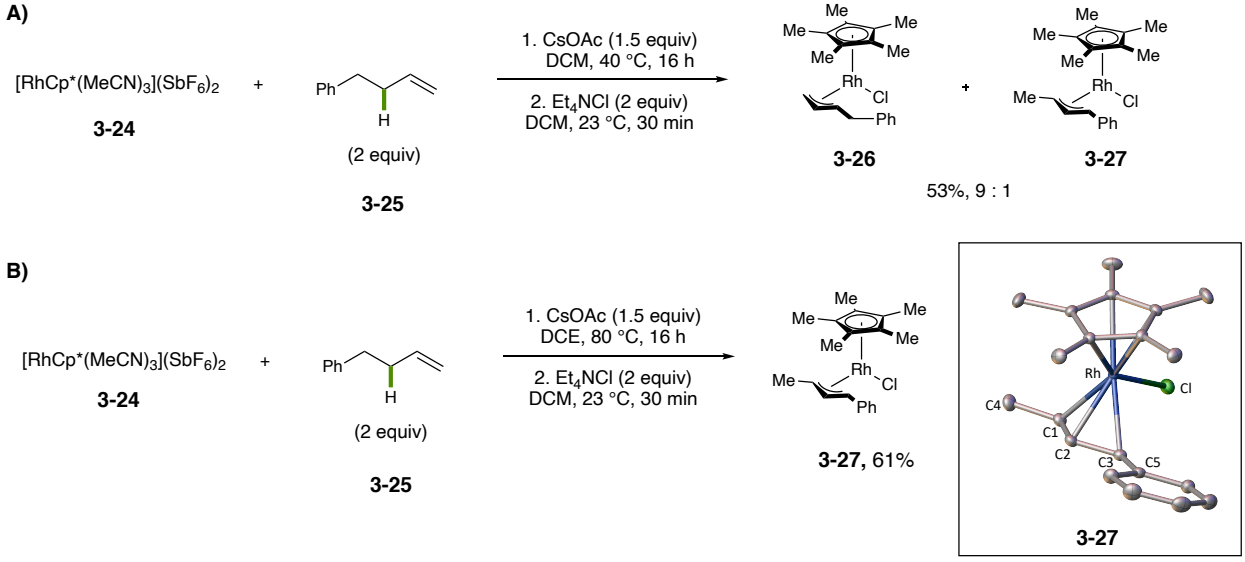

Figure 3-8. RhCp*-π-allyl Chloro Complex Formation

To support the intermediacy of a RhCp*-π-allyl complex, complex **3-27** was subjected to catalytically relevant reaction conditions with and without $AgSbF_6$ as the halide scavenger. As expected, without a halide scavenger to activate the complex no desired product was observed. On the other hand, when a halide scavenger was used with complex **3-27**, Allylic amine **3-29** was observed in 43% yield as well as a surprisingly high yield of allylic acetate (**3-28,** 31%) (**Figure 3-9**). While complex **3-27** cannot be the catalytic

intermediate, the cationic complex resulting from halide abstraction was supported as an intermediate from this experiment. Furthermore, the large quantity of allylic acetate **3-28** further supports the intermediacy of an allylic acetate in this reaction.

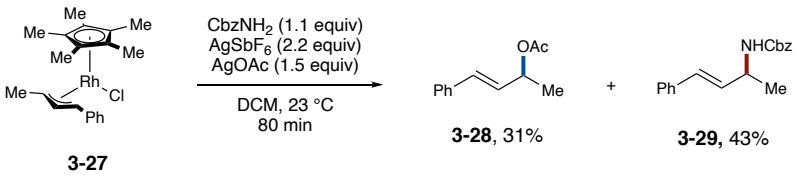

Figure 3-9. Stoichiometric Reactivity of Complex 3-27

To further probe our hypotheses, complexes **3-30, 3-31,** and **3-32** were synthesized (**Figure 3-10**). Dr. Harris determined that complex **3-27** would be an ideal starting point for diversification as a cationic complex can be formed after halide abstraction to react with various coordinating ligands. To afford a complex to test for direct reductive elimination of the C–N bond, complex **3-27** was subjected to $AgSbF_6$ (1.0 equiv) for 45 min, followed by KHNTs (1.1 equiv) for 3 h to afford complex **3-30** in 53% yield. Next, complex **3-27** was subjected to $AgSbF_6$ (1.1 equiv) in MeCN for 2 h resulting in 95% yield of complex **3-31**. Complex **3-31** would provide us with a means to test a cationic complex without the need of silver salt activation. Lastly, since allylic acetate **3-28** had been observed in such large quantities, complex **3-32** was synthesized by reacting complex **3-27** with AgOAc (25 min) to test direct reductive elimination from the metal center. Now that all of these complexes had been formed, stoichiometric reactivity could be performed to provide further insight.

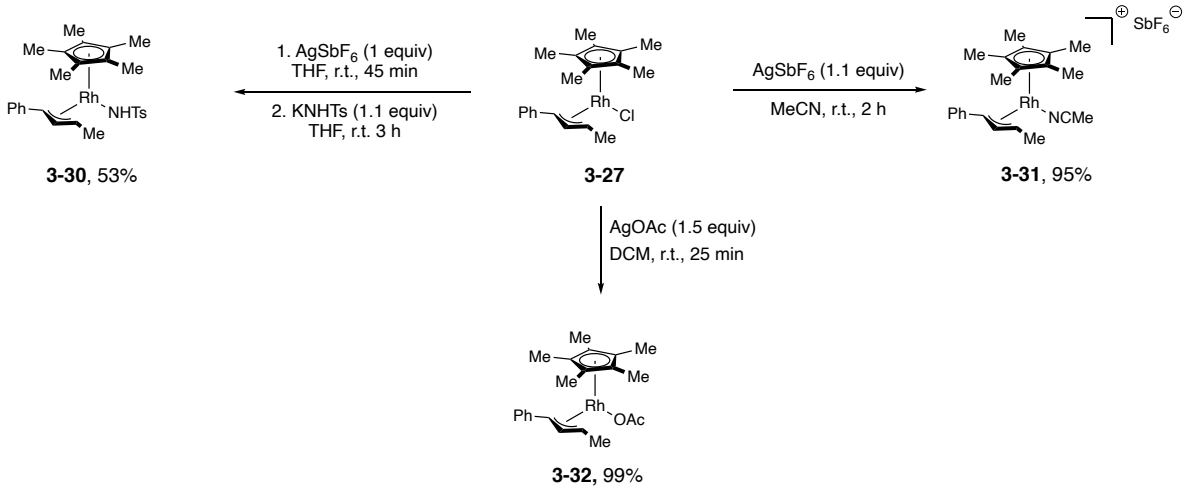

Figure 3-10. Synthesis of RhCp*-π-allyl Complexes

Firstly, to determine if a Rh(III)/Rh(I) catalytic cycle was possible, complexes **3-30** and **3-32** were heated to 60 °C for 6 h with no thermally induced reductive elimination product observed. Furthermore, when complex **3-30** was subjected to benzylcarbamate in DCM at 40 °C for 14 h, no desired allylic products were observed, rather after a chloride quench complex **3-27** was isolated in 92% yield (**Figure 3-11A**). To test the inner sphere vs. outersphere attack to form the C–N bond, complex **3-30** was subjected to $AgSbF_6$ (2 equiv) as an oxidant, and benzenesulformamide (2 equiv), as an outersphere nucleophile, resulting in a 10% combined yield of **3-33** and **3-34** in a 1:1.5 ratio. While 10% combined yield was observed, the equivalent ratio of amine products provides ambiguous results for inner sphere or outersphere bond formation (**Figure 3-11B**). On the other hand, when complex **3-32** was subjected to $AgSbF_6$ (2 equiv) at 25 °C, facile conversion to allylic acetate (**3-28**) was observed. After 5 min, allylic acetate **3-28** was observed in 50% yield and after 20 min in 70% yield (**Figure 3-11C**). This experiment led us to conclude that direct oxidatively induced reductive elimination of allylic acetate **3-28** from complex **3-32** was the

key bond forming step rather than direct C–N bond formation from **3-30**. With this in mind, we hypothesized that allylic amination is likely proceeding through a transient allylic acetate **3-28** via an off-cycle pathway.

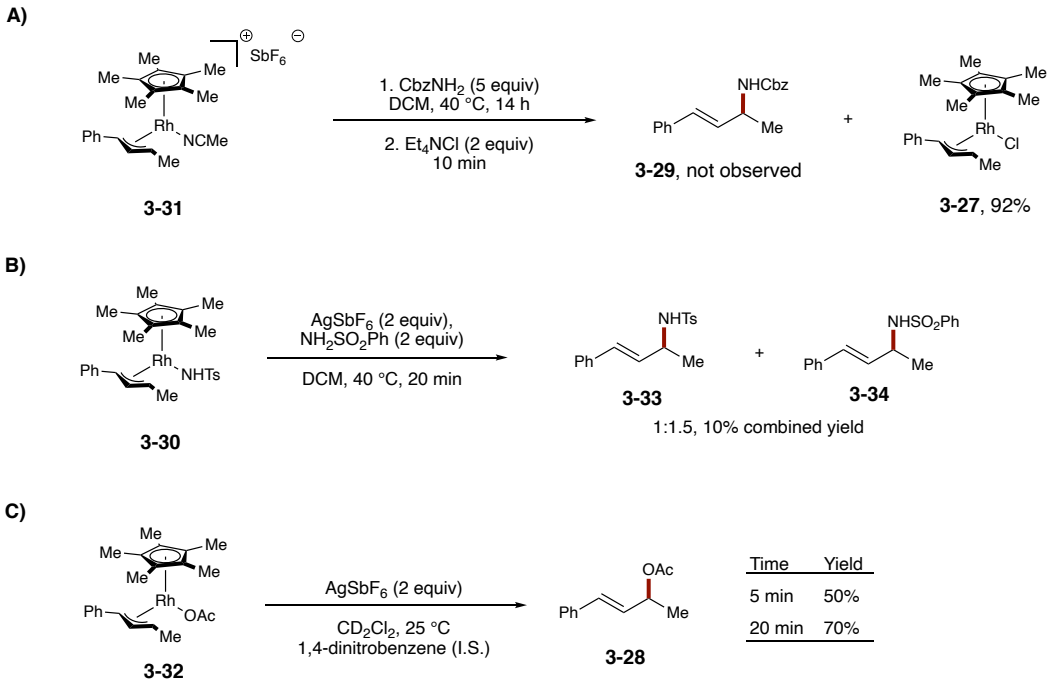

Figure 3-11. Stoichiometric Reactivity of RhCp*-π-allyl Complexes

II.3. Lewis-acid Catalyst Investigations

We hypothesized that Lewis-acid catalyzed substitution of acetate **3-28** was forming **3-29** in an off-cycle pathway**.** In order to support this hypothesis, we tested several reagents found in the catalytic reaction that could act as a Lewis-acid catalyst. In this case, $AgSbF_6$, $AgBF_4$, $[RhCp^*Cl_2]_2$ with $AgSbF_6$, and $[RhCp^*(MeCN)_3](SbF_6)_2$ were all shown to catalyze the reaction at 60 °C for 3 hours (**Table 3-1, Entries 1-4**). When no Lewis-acid was used not conversion was observed (**Table 3-1, Entry 5**). I then began investigating the relative rates

of these components at 0 °C for us to determine the predominant Lewis-acid catalyst. The Lewis-acid could either be Ag^+ or $RhCp^{*2+}$ for this reaction. Because the activation of $[RhCp^*Cl_2]_2$ with $AgSbF_6$ would not provide a clear answer to this question, I focused on $AgSbF_6$ and $[RhCp^*(MeCN)_3](SbF_6)_2$ as the Lewis-acids with noncoordinating counter ions. After 5 min at 0 °C $[RhCp^*(MeCN)_3](SbF_6)_2$ when reacted with acetate **3-20** resulted in 97% yield of amine **3-22**, while $AgSbF_6$ resulted in only 47% yield (**Table 3-1**, **Entries 6-7**). It was not until 2.5 h that $AgSbF_6$ was able to afford 90% yield of amine (**3-22, Table 3-1, Entry 8**). These results led us to conclude that $RhCp^{*2+}$ was the active Lewis-acid catalyst over Ag(I). Full time course studies with $[RhCp^*(MeCN)_3](SbF_6)_2$ and $AgSbF_6$ supported the facile conversion of allylic acetate **3-20** to amine **3-22** when $RhCp^{*2+}$ is employed as the Lewis-acid catalyst.

Table 3-1. Reactivity of Allylic Acetate and Benzyl Carbamate in the Presence of Ag(I) or Rh(III) as a Catalyst

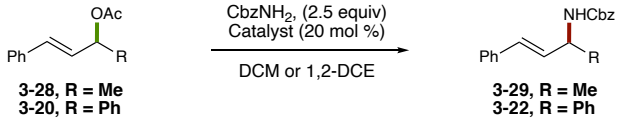

3-28, R = Me
3-20, R = Ph

3-29, R = Me
3-22, R = Ph

Entry	Time	R	Temp (°C)	Catalyst	Yield
1	3 h	Me	60	$AgSbF_6$	91%[a]
2	3 h	Me	60	$AgBF_4$	76%[a]
3	3 h	Me	60	$[RhCp^*Cl_2]_2/AgSbF_6$[c]	73%[a]
4	3 h	Me	60	$[RhCp^*(MeCN)_3](SbF_6)_2$	84%[a]
5	3 h	Me	60	none	0%[b,d]
6	5 min	Ph	0	$[RhCp^*(MeCN)_3](SbF_6)_2$	97%[b]
7	5 min	Ph	0	$AgSbF_6$	47%[b]
8	2.5 h	Ph	0	$AgSbF_6$	90%[b]

[a]Reactions were performed in 1,2-DCE and yield was determined using crude reaction analysis by ^1H NMR against 1,4-dinitrobenzene. [b]Reactions were performed in DCM and yield was determined by GC analysis against nonane as internal standard. [c]$[RhCp^*Cl_2]_2$ (25 mM) and $AgSbF_6$ (40 mM) were stirred in DCM with benzyl carbamate (2) at 60 °C for 30 min before allylic acetate 4 was added to be sure that there was no Ag+ in solution.[d]Allylic amine was not observed by ^1H NMR.

II.4. Computational Investigation of the Key Steps in the Catalytic Cycle

To further support our experimental analysis and resulting conclusions, we turned to computational analysis provided by Dr. Jiyong Park and Dr. Nafees Iqbal of Dr. Baik's group. After determining that complex **3-32** was the key intermediate for bond formation, and since an oxidant was determined to be necessary for the reductive elimination to take place, the calculated energy profiles of Rh(III/I), Rh(IV/II), and Rh(V/III) reductive elimination were performed. Reductive elimination of Rh(IV) to Rh(II) of allylic acetate **3-20** required the lowest calculated energy at 17.64 kcal/mol with the Rh(V) to Rh(III) reductive elimination energy being slightly higher at 19.45 kcal/mol (**Figure 3-12 A-B**). The corresponding Rh(III) to Rh(I) energy was much higher at 38.35 kcal/mol, which corresponded to our experimental results (**Figure 3-12 C**). An important distinction of the three calculated pathways is for the reductive elimination from the Rh(III) complex, the oxygen directly connected to the rhodium-center is reductively eliminated. This is not the case for the corresponding Rh(IV) and Rh(V) calculations where the distal oxygen is found to form the desired C–O bond while the Rh–O bond is broken to form the oxygen of the resulting ketone. While these calculations support Rh(IV)/Rh(II) reductive elimination over Rh(V)/Rh(III), we wanted to confirm these results experimentally as well.

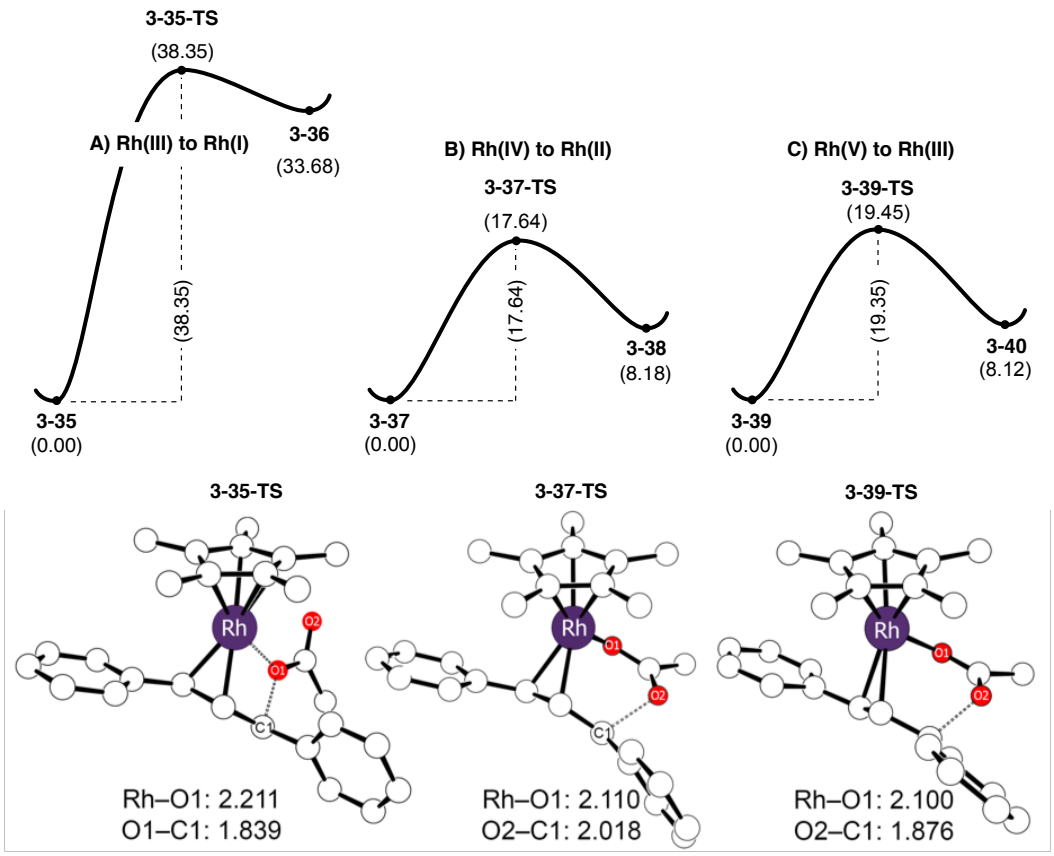

Figure 3-12.Calculated Energy Profiles for Reductive Elimination of A) Rh(III)/Rh(I), B) Rh(IV)/Rh(II), C) Rh(V)/Rh(III) Pathways

II.5.Electrochemical Characterization of 3-32

To support these claims experimentally, we turned to the lab of Dr. MacBeth for their cyclic voltammetry expertise. Cyclic Voltammetry would provide insight into the oxidation events and oxidation potentials of complex **3-32**. Analysis of complex **3-32** by cyclic voltammetry revealed two irreversible redox events at 0.42 V and 0.85 V against Fc/Fc^+ in DCM at varied scan rates (**Figure 3-13 A-B**). Further isolation of each oxidation event revealed an expected scan-rate dependence on the relative position of the peaks (**Figure**

3-13 C-D). Scan-rate dependence supports the coupling of an electrochemical event with a chemical step and would be expected for any of the routes described. The 0.42 V peak was tentatively assigned to a Rh(III/IV) couple and the following 0.85 V peak to a Rh(IV/V) couple. While both oxidation events are accessible on an electrochemical timescale, Ag^+ [18, 19] in DCM has an oxidation potential of 0.65 V making the Rh(IV) intermediate favored theoretically. To further support this fact, $Fe(\eta^5\text{-}C_5H_4COMe)_2SbF_6$ (1,1′-diacetylferrocenium hexafluoro antimonate, E1/2 = +0.49 V vs Fc/Fc+) was utilized as the outersphere oxidant with complex **3-32** resulting in a 25% yield of allylic acetate **3-28**. Since $Fe(\eta^5\text{-}C_5H_4COMe)_2SbF_6$ would only provide enough oxidation potential for the Rh(III)/Rh(IV) couple, these experiments support the Rh(IV) to Rh(II) reductively elimination pathway to form allylic acetate **3-28**. While oxidatively induced reductive elimination pathways proceeding thru a M(IV) oxidation state have been reported, this confirmation, along with Lewis-acid catalyzed substitution supports a new mechanistic paradigm.

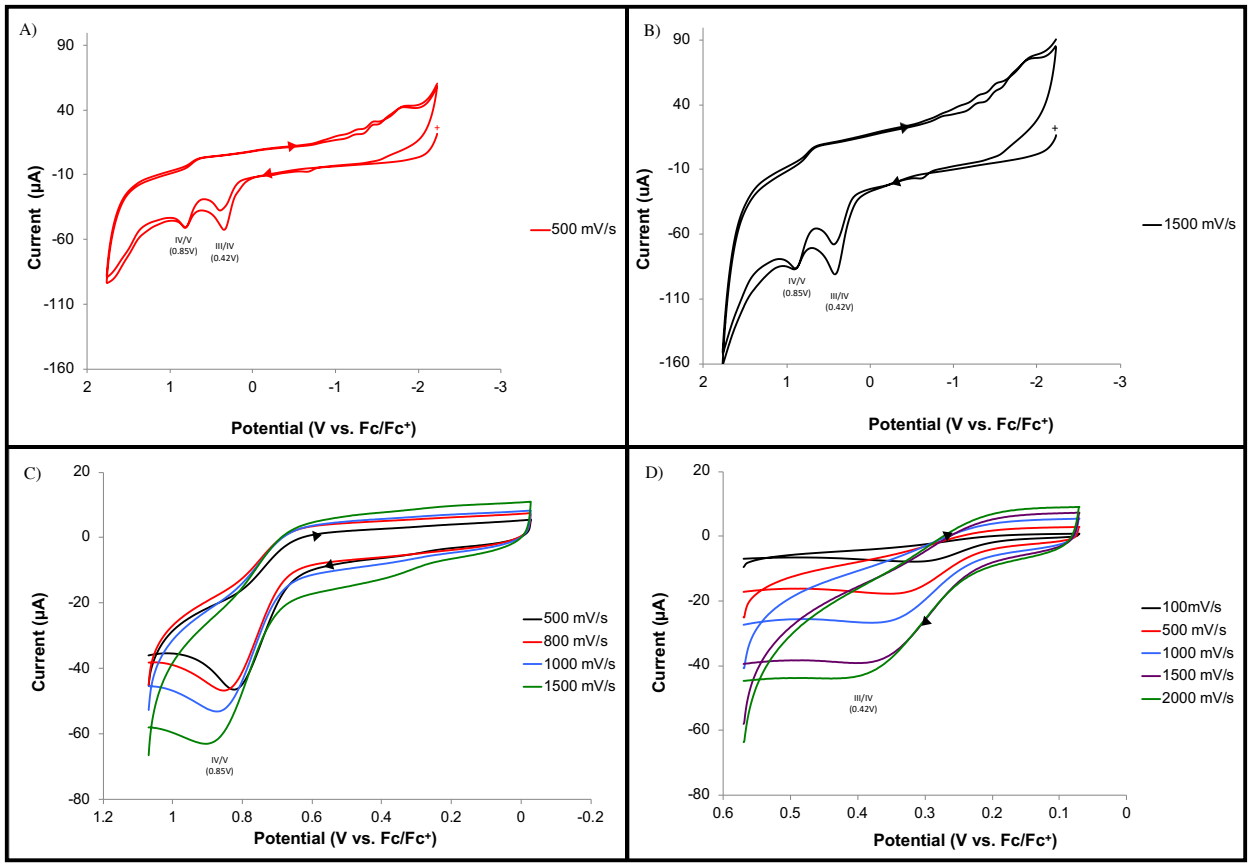

Figure 3-13. Cyclic voltammogram of 3-32 recorded at room temperature in DCM (0.001 M in 0.10 M n-Bu_4NPF_6). (see supplemental for details)

This cyclic voltammetry work provided key insight but also suggested that reductive elimination could likely be induced by electrochemical oxidation for electrocatalysis. Bulk electrolysis of complex **3-32** would provide stoichiometric results to begin an electrocatalytic investigation. The electrasyn 2.0 provided a simple means to test the bulk electrolysis of complex **3-32** under a variety of conditions due to its modularity and ease of use. To begin this study, I utilized similar conditions to those of our cyclic

voltammetry studies. When complex **3-32** was subjected to 2.0 V at 400 rpm (0.1 M in 0.3 M n-Bu_4NPF_6 in DCM) for 1.5 h and then quenched with Et_4NCl, 9% of acetate **3-28** and 49% of complex **3-27** was observed (**Figure 3-14 A**). Complex **3-27** results from the Et_4NCl quench as chloro π-allyl complexes have been found to be more stable for analysis. Varying the voltage, rpm, and time resulted in no increase in yield. While n-Bu_4NPF_6 had been used for the cyclic voltammetry studies, other electrolytes have been utilized for RhCp* electrocatalytic methods in C–H functionalization. When n-Bu_4NOAc was used as the electrolyte (0.01 M in 0.3 M n-Bu_4NOAc in DCM) at 2.0 V, 400 rpm for 19 h, 35 % of acetate **3-28** was observed with 0% of complex **3-27** (**Figure 3-14 B**). The observation of 0% of complex **3-27** supports consumption of starting complex **3-27**. Further analysis of the crude ^1H NMR assay revealed that ketone **3-41** was formed in 9% yield. I hypothesized that the observation of ketone **3-41** in such high yield could be the result of residual water in the reagents. Adding 4Å molecular sieves to the reaction to adsorb water, unfortunately, provided acetate **3-28** in only 12% yield and complex **3-27** in 14% yield (**Figure 3-14 C**). Trace quantities of diene **3-42** were also observed, which may be the result of increased β-hydride elimination. Further optimization studies were not pursued, but these results stand as a proof-of-concept for the bulk electrolysis of complex **3-27**. More so, these bulk electrolysis studies also support the further development of an electrocatalytic method, as super stoichiometric amounts of AgOAc are not ideal for the scalability of this transformation.

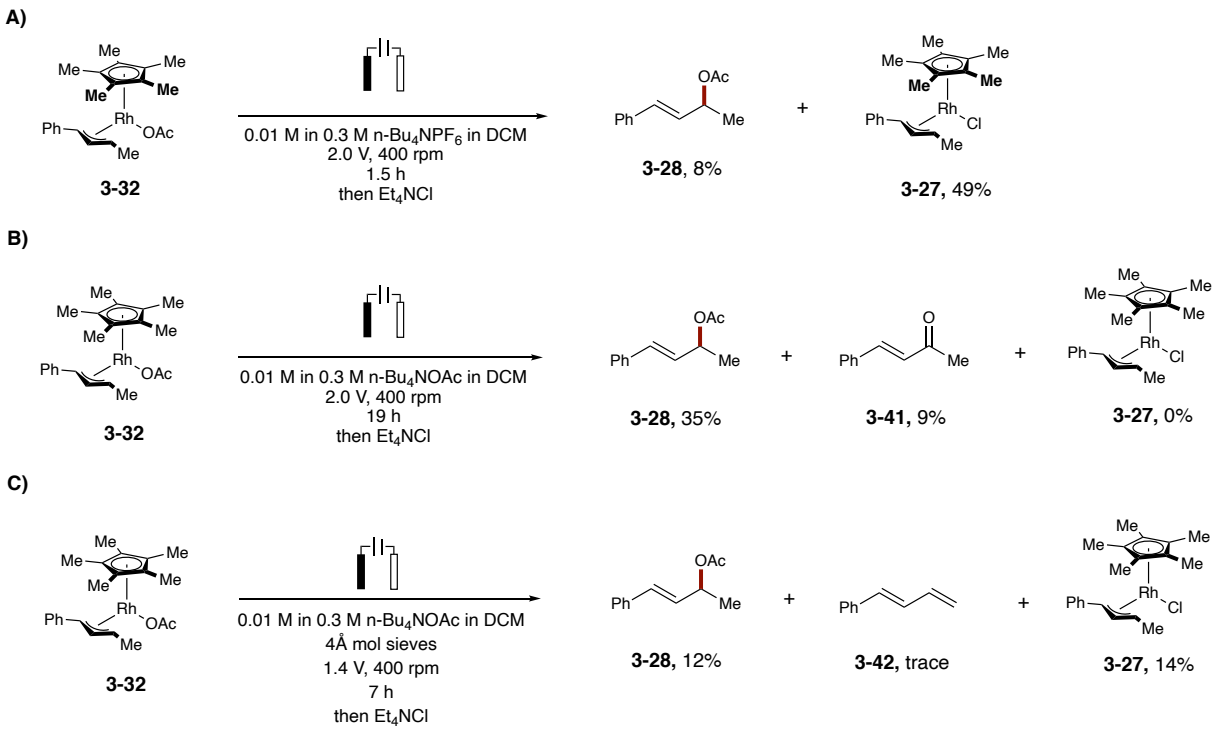

Figure 3-14. Bulk Electrolysis of Complex 3-32 Under Varied Conditions

With all of this information in hand a full catalytic cycle can now be proposed (**Figure 3-15**). First the RhCp* precatalyst (**3-1**) is activated by halide abstraction resulting in Rh(III) complex **3-2**. Complex **3-2** then coordinates to the olefin coupling partner (**3-20**) as well as an acetate. This coordination step results in complex **3-43** which is poised for concerted metalation-deprotonation. Allylic C–H activation yields Rh(III) complex **3-44** with an open coordination site. Following acetate coordination, complex **3-44** is then oxidized to Rh(IV) complex **3-37** which is poised for reductive elimination to form acetate **3-23**. This reductive elimination results in a Rh(II) intermediate (**3-38**) with acetate **3-23** coordinated by the olefin. To complete the catalytic cycle, intermediate **3-38** is reoxidized to Rh(III) complex **3-2** and acetate **3-23** is disassociated. The Baik group was also able to

calculate a full energy diagram further supporting the steps stated above. Detailed calculations were also performed for the Lewis-acid mediated allylic substitution to form amine **3-22** from acetate **3-23**. In agreement with our experimental data, $RhCp^{*2+}$ was confirmed as the Lewis-acid via an S_N1 mechanism.

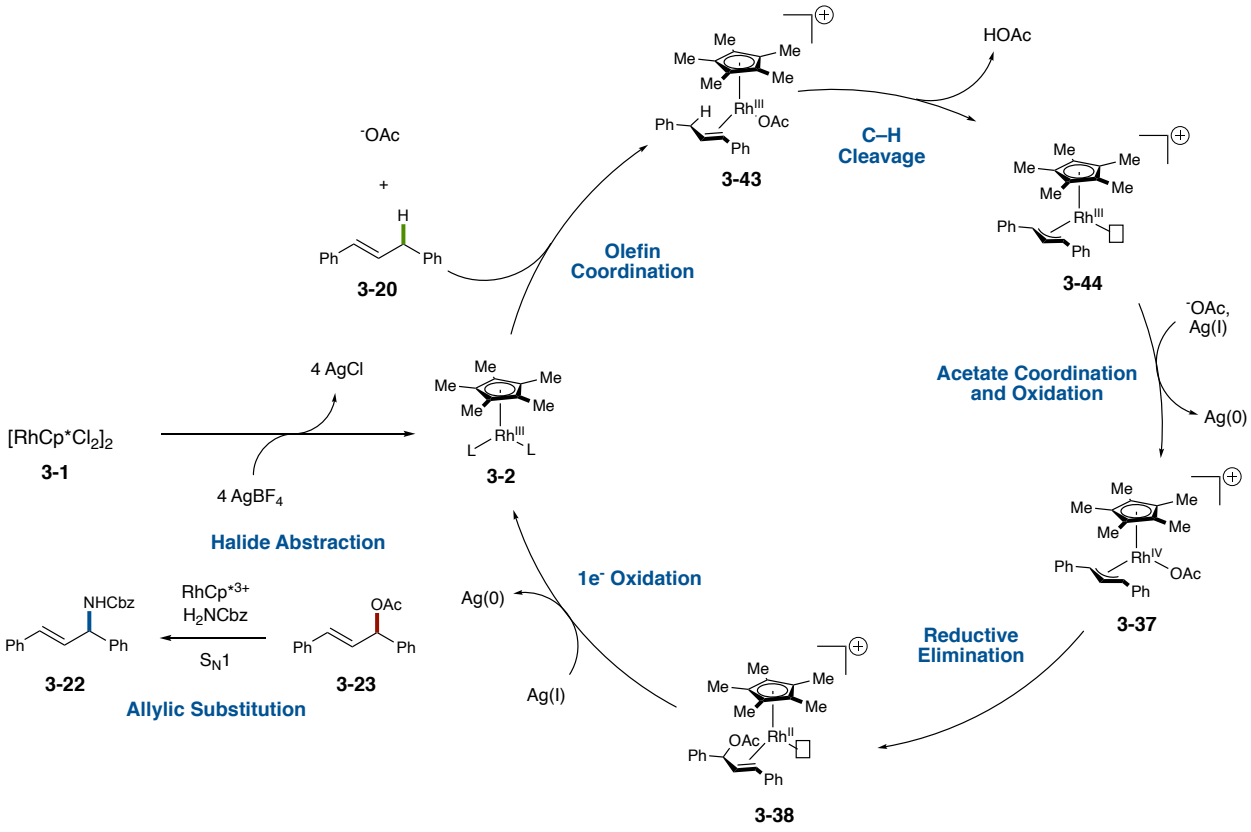

Figure 3-15. New Proposed Rh(III)/Rh(IV)/Rh(II) Catalytic Cycle

III. Conclusion

In conclusion, we have described a detailed investigation to determine the mechanism of our previously disclosed allylic C–H amination protocol. We first performed

kinetic analyses revealing that the olefin and rhodium were first order dependent, and an inverse order dependence was observed for carbamate **3-21**. Kinetic isotope effect and deuterium exchange studies along with our initial-rate analyses support C–H activation as the rate-determining step. This conclusion was further supported by computational calculations. Stoichiometric isolation and further reactivity of π-allyl complexes **3-27, 3-30, 3-31,** and **3-32** revealed that allylic acetate **3-23** reductively eliminates from a Rh(IV)-acetate intermediate (**3-37**), confirming a Rh(III)/Rh(IV)/Rh(II) catalytic cycle. Further computational and time-course analysis confirmed that allylic acetate **3-23** was converted to amine **3-22** via RhCp* Lewis-acid catalyzed allylic substitution. While this study focused on the allylic amination protocol, these results are consistent with the allylic C–H etherification previously discussed[13] and a heteroarylation disclosed by Glorius *et. al*.[20] This study confirms that enantioselectivity induced by the metal-center would not be possible under this mechanistic paradigm. While enantioselectivity could be induced by other means, catalyst-controlled enantioselectivity would require a change in mechanism to provide asymmetric allylic products.

IV. Experimental Procedures:

IV.1. General Information

Reactions were performed under a nitrogen atmosphere employing standard Schlenk and glovebox techniques using anhydrous solvents unless otherwise specified. Anhydrous tetrahydrofuran (THF), diethyl ether (Et_2O), and dichloromethane (DCM) were obtained by passage through activated alumina using a *Glass Contours* solvent purification system. Anhydrous dichloroethane (1,2-DCE) was obtained by distillation over calcium

hydride and stored over 4 Å molecular sieves. All other reagents were obtained from commercial suppliers and used as received. Analytical thin layer chromatography (TLC) was performed on precoated aluminum backed Silicycle SiliaPure® 0.25 mm silica gel 60 plates. Visualization was accomplished with UV light, ethanolic *p*-anisaldehyde, or aqueous potassium permanganate. Flash column chromatography was performed employing 200-400 mesh silica gel (EM) on a Biotage Isolera One flash chromatography system. NMR spectra were obtained on a Varian spectrometer at 25 °C operating at 400 MHz for ^{1}H NMR, 125 MHz for ^{13}C NMR, and 376 MHz for ^{19}F $CDCl_3$ unless noted otherwise; ^{13}C NMR was referenced relative to $CDCl_3$ (δ = 77.16), ^{1}H NMR was referenced relative to residual $CHCl_3$ (δ = 7.26) for $CDCl_3$ and $CHDCl_2$ (δ = 5.32) for CD_2Cl_2, and ^{19}F was reported unreferenced. Chemical shifts (δ values) were reported in parts per million (ppm) and coupling constants (*J* values) in Hz. Multiplicity is indicated using the following abbreviations: s = singlet, d = doublet, t = triplet, q = quartet, qn = quintet, hep = heptet, m = multiplet, b = broad signal). Infrared (IR) spectra were recorded using Thermo Electron Corporation Nicolet 380 FT-IR spectrometer. High resolution mass spectra were obtained using a Thermo Electron Corporation Finigan LTQFTMS (at the Mass Spectrometry Facility, Emory University). All gas chromatograph spectra were taken on an Agilent Technologies 6850 series gas chromatograph equipped with a flame ionization detector and with a HP-1 column (30 m wide bore 0.32mm x 0.25 μm) manufactured by J&W. Method for GC analysis: injector, splitless at 225 °C, 9.14 psi, 54.5 mL/min Helium, split ratio 24.5:1, split flow 49.2 mL/min; Oven, 40 °C 2 min, 15 °C/min until 300 °C; FID, 250 °C, 40.0 mL/min hydrogen, 450 mL/min air. Cyclic voltammetry experiments were carried out using a CH Instruments (Austin, TX) Model 660C potentiostat. All cyclic voltammetry experiments were conducted in DCM with

0.10 M tetrabutylammonium hexafluorophosphate (electrochemical grade Sigma-Aldrich) as the supporting electrolyte in a three-S4 component cell consisting of a Pt-wire auxiliary electrode, a non-aqueous reference electrode ($Ag/AgNO_3$), and a glassy-carbon working electrode. Bulk electrolysis was performed using an IKA electrasyn 2.0 with a platinum plated counter electrode, non-aqueous reference electrode ($Ag/AgNO_3$), and glassy-carbon working electrode. All electrodes for bulk electrolysis were purchased from IKA and used as received.

IV.2. Detailed Catalytic Cycle

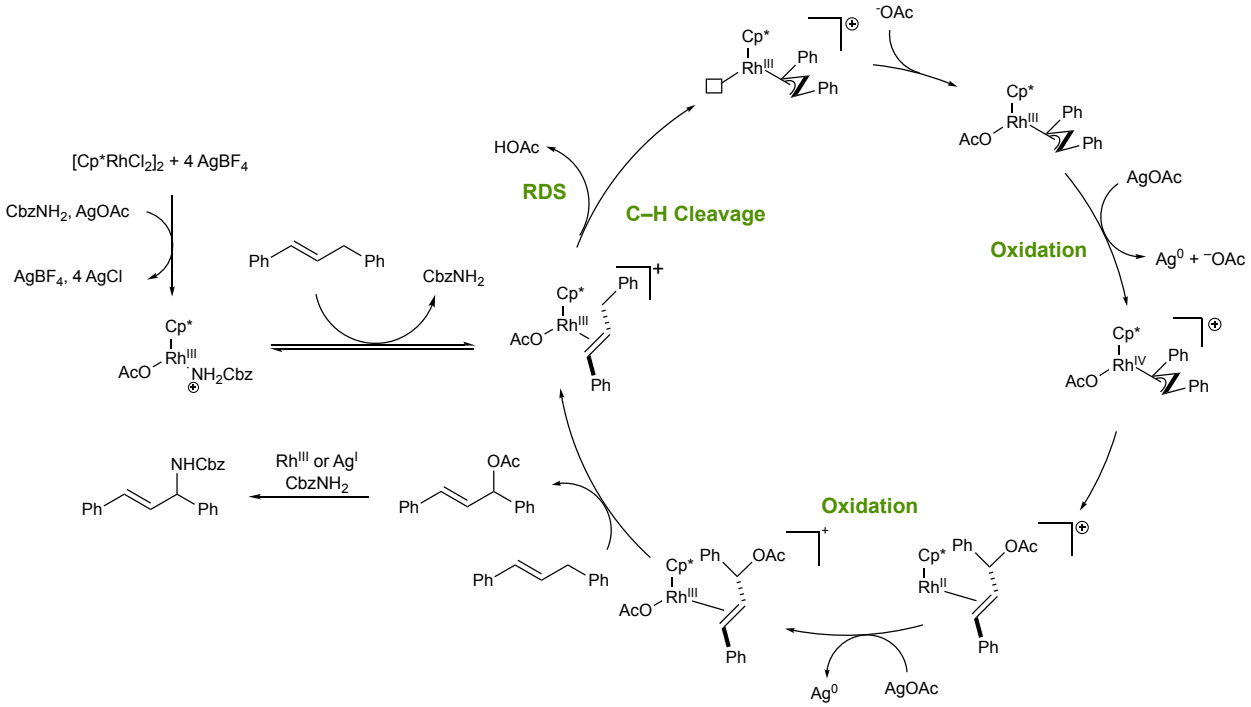

Figure 3-16. Detailed Catalytic Cycle for Visualization of All Components

IV.3. Experimental Rate Law Determination

IV.3.1. Representative Procedure for Initial Rate Kinetic Experiments

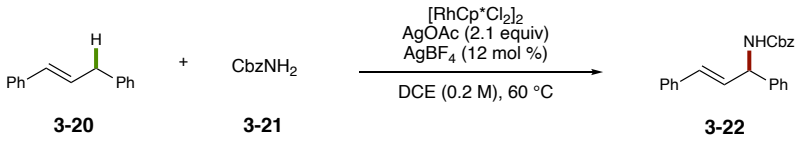

In a nitrogen filled glove box, benzyl carbamate (194 mg, 1.28 mmol) and silver acetate (180 mg, 1.08 mmol) were added to a 7 mL reaction vial equipped with a magnetic stir bar. Silver tetrafluoroborate (40 mg, 0.2 mmol) and $[RhCp^*Cl_2]_2$ (96 mg, 0.3 mmol) were added to two separate 4 mL vials. All three vials were fitted with septum caps and removed from the glove box. Nonane (internal standard, 134.6 mg, 1.05 mmol) was added to a 10 mL volumetric flask followed by the addition of distilled 1,2-dichloroethane to create a 0.105 M solution. 2.3 mL of the resulting solution was added to the 7 mL reaction vial containing benzyl carbamate and silver acetate. 1 mL of the solution containing the internal standard was added to each of the 4 mL vials containing silver tetrafluoroborate and $[RhCp^*Cl_2]_2$ to create stock solutions of silver tetrafluoroborate (0.2 M) and the rhodium catalyst (0.3 M). 1,3-diphenyl propene (0.1 mL, 0.51 mmol) was added via syringe to the 7 mL reaction vial followed by 0.1mL from each of the stock solutions of silver tetrafluoroborate (0.02 mmol) and $[RhCp^*Cl_2]_2$ (0.03 mmol). The reaction vial was then placed in a heating block at 60 °C. Placing the vial in the heating block was considered the t=0 time point for kinetic analysis. Reaction progress was monitored by removing an aliquot of the reaction mixture (~50 μL). Each aliquot was taken using a fresh syringe (1mL) and a clean reusable needle. Each sample was worked up by filtering through diatomaceous silica using ethyl acetate as the eluent and then analyzed by gas chromatography equipped with a flame ionization detector.

Table 3-2. Initial Rates for the Rhodium–catalyzed Allylic Amination of Diphenylpropene 3-20 with Benzylcarbamate 3-21

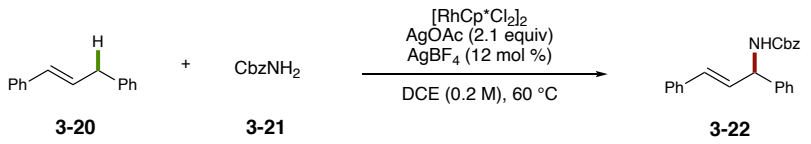

3-20 **3-21** **3-22**

entry	[Rh] (mM)	[**3-20**] (M)	[$CbzNH_2$] (M)	Rate ($10^6 \times Ms^{-1}$)[a]
1	12	0.20	0.49	2.1 ± 0.2
2	12[b]	0.20	0.49	3.2 ± 0.2
3	12	0.20	0.49	2.3 ± 0.3
4	4[b]	0.20	0.49	1.2 ± 0.1
5	8	0.20	0.49	1.9 ± 0.2
6	16	0.20	0.49	4.2 ± 0.5
7	12	0.10	0.49	0.34 ± 0.04
8	12	0.40	0.49	4.2 ± 0.3
9	12	0.40	0.49	5.4 ± 0.2
10	12	0.50	0.49	7.7 ± 0.9
11	12	0.50	0.49	6.5 ± 0.2
12	12	0.20	0.25	4.7 ± 0.8
13	12	0.20	0.25	4.5 ± 0.2
14	12	0.20	0.40	3.5 ± 0.4
15	12	0.20	0.74	1.0 ± 0.1
16	12	0.20	0.79	0.91 ± 0.05

17	12	0.20	0.99	0.44 ± 0.09
18	12	0.20	1.1	0.31 ± 0.03

[a]Errors represent 1 standard deviation obtained by least square analysis and do not reflect systematic experimental errors [b]4 mol % $AgBF_4$ was used.

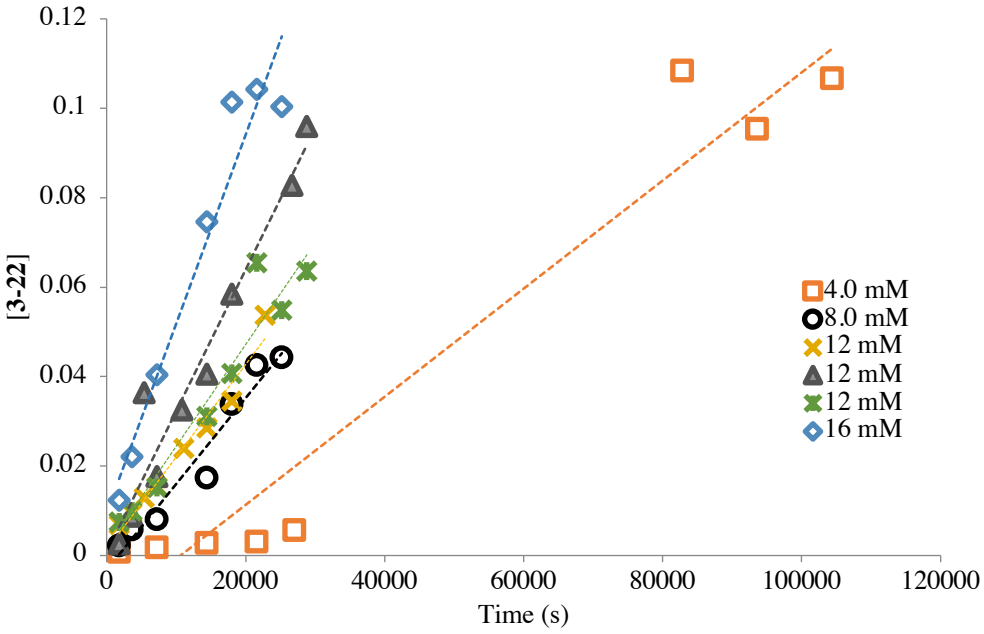

Figure 3-17. Initial-Rate Plots for the Allylic Amination of Diphenylpropene (3-20) (0.20 M) with Benzyl carbamate (3-21) (0.50M) Catalyzed by a Mixture of [RhCp*Cl$_2$]$_2$ ([Rh] = 4.0–16 mM) and $AgBF_4$ (24 mM) in the Presence of AgOAc (0.42 M).

For [Rh] = 4.0 and 8.0 mM a reduced amount of $AgBF_4$ (8.0 mM) was used; however, since the abstraction of Cl^- is much faster than the oxidation of Rh, the excess AgOAc can also serve to abstract the Cl^- once a small amount of acetic acid has been generated.

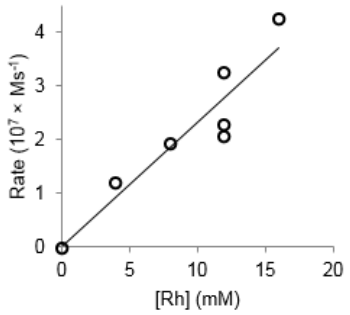

Figure 3-18. Rhodium Concentration Dependence for the Rate of Allylic Amination of Diphenylpropene (3-20) (0.20 M) with Benzylcarbamate (3-21) (0.49 M) Catalyzed by a Mixture of $[RhCp^*Cl_2]_2$ and $AgBF_4$ in the Presence of AgOAc in DCE at 60 °C.

A slope of k_1 = 2.4 ± 0.4 × 10−4 s^{-1} was calculated and established a first–order dependence of the rate on rhodium concentration.

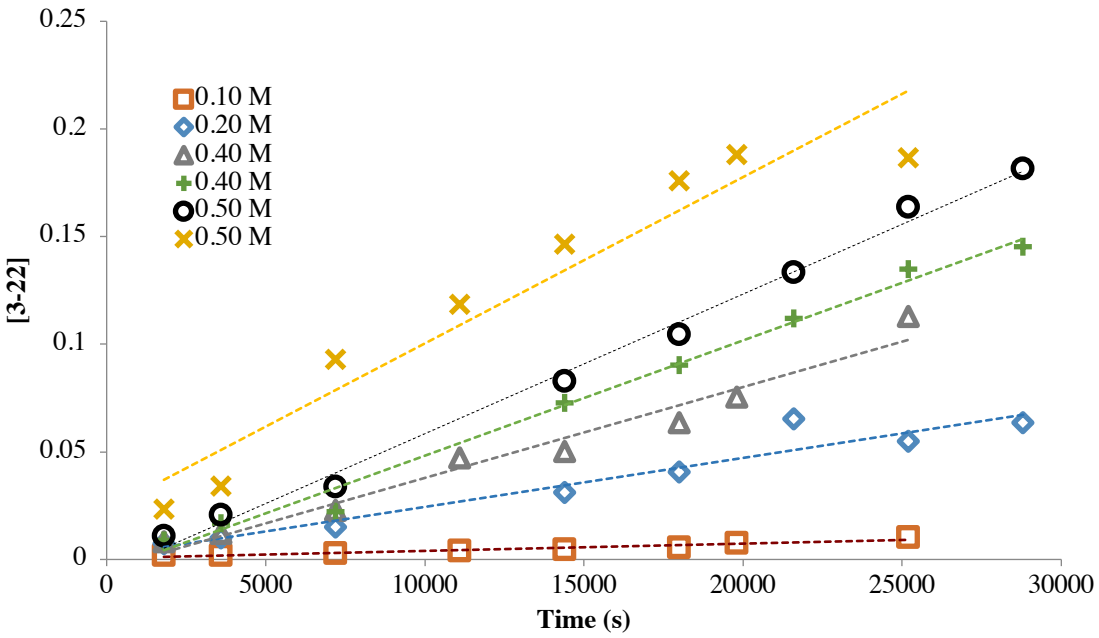

Figure 3-19. Initial Rate Plots for the Allylic Amination of Diphenylpropene (3-20) (0.10 – 0.50 M) with Benzyl Carbamate (3-21) (0.49M) Catalyzed by a Mixture of $[RhCp^*Cl_2]_2$ ([Rh] = 12 mM) and $AgBF_4$ (24 mM) in the Presence of AgOAc (0.42 M).

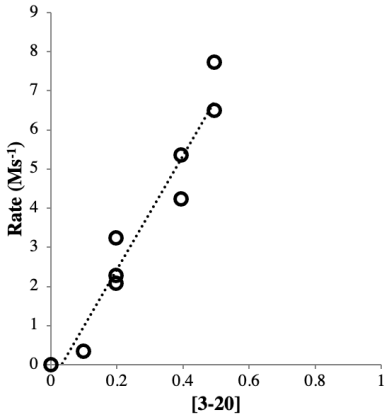

Figure 3-20. Concentration Dependence for the Rate of Allylic Amination of Diphenylpropene (3-20) with Benzylcarbamate (3-21) (0.49 M) Catalyzed by a Mixture of $[RhCp^*Cl_2]_2$ and $AgBF_4$ in the Presence of AgOAc in DCE at 60 °C.

A plot of rate versus [3-20] was linear with a slope of $k_2 = 1.5 \pm 0.1 \times 10^{-5}$ s^{-1}.

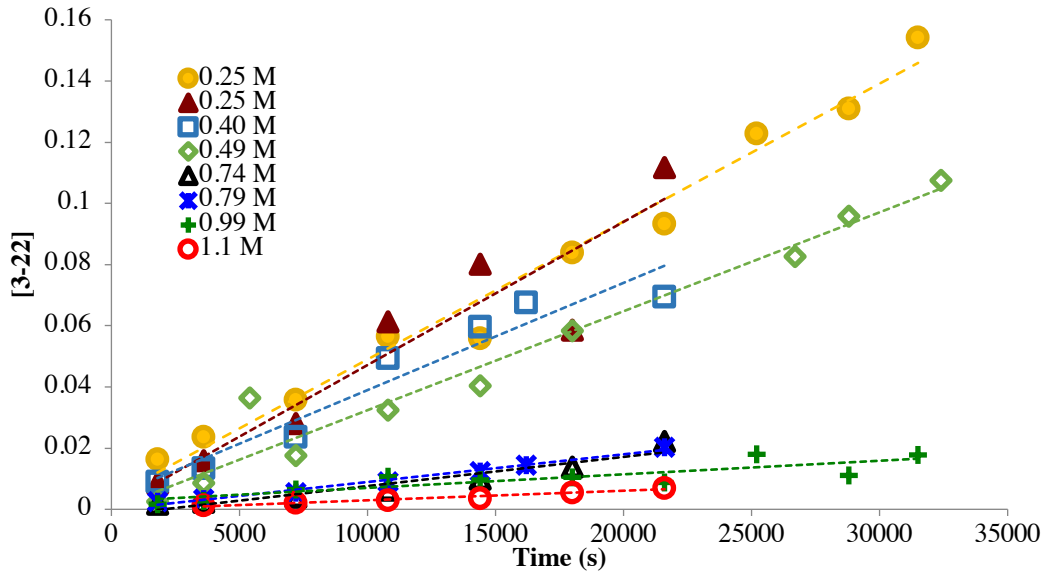

Figure 3-21. Initial Rate Plots for the Allylic Amination of Diphenylpropene (3-20) (0.20 M) with Benzyl carbamate (3-21) (0.25 – 1.1 M) Catalyzed by a Mixture of $[RhCp^*Cl_2]_2$ ([Rh] = 12 mM) and $AgBF_4$ (24 mM) in thePpresence of AgOAc (0.42 M).

For $[CbzNH_2]$ = 0.49 M a reduced amount of $AgBF_4$ (8.0 mM) was used; however, since the abstraction of Cl^- is much faster than the oxidation of Rh, the excess AgOAc can also serve to abstract the Cl^- once a small amount of acetic acid has been generated.

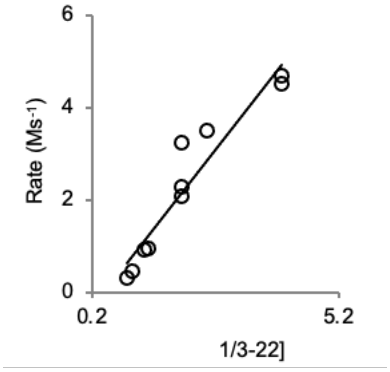

Figure 3-22. Concentration Dependence for Rate of Allylic Amination of 3-20 (4.9 M) with 3-21 Catalyzed by a Mixture of $[RhCp^*Cl_2]_2$ and $AgBF_4$ in the Presence of AgOAc in DCE at 60 °C.

A plot of rate versus 1/[**3-22**] was nearly linear with a slope of $k_3 = 1.4 \pm 0.2 \times 10{-}6\ M^2s^{-1}$.

IV.3.2. Determination of KIE

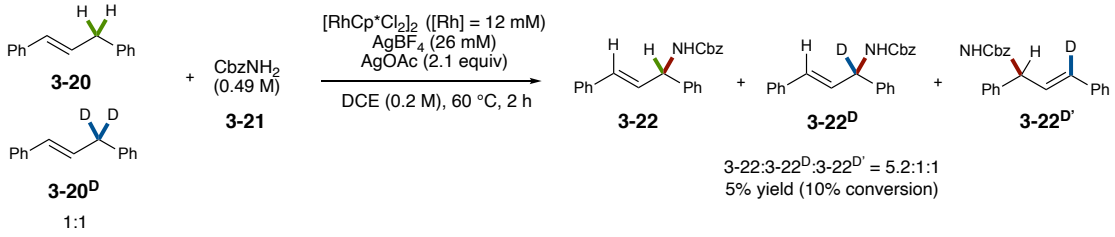

In a nitrogen filled glove box, $[RhCp^*Cl_2]_2$ (9.9 mg, 0.016 mmol), silver tetrafluoroborate (12 mg, 0.069 mmol), benzyl carbamate (194.5 mg, 1.29 mmol), and silver acetate (180 mg, 1.10 mmol) were added to a 7 mL reaction vial equipped with a magnetic stir bar. The vial was fitted with a septum cap and removed from the glove box. In a separate vial, 100 µL each of diphenylpropene (**3-20**) and **3-20D** were added. A ^1H NMR of the

resulting mixture of **3-20** and **3-20^{D}** was obtained to determine a 1.05:1 mixture of **3-20**:**3-20**^{D}. Dichloroethane (2.6 mL) and the mixture of diphenylpropene (101.2 mg) were added to the reaction vial via syringe and the resulting mixture was mixed thoroughly and stirred at 60 °C for 2 h. After 2 h the reaction was stopped by filtering through silica gel and eluting with EtOAc. Preparatory thin layer chromatography in 2% EtOAc in toluene afforded 3-22:3-22^{D}:3-22$^{D'}$ in a 5.2:1:1 ratio (6.3 mg, 5 %).

IV.4. Synthesis and Reactivity of Rhodium Complexes

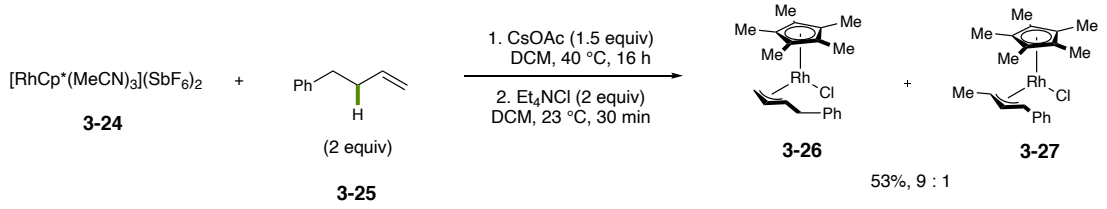

Chloro-(η3-1-benzylallyl)-(η5-pentamethylcyclopentadienyl)-rhodium, (**3-26**).

[Cp*Rh(MeCN)$_3$](SbF$_6$)$_2$ (650 mg, 0.78 mmol) and CsOAc (243 mg, 1.27 mmol) were added to a 100 mL oven-dried round bottom flask charged with a magnetic stir bar in a glove box. The flask was capped with a rubber septum and removed from the glovebox. Dichloromethane (30 mL) and 1-phenyl-4-butene (250 μL, 1.66 mmol) were added via syringe, and the reaction was stirred at 40 °C for 16 h. After 16 h, the reaction was cooled to room temperature. Et$_4$NCl (300 mg, 1.81 mmol) was dissolved in dichloromethane (3 mL) and the resulting solution was added to the reaction via syringe and allowed to stir for 30 min. The reaction mixture was then filtered through celite, eluted with dichloromethane, and concentrated under reduce pressure. The resulting solid was chromatographed (Hexanes-EtOAc = 9:1 to 7:3) to give **3-26** and **3-27** as a red solid in a 9:1 ratio (53%). The two isomers could be separated by column chromatography to yield **3-26** cleanly.

^{1}H NMR ($CDCl_3$, 400 MHz): δ 7.37 (d, J = 7.5 Hz, 2H), 7.30 (t, J = 7.6 Hz, 2H), 7.20 (t, J = 7.3 Hz, 1H), 4.08 (tdd, J = 10.9, 6.9, 2.0 Hz, 1H), 3.67 (td, J = 9.6, 6.0 Hz, 1H), 3.35-3.27 (m, 2H), 3.05-2.96 (m, 2H), 1.71 (s, 14H).

HRMS (ESI): calcd for $C_{20}H_{26}ClRh$ $[M+]^+$: 404.07781, found 404.07783.

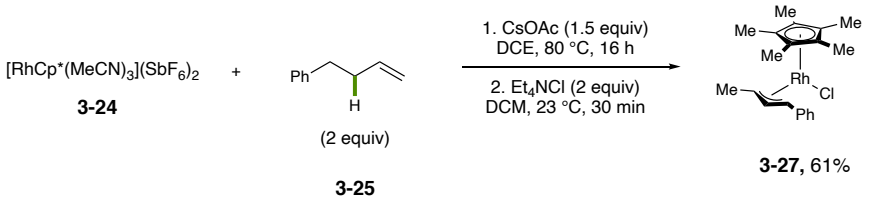

Chloro-(η3-1-methyl-3-phenylallyl)-(η5-pentamethylcyclopentadienyl)-rhodium, (**3-27**).

$[Cp^*Rh(MeCN)_3](SbF_6)_2$ (650 mg, 0.78 mmol) and CsOAc (243 mg, 1.27 mmol) were added to a 100 mL oven-dried round bottom flask charged with a magnetic stir bar in a glove box. The flask was capped with a rubber septum and removed from the glovebox. 1,2-Dichloroethane (30 mL) and 1-phenyl-4-butene (250 μL, 1.66 mmol) were added via syringe, and the reaction was stirred at 80 °C for 16 h. After 16 h, the reaction was cooled to room temperature. Et_4NCl (300 mg, 1.81 mmol) was dissolved in dichloromethane (3 mL) and the resulting solution was added to the reaction via syringe and allowed to stir for 30 min. The reaction mixture was then filtered through celite, eluted with dichloromethane, and concentrated under reduce pressure. The resulting solid was chromatographed (Hexanes-EtOAc = 9:1 to 7:3) to give **3-27** as a red solid (61%).

^{1}H NMR ($CDCl_3$, 400 MHz): δ 7.33-7.29 (m, 4 H), 7.22-7.16, (m, 1 H), 4.67 (d, J = 10.7, 1 H), 4.55 (td, J_{HH} = 11.1 Hz, J_{RhH} = 2.0, 1 H), 3.73(dq, J = 10.7, 6.3 Hz, 1 H), 1.69 (d, J = 6.3 Hz, 3 H), 1.35 (s, 15 H).

^{13}C NMR ($CDCl_3$, 125 MHz): δ 139.0, 128.7, 126.1, 126.0, 97.8 (d, J_{RhC} = 6.8 Hz), 89.0 (d, J_{RhC} = 6.3 Hz), 77.3 (d, J_{RhC} = 7.3 Hz), 58.4 (d, J_{RhC} = 10.9 Hz), 8.6.

HRMS (ESI): calculated for $C_{20}H_{26}ClRh$ $[M+]^+$: 404.07781, found 404.07783.

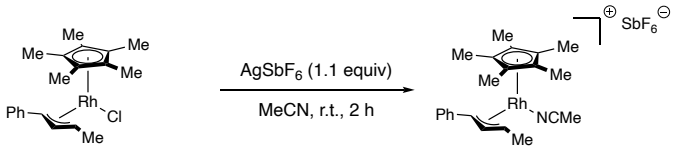

3-27 **3-31**, 95%

[(η3-1-methyl-3-phenylallyl) -(η5-pentamethylcyclopentadienyl)-rhodium acetonitrile] hexafluoroanimonate, (3-31).

Complex **3-27** (87.5 mg, 0.22 mmol) and $AgSbF_6$ (83 mg, 0.24 mmol) were suspended in MeCN (4 mL) inside a glovebox. The reaction was capped, removed from box, and stirred at room temperature for 2 h. The resulting mixture was filtered through celite, eluted with DCM, and concentrated under reduced pressure. The resulting solid was crystalized by layer hexanes on top of dichloromethane. The supernatant was decanted, and the solids were washed with hexanes (x 3). The resulting solids were redissolved in dichloromethane and filtered through celite to remove any remaining silver. The resulting yellow-orange solution was concentrated under reduced pressure to afford a yellow-orange solid in 95% yield.

^{1}H NMR ($CDCl_3$, 400MHz): δ 7.39 (t, J = 7.7 Hz, 2 H), 7.31-7.29 (m, 3 H), 4.61 (td, J_{HH} = 11.0 Hz, J_{RhH} = 1.6, 1 H), 4.24 (d, J = 11.2, 1 H), 3.42(dq, J = 11.2, 5.8 Hz, 1 H), 2.48 (s, 3 H), 1.76 (d, J = 6.3 Hz, 2 H), 1.38 (s, 15 H).

^{13}C NMR ($CDCl_3$, 125 MHz): δ 137.0, 129.3, 127.4, 126.7, 124.8 (d, J_{RhC} = 7.6 Hz), 99.6(d, J_{RhC} = 6.5 Hz), 90.6 (d, J_{RhC} = 5.7 Hz), 75.5 (d, J_{RhC} = 7.0 Hz), 72.0 (d, J_{RhC} = 8.5 Hz), 18.1, 8.2, 3.4. **HRMS** (ESI): calculated for $C_{22}H_{29}NRh$ [M-SbF_6]: 410.13550, found 410.13517.

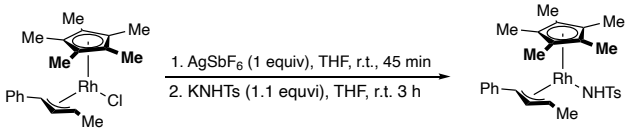

3-30, 53%

[(η3-1-methyl-3-phenylallyl)-(η5-pentamethylcyclopentadienyl)-rhodium tosylamide], (**3-30**)**.**

Complex **3-27** (202.4 mg, 0.5 mmol) and $AgSbF_6$ (171.8 mg, 0.5 mmol) were suspended in THF (15 mL) inside a glovebox. The reaction was stirred for 45 min at room temperature. Potassium tosylamide (KNHTs, 106.7 mg, 0.55 mmol) was added to the reaction as a solid. The reaction was capped, removed from box, and stirred at room temperature for 3 hours. The resulting mixture was filtered through celite, eluted with DCM, and concentrated under reduced pressure. The resulting solid was redissolved in 2 mL DCM, 6 ml of hexanes were added to the DCM solution and concentrated under reduced pressure until solids began to crash out. The solids were collected via vacuum filtration and resulted in a 10:1 mixture of the product (**3-30**) : starting material (**3-27**). This mixture was further purified by dissolving in Et_2O and concentrating until solids began to precipitate. The resulting Et_2O suspension was and further **3-30** precipitated. The solids were collected by vacuum filtration and washed with pentane to afford **3-30** as an orange powder in 53% yield (145 mg).

^{1}H NMR ($CDCl_3$, 400MHz): δ 7.64 (d, *J* = 8.2 Hz, 2H), 7.41 (d, *J* = 7.3 Hz, 2H), 7.29 (t, *J* = 7.7 Hz, 2H), 7.17(t, *J* = 7.4 Hz, 1H), 7.10 (d, *J* = 7.9 Hz, 2H), 4.45 (td, J_{HH} = 10.6 Hz, J_{RhH} = 1.8 Hz, 1H), 4.32 (d, *J* = 11.1 Hz, 1H), 3.20 (dq, *J* = 10.9, 5.7 Hz, 1H), 2.30 (s, 3H), 1.63 (d, *J* = 6.4 Hz, 3H), 1.38 (s, 15H).

^{13}C NMR ($CDCl_3$, 125 MHz): δ 146.67, 139.70, 139.65, 128.79, 128.69, 126.61, 125.96, 125.44, 97.52 (d, J_{RhC} = 5.9 Hz), 89.32 (d, J_{RhC} = 6.2 Hz), 72.40 (d, J_{RhC} = 8.6 Hz), 69.68 (d, J_{RhC} = 9.6 Hz), 21.22, 18.32, 8.60.

HRMS (ESI): calculated for $C_{27}H_{35}O_2NRhS$ $[M+H]^+$: 540.14435, found 540.14417.

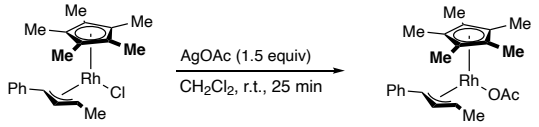

3-32, >99%

[(η3-1-methyl-3-phenylallyl)-(η5-pentamethylcyclopentadienyl)-rhodium acetate], (3-32).

Complex 3-**27** (100 mg, 0.25 mmol) and AgOAc (61.8, 0.37 mmol) were suspended in DCM (10 mL) inside a glovebox. The reaction was capped, removed from the glove box, and stirred at room temperature for 25 min. The resulting mixture was filtered through celite, eluted with DCM, and concentrated under reduced pressure to afford complex **3-32** as a red powder in quantitative yield (105.3 mg)

^{1}H NMR ($CDCl_3$, 400MHz): δ 7.56 (d, *J* = 7.5 Hz, 2H), 7.30 (t, *J* = 7.5 Hz, 2H), 7.17 (t, *J* = 7.4 Hz, 1H), 4.58 (t, *J* = 10.8 Hz, 1H), 4.24 (d, *J* = 11.2 Hz, 1H), 3.04 (dq, *J* = 11.1, 5.7 Hz, 1H), 1.96 (s, 3H), 1.78 (d, *J* = 6.3 Hz, 3H), 1.31 (s, 15H).

^{13}CNMR ($CDCl_3$, 125 MHz): δ 176.6, 139.8, 128.4, 127.1, 125.9, 96.4 (d, J_{RhC} = 6.8 Hz), 90.6 (d, J_{RhC} = 6.4 Hz), 76.0 (d, J_{RhC} = 8.7 Hz), 74.0 (d, J_{RhC} = 9.5 Hz), 25.7, 18.3, 8.4.

HRMS (ESI): calculated for $C_{22}H_{329}O_2NRh$ [M^+]: 428.12226, found 428.12275.

IV.5. Reactions of Complexes with a halide abstractor, silver oxidant, and base

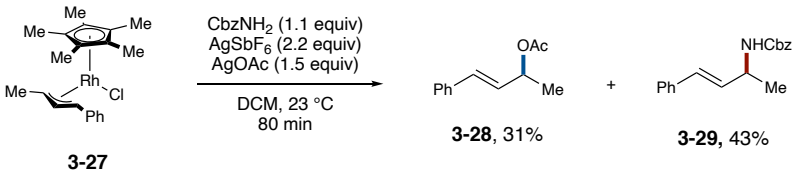

Complex **3-27** (20.4 mg, 0.05 mmol), $CbzNH_2$ (8.8 mg, 0.058 mmol), $AgSbF_6$ (38.8 mg, 0.11 mmol), and AgOAc (13.9 mg, 0.08 mmol) were dissolved in DCM (2 mL) under N_2 and stirred at room temperature for 80 min. The reaction was monitored by TLC for consumption of **3-27**. After consumption of **3-27** was observed (80 min), the reaction was filtered through celite, eluted with DCM, and concentrated under reduced pressure. The remaining residue was purified by column chromatography (Hexanes:EtOAc, 10:0 to 8:2) to afford allylic acetate **3-28** in 31% yield and allylic carbamate **3-29** in 43% yield.

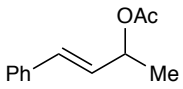

Allylic acetate (3-28): ^{1}H NMR (CDCl3, 400 MHz): δ 7.38 (d, J = 7.6 Hz, 2H), 7.32 (t, J = 7.4 Hz, 2H), 7.27-7.24 (m, 1H), 6.60 (d, J = 15.9 Hz, 1H), 6.19 (dd, J = 16.0, 6.8 Hz, 1H), 5.52 (quintet, J = 6.6 Hz, 1H), 2.08 (s, 3H), 1.41 (d, J = 6.5 Hz, 4H).[21]

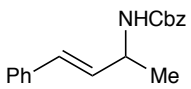

Allylic carbamate (3-29): ^{1}H NMR (CDCl3, 400 MHz): δ 7.37-7.28 (m, 9H), 7.25-7.21 (m, 1H), 6.51 (d, *J* = 16.0 Hz, 1H), 6.16 (dd, *J* = 16.0, 5.8 Hz, 1H), 5.13 (3, 2H), 4.77 (bs, 1H), 4.49 (bs, 1H), 1.34 (d, *J* = 6.8 Hz, 4H). [22]

Reactions of Complex 3-31 in the presence and absence of $AgSbF_6$ and CsOAc.

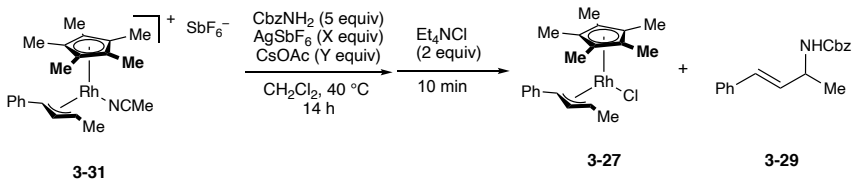

Complex **3-31** (33.3 mg, 0.05 mmol), $CbzNH_2$ (37.8 mg, 0.25 mmol), $AgSbF_6$ (0–34.7 mg, 0–0.1 mmol), and CsOAc (0–19.2 mg, 0–0.1 mmol) were dissolved in DCM (2 mL) under N_2 and stirred at 40 °C. The reaction was monitored by TLC by removing small aliquots with a microliter syringe, adding the aliquot to a solution of Et_4NCl, and monitoring for the chloro-complex **3-27**. In all cases, reactions were not complete within 2 h and were left overnight for 14 h at which point the reactions were quenched with Et_4NCl, filtered through celite, eluted with DCM, and concentrated under reduced pressure. The remaining residue was purified by column chromatography (Hexanes:EtOAc, 10:0 to 8:2) to afford allylic carbamate **3-29** and/or chloro-complex **3-27**.

entry	*$AgSbF_6$ (equiv)*	*CsOAc (equiv)*	*% yield 3-27*	*% yield 3-29*
1	0	0	92%	0%

2	2	0	0%	7%
3	0	2	30%	0%
4	2	2	0%	29%

Reactions of Complex 3-30 in the presence of a silver oxidant.

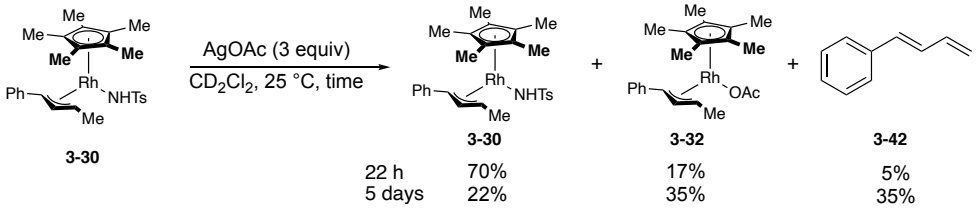

Complex **3-30** (8.3 mg, 0.015) and AgOAc (7.5 mg, 0.045 mmol) were added to an NMR tube and the tube was capped with a septum in a glovebox. CD_2Cl_2 (0.6 mL) and a solution of 1,4-dinitrobenzene in CD_2Cl_2 (internal standard, 0.32 M, 20 μL, 0.006 mmol) were added to the NMR tube via syringe. A ^1H NMR spectrum was acquired immediately and treated as t=0. After 22 h, 1-phenylbutadiene was observed in 5% yield, acetate complex **3-32** was observed in 17% yield, and 70% of complex **3-30** remained unreacted. After 5 days, 1-phenylbutadiene (**3-42**) was observed in 35% yield, acetate complex **3-32** was observed in 35% yield, and 22% of complex **3-30** remained unreacted.

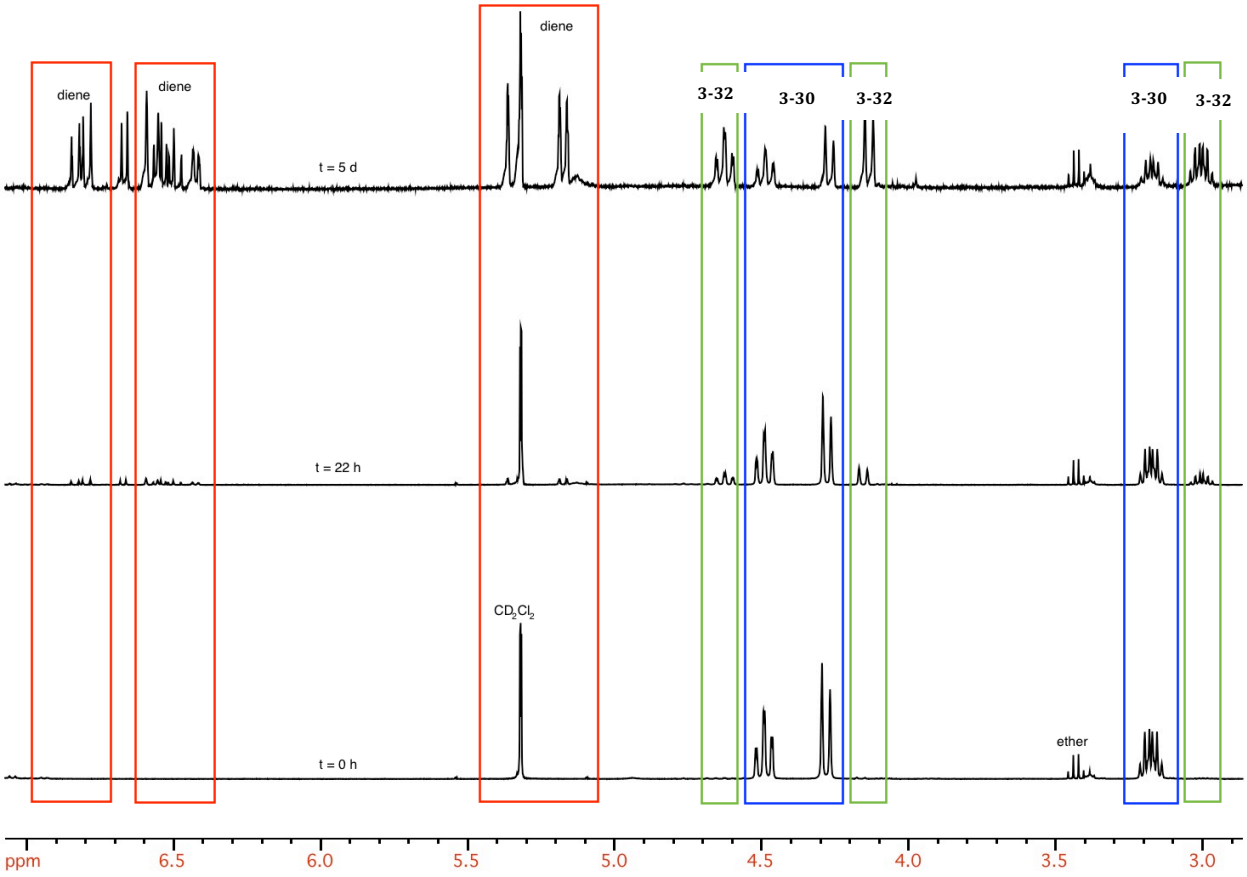

Figure 3-23. ^{1}H-NMR Spectra of the Reaction Between Complex 3-30 (24 mM) and AgOAc (72 mM).

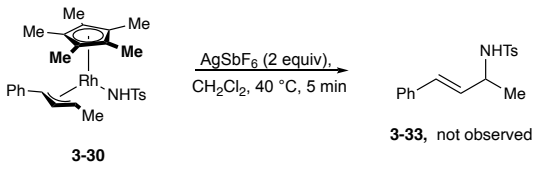

Complex **3-30** (27.0 mg, 0.05 mmol) and $AgSbF_6$ (37.8 mg, 0.11 mmol) were dissolve in DCM (2.0 mL) under N_2 and stirred at 40 °C. The reaction was monitored by TLC by removing

small aliquots with a microliter syringe, diluting with DCM, washing with 1 N HCl (aq) and monitoring for the chloro-complex **3-27**. After 5 min, complex **3-27** was not observed by TLC. The reaction was filtered through celite and concentrated under reduced pressure. Allylic amine **3-33** was not observed by crude ^{1}H NMR.

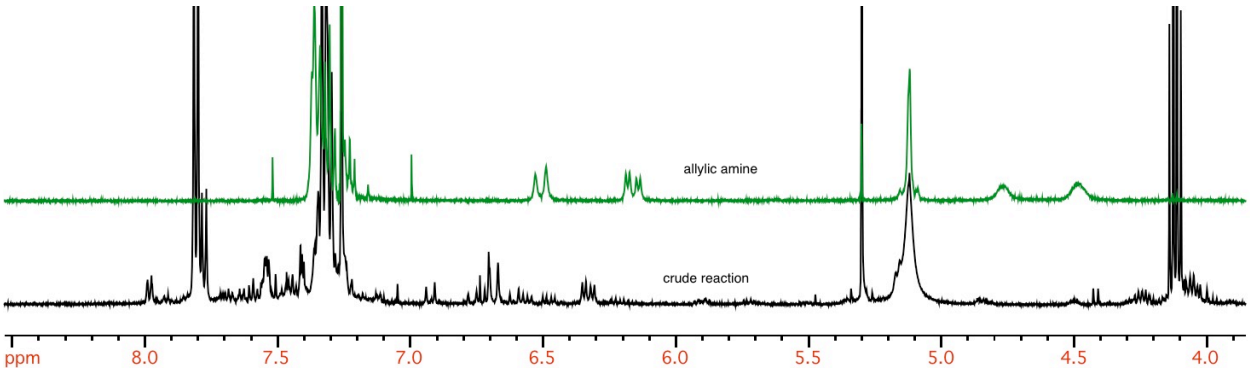

Figure 3-24. ^{1}H-NMR spectrum of the crude reaction mixture between complex 3-30 (25 mM) and $AgSbF_6$ (55 mM) with a 1H-NMR spectrum of an authentic sample of allylic amine 3-33 overlayed.

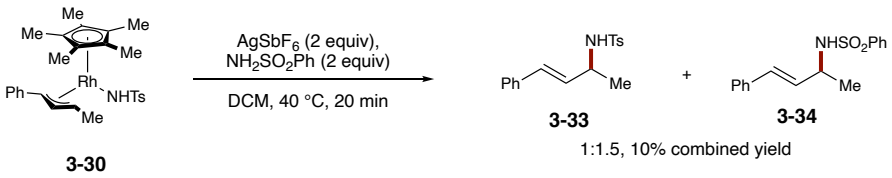

Complex **3-30** (26.7 mg, 0.05 mmol), $AgSbF_6$ (38.1 mg, 0.11 mmol), and benzensulfonamide (17.1, 0.11 mmol) were dissolved in DCM (2.0 mL) under N_2 and stirred at 40 °C. The reaction was monitored by TLC by removing small aliquots with a microliter syringe, diluting with DCM, washing with 1 N HCl (aq) and monitoring for the chloro-complex **3-27**. After 20 min, complex **3-30** was not observed by TLC. The reaction was filtered through

celite and concentrated under reduced pressure. The residue was purified by column chromatography (Hexanes:EtOAc, 10:0 to 8:2) to afford allylic sulfonamides **3-33** and **3-34** in a 1:1.5 ratio and a combined 10% yield.

Reaction of Complex 3-32 in the presence of an oxidant.

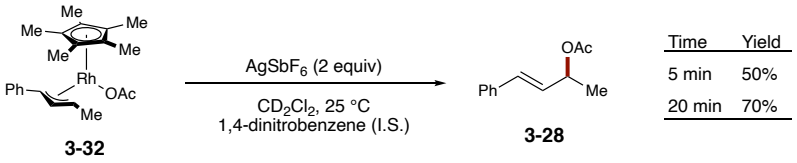

Complex **3-32** (6.7 mg, 0.016 mmol) and AgOAc (11.9 mg, 0.035 mmol) were added to an NMR tube and the tube was capped with a septum in a glovebox. CD_2Cl_2 (0.6 mL) and a solution of 1,4-dinitrobenzene in CD_2Cl_2 (internal standard, 0.32 M, 20 µL, 0.006 mmol) were added to the NMR tube via syringe. A ^{1}H NMR spectrum was acquired after 5 min allylic acetate **3-28** was observed in 50% yield. After 20 min, full consumption of complex **3-32** was observed and allylic acetate **3-28** was observed in 70% yield.

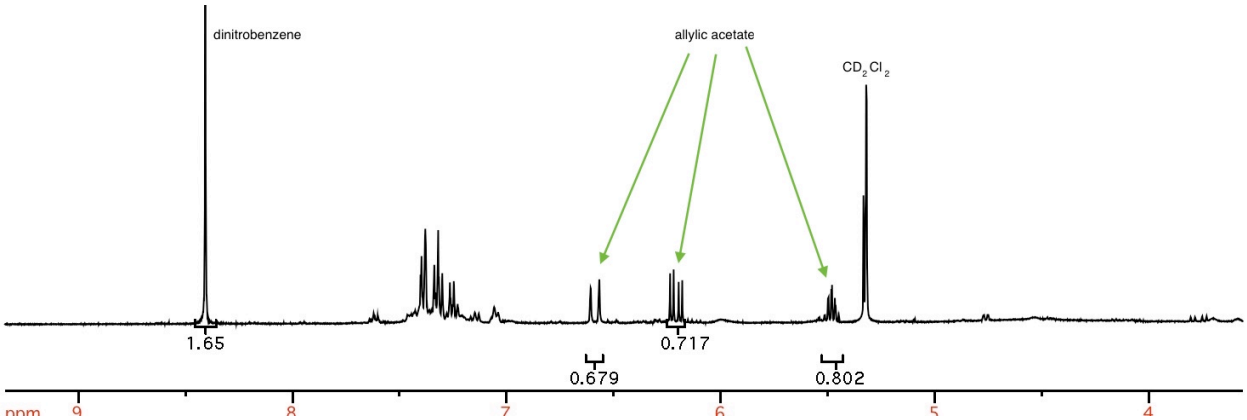

Figure 3-25. ^{1}H-NMR spectrum of the reaction between complex 3-32 (26 mM) and $AgSbF_6$ (56 mM) after 20 min at room temperature.

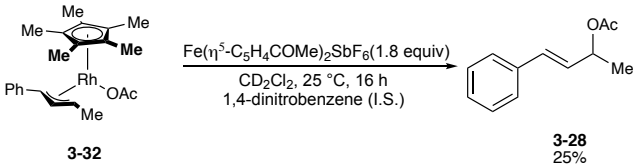

Complex **3-32**(7.7 mg, 0.018 mmol) and $Fe(\eta^5\text{-}C_5H_4COMe)_2SbF_6$ (16.4 mg, 0.032 mmol) were added to an NMR tube and the tube was capped with a septum in a glovebox. 1,4 - Dinitrobenzene (5.1 mg, 0.03 mmol) was dissolve in CD_2Cl_2 (2.8 mL) resulting in a 11 mM solution. 0.6 mL of the resulting solution were added to the NMR tube via syringe. A ^1H NMR spectra at 5 min and 1 h were broadened due to the paramagnetic ferrocenium salt. After 16 h, the ferrocenium was completely consumed, and allylic acetate **3-28** was observed in 25% NMR yield.

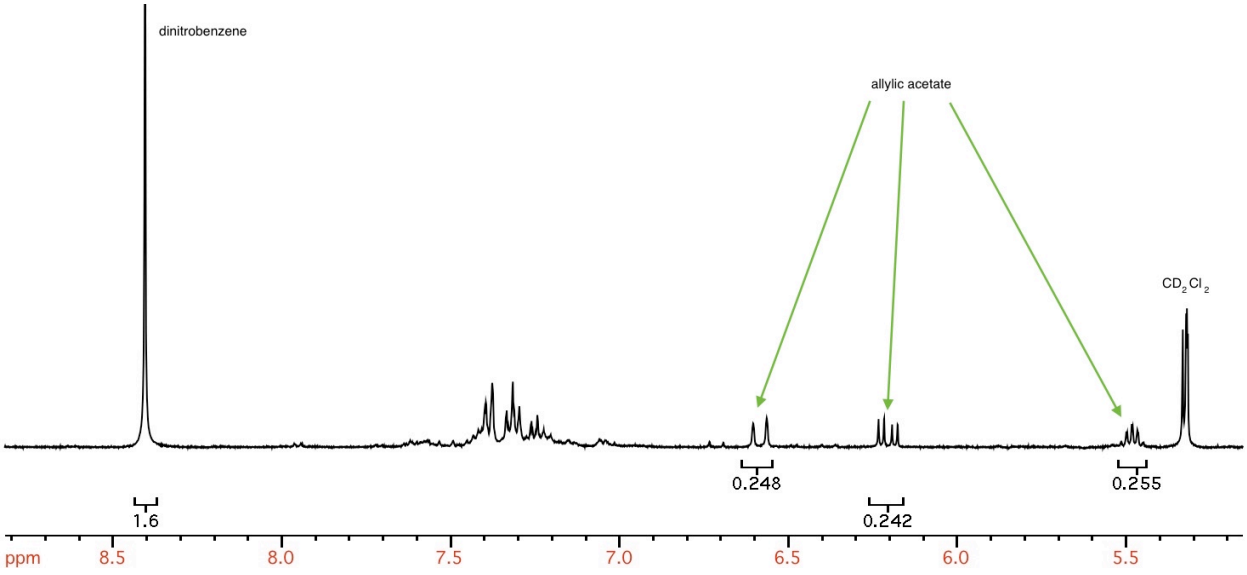

Figure 3-26. ^1H-NMR spectrum of the reaction between complex 3-32 (30 mM) and $Fe(\eta^5\text{-}C_5H_4COMe)_2SbF_6$ (53 mM) after 16 h at room temperature.

IV.6. Reactivity of Allylic Acetate

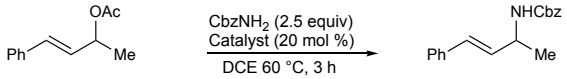

3-28 **3-29**

Benzyl carbamate (75.6 mg, 0.5 mmol) and the catalyst (0.04 mmol) were added to a vial equipped with a stir bar and capped with a septum inside a glove box. The vial was removed from the box, 1,2-dichloroethane (1 mL) was added via syringe and the vial was heated to 60 °C for five minutes. After equilibration, the allylic acetate **3-28** (37.5 μL, d = 1.02 g/mL, 0.2 mmol) was added via syringe, and the reaction was monitored by TLC. After 100 min, starting material was still present in all cases, but a new spot was observed for all reactions with a catalyst present. After 3 h, no discernable change was noticed by TLC from the 100 min time point. The reactions were stopped by filtering through celite and concentrating under reduced pressure. Crude ^{1}H NMR showed no conversion for the reaction with no catalyst, and complete consumption of the allylic acetate for all reactions with a catalyst present. The reaction mixture was purified by column chromatography (Hexanes:EtOAc, 10:0 to 8:2) to afford the allylic carbamate **3-29**.

Table 3-3. Lewis-acid Catalyzed Substitution to Form Amine 3-29

entry	Catalyst	Yield of **3-29**
1	–	0%
2	$AgSbF_6$	91%
3	$AgBF_4$	76%

4	$[RhCp^*Cl_2]_2/AgSbF_6$[a]	73%
5	$[RhCp^*(NCMe)_3](SbF_6)_2$	84%

[a]A mixture of $[RhCp^*Cl_2]_2$ (0.022 mmol) and $AgSF_6$ (0.04 mmol) was stirred in DCE for 30 min before the addition

IV.7. General Procedure for Silver ($AgSbF_6$) or Rhodium ($RhCp^*(MeCN)_3(SbF_6)_2$) as the Lewis-Acid

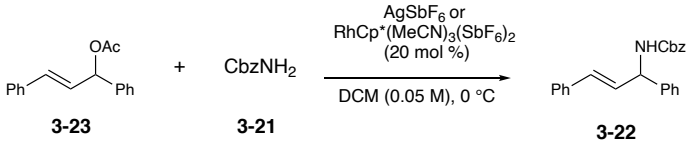

In a nitrogen filled glovebox was weighed $AgSbF_6$ or $RhCp^*(MeCN)_3(SbF_6)_2$ (20 mol %), and benzyl carbamate (2.0 equiv) into a 7 mL oven-dried vial charged with a stir bar. After sealing with a cap and septa, the vial was removed from the glovebox. In another oven dried 7 mL vial was weighed allylic acetate **3-23** to afford a stock solution (50 mg/ 2 mL) in DCM. To the acetate stock solution was then added nonane (1.0 equiv) by microliter syringe. In an ice bath the reaction vial with silver or rhodium was submersed followed by addition of 2 mL of DCM and the dispersion allowed to mix. The acetate stock solution was also cooled in the ice bath to 0°C after which 2 mL of the stock solution was added to the reaction vial. A 1 mL disposal syringe with needle was already placed in the reaction vial and ~50 μL was taken and filtered over a small pad of silica with ethyl acetate into a GC vial and treated as

t=0. Each time point was then analyzed against nonane internal standard utilizing flame ionization GC traces. Error bars show standard deviation of three separate reactions.

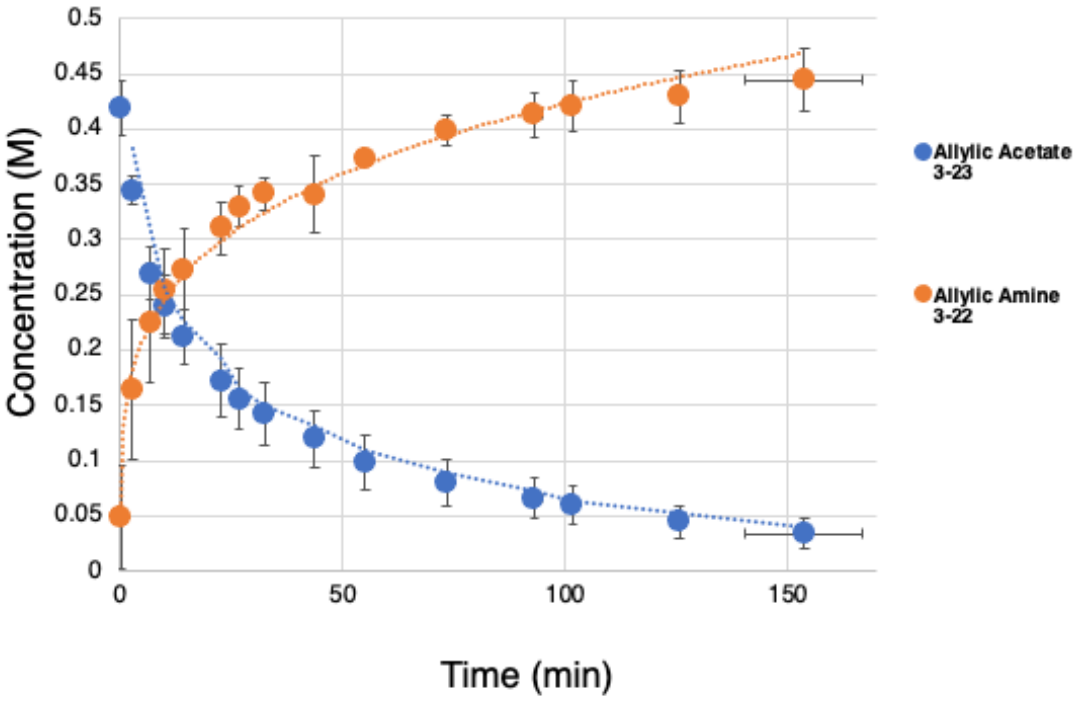

Figure 3-27. Silver ($AgSbF_6$) catalyzed allylic substitution of allylic acetate 3-23 to allylic amine 3-22.

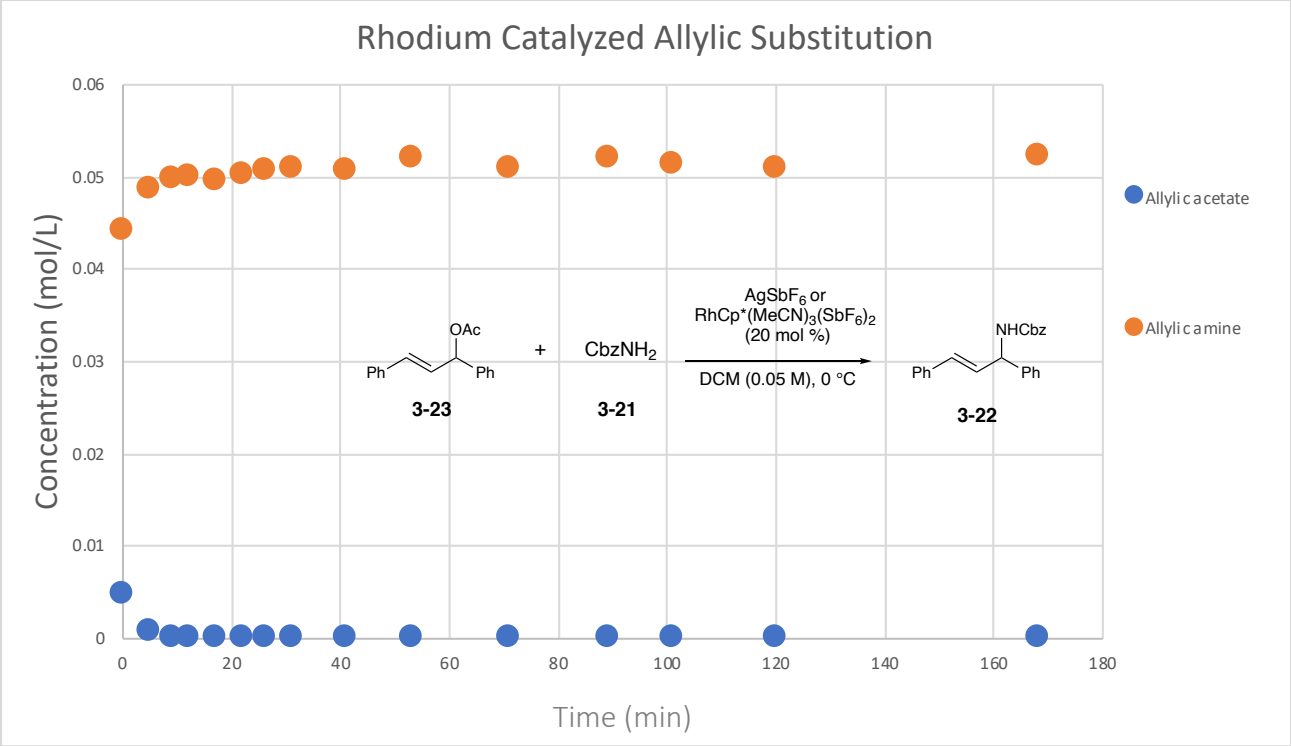

Figure 3-28. Rhodium catalyzed allylic substitution of allylic acetate 3-23 to allylic amine 3-22. Reaction was complete within minutes.

IV.8. General procedure for Cyclic Voltammetry Experiments

Electrochemical measurements **3-32** were conducted using cyclic voltammetry in a 3-electrode cell consisting of a 3mm glassy carbon disc working electrode, a Ag/Ag^+ reference electrode with a Ag wire in a fritted chamber containing a solution of $AgNO_3$ (0.01 M) and nBu$_4$PF$_6$ (0.1 M) in DCM and a Pt wire counter electrode. Experiments were conducted at room temperature inside a N_2 filled glovebox. A solution of **3-32** (0.001 M) and nBu$_4$PF$_6$ (0.1 M) in DCM was added to the electrochemical cell. Cyclic voltammetry scans were taken at selected scan rates (100 mV/s to 2000 mV/s) in the selected potential

window. The cyclic voltammograms of **3-32** were referenced to Fc/Fc^{+} redox couple (Note: The redox potentials reported in this manuscript are determined using Fc/Fc^{+} as an external standard.)

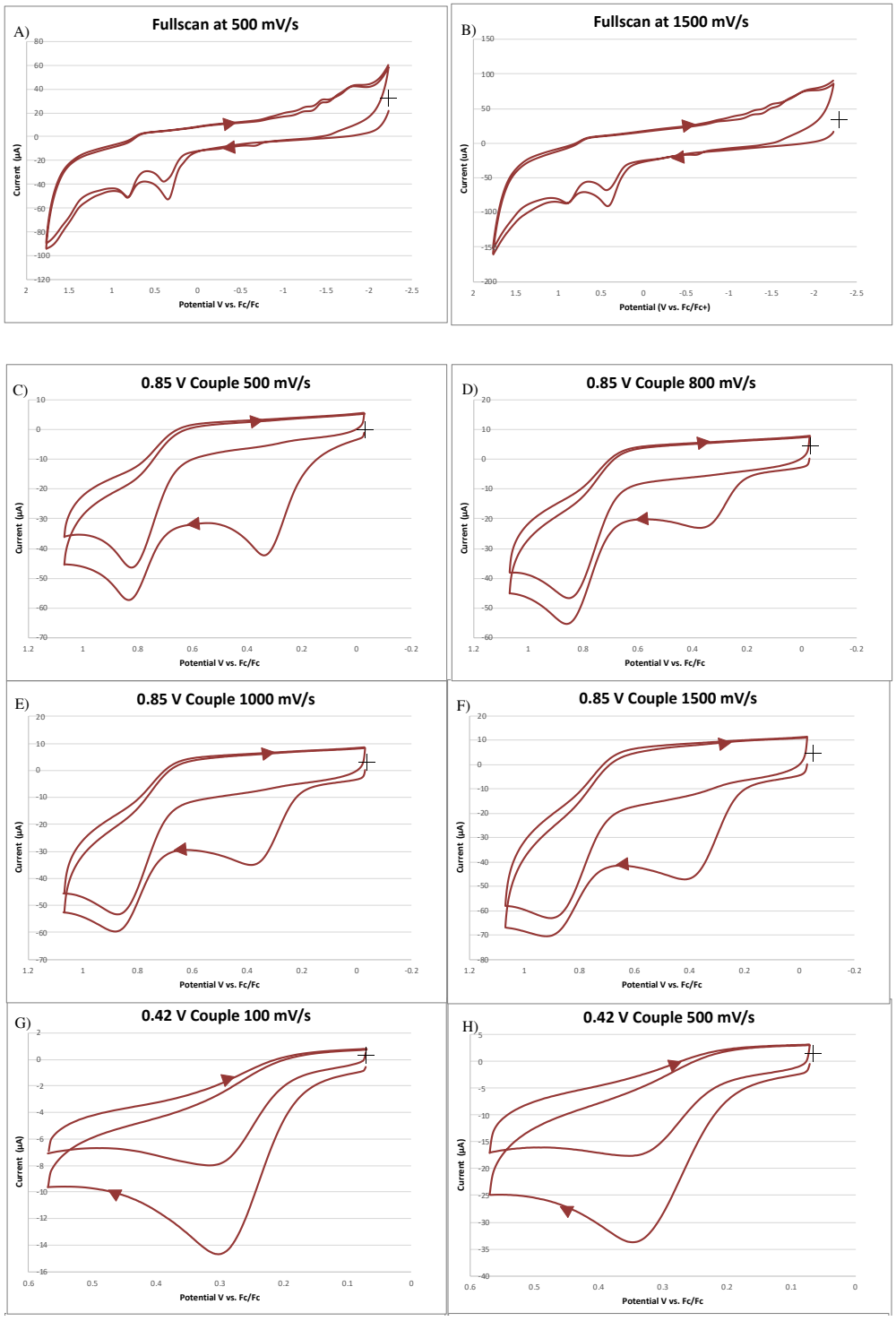

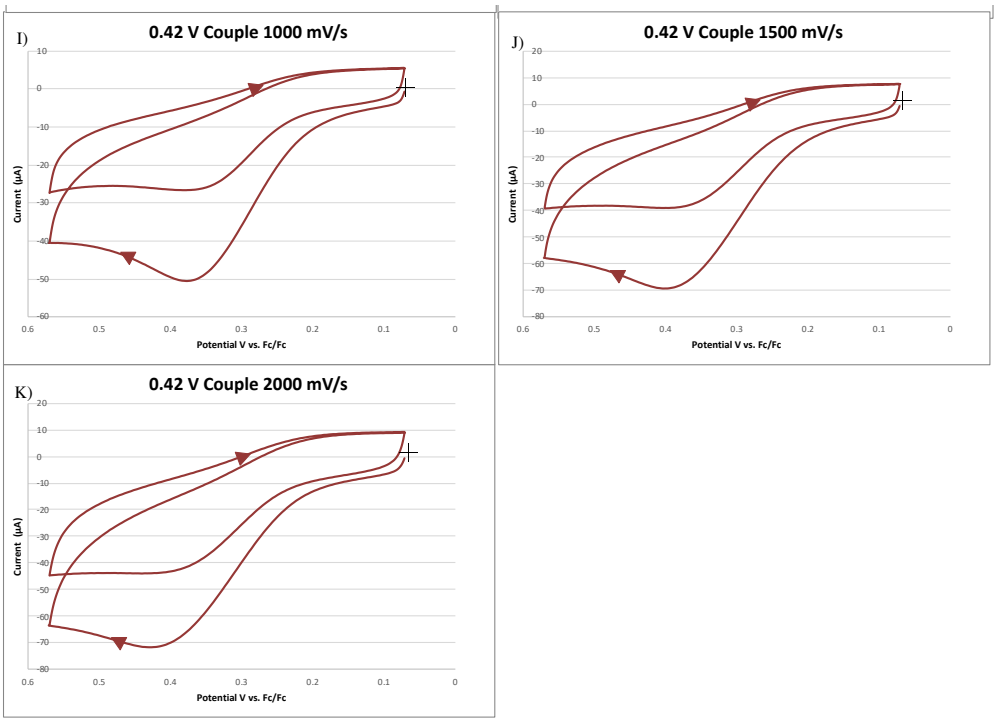

Figure 3-29. Cyclic voltammogram of 3-32 recorded at room temperature in DCM (0.001 M in 0.10 M n-Bu_4NPF_6).

A)Full scan width of cyclic voltammogram 1.7 V to -2.2 V at 500 mV/s showing two quasireversible couples for Rh(IV/V) at ~0.85 V and Rh(III/IV) at ~0.42 V B) Full scan width of cyclic voltammagram 1.7 V to -2.2 V at 1000 mV/s showing two quasireversible couples for Rh(IV/V) at ~0.85 V and Rh(III/IV) at ~0.42 V C) Scan width for proposed Rh(IV/V) voltammogram 1.1V to -0.03 V at 500 mV/s showing quasireversible ~0.85 V couple and scan rate dependence on E^2 (0.85 V) D) Scan width for proposed Rh(IV/V) voltammogram 1.1V to -0.03 V at 800 mV/s showing quasireversible ~0.85 V couple and scan rate dependence on E^2 (0.85 V) E) Scan width for proposed Rh(IV/V) voltammogram 1.1V to -0.03 V at 1000 mV/s showing quasireversible ~0.85 V couple and scan rate dependence on E^2(0.85 V) F) Scan

width for proposed Rh(IV/V) voltammogram 1.1V to -0.03 V at 1500 mV/s showing quasireversible ~0.85 V couple and scan rate dependence on E^2 (0.85 V) G) Scan width for proposed Rh(III/IV) voltammogram 0.60 V to 0.03 V at 100 mV/s showing quasireversible ~0.42 V couple and scan rate dependence on E^1(0.42 V) H) Scan width for proposed Rh(III/IV) voltammogram 0.60 V to 0.03 V at 500 mV/s showing quasireversible ~0.42 V couple and scan rate dependence on E^1 (0.42 V) I) Scan width for proposed Rh(III/IV) voltammogram 0.60 V to 0.03 V at 1000 mV/s showing quasireversible ~0.42 V couple and scan rate dependence on E^1 (0.42 V) J) Scan width for proposed Rh(III/IV) voltammogram 0.60 V to 0.03 V at 1500 mV/s showing quasireversible ~0.42 V couple and scan rate dependence on E^1 (0.42 V) K) Scan width for proposed Rh(III/IV) voltammogram 0.60 V to 0.03 V at 2000 mV/s showing quasireversible ~0.42 V couple and scan rate dependence on E^1 (0.42 V).

IV.9. General Procedure for Allylic Amination Time Course

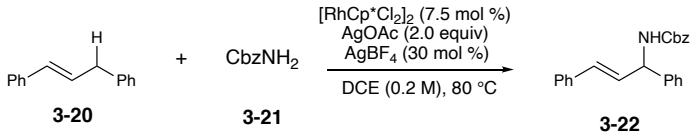

3-20 **3-21** **3-22**

In a nitrogen filled glovebox was weighed $(RhCp^*Cl_2)_2$ (7.5 mol %), benzyl carbamate (2.0 equiv), $AgBF_4$ (30 mol %), and AgOAc (2.0 equiv) into a 7 mL oven-dried vial. The vial was charged with a stir bar and fitted with a septa and cap. The vial was then removed from the glovebox. In a separate 7 mL oven-dried vial was weighed 1,3-diphenylpropene which was purged of air followed by addition of 1,2-DCE to afford a stock solution (200 mg/4 mL). To this stock solution was added nonane (1 equiv) by µliter syringe. To the reaction solids was added 4 mL of the stock solution via syringe after which the vial was placed in a 7 mL heating

block at 80 °C. Aliquots were taken at specified times, filtered through a short pad of silica with ethyl acetate and analyzed by gas chromatography. The reaction was performed in triplicate with standard deviation error bar showing error in yield and time acquired.

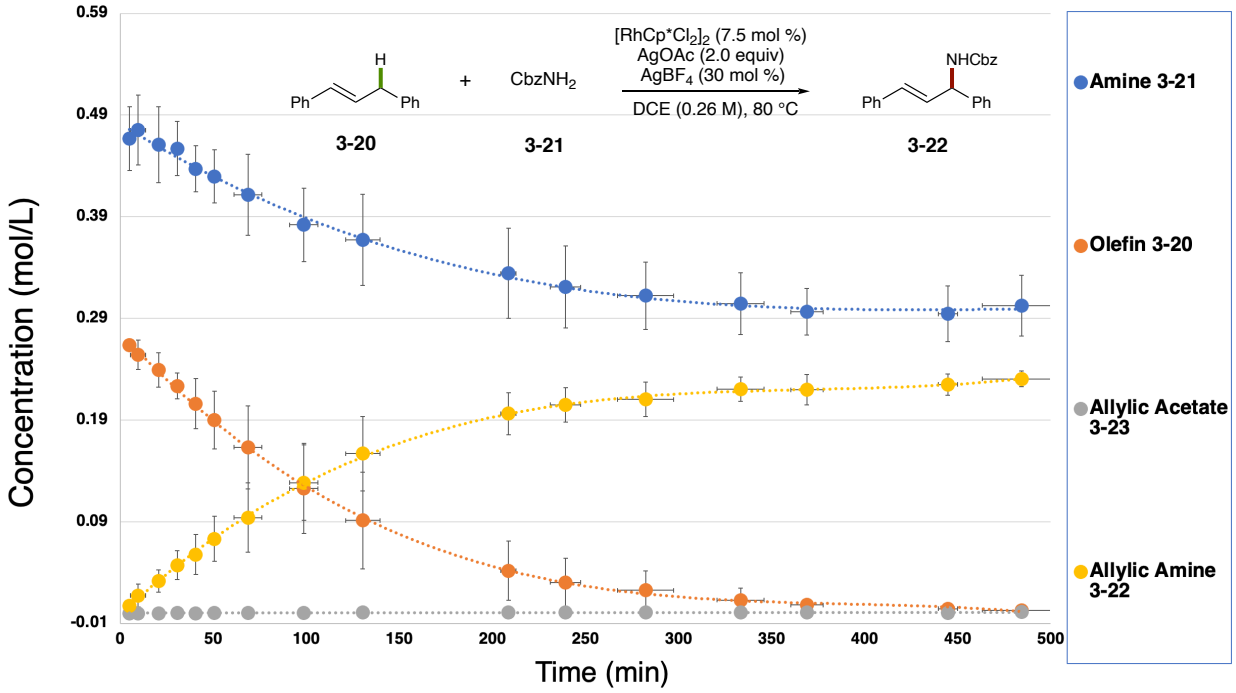

Figure 3-30. Average reaction time course of allylic C–H amination of 1,3-diphenylpropene with benzyl carbamate. Standard deviation is reported from triplicate analysis.

IV.10. Computational details

We performed density functional theory (DFT) calculations using the Jaguar 9.1. software.[23] The Becke's three-parameter exchange functional augmented with Grimme's

D3 correction (B3LYP-D3)[24, 25] in combination with the Pople basis set with *d*- and *p*-orbital polarization functions for hydrogen atoms (6-31G(d,p) basis set)[26] and Los Alamos effective core potential (LANL2DZ) for the transition metal (Rh) was used to optimize the ground state geometries at the given oxidation state of the metal center.[27] Upon completion of the geometry optimizations, single-point electronic structure calculations were followed at the triple-zeta quality basis sets (cc-pVTZ(-f) for main group elements and LACV3P for the transition metal)[28] to reevaluate the energies of optimized structures. The zero-point energy (ZPE) values and vibrational entropy corrections were obtained from the vibrational frequency calculations at the same level of theory as the geometry optimization calculations. Solvation energies were evaluated based on a self-consistent reaction field (SCRF)[29] approach with the dielectric constant (ε) dichloroethane (ε = 10.36) using the optimized gas phase structures.

The free energy in solution phase G(sol) has been calculated as follows:

$$G(sol) = G(gas) + G(solv) \quad (1)$$

$$G(gas) = H(gas) - TS(gas) \quad (2)$$

$$H(gas) = E(SCF) + ZPE \quad (3)$$

$$\Delta E(SCF) = \sum E(SCF) \text{ for products} - \sum E(SCF) \text{ for reactants} \quad (4)$$

$$\Delta G(sol) = \sum G(sol) \text{ for products} - \sum G(sol) \text{ for reactants} \quad (5)$$

G(gas) is the free energy in gas phase; G(solv) is the free energy of solvation as computed using the continuum solvation model; H(gas) is the enthalpy in gas phase; T is

the temperature (298.15K); S(gas) is the entropy in gas phase; E(SCF) is the self-consistent field energy computed at the triple-zeta quality basis set and ZPE is the zero-point energy. Note that by entropy here we refer specifically to the vibrational/rotational/translational entropy of the solute(s) and the entropy of the solvent is incorporated implicitly in the continuum solvation model.

Table S2 Computed Energy Components for Optimized Structures. Units of energies are kcal/mol, except for that of the SCF electronic energy (E(SCF)) which is in eV. The gas phase entropy (-TS(gas)) is computed at 298.15 K.

Structure	E(SCF)	ZPE	-TS(gas)	G(solv)
3-20	-15788.563	152.89	-34.77	-5.08
Methylcarbamate	-7743.108	49.95	-22.24	-9.62
Acetate	-6220.611	30.17	-20.58	-68.71
Acetic acid	-6236.252	38.89	-20.45	-7.75
3-23	-21991.794	179.28	-42.25	-9.69
3-35	-35593.844	319.46	-57.80	-9.82
3-35-TS	-35592.086	318.44	-59.33	-9.46
3-36	-35592.328	319.36	-59.84	-8.96
3-37	-35587.594	319.21	-61.98	-38.36
3-37-TS	-35586.871	318.91	-61.34	-37.74
3-38	-35587.343	320.32	-61.05	-38.01
3-39	-35578.605	319.64	-62.98	-125.12
3-39-TS	-35577.813	319.55	-59.56	-127.26
3-40	-35578.152	320.09	-59.34	-131.54

IV.11. X-ray Crystal Structure Reports

IV.11.1. RhCp*-π-allyl-acetate (3-32)

CCDC 1918703

Crystal Data and Experimental

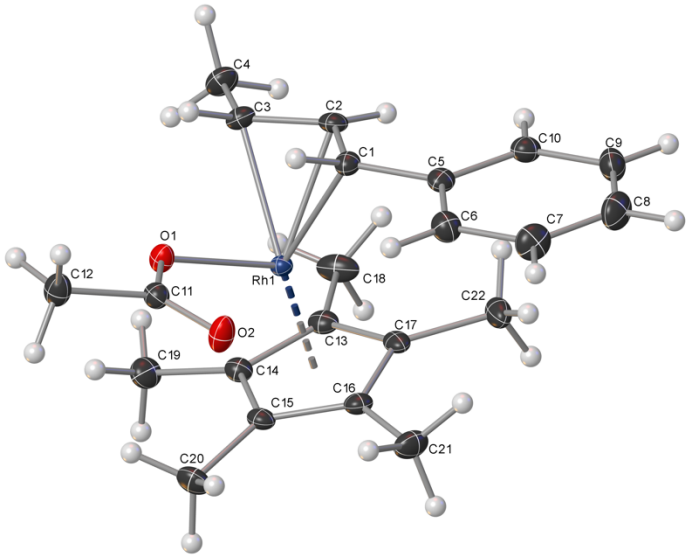

Experimental. Single orange prism shaped crystals of **3-32** were obtained by vapor diffusion of pentane into the ether solution. A suitable crystal 0.13×0.08×0.03 mm^3 was selected and mounted on a suitable support on an XtaLAB Synergy, Dualflex, HyPix diffractometer. The crystal was cooled to T = 100(2) K during data collection. The structure was solved with the **ShelXT** (Sheldrick, 2015) structure solution program using the Intrinsic Phasing solution method and by using **Olex2** (Dolomanov et al., 2009) as the graphical interface. The model was refined with version 2018/3 of **ShelXL-2014** (Sheldrick, 2015) using Least Squares minimisation.

Crystal Data. $C_{22}H_{29}O_2Rh$, M_r = 428.36, monoclinic, $P2_1/c$ (No. 14), a = 7.2611(2) Å, b = 14.6975(3) Å, c = 18.0948(5) Å, β = 95.564(2)°, $\alpha = \gamma$ = 90°, V = 1921.98(8) $Å^3$, T = 100(2) K,

Z = 4, Z' = 1, μ(MoK$_\alpha$) = 0.900, 36145 reflections measured, 5883 unique (R_{int} = 0.0581) which were used in all calculations. The final wR_2 was 0.0649 (all data) and R_1 was 0.0280 (I > 2σ(I)).

Compound	**Rh-pi-allyl-complex**
Formula	$C_{22}H_{29}O_2Rh$
$D_{calc.}$/ g cm^{-3}	1.480
μ/mm^{-1}	0.900
Formula Weight	428.36
Colour	orange
Shape	prism
Size/mm^3	0.13×0.08×0.03
T/K	100(2)
Crystal System	monoclinic
Space Group	$P2_1/c$
a/Å	7.2611(2)
b/Å	14.6975(3)
c/Å	18.0948(5)
α/°	90
β/°	95.564(2)
γ/°	90
V/Å^3	1921.98(8)
Z	4
Z'	1
Wavelength/Å	0.71073
Radiation type	MoK$_\alpha$
Θ_{min}/°	1.788
Θ_{max}/°	30.508

Measured Refl.	36145
Independent Refl.	5883
Reflections with I > 2σ(I)	4968
R_{int}	0.0581
Parameters	243
Restraints	3
Largest Peak	0.555
Deepest Hole	-0.410
GooF	1.049
wR_2 (all data)	0.0649
wR_2	0.0624
R_1 (all data)	0.0371
R_1	0.0280

Structure Quality Indicators

Reflections:	d min (Mo) 0.70	I/σ 24.8	Rint 5.81%	complete 100% (IUCr) 100%
Refinement:	Shift 0.001	Max Peak 0.6	Min Peak -0.4	GooF 1.049

A orange prism shaped crystal with dimensions 0.13×0.08×0.03 mm^3 was mounted on a suitable support. Data were collected using an XtaLAB Synergy, Dualflex, HyPix diffractometer equipped with an Oxford Cryosystems low-temperature device, operating at T = 100(2) K.

Data were measured using ω scans of 0.5° per frame for 10.0 s using MoK$_\alpha$ radiation (micro-focus sealed X-ray tube, 50 kV, 1.0 mA). The total number of runs and images was based on the strategy calculation from the program **CrysAlisPro** (Rigaku, V1.171.39.43c, 2018). The maximum resolution that was achieved was Θ = 30.508°.

The diffraction patterns were indexed using **CrysAlisPro** (Rigaku, V1.171.39.43c, 2018) and the unit cells were refined using **CrysAlisPro** (Rigaku, V1.171.39.43c, 2018) on 18003 reflections, 50 % of the observed reflections. Data reduction, scaling and absorption corrections were performed using **CrysAlisPro** (Rigaku, V1.171.39.43c, 2018) and CrysAlisPro 1.171.39.43c (Rigaku Oxford Diffraction, 2018). A numerical absorption correction based on Gaussian integration over a multifaceted crystal model was used. An empirical absorption correction using spherical harmonics as implemented in SCALE3 ABSPACK was also used. The final completeness is 100.00% out to 30.508° in Θ. The absorption coefficient μ of this material is 0.900 mm^{-1} at this wavelength (λ = 0.711Å) and the minimum and maximum transmissions are 0.855 and 1.000.

The structure was solved and the space group $P2_1/c$ (# 14) determined by the **ShelXT** (Sheldrick, 2015) structure solution program using Intrinsic Phasing and refined by Least Squares using version 2018/3 of **ShelXL-2014** (Sheldrick, 2015). All non-hydrogen atoms were refined anisotropically. Hydrogen atom positions were calculated geometrically and refined using the riding model.

There is a single molecule in the asymmetric unit, which is represented by the reported sum formula. In other words: Z is 4 and Z' is 1.

Images of the Crystal on the Diffractometer

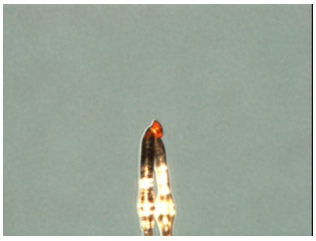

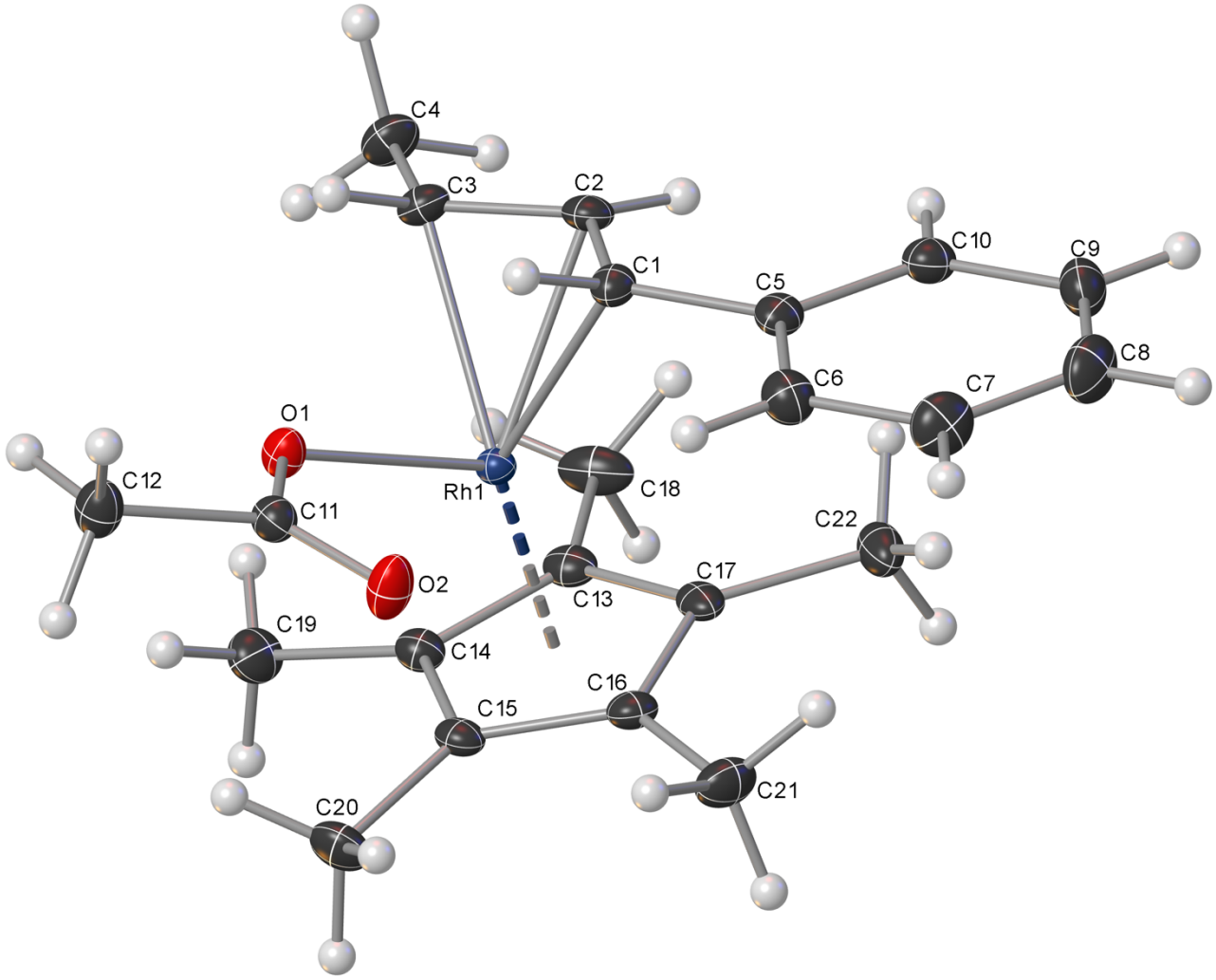

Figure 3-31. Structure Complex 3-32

Data Plots: Diffraction Data

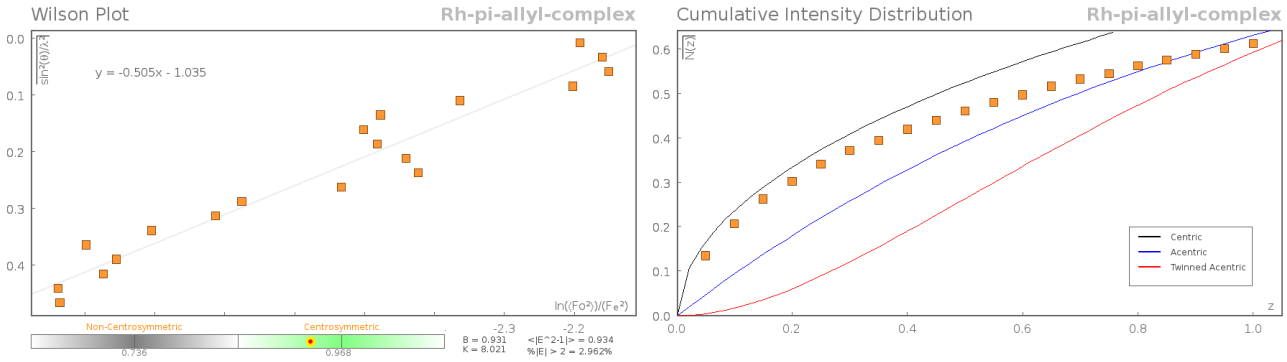

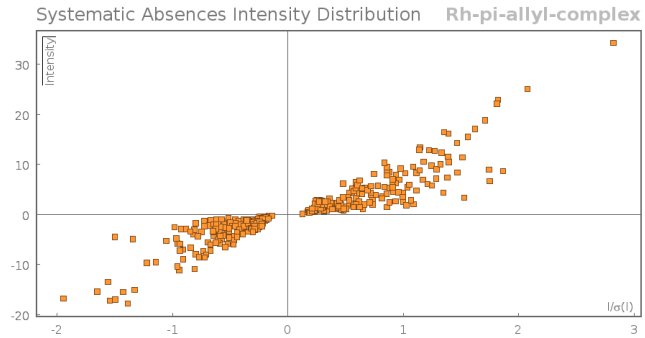

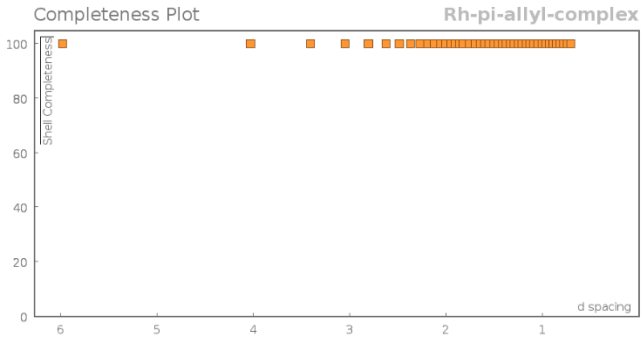

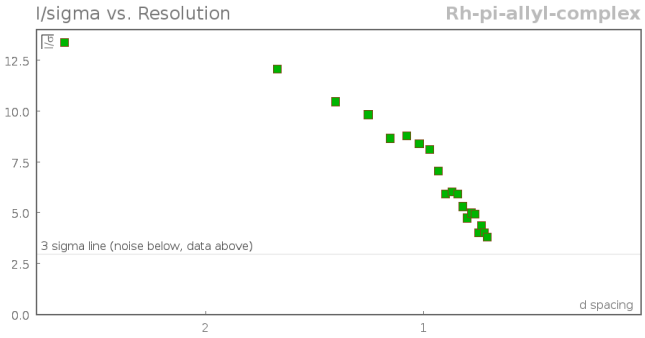

Data Plots: Refinement and Data

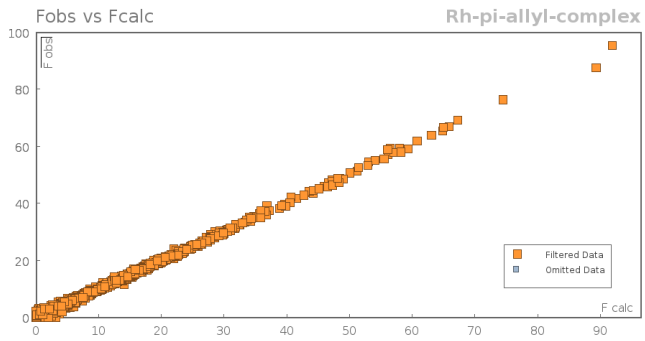

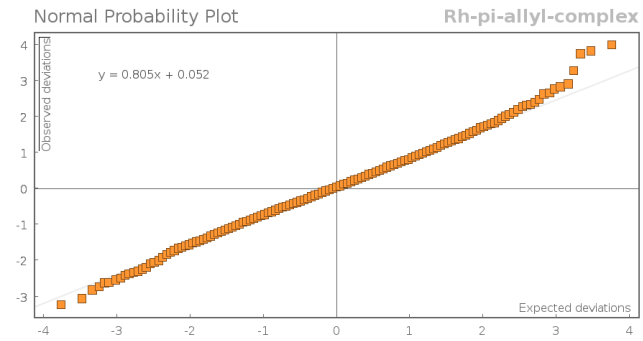

Reflection Statistics

Total reflections (after filtering)	36810	Unique reflections	5883
Completeness	1.0	Mean I/σ	17.87
hkl_{max} collected	(10, 20, 25)	hkl_{min} collected	(-10, -20, -25)
hkl_{max} used	(10, 20, 25)	hkl_{min} used	(-10, 0, 0)

Lim d_{max} collected	100.0	Lim d_{min} collected	0.36
d_{max} used	11.39	d_{min} used	0.7
Friedel pairs	7871	Friedel pairs merged	1
Inconsistent equivalents	0	R_{int}	0.0581
R_{sigma}	0.0403	Intensity transformed	0
Omitted reflections	0	Omitted by user (OMIT hkl)	0
Multiplicity	(8654, 6755, 2932, 840, 249, 111, 52, 20, 5, 1)	Maximum multiplicity	18
Removed systematic absences	665	Filtered off (Shel/OMIT)	0

Table 3-4. Fractional Atomic Coordinates (×10⁴) and Equivalent Isotropic Displacement Parameters (Å2×10³) for Rh-pi-allyl-complex 3-32. U_{eq} is defined as 1/3 of the trace of the orthogonalised U_{ij}.

Atom	**x**	**y**	**z**	***U_{eq}***
Rh1	3584.1(2)	3831.9(2)	1862.0(2)	10.23(4)
O1	4843.6(17)	4695.9(8)	1128.6(7)	14.7(2)
O2	5749.0(19)	5820.5(9)	1925.4(7)	21.1(3)
C11	5549(2)	5482.8(11)	1299.9(10)	14.6(3)
C2	5612(2)	2780.6(11)	2043.1(10)	14.8(3)
C3	5030(2)	2784.3(11)	1276.5(10)	15.1(3)
C1	6400(2)	3579.4(12)	2379.4(10)	13.9(3)
C14	619(2)	3960.5(11)	1501.2(10)	13.8(3)
C17	1717(2)	3563.0(12)	2706.1(10)	15.4(3)
C5	6904(2)	3684.8(12)	3180.0(10)	14.8(3)

Atom	x	y	z	U_{eq}
C13	914(2)	3216.2(11)	2003.6(10)	15.0(3)
C15	1258(2)	4768.3(11)	1905.2(10)	14.0(3)
C16	1893(2)	4528.5(11)	2646.4(10)	14.8(3)
C10	6794(2)	2973.8(12)	3684.7(10)	17.8(4)
C9	7328(3)	3099.9(13)	4434.2(10)	21.6(4)
C22	2076(3)	3013.5(14)	3399.8(11)	22.5(4)
C6	7562(3)	4530.2(12)	3451.7(11)	19.5(4)
C19	-247(3)	3936.8(13)	721.2(11)	21.1(4)
C12	6136(3)	6002.4(12)	636.7(10)	19.5(4)
C21	2609(3)	5166.0(13)	3253.1(11)	21.8(4)
C8	7978(3)	3937.4(14)	4695.0(11)	25.9(4)
C4	4074(3)	1979.8(12)	900.1(11)	20.1(4)
C18	338(3)	2252.1(12)	1862.1(12)	23.2(4)
C7	8083(3)	4651.2(14)	4200.3(11)	24.5(4)
C20	1149(3)	5708.9(12)	1595.5(11)	20.7(4)

Table 3-5. Anisotropic Displacement Parameters (×10⁴) Rh-pi-allyl-complex 3-32.

The anisotropic displacement factor exponent takes the form: $-2\pi^2[h^2a^{*2} \times U_{11} + ... + 2hka^* \times b^* \times U_{12}]$

Atom	U_{11}	U_{22}	U_{33}	U_{23}	U_{13}	U_{12}
Rh1	9.60(7)	9.61(6)	11.67(7)	0.25(5)	2.07(4)	0.07(4)
O1	18.5(6)	12.4(6)	13.7(6)	0.3(4)	3.3(5)	-2.8(5)
O2	31.5(8)	18.4(6)	13.7(6)	-1.8(5)	3.6(5)	-5.7(5)
C11	13.4(8)	15.1(8)	15.6(8)	1.8(6)	2.2(6)	-0.2(6)
C2	11.9(8)	13.7(8)	19.2(9)	0.1(6)	3.3(6)	3.9(6)

Atom	U_{11}	U_{22}	U_{33}	U_{23}	U_{13}	U_{12}
C3	14.5(8)	14.3(8)	17.2(9)	-2.9(6)	5.4(7)	0.3(6)
C1	10.8(7)	17.0(8)	14.0(8)	0.0(6)	2.0(6)	1.0(6)
C14	10.3(7)	13.7(8)	17.4(8)	0.3(6)	1.1(6)	-0.6(6)
C17	9.9(7)	18.2(8)	19.1(9)	4.8(7)	5.8(6)	3.9(6)
C5	9.9(7)	18.6(9)	15.7(8)	-0.6(6)	0.1(6)	1.9(6)
C13	9.6(7)	14.9(8)	21.2(9)	0.6(6)	4.4(6)	-0.3(6)
C15	9.7(7)	13.7(8)	18.8(9)	1.8(6)	2.6(6)	2.3(6)
C16	11.5(8)	16.0(8)	17.1(8)	-1.8(6)	3.1(6)	2.6(6)
C10	16.0(8)	18.3(8)	19.2(9)	-0.9(7)	1.6(7)	2.7(6)
C9	20.5(9)	27.1(10)	16.9(9)	5.7(7)	1.0(7)	1.9(7)
C22	17.9(9)	29.6(10)	20.9(10)	10.6(8)	6.8(7)	5.3(7)
C6	17.4(9)	20.5(9)	20.4(9)	1.3(7)	0.7(7)	-1.2(7)
C19	17.7(9)	25.4(10)	19.4(9)	-1.3(7)	-2.3(7)	1.4(7)
C12	25.7(10)	16.2(8)	16.8(9)	0.7(7)	3.7(7)	-3.3(7)
C21	20.4(9)	24.7(9)	20.3(9)	-8.0(7)	1.5(7)	2.6(7)
C8	24.3(10)	36.6(11)	15.9(9)	-3.1(8)	-3.0(8)	-1.9(8)
C4	23.0(9)	18.1(9)	19.8(9)	-5.5(7)	4.7(7)	-0.8(7)
C18	15.5(9)	13.3(8)	41.9(12)	-0.1(8)	7.7(8)	-2.8(7)
C7	22.8(10)	26.7(10)	23.3(10)	-5.8(8)	-1.9(8)	-5.2(8)
C20	21.1(9)	12.8(8)	27.9(10)	3.2(7)	1.1(8)	2.5(7)

Table 3-6. Bond Lengths in Å for Rh-pi-allyl-complex 3-32.

Atom	Atom	Length/Å
Rh1	O1	2.1084(12)

Atom	Atom	Length/Å
Rh1	C2	2.1379(16)
Rh1	C3	2.1935(17)
Rh1	C1	2.1963(17)
Rh1	C14	2.1966(17)
Rh1	C17	2.1743(17)
Rh1	C13	2.1772(16)
Rh1	C15	2.1860(16)
Rh1	C16	2.2155(17)
O1	C11	1.290(2)
O2	C11	1.232(2)
C11	C12	1.518(2)
C2	C3	1.410(3)
C2	C1	1.417(2)
C3	C4	1.501(2)
C1	C5	1.468(2)
C14	C13	1.425(2)
C14	C15	1.447(2)
C14	C19	1.489(3)
C17	C13	1.440(3)
C17	C16	1.430(2)
C17	C22	1.494(2)
C5	C10	1.395(2)
C5	C6	1.403(2)
C13	C18	1.493(2)
C15	C16	1.420(2)
C15	C20	1.491(2)

Atom	Atom	Length/Å
C16	C21	1.498(2)
C10	C9	1.386(3)
C9	C8	1.385(3)
C6	C7	1.382(3)
C8	C7	1.386(3)

Table 3-7. Bond Angles in ° for Rh-pi-allyl-complex 3-32.

Atom	Atom	Atom	Angle/˚
O1	Rh1	C2	101.38(6)
O1	Rh1	C3	82.04(6)
O1	Rh1	C1	85.83(6)
O1	Rh1	C14	103.51(6)
O1	Rh1	C17	152.83(6)
O1	Rh1	C13	140.35(6)
O1	Rh1	C15	91.55(5)
O1	Rh1	C16	115.22(6)
C2	Rh1	C3	37.98(7)
C2	Rh1	C1	38.14(6)
C2	Rh1	C14	138.46(6)
C2	Rh1	C17	103.18(7)
C2	Rh1	C13	106.83(6)
C2	Rh1	C15	166.59(7)
C2	Rh1	C16	130.71(7)
C3	Rh1	C1	67.53(6)

Atom	Atom	Atom	Angle/°
C3	Rh1	C14	114.72(7)
C3	Rh1	C16	162.71(7)
C1	Rh1	C14	170.55(6)
C1	Rh1	C16	110.85(6)
C14	Rh1	C16	64.05(6)
C17	Rh1	C3	124.88(7)
C17	Rh1	C1	106.73(6)
C17	Rh1	C14	64.19(7)
C17	Rh1	C13	38.64(7)
C17	Rh1	C15	63.44(6)
C17	Rh1	C16	38.00(6)
C13	Rh1	C3	103.80(6)
C13	Rh1	C1	133.04(6)
C13	Rh1	C14	38.03(6)
C13	Rh1	C15	63.74(6)
C13	Rh1	C16	63.99(6)
C15	Rh1	C3	150.10(7)
C15	Rh1	C1	141.42(6)
C15	Rh1	C14	38.56(6)
C15	Rh1	C16	37.63(6)
C11	O1	Rh1	125.09(11)
O1	C11	C12	113.36(15)
O2	C11	O1	126.21(16)
O2	C11	C12	120.43(15)
C3	C2	Rh1	73.15(10)
C3	C2	C1	119.28(16)

Atom	Atom	Atom	Angle/°
C1	C2	Rh1	73.16(10)
C2	C3	Rh1	68.87(9)
C2	C3	C4	121.64(16)
C4	C3	Rh1	123.38(12)
C2	C1	Rh1	68.69(9)
C2	C1	C5	124.26(16)
C5	C1	Rh1	122.39(12)
C13	C14	Rh1	70.25(10)
C13	C14	C15	106.65(15)
C13	C14	C19	127.60(15)
C15	C14	Rh1	70.33(9)
C15	C14	C19	125.70(15)
C19	C14	Rh1	126.27(13)
C13	C17	Rh1	70.79(10)
C13	C17	C22	124.97(16)
C16	C17	Rh1	72.56(10)
C16	C17	C13	108.43(15)
C16	C17	C22	126.19(17)
C22	C17	Rh1	128.23(12)
C10	C5	C1	122.85(16)
C10	C5	C6	118.24(17)
C6	C5	C1	118.89(16)
C14	C13	Rh1	71.72(10)
C14	C13	C17	108.33(15)
C14	C13	C18	126.66(17)
C17	C13	Rh1	70.57(9)

Atom	Atom	Atom	Angle/°
C17	C13	C18	124.78(16)
C18	C13	Rh1	127.76(12)
C14	C15	Rh1	71.12(9)
C14	C15	C20	124.63(16)
C16	C15	Rh1	72.31(9)
C16	C15	C14	109.41(14)
C16	C15	C20	125.86(16)
C20	C15	Rh1	125.68(12)
C17	C16	Rh1	69.44(9)
C17	C16	C21	126.35(16)
C15	C16	Rh1	70.06(10)
C15	C16	C17	107.14(15)
C15	C16	C21	126.51(16)
C21	C16	Rh1	125.73(12)
C9	C10	C5	120.79(17)
C8	C9	C10	120.39(18)
C7	C6	C5	120.59(17)
C9	C8	C7	119.41(18)
C6	C7	C8	120.57(18)

Table 3-8. Hydrogen Fractional Atomic Coordinates (×10⁴) and Equivalent Isotropic Displacement Parameters (Å²×10³) for Rh-pi-allyl-complex 3-32

U_{eq} is defined as 1/3 of the trace of the orthogonalised U_{ij}.

Atom	x	y	z	U_{eq}
H10	6356.85	2408.59	3516.36	21
H9	7248.09	2619.23	4763.86	26
H22A	2530.65	2423.78	3279.53	34
H22B	946.69	2946.87	3630.05	34
H22C	2980.21	3316.79	3735.45	34
H6	7648.59	5013.51	3125.11	23
H19A	394.01	4348.9	423.84	32
H19B	-1521.57	4115.24	708.83	32
H19C	-172.26	3331.04	527.98	32
H12A	5882.29	5642.37	195.94	29
H12B	7437.86	6129.61	712.5	29
H12C	5460.9	6563.7	582.33	29
H21A	3449.98	4846.97	3604.44	33
H21B	1592.98	5396.78	3499.25	33
H21C	3243.4	5662.79	3044.42	33
H8	8341.52	4020.17	5197.55	31
H4A	3492.57	1626.93	1258.77	30
H4B	4964.57	1610.54	679.81	30
H4C	3153.42	2187.39	521	30
H18A	289.32	2127.15	1339.82	35
H18B	-862.66	2156.22	2028.73	35

Atom	x	y	z	U_{eq}
H18C	1216.44	1852.7	2126.75	35
H7	8508.08	5216.41	4373.62	29
H20A	2034.43	6089.8	1876.49	31
H20B	-72.71	5947.2	1624.42	31
H20C	1415.95	5695.43	1086.29	31
H1	7030(30)	3967(11)	2067(10)	16(3)
H3	5670(20)	3161(12)	960(10)	16(3)
H2	5210(30)	2307(11)	2346(10)	16(3)

Citations for Crystallography

CrysAlisPro Software System, Rigaku Oxford Diffraction, (2018).

O.V. Dolomanov and L.J. Bourhis and R.J. Gildea and J.A.K. Howard and H. Puschmann, Olex2: A complete structure solution, refinement and analysis program, *J. Appl. Cryst.*, (2009), **42**, 339-341.

Sheldrick, G.M., Crystal structure refinement with ShelXL, *Acta Cryst.*, (2015), **C27**, 3-8.

Sheldrick, G.M., ShelXT-Integrated space-group and crystal-structure determination, *Acta Cryst.*, (2015), **A71**, 3-8.

```
#===============================================================================
# PLATON/CHECK-( 70414) versus check.def version of 310314   for Entry: rh-pi-al
# Data: Rh-pi-allyl-complex.cif - Type: CIF      Bond Precision   C-C = 0.0026 A
# Refl: Rh-pi-allyl-complex.fcf - Type: LIST4                      Temp = 100 K
#                                              X-Ray         Nref/Npar =  24.2
# Cell   7.2611(2)  14.6975(3)  18.0948(5)           90    95.564(2)          90
# Wavelength 0.71073    Volume Reported    1921.98(8)   Calculated    1921.98(8)
# SpaceGroup from Symmetry P 21/c     Hall: -P 2ybc               monoclinic
#                 Reported P 1 21/c 1       -P 2ybc               monoclinic
# MoietyFormula C22 H29 O2 Rh
#      Reported C22 H29 O2 Rh
#    SumFormula C22 H29 O2 Rh
#      Reported C22 H29 O2 Rh
# Mr        =    428.36[Calc],    428.36[Rep]
# Dx,gcm-3  =     1.480[Calc],     1.480[Rep]
# Z         =         4[Calc],         4[Rep]
# Mu (mm-1) =     0.900[Calc],     0.900[Rep]
# F000      =     888.0[Calc],     888.0[Rep]  or F000' =    883.82[Calc]
# Reported   T Limits: Tmin=0.855             Tmax=1.000  AbsCorr=GAUSSIAN
# Calculated T Limits: Tmin=0.915 Tmin'=0.887  Tmax=0.972
# Reported   Hmax= 10, Kmax= 20, Lmax= 25, Nref=   5883        , Th(max)= 30.508
# Obs in FCF Hmax= 10, Kmax= 20, Lmax= 25, Nref=   5883[  5883], Th(max)= 30.508
# Calculated Hmax= 10, Kmax= 20, Lmax= 25, Nref=   5883        , Ratio  =  1.000
# Reported   Rho(min) = -0.41, Rho(max) =  0.56 e/Ang**3 (From CIF)
# Calculated Rho(min) = -0.42, Rho(max) =  0.60 e/Ang**3 (From CIF+FCF data)
# w=1/[sigma**2(Fo**2)+(0.0269P)**2+  0.4570P], P=(Fo**2+2*Fc**2)/3
# R= 0.0280(  4968), wR2= 0.0649(  5883), S = 1.049      (From CIF+FCF data)
# R= 0.0280(  4968), wR2= 0.0649(  5883), S = 1.049      (From FCF data only)
# R= 0.0280(  4968), wR2= 0.0649(  5883), S = 1.049, Npar=  243
#===============================================================================
For Documentation: http://http://www.platonsoft.nl/CIF-VALIDATION.pdf
```

```
#==============================================================================

#==============================================================================
>>> The Following Improvement and Query ALERTS were generated - (Acta-Mode) <<<
#==============================================================================
Format: alert-number_ALERT_alert-type_alert-level text

761_ALERT_1_C CIF Contains no X-H Bonds .....................     Please Check
762_ALERT_1_C CIF Contains no X-Y-H or H-Y-H Angles ..........     Please Check
906_ALERT_3_C Large K value in the Analysis of Variance ......      2.018 Check
#==============================================================================
002_ALERT_2_G Number of Distance or Angle Restraints on AtSite          6 Note
008_ALERT_5_G No _iucr_refine_reflections_details   in the CIF     Please Do !
164_ALERT_4_G Nr. of Refined C-H H-Atoms in Heavy-Atom Struct.          3 Note
380_ALERT_4_G Incorrectly? Oriented X(sp2)-Methyl Moiety .....         C4 Check
380_ALERT_4_G Incorrectly? Oriented X(sp2)-Methyl Moiety .....        C12 Check
760_ALERT_1_G CIF Contains no Torsion Angles .................          ? Info
795_ALERT_4_G C-Atom in CIF Coordinate List out of Sequence ..         C2 Note
802_ALERT_4_G CIF Input Record(s) with more than 80 Characters          ! Info
860_ALERT_3_G Number of Least-Squares Restraints .............          3 Note
#==============================================================================

ALERT_Level and ALERT_Type Summary
==================================
3 ALERT_Level_C = Check. Ensure it is Not caused by an Omission or Oversight
9 ALERT_Level_G = General Info/Check that it is not Something Unexpected

3 ALERT_Type_1 CIF Construction/Syntax Error, Inconsistent or Missing Data.
1 ALERT_Type_2 Indicator that the Structure Model may be Wrong or Deficient.
2 ALERT_Type_3 Indicator that the Structure Quality may be Low.
5 ALERT_Type_4 Improvement, Methodology, Query or Suggestion.
```

```
1 ALERT_Type_5 Informative Message, Check.

#==============================================================================

1 Missing  Experimental  Info Issue(s) (Out of  54 Tests) -   98 % Satisfied

0 Experimental  Data  Related Issue(s) (Out of  28 Tests) -  100 % Satisfied

6 Structural  Model   Related Issue(s) (Out of 117 Tests) -   95 % Satisfied

5 Unresolved or to be Checked Issue(s) (Out of 223 Tests) -   98 % Satisfied

#==============================================================================
```

IV.11.2. RhCp*-π-allyl-Cl (3-27)

CCDC 1899790

Crystal Data and Experimental

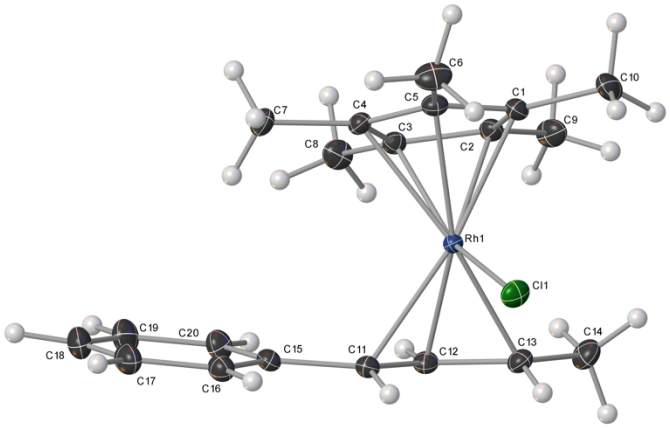

Experimental. Single orange block-shaped crystals of **Rh-p-allyl-Cl 3-27** were recrystallised from a mixture of DCM and pentane by vapor diffusion. A suitable crystal 0.37×0.32×0.28 mm^3 was selected and mounted on a loop with paratone oil on an XtaLAB Synergy-S diffractometer. The crystal was kept at a steady T = 100.02(10) K during data collection. The structure was solved with the **ShelXT** (Sheldrick, 2015) structure solution program using the Intrinsic Phasing solution method and by using **Olex2** (Dolomanov et al., 2009) as the graphical interface. The model was refined with version 2018/3 of **ShelXL** (Sheldrick, 2015) using Least Squares minimisation.

Crystal Data. $C_{20}H_{26}ClRh$, M_r = 404.77, monoclinic, $P2_1/c$ (No. 14), a = 7.4511(10) Å, b = 12.8249(10) Å, c = 18.6937(10) Å, β = 94.110(10)°, $\alpha = \gamma$ = 90°, V = 1781.8(3) Å^3, T = 100.02(10) K, Z = 4, Z' = 1, μ(MoK$_\alpha$) = 1.103 mm^{-1}, 119524 reflections measured, 15581 unique (R_{int} = 0.0215) which were used in all calculations. The final wR_2 was 0.0482 (all data) and R_1 was 0.0201 (I > 2σ(I)).

Compound	**Rh-p-allyl-Cl 3-27**
Formula	$C_{20}H_{26}ClRh$
$D_{calc.}$/ g cm^{-3}	1.509
μ/mm^{-1}	1.103
Formula Weight	404.77
Colour	orange
Shape	block
Size/mm^3	0.37×0.32×0.28
T/K	100.02(10)
Crystal System	monoclinic
Space Group	$P2_1/c$
a/Å	7.4511(10)
b/Å	12.8249(10)
c/Å	18.6937(10)
α/°	90
β/°	94.110(10)
γ/°	90
V/Å^3	1781.8(3)
Z	4
Z'	1
Wavelength/Å	0.71073
Radiation type	MoK_α
Θ_{min}/°	1.927
Θ_{max}/°	46.218
Measured Refl.	119524

Independent Refl.	15581
Reflections with I >2σ(I)	14700
R_{int}	0.0215
Parameters	284
Restraints	317
Largest Peak	1.343
Deepest Hole	-1.100
GooF	1.197
wR_2 (all data)	0.0482
wR_2	0.0477
R_1 (all data)	0.0221
R_1	0.0201

Structure Quality Indicators

Reflections:	d min (Mo) 0.49	I/σ 88.7	Rint 2.15%	complete 98% (IUCr) 100%
Refinement:	Shift -0.010	Max Peak 1.3	Min Peak -1.1	GooF 1.197

An orange block-shaped crystal with dimensions 0.37×0.32×0.28 mm^3 was mounted on a loop with paratone oil. Data were collected using an XtaLAB Synergy, Dualflex, HyPix diffractometer equipped with an Oxford Cryosystems low-temperature device operating at T = 100.02(10) K.

Data were measured using ω scans using MoK_α radiation. The total number of runs and images was based on the strategy calculation from the program **CrysAlisPro** (Rigaku, V1.171.40.37a, 2019). The maximum resolution that was achieved was Θ = 46.218° (0.49 Å).

The diffraction pattern was indexed. The total number of runs and images was based on the strategy calculation from the program **CrysAlisPro** (Rigaku, V1.171.40.37a, 2019) and the unit cell was refined using **CrysAlisPro** on 85788 reflections, 72% of the observed reflections.

Data reduction, scaling and absorption corrections were performed using **CrysAlisPro** (Rigaku, V1.171.40.37a, 2019). The final completeness is 100.00 % out to 46.218° in Θ. A numerical absorption correction based on Gaussian integration over a multifaceted crystal model was performed using **CrysAlisPro** (Rigaku, V1.171.40.37a, 2019). An empirical absorption correction using spherical harmonics as implemented in SCALE3 ABSPACK in **CrysAlisPro** (Rigaku, V1.171.40.37a, 2019) was also applied. The absorption coefficient μ of this material is 1.103 mm^{-1} at this wavelength (λ = 0.711Å) and the minimum and maximum transmissions are 0.564 and 1.000.

The structure was solved and the space group $P2_1/c$ (# 14) determined by the **ShelXT** (Sheldrick, 2015) structure solution program using Intrinsic Phasing and refined by Least Squares using version 2018/3 of **ShelXL** (Sheldrick, 2015). All non-hydrogen atoms were refined anisotropically. All hydrogen atom positions were located from the electron density maps and refined using restraints.

Images of the Crystal on the Diffractometer

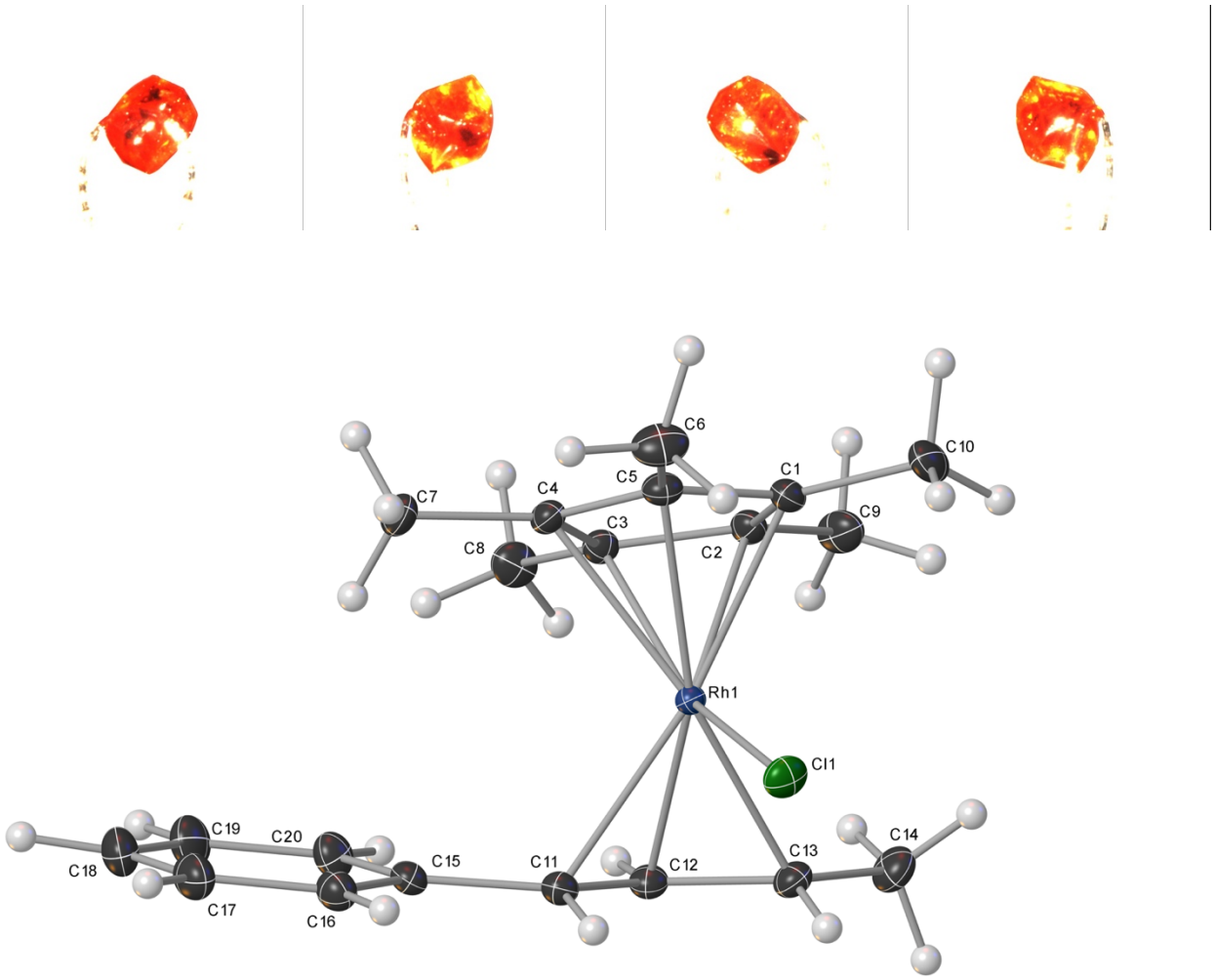

Figure 3-32. Thermal ellipsoid representation of the molecular structure of 3-27.

Data Plots: Diffraction Data

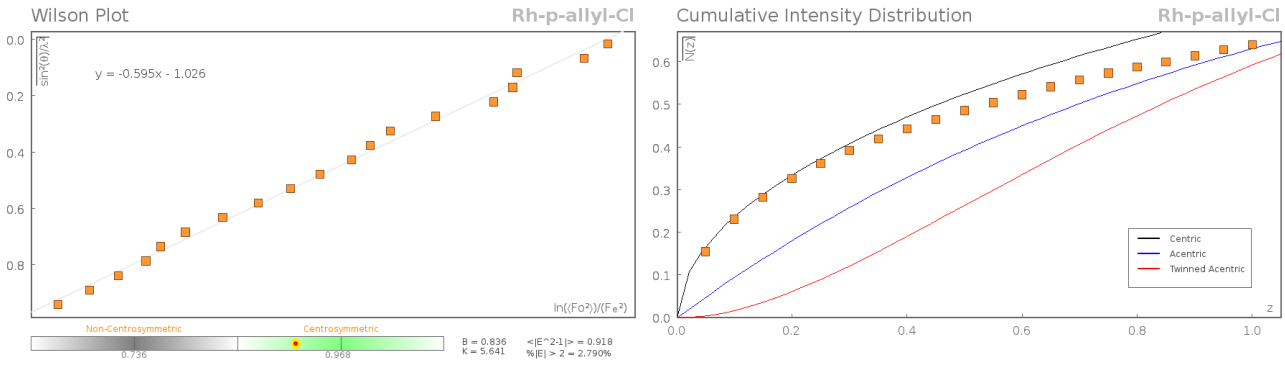

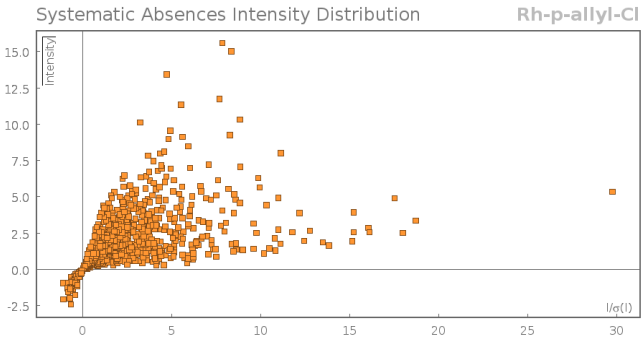

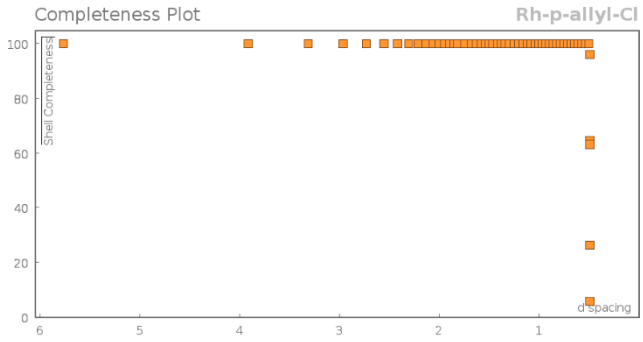

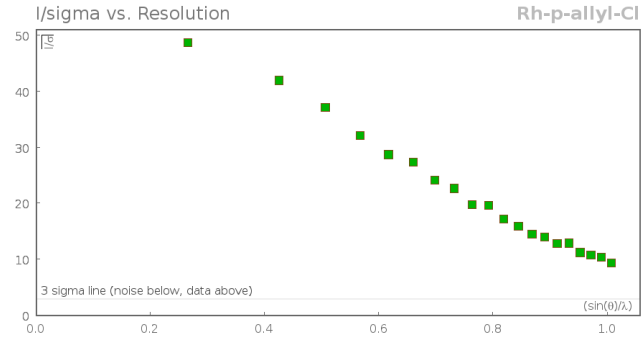

Data Plots: Refinement and Data

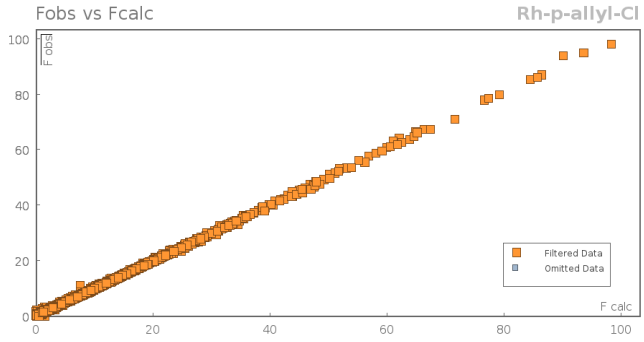

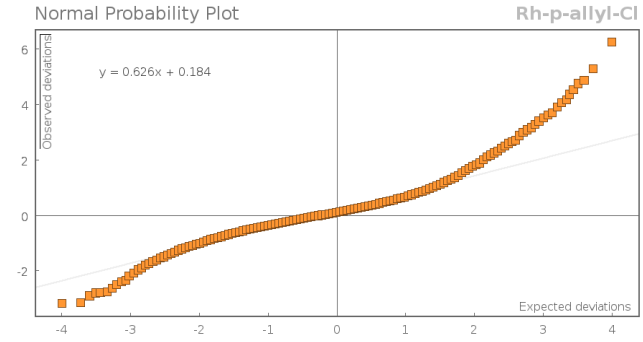

Reflection Statistics

Total reflections (after filtering)	121235	Unique reflections	15581
Completeness	0.997	Mean I/σ	57.92
hkl_{max} collected	(15, 25, 37)	hkl_{min} collected	(-15, -26, -37)
hkl_{max} used	(15, 26, 37)	hkl_{min} used	(-15, 0, 0)

Lim d_{max} collected	100.0	Lim d_{min} collected	0.36
d_{max} used	12.82	d_{min} used	0.49
Friedel pairs	22515	Friedel pairs merged	1
Inconsistent equivalents	2	R_{int}	0.0215
R_{sigma}	0.0113	Intensity transformed	0
Omitted reflections	0	Omitted by user (OMIT hkl)	0
Multiplicity	(17090, 17005, 9592, 5123, 2113, 964, 511, 103, 13)	Maximum multiplicity	21
Removed systematic absences	1711	Filtered off (Shel/OMIT)	0

Table 3-9. Fractional Atomic Coordinates (×10⁴) and Equivalent Isotropic Displacement Parameters (Å²×10³) for Rh-p-allyl-Cl 3-27.

U_{eq} is defined as 1/3 of the trace of the orthogonalised U_{ij}.

Atom	x	y	z	U_{eq}
Rh1	5419.0(2)	8666.3(2)	1743.9(2)	9.52(1)
Cl1	3969.0(2)	10355.2(2)	1616.0(2)	17.35(3)
C1	8193.1(8)	9251.4(5)	1765.4(4)	14.39(8)
C2	8224.6(8)	8236.7(5)	2065.5(3)	13.69(8)
C3	7469.4(8)	7528.6(5)	1520.5(3)	12.77(8)
C4	7092.3(8)	8109.3(5)	864.8(3)	13.00(8)
C5	7492.9(8)	9166.2(5)	1016.8(3)	14.17(8)
C6	7417.0(12)	10056.7(6)	501.7(5)	22.90(13)
C7	6428.2(10)	7654.8(6)	157.7(4)	19.22(11)
C8	7454.8(11)	6367.3(5)	1577.7(5)	19.63(11)
C9	8989.2(10)	7927.6(7)	2796.1(4)	20.67(12)
C10	8891.3(11)	10234.4(6)	2110.2(5)	22.98(13)

Atom	x	y	z	U_{eq}
C11	2716.2(8)	7938.7(5)	1561.9(3)	13.92(8)
C12	3573.9(9)	7666.3(5)	2237.1(3)	14.51(8)
C13	4019.0(9)	8476.8(5)	2733.2(3)	15.32(9)
C14	4965.5(11)	8261.7(7)	3452.6(4)	20.60(11)
C15	2321.7(8)	7213.5(5)	963.1(3)	14.32(8)
C16	1421.4(10)	7606.1(6)	337.5(4)	17.75(10)
C17	1058.5(12)	6982.1(7)	-263.1(4)	23.05(13)
C18	1571.4(12)	5938.6(7)	-247.6(5)	25.34(14)
C19	2435.6(13)	5530.9(6)	374.5(5)	24.68(14)
C20	2808.1(11)	6156.6(5)	976.5(4)	19.25(11)

Table 3-10. Anisotropic Displacement Parameters (×10⁴) Rh-p-allyl-Cl 3-27.

The anisotropic displacement factor exponent takes the form: $-2\pi^2[h^2a^{*2} \times U_{11} + ... + 2hka^* \times b^* \times U_{12}]$

Atom	U_{11}	U_{22}	U_{33}	U_{23}	U_{13}	U_{12}
Rh1	9.36(1)	9.68(1)	9.62(1)	-0.32(1)	1.29(1)	-0.06(1)
Cl1	19.64(6)	12.10(5)	20.69(6)	0.24(4)	4.23(5)	3.33(4)
C1	11.76(19)	14.7(2)	16.9(2)	-2.33(16)	2.17(16)	-2.43(15)
C2	11.08(18)	16.8(2)	13.01(19)	-0.54(16)	-0.10(15)	0.55(15)
C3	11.81(18)	12.56(18)	13.98(19)	-0.10(14)	1.26(15)	1.28(14)
C4	12.66(19)	15.13(19)	11.37(18)	-0.83(15)	2.07(14)	0.82(15)
C5	13.3(2)	14.37(19)	15.2(2)	1.90(16)	3.70(16)	-0.51(15)
C6	24.4(3)	20.6(3)	24.6(3)	9.2(2)	8.3(2)	0.5(2)
C7	18.9(3)	25.8(3)	13.1(2)	-5.0(2)	1.49(18)	0.8(2)

Atom	U_{11}	U_{22}	U_{33}	U_{23}	U_{13}	U_{12}
C8	20.2(3)	12.9(2)	25.7(3)	0.8(2)	1.3(2)	3.00(19)
C9	15.5(2)	30.9(3)	15.1(2)	1.8(2)	-2.49(18)	3.2(2)
C10	18.4(3)	19.7(3)	31.1(4)	-8.9(2)	3.5(2)	-6.5(2)
C11	11.95(19)	14.64(19)	15.3(2)	-0.84(16)	1.89(15)	-0.96(15)
C12	14.6(2)	15.2(2)	14.1(2)	0.68(16)	3.72(16)	-2.28(16)
C13	16.1(2)	17.4(2)	12.90(19)	-0.57(16)	3.97(16)	0.33(17)
C14	24.4(3)	25.2(3)	12.5(2)	-0.1(2)	3.4(2)	1.3(2)
C15	12.14(19)	15.2(2)	15.7(2)	-0.77(16)	1.59(16)	-3.11(15)
C16	16.9(2)	19.9(2)	16.2(2)	0.31(18)	0.07(18)	-2.02(19)
C17	21.5(3)	30.4(3)	16.9(3)	-2.7(2)	-1.1(2)	-4.2(3)
C18	25.3(3)	28.0(3)	22.6(3)	-9.2(3)	1.2(2)	-7.6(3)
C19	28.0(4)	17.7(3)	28.2(3)	-6.4(2)	0.8(3)	-4.2(2)
C20	20.9(3)	14.6(2)	22.0(3)	-1.71(19)	-0.3(2)	-2.40(19)

Table 3-11. Bond Lengths in Å for Rh-p-allyl-Cl 3-27.

Atom	Atom	Length/Å
Rh1	Cl1	2.4247(2)
Rh1	C1	2.1967(7)
Rh1	C2	2.2034(7)
Rh1	C3	2.1746(6)
Rh1	C4	2.2494(6)
Rh1	C5	2.2244(6)
Rh1	C11	2.2235(7)
Rh1	C12	2.1368(6)

Atom	Atom	Length/Å
Rh1	C13	2.2008(7)
C1	C2	1.4166(9)
C1	C5	1.4621(9)
C1	C10	1.4924(9)
C2	C3	1.4482(8)
C2	C9	1.4950(9)
C3	C4	1.4446(8)
C3	C8	1.4933(9)
C4	C5	1.4125(9)
C4	C7	1.4960(9)
C5	C6	1.4923(9)
C11	C12	1.4170(9)
C11	C15	1.4686(9)
C12	C13	1.4165(9)
C13	C14	1.4988(10)
C15	C16	1.3996(10)
C15	C20	1.4028(10)
C16	C17	1.3894(11)
C17	C18	1.3915(14)
C18	C19	1.3904(14)
C19	C20	1.3937(11)

Table 3-12. Bond Angles in ° for Rh-π-allyl-Cl 3-27.

Atom	Atom	Atom	Angle/°
C1	Rh1	Cl1	96.237(19)
C1	Rh1	C2	37.56(2)
C1	Rh1	C4	63.37(2)
C1	Rh1	C5	38.62(2)
C1	Rh1	C11	170.72(2)
C1	Rh1	C13	121.63(3)
C2	Rh1	Cl1	131.115(17)
C2	Rh1	C4	63.59(2)
C2	Rh1	C5	63.36(2)
C2	Rh1	C11	140.18(2)
C3	Rh1	Cl1	153.463(17)
C3	Rh1	C1	63.87(2)
C3	Rh1	C2	38.63(2)
C3	Rh1	C4	38.07(2)
C3	Rh1	C5	63.10(2)
C3	Rh1	C11	109.27(2)
C3	Rh1	C13	117.98(2)
C4	Rh1	Cl1	118.558(16)
C5	Rh1	Cl1	90.366(18)
C5	Rh1	C4	36.80(2)
C11	Rh1	Cl1	88.140(18)
C11	Rh1	C4	107.35(2)
C11	Rh1	C5	133.53(2)

Atom	Atom	Atom	Angle/°
C12	Rh1	Cl1	106.43(2)
C12	Rh1	C1	146.18(3)
C12	Rh1	C2	111.06(3)
C12	Rh1	C3	99.37(3)
C12	Rh1	C4	122.14(2)
C12	Rh1	C5	158.94(2)
C12	Rh1	C11	37.86(2)
C12	Rh1	C13	38.08(2)
C13	Rh1	Cl1	86.953(19)
C13	Rh1	C2	103.93(3)
C13	Rh1	C4	154.13(2)
C13	Rh1	C5	159.58(2)
C13	Rh1	C11	66.65(3)
C2	C1	Rh1	71.48(3)
C2	C1	C5	107.76(5)
C2	C1	C10	127.56(7)
C5	C1	Rh1	71.72(4)
C5	C1	C10	124.46(6)
C10	C1	Rh1	126.51(5)
C1	C2	Rh1	70.96(3)
C1	C2	C3	107.63(5)
C1	C2	C9	126.85(6)
C3	C2	Rh1	69.61(3)
C3	C2	C9	125.43(6)
C9	C2	Rh1	127.41(5)
C2	C3	Rh1	71.76(3)

Atom	Atom	Atom	Angle/°
C2	C3	C8	125.42(6)
C4	C3	Rh1	73.77(3)
C4	C3	C2	108.41(5)
C4	C3	C8	124.95(6)
C8	C3	Rh1	130.29(5)
C3	C4	Rh1	68.16(3)
C3	C4	C7	125.51(6)
C5	C4	Rh1	70.64(3)
C5	C4	C3	107.37(5)
C5	C4	C7	127.12(6)
C7	C4	Rh1	127.14(5)
C1	C5	Rh1	69.67(3)
C1	C5	C6	123.70(6)
C4	C5	Rh1	72.56(3)
C4	C5	C1	108.67(5)
C4	C5	C6	127.36(6)
C6	C5	Rh1	128.25(5)
C12	C11	Rh1	67.75(4)
C12	C11	C15	125.14(6)
C15	C11	Rh1	120.80(4)
C11	C12	Rh1	74.39(4)
C13	C12	Rh1	73.40(4)
C13	C12	C11	118.15(6)
C12	C13	Rh1	68.51(3)
C12	C13	C14	121.70(6)
C14	C13	Rh1	123.61(5)

Atom	Atom	Atom	Angle/˚
C16	C15	C11	117.83(6)
C16	C15	C20	118.05(6)
C20	C15	C11	124.12(6)
C17	C16	C15	121.46(7)
C16	C17	C18	119.99(8)
C19	C18	C17	119.29(7)
C18	C19	C20	120.81(8)
C19	C20	C15	120.38(7)

Table 3-13. Torsion Angles in ° for Rh-π-allyl-Cl 3-27.

Atom	Atom	Atom	Atom	Angle/˚
Rh1	C1	C2	C3	60.24(4)
Rh1	C1	C2	C9	-122.99(7)
Rh1	C1	C5	C4	-62.45(4)
Rh1	C1	C5	C6	123.12(7)
Rh1	C2	C3	C4	65.17(4)
Rh1	C2	C3	C8	-126.95(7)
Rh1	C3	C4	C5	60.03(4)
Rh1	C3	C4	C7	-120.87(6)
Rh1	C4	C5	C1	60.62(4)
Rh1	C4	C5	C6	-125.21(7)
Rh1	C11	C12	C13	60.93(5)
Rh1	C11	C15	C16	-98.52(6)
Rh1	C11	C15	C20	80.74(8)

Atom	Atom	Atom	Atom	Angle/˚
Rh1	C12	C13	C14	-117.13(6)
C1	C2	C3	Rh1	-61.10(4)
C1	C2	C3	C4	4.07(7)
C1	C2	C3	C8	171.95(6)
C2	C1	C5	Rh1	62.80(4)
C2	C1	C5	C4	0.35(7)
C2	C1	C5	C6	-174.09(6)
C2	C3	C4	Rh1	-63.87(4)
C2	C3	C4	C5	-3.84(7)
C2	C3	C4	C7	175.26(6)
C3	C4	C5	Rh1	-58.46(4)
C3	C4	C5	C1	2.16(7)
C3	C4	C5	C6	176.33(7)
C5	C1	C2	Rh1	-62.95(4)
C5	C1	C2	C3	-2.71(7)
C5	C1	C2	C9	174.06(6)
C7	C4	C5	Rh1	122.45(7)
C7	C4	C5	C1	-176.93(6)
C7	C4	C5	C6	-2.75(11)
C8	C3	C4	Rh1	128.18(7)
C8	C3	C4	C5	-171.79(6)
C8	C3	C4	C7	7.32(10)
C9	C2	C3	Rh1	122.07(6)
C9	C2	C3	C4	-172.76(6)
C9	C2	C3	C8	-4.88(10)
C10	C1	C2	Rh1	122.27(7)

Atom	Atom	Atom	Atom	Angle/°
C10	C1	C2	C3	-177.49(6)
C10	C1	C2	C9	-0.72(11)
C10	C1	C5	Rh1	-122.22(7)
C10	C1	C5	C4	175.33(6)
C10	C1	C5	C6	0.90(10)
C11	C12	C13	Rh1	-61.45(5)
C11	C12	C13	C14	-178.57(6)
C11	C15	C16	C17	177.50(7)
C11	C15	C20	C19	-177.76(7)
C12	C11	C15	C16	178.34(6)
C12	C11	C15	C20	-2.40(10)
C15	C11	C12	Rh1	112.86(6)
C15	C11	C12	C13	173.79(6)
C15	C16	C17	C18	0.87(12)
C16	C15	C20	C19	1.50(11)
C16	C17	C18	C19	0.40(13)
C17	C18	C19	C20	-0.69(14)
C18	C19	C20	C15	-0.27(13)
C20	C15	C16	C17	-1.81(11)

Table 3-14. Hydrogen Fractional Atomic Coordinates (×10⁴) and Equivalent Isotropic Displacement Parameters (Å²×10³) for Rh-π-allyl-Cl 3-27

U_{eq} is defined as 1/3 of the trace of the orthogonalised U_{ij}.

Atom	x	y	z	U_{eq}
H9A	8395(14)	7338(6)	2988(6)	33.2(10)
H8A	7185(15)	6142(10)	2047(3)	33.2(10)
H10A	8915(15)	10203(10)	2623(2)	33.2(10)
H9B	8863(16)	8509(6)	3111(6)	33.2(10)
H8B	6596(12)	6062(10)	1233(5)	33.2(10)
H10B	8149(14)	10811(7)	1949(6)	33.2(10)
H10C	10090(7)	10361(10)	1976(6)	33.2(10)
H7A	7375(12)	7257(7)	-31(6)	33.2(10)
H9C	10244(6)	7770(8)	2783(7)	33.2(10)
H6A	6858(13)	9876(10)	41(4)	33(4)
H6B	6784(13)	10638(7)	686(6)	33.2(10)
H7B	6074(14)	8193(7)	-179(6)	33.2(10)
H8C	8630(8)	6119(10)	1487(6)	33.2(10)
H7C	5419(10)	7204(7)	208(7)	33.2(10)
H6C	8629(8)	10271(9)	441(6)	33.2(10)
H14A	5613(13)	7616(5)	3450(7)	29(2)
H14B	4098(13)	8217(8)	3806(5)	29(2)
H14C	5797(12)	8810(6)	3588(7)	29(2)
H20	3380(18)	5848(11)	1409(5)	26(2)
H19	2790(20)	4802(6)	391(9)	37(2)

Atom	x	y	z	U_{eq}
H16	1011(19)	8325(6)	311(8)	26(2)
H17	457(19)	7287(12)	-692(6)	37(2)
H18	1390(20)	5503(11)	-672(6)	37(2)
H11	2012(18)	8553(9)	1529(8)	23(2)
H12	4070(17)	6983(10)	2339(7)	17(3)
H13	3256(17)	9066(9)	2727(8)	23(2)

Citations for Crystallography

CrysAlisPro Software System, Rigaku Oxford Diffraction, (2019).

O.V. Dolomanov and L.J. Bourhis and R.J. Gildea and J.A.K. Howard and H. Puschmann, Olex2: A complete structure solution, refinement and analysis program, *J. Appl. Cryst.*, (2009), **42**, 339-341.

Sheldrick, G.M., Crystal structure refinement with ShelXL, *Acta Cryst.*, (2015), **C27**, 3-8.

Sheldrick, G.M., ShelXT-Integrated space-group and crystal-structure determination, *Acta Cryst.*, (2015), **A71**, 3-8.

```
#===============================================================================
# PLATON/CHECK-( 70414) versus check.def version of 310314   for Entry: rh-p-all
# Data: Rh-p-allyl-Cl.cif - Type: CIF            Bond Precision   C-C = 0.0010 A
# Refl: Rh-p-allyl-Cl.fcf - Type: LIST4                             Temp = 100 K
#                                                X-Ray         Nref/Npar =  54.9
# Cell  7.4511(10) 12.8249(10) 18.6937(10)           90     94.11(1)          90
# Wavelength 0.71073    Volume Reported     1781.8(3)   Calculated     1781.8(3)
# SpaceGroup from Symmetry P 21/c     Hall: -P 2ybc               monoclinic
#                 Reported P 1 21/c 1       -P 2ybc               monoclinic
# MoietyFormula C20 H26 Cl Rh
#      Reported C20 H26 Cl Rh
#    SumFormula C20 H26 Cl Rh
#      Reported C20 H26 Cl Rh
# Mr        =    404.77[Calc],    404.77[Rep]
# Dx,gcm-3  =     1.509[Calc],     1.509[Rep]
# Z         =         4[Calc],         4[Rep]
# Mu (mm-1) =     1.103[Calc],     1.103[Rep]
# F000      =     832.0[Calc],     832.0[Rep]  or F000' =    828.32[Calc]
# Reported   T Limits: Tmin=0.564             Tmax=1.000  AbsCorr=GAUSSIAN
# Calculated T Limits: Tmin=0.674 Tmin'=0.661  Tmax=0.736
# Reported   Hmax= 15, Kmax= 26, Lmax= 37, Nref=  15581        , Th(max)= 46.218
# Obs in FCF Hmax= 15, Kmax= 26, Lmax= 37, Nref=  15581[ 15581], Th(max)= 46.218
# Calculated Hmax= 15, Kmax= 26, Lmax= 37, Nref=  15624        , Ratio  =  0.997
# Reported   Rho(min) = -1.10, Rho(max) =  1.34 e/Ang**3 (From CIF)
# Calculated Rho(min) = -1.24, Rho(max) =  1.35 e/Ang**3 (From CIF+FCF data)
# w=1/[sigma**2(Fo**2)+(0.0153P)**2+  0.5675P], P=(Fo**2+2*Fc**2)/3
# R= 0.0201( 14700), wR2= 0.0482( 15581), S = 1.197      (From CIF+FCF data)
# R= 0.0201( 14700), wR2= 0.0482( 15581), S = 1.197      (From FCF data only)
# R= 0.0201( 14700), wR2= 0.0482( 15581), S = 1.197, Npar=  284
#===============================================================================
For Documentation: http://http://www.platonsoft.nl/CIF-VALIDATION.pdf
```

```
#===============================================================================

#===============================================================================
>>> The Following Improvement and Query ALERTS were generated - (Acta-Mode) <<<
#===============================================================================
Format: alert-number_ALERT_alert-type_alert-level text

731_ALERT_1_C Bond    Calc   2.4247(5), Rep   2.4247(2) ......          3 su-Rat
RH1  -CL1     1.555   1.555                    #          1
906_ALERT_3_C Large K value in the Analysis of Variance ......      2.581 Check
#===============================================================================
002_ALERT_2_G Number of Distance or Angle Restraints on AtSite         38 Note
153_ALERT_1_G The su's on the Cell Axes   are Equal ..........    0.00100 Ang.
164_ALERT_4_G Nr. of Refined C-H H-Atoms in Heavy-Atom Struct.         26 Note
232_ALERT_2_G Hirshfeld Test Diff (M-X)  Rh1    --  Cl1     ..       23.5 su
232_ALERT_2_G Hirshfeld Test Diff (M-X)  Rh1    --  C1      ..        6.0 su
232_ALERT_2_G Hirshfeld Test Diff (M-X)  Rh1    --  C2      ..        6.8 su
232_ALERT_2_G Hirshfeld Test Diff (M-X)  Rh1    --  C3      ..        8.9 su
232_ALERT_2_G Hirshfeld Test Diff (M-X)  Rh1    --  C4      ..        7.8 su
232_ALERT_2_G Hirshfeld Test Diff (M-X)  Rh1    --  C5      ..        8.0 su
232_ALERT_2_G Hirshfeld Test Diff (M-X)  Rh1    --  C11     ..       12.5 su
232_ALERT_2_G Hirshfeld Test Diff (M-X)  Rh1    --  C12     ..        7.0 su
232_ALERT_2_G Hirshfeld Test Diff (M-X)  Rh1    --  C13     ..       11.0 su
860_ALERT_3_G Number of Least-Squares Restraints .............        317 Note
912_ALERT_4_G Missing # of FCF Reflections Above STh/L=  0.600         44 Note
#===============================================================================

ALERT_Level and ALERT_Type Summary
==================================
2 ALERT_Level_C = Check. Ensure it is Not caused by an Omission or Oversight
14 ALERT_Level_G = General Info/Check that it is not Something Unexpected
```

```
2 ALERT_Type_1 CIF Construction/Syntax Error, Inconsistent or Missing Data.
10 ALERT_Type_2 Indicator that the Structure Model may be Wrong or Deficient.
2 ALERT_Type_3 Indicator that the Structure Quality may be Low.
2 ALERT_Type_4 Improvement, Methodology, Query or Suggestion.
#===============================================================================

0 Missing  Experimental  Info Issue(s) (Out of  54 Tests) -  100 % Satisfied
0 Experimental  Data  Related Issue(s) (Out of  28 Tests) -  100 % Satisfied
13 Structural  Model   Related Issue(s) (Out of 117 Tests) -   89 % Satisfied
3 Unresolved or to be Checked Issue(s) (Out of 223 Tests) -   99 % Satisfied

#===============================================================================
```

IV.11.3. Rhodium Cp*-π-allyl-NHTs (3-30)

CCDC 1918704

Crystal Data and Experimental

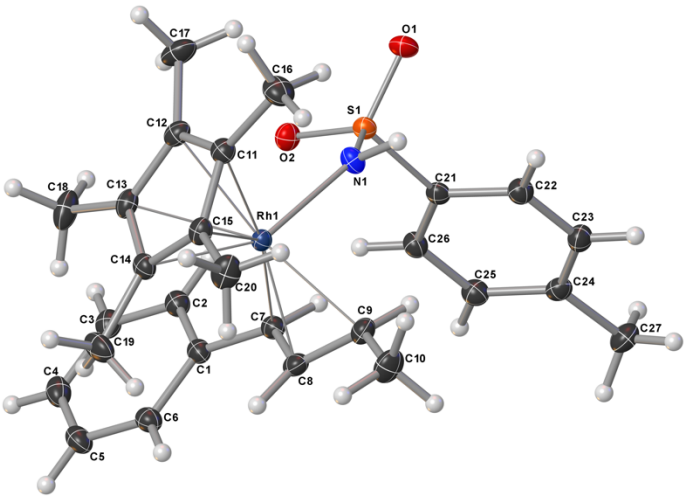

Experimental. Single orange plate-shaped crystals of **RJH-II-091 3-30** were recrystallised from a

mixture of DCM and pentane by vapor diffusion. A suitable crystal 0.25×0.15×0.05 mm^3 was selected and mounted on a loop with paratone oilon an XtaLAB Synergy, Dualflex, HyPix diffractometer.The crystal was kept at a steady T = 102(4) K during data collection. The structure was solved with the **ShelXT** (Sheldrick, 2015) structure solution program usingthe Intrinsic Phasing solution method and by using **Olex2** (Dolomanov et al., 2009) as the graphical interface.The model was refined with version 2018/3 of **ShelXL-2014** (Sheldrick, 2015) using Least Squares minimisation.

Crystal Data. $C_{27}H_{34}NO_2RhS$, M_r = 539.52, monoclinic, $P2_1/n$ (No. 14), a = 9.08450(13) Å, b = 26.7256(4) Å, c = 10.28003(15) Å, β = 94.9110(13)°, $\alpha = \gamma$ = 90°, V = 2486.71(6) $Å^3$, T = 102(4) K, Z = 4, Z' = 1, $\mu(MoK_\alpha)$ = 0.794 mm^{-1}, 44992 reflections measured, 11459 unique (R_{int} = 0.0407) which were used in all calculations. The final wR_2 was 0.0689 (all data) and R_1 was 0.0269 (I > 2σ(I)).

Compound	**RJH-II-091 3-30**
Formula	$C_{27}H_{34}NO_2RhS$
$D_{calc.}$/ g cm^{-3}	1.441
μ/mm^{-1}	0.794
Formula Weight	539.52
Colour	orange
Shape	plate
Size/mm^3	0.25×0.15×0.05
T/K	102(4)
Crystal System	monoclinic
Space Group	$P2_1/n$
a/Å	9.08450(13)
b/Å	26.7256(4)
c/Å	10.28003(15)
α/°	90
β/°	94.9110(13)
γ/°	90
V/Å^3	2486.71(6)
Z	4
Z'	1
Wavelength/Å	0.71073
Radiation type	MoK_α
Θ_{min}/°	2.129
Θ_{max}/°	35.630
Measured Refl.	44992

Independent Refl.	11459
Reflections with I > 2σ(I)	9946
R_{int}	0.0407
Parameters	311
Restraints	4
Largest Peak	0.931
Deepest Hole	-0.348
GooF	1.035
wR_2 (all data)	0.0689
wR_2	0.0667
R_1 (all data)	0.0334
R_1	0.0269

Structure Quality Indicators

Reflections:	d min (Mo) 0.61	I/σ 20.8	Rint 4.07%	complete at 2θ=72° 100%
Refinement:	Shift 0.002	Max Peak 0.9	Min Peak -0.3	GooF 1.035

An orange plate-shaped crystal with dimensions 0.25×0.15×0.05 mm^3 was mounted on a loop with paratone oil. Data were collected using an XtaLAB Synergy, Dualflex, HyPix diffractometer equipped with an Oxford Cryosystems low-temperature device operating at T = 102(4) K.

Data were measured using ω scans of 0.5° per frame for s using MoK_α radiation. The total number of runs and images was based on the strategy calculation from the program **CrysAlisPro** (Rigaku, V1.171.39.43c, 2018). The maximum resolution that was achieved was Θ = 35.630°.

The diffraction pattern was indexed using **CrysAlisPro** (Rigaku, V1.171.39.43c, 2018) and the unit cell was refined using **CrysAlisPro** (Rigaku, V1.171.39.43c, 2018) on 29649 reflections, 66% of the observed reflections.

Data reduction, scaling and absorption corrections were performed using **CrysAlisPro** (Rigaku, V1.171.39.43c, 2018). The final completeness is 100.00 % out to 35.630° in Θ. A Gaussian absorption correction was performed using CrysAlisPro 1.171.39.43c (Rigaku Oxford Diffraction, 2018). This is a numerical absorption correction based on Gaussian integration over a multifaceted crystal model. An empirical absorption correction using spherical harmonics as implemented in SCALE3 ABSPACK was also carried out. The absorption coefficient μ of this material is 0.794 mm^{-1} at this wavelength (λ = 0.71073Å) and the minimum and maximum transmissions are 0.736 and 1.000.

The structure was solved and the space group $P2_1/n$ (# 14) determined by the **ShelXT** (Sheldrick, 2015) structure solution program using Intrinsic Phasing and refined by Least Squares using version 2018/3 of **ShelXL-2014** (Sheldrick, 2015). All non-hydrogen atoms were refined anisotropically. Hydrogen atom positions were calculated geometrically and refined using the riding model. Most hydrogen atom positions were calculated geometrically and refined using the riding model, but some hydrogen atoms were refined freely.

There is a single molecule in the asymmetric unit, which is represented by the reported sum formula. In other words: Z is 4 and Z' is 1.

Images of the Crystal on the Diffractometer

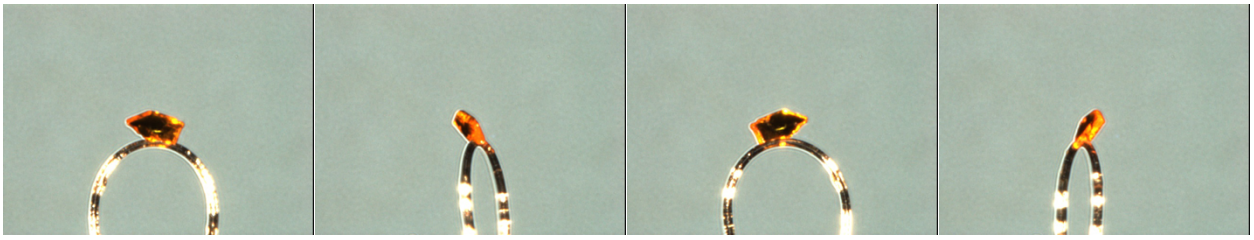

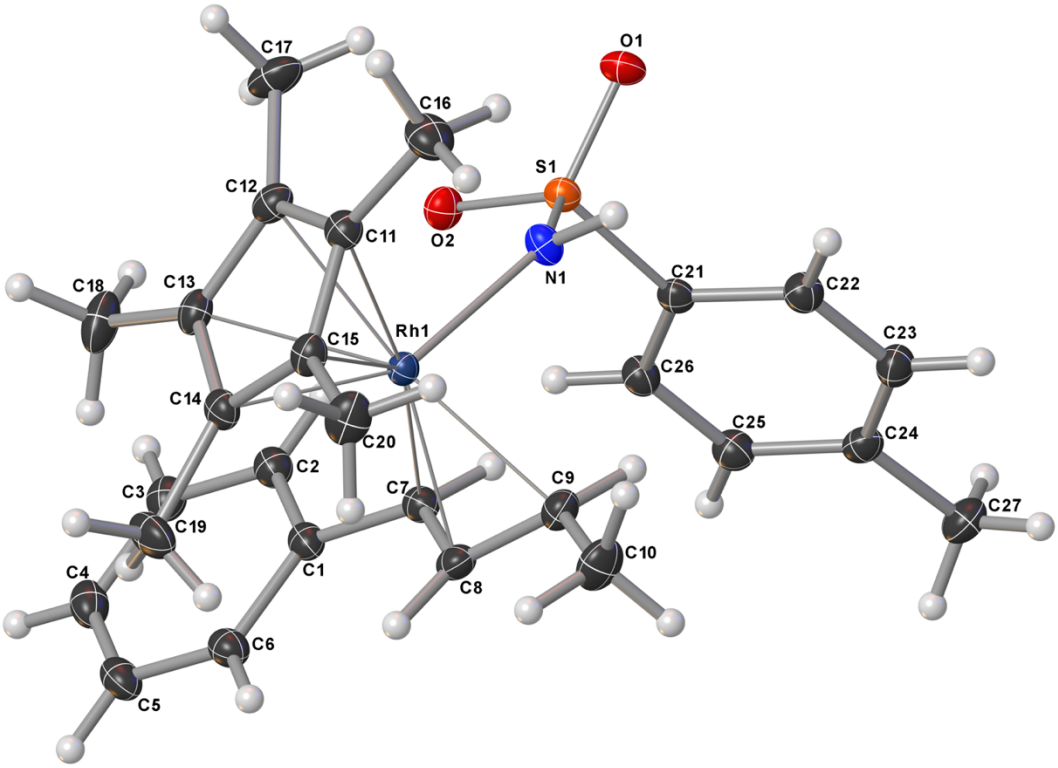

Figure 3-33. Thermal Ellipsoid Representation of Complex 3-30

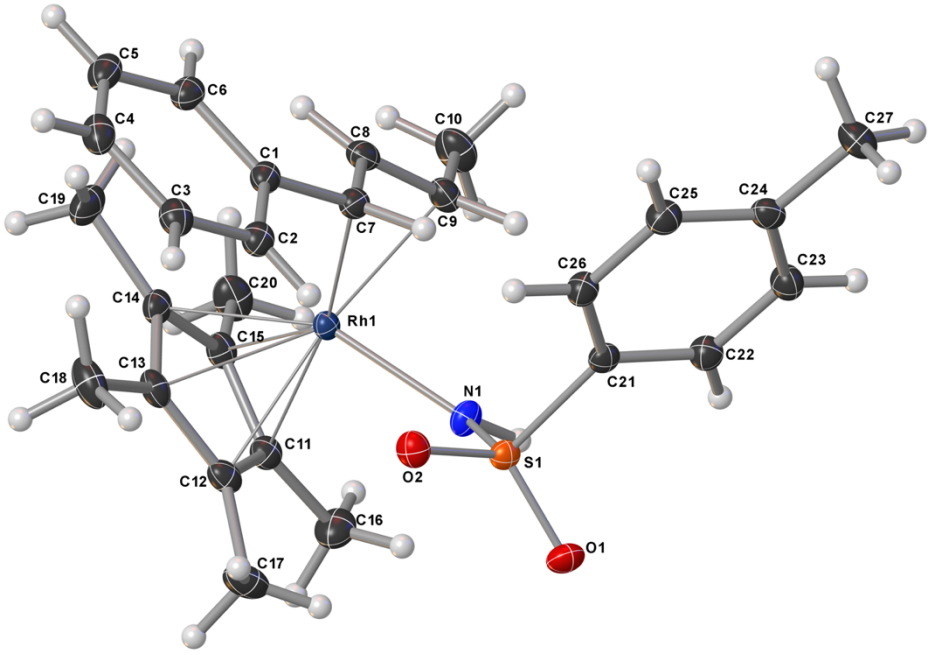

Figure 3-34. Thermal Ellipsoid Representation of Complex 3-30 Second View

Data Plots: Diffraction Data

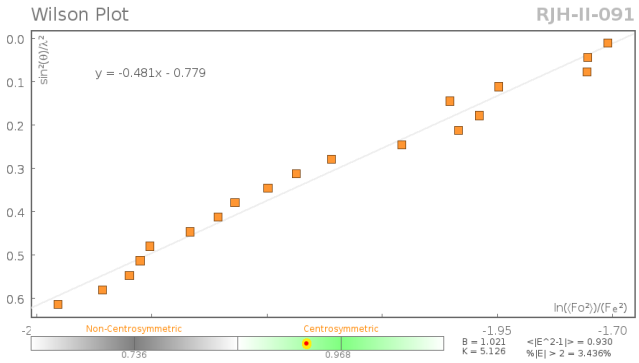

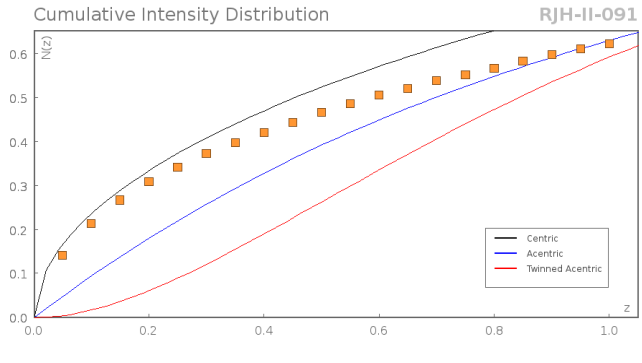

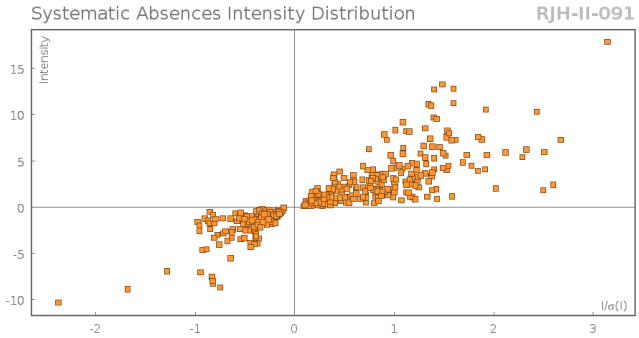

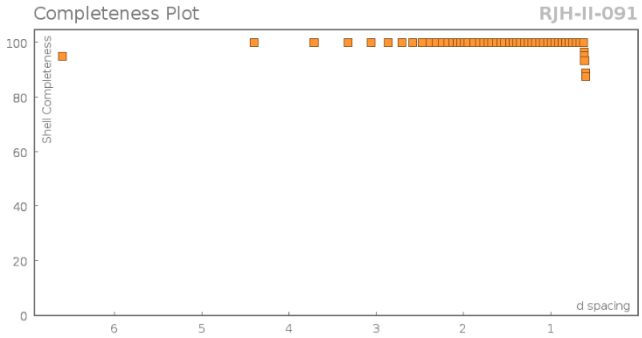

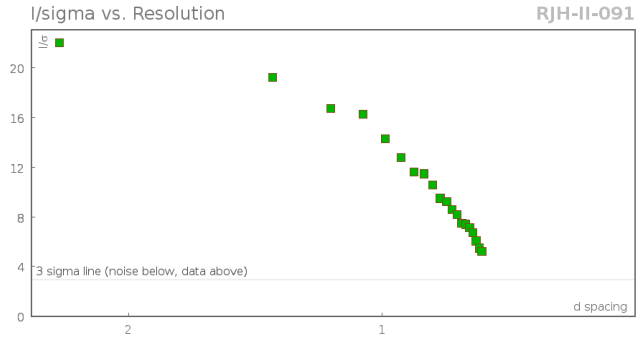

Data Plots: Refinement and Data

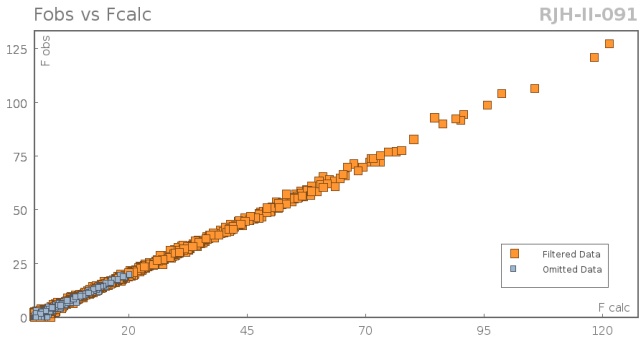

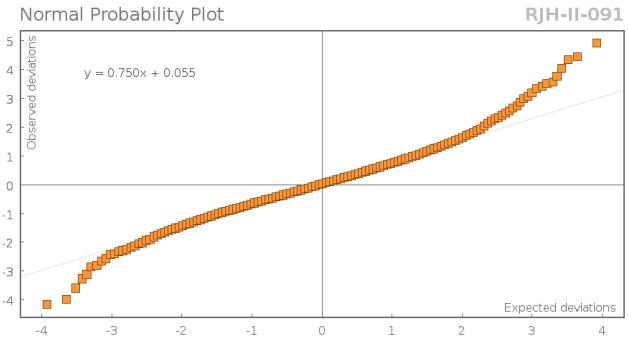

Reflection Statistics

Total reflections (after filtering)	45369	Unique reflections	11459
Completeness	1.0	Mean I/σ	21.05
hkl_{max} collected	(15, 44, 17)	hkl_{min} collected	(-15, -41, -15)
hkl_{max} used	(14, 43, 16)	hkl_{min} used	(-14, 0, 0)
Lim d_{max} collected	20.0	Lim d_{min} collected	0.61
d_{max} used	10.24	d_{min} used	0.61
Friedel pairs	9750	Friedel pairs merged	1
Inconsistent equivalents	3	R_{int}	0.0397
R_{sigma}	0.0329	Intensity transformed	0
Omitted reflections	0	Omitted by user (OMIT hkl)	0
Multiplicity	(19892, 8556, 2355, 526, 89, 16, 4)	Maximum multiplicity	15
Removed systematic absences	510	Filtered off (Shel/OMIT)	1373

Images of the Crystal on the Diffractometer

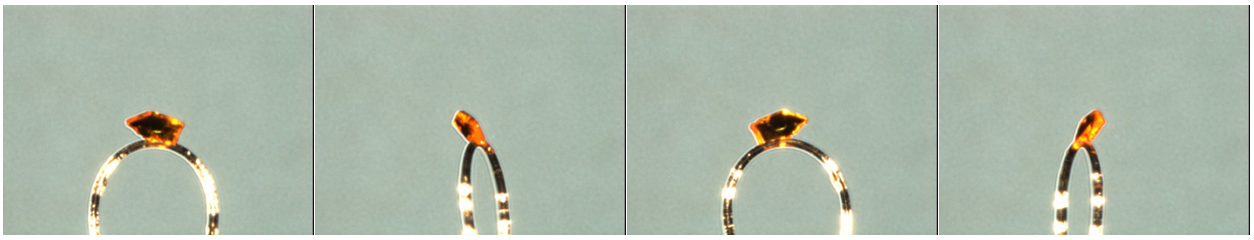

Table 3-15. Fractional Atomic Coordinates (×10⁴) and Equivalent Isotropic Displacement Parameters (Å²×10³) for RJH-II-091 3-30.

U_{eq} is defined as 1/3 of the trace of the orthogonalised U_{ij}.

Atom	x	y	z	U_{eq}
Rh1	5796.2(2)	3739.2(2)	7705.4(2)	12.28(2)
S1	5415.0(3)	4177.3(2)	4636.0(2)	14.40(5)
O2	4974.9(10)	3666.6(3)	4336.7(9)	18.99(15)
O1	4540.4(10)	4571.0(3)	3972.6(8)	19.66(16)
N1	5551.4(11)	4260.7(4)	6152.6(9)	16.46(16)
C8	8059.7(12)	3524.4(5)	7948.2(11)	18.02(19)
C14	4970.1(13)	3252.8(4)	9181.8(11)	17.33(19)
C2	6590.4(13)	2623.4(4)	5288.2(11)	18.18(19)
C13	4031.8(13)	3175.0(4)	7994.4(11)	17.91(19)
C9	8036.1(13)	4048.5(5)	8122.2(12)	18.87(19)
C25	9304.8(13)	3926.0(5)	3061.0(12)	19.7(2)
C24	9943.6(13)	4401.9(5)	3063.5(11)	18.13(19)
C21	7194.6(12)	4249.1(4)	4055(1)	14.89(17)
C11	3848.6(13)	4007.9(4)	8633.4(11)	17.18(18)
C1	7314.6(12)	2779.5(4)	6481.9(11)	16.67(18)
C3	6400.9(14)	2118.6(5)	5004.7(12)	20.3(2)
C26	7939.7(13)	3849.3(4)	3543.5(11)	17.80(19)

Atom	x	y	z	U_{eq}
C6	7843.6(13)	2410.4(4)	7371.6(12)	19.6(2)
C7	7495.2(12)	3320.3(4)	6734.0(11)	16.12(18)
C12	3378.2(13)	3640.3(5)	7633.9(11)	18.13(19)
C22	7835.4(13)	4723.1(4)	4104.3(11)	18.74(19)
C23	9188.7(13)	4795.0(5)	3598.2(12)	19.9(2)
C4	6917.3(14)	1756.2(5)	5908.4(13)	22.8(2)
C15	4785.7(13)	3763.0(4)	9595.0(11)	16.87(19)
C19	5762.0(16)	2850.8(5)	9975.9(14)	27.5(3)
C16	3324.2(16)	4539.3(5)	8683.6(14)	26.9(3)
C5	7641.5(15)	1904.0(5)	7091.0(13)	22.7(2)
C20	5417.2(16)	3979.7(6)	10863.7(12)	25.9(2)
C27	11389.2(14)	4490.2(5)	2486.6(14)	24.8(2)
C18	3765.0(16)	2689.9(5)	7291.3(14)	27.7(3)
C17	2290.7(15)	3741.3(6)	6487.9(14)	27.3(3)
C10	8575.6(16)	4286.7(6)	9396.5(13)	27.0(3)

Table 3-16. Anisotropic Displacement Parameters (×10⁴) RJH-II-091 3-30.

The anisotropic displacement factor exponent takes the form: $-2\pi^2[h^2a^{*2} \times U_{11} + ... + 2hka^* \times b^* \times U_{12}]$

Atom	U_{11}	U_{22}	U_{33}	U_{23}	U_{13}	U_{12}
Rh1	12.71(4)	13.41(4)	10.83(4)	0.33(2)	1.72(2)	-0.82(2)
S1	15.22(11)	15.91(11)	11.99(10)	0.79(8)	0.72(8)	0.81(9)
O2	20.4(4)	18.7(4)	17.7(4)	-2.1(3)	1.0(3)	-2.8(3)
O1	19.0(4)	22.0(4)	17.4(4)	3.1(3)	-1.8(3)	4.7(3)
N1	22.7(4)	15.3(4)	11.6(4)	0.7(3)	3.0(3)	1.0(3)

Atom	U_{11}	U_{22}	U_{33}	U_{23}	U_{13}	U_{12}
C8	12.9(4)	22.2(5)	18.9(5)	1.7(4)	1.2(3)	-0.1(4)
C14	18.6(5)	17.7(4)	16.4(4)	3.3(3)	5.8(4)	0.0(4)
C2	18.7(5)	18.0(5)	18.5(5)	0.6(4)	5.6(4)	1.2(4)
C13	17.0(4)	18.7(5)	19.0(5)	-3.1(4)	6.9(4)	-4.5(4)
C9	15.9(4)	21.3(5)	19.4(5)	0.2(4)	1.7(4)	-3.5(4)
C25	20.2(5)	20.2(5)	19.1(5)	-0.1(4)	4.0(4)	2.5(4)
C24	15.2(4)	22.2(5)	16.7(5)	1.0(4)	-0.1(3)	0.1(4)
C21	16.0(4)	16.7(4)	11.8(4)	1.6(3)	0.2(3)	1.1(3)
C11	16.9(4)	18.7(5)	16.5(4)	0.3(4)	4.8(4)	0.5(4)
C1	15.8(4)	16.5(4)	18.4(5)	1.7(3)	5.8(4)	1.7(4)
C3	20.0(5)	20.0(5)	21.9(5)	-1.5(4)	7.1(4)	-0.4(4)
C26	19.9(5)	16.4(4)	17.5(5)	0.7(3)	3.8(4)	1.0(4)
C6	19.2(5)	19.4(5)	20.7(5)	2.9(4)	4.5(4)	3.3(4)
C7	15.1(4)	17.4(4)	16.2(4)	1.6(3)	3.3(3)	1.1(4)
C12	14.3(4)	24.5(5)	15.8(5)	-0.7(4)	3.1(3)	-1.8(4)
C22	19.5(5)	18.0(5)	18.9(5)	-0.4(4)	2.3(4)	0.4(4)
C23	19.2(5)	18.7(5)	21.9(5)	-0.5(4)	1.8(4)	-2.3(4)
C4	23.5(5)	16.4(5)	30.0(6)	0.0(4)	10.7(5)	1.0(4)
C15	18.5(5)	19.9(5)	12.7(4)	-0.4(3)	4.3(3)	-2.9(4)
C19	29.6(6)	27.3(6)	27.0(6)	12.9(5)	10.3(5)	6.4(5)
C16	28.1(6)	22.1(6)	31.4(6)	0.7(5)	8.6(5)	7.1(5)
C5	24.0(5)	18.3(5)	26.8(6)	5.0(4)	8.0(4)	4.9(4)
C20	30.0(6)	32.4(6)	15.3(5)	-2.9(4)	2.7(4)	-6.6(5)
C27	17.0(5)	29.4(6)	28.4(6)	-1.3(5)	4.1(4)	-3.1(4)
C18	28.5(6)	23.8(6)	32.8(7)	-10.8(5)	14.0(5)	-10.8(5)
C17	16.7(5)	44.3(8)	20.3(6)	0.9(5)	-2.5(4)	-1.0(5)

Atom	U_{11}	U_{22}	U_{33}	U_{23}	U_{13}	U_{12}
C10	24.8(6)	32.8(7)	22.8(6)	-5.1(5)	-1.3(4)	-8.8(5)

Table 3-17. Bond Lengths in Å for RJH-II-091 (3-30).

Atom	Atom	Length/Å
Rh1	N1	2.1165(9)
Rh1	C8	2.1290(11)
Rh1	C14	2.1798(11)
Rh1	C13	2.2390(11)
Rh1	C9	2.2041(12)
Rh1	C11	2.2012(11)
Rh1	C7	2.2128(11)
Rh1	C12	2.2074(11)
Rh1	C15	2.2193(11)
S1	O2	1.4480(9)
S1	O1	1.4528(9)
S1	N1	1.5693(9)
S1	C21	1.7812(11)
C8	C9	1.4126(17)
C8	C7	1.4172(16)
C14	C13	1.4428(17)
C14	C15	1.4420(16)
C14	C19	1.4958(17)
C2	C1	1.4052(16)
C2	C3	1.3878(17)

Atom	Atom	Length/Å
C13	C12	1.4139(17)
C13	C18	1.4939(17)
C9	C10	1.5006(17)
C25	C24	1.3978(17)
C25	C26	1.3897(17)
C24	C23	1.3931(17)
C24	C27	1.5052(17)
C21	C26	1.3919(16)
C21	C22	1.3932(16)
C11	C12	1.4590(16)
C11	C15	1.4094(17)
C11	C16	1.5002(17)
C1	C6	1.4020(16)
C1	C7	1.4750(16)
C3	C4	1.3952(18)
C6	C5	1.3926(18)
C12	C17	1.4958(18)
C22	C23	1.3887(17)
C4	C5	1.3892(19)
C15	C20	1.4957(17)

Table 3-18. Bond Angles in ° for RJH-II-091 (3-30).

Atom	Atom	Atom	Angle/°
N1	Rh1	C8	107.70(4)
N1	Rh1	C14	153.85(4)

Atom	Atom	Atom	Angle/°
N1	Rh1	C13	120.90(4)
N1	Rh1	C9	86.29(4)
N1	Rh1	C11	94.33(4)
N1	Rh1	C7	91.44(4)
N1	Rh1	C12	90.79(4)
N1	Rh1	C15	128.07(4)
C8	Rh1	C14	98.29(4)
C8	Rh1	C13	119.87(4)
C8	Rh1	C9	38.00(5)
C8	Rh1	C11	147.28(4)
C8	Rh1	C7	38.04(4)
C8	Rh1	C12	156.93(5)
C8	Rh1	C15	111.89(4)
C14	Rh1	C13	38.09(4)
C14	Rh1	C9	117.09(4)
C14	Rh1	C11	63.60(4)
C14	Rh1	C7	107.91(4)
C14	Rh1	C12	63.31(4)
C14	Rh1	C15	38.26(4)
C9	Rh1	C13	152.41(5)
C9	Rh1	C7	67.01(4)
C9	Rh1	C12	161.96(5)
C9	Rh1	C15	105.26(4)
C11	Rh1	C13	63.33(4)
C11	Rh1	C9	123.80(4)
C11	Rh1	C7	168.02(4)

Atom	Atom	Atom	Angle/°
C11	Rh1	C12	38.65(4)
C11	Rh1	C15	37.18(4)
C7	Rh1	C13	104.72(4)
C7	Rh1	C15	140.01(4)
C12	Rh1	C13	37.07(4)
C12	Rh1	C7	130.92(4)
C12	Rh1	C15	63.10(4)
C15	Rh1	C13	63.17(4)
O2	S1	O1	116.93(5)
O2	S1	N1	110.00(5)
O2	S1	C21	105.80(5)
O1	S1	N1	110.92(5)
O1	S1	C21	103.90(5)
N1	S1	C21	108.73(5)
S1	N1	Rh1	130.54(6)
C9	C8	Rh1	73.88(7)
C9	C8	C7	119.00(10)
C7	C8	Rh1	74.19(6)
C13	C14	Rh1	73.18(6)
C13	C14	C19	125.43(11)
C15	C14	Rh1	72.36(6)
C15	C14	C13	108.09(10)
C15	C14	C19	125.51(11)
C19	C14	Rh1	129.06(8)
C3	C2	C1	120.83(11)
C14	C13	Rh1	68.73(6)

Atom	Atom	Atom	Angle/°
C14	C13	C18	126.45(12)
C12	C13	Rh1	70.25(6)
C12	C13	C14	107.42(10)
C12	C13	C18	126.11(12)
C18	C13	Rh1	127.49(8)
C8	C9	Rh1	68.11(6)
C8	C9	C10	121.59(11)
C10	C9	Rh1	123.77(9)
C26	C25	C24	121.10(11)
C25	C24	C27	121.19(11)
C23	C24	C25	117.94(11)
C23	C24	C27	120.86(11)
C26	C21	S1	121.92(9)
C26	C21	C22	119.77(10)
C22	C21	S1	118.30(8)
C12	C11	Rh1	70.91(6)
C12	C11	C16	125.94(11)
C15	C11	Rh1	72.11(6)
C15	C11	C12	107.70(10)
C15	C11	C16	126.17(11)
C16	C11	Rh1	126.38(8)
C2	C1	C7	118.76(10)
C6	C1	C2	117.99(11)
C6	C1	C7	123.24(11)
C2	C3	C4	120.42(12)
C25	C26	C21	119.95(11)

Atom	Atom	Atom	Angle/°
C5	C6	C1	121.13(12)
C8	C7	Rh1	67.77(6)
C8	C7	C1	123.93(10)
C1	C7	Rh1	120.24(7)
C13	C12	Rh1	72.68(7)
C13	C12	C11	108.46(10)
C13	C12	C17	126.83(11)
C11	C12	Rh1	70.44(6)
C11	C12	C17	124.55(11)
C17	C12	Rh1	126.36(9)
C23	C22	C21	119.52(11)
C22	C23	C24	121.66(11)
C5	C4	C3	119.50(11)
C14	C15	Rh1	69.39(6)
C14	C15	C20	125.27(11)
C11	C15	Rh1	70.71(6)
C11	C15	C14	108.12(10)
C11	C15	C20	126.53(11)
C20	C15	Rh1	128.15(8)
C4	C5	C6	120.12(11)

Table 3-19. Hydrogen Fractional Atomic Coordinates (×10⁴) and Equivalent Isotropic Displacement Parameters (Å²×10³) for RJH-II-091 (3-30).

U_{eq} is defined as 1/3 of the trace of the orthogonalised U_{ij}.

Atom	x	y	z	U_{eq}
H2	6225.95	2866.38	4667.49	22
H25	9812.35	3650.46	2723.82	24
H3	5916.51	2019.12	4190.09	24
H26	7515.48	3524.2	3524.29	21
H6	8348.64	2507.32	8179.73	24
H22	7350.06	4995.11	4481.35	22
H23	9610.28	5120.48	3617.08	24
H4	6774.79	1410.97	5716.54	27
H19A	6085.09	2589.86	9394.06	41
H19B	5094.92	2705.08	10573.62	41
H19C	6624.87	2994.23	10480.08	41
H16A	3835.16	4708.35	9438.67	40
H16B	2256.94	4543.59	8763.31	40
H16C	3537.77	4713.08	7881.66	40
H5	7999.53	1659.19	7709.41	27
H20A	6360.36	3816.23	11131.62	39
H20B	4726.93	3925.31	11532.15	39
H20C	5578.09	4339.47	10758.38	39
H27A	12076.92	4218.58	2747.66	37
H27B	11809.3	4809.74	2804.19	37
H27C	11222.74	4499.61	1532.36	37

Atom	x	y	z	U_{eq}
H18A	3600.67	2752.75	6350.86	42
H18B	2891.99	2526.72	7596.79	42
H18C	4627.16	2472.07	7464.91	42
H17A	2423.84	4083.68	6177.47	41
H17B	1284.69	3702	6749.21	41
H17C	2450.99	3504.38	5786.27	41
H10A	7942.9	4572.24	9566.54	40
H10B	9594.17	4402.16	9353.58	40
H10C	8542.01	4041.3	10101.69	40
H8	8250(18)	3299(5)	8720(10)	18(4)
H7	7628(18)	3521(5)	5936(10)	19(3)
H9	8144(18)	4267(5)	7351(10)	19(3)
H1	5580(30)	4614(2)	6370(20)	55(7)

Citations for Crystallography

CrysAlisPro Software System, Rigaku Oxford Diffraction, (2018).

O.V. Dolomanov and L.J. Bourhis and R.J. Gildea and J.A.K. Howard and H. Puschmann, Olex2: A complete structure solution, refinement and analysis program, *J. Appl. Cryst.*, (2009), **42**, 339-341.

Sheldrick, G.M., Crystal structure refinement with ShelXL, *Acta Cryst.*, (2015), **C27**, 3-8.

Sheldrick, G.M., ShelXT-Integrated space-group and crystal-structure determination, *Acta Cryst.*, (2015), **A71**, 3-8.

```
#===============================================================================
# PLATON/CHECK-( 70414) versus check.def version of 310314   for Entry: rjh-ii-0
# Data: RJH-II-091.cif - Type: CIF               Bond Precision   C-C = 0.0017 A
# Refl: RJH-II-091.fcf - Type: LIST6                                Temp = 102 K
#                                                X-Ray         Nref/Npar =  36.8
# Cell 9.08450(13)  26.7256(4)10.28003(15)           90  94.9110(13)          90
# Wavelength 0.71073    Volume Reported    2486.71(6)   Calculated    2486.71(6)
# SpaceGroup from Symmetry P 21/n     Hall: -P 2yn                monoclinic
#                 Reported P 1 21/n 1       -P 2yn                monoclinic
# MoietyFormula C27 H34 N O2 Rh S
#      Reported C27 H34 N O2 Rh S
#    SumFormula C27 H34 N O2 Rh S
#      Reported C27 H34 N O2 Rh S
# Mr        =    539.53[Calc],    539.52[Rep]
# Dx,gcm-3  =     1.441[Calc],     1.441[Rep]
# Z         =         4[Calc],         4[Rep]
# Mu (mm-1) =     0.794[Calc],     0.794[Rep]
# F000      =    1120.0[Calc],    1120.0[Rep]  or F000' =   1116.37[Calc]
# Reported   T Limits: Tmin=0.736             Tmax=1.000  AbsCorr=GAUSSIAN
# Calculated T Limits: Tmin=0.867 Tmin'=0.820  Tmax=0.961
# Reported   Hmax= 14, Kmax= 43, Lmax= 16, Nref=  11459        , Th(max)= 35.630
# Obs in FCF Hmax= 14, Kmax= 43, Lmax= 16, Nref=  11459[ 11459], Th(max)= 35.630
# Calculated Hmax= 14, Kmax= 43, Lmax= 16, Nref=  11463        , Ratio  =  1.000
# Reported   Rho(min) = -0.35, Rho(max) =  0.93 e/Ang**3 (From CIF)
# w=1/[sigma**2(Fo**2)+(0.0316P)**2+  0.7328P], P=(Fo**2+2*Fc**2)/3
# R= 0.0267(  9921), wR2= 0.0636( 11459), S = 1.791      (From FCF data only)
# R= 0.0269(  9946), wR2= 0.0689( 11459), S = 1.035, Npar=  311
#===============================================================================
For Documentation: http://http://www.platonsoft.nl/CIF-VALIDATION.pdf
#===============================================================================
```

```
#===============================================================================

>>> The Following Improvement and Query ALERTS were generated - (Acta-Mode) <<<

#===============================================================================

Format: alert-number_ALERT_alert-type_alert-level text


#===============================================================================

094_ALERT_2_C Ratio of Maximum / Minimum Residual Density ....       2.68 Why ?

#===============================================================================

002_ALERT_2_G Number of Distance or Angle Restraints on AtSite          8 Note

008_ALERT_5_G No _iucr_refine_reflections_details   in the CIF     Please Do !

164_ALERT_4_G Nr. of Refined C-H H-Atoms in Heavy-Atom Struct.          3 Note

760_ALERT_1_G CIF Contains no Torsion Angles .................          ? Info

795_ALERT_4_G C-Atom in CIF Coordinate List out of Sequence ..         C2 Note

796_ALERT_4_G O-Atom in CIF Coordinate List out of Sequence ..         O1 Note

802_ALERT_4_G CIF Input Record(s) with more than 80 Characters          ! Info

860_ALERT_3_G Number of Least-Squares Restraints .............          4 Note

910_ALERT_3_G Missing # of FCF Reflections Below Th(Min) .....          1 Why ?

912_ALERT_4_G Missing # of FCF Reflections Above STh/L=  0.600          4 Note

961_ALERT_5_G Dataset Contains no Negative Intensities .......     Please Check

#===============================================================================


ALERT_Level and ALERT_Type Summary

==================================

2 ALERT_Level_A = Most Likely a Serious Problem - Resolve or Explain

2 ALERT_Level_B = A Potentially Serious Problem - Consider Carefully

1 ALERT_Level_C = Check. Ensure it is Not caused by an Omission or Oversight

11 ALERT_Level_G = General Info/Check that it is not Something Unexpected


4 ALERT_Type_1 CIF Construction/Syntax Error, Inconsistent or Missing Data.

2 ALERT_Type_2 Indicator that the Structure Model may be Wrong or Deficient.

3 ALERT_Type_3 Indicator that the Structure Quality may be Low.
```

5 ALERT_Type_4 Improvement, Methodology, Query or Suggestion.

2 ALERT_Type_5 Informative Message, Check.

#==

1 Missing Experimental Info Issue(s) (Out of 54 Tests) - 98 % Satisfied

0 Experimental Data Related Issue(s) (Out of 28 Tests) - 100 % Satisfied

5 Structural Model Related Issue(s) (Out of 117 Tests) - 96 % Satisfied

10 Unresolved or to be Checked Issue(s) (Out of 223 Tests) - 96 % Satisfied

#==

IV.12. DFT Optimized Geometries and Computed Vibrational Frequencies

IV.12.1. XYZ coordinates

==========

3-20

==========

C	-1.8333	-1.1124	-3.7063
C	-3.0985	-1.2594	-3.1403
C	-1.2617	0.1548	-3.8224
H	-3.5366	-2.2508	-3.0531
H	-0.2731	0.2734	-4.2564
C	-3.8265	-0.1475	-2.6822
C	-1.9677	1.2707	-3.3631
H	-1.5252	2.2605	-3.4356
C	-3.2311	1.1224	-2.7988
H	-3.7513	1.9985	-2.4244
H	-1.2927	-1.9887	-4.0532
C	-5.1556	-0.3610	-2.0899
H	-5.4130	-1.4047	-1.9031
C	-6.0681	0.5710	-1.7791
H	-5.8610	1.6248	-1.9599
C	-7.3848	0.2783	-1.1122
H	-8.2094	0.6903	-1.7085
H	-7.5406	-0.8076	-1.0675
C	-7.4495	0.8623	0.2927
C	-8.4764	1.7317	0.6741
C	-6.4635	0.5343	1.2337
C	-8.5245	2.2576	1.9674
C	-6.5095	1.0546	2.5257
C	-7.5414	1.9202	2.8973
H	-9.2463	1.9989	-0.0461
H	-5.6505	-0.1245	0.9400
H	-9.3287	2.9333	2.2457
H	-5.7369	0.7895	3.2424
H	-7.5758	2.3297	3.9029

==========

Methylcarbamate

==========

C	1.2749	-0.2819	1.5104

O	0.9785	-1.1598	2.2968
N	1.1336	-0.3525	0.1509
H	1.1912	0.4964	-0.3892
H	0.5465	-1.0946	-0.1931
O	1.8308	0.9103	1.8595
C	2.0705	1.0617	3.2649
H	2.5138	2.0512	3.3831
H	2.7562	0.2910	3.6284
H	1.1367	0.9916	3.8300

==========

Acetate

==========

O	-0.7844	-2.6066	-0.2122
C	-0.7982	-2.0690	0.9258
C	-1.0476	-3.0764	2.1123
O	-0.6334	-0.8669	1.2515
H	-1.9539	-3.6674	1.9213
H	-1.1416	-2.5711	3.0819
H	-0.2161	-3.7935	2.1680

==========

Acetatic acid

==========

O	-0.7569	-2.6508	-0.1997
C	-0.7986	-2.0538	1.0189
C	-1.0895	-3.0517	2.1134
O	-0.6090	-0.8674	1.1679
H	-1.9795	-3.6367	1.8666
H	-1.2286	-2.5269	3.0582
H	-0.2524	-3.7517	2.1992
H	-0.5575	-1.9468	-0.8400

==========

3-23

==========

C	-0.0510	2.2571	0.9857
C	0.7153	1.4734	0.1249
C	-0.7933	1.6567	2.0034
H	1.2902	1.9478	-0.6668
H	-1.3913	2.2637	2.6766
C	0.7581	0.0742	0.2568
C	-0.7570	0.2668	2.1518
H	-1.3270	-0.2095	2.9446
C	0.0101	-0.5149	1.2932
H	0.0321	-1.5914	1.4322
H	-0.0674	3.3362	0.8615
C	1.5780	-0.6994	-0.6857
H	2.1665	-0.0982	-1.3793
C	1.6811	-2.0324	-0.7785
H	1.1264	-2.6990	-0.1222
C	2.6080	-2.7157	-1.7403
H	3.0581	-1.9943	-2.4283
C	3.7044	-3.4677	-1.0065
C	3.4671	-4.7407	-0.4780
C	4.9475	-2.8620	-0.8016
C	4.4626	-5.4002	0.2430
C	5.9419	-3.5188	-0.0775
C	5.7016	-4.7901	0.4475
H	2.5051	-5.2150	-0.6472
H	5.1385	-1.8756	-1.2165
H	4.2709	-6.3908	0.6463
H	6.9067	-3.0418	0.0706
H	6.4770	-5.3039	1.0086

O	1.7875	-3.6419	-2.5097
C	2.3071	-4.0457	-3.6975
O	3.3591	-3.6472	-4.1443
C	1.3923	-5.0476	-4.3595
H	0.3822	-4.6378	-4.4468
H	1.3287	-5.9485	-3.7412
H	1.7853	-5.3017	-5.3435

==========

3-35

==========

Rh	4.4079	9.2197	14.3212
O	3.4372	7.7522	15.5174
O	4.6150	8.2586	17.3857
C	3.7858	7.5873	16.7594
C	2.7810	10.6413	14.0800
C	3.1473	10.6785	15.4485
C	2.3316	9.4320	13.4940
C	6.6401	9.3227	14.7876
C	5.8199	9.6099	12.6220
C	2.1016	9.2459	12.0548
C	6.3212	10.2994	13.7933
C	6.2982	8.0315	14.2386
C	5.8392	8.1989	12.8853
C	2.0735	10.3044	11.1299
H	2.1910	11.3278	11.4730
C	1.8803	10.0612	9.7709
H	1.8589	10.8953	9.0746
C	1.9085	7.9383	11.5706
H	1.9275	7.1126	12.2775
C	3.0576	6.4268	17.4346
H	3.3072	5.4889	16.9272
H	3.3435	6.3632	18.4855
H	1.9747	6.5611	17.3494
C	1.7069	8.7569	9.3037
H	1.5566	8.5700	8.2443
C	1.7181	7.6953	10.2133
H	1.5776	6.6763	9.8630
H	1.8651	8.6961	14.1433
H	2.6722	9.9760	16.1249
H	3.0567	11.4741	13.4385
C	3.8078	11.8305	16.0854
C	4.4790	11.6195	17.3049
C	3.8172	13.1199	15.5264
C	5.1461	12.6656	17.9368
C	4.4850	14.1656	16.1644
C	5.1550	13.9438	17.3690
H	4.4999	10.6133	17.7156
H	3.2837	13.3171	14.6010
H	5.6653	12.4829	18.8740
H	4.4758	15.1587	15.7229
H	5.6740	14.7601	17.8640
C	5.4770	7.1177	11.9128
H	6.3100	6.9077	11.2286
H	5.2313	6.1878	12.4319
H	4.6096	7.3999	11.3084
C	6.4620	6.7260	14.9556
H	5.6794	6.0199	14.6678
H	7.4342	6.2775	14.7139
H	6.4047	6.8719	16.0356
C	7.2454	9.5781	16.1340
H	6.7359	8.9850	16.8957
H	8.3152	9.3303	16.1369
H	7.1415	10.6286	16.4153

C	6.5482	11.7748	13.9144
H	6.4061	12.1170	14.9410
H	7.5699	12.0306	13.6073
H	5.8592	12.3414	13.2838
C	5.4729	10.2480	11.3123
H	6.3664	10.3272	10.6795
H	4.7233	9.6701	10.7687
H	5.0752	11.2566	11.4504

==========

3-35-TS

==========

Rh	4.7528	9.4139	14.2506
O	3.1650	7.9054	14.5553
O	4.0999	6.0433	15.3519
C	3.1050	6.6479	14.9802
C	2.7941	10.2320	13.8263
C	3.2598	10.6997	15.1062
C	1.9499	9.0508	13.7830
C	6.7884	8.6235	14.8306
C	6.4951	10.5093	13.5379
C	1.5480	8.4977	12.4786
C	6.8519	10.0393	14.8620
C	6.5366	8.2025	13.4458
C	6.4144	9.3544	12.6469
C	2.4471	8.4764	11.3977
H	3.4596	8.8342	11.5539
C	2.0480	7.9760	10.1627
H	2.7518	7.9594	9.3350
C	0.2505	7.9937	12.2957
H	-0.4483	8.0022	13.1286
C	1.7226	6.0250	14.9596
H	1.3314	6.0186	13.9377
H	1.7762	5.0063	15.3439
H	1.0328	6.6146	15.5728
C	0.7501	7.4844	9.9875
H	0.4437	7.0885	9.0233
C	-0.1485	7.4956	11.0556
H	-1.1570	7.1140	10.9247
H	1.2063	8.9297	14.5714
H	2.8617	10.1726	15.9750
H	2.8041	10.8516	12.9354
C	3.6637	12.0868	15.3904
C	4.0329	12.4398	16.7029
C	3.7026	13.0957	14.4092
C	4.4338	13.7353	17.0206
C	4.1024	14.3926	14.7270
C	4.4737	14.7225	16.0326
H	4.0107	11.6747	17.4755
H	3.4183	12.8652	13.3872
H	4.7157	13.9757	18.0426
H	4.1225	15.1519	13.9491
H	4.7849	15.7341	16.2771
C	6.2272	9.4262	11.1617
H	7.1814	9.6117	10.6497
H	5.8163	8.4949	10.7618
H	5.5493	10.2398	10.8859
C	6.4667	6.7703	13.0076
H	6.0202	6.6766	12.0138
H	7.4700	6.3261	12.9669
H	5.8649	6.1861	13.7075
C	7.0327	7.6689	15.9605
H	6.2742	6.8829	15.9649
H	8.0198	7.1968	15.8643

H	6.9984	8.1790	16.9265
C	7.1984	10.9173	16.0244
H	7.1557	10.3655	16.9668
H	8.2143	11.3198	15.9174
H	6.5115	11.7641	16.1051
C	6.5537	11.9374	13.0874
H	7.5667	12.1894	12.7456
H	5.8674	12.1260	12.2566
H	6.2876	12.6205	13.8949

==========

3-36

==========

Rh	4.7831	9.4438	14.2503
O	3.0630	7.9533	14.5551
O	3.8618	6.0352	15.3008
C	2.8867	6.6662	14.9644
C	2.8250	10.1582	13.8948
C	3.2761	10.6794	15.1551
C	2.0516	8.8564	13.9281
C	6.8752	8.6363	14.7482
C	6.4953	10.5641	13.5434
C	1.6429	8.3487	12.5686
C	6.9203	10.0401	14.8387
C	6.5525	8.2723	13.3603
C	6.4021	9.4519	12.6053
C	2.6173	7.9829	11.6283
H	3.6640	8.0561	11.9069
C	2.2377	7.5349	10.3647
H	2.9983	7.2518	9.6421
C	0.2911	8.2569	12.2251
H	-0.4684	8.5339	12.9530
C	1.4745	6.1304	14.9589
H	1.0872	6.1047	13.9363
H	1.4864	5.1245	15.3777
H	0.8101	6.7698	15.5477
C	0.8845	7.4521	10.0241
H	0.5903	7.1042	9.0377
C	-0.0881	7.8164	10.9553
H	-1.1415	7.7533	10.6976
H	1.1850	8.8851	14.6029
H	2.9575	10.1495	16.0552
H	2.6193	10.7972	13.0415
C	3.6244	12.0908	15.4006
C	4.0498	12.4792	16.6860
C	3.5644	13.0883	14.4095
C	4.4103	13.7955	16.9669
C	3.9224	14.4059	14.6900
C	4.3516	14.7715	15.9683
H	4.1049	11.7252	17.4681
H	3.2408	12.8310	13.4057
H	4.7381	14.0601	17.9691
H	3.8661	15.1532	13.9022
H	4.6315	15.7987	16.1835
C	6.1841	9.5805	11.1272
H	7.1210	9.8255	10.6076
H	5.8041	8.6518	10.6916
H	5.4654	10.3726	10.8971
C	6.4552	6.8543	12.8769
H	5.9731	6.7951	11.8969
H	7.4494	6.3966	12.7868
H	5.8713	6.2477	13.5756
C	7.1610	7.6304	15.8240
H	6.3919	6.8526	15.8400

H	8.1318	7.1434	15.6607
H	7.1832	8.0978	16.8118
C	7.2889	10.8816	16.0225
H	7.2990	10.2917	16.9427
H	8.2872	11.3217	15.8963
H	6.5810	11.7044	16.1627
C	6.5189	12.0131	13.1619
H	7.5251	12.3090	12.8339
H	5.8263	12.2211	12.3418
H	6.2336	12.6495	14.0006

==========

3-37

==========

Rh	4.4723	9.1710	14.4089
O	3.3912	7.4852	15.2419
O	4.4199	8.4995	16.9178
C	3.7218	7.5486	16.4880
C	2.8318	10.6901	14.0464
C	3.0694	10.8032	15.4304
C	2.3240	9.5008	13.4838
C	6.7315	9.2617	14.8068
C	5.8335	9.6630	12.6873
C	2.0914	9.2582	12.0679
C	6.3585	10.2954	13.8807
C	6.3330	7.9990	14.2286
C	5.8272	8.2389	12.8933
C	2.1261	10.2739	11.0923
H	2.3138	11.3038	11.3805
C	1.8986	9.9720	9.7532
H	1.9174	10.7647	9.0114
C	1.8004	7.9382	11.6640
H	1.7627	7.1530	12.4146
C	3.2374	6.4433	17.3950
H	3.5326	5.4730	16.9857
H	3.6451	6.5676	18.3987
H	2.1438	6.4586	17.4384
C	1.6352	8.6544	9.3633
H	1.4589	8.4237	8.3171
C	1.5835	7.6382	10.3232
H	1.3676	6.6167	10.0250
H	1.9000	8.7653	14.1620
H	2.6301	10.0591	16.0889
H	3.1660	11.4871	13.3892
C	3.7257	11.9288	16.0756
C	4.2393	11.7450	17.3777
C	3.8820	13.1828	15.4483
C	4.9120	12.7790	18.0195
C	4.5416	14.2174	16.1031
C	5.0655	14.0167	17.3852
H	4.1354	10.7725	17.8497
H	3.4601	13.3598	14.4634
H	5.3127	12.6250	19.0169
H	4.6445	15.1841	15.6196
H	5.5832	14.8259	17.8916
C	5.4157	7.1982	11.8997
H	6.2608	6.9419	11.2481
H	5.0888	6.2832	12.3993
H	4.5962	7.5509	11.2680
C	6.5256	6.6568	14.8606
H	5.6971	5.9879	14.6169
H	7.4542	6.2010	14.4970
H	6.5881	6.7445	15.9471
C	7.3691	9.4361	16.1471

H	6.7666	8.9497	16.9191
H	8.3664	8.9798	16.1500
H	7.4732	10.4910	16.4073
C	6.6248	11.7587	14.0564
H	6.4809	12.0699	15.0927
H	7.6585	11.9868	13.7698
H	5.9644	12.3680	13.4357
C	5.4988	10.3576	11.4081
H	6.3989	10.4135	10.7841
H	4.7312	9.8235	10.8467
H	5.1521	11.3804	11.5782

==========

3-37-TS

==========

Rh	4.9458	9.3298	14.7827
O	2.7896	7.1825	14.2303
O	4.0231	7.8635	15.9873
C	3.3227	6.9983	15.3689
C	3.0238	10.1197	14.0039
C	3.2445	10.7356	15.2579
C	2.0806	9.0326	13.8478
C	7.1196	9.0164	15.2113
C	6.4077	10.3109	13.4152
C	1.5069	8.7157	12.5510
C	6.9514	10.3706	14.7474
C	6.7183	8.1267	14.1458
C	6.3089	8.9210	13.0251
C	2.1560	9.0314	11.3407
H	3.1331	9.5019	11.3525
C	1.5578	8.7269	10.1248
H	2.0619	8.9730	9.1954
C	0.2580	8.0674	12.5084
H	-0.2354	7.8008	13.4386
C	3.1460	5.6468	16.0266
H	3.9848	5.0065	15.7306
H	3.1675	5.7513	17.1130
H	2.2200	5.1752	15.6963
C	0.3043	8.1045	10.0975
H	-0.1645	7.8754	9.1452
C	-0.3440	7.7737	11.2903
H	-1.3134	7.2862	11.2673
H	1.4419	8.8406	14.7027
H	2.8327	10.2349	16.1343
H	3.2853	10.6624	13.1034
C	3.7022	12.1041	15.4771
C	4.0436	12.4951	16.7882
C	3.8112	13.0531	14.4402
C	4.5080	13.7794	17.0507
C	4.2725	14.3387	14.7071
C	4.6298	14.7048	16.0099
H	3.9526	11.7732	17.5958
H	3.5095	12.7940	13.4308
H	4.7710	14.0627	18.0653
H	4.3413	15.0643	13.9022
H	4.9866	15.7098	16.2134
C	5.8681	8.3847	11.6987
H	6.6958	7.8646	11.2020
H	5.0471	7.6696	11.8120
H	5.5356	9.1843	11.0343
C	6.7419	6.6306	14.1919
H	5.9922	6.2047	13.5204
H	7.7242	6.2524	13.8833
H	6.5468	6.2634	15.2023

C	7.6601	8.5836	16.5375
H	7.1387	7.6961	16.9049
H	8.7249	8.3340	16.4509
H	7.5602	9.3693	17.2887
C	7.2952	11.6183	15.4961
H	7.2776	11.4552	16.5752
H	8.3028	11.9553	15.2232
H	6.5958	12.4256	15.2697
C	6.1860	11.4830	12.5096
H	7.0760	11.6501	11.8918
H	5.3432	11.3210	11.8319
H	5.9951	12.3939	13.0768

==========

3-38

==========

Rh	1.3336	0.0702	-2.2606
C	0.1656	2.0128	-2.7969
C	-0.1647	0.9421	-3.6962
C	-0.8217	-0.1102	-2.9481
C	-0.7679	0.2596	-1.5643
C	-0.1473	1.5737	-1.4693
C	2.6558	2.2833	2.2472
C	2.9334	1.6083	1.0619
C	1.7973	1.7136	3.1910
H	3.5986	2.0546	0.3264
H	1.5802	2.2372	4.1171
C	2.3546	0.3547	0.7926
C	1.2379	0.4551	2.9498
H	0.5949	-0.0048	3.6945
C	1.5190	-0.2237	1.7662
H	1.1138	-1.2189	1.6124
H	3.1093	3.2514	2.4373
C	2.6856	-0.3218	-0.4659
H	3.6408	-0.0180	-0.9004
C	2.1141	-1.5006	-0.9653
H	1.2946	-1.9738	-0.4299
C	3.0153	-2.4631	-1.7159
H	3.9311	-1.9431	-2.0134
C	3.3344	-3.6433	-0.8307
C	2.4330	-4.7058	-0.6947
C	4.4996	-3.6171	-0.0582
C	2.7059	-5.7397	0.1995
C	4.7659	-4.6486	0.8420
C	3.8698	-5.7109	0.9716
H	1.5312	-4.7295	-1.2994
H	5.1980	-2.7895	-0.1563
H	2.0102	-6.5680	0.2954
H	5.6735	-4.6241	1.4376
H	4.0781	-6.5151	1.6708
O	2.4235	-2.9922	-2.9531
C	2.3061	-2.1604	-3.9724
O	2.4488	-0.9305	-3.8791
C	2.0175	-2.8504	-5.2717
H	1.3127	-3.6705	-5.1160
H	2.9473	-3.2858	-5.6544
H	1.6348	-2.1338	-5.9978
C	-1.3924	-0.4878	-0.4277
H	-2.4367	-0.1742	-0.3071
H	-1.3879	-1.5660	-0.6026
H	-0.8758	-0.2861	0.5126
C	-1.4301	-1.3520	-3.5223
H	-0.8773	-1.7010	-4.3984
H	-1.4518	-2.1624	-2.7902

H	-2.4617	-1.1624	-3.8421
C	0.0346	0.9700	-5.1815
H	1.0007	1.4085	-5.4433
H	-0.0059	-0.0329	-5.6102
H	-0.7489	1.5707	-5.6582
C	0.7573	3.3326	-3.1812
H	1.3674	3.7492	-2.3765
H	1.3790	3.2467	-4.0752
H	-0.0389	4.0552	-3.4021
C	-0.0684	2.4160	-0.2365
H	-0.0163	1.8122	0.6693
H	0.8062	3.0686	-0.2508
H	-0.9621	3.0483	-0.1748

==========

3-39

==========

Rh	4.8322	9.0895	14.5811
O	3.7122	7.2776	15.0997
O	4.4003	8.6144	16.6829
C	3.8358	7.5131	16.3528
C	2.9010	10.5714	14.0921
C	3.0283	10.8852	15.4578
C	2.2502	9.4019	13.6524
C	6.9888	8.8237	14.8248
C	6.1450	10.2477	13.1748
C	1.9593	9.0338	12.3084
C	6.7168	10.2145	14.4942
C	6.5362	8.0080	13.7247
C	5.9793	8.8892	12.7132
C	2.1774	9.8938	11.1966
H	2.5554	10.8994	11.3468
C	1.8699	9.4667	9.9176
H	2.0178	10.1292	9.0709
C	1.4169	7.7395	12.0809
H	1.2484	7.0791	12.9271
C	3.3227	6.5565	17.3813
H	3.4750	5.5286	17.0447
H	3.8177	6.7262	18.3387
H	2.2452	6.7090	17.5124
C	1.3449	8.1770	9.7122
H	1.1021	7.8514	8.7052
C	1.1203	7.3160	10.7938
H	0.7077	6.3265	10.6264
H	1.9144	8.7071	14.4187
H	2.6546	10.1574	16.1736
H	3.2276	11.2980	13.3573
C	3.5711	12.0820	16.0145
C	3.8218	12.1046	17.4116
C	3.8718	13.2336	15.2374
C	4.3783	13.2278	18.0066
C	4.4102	14.3559	15.8432
C	4.6712	14.3522	17.2255
H	3.5941	11.2239	18.0053
H	3.6352	13.2593	14.1786
H	4.5749	13.2393	19.0737
H	4.6163	15.2463	15.2580
H	5.0918	15.2377	17.6931
C	6.6106	6.5234	13.6174
H	6.8063	6.0522	14.5807
H	5.6828	6.1101	13.2149
H	7.4243	6.2534	12.9326
C	7.6337	8.3674	16.0897
H	7.0761	8.7253	16.9604

H	7.7020	7.2813	16.1456
H	8.6482	8.7780	16.1473
C	7.0870	11.3777	15.3549
H	6.5164	12.2724	15.1027
H	6.9215	11.1513	16.4111
H	8.1522	11.6046	15.2262
C	5.8257	11.4807	12.3957
H	6.7090	11.7674	11.8108
H	5.0090	11.3172	11.6904
H	5.5793	12.3215	13.0463
C	5.4656	8.4409	11.3836
H	6.3091	8.2455	10.7101
H	4.8920	7.5150	11.4739
H	4.8283	9.1912	10.9153

==========

3-39-TS

==========

Rh	1.3945	0.1503	-1.7288
C	-0.1688	1.3741	-2.6653
C	-0.0537	0.1385	-3.3783
C	-0.3513	-0.9434	-2.4538
C	-0.7182	-0.3509	-1.1722
C	-0.6053	1.0648	-1.3007
C	2.6683	3.2197	0.9963
C	3.0925	2.1080	0.2725
C	1.8024	3.0508	2.0791
H	3.8025	2.2212	-0.5427
H	1.4969	3.9122	2.6656
C	2.6138	0.8128	0.6050
C	1.3462	1.7682	2.4396
H	0.7054	1.6495	3.3078
C	1.7332	0.6597	1.7076
H	1.4118	-0.3329	2.0078
H	3.0364	4.2077	0.7391
C	3.0877	-0.3047	-0.1948
H	4.0123	-0.1220	-0.7404
C	2.4746	-1.5297	-0.3914
H	1.6130	-1.8161	0.1988
C	3.1623	-2.5663	-1.1830
H	4.2337	-2.4089	-1.2703
C	2.7685	-3.9611	-1.1107
C	1.5579	-4.3956	-0.5275
C	3.6557	-4.9235	-1.6411
C	1.2515	-5.7484	-0.4725
C	3.3428	-6.2752	-1.5923
C	2.1412	-6.6890	-1.0070
H	0.8659	-3.6847	-0.0894
H	4.5862	-4.5971	-2.0964
H	0.3286	-6.0791	-0.0072
H	4.0316	-7.0081	-1.9993
H	1.8999	-7.7465	-0.9583
O	3.0162	-2.2193	-3.0206
C	3.3339	-1.0871	-3.5366
O	3.0280	0.0468	-3.0442
C	4.1236	-1.1203	-4.8176
H	3.7398	-1.9099	-5.4685
H	5.1625	-1.3762	-4.5792
H	4.0969	-0.1529	-5.3185
C	-1.2130	-1.0875	0.0306
H	-2.3095	-1.0969	0.0282
H	-0.8813	-2.1271	0.0386
H	-0.8883	-0.6084	0.9565
C	-0.3868	-2.3860	-2.8265

H	0.5324	-2.6804	-3.3403
H	-0.5155	-3.0338	-1.9606
H	-1.2273	-2.5600	-3.5103
C	0.3137	-0.0250	-4.8141
H	1.0291	0.7354	-5.1323
H	0.7335	-1.0126	-5.0135
H	-0.5882	0.0840	-5.4292
C	0.0247	2.7448	-3.2235
H	0.3577	3.4487	-2.4580
H	0.7479	2.7496	-4.0415
H	-0.9304	3.1135	-3.6209
C	-0.9159	2.0921	-0.2673
H	-1.0805	1.6521	0.7152
H	-0.1135	2.8315	-0.1855
H	-1.8264	2.6291	-0.5622

==========

3-40

==========

Rh	1.3171	0.1168	-2.4500
C	0.2413	1.9829	-3.1988
C	-0.2106	0.8473	-3.9203
C	-0.7574	-0.1042	-2.9533
C	-0.6983	0.5077	-1.6308
C	-0.0275	1.7608	-1.7727
C	2.1825	1.6665	2.6477
C	2.5509	1.2134	1.3884
C	1.3338	0.8885	3.4461
H	3.2262	1.8043	0.7744
H	1.0589	1.2341	4.4380
C	2.0594	-0.0180	0.8944
C	0.8617	-0.3477	2.9845
H	0.2339	-0.9607	3.6233
C	1.2205	-0.8023	1.7223
H	0.8912	-1.7821	1.3916
H	2.5651	2.6110	3.0208
C	2.5166	-0.4853	-0.3943
H	3.4453	-0.0218	-0.7457
C	2.0481	-1.5745	-1.1331
H	1.1832	-2.1262	-0.7708
C	3.0725	-2.4093	-1.8825
H	3.9633	-1.8073	-2.0882
C	3.4141	-3.6077	-1.0342
C	2.4934	-4.6551	-0.8859
C	4.6229	-3.6299	-0.3306
C	2.7942	-5.7288	-0.0514
C	4.9156	-4.7032	0.5108
C	4.0031	-5.7511	0.6506
H	1.5614	-4.6453	-1.4455
H	5.3400	-2.8204	-0.4443
H	2.0908	-6.5493	0.0503
H	5.8587	-4.7262	1.0475
H	4.2351	-6.5876	1.3025
O	2.6008	-2.9130	-3.1817
C	2.4767	-2.0655	-4.1764
O	2.4155	-0.8247	-4.0197
C	2.4470	-2.6999	-5.5283
H	1.9232	-3.6579	-5.4879
H	3.4806	-2.9090	-5.8311
H	1.9977	-2.0270	-6.2579
C	-1.3129	-0.0403	-0.3897
H	-2.3465	0.3233	-0.3186
H	-1.3505	-1.1316	-0.3973
H	-0.7842	0.2846	0.5067

C	-1.4135	-1.4011	-3.2775
H	-0.9983	-1.8574	-4.1779
H	-1.3374	-2.1105	-2.4512
H	-2.4824	-1.2229	-3.4618
C	-0.1283	0.6408	-5.3962
H	0.7786	1.0831	-5.8131
H	-0.1448	-0.4182	-5.6574
H	-0.9904	1.1161	-5.8795
C	0.8897	3.2003	-3.7590
H	1.7116	3.5480	-3.1270
H	1.2653	3.0364	-4.7694
H	0.1520	4.0134	-3.8018
C	0.2251	2.7612	-0.6969
H	0.2624	2.2993	0.2889
H	1.1562	3.3081	-0.8620
H	-0.5905	3.4965	-0.6995

IV.12.2. Frequencies

==========

3-20

==========

21.01 23.35 35.97 90.80 139.34 172.04

247.99 287.14 294.15 385.53 414.05 417.13

442.89 500.91 509.18 596.44 626.06 630.03

636.48 705.28 714.53 757.20 763.16 807.78

833.91 852.36 861.44 879.45 922.81 928.90

947.87 970.76 974.88 994.31 998.74 1011.10

1013.52 1016.21 1058.29 1058.94 1086.43 1112.74

1118.85 1194.90 1196.22 1200.73 1215.75 1217.02

1220.56 1244.92 1299.47 1334.74 1345.48 1363.71

1368.49 1370.72 1387.01 1486.61 1492.84 1498.02

1539.56 1541.20 1633.07 1642.77 1661.31 1662.83

1726.43 3023.90 3065.45 3130.29 3158.23 3167.81

3169.97 3174.50 3177.59 3184.34 3188.17 3192.45

3198.31 3203.71 3206.55

==========

Methylcarbamate

==========

116.07 167.78 297.22 357.23 471.06 512.29

668.59 773.81 880.58 1099.22 1130.46 1183.85

1217.72 1375.66 1488.13 1494.35 1513.84 1624.59

1848.06 3056.14 3131.29 3162.90 3618.69 3753.27

==========

Acetate

==========

47.30 420.68 600.99 614.18 859.65 985.69

1020.71 1318.23 1373.55 1479.68 1493.62 1756.78

2994.40 3059.37 3077.99

==========

Acetatic acid

==========

81.31 422.15 542.60 584.71 680.10 864.63

1003.55 1069.34 1218.77 1354.20 1421.10 1482.56

1489.15 1855.46 3066.21 3134.31 3182.19 3751.42

==========

3-23

==========

18.31 22.89 30.49 49.08 55.43 63.37

87.35 95.37 147.25 177.99 224.72 244.36

255.45 314.28 335.97 377.32 413.08 413.69

450.58 490.64 547.18 550.93 594.58 613.75

632.28 633.73 639.74 684.67 704.40 713.96

762.08 778.09 820.05 847.87 856.26 860.46

898.75 924.24 927.24 938.43 971.59 975.90

979.78 994.47 999.89 1009.13 1013.53 1016.57

1041.01 1058.15 1058.88 1065.91 1112.24 1114.38

1146.38 1196.21 1196.50 1212.55 1218.94 1222.08

1245.35 1260.38 1271.43 1327.23 1337.29 1347.47

1365.71 1370.12 1388.99 1395.98 1410.52 1481.96

1488.49 1492.91 1497.09 1539.35 1541.33 1633.13

1645.37 1660.87 1663.51 1727.37 1834.44 3064.12

3090.07 3132.47 3139.87 3171.07 3172.91 3175.73

3179.26 3179.69 3180.53 3189.60 3189.94 3199.04

3199.37 3206.53 3208.29

==========

3-35

==========

8.94 37.99 43.22 49.28 57.11 58.85

67.21 70.62 81.70 87.06 110.89 111.93

129.69 132.97 137.59 140.48 154.25 158.78

171.60 178.88 185.60 192.60 198.95 206.16

209.24 222.62 237.95 240.87 260.58 305.45

312.56 315.05 316.89 318.88 360.03 371.80

407.05 413.09 416.60 417.88 424.04 499.63

501.53 515.03 531.66 538.55 552.61 562.99

564.32 593.67 601.17 606.43 611.76 617.41

633.67 633.76 640.73 668.79 707.74 712.73

775.69 777.89 814.49 816.26 817.18 855.40

865.40 876.79 886.10 910.74 926.45 930.95

938.47 969.78 971.19 975.16 979.41 992.66

997.80 1009.37 1013.92 1017.41 1029.77 1049.91

1050.57 1057.59 1058.04 1059.24 1060.60 1060.93

1064.92 1102.06 1102.47 1111.91 1113.84 1133.67

1175.24 1180.74 1195.73 1196.28 1206.51 1217.13

1224.37 1234.01 1238.21 1292.70 1297.67 1343.59

1350.54 1354.23 1367.76 1372.13 1397.46 1401.32

1404.38 1424.22 1427.28 1428.62 1441.49 1443.28

1444.00 1458.15 1459.07 1468.34 1480.65 1483.48

1486.54 1490.61 1490.86 1493.55 1503.07 1504.28

1506.21 1510.89 1515.89 1519.71 1527.36 1534.03

1536.85 1544.60 1584.76 1629.69 1631.47 1657.10

1658.46 1698.85 3027.57 3028.79 3036.28 3039.30

3041.76 3051.08 3096.89 3109.18 3115.30 3116.42

3116.97 3118.03 3132.15 3150.11 3152.31 3154.72

3157.87 3159.53 3169.75 3172.38 3175.20 3178.25

3179.78 3185.75 3189.01 3190.20 3195.77 3196.74

3202.30 3205.54 3207.49

==========

3-35-TS

==========

-331.37 12.76 34.10 36.26 47.28 52.92

60.80 67.13 72.21 102.21 110.58 114.72

125.83 133.31 147.79 154.25 160.01 164.49

165.95 167.25 175.27 180.93 185.29 200.20

203.27 214.31 228.64 236.51 254.02 292.75

299.29 308.56 310.51 313.06 348.41 371.66

383.77 415.17 415.85 418.07 432.30 486.63

495.38 529.36 537.44 545.46 552.00 563.21

575.79 576.06 590.35 611.45 621.54 626.60

632.65 637.52 643.79 665.63 706.43 708.46

763.80 777.53 783.68 810.93 813.31 822.10

850.59 864.89 869.29 903.06 908.39 931.60

942.27 961.81 966.57 974.14 982.90 987.60

1006.25 1012.52 1015.66 1022.51 1049.71 1053.01

1056.79 1057.83 1059.53 1060.75 1062.97 1067.33

1099.61 1100.20 1104.31 1109.80 1113.33 1130.79

1159.85 1173.34 1180.54 1190.16 1195.78 1197.83

1213.96 1217.99 1234.81 1263.97 1268.18 1310.46

1336.52 1352.76 1366.43 1366.82 1382.10 1393.67

1402.91 1418.01 1418.81 1424.11 1429.06 1434.88

1438.97 1449.88 1475.54 1480.07 1482.60 1485.31

1486.64 1491.66 1495.44 1499.05 1500.77 1501.37

1505.22 1510.32 1512.23 1519.17 1521.03 1538.47

1540.47 1546.09 1568.17 1628.06 1635.02 1655.79

1657.33 1759.68 3022.01 3025.77 3028.26 3029.30

3030.65 3054.59 3086.27 3100.16 3101.53 3102.87

3107.87 3113.82 3121.17 3122.05 3123.84 3135.54

3144.10 3149.51 3156.43 3165.91 3171.79 3171.94

3175.03 3181.96 3183.62 3191.44 3193.24 3198.40

3203.63 3205.32 3214.90

==========

3-36

==========

19.83 26.09 34.17 40.53 45.47 55.03

63.51 65.62 78.96 98.23 109.76 135.03

141.65 150.49 151.46 157.37 160.34 162.29

168.70 174.68 179.49 195.28 198.57 204.01

212.63 227.19 235.30 257.06 296.72 303.60

306.88 309.51 326.50 343.97 362.21 379.26

409.94 414.17 415.42 432.83 462.15 497.05

512.63 531.47 540.66 560.33 564.42 566.83

583.89 589.38 600.57 616.48 623.23 633.23

634.39 649.57 679.66 706.63 713.58 768.04

780.17 803.26 810.00 810.94 822.50 849.70

855.69 863.37 872.05 906.00 928.44 933.48

961.85 963.80 972.06 975.07 980.01 986.60

1001.36 1012.26 1016.89 1027.38 1050.60 1053.58

1056.24 1057.64 1058.28 1062.58 1062.94 1066.77

1072.28 1097.22 1098.40 1106.95 1116.16 1128.70

1167.78 1180.67 1190.57 1196.12 1196.88 1213.71

1218.22 1226.40 1241.99 1257.81 1264.33 1310.68

1329.03 1350.10 1365.22 1365.83 1379.93 1390.49

1393.20 1407.42 1414.47 1424.85 1429.01 1433.93

1436.51 1446.30 1469.52 1482.02 1482.69 1483.21

1486.89 1490.67 1493.47 1497.39 1498.12 1500.37

1502.69 1508.25 1510.36 1512.08 1516.93 1538.38

1541.31 1545.05 1573.88 1627.57 1641.57 1655.47

1662.60 1829.01 3018.95 3020.88 3023.92 3025.10

3025.68 3028.24 3064.06 3087.44 3092.11 3095.53

3099.86 3101.90 3104.65 3121.18 3126.88 3128.27

3133.11 3134.12 3155.41 3164.15 3168.46 3170.97

3178.37 3178.87 3182.09 3184.44 3190.09 3195.78

3201.54 3203.15 3206.77

==========

3-37

==========

11.85 33.17 33.80 36.66 49.97 52.32

62.85 69.68 82.54 88.15 94.60 106.88

113.73 127.94 130.55 138.97 142.44 151.73

154.38 166.48 173.03 179.95 189.41 193.19

199.74 204.90 216.52 239.58 264.50 301.92

304.54 307.19 313.71 319.26 361.09 367.64

383.68 408.21 410.39 413.82 418.52 447.17

469.08 496.48 519.52 522.27 533.53 541.33

567.49 590.48 592.82 598.95 603.59 620.31

629.25 630.62 638.24 669.37 701.78 702.13

780.93 783.86 812.21 815.63 818.97 858.46

861.37 881.81 900.17 916.95 943.65 947.40

952.64 962.69 969.71 985.98 993.02 1008.08

1012.46 1015.58 1018.42 1021.64 1027.54 1039.20

1041.37 1045.97 1050.19 1054.88 1055.11 1055.92

1068.38 1100.51 1102.96 1117.76 1119.82 1133.80

1168.20 1171.73 1202.83 1203.28 1213.90 1218.92

1223.79 1246.89 1252.03 1296.04 1317.61 1352.02

1364.16 1372.56 1374.95 1386.00 1390.66 1394.08

1419.72 1424.30 1425.23 1433.75 1436.45 1442.62

1447.44 1450.91 1456.76 1459.94 1470.84 1476.50

1484.97 1485.62 1489.57 1491.29 1493.49 1498.76

1502.66 1508.68 1514.12 1517.30 1517.99 1525.98

1534.44 1543.50 1589.58 1593.34 1621.53 1626.62

1648.07 1651.00 3042.15 3047.12 3049.76 3051.40

3052.51 3062.59 3114.62 3116.99 3119.93 3125.17

3126.32 3131.73 3146.58 3152.54 3155.92 3157.11

3161.71 3171.50 3183.96 3185.63 3188.20 3189.94

3194.34 3197.01 3199.46 3203.48 3206.08 3208.63

3211.51 3216.93 3217.47

==========

3-37-TS

==========

-185.63 13.23 26.05 36.91 45.12 53.13

55.60 60.66 68.44 72.41 80.66 98.11

106.88 111.05 113.34 126.38 135.26 147.21

148.94 162.49 166.25 174.90 185.13 191.11

198.22 206.34 220.81 233.56 281.18 294.95

297.43 307.93 314.04 317.40 346.70 374.73

390.48 404.50 412.80 414.42 421.03 469.95

492.42 511.78 518.80 531.06 537.76 559.59

564.44 590.75 598.20 604.00 608.85 617.38

627.60 629.88 636.16 671.53 697.01 703.87

777.89 784.88 811.16 816.47 823.20 851.49

855.50 876.63 884.65 935.69 947.72 950.16

960.37 964.33 973.44 984.83 985.10 1010.09

1012.07 1013.99 1020.54 1035.16 1039.74 1042.13

1046.00 1050.02 1053.35 1054.11 1055.18 1063.18

1075.67 1098.26 1100.91 1114.33 1118.46 1131.04

1169.92 1175.56 1180.01 1202.06 1205.06 1215.54

1220.46 1231.53 1242.30 1288.61 1300.98 1348.55

1361.62 1370.67 1376.86 1391.05 1396.82 1400.10

1424.31 1425.63 1426.79 1434.33 1434.62 1440.75

1442.69 1452.39 1453.65 1463.50 1467.48 1482.21

1485.64 1488.33 1489.14 1492.73 1494.48 1502.09

1505.40 1507.80 1510.89 1514.46 1519.57 1524.88

1529.10 1540.31 1551.21 1581.41 1624.07 1630.16

1647.09 1654.90 3045.52 3045.62 3046.93 3047.90

3051.74 3059.98 3106.62 3112.30 3115.22 3116.97

3123.97 3136.46 3144.41 3146.70 3149.86 3151.42

3156.43 3165.22 3178.88 3181.43 3191.35 3191.63

3196.33 3200.77 3202.71 3206.54 3208.39 3214.17

3217.06 3219.67 3223.47

==========

3-38

==========

14.24 26.07 26.66 41.76 51.54 66.41

68.99 75.54 79.55 92.24 99.24 104.24

109.04 113.23 121.26 143.44 145.32 147.56

159.83 178.09 180.07 184.53 196.21 212.81

219.42 233.15 260.41 279.09 302.46 305.32

311.04 314.77 317.31 341.51 363.20 388.40

391.88 410.87 414.02 419.14 446.48 472.87

508.71 529.32 536.47 552.94 563.27 566.81

590.00 591.97 598.54 611.82 622.14 630.06

630.84 642.63 682.46 709.27 713.61 777.01

778.01 810.18 813.56 835.46 855.77 857.88

862.26 885.52 931.25 936.91 942.07 956.47

965.66 976.92 984.19 987.68 998.92 1012.34

1013.03 1015.40 1016.15 1036.25 1038.42 1045.05

1046.88 1048.33 1050.21 1057.37 1057.74 1066.50

1090.24 1096.34 1099.46 1117.65 1123.93 1130.12

1161.50 1176.10 1201.55 1201.85 1214.06 1216.17

1220.33 1228.59 1258.36 1286.51 1330.32 1343.05

1353.02 1367.61 1369.52 1385.12 1388.76 1393.01

1402.53 1423.55 1425.03 1426.49 1430.01 1433.68

1434.41 1451.97 1453.77 1464.32 1469.49 1480.80

1482.62 1485.26 1485.98 1488.83 1495.96 1497.54

1499.18 1506.56 1508.20 1513.68 1518.98 1526.18

1531.45 1540.02 1563.51 1630.71 1642.80 1652.37

1660.70 1682.03 3040.84 3046.53 3048.13 3053.05

3053.70 3065.61 3082.05 3111.38 3112.68 3116.39

3118.75 3122.40 3132.59 3137.24 3140.98 3147.33

3151.29 3154.78 3173.50 3174.95 3175.22 3176.04

3185.68 3187.48 3189.37 3196.82 3198.75 3205.49

3205.91 3215.33 3215.72

==========

3-39

==========

13.44 17.58 27.90 35.36 35.56 40.85

62.26 67.19 68.87 75.39 79.43 84.35

107.64 113.44 118.20 132.30 137.73 149.81

162.19 170.25 174.48 184.38 188.34 193.52

210.58 213.64 229.84 247.41 248.31 290.09

300.28 309.10 318.55 318.99 352.34 365.46

391.04 403.53 408.04 420.67 426.97 445.91

469.70 480.66 499.23 529.46 530.22 534.18

564.91 590.26 595.87 597.97 599.79 616.90

621.11 623.64 636.07 676.49 681.52 682.08

785.52 790.05 807.20 814.90 826.64 845.21

850.92 899.49 930.51 941.96 955.84 966.76

968.82 971.27 973.18 1001.58 1002.27 1007.97

1009.63 1020.96 1031.67 1032.46 1035.72 1037.64

1038.42 1041.87 1043.05 1045.35 1046.37 1048.24

1070.10 1095.70 1104.72 1122.96 1123.82 1129.18

1177.91 1179.64 1210.50 1211.01 1217.99 1222.07

1226.38 1264.62 1281.06 1319.86 1336.35 1368.56

1370.57 1391.28 1395.24 1396.11 1397.73 1399.64

1419.99 1422.60 1423.85 1432.92 1435.49 1441.70

1446.90 1448.01 1452.36 1470.65 1471.61 1475.31

1479.90 1483.82 1489.44 1490.27 1492.00 1499.80

1500.61 1507.55 1513.02 1518.96 1521.60 1523.52

1528.12 1535.33 1558.94 1601.69 1603.37 1606.76

1646.03 1648.04 3052.16 3052.85 3053.78 3054.60

3057.82 3061.15 3123.15 3124.21 3125.52 3126.67

3129.28 3136.01 3161.75 3165.68 3167.94 3168.87

3174.18 3175.90 3190.61 3194.67 3198.57 3200.43

3201.58 3204.13 3209.45 3212.08 3219.99 3221.72

3225.92 3227.63 3229.84

==========

3-39-TS

==========

-243.74 19.38 27.70 34.61 49.47 56.03

67.69 73.79 77.62 90.38 96.87 111.35

119.32 123.09 130.92 136.77 141.20 151.62

156.03 162.50 170.40 172.57 185.11 190.79

206.11 218.87 223.10 228.32 260.13 292.76

304.77 310.09 313.03 317.30 353.55 398.09

406.96 408.01 416.21 432.11 441.14 455.96

484.21 492.59 515.69 528.57 533.98 552.97

564.93 591.06 591.49 598.11 608.93 621.84

622.63 629.59 639.50 677.39 691.62 693.37

779.38 785.64 807.65 814.69 817.59 845.40

857.29 880.57 897.15 945.35 952.81 959.60

963.90 975.99 992.03 1002.85 1004.25 1012.93

1019.12 1028.37 1029.02 1032.56 1033.82 1034.80

1035.66 1038.50 1039.03 1045.54 1053.05 1062.91

1096.95 1098.37 1102.23 1119.62 1129.98 1131.82

1169.93 1178.12 1180.13 1209.61 1210.99 1216.02

1222.80 1249.71 1251.26 1292.05 1328.65 1353.49

1370.60 1382.34 1386.06 1388.56 1391.81 1393.54

1413.88 1419.94 1422.29 1422.63 1426.41 1428.95

1435.12 1449.82 1454.93 1455.53 1461.12 1469.13

1477.58 1479.23 1482.86 1486.46 1489.72 1490.95

1499.58 1503.29 1504.17 1513.83 1517.77 1523.87

1530.52 1537.08 1549.87 1598.84 1611.56 1622.79

1641.14 1650.47 3044.63 3049.25 3050.40 3054.99

3058.69 3061.37 3113.59 3123.63 3124.58 3128.68

3130.50 3133.79 3160.10 3160.47 3166.52 3171.43

3178.03 3178.50 3180.48 3185.35 3192.87 3197.81

3198.41 3199.85 3208.13 3209.35 3216.89 3219.10

3224.34 3226.19 3234.95

==========

3-40

==========

-14.05 12.19 32.59 37.82 49.98 58.46

65.20 65.84 80.39 89.34 95.12 99.42

107.00 120.00 124.53 131.78 136.51 137.73

148.73 163.63 180.95 185.40 198.15 199.16

206.63 224.51 268.09 281.01 302.49 306.90

311.89 317.95 321.00 328.71 387.23 393.54

409.25 409.92 419.58 429.58 448.46 463.90

499.67 525.78 528.23 538.35 565.36 572.16

587.02 593.41 595.08 600.92 622.81 624.93

628.42 635.95 682.05 691.76 710.86 777.20

781.24 806.59 812.45 838.92 851.78 853.50

855.82 892.54 927.07 940.34 959.87 965.57

970.79 983.95 991.83 997.15 1009.60 1014.03

1018.16 1022.29 1024.50 1027.12 1028.61 1031.67

1033.96 1035.01 1048.29 1050.98 1054.71 1064.41

1083.10 1099.28 1101.55 1120.81 1128.34 1129.36

1178.43 1179.12 1206.46 1207.15 1209.79 1219.04

1220.56 1240.78 1258.79 1301.01 1324.26 1353.09

1363.19 1369.23 1378.19 1385.06 1388.13 1389.82

1404.07 1408.51 1420.38 1421.84 1423.16 1428.32

1429.52 1432.86 1451.22 1459.05 1460.55 1464.37

1478.35 1479.58 1480.54 1482.64 1486.34 1489.24

1497.86 1499.09 1501.46 1514.09 1520.34 1525.99

1535.65 1538.16 1574.24 1613.31 1631.19 1641.30

1645.05 1649.91 3039.41 3041.21 3047.36 3048.64

3057.62 3059.84 3082.27 3088.01 3113.40 3121.88

3125.09 3126.42 3133.11 3134.32 3161.81 3165.80

3168.80 3170.16 3174.29 3177.45 3179.26 3179.90

3183.08 3190.02 3201.73 3203.49 3209.33 3212.83

3218.29 3222.26 3225.08

V. References

1. Chu, J. C. K.; Rovis, T., Complementary Strategies for Directed C(sp^3)–H Functionalization: A Comparison of Transition-Metal-Catalyzed Activation, Hydrogen Atom Transfer, and Carbene/Nitrene Transfer. *Angew. Chem. Int. Ed.* **2018,** *57*, 62-101.

2. Wang, R.; Luan, Y.; Ye, M., Transition Metal–Catalyzed Allylic C(sp^3)–H Functionalization via η^3 -Allylmetal Intermediate. *Chin. J. Chem.* **2019,** *37*, 720-743.

3. Hull, K. L.; Lanni, E. L.; Sanford, M. S., Highly Regioselective Catalytic Oxidative Coupling Reactions: Synthetic and Mechanistic Investigations. *J. Am. Chem. Soc*. **2006,** *128,* 14047-14049

4. Vásquez-Céspedes, S.; Wang, X.; Glorius, F., Plausible Rh(V) Intermediates in Catalytic C–H Activation Reactions. *ACS Catal.* **2018,** *8*, 242-257.

5. Cochet, T.; Bellosta, V.; Roche, D.; Ortholand, J.-Y.; Greiner, A.; Cossy, J., Rhodium (III)-catalyzed allylic C–H bond amination. Synthesis of cyclic amines from ω-unsaturated N-sulfonylamines. *Chem. Commun.* **2012,** *48*, 10745-10747.

6. Kim, J.; Shin, K.; Jin, S.; Kim, D.; Chang, S., Oxidatively Induced Reductive Elimination: Exploring the Scope and Catalyst Systems with Ir, Rh, and Ru Complexes. *J. Am. Chem. Soc.* **2019,** *141*, 4137-4146.

7. Shin, K.; Park, Y.; Baik, M.-H.; Chang, S., Iridium-catalysed arylation of C–H bonds enabled by oxidatively induced reductive elimination. *Nat. Chem.* **2017,** *10*, 218-224.

8. Li, X.; Ouyang, W.; Nie, J.; Ji, S.; Chen, Q.; Huo, Y., Recent Development on Cp*Ir(III)-Catalyzed C−H Bond Functionalization. *ChemCatChem* **2020**, *12, 2358-2384*

9. Periana, R. A.; Bergman, R. G., Rapid intramolecular rearrangement of a hydrido(cyclopropyl)rhodium complex to a rhodacyclobutane. Independent synthesis of the metallacycle by addition of hydride to the central carbon atom of a cationic rhodium π-allyl complex. *J. Am. Chem. Soc.* **1984,** *106*, 7272-7273.

10. Wakefield, J. B.; Stryker, J. M., Metallacyclobutanes from kinetic nucleophilic addition to η^3-allyl ethylene complexes of iridium. Regioselectivity dependence on nucleophile and allyl orientation. *J. Am. Chem. Soc.* **1991,** *113*, 7057-7059.

11. Shibata, Y.; Kudo, E.; Sugiyama, H.; Uekusa, H.; Tanaka, K., Facile Generation and Isolation of π-Allyl Complexes from Aliphatic Alkenes and an Electron-Deficient Rh(III) Complex: Key Intermediates of Allylic C–H Functionalization. *Organometallics* **2016,** *35*, 1547-1552.

12. Burman, J. S.; Blakey, S. B., Regioselective Intermolecular Allylic C–H Amination of Disubstituted Olefins via Rhodium/π-Allyl Intermediates. *Angew. Chem. Int. Ed.* **2017,** *56*, 13666-13669.

13. Nelson, T. A. F.; Blakey, S. B., Intermolecular Allylic C–H Etherification of Internal Olefins. *Angew. Chem. Int. Ed.* **2018,** *57*, 14911-14915.

14. Mas-Roselló, J.; Herraiz, A. G.; Audic, B.; Laverny, A.; Cramer, N., Chiral Cyclopentadienyl Ligands: Design, Syntheses, and Applications in Asymmetric Catalysis. *Angew. Chem. Int. Ed.* **2020**. Early View, doi/10.1002/anie.202008166

15. Duchemin, C.; Smits, G.; Cramer, N., Rh^{I}, Ir^{III}, and Co^{III} Complexes with Atropchiral Biaryl Cyclopentadienyl Ligands: Syntheses, Structures, and Catalytic Activities. *Organometallics* **2019**, *38,* 3939-3947

16. Harris, R. J.; Park, J.; Nelson, T. A. F.; Iqbal, N.; Salgueiro, D. C.; Bacsa, J.; Macbeth, C. E.; Baik, M.-H.; Blakey, S. B., The Mechanism of Rhodium-Catalyzed Allylic C–H Amination. *J. Am. Chem. Soc.* **2020,** *142*, 5842-5851.

17. Simmons, E. M.; Hartwig, J. F., On the Interpretation of Deuterium Kinetic Isotope Effects in C–H Bond Functionalizations by Transition-Metal Complexes. *Angew. Chem. Int. Ed.* **2012,** *51*, 3066-3072.

18. Song, L.; Trogler, W. C., $[(CO)_3(PPh_3)_2OsAg(O_2CCF_3)]$: A Model for an Intermediate on the Reaction Coordinate in Electron Transfer. *Angew. Chem., Int. Ed.* **1992,** *31*, 770-772.

19. Connelly, N. G.; Geiger, W. E., Chemical Redox Agents for Organometallic Chemistry. *Chem. Rev.* **1996,** *96*, 877-910.

20. Lerchen, A.; Knecht, T.; Koy, M.; Ernst, J. B.; Bergander, K.; Daniliuc, C. G.; Glorius, F., Non-Directed Cross-Dehydrogenative (Hetero)arylation of Allylic C(sp^3)–H bonds enabled by C–H Activation. *Angew. Chem. Int. Ed.* **2018,** *57*, 15248-15252.

21. Xia, C.; Shen, J.; Liu, D.; Zhang, W., Synthesis of Chiral α,β-Unsaturated γ-Amino Esters via Pd-Catalyzed Asymmetric Allylic Amination. *Org. Lett.* **2017,** *19*, 4251-4254.

22. Das, B. G.; Nallagonda, R.; Ghorai, P., Direct Substitution of Hydroxy Group of π-Activated Alcohols with Electron-Deficient Amines Using Re_2O_7 Catalyst. *J. Org. Chem.***2012,** *77*, 5577-5583.

23. Bochevarov, A.; Harder, E.; Hughes, T.; Greenwood, J.; Braden, D.; Philipp, D.; Rinaldo, D.; Halls, M.; Zhang, J.; Friesner, R., Jaguar: A high-performance quantum chemistry software program with strengths in life and materials sciences. *Int. J. Quantum Chem.* **2013,** *113*, 2110-2142.

24. Becke, A. D., Density-Functional Theromochemistry 3. The Role of Exact Exchange. *J. Chem. Phys.* **1993,** *98*, 5648-5652.

25. Grimme, S.; Antony, J.; Ehrlich, S.; Krieg, H., A consistent and accurate ab initio parametrization of density functional dispersion correction (DFT-D) for the 94 elements H-Pu. *J. Chem. Phys.* **2010,** *132*.

26. Ditchfield, R.; Hehre, W. J.; Pople, J. A., Self-consistent Molecular-Orbital Methods IV. Extended Gaussian-Type Basis For Molecular-Orbital Studies Of Organic Molecules. *J. Chem. Phys.* **1971,** *54*, 724-728.

27. Hay, P. J.; Jeffrey Hay, P.; Wadt, W. R., Ab initio effective core potentials for molecular calculations. Potentials for the transition metal atoms Sc to Hg. *J. Chem. Phys.* **1985,** *82*, 270-283.

28. Dunning, T. H., Gaussian-Basis Sets for Use in Correlated Molecular Calculations 1. The AToms Boron Through Neon and Hydrogen. *J. Chem. Phys.* **1989,** *90*, 1007-1023.

29. Marten, B.; Kim, K.; Cortis, C.; Friesner, R.; Murphy, R.; Ringnalda, M.; Sitkoff, D.; Honig, B., New model for calculation of solvation free energies: Correction of self-consistent reaction field continuum dielectric theory for short-range hydrogen-bonding effects. *J. Phys. Chem.* **1996,** *100*, 11775-11788.

Complex 3-27 (^{1}H, 400 MHz, $CDCl_3$)

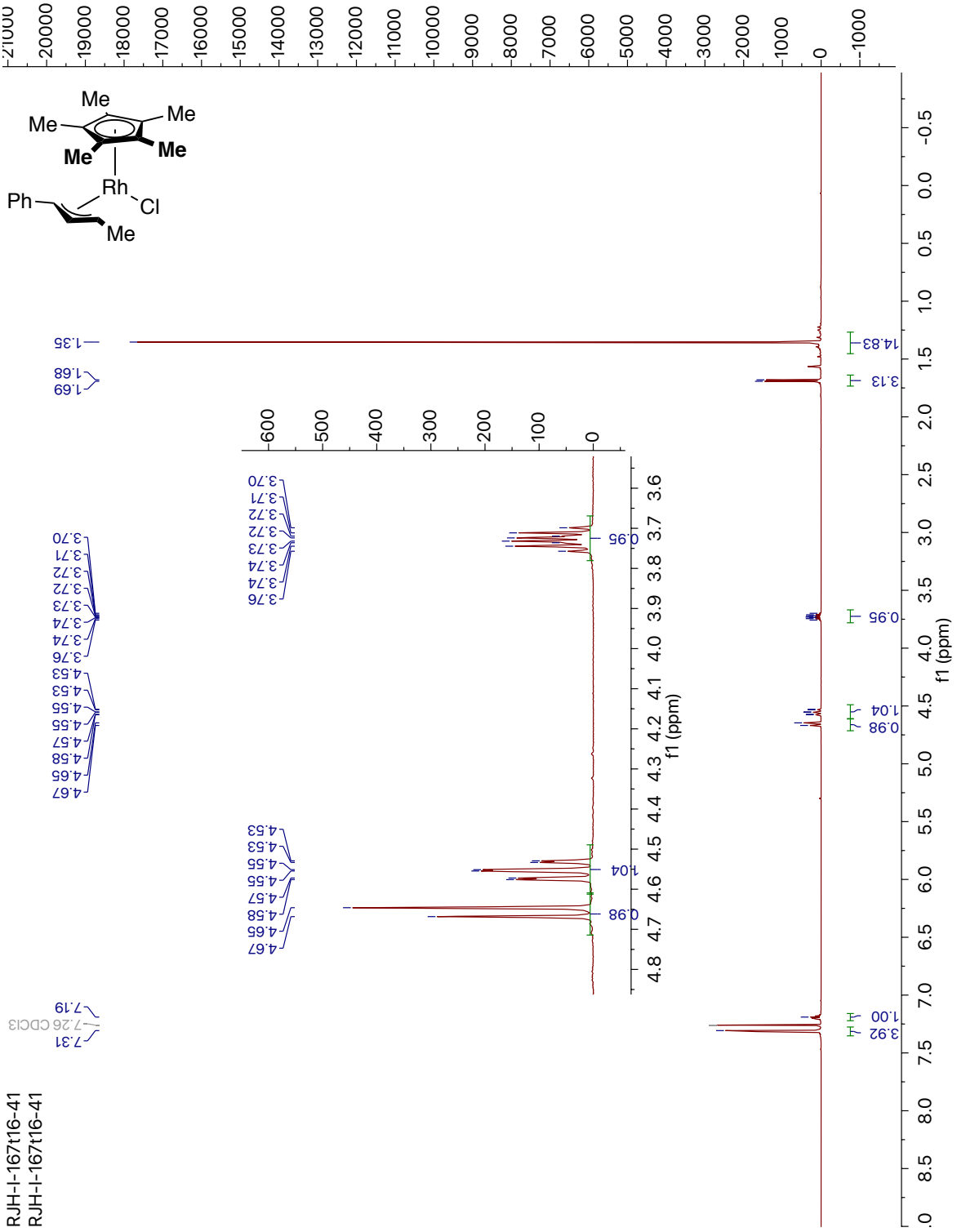

Complex 3-27 (^{13}C, 125 MHz, $CDCl_3$)

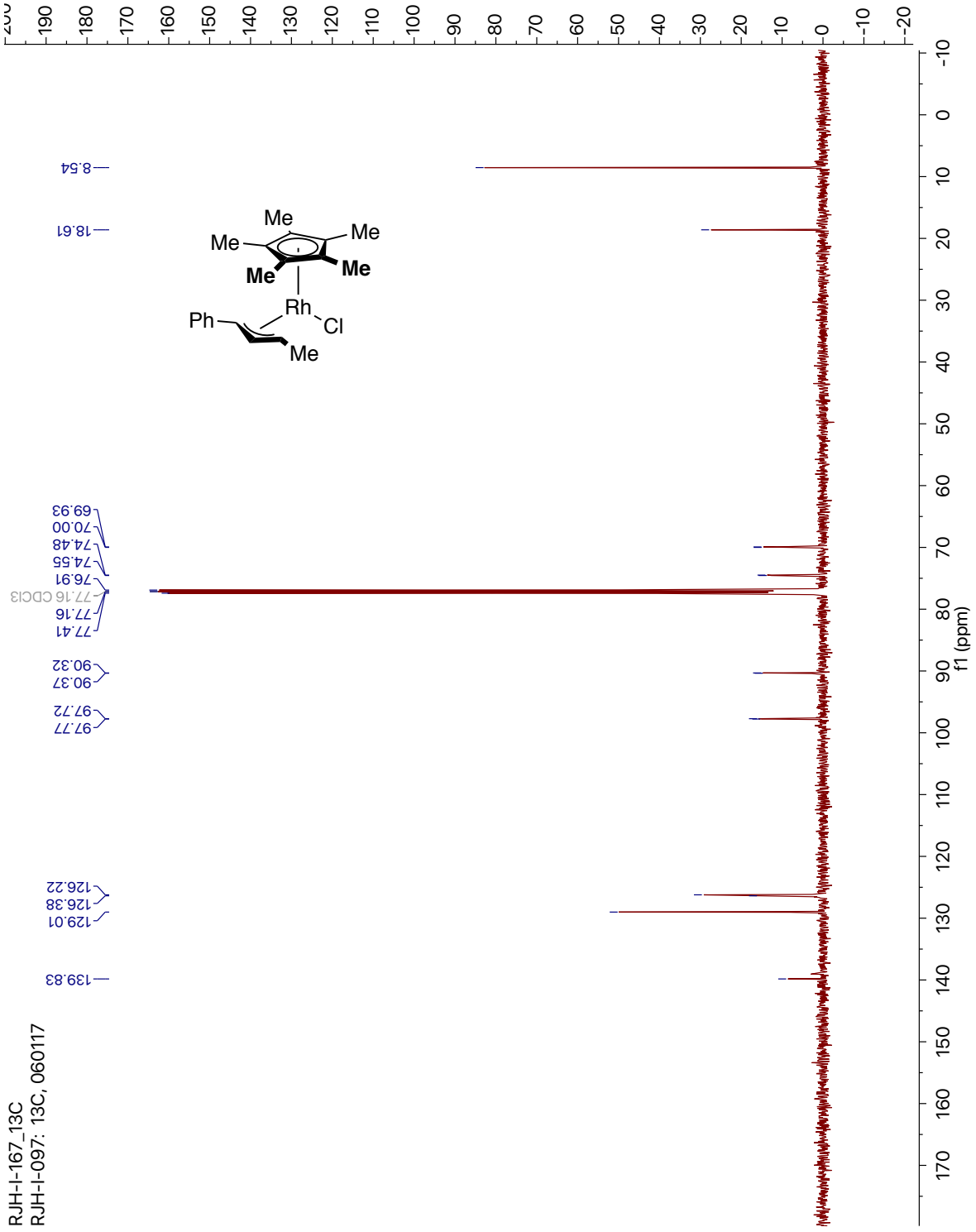

Complex 3-31 (^{1}H, 400 MHz, $CDCl_3$)

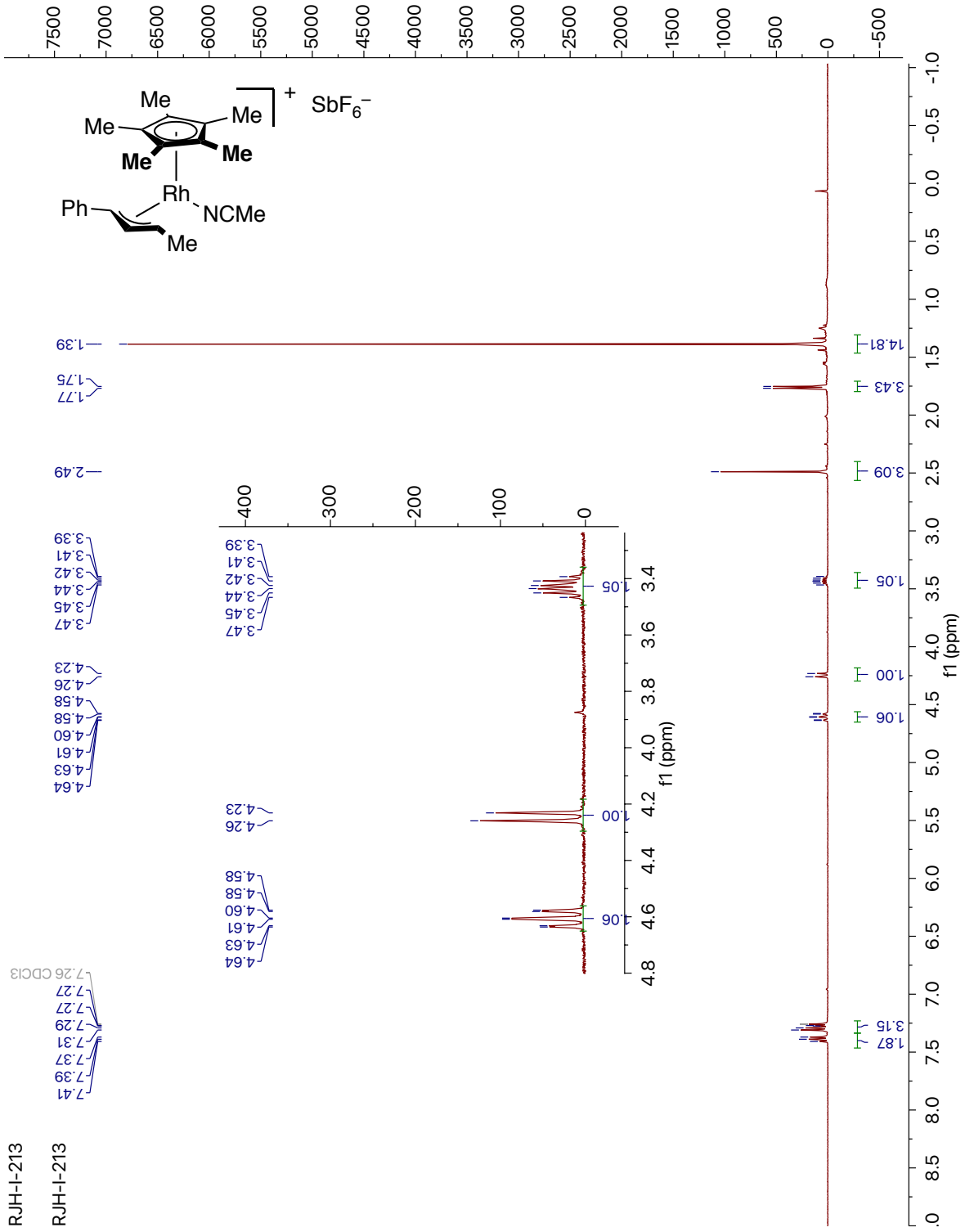

Complex 3-31 (^{13}C, 125 MHz, $CDCl_3$)

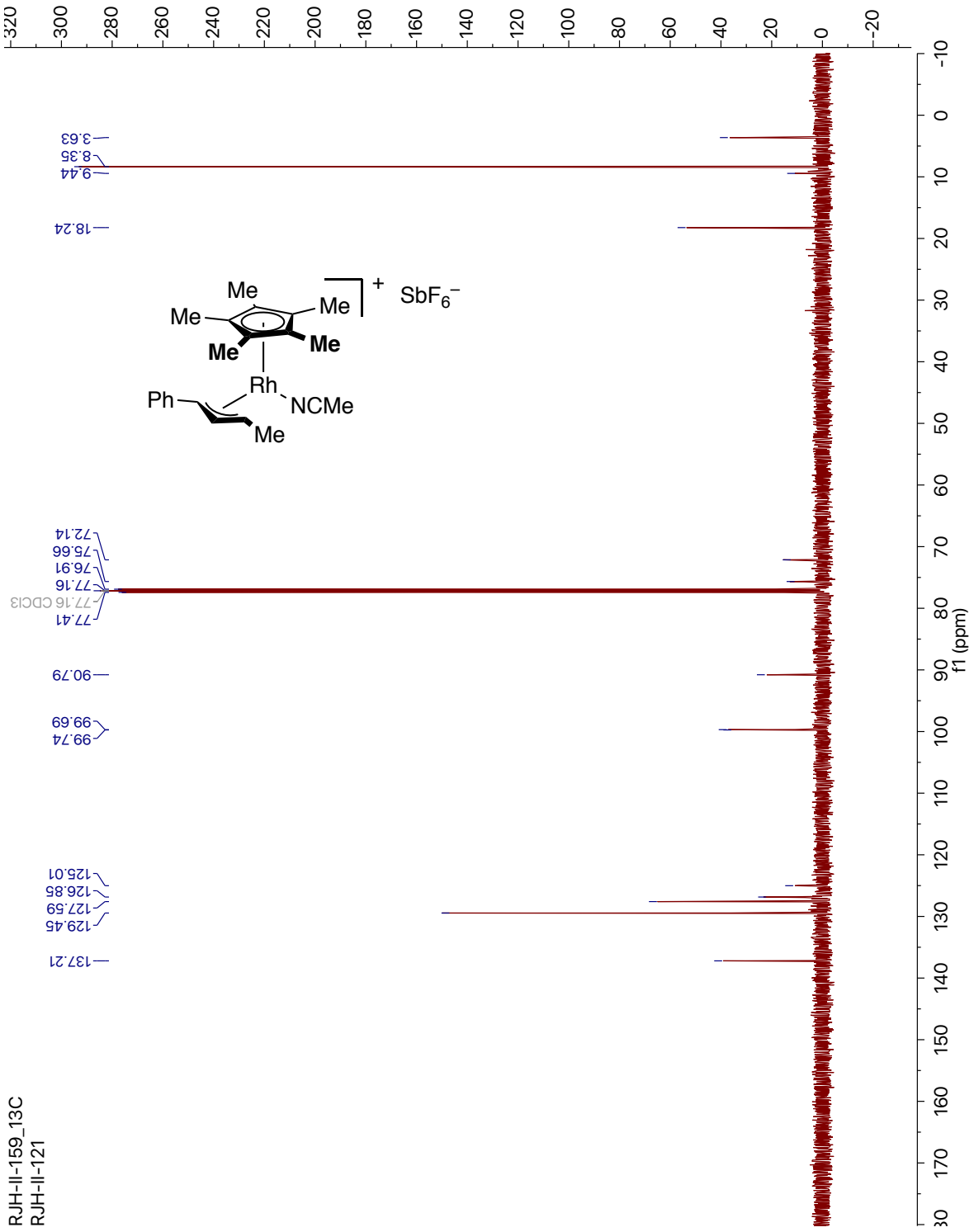

Complex 3-30 (^{1}H, 400 MHz, $CDCl_3$)

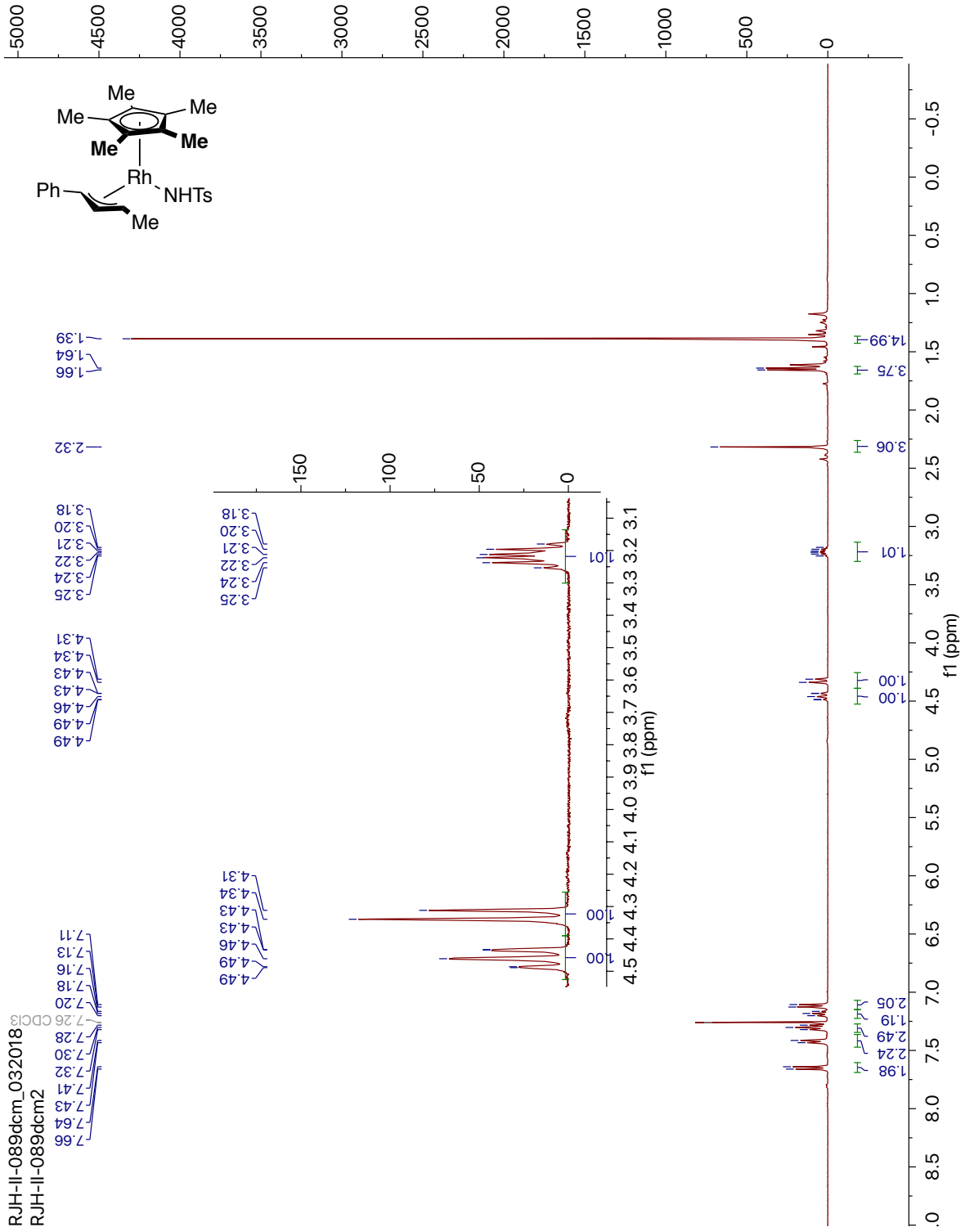

Complex 3-30 (^{13}C, 125 MHz, $CDCl_3$)

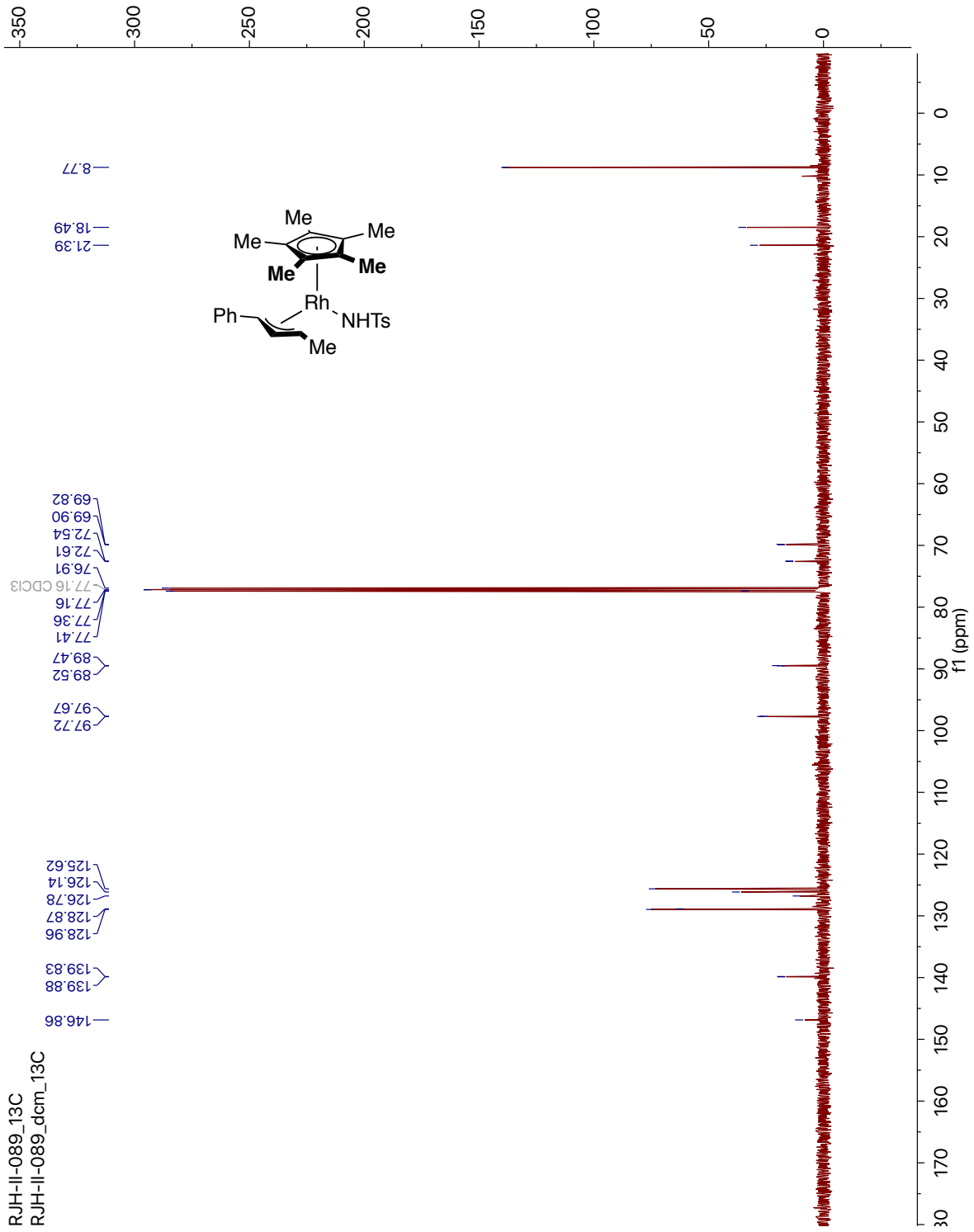

Complex 3-32 (^{1}H, 400 MHz, $CDCl_3$)

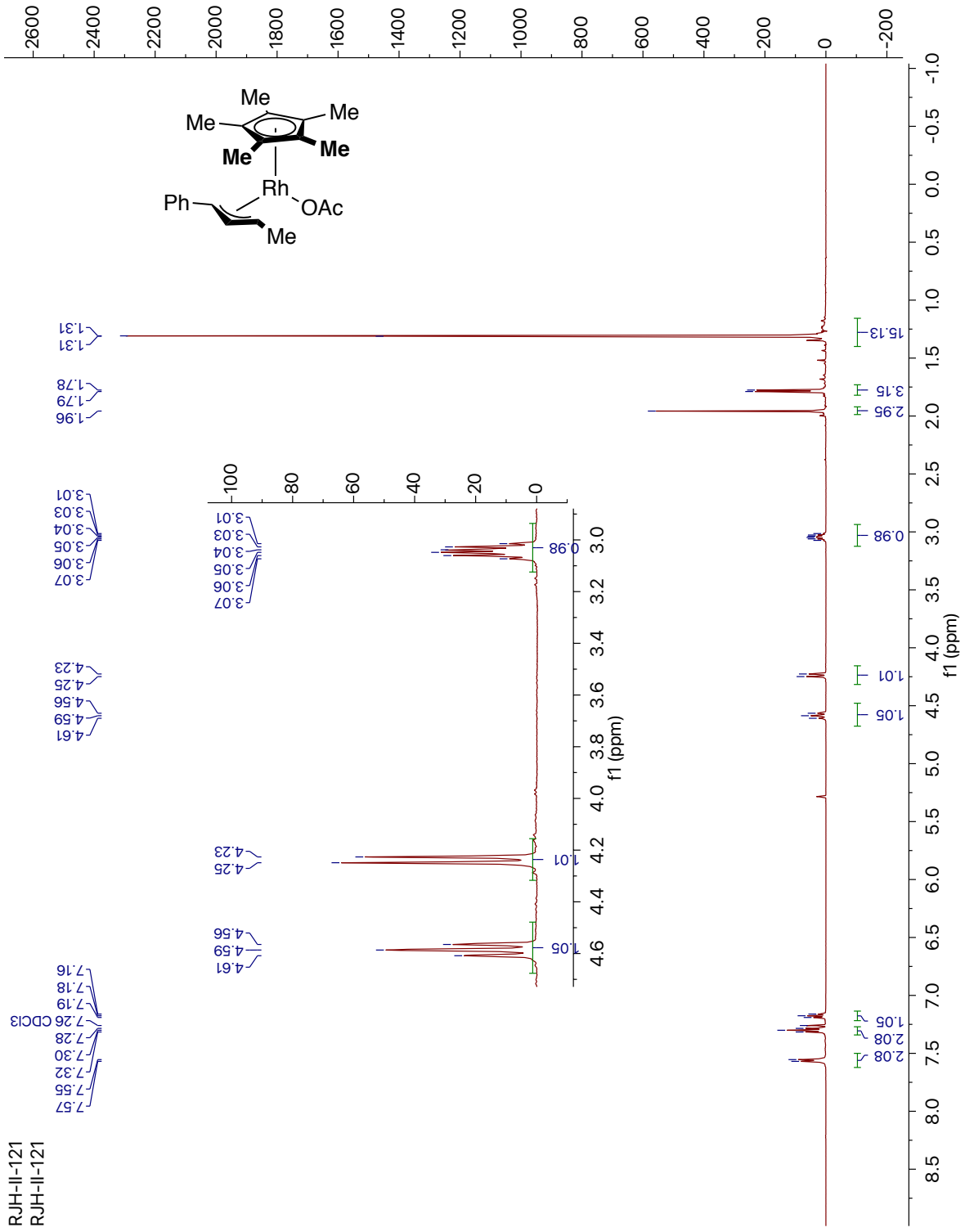

Complex 3-32 (^{13}C, 125 MHz, $CDCl_3$)

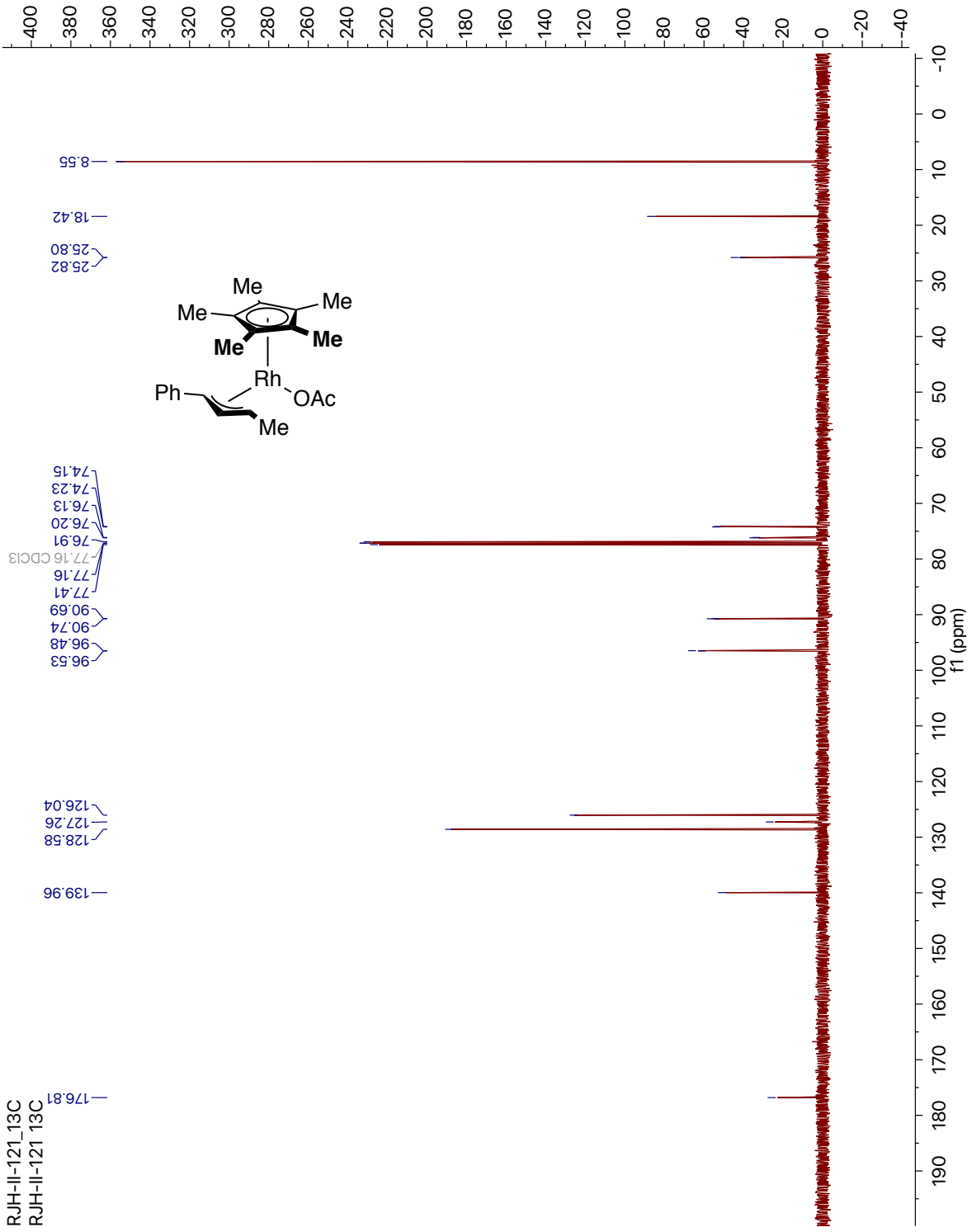

Chapter 4: Regiodivergent Allylic C–H Sulfamidation of Allylbenzene Derivatives via a Ir(V)Cp*-π-allyl Nitrenoid Intermediate

I. Introduction

I.1. MCp*-catalyzed Allylic C–N Bond Formation

Now that the mechanism for our first-generation allylic amination had been disclosed,[1] our group turned our focus toward developing an enantioselective protocol for allylic C–H functionalization. Since the first-generation procedure to form C–O,[2] C–N,[3] and C–C[4] bonds precludes catalyst-controlled enantioselectivity, a change in mechanism was desired (**Figure 4-1A**). We hypothesized that one means to provide enantioselectivity would be through the direct reductive elimination of the desired C–X bond from the metal center of the catalyst. We believed this could be induced via oxidative coupling reagents. As was mentioned earlier, Glorius and co-workers disclosed a perspective on Rh(V) intermediates in C–H functionalization (Chapter 3).[5] The main source of these high-valent RhCp* species was through the use of oxidizing coupling partners and directing groups. Nitrene precursors are one well-known class of oxidizing coupling reagents that we began to consider to provide important allylic products. Sukbok Chang had also recently introduced the use of dioxazolone nitrenoid precursors for directed sp^2 C–H functionalization (**Figure 4-1B**).[6, 7] These reagents quickly gained popularity with group(IX)Cp* catalyzed C–H functionalization. Furthermore, utilization of dioxazolone reagents as the nitrene precursors could allow access to allylic amides, which had previously been elusive in the first-generation reactions.

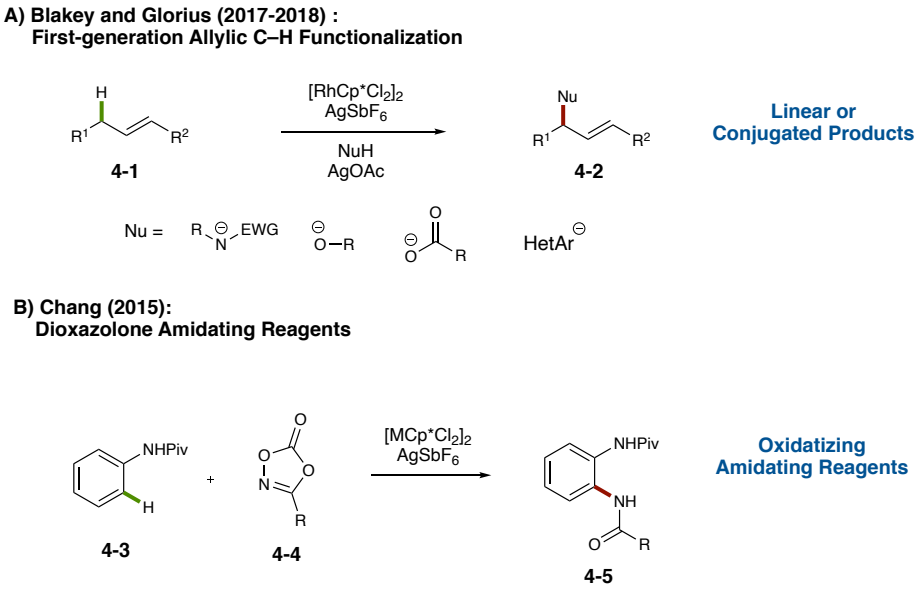

Figure 4-1. Previous Group(IX)Cp*-Catalyzed C–H Functionalization Reactions

With this information in hand, Dr. Jacob Burman, Dr. Caitlin Farr, and Dr. Robert Harris from our group developed an allylic C–H amidation protocol with complementary regioselectivity observed in the first-generation methods.[8] Speaking to the importance of this reaction, analogous methods were concomitantly reported by both Glorius and Rovis (**Figure 4-2**).[9, 10] In all disclosures, when terminal olefins were utilized, an IrCp*-catalyst afforded greater regiocontrol for the branched product. While not a large focus of any of the first-generation reports, linear products were favored for C–N, C–O, and C–C bond formation. Our group also focused on the reactivity of internal olefins and found that RhCp*-precatalysts provided greater regioselectivity for the benzylic isomer and IrCp*-precatalysts provided modest regioselectivity for the conjugated isomer, providing complementary

reactivity to previous disclosed methods. A wide variety of allylic amides were formed across all three disclosures. Mechanistic studies were performed by our group to determine the origins of the regioselectivity provided by the metal catalysts but, unfortunately, little insight was provided. While further studies would have to be performed to confirm the mechanism of the amidation procedure, a M(V)-nitrenoid intermediate is likely.

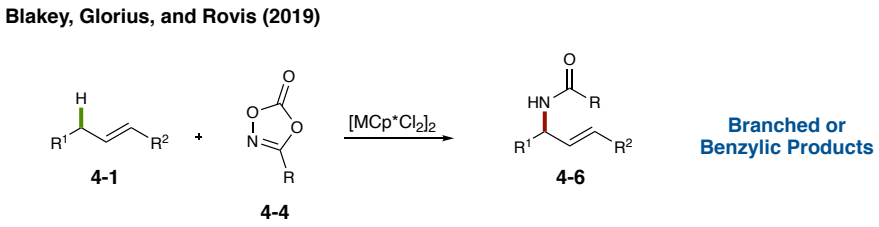

Figure 4-2. Allylic C–H Amidation using Dioxazolone Nitrenoid Precursors

The proposed catalytic cycle for allylic C–H amidation likely starts much like the first-generation disclosures. Catalyst activation followed by olefin (**4-7**) and carboxylate coordination provides complex **4-8** (**Figure 4-3**). Complex **4-8** through concerted metalation-deprotonation produces π-allyl complex **4-9** with an open coordination site. Dioxazolone (**4-4**) decomposition releases CO_2 to produce M(V) nitrene complex **4-10**. Complex **4-10** is proposed to reductively eliminate amide **4-12** to complete the catalytic cycle. We believed that this second-generation mechanistic pathway could afford asymmetric products if an enantioselective catalyst system could be used, and therefore, is a key focus for further development.

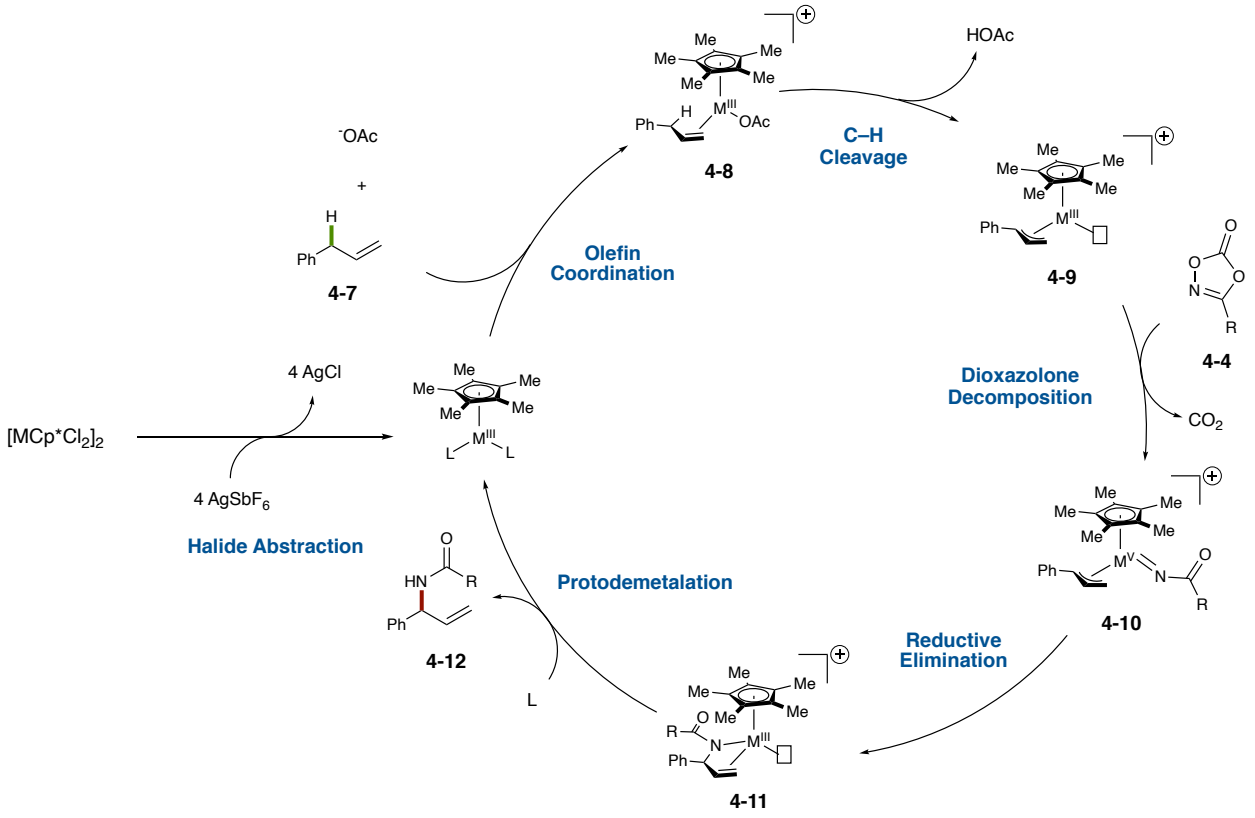

Figure 4-3. Allylic C–H Amidation Proposed Catalytic Cycle

I.2. A Novel Allylic C–H Amination Protocol

A drawback of dioxazolone reagents is that they only result in the formation of amide products. Amides are indispensable for the formation of amino acids, proteins, and important drug molecules.[11] Unfortunately, to form the corresponding allylic amines from these amide products, relatively harsh conditions are required.[12] With this in mind, we turned our focus towards developing an allylic C–H amination protocol proceeding through the second-generation mechanism. If a second-generation allylic C–H amination protocol could be investigated complementary regioselectivity to the first-generation methods would

be observed, but our first-generation amination report was never optimized for terminal olefins. Optimization of the first-generation methods and the development of a second-generation amination could allow for a regiodivergent report for allylic C–H amination to be developed based on reagent and catalyst choice (**Figure 4-4**).[3]

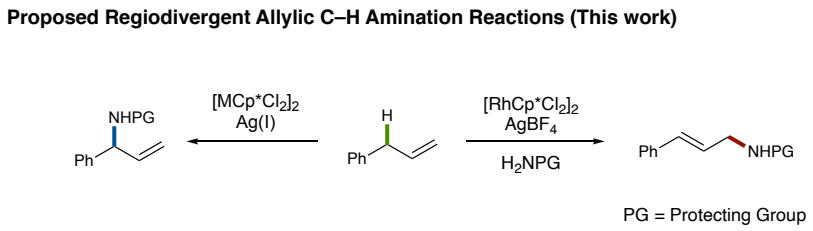

Figure 4-4. Proposed Regiodivergent Allylic C–H Amination

I performed this investigation as a collaborative study with Amaan Kazerouni, Steven Chen, and Kim Sharp. Initially, Amaan Kazerouni (a graduate student in our lab) and Steven Chen (an undergraduate researcher) focused on developing a branched-selective allylic C–H amination reaction. While this was occurring, I worked with Kim Sharp (an undergraduate researcher) to further optimize and study our first-generation linear-selective amination procedure.

II. Results and Discussion

II.1. Branched-selective Optimization

Amaan and Steven began their investigation by performing a short screen of nitrene precursors that would result in protected allylic amine products. After this nitrene screen,

N-tosylazide was chosen for the rest of this investigation.[13] Furthermore, tosyl protecting groups can be readily cleaved via reductive conditions to afford the corresponding allylic amine.[14] Amaan then began an optimization study utilizing similar conditions to those of our previous reports. In this case, $[RhCp^*Cl_2]_2$ was utilized as the precatalyst, $AgSbF_6$ as the halide scavenger, *N*-tosylazide as the nitrene precursor, and CsOAc as the carboxylate source in DCE at 80 °C for 24 h resulting in 13% yield of amine **4-13**, and 4% yield of linear amine **4-14** (**Table 4-1**, **Entry 1**). Substituting $[IrCp^*Cl_2]_2$ for the rhodium precatalyst afforded fairly similar results (**4-13**, 17%; **4-14**, 8%; **Table 4-1**, **Entry 2**). During the development of the allylic C–H amidation procedure utilizing dioxazolones as the nitrene precursor it was found that a 10 mol% excess of $AgSbF_6$ increased the yield.[3] Surprisingly, increasing the silver loading to 40 mol% from 30 mol% with either the RhCp* or IrCp* precatalyst proved deleterious to the reaction (**Table 4-1**, **Entries 3-4**). During the etherification investigation, I found that the counterion of the silver (I) halide scavenger had a significant impact on the overall reaction efficiency.[2] For this reason, a small screen of silver salts was performed. Both $AgBF_4$ and AgOTs at 10 mol% loading resulted in trace product observed, while $AgNTf_2$ increased the yield to 23% for amine **4-13** and, more importantly, resulted in none of the undesired linear amine (**4-14, Table 4-1**, **Entries 5-7**). Furthermore, using 2,2,2-trifluoroethanol (TFE, 55%), and 1,1,1,3,3,3-hexafluorisopropanol (HFIP, 60%) as the solvent resulted in a further increase in yield (**Table 4-1**, **Entries 8-9**). In these cases, sealed tubes were utilized to prevent undesired solvent evaporation and a reproducible environment. The conditions found in Entry 9 were chosen for the rest of this study.

Table 4-1. Optimization of Branched-Selective C–H Amination of Allylbenzene

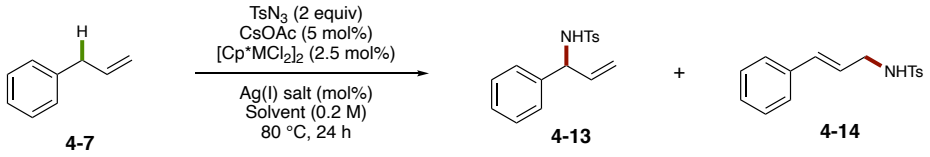

4-7 **4-13** **4-14**

Entry	$[MCp^*Cl_2]_2$	Ag(I) (mol%)	Solvent	% yield (**4-13**)[b]	% yield (**4-14**)[b]
1	$[RhCp^*Cl_2]_2$	$AgSbF_6$ (10)	DCE	13	4
2	$[IrCp^*Cl_2]_2$	$AgSbF_6$ (10)	DCE	17	8
3	$[RhCp^*Cl_2]_2$	$AgSbF_6$ (40)	DCE	trace	0
4	$[IrCp^*Cl_2]_2$	$AgSbF_6$ (40)	DCE	trace	0
5	$[IrCp^*Cl_2]_2$	$AgBF_4$ (10)	DCE	<5	trace
6	$[IrCp^*Cl_2]_2$	AgOTs (10)	DCE	<5	trace
7	$[IrCp^*Cl_2]_2$	$AgNTf_2$ (10)	DCE	23	0
8	$[IrCp^*Cl_2]_2$	$AgNTf_2$ (10)	TFE	55	0
9	$[IrCp^*Cl_2]_2$	$AgNTf_2$ (10)	HFIP	60	0

[a]Reactions were run using 1a (0.10 mmol), TsN_3 (0.40 mmol), CsOAc (0.005 mmol), $AgNTf_2$ (0.0025 mmol), $[Cp^*IrCl_2]_2$ (0.0025 mmol). [b]Isolated yields.

II.2.Linear-selective Optimization

Now that we could form the branched products selectively by the use of nitrenoid precursors we decided to further optimize the first-generation amination protocol to afford a regiodivergent sulfamidation based on reagent choice. The unoptimized reaction conditions previously disclosed resulted in only 40% yield of the desired product under standard reaction conditions (**Figure 4-5**). Since terminal olefins were not the focus of that manuscript, further optimization was never performed. Increasing the temperature to 60 °C for 24 h with $TsNH_2$ (2.5 equiv), AgOAc (2.1 equiv), $[RhCp^*Cl_2]_2$ (2 mol%), and $AgBF_4$ (8 mol%) resulted in 61% yield of **4-14** (**Table 4-2**, **Entry 1**). Increasing the temperature further to 80 °C (62% yield) provided little increase in yield (**Table 4-2**, **Entry 2**). A short

Ag(I) halide scavenger salt screen was then undertaken. Unfortunately, $AgSbF_6$ (29%), $AgNTf_2$ (55%), and $AgBAr^F{}_4$ (15%) did not provide superior results in comparison to $AgBF_4$ (**Table 4-2**, **Entries 3-5**). For this reason, Kim continued this investigation with $AgBF_4$ as the halide scavenger. Furthermore, when THF was used as the solvent at 60 °C, amine **4-14** was observed in 70% yield (**Table 4-2**, **Entry 6**). When trifluorotoluene was used at 80 °C (35%) or 100 °C (70%) similar yields were observed (**Table 4-2, Entries 7-8**). Likewise, chlorobenzene was used as the solvent resulting in 72% (80 °C) and 67% (100 °C) yield of amine (**4-14, Table 4-2, Entries 9-10**)**.** Furthermore, when the reaction was performed in 1,4-dioxane as the solvent, amine **4-14** was observed in 64% yield at 80 °C and 81% yield at 100 °C (**Table 4-2, Entries 11-12**). Overall, ethereal solvents were found to increase the yield of the reaction modestly with the entry 12 providing the best results. For this reason, conditions found in entry 12 were chosen for the continuation of this study.

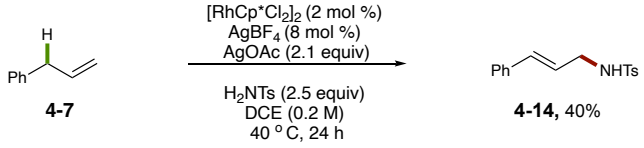

Figure 4-5. Previously Disclosed Allylic C–H Amination of Allylbenzene

Table 4-2. Optimization of Linear-Selective Amination of Allylbenzene

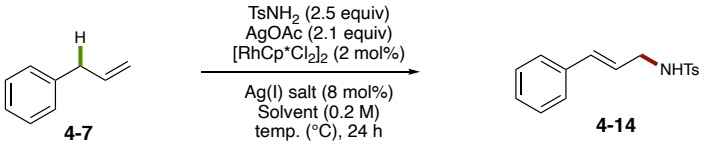

Entry	Ag(I) (mol%)	Solvent	temp (°C)	% yield (**4-14**)
1	$AgBF_4$	DCE	60	61
2	$AgBF_4$	DCE	80	62
3	$AgSbF_6$	DCE	80	29
4	$AgNTf_2$	DCE	80	55
5	$AgBAr^F_4$	DCE	80	15
6	$AgBF_4$	THF	60	70
7	$AgBF_4$	TFT	80	35
8	$AgBF_4$	TFT	100	70
9	$AgBF_4$	PhCl	80	72
10	$AgBF_4$	PhCl	100	67
11	$AgBF_4$	1,4-dioxane	80	64
12	$AgBF_4$	1,4-dioxane	100	81

Yields were determined by crude GC analysis with nonane as an internal standard

II.3. Scope of Linear Selective Sulfamidation

Now that we had optimized the reaction conditions of the linear-selective amination, Kim and I set out to study the effect steric and electronic bias of the olefin coupling partner had on the reaction efficiency (**Figure 4-6**). Unfortunately, conditions from Entry 12 only provided **4-14** in 66% isolated yield. Likewise, using halogenated allylbenzenes as the olefin coupling partner afforded product **4-17** (*para*-F) in 48% yield and **4-18** (*para*-Br) in only 7% yield. To test the effect electron-poor and electron-rich arenes had on the reaction, *para*-CF_3-allylbenzene (**4-20**, 11%), *para*-*t*-Bu-allylbenzene (**4-21**, 32%), and *para*-OMe-allylbenzene (**4-21**, trace) were utilized providing low yields of the corresponding products. *ortho*-Tolyl (**4-22**, 20%) and safrole (**4-23**, 18%) allylbenzene derivatives also provided low yield of their corresponding cinnamyl amine products. Furthermore, using 4-phenyl-1-

butene as a non-allylbenzene terminal olefin provided **4-24** in only 13% yield as a 1:1 mixture of regioisomers of amination at the 1 and 2 position. These results suggested that the optimized conditions were specific for neutral allylbenzenes and further electronic or steric perturbations would be deleterious to this reaction. With this in mind we decided to turn our focus to the branched selective method for the remainder of the investigation.

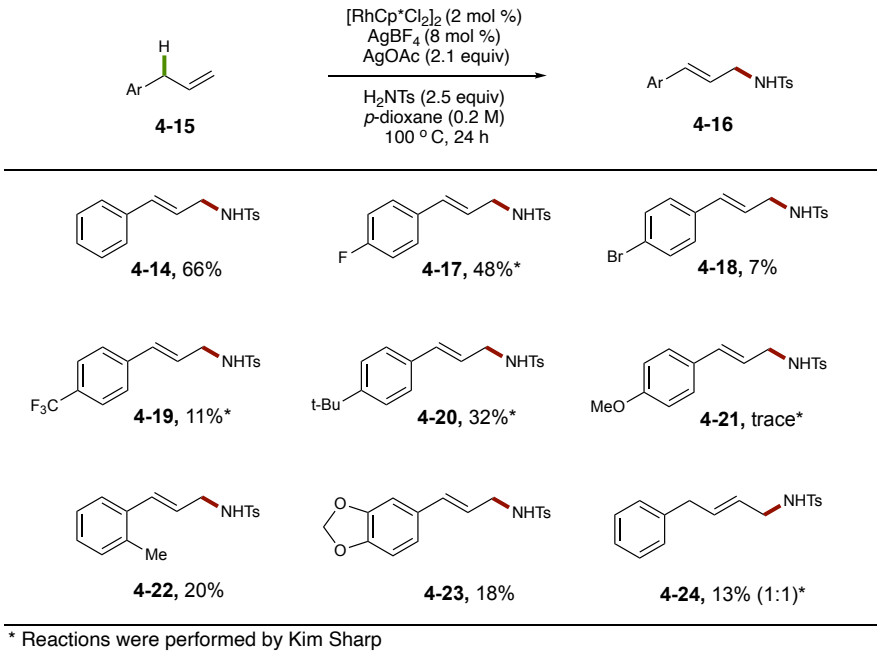

Figure 4-6. Linear-selective Allylic C–H Amination

II.4.Scope of Branched-selective Sulfamidation

Amaan, Steven, and I then studied the effects of electronics, steric bias, and functional group tolerance on the overall reaction efficiency of the branched-selective system. Overall, a variety of allylbenzene derivatives were tolerated under the reaction conditions, resulting

in the branched allylic amine **4-25** (**Figure 4-7**). Allylbenzenes with a *para*-OMe (**4-26**, 57%) or *para*-*t*-butyl (**4-27**, 61%) group provided good yields, illustrating that an increase in electron density had little effect on the overall reaction efficiency. Furthermore, allylbenzenes with electron-deficient substituents such as *para*-methyl ester (**4-28,** 52%,) and *para*-CF_3(**4-30,** 46%) provided the desired product in mildly lower yields. *Para*-fluorinated allylbenzene was also well tolerated resulting in a 67% yield of amine **4-29**. Surprisingly, increasing the electron-density on the arene further by utilizing safrole hindered the reaction slightly, resulting in a 47% yield (**4-31**) even under an extended reaction time of 48 h. Next, we investigated the effect of steric bulk ortho to the presumed π-allyl intermediate with *o*-allyltoluene resulting in 60% yield of **4-32** after 48 h. We then proceeded to utilize 4-phenyl-1-butene and 1-hexene as the olefin coupling partner to determine the necessity of the arene substituent for reactivity. In this case, 4-phenyl-1-butene resulted in a 75% yield of **4-33** after extended reaction times (48 h), and 1-hexene provided the corresponding amine **4-34** in only 49% yield as a 4.5:1.5:1 mixture of regioisomers. Furthermore, when *N*-Cbz azide was used as the nitrene precursor, amine **4-35** was afforded in a modest 17% yield, illustrating the importance of the tosyl protecting group for compatibility. A disubstituted olefin was also able to engage in this reaction, providing amine **4-36** in 54% yield. Likewise, a phenylalanine derivative and estrone derivative provided the corresponding allylic amines **4-37** and **4-38** in 50% and 62% yield, respectively. These results taken together show that this reaction provides good yield for a wide variety of allylbenzene derivatives regardless of steric bulk, electronic perturbation, and functionality.

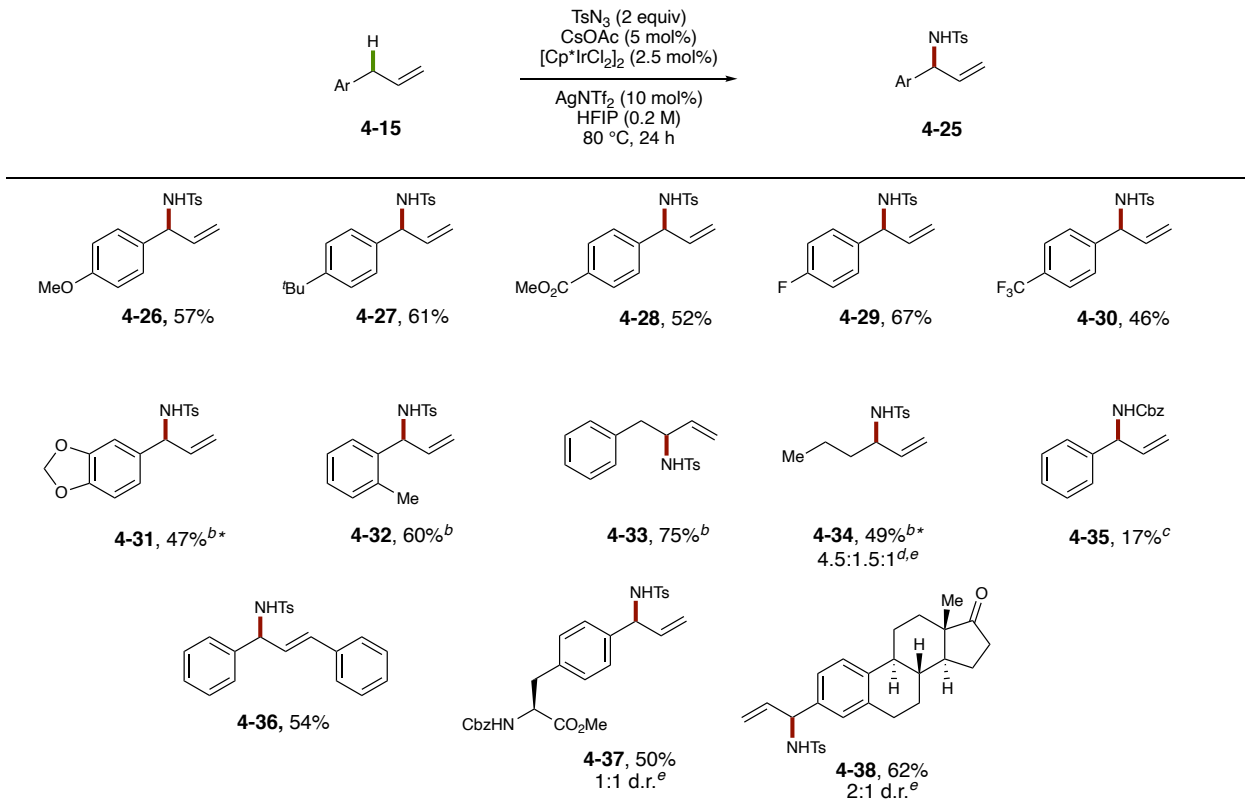

[a]Isolated yields. [b]Isolated yields after 48 hours. [c]$CbzN_3$ (0.40 mmol, 2 equiv) was used instead of TsN_3. [d]Isolated as mixture of regioisomers of allylic sulfonamide products at the 3-, 4-, and 2-positions, respectively (major isomer shown) [e]Determined by integration of crude reaction ^1H NMR spectrum. * Reactions were performed by Taylor Nelson, all other reactions were perforemd by Amaan Kazerouni or Steven Chen. (see supplemental for details)

Figure 4-7. Scope of Branched-selective Allylic C–H Sulfamidation of Allylbenzenes

II.5. Proposed Catalytic Cycle of Branched Selective Allylic C–H Amination

Allylic C–H sulfamidation utilizing *N*-tosylazide as the nitrenoid precursor provided similar regiochemical results to that of the amidation procedure utilizing dioxazolone reagents.[8] For this reason, we propose that the reaction proceeds via a similar mechanism. While further mechanistic investigations would be necessary to confirm the proposed catalytic cycle, an Ir(V) nitrenoid intermediate is likely (**Figure 4-8**). Complex **4-39** is first formed from the activation of $[IrCp^*Cl_2]_2$ with $AgNTf_2$, as the halide scavenger. Olefin (**4-7**)

coordination to form complex **4-40** followed by C–H activation via a concerted-metalation-deprotonation forms complex **4-41**. After the formation of Ir(III) complex **4-41**, TsN_3 decomposition releases N_2 gas to afford nitrene-Ir(V)-complex **4-42**. The oxidation of the Ir center is then followed by rapid reductive elimination to provide the corresponding C–N bond at the electron-rich carbon of the π-allyl group. This reductive elimination is then followed by protodemetalation to afford allylic sulfamide **4-13** and also regenerates the Ir(III) complex **4-39** to complete the catalytic cycle. To fully support this mechanism further studies would need to be performed.

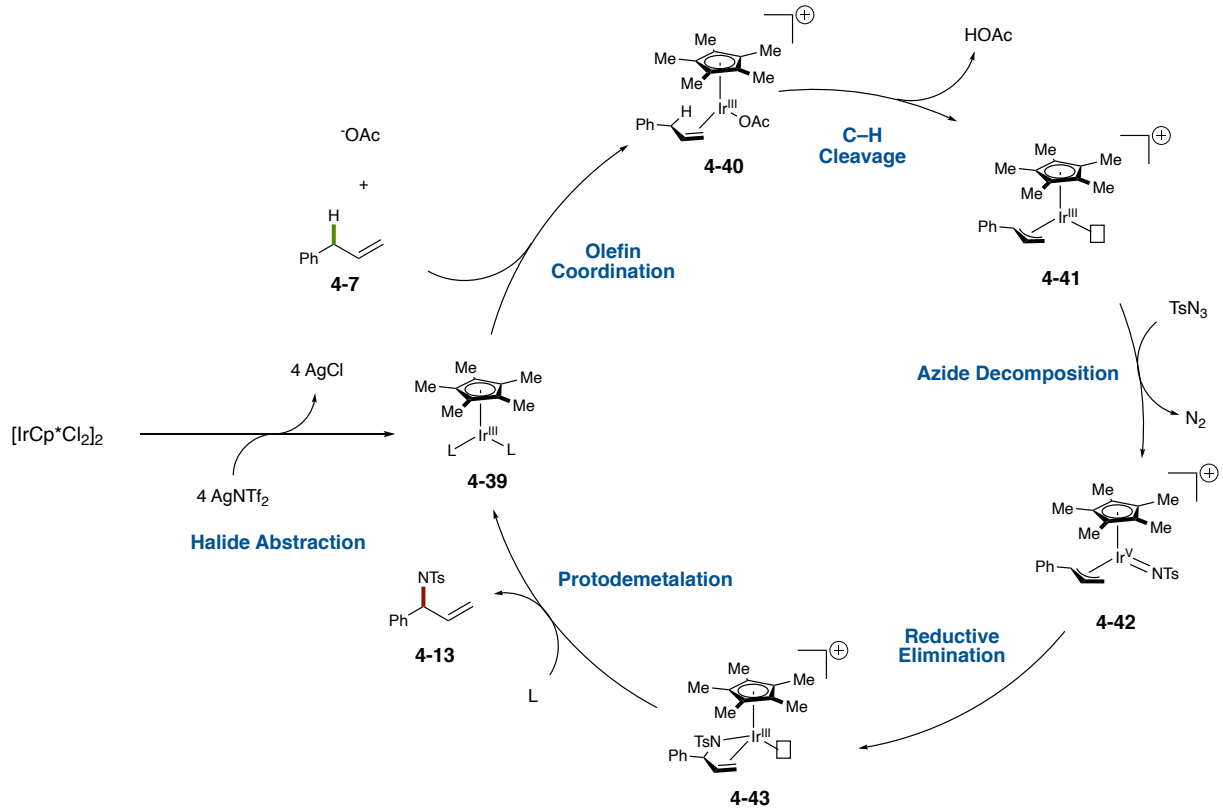

Figure 4-8. Proposed Catalytic Cycle of Branched Selective Allylic C–H Sulfamidation

II.6. Diversification of Branched Products to form Heterocycles

To support the utility of this novel reaction we set out to diversify the products to form important heterocycles. *Para*-*t*-butyl amide **4-27** was first allylated using allylbromide to afford diene **4-44** in 70% yield. Diene **4-44** was then subjected to ring-closing metathesis conditions to provide the resulting dihydropyrrole **4-45** in 61% yield. Likewise, I was able to isolate sulfamide product **4-46** in 9% unoptimized yield from the parent olefin. Cyclization of olefin **4-46** under basic conditions resulted in the corresponding 2-vinylpyrrolidine (**4-47**) in 96% yield. These results suggest that the utility of this allylic C–H sulfamidation protocol is not limited to the formation of allylic amines, but also the products resulting from further diversification.

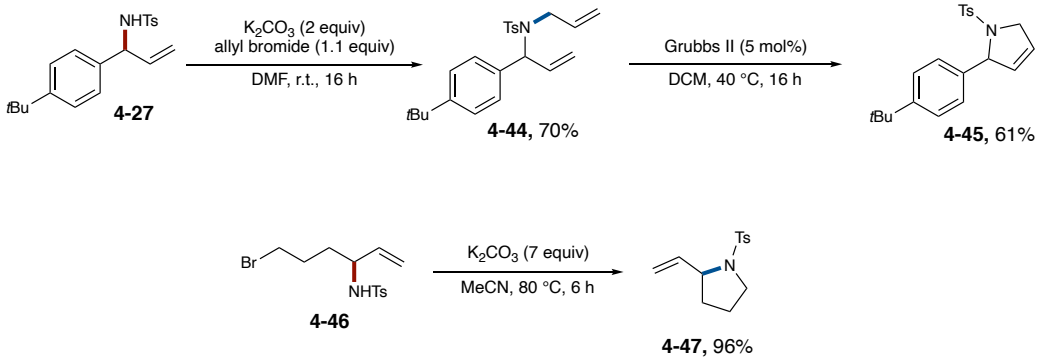

Figure 4-9. Diversification of Sulfamide Products

III. Conclusion

In conclusion, we have developed a branched selective allylic C–H sulfamidation procedure which proceeds via an Ir(V) nitrenoid intermediate. Optimized conditions were tolerant of a wide variety of allylbenzene derivatives. We also demonstrated that non-allylbenzene terminal olefins and 1,2-disubstituted olefins provided product in good yield. In hopes to develop regiodivergent methods based on reagent choice, we further optimized the linear-selective system previously disclosed by our group. Unfortunately, when the optimized conditions were tested on a variety of allylbenzene derivatives very low yields were observed suggesting these conditions were specific for the neutral olefin. We then proceeded to take the sulfamide products of the branched-selective reaction forward to form heterocycles showing the utility of this reaction. While a complete mechanistic investigation has not been performed, the C–N bond formation is likely due to direct reductive elimination from the Ir-metal center. Portions of this study were presented in an invited communication in the Journal of Organic Chemistry.[15] Following this investigation, an enantioselective allylic amidation protocol using a metal indene precatalyst and dioxazolone reagents was reported by our group.[16] Furthermore, a regioselective allylic C–H amination using oxidizing coupling reagents was reported by Rovis relying on minor electronic effects for regioselectivity.[17]

IV. Experimental Procedures:

IV.1. General Information

All reactions were carried out under nitrogen atmospheres with anhydrous solvents in oven- or flame-dried glassware using standard Schlenk technique, unless otherwise stated. Anhydrous dichloromethane (DCM), diethyl ether (Et_2O), tetrahydrofuran (THF), and

toluene were obtained by passage through activated alumina using a *Glass Contours* solvent purification system. 1,2-dichloroethane (DCE), 2,2,2-trifluoroethanol (TFE), and 1,1,1,3,3,3-hexafluoroisopropanol (HFIP) were distilled over CaH_2 and stored over activated molecular sieves. Solvents for workup, extraction, and column chromatography were used as received from commercial suppliers without further purification. $Pd(PPh_3)_4$, LiCl, $AgSbF_6$, $AgBF_4$, AgOTs, $AgNTf_2$, CsOAc, $[Cp^*IrCl_2]_2$, and $[Cp^*RhCl_2]_2$ were stored and weighed in a nitrogen-filled glovebox. Tosyl azide (TsN_3),[18] $[Cp^*IrCl_2]_2$, and $[Cp^*RhCl_2]_2$[19] were synthesized according to previously reported methods. All other chemicals were purchased from Sigma-Aldrich, Strem Chemicals, Oakwood Chemicals, Alfa Aesar, or Combi-Blocks, and used as received without further purification. ^1H and ^{13}C nuclear magnetic resonance (NMR) spectra were recorded on a Varian Inova 600 spectrometer (600 MHz ^1H, 151 MHz ^{13}C), a Bruker 600 spectrometer (600 MHz ^1H, 151 MHz ^{13}C), a Varian Inova 500 spectrometer (500 MHz ^1H, 126 MHz ^{13}C), and a Varian Inova 400 spectrometer (400 MHz ^1H, 100 MHz ^{13}C) at room temperature in $CDCl_3$ (neutralized and dried over anhydrous K_2CO_3) with internal $CHCl_3$ as the reference (7.26 ppm for ^1H, 77.16 ppm for ^{13}C), unless otherwise stated. Chemical shifts (δ values) were reported in parts per million (ppm) and coupling constants (*J* values) in Hz. Multiplicity was indicated using the following abbreviations: s = singlet, d = doublet, t = triplet, q = quartet, qn = quintet, m = mutiplet, br = broad. Infrared (IR) spectra were recorded using a Thermo Electron Corporation Nicolet 380 FT-IR spectrometer. High resolution mass spectra (HRMS) were obtained using a Thermo Electron Corporation Finigan LTQFTMS (at the Mass Spectrometry Facility, Emory University). Analytical thin layer chromatography (TLC) was performed on precoated glass backed Silicycle SiliaPure® 0.25 mm silica gel 60 plates and visualized with UV light, ethanolic *p*-anisaldehyde, or

aqueous potassium permanganate ($KMnO_4$). Flash column chromatography was performed using Silicycle SiliaFlash® F60 silica gel (40-63 μm) on a Biotage Isolera One system. Preparatory TLC was performed on precoated glass backed Silicycle SiliaPure® 1.0 mm silica gel 60 plates. We acknowledge the use of shared instrumentation provided by grants from the NIH and the NSF.

IV.2. Preparation of Olefin Coupling Partners

4-7, *para*-OMe-allylbenzene, *para*-F-allylbenzene, *para*-CF_3-allylbenzene, safrole, *ortho*-allyltoluene, 4-phenyl-1-butene, and 1-hexene were purchased from commercial sources and used as received without further purification. *para*-tert-butyl-allylbenzene,[9] *para*-MeO_2C-allylbenzene,[20] 1,3-diphenyl-1-propene,[21] and estrone-derived allylbenzene[22] were prepared according to previously reported procedures, $Pd(PPh_3)_4$ was used as the palladium precatalyst in all cases.

Phenylalanine-derived allylbenzene (4-S1):

In a nitrogen-filled glovebox, $Pd(PPh_3)_4$ (0.0553 g, 0.048 mmol, 0.031 equiv) and LiCl (0.3022 g, 7.13 mmol, 4.75 equiv) were added to an oven dried 15 mL vial equipped with a magnetic stir-bar and teflon-septum screw cap. The vial was capped and brought out of the glovebox. A solution of *N*-Cbz-(*p*-OTf)-Phe-OMe (0.7003 g, 1.50 mmol, 1 equiv) in DMF (6.30 mL) was added, followed by neat allyltributylstannane (0.600 mL, 1.67 mmol, 1.1 equiv). The vial was placed in an aluminum heating block pre-heated to 100 °C and stirred for 12.5 hours. The reaction was removed from heat, allowed to cool to room temperature, and quenched

with aqueous NH_4OH (1N, 7.0 mL). The layers were separated, and the aqueous layer was extracted with EtOAc (3 x 10.0 mL). The combined organic extracts were washed with brine (2 x 15.0 mL), dried over anhydrous Na_2SO_4, filtered, and concentrated under reduced pressure. Purification by flash chromatography on silica gel (0-100% EtOAc in Hexanes) provided **4-S1** (0.297 g, 55% yield).

^{1}H NMR ($CDCl_3$, 600 MHz) δ 7.43 – 7.31 (m, 5H), 7.14 – 7.08 (m, 2H), 7.06 – 7.00 (m, 2H), 5.95 (ddt, *J* = 17.5, 9.5, 6.7 Hz 1H), 5.21 (d, *J* = 8.3 Hz, 1H) 5.15 – 4.92 (m, 4H), 4.66 (dt, *J* = 8.3, 5.8 Hz, 1H), 3.73 (s, 3H), 3.36 (dd, *J* = 6.8, 1.6 Hz, 2H), 3.10 (dd, *J* = 14.9, 5.8 Hz, 2H) ppm; **^{13}CNMR** ($CDCl_3$, 151 MHz) 172.1, 155.7, 139.0, 137.4, 136.4, 133.4, 129.4, 129.0, 128.6, 128.6, 128.30, 128.2, 116.0, 67.1, 54.9, 52.4, 39.9, 37.9 ppm

HRMS (+ NSI) calculated for $C_{21}H_{24}O_4N$ $[M+H]^+$ 354.1705, found 354.1706.

IV.3. General Procedure for Linear-Selective Reaction Optimization

To an oven-dried 4 mL vial in an N_2 atmosphere glovebox was added p-toluenesulfonamide (0.325 mmol, 2.5 equiv), AgOAc (0.273 mmol, 2.1 equiv), halide scavenger (2.02 mmol, 8 mol %), and $[RhCp^*Cl_2]_2$ (1.61 mmol, 2 mol%) and a stir bar. The reaction vial was teflon-septum screw capped and removed from the glovebox. Then 0.65 mL of anhydrous solvent was added to the vial via syringe, followed by nonane (0.065 mmol, 0.5 equiv) and allylbenzene (0.13 mmol, 1 equiv) via microliter syringes. The vial was then heated to temperature and stirred for 24 hours. At 24 hours the reaction was allowed to cool and a 50 μL sample was taken via syringe and needle and filtered with DCM as the eluent through celite into a 2 mL GC vial. Each sample was injected and analyzed via a gas-

chromatography flame-ionization detector. The concentration was calculated using nonane as an internal standard and compared to the 0.2 M theoretical yield.

IV.4. General Procedure A: Optimization of Allylic C–H Sulfamidation Reaction

In a nitrogen-filled glovebox, CsOAc (0.0009 g, 0.005 mmol, 0.05 equiv), the Ag halide scavenger (0.010-0.040 mmol, 0.10-0.40 equiv, as indicated), and $[Cp^*MCl_2]_2$ (0.0025 mmol, 0.025 equiv) were added to an oven-dried 4 mL vial equipped with a magnetic stir-bar and a teflon-septum screw cap. After the vial was capped it was brought out of the glovebox. The indicated solvent (0.50 mL), allylbenzene (**4-7**) (0.013 mL, 0.10 mmol, 1 equiv, with a microsyringe), and TsN_3 (0.030 mL, 0.20 mmol, 2 equiv., with a microsyringe) were added. The vial was sealed with teflon tape and parafilm and placed in an aluminum heating block pre-heated to 80 °C and stirred for 24 hours. The vial was removed from heat and allowed to cool to room temperature. The reaction was filtered through a pipette containing celite with EtOAc (10 mL) and the filtrate was concentrated under reduced pressure. Purification by flash chromatography on silica gel (10-30% EtOAc in Hexanes) provided branched tosylamide **4-13** and linear tosylamide **4-14**. Spectral data matches those previously reported in the literature.[3, 23]

4-methyl-N-(1-phenylallyl)benzenesulfonamide (4-13):

^{1}H NMR ($CDCl_3$, 500 MHz) δ 7.63 (d, *J* = 8.3 Hz, 2H), 7.24 – 7.18 (m, 5H), 7.12 – 7.07 (m, 2H), 5.86 (ddd, *J* = 16.9, 10.5, 5.7 Hz, 1H), 5.16 – 5.08 (m, 2H), 4.97 – 4.86 (m, 2H), 2.39 (s, 1H) ppm.

N-cinnamyl-4-methylbenzenesulfonamide (4-14):

^{1}H NMR ($CDCl_3$, 400 MHz) δ 7.78 (d, *J* = 8.3 Hz, 2H), 7.42 – 7.10 (m, 7H), 6.44 (d, *J* = 15.9 Hz, 1H), 6.02 (dt, *J* = 15.8, 6.4 Hz, 1H), 4.46 (t, *J* = 6.2 Hz, 1H), 3.76 (td, *J* = 6.3, 1.5 Hz, 2H), 2.42 (s, 3H) ppm.

IV.5. General procedure B: Allylic C–H Sulfamidation of Allylbenzene Derivatives

In a nitrogen-filled glovebox, CsOAc (0.0019 g, 0.010 mmol, 0.05 equiv.), the $AgNTf_2$ (0.0078 g, 0.020 mmol, 0.10 equiv., as indicated), and $[Cp^*IrCl_2]_2$ (0.0040 g, 0.005 mmol, 0.025 equiv.) were added to an oven-dried 7 mL side-arm pressure tube equipped with a magnetic stir-bar and a screw cap. The tube was sealed and brought out of the glovebox. The tube was un-sealed via and HFIP (0.5 mL) and TsN_3 (0.40 mmol, 2 equiv) were added through the side-arm of the tube. For allylbenzene derivatives with known densities, a microsyringe was used for addition through the side-arm of the pressure tube (0.20 mmol, 1 equiv), followed by HFIP (0.5 mL) to wash the sides of the tube. All other allylbenzene derivatives (0.20 mmol, 1 equiv) were added as stock solutions in HFIP (0.5 mL). The tube was sealed and placed in an aluminum heating block pre-heated to 80 °C, and stirred for 24-48 hours, as indicated. The tube was removed from heat and allowed to cool to room temperature. The tube was opened to the side-arm and the septum was carefully removed to release pressure. The reaction was filtered through a pipette containing celite with EtOAc (15 mL) and the filtrate was concentrated under reduced pressure. Purification by flash chromatography on silica gel (10-30% EtOAc in Hexanes) providing the tosylamide products.

IV.6. General Procedure C: Linear Selective Amination of Allylbenzene Derivatives

To an oven-dried 7 mL vial in an N_2 atmosphere glovebox was added p-toluenesulfonamide (0.625 mmol 2.5 equiv), AgOAc (0.525 mmol, 2.1 equiv), $AgBF_4$ (0.02 mmol, 8 mol %), and $[RhCp^*Cl_2]_2$ (0.005 mmol, 2 mol%). After the solids were weighed, the reaction vial was capped with a Teflon septa cap and removed from the glovebox. 1.25 mL of anhydrous p-dioxane were added to the vial via syringe and needle, followed by the olefin (0.13 mmol, 1 eq) via microliter syringe. The vial was then heated to the temperature indicated and stirred for 24 hours. At 24 hours, the reaction was allowed to cool to room temperature and was filtered through a pipette containing celite with ethyl acetate as the eluent, then purified by flash column chromatography on silica gel as indicated to afford the corresponding sulfamide product.

IV.7. Characterization of Allylic C–H Sulfamidation Products

***N*-cinnamyl-4-methylbenzenesulfonamide (4-14):**

Following General Procedure C, NH_2Ts (43.4 mg, 0.25mmol, 2.5 equiv), AgOAc (35.6 mg, 0.21 mmol, 2.1 equiv), $AgBF_4$ (4.9 mg, 0.025 mmol, 25 mol%), $[RhCp^*Cl_2]_2$ (1.5 mg, 0.0024 mmol, 2.5 mol%), and allylbenzene (13 μL, 0.10 mmol, 1.0 equiv) were used for 22 h at 100 °C in 0.5 mL p-dioxane. Purification by flash column chromatography on silica gel (0% to 100% EtOAc/Hexanes) afforded amine **4-14** in 66% yield (19.2 mg, 0.066 mmol).

(*E*)-*N*-(3-(4-fluorophenyl)allyl)-4-methylbenzenesulfonamide (4-17):

Following General Procedure C, NH_2Ts (107.2 mg, 0.625 mmol, 2.5 equiv), AgOAc (87.7 mg, 0.525 mmol, 2.1 equiv), $AgBF_4$ (3.9 mg, 0.02 mmol, 8 mol%), $[RhCp^*Cl_2]_2$ (3.1 mg, 0.005 mmol, 2 mol%), and para-F-allylbenzene (33.7 μL, 0.25 mmol, 1.0 equiv) were used for 27 h at 100 °C in 1.25 mL p-dioxane. Purification by flash column chromatography on silica gel (0% to 100% EtOAc/Hexanes) afforded amine **4-17** in 68% yield (36.5 mg, 0.1195 mmol). Spectral data matches those previously reported in the literature.[23] This reaction was performed by Kim Sharp.

(*E*)-*N*-(3-(4-bromophenyl)allyl)-4-methylbenzenesulfonamide (4-18):

Following General Procedure C, NH_2Ts (114.2 mg, 0.667 mmol, 2.7 equiv), AgOAc (97.3 mg, 0.583 mmol, 2.3 equiv), $AgBF_4$ (5.1 mg, 0.026 mmol, 10 mol%), $[RhCp^*Cl_2]_2$ (4.3 mg, 0.007 mmol, 2.8 mol%), and para-Br-allylbenzene (39 mg, 0.25 mmol, 1.0 equiv) were used for 25 h at 100 °C in 1.25 mL p-dioxane. Purification by flash column chromatography on silica gel (0% to 100% EtOAc/Hexanes) afforded amine **4-18** in 7% yield (6.7 mg, 0.018 mmol). Spectral data matches those previously reported in the literature.[24]

(E)-4-methyl-N-(3-(4-(trifluoromethyl)phenyl)allyl)benzenesulfonamide (4-19):

Following General Procedure C, NH_2Ts (107.2 mg, 0.625 mmol, 2.5 equiv), AgOAc (87.8 mg, 0.525 mmol, 2.1 equiv), $AgBF_4$ (4.0 mg, 0.02 mmol, 8 mol%), $[RhCp^*Cl_2]_2$ (3.1 mg, 0.005 mmol, 2 mol%), and para-CF_3-allylbenzene (41.9 μL, 0.25 mmol, 1.0 equiv) were used for 26 h at 100 °C in 1.25 mL p-dioxane. Purification by flash column chromatography on silica gel (0% to 80% EtOAc/Hexanes) afforded amine **4-19** in 11% yield (9.6 mg, 0.032 mmol).

Spectral data matches those previously reported in the literature.[25] This reaction was performed by Kim Sharp.

(E)-N-(3-(4-(tert-butyl)phenyl)allyl)-4-methylbenzenesulfonamide (4-20):

Following General Procedure C, NH_2Ts (107.1 mg, 0.625 mmol, 2.5 equiv), AgOAc (87.7 mg, 0.525 mmol, 2.1 equiv), $AgBF_4$ (4.1 mg, 0.02 mmol, 8 mol%), $[RhCp^*Cl_2]_2$ (3.1 mg, 0.005 mmol, 2 mol%), and para-t-Butyl-allylbenzene (50.1 µL, 0.25 mmol, 1.0 equiv) were used for 26 h at 100 °C in 1.25 mL p-dioxane. Purification by flash column chromatography on silica gel (0% to 40% Et_2O/Hexanes) afforded amine **4-20** in 32% yield (27.4 mg, 0.079 mmol). Spectral data matches those previously reported in the literature. [18] This reaction was performed by Kim Sharp.

(E)-N-(3-(4-methoxyphenyl)allyl)-4-methylbenzenesulfonamide (4-21):

Following General Procedure C, NH_2Ts (107.2 mg, 0.625 mmol, 2.5 equiv), AgOAc (87.8 mg, 0.525 mmol, 2.1 equiv), $AgBF_4$ (4.0 mg, 0.02 mmol, 8 mol%), $[RhCp^*Cl_2]_2$ (3.1 mg, 0.005 mmol, 2 mol%), and para-OMe-allylbenzene (38.4 µL, 0.25 mmol, 1.0 equiv) were used for 26 h at 100 °C in 1.25 mL p-dioxane. Purification by flash column chromatography on silica gel (0% to 75% Et_2O/Hexanes) afforded amine **4-21** in trace yield. Spectral data matches those previously reported in the literature. [23] This reaction was performed by Kim Sharp.

(E)-4-methyl-N-(3-(o-tolyl)allyl)benzenesulfonamide (4-22):

Following General Procedure C, NH_2Ts (133.3mg, 0.777 mmol, 3.1 equiv), AgOAc (93.7 mg, 0.56 mmol, 2.2 equiv), $AgBF_4$ (6.6 mg, 0.034 mmol, 14 mol%), $[RhCp^*Cl_2]_2$ (7.4 mg, 0.012 mmol, 4.8 mol%), and o-tolylallylbenzene (37.0 μL, 0.25 mmol, 1.0 equiv) were used for 24 h at 100 °C in 1.25 mL p-dioxane. Purification by flash column chromatography on silica gel (0% to 80% EtOAc/Hexanes) afforded amine **4-22** in 20% yield (14.8 mg, 0.049 mmol). Spectral data matches those previously reported in the literature. [26]

(*E*)-*N*-(3-(benzo[*d*][1,3]dioxol-5-yl)allyl)-4-methylbenzenesulfonamide (4-23):

Following General Procedure C, NH_2Ts (116.7 mg, 0.68 mmol, 2.7 equiv), AgOAc (90.2 mg, 0.54 mmol, 2.2 equiv), $AgBF_4$ (6.0 mg, 0.031 mmol, 12 mol%), $[RhCp^*Cl_2]_2$ (5.6 mg, 0.009 mmol, 3.6 mol%), and safrole (37 μL, 0.25 mmol, 1.0 equiv) were used for 24 h at 100 °C in 1.25 mL p-dioxane. Purification by preparatory thin layer chromatography (50% petroleum ether: ether) afforded amine **4-23** in 18% yield (14.8 mg, 0.045 mmol).

^{1}H NMR (400 MHz, $CDCl_3$): δ 7.75 (d, *J* = 8.3 Hz, 2H), 7.30 (d, *J* = 8.7 Hz, 2H), 6.92 – 6.54 (m, 3H), 6.33 (d, *J* = 15.8 Hz, 1H), 5.93 (s, 2H), 5.81 (dt, *J* = 15.8, 6.5 Hz, 1H), 4.38 (t, *J* = 6.5 Hz, 1H), 3.71 (td, *J* = 6.3, 1.4 Hz, 2H), 2.42 (s, 3H).

^{13}C NMR (126 MHz, $CDCl_3$) δ 148.16, 143.74, 137.24, 133.01, 130.62, 129.92, 127.36, 122.31, 121.40, 108.41, 105.75, 101.29, 45.67, 21.67.

(*E*)-4-methyl-*N*-(4-phenylbut-2-en-1-yl)benzenesulfonamide (4-24):

Following General Procedure C, NH_2Ts (107.1 mg, 0.625 mmol, 2.5 equiv), AgOAc (87.7 mg, 0.525 mmol, 2.1 equiv), $AgBF_4$ (4.0 mg, 0.02 mmol, 8 mol%), $[RhCp^*Cl_2]_2$ (3.1 mg, 0.005

mmol, 2 mol%), and 4-phenyl-1-butene (37.1 μL, 0.25 mmol, 1.0 equiv) were used for 25 h at 100 °C in 1.25 mL p-dioxane. Purification by flash column chromatography on silica gel (0% to 50% EtOAc/Hexanes) afforded amine **4-24** in 13% yield (10 mg, 0.033 mmol). Spectral data matches those previously reported in the literature. [27, 28] This reaction was performed by Kim Sharp.

N-(1-(4-methoxyphenyl)allyl)-4-methylbenzenesulfonamide (4-26):

Prepared according to General Procedure B, using 4-allylanisole (0.031 mL, 0.20 mmol, 1 equiv), TsN_3 (0.061 mL, 0.40 mmol, 1 equiv), $[Cp^*IrCl_2]_2$ (0.0040 g, 0.005 mmol, 0.0025 equiv), $AgNTf_2$ (0.0078 g, 0.02 mmol, 0.10 equiv), and CsOAc (0.0019 g, 0.01 mmol. 0.05 equiv) in HFIP (1.0 mL) at 80 °C for 24 hours. Purified by flash chromatography on silica gel (10-30% EtOAc in Hexanes) to provide **4-26** (0.0365 g, 57% yield). Spectral data matches those previously reported in the literature.[29] This reaction was performed by Steven Chen.

^{1}H NMR ($CDCl_3$, 500 MHz) δ 7.63 (d, *J* = 8.5 Hz, 2H), 7.20 (d, *J* = 8.6 Hz, 2H), 7.01 (d, *J* = 8.7 Hz, 2H), 6.74 (d, *J* = 8.9 Hz, 2H), 5.85 (ddd, *J* = 17.2, 10.1, 5.7 Hz, 1H), 5.14 – 5.08 (m, 2H), 4.95 (d, *J* = 7.5 Hz, 1H), 4.90 – 4.85 (m, 1H), 3.75 (s, 3H), 2.39 (s, 3H) ppm.

N-(1-(4-(tert-butyl)phenyl)allyl)-4-methylbenzenesulfonamide (4-27): Prepared according to General Procedure B, using 1-allyl-4-(*tert*-butyl)benzene (0.0350 g, 0.20 mmol, 1 equiv), TsN_3 (0.061 mL, 0.40 mmol, 1 equiv), $[Cp^*IrCl_2]_2$ (0.0040 g, 0.005 mmol, 0.0025 equiv), $AgNTf_2$ (0.0078 g, 0.02 mmol, 0.10 equiv), and CsOAc (0.0019 g, 0.01 mmol. 0.05 equiv) in HFIP (1.0 mL) at 80 °C for 24 hours. Purified by flash chromatography on silica gel

(10-30% EtOAc in Hexanes) to provide **4-27** (0.0422 g, 61% yield). This reaction was performed by Amaan Kazerouni.

^{1}H NMR ($CDCl_3$, 600 MHz) δ 7.61 (d, *J* = 8.3 Hz, 2H), 7.21 (d, *J* = 8.4 Hz, 2H), 7.16 (d, *J* = 7.8 Hz, 2H), 7.01 (d, *J* = 8.1 Hz, 2H), 5.87 (ddd, *J* = 17.1, 10.3, 5.9 Hz, 1H), 5.20 – 5.05 (m, 2H), 5.01 (d, *J* = 7.3 Hz, 1H), 4.95 – 4.91 (m, 1H), 2.37 (s, 3H), 1.27 (s, 9H) ppm

^{13}C NMR ($CDCl_3$, 151 MHz) δ 150.8, 143.1, 137.9, 137.4, 136.4, 129.4, 127.4, 126.9, 125.6, 116.7, 59.8, 34.6, 31.4, 21.6 ppm

HRMS (+ APCI) calculated for $C_{20}H_{29}N_2O_2S$ $[M+NH_4]^+$ 361.1950, found 361.1940.

Methyl-4-(1-((4-methylphenyl)sulfonamido)allyl)benzoate (4-28):

Prepared according to General Procedure B, using 4-methylallylbenzoate (0.0350 g, 0.20 mmol, 1 equiv), TsN_3 (0.061 mL, 0.40 mmol, 1 equiv), $[Cp^*IrCl_2]_2$ (0.0040 g, 0.005 mmol, 0.0025 equiv), $AgNTf_2$ (0.0078 g, 0.02 mmol, 0.10 equiv), and CsOAc (0.0019 g, 0.01 mmol. 0.05 equiv) in HFIP (1.0 mL) at 80 °C for 24 hours. Purified by flash chromatography on silica gel (10-30% EtOAc in Hexanes) to provide **4-28** (0.0361 g, 52% yield). This reaction was performed by Amaan Kazerouni.

^{1}H NMR ($CDCl_3$, 600 MHz) δ 7.85 (d, *J* = 8.3 Hz, 2H), 7.61 (d, *J* = 8.3 Hz, 2H), 7.18 (d, *J* = 8.3 Hz, 2H), 7.16 (d, *J* = 8.0 Hz, 2H), 5.83 (ddd, *J* = 16.7, 10.3, 6.0 Hz, 1H), 5.37 (d, *J* = 7.7 Hz, 1H), 5.16 – 5.03 (m, 2H), 5.01 – 4.95 (m, 1H), 3.89 (s, 3H), 2.37 (s, 3H) ppm

^{13}C NMR ($CDCl_3$, 151 MHz) δ 166.8, 144.5, 143.6, 137.6, 136.5, 130.0, 129.8, 129.6, 127.3, 126.5, 117.7, 59.7, 52.3, 21.6 ppm

HRMS (+ APCI) calculated for $C_{18}H_{23}N_2O_4S$ $[M+NH_4]^+$ 363.1379, found 363.1376.

N-(1-(4-fluorophenyl)allyl)-4-methylbenzenesulfonamide (4-29):

Prepared according to General Procedure B, using 1-allyl-4-fluorobenzene (0.027 mL, 0.20 mmol, 1 equiv), TsN_3 (0.061 mL, 0.40 mmol, 1 equiv), $[Cp^*IrCl_2]_2$ (0.0040 g, 0.005 mmol, 0.0025 equiv), $AgNTf_2$ (0.0078 g, 0.02 mmol, 0.10 equiv), and CsOAc (0.0019 g, 0.01 mmol. 0.05 equiv) in HFIP (1.0 mL) at 80 °C for 24 hours. Purified by flash chromatography on silica gel (10-30% EtOAc in Hexanes) to provide **4-29** (0.0422 g, 67% yield). This reaction was performed by Steven Chen.

^{1}H NMR ($CDCl_3$, 600 MHz) δ 7.61 (d, *J* = 8.3 Hz, 2H), 7.19 (dd, *J* = 8.6, 0.8 Hz, 2H), 7.11 – 7.05 (m, 2H), 6.89 (t, *J* = 8.7 Hz, 2H), 5.83 (ddd, *J* = 17.0, 10.3, 5.8 Hz, 1H), 5.13 (d, *J* = 10.3 Hz, 1H), 5.10 – 5.06 (m, 2H), 4.96 – 4.90 (m, 1H), 2.39 (s, 3H) ppm

^{13}C NMR ($CDCl_3$, 151 MHz) δ 162.2 (d, $J_{C=F}$ = 246.3 Hz), 143.5, 137.6, 136.9, 135.3 (d, $J_{C=F}$ = 3.2 Hz), 129.5, 129.0 (d, $J_{C=F}$ = 8.2 Hz), 127.3, 117.1, 115.5 (d, $J_{C=F}$ = 21.5 Hz), 59.3, 21.6 ppm

HRMS (+ APCI) calculated for $C_{16}H_{17}FNO_2S$ $[M+H]^+$ 306.0964, found 306.0954.

4-methyl-N-(1-(4-(trifluoromethyl)phenyl)allyl)benzenesulfonamide (4-30):

Prepared according to General Procedure B, using 4-allyltriflourotoluene (0.033 mL, 0.20 mmol, 1 equiv), TsN_3 (0.061 mL, 0.40 mmol, 1 equiv), $[Cp^*IrCl_2]_2$ (0.0040 g, 0.005 mmol, 0.0025 equiv), $AgNTf_2$ (0.0078 g, 0.02 mmol, 0.10 equiv), and CsOAc (0.0019 g, 0.01 mmol. 0.05 equiv) in HFIP (1.0 mL) at 80 °C for 24 hours. Purified by flash chromatography on silica gel (10-30% EtOAc in Hexanes) to provide **4-30** (0.033 g, 46% yield). Spectral data matches those previously reported in the literature.[9] This reaction was performed by Steven Chen.

^{1}H NMR ($CDCl_3$, 500 MHz) δ 7.56 (d, *J* = 8.3 Hz, 2H), 7.41 (d, *J* = 8.4 Hz, 2H), 7.21 (d, *J* = 8.5 Hz, 2H), 7.13 (d, *J* = 8.0 Hz, 2H), 5.84 (ddd, *J* = 16.3, 10.3, 5.9 Hz, 1H), 5.37 (d, *J* = 7.4 Hz, 1H), 5.16 (d, *J* = 10.3 Hz, 1H), 5.11 – 4.97 (m, 2H), 2.36 (s, 3H) ppm

^{13}C NMR ($CDCl_3$, 126 MHz) δ 143.7, 143.27, 143.25, 137.4, 136.4, 130.1 (q, J_{C-F} = 32.5 Hz), 129.6, 129.5, 127.7, 127.3, 125.5 (q, J_{C-F} = 3.8 Hz), 117.9, 59.6, 21.5 ppm

HRMS (+ APCI) calculated for $C_{17}H_{20}F_3N_2O_2S$ $[M+NH_4]^+$ 373.1198, found 373.1192.

N-(1-(benzo[d][1,3]dioxol-5-yl)allyl)-4-methylbenzenesulfonamide (4-31):

Prepared according to General Procedure B, using safrole (0.029 mL, 0.20 mmol, 1 equiv), TsN_3 (0.061 mL, 0.40 mmol, 1 equiv), $[Cp^*IrCl_2]_2$ (0.0040 g, 0.005 mmol, 0.0025 equiv), $AgNTf_2$ (0.0078 g, 0.02 mmol, 0.10 equiv), and CsOAc (0.0019 g, 0.01 mmol. 0.05 equiv) in HFIP (1.0 mL) at 80 °C for 48 hours. Purified by flash chromatography on silica gel (10-30% EtOAc in Hexanes) to provide **4-31** (0.0311 g, 47% yield).

^{1}H NMR ($CDCl_3$, 500 MHz) δ 7.63 (d, *J* = 8.3 Hz, 2H), 7.21 (d, *J* = 8.5 Hz 1H), 6.64 (d, *J* = 8.0 Hz, 1H), 6.57 (dd, *J* = 8.0, 1.8 Hz, 1H), 6.53 (d, *J* = 1.8 Hz, 1H), 5.90 (d, *J* = 1.5 Hz, 1H), 5.89 (d, *J* = 1.4 Hz, 1H), 5.82 (ddd, *J* = 17.2, 10.1, 5.4 Hz, 1H), 5.16 – 5.08 (m, 2H), 4.88 – 4.81 (m, 2H), 2.40 (s, 3H) ppm

^{13}C NMR ($CDCl_3$, 151 MHz) δ 147.9, 147.3, 143.4, 137.8, 137.2, 133.4, 129.5, 127.4, 120.8, 116.9, 108.3, 107.7, 101.26, 77.2, 59.8, 21.6 ppm

HRMS (+ APCI) calculated for $C_{17}H_{18}NO_4S$ $[M+H]^+$ 332.0957, found 332.0943.

4-methyl-N-(1-(o-tolyl)allyl)benzenesulfonamide (4-32):

Prepared according to General Procedure B using 1-allyl-2-methylbenzene (0.029 mL, 0.20 mmol, 1 equiv), TsN_3 (0.061 mL, 0.40 mmol, 1 equiv), $[Cp^*IrCl_2]_2$ (0.0040 g, 0.005 mmol, 0.0025 equiv), $AgNTf_2$ (0.0078 g, 0.02 mmol, 0.10 equiv), and CsOAc (0.0019 g, 0.01 mmol. 0.05 equiv) in HFIP (1.0 mL) at 80 °C for 48 hours. Purified by flash chromatography on silica gel (10-30% EtOAc in Hexanes) to provide **4-32** (0.0359 g, 60% yield). This reaction was performed by Amaan Kazerouni.

^{1}H NMR ($CDCl_3$, 600 MHz) δ 7.60 (d, *J* = 8.2 Hz, 2H), 7.16 (d, *J* = 8.4 Hz, 2H), 7.07 – 7.01 (m, 3H), 5.85 (ddd, *J* = 17.1, 10.3, 5.5 Hz, 1H), 5.21-5.15 (m, 1H), 5.10 (dd, *J* = 10.3, 1.3 Hz, 1H), 5.06 – 4.96 (m, 1H), 4.85 (d, *J* = 7.2 Hz, 1H), 2.37 (s, 3H), 2.21 (s, 3H) ppm

^{13}C NMR ($CDCl_3$, 126 MHz) δ 143.3, 137.8, 137.4, 137.1, 135.6, 130.8, 129.5, 127.8, 127.2, 126.9, 126.4, 116.9, 56.5, 21.6, 19.3 ppm

HRMS (+ APCI) calculated for $C_{17}H_{20}NO_2S$ $[M+H]^+$ 302.1215, found 302.1204.

4-methyl-N-(1-phenylbut-3-en-2-yl)benzenesulfonamide (4-33):

Prepared according to General Procedure B, using 4-phenylbutene (0.030 mL, 0.20 mmol, 1 equiv), TsN_3 (0.061 mL, 0.40 mmol, 1 equiv), $[Cp^*IrCl_2]_2$ (0.0040 g, 0.005 mmol, 0.0025 equiv), $AgNTf_2$ (0.0078 g, 0.02 mmol, 0.10 equiv), and CsOAc (0.0019 g, 0.01 mmol. 0.05 equiv) in HFIP (1.0 mL) at 80 °C for 48 hours. Purified by flash chromatography on silica gel (10-40% EtOAc in Hexanes) to provide **4-33** (0.045 g, 75% yield). Spectral data matches those previously reported in the literature.[30] This reaction was performed by Amaan Kazerouni.

^{1}H NMR ($CDCl_3$, 400 MHz): δ 7.60 (d, *J* = 8.3 Hz, 2H), 7.27 – 7.16 (m, 5H), 7.05 – 7.00 (m. 2H), 5.68 (ddd, *J* = 16.8, 10.4, 6.1 Hz, 1H), 5.10 – 4.96 (m, 2H), 4.49 (d, *J* = 7.3 Hz, 1H), 4.07 – 3.95 (m, 1H), 3.08 – 2.61 (m, 2H), 2.41 (3H, s) ppm.

N-(hex-1-en-3-yl)-4-methylbenzenesulfonamide (4-34):

Prepared following General Procedure B using 1-hexene (0.025 mL, 0.20 mmol, 1 equiv). Purified by flash chromatography on silica gel (0-100% Et_2O in Hexanes) to provide **4-34** (0.025 g, 49% yield) as an inseparable mixture of regioisomers (4.5:1.5:1 r.r.). Spectral data matches those previously reported in the literature.[31, 32]

^{1}H NMR ($CDCl_3$, 399 MHz) δ 7.73 (m, 28H), 7.28 (m, 28H), 5.53 (ddd, J = 17.0, 10.3, 6.6 Hz, 9H), 5.45 (dt, J = 15.4, 6.3 Hz, 2H), 5.41 – 5.28 (m, 3H), 5.14 (dd, J = 15.4, 6.6 Hz, 2H), 5.05 (ddd, J = 15.3, 7.4, 1.7 Hz, 3H), 5.00 – 4.93 (m, 18 H), 4.58 (d, J = 7.9 Hz, 9H), 4.50 (d, J = 7.6 Hz, 5H), 3.97 – 3.82 (m, 2H), 3.76 (quint, J = 6.8 Hz, 9H), 3.61 (quint, J = 7.2 Hz, 3H), 2.42 (s, 42H), 1.95 – 1.80 (m, 5H), 1.56 – 1.16 (m, 33H), 0.83 (t, J = 7.3 Hz, 42H) ppm.

Benzyl (1-phenylallyl)carbamate (4-35):

Prepared according to General Procedure B using allylbenzene (0.026 mL, 0.20 mmol, 1 equiv), $CbzN_3$ (0.071 g, 0.40 mmol, 2 equiv), $[Cp^*IrCl_2]_2$ (0.0040 g, 0.005 mmol, 0.0025 equiv), $AgNTf_2$ (0.0078 g, 0.02 mmol, 0.10 equiv), and CsOAc (0.0019 g, 0.01 mmol. 0.05 equiv) in HFIP (1.0 mL) at 80 °C for 24 hours. Purified by flash chromatography on silica gel (10-30% EtOAc in Hexanes) to provide **4-35** (0.0091 g, 17% yield). Spectral data matches those previously reported in the literature.[33] This reaction was performed by Amaan Kazerouni.

^{1}H NMR ($CDCl_3$, 500 MHz) δ 7.40 – 7.27 (m, 10H), 6.01 (ddd, *J* = 16.3, 10.6, 5.3 Hz, 1H), 5.37 (br s, 1H), 5.26 (br s, 1H), 5.24 – 5.20 (m, 2H), 5.16 – 5.09 (m, 2H) ppm.

(E)-N-(1,3-diphenylallyl)-4-methylbenzenesulfonamide (4-36):

Prepared following General Procedure B using 1,3-*trans*-diphenylpropene (0.038 mL, 0.20 mmol, 1 equiv). Purified by flash chromatography on silica gel (10-30% EtOAc in Hexanes) to provide **4-36** (0.0393 g, 54% yield). Spectral data matches those previously reported in the literature.[3] This reaction was performed by Amaan Kazerouni.

^{1}H NMR ($CDCl_3$, 500 MHz) δ 7.65 (d, *J* = 8.3 Hz, 2H), 7.28 – 7.10 (m, 12H), 6.33 (dd, *J* = 15.8, 1.2 Hz, 1H), 6.07 (dd, *J* = 15.8, 6.8 Hz, 1H), 5.22 (d, *J* = 7.3 Hz, 1H), 5.11 (td, *J* = 7.1, 1.3 Hz, 1H), 2.31 (s, 3H) ppm.

Phenylalanine-derived allylbenzene tosylamide (4-37):

Prepared according to General Procedure B using Cbz-(*p*-allyl)-Phe-OMe (0.071 g, 0.20 mmol, 1 equiv), TsN_3 (0.061 mL, 0.40 mmol, 1 equiv), $[Cp^*IrCl_2]_2$ (0.0040 g, 0.005 mmol, 0.0025 equiv), $AgNTf_2$ (0.0078 g, 0.02 mmol, 0.10 equiv), and CsOAc (0.0019 g, 0.01 mmol. 0.05 equiv) in HFIP (1.0 mL) at 80 °C for 24 hours. Purified by flash chromatography on silica gel (30-50% EtOAc in Hexanes) to provide the desired product with $TsNH_2$ impurities. Additional purification by preparatory TLC (30% EtOAc in Hexanes, 2 sweeps) provided **4-37** (0.0495 g, 50% yield) as an inseparable mixture of diastereomers (1:1 d.r.). This reaction was performed by Amaan Kazerouni.

^{1}H NMR ($CDCl_3$, 600 MHz) δ 7.64 (d, *J* = 8.4 Hz, 2H), 7.63 (d, *J* = 8.3 Hz, 2H), 7.40 – 7.30 (m, 10H), 7.21 (d, *J* = 8.3 Hz, 2H), 7.21 (d, *J* = 7.9 Hz, 2H), 7.03 (d, *J* = 8.1 Hz, 4H), 6.96 (d, *J* = 8.2

Hz, 2H), 6.95 (d, *J* = 8.1 Hz, 2H), 5.82 (ddd, *J* = 16.1, 10.3, 6.0 Hz, 1H), 5.82, (ddd, *J* = 17.0, 10.3, 6.0 Hz, 1H), 5.19 – 5.05 (m, 10H), 4.90 (q, *J* = 5.7 Hz, 2H), 4.73 (d, *J* = 7.3 Hz, 1H), 4.73 (d, *J* = 7.3 Hz, 1H), 4.62 (q, *J* = 6.0 Hz, 2H), 3.72 (s, 3H), 3.71 (s, 3H), 3.09 (dd, *J* = 13.9, 5.7 Hz, 1H), 3.08 (dd, *J* = 14.0, 5.7 Hz, 1H), 3.03 (dd, *J* = 14.2, 6.2 Hz, 2H), 2.39 (s, 3H), 2.39 (s, 3H) ppm;

^{13}C NMR ($CDCl_3$, 151 MHz) δ 171.9, 155.7, 143.5, 138.5, 137.8, 137.07, 137.05, 136.3, 135.1, 129.73, 129.71, 129.6, 129.5, 128.7, 128.4, 128.3, 127.5, 127.4, 117.2, 117.1, 67.2, 59.6, 54.8, 52.5, 37.9, 37.9, 21.6 ppm

HRMS (– APCI) calculated for $C_{28}H_{29}N_2O_6S$ $[M–H]^-$ 521.1746, found 521.1748.

Estrone-derived allylbenzene tosylamide (4-38):

Prepared following General Procedure B using estrone allylbenzene (0.0503 g, 0.171mmol, 1 equiv), TsN_3 (0.0524 mL,0.342 mmol, 2 equiv), $[Cp^*IrCl_2]_2$ (0.0034 g, 0.0043 mmol, 0.0025 equiv), $AgNTf_2$ (0.0063 g, 0.0171 mmol, 0.10 equiv) and CsOAc (0.0016 g, 0.0085 mmol, 0.05 equiv) in HFIP (1.0 mL) at 80 °C for 24 hours. Purified by flash chromatography on silica gel (30-50% EtOAc in Hexanes) to provide **4-38** (0.0494 g, 62% yield) as an inseparable mixture of diastereomers (2:1 d.r.). This reaction was performed by Amaan Kazerouni.

^{1}H NMR ($CDCl_3$, 500 MHz) 7.81 (d, *J* = 8.3 Hz, 2H), 7.63 (d, *J* = 8.4, 4H), 7.30 (d, *J* = 8.3 Hz, 2H), 7.19 (d, 8.6 Hz, 4H), 7.14 (dd, *J* = 8.0, 2.9 Hz, 3H), 6.89 (ddd, *J* = 7.9, 5.6, 2.0 Hz, 3H), 6.78 (dd, *J* = 3.5, 2.0 Hz, 3H), 5.84 (ddd, *J* = 15.4, 10.3, 6.0 Hz, 1H), 5.84 (ddd, *J* = 16.3, 10.3 Hz, 6.0 Hz, 2H), 5.17 - 5.08 (m, 3H), 4.99 (d, *J* = 7.0 Hz, 3H), 4.85 (q, *J* = 5.9 Hz, 3H), 2.85 - 2.69 (m, 5H), 2.50 (dd, *J* = 19.1, 8.8 Hz, 3H), 2.42 (s, 3H), 2.40 (s, 6H), 2.40 - 2.33 (m, 3H), 2.26 - 2.19 (m, 3H), 2.14 (dt, *J* = 19.0, 8.9 Hz, 3H), 2.08 - 2.02 (m, 3H), 2.01 - 1.91 (m, 6H), 1.69 - 1.56 (m, 4H), 1.56 - 1.44 (m, 12H), 1.44 - 1.32 (m, 3H), 0.90 (s, 3H), 0.90 (s, 6H) ppm

^{13}C NMR ($CDCl_3$, 126 MHz) δ 220.8, 143.6, 143.2, 139.53, 139.51, 139.4, 137.95, 137.92, 137.27, 137.26, 137.01, 136.98, 136.90, 129.8, 129.44, 129.42, 127.80, 127.78, 127.4, 126.6, 125.8, 124.6, 124.7, 116.71, 116.68, 59.80, 59.79, 50.6, 48.1, 44.4, 38.23, 38.22, 36.0, 31.7, 29.4, 26.5, 25.83, 25.82, 21.70, 21.66, 21.65, 21.63, 14.0 ppm

HRMS (+ APCI) calculated for $C_{28}H_{34}NO_3S$ $[M+H]^+$ 464.2259, found 464.2264.

Synthesis of dihydropyrrole 4-45

N-allyl-N-(1-(4-(tert-butyl)phenyl)allyl)-4-methylbenzenesulfonamide (4-44):

Allyl bromide (0.011 mL, 0.126 mmol, 1.1 equiv) and K_2CO_3 0.0316 g, 0.229 mmol, 2 equiv) were added to a solution of *N*-(1-(4-(*tert*-butyl)phenyl)allyl)-4-methylbenzenesulfonamide (**4-27**) (0.0393 g, 0.114 mmol, 1 equiv) in DMF (0.50 mL), and the resulting mixture was stirred at room temperature. After 16 hours, the reaction was diluted with water (5.0 mL) and EtOAc (5.0 mL). The layers were separated, and the aqueous layer was extracted with EtOAc (3 x 5.0 mL). The combined organic extracts were washed with brine (2 x 15.0 mL), dried over anhydrous Na_2SO_4, filtered, and concentrated under reduced pressure. Purification by flash chromatography on silica gel (5-20% EtOAc in Hexanes) to provide **4-44** (0.0305 g, 70% yield). This reaction was performed by Amaan Kazerouni.

^{1}H NMR ($CDCl_3$, 500 MHz) δ 7.69 (d, *J* = 8.3 Hz, 2H), 7.29 (d, *J* = 8.2 Hz, 2H), 7.24 (d, *J* = 8.6 Hz, 2H), 7.14 (d, *J* = 8.9 Hz, 2H), 6.05 (ddd, *J* = 17.2, 10.3, 7.0 Hz, 1H), 5.62 (d, *J* = 7.0 Hz, 1H), 5.50 (ddt, *J* = 16.2, 10.2, 6.3 Hz, 1H), 5.26 (d, *J* = 10.3 Hz, 1H), 5.14 (d, *J* = 17.1 Hz, 1H), 4.97 – 4.84 (m, 2H), 3.83 (dd, *J* = 16.3, 6.1 Hz, 1H), 3.71 (dd, *J* = 16.2, 6.6 Hz, 1H), 2.42 (s, 3H), 1.30 (s, 9H) ppm

^{13}C NMR ($CDCl_3$, 126 MHz) δ 151.0, 143.0, 138.4, 135.5, 135.4, 135.1, 129.5, 128.2, 127.7, 125.4, 119.0, 117.2, 63.4, 48.1, 34.6, 31.5, 21.7 ppm.

HRMS (+ APCI) calculated for $C_{23}H_{30}NO_2S$ $[M+H]^+$ 384.1997, found 384.1987.

2-(4-(tert-butyl)phenyl)-1-tosyl-2,5-dihydro-1H-pyrrole (4-45):

Grubbs II (0.0034 g, 0.00398 mmol, 0.05 equiv) was added to a solution of *N*-allyl-*N*-(1-(4-(*tert*-butyl)phenyl)allyl)-4-methylbenzenesulfonamide **4-44** (0.0305 g, 0.0795 mmol, 1 equiv) in DCM (1.50 mL) and the resulting mixture was stirred in an aluminum heating block pre-heated to 40 °C. After 16 hours, the reaction was quenched with saturated aqueous $NaHCO_3$ (3.0 mL) and diluted with DCM (3.0 mL). The layers were separated, and the aqueous layer was extracted with DCM (3 x 3.0 mL). The combined organic extracts were washed with brine (8.0 mL), dried over anhydrous Na_2SO_4, filtered, and concentrated under reduced pressure. Purification by flash chromatography (10-30% EtOAc in Hexanes) provided **4-45** (0.0171 g, 61% yield). This reaction was performed by Amaan Kazerouni.

^{1}H NMR ($CDCl_3$, 600 MHz) δ 7.46 (d, *J* = 8.3 Hz, 2H), 7.27 (d, *J* = 8.4 Hz, 2H), 7.14 (d, *J* = 8.4Hz, 2H), 7.14 (d, *J* = 8.5 Hz, 2H), 5.79 (dq, *J* = 6.1, 2.0 Hz, 1H), 5.66 (dq, *J* = 6.5, 2.2 Hz, 1H), 5.51 (dq, *J* = 6.3, 2.2 Hz, 1H), 4.37 (dq, *J* = 14.5, 2.3 Hz, 1H), 4.25 (ddt, *J* = 14.5, 5.7, 2.1 Hz, 1H), 2.36 (s, 3H), 1.30 (s, 9H) ppm

^{13}C NMR ($CDCl_3$, 126 MHz) δ 150.9, 143.0, 137.3, 136.1, 130.8, 129.4, 127.3, 127.2, 125.4, 124.5, 70.0, 55.4, 34.6, 31.5, 21.6 ppm

HRMS (+ APCI) calculated for $C_{21}H_{26}NO_2S$ $[M+H]^+$ 356.1684, found 356.1670.

Synthesis of 2-vinylpyrrolidine 4-47

N-(6-bromohex-1-en-3-yl)-4-methylbenzenesulfonamide (4-46):

Prepared according to General Procedure B, using 6-bromohexene (0.025 mL, 0.20 mmol, 1 equiv), TsN3 (0.061 mL, 0.40 mmol, 1 equiv), [Cp*IrCl2]2 (0.0040 g, 0.005 mmol, 0.0025 equiv), AgNTf2 (0.0078 g, 0.02 mmol, 0.10 equiv), and CsOAc (0.0019 g, 0.01 mmol. 0.05 equiv) in HFIP (1.0 mL) at 80 °C for 40 hours. Purified by flash chromatography on silica gel (0-100% EtOAc in Hexanes) to provide **4-46** (4.5 mg, 9% yield).

^{1}H NMR ($CDCl_3$, 400 MHz) δ 7.72 (d, *J* = 8.1 Hz, 2H), 7.31 (d, *J* = 8.0 Hz, 2H), 5.81 (ddd, *J* = 16.8, 10.3, 6.0 Hz, 1H), 5.28 (d, *J* = 17.0 Hz, 1H), 5.12 (d, *J* = 10.2 Hz, 1H), 4.13 (q, *J* = 6.9, 6.3 Hz, 1H), 3.45 (ddd, *J* = 9.8, 7.2, 4.1 Hz, 1H), 3.23 (dt, *J* = 10.0, 7.5 Hz, 1H), 2.43 (s, 3H), 2.08 – 1.57 (m, 4H) ppm

^{13}C NMR ($CDCl_3$, 151 MHz) δ 143.4, 138.8, 135.4, 129.7, 127.7, 115.5, 62.1, 48.9, 32.4, 23.9, 21.7 ppm

HRMS (+ NSI) calculated for $C_{13}H_{18}NO_2S$ $[M-Br]^+$ 252.1058, found 252.1050.

1-tosyl-2-vinylpyrrolidine (4-47):

K_2CO_3 (0.0123 g, 0.0890 mmol, 7 equiv) was added to a solution of tosylamide **4-46** (0.0044 g, 0.013 mmol, 1 equiv) in CH_3CN (0.40 mL). The vial was placed in a sand bath pre-heated to 80 °C and stirred for 6 hours. The vial was removed heat and allowed to cool to room temperature. The reaction was filtered through a celite plug with EtOAc (10.0 mL) and the filtrate was concentrated under reduced pressure to provide **4-47** (0.0032 g, 96% yield). Spectral data matches those previously reported in the literature.[34]

^{1}H NMR ($CDCl_3$, 400 MHz) δ 7.73 (d, *J* = 8.0 Hz, 2H), 7.34 – 7.29 (m, 2H), 5.81 (ddd, *J* = 17.1, 10.2, 6.0 Hz, 1H), 5.13 (dt, *J* = 10.3, 1.3 Hz, 1H), 3.46 (ddd, *J* = 11.2, 7.2, 4.1 Hz, 1H), 3.28 – 3.09 (m, 1H), 2.43 (s, 3H), 1.86 – 1.57 (m, 4H) ppm.

IV.8. Spectra of Compounds

^{1}H NMR ($CDCl_3$, 600 MHz) **4-37 starting olefin**

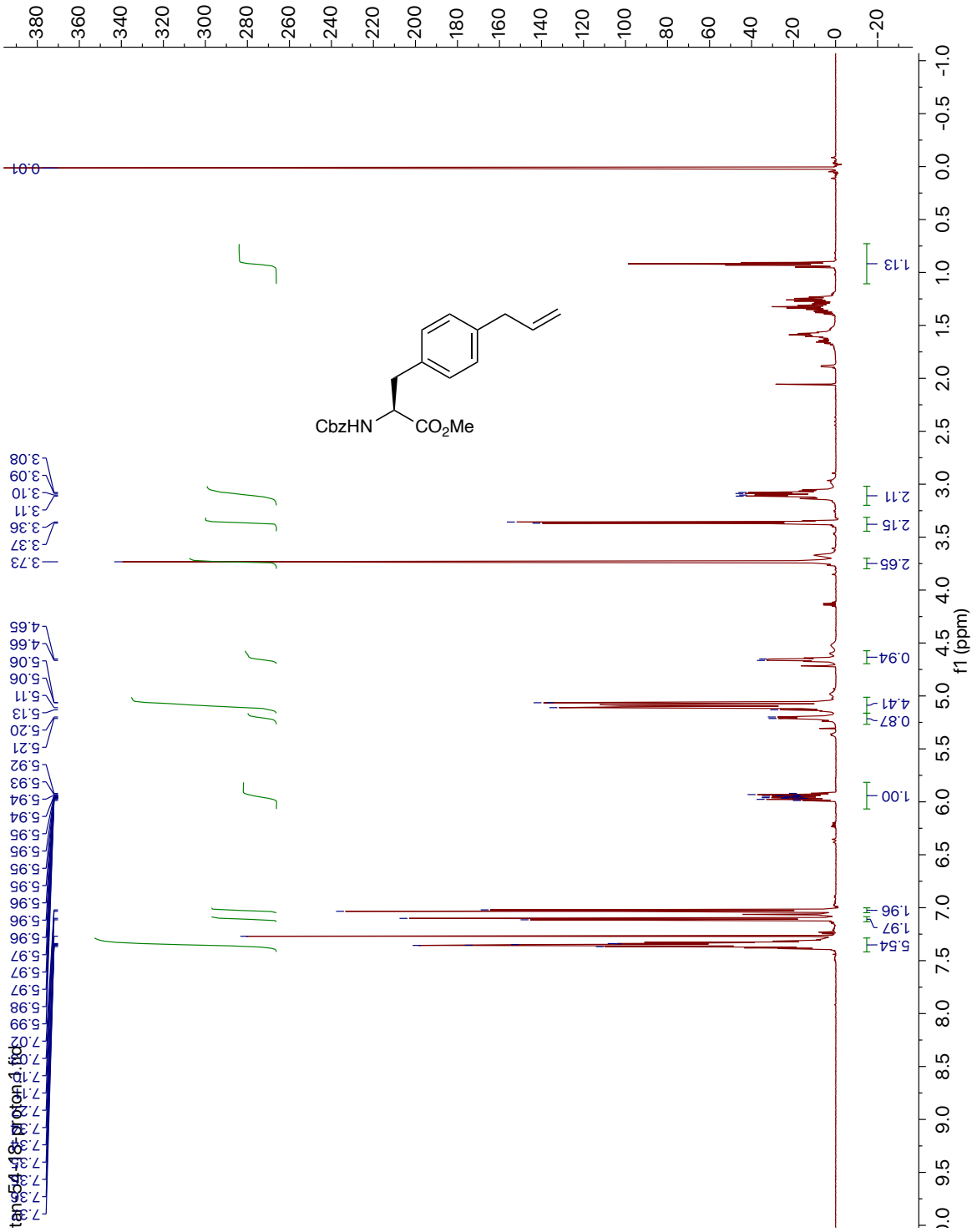

^{13}C NMR ($CDCl_3$, 151 MHz)

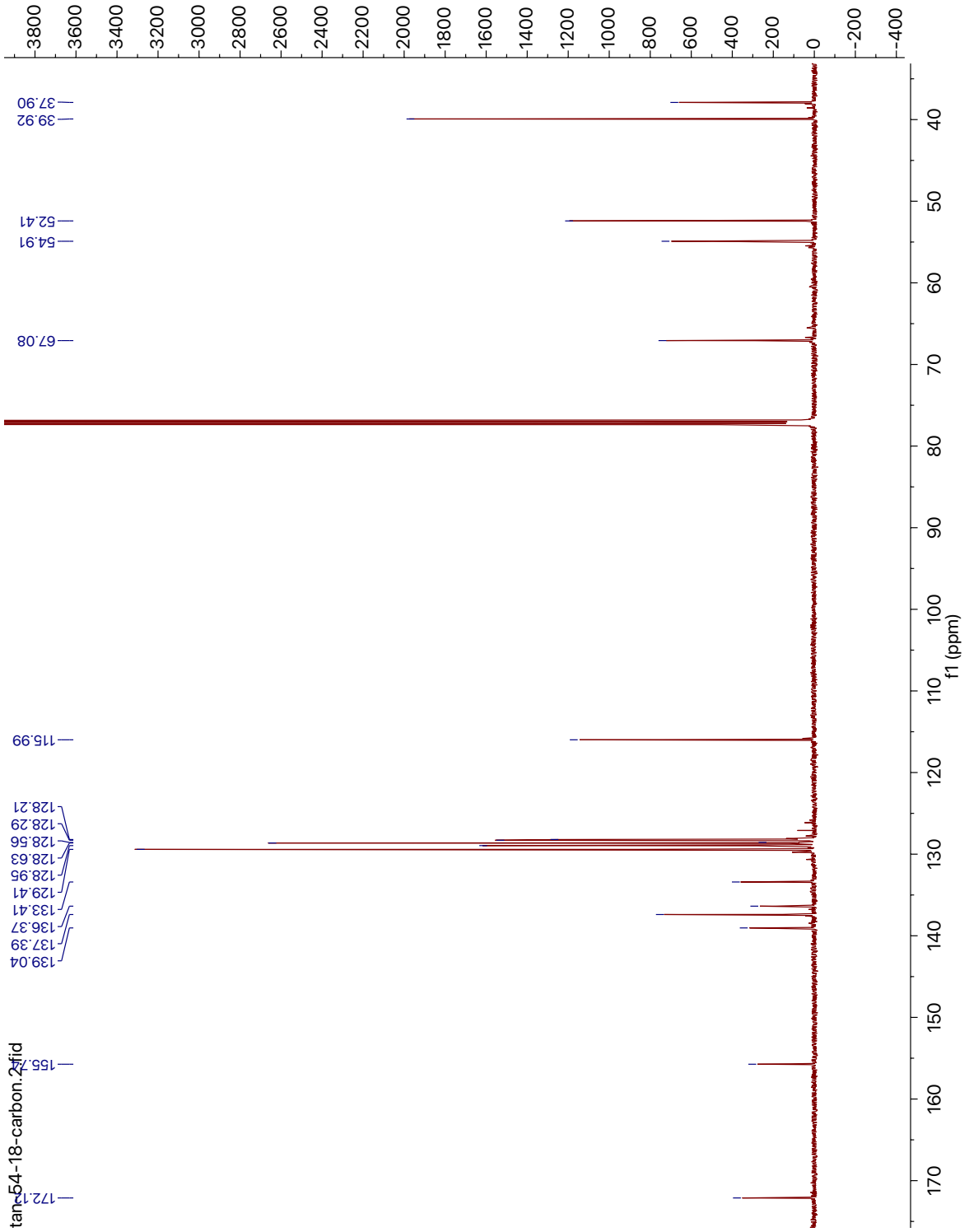

^{1}H NMR ($CDCl_3$, 500 MHz) **4-13**

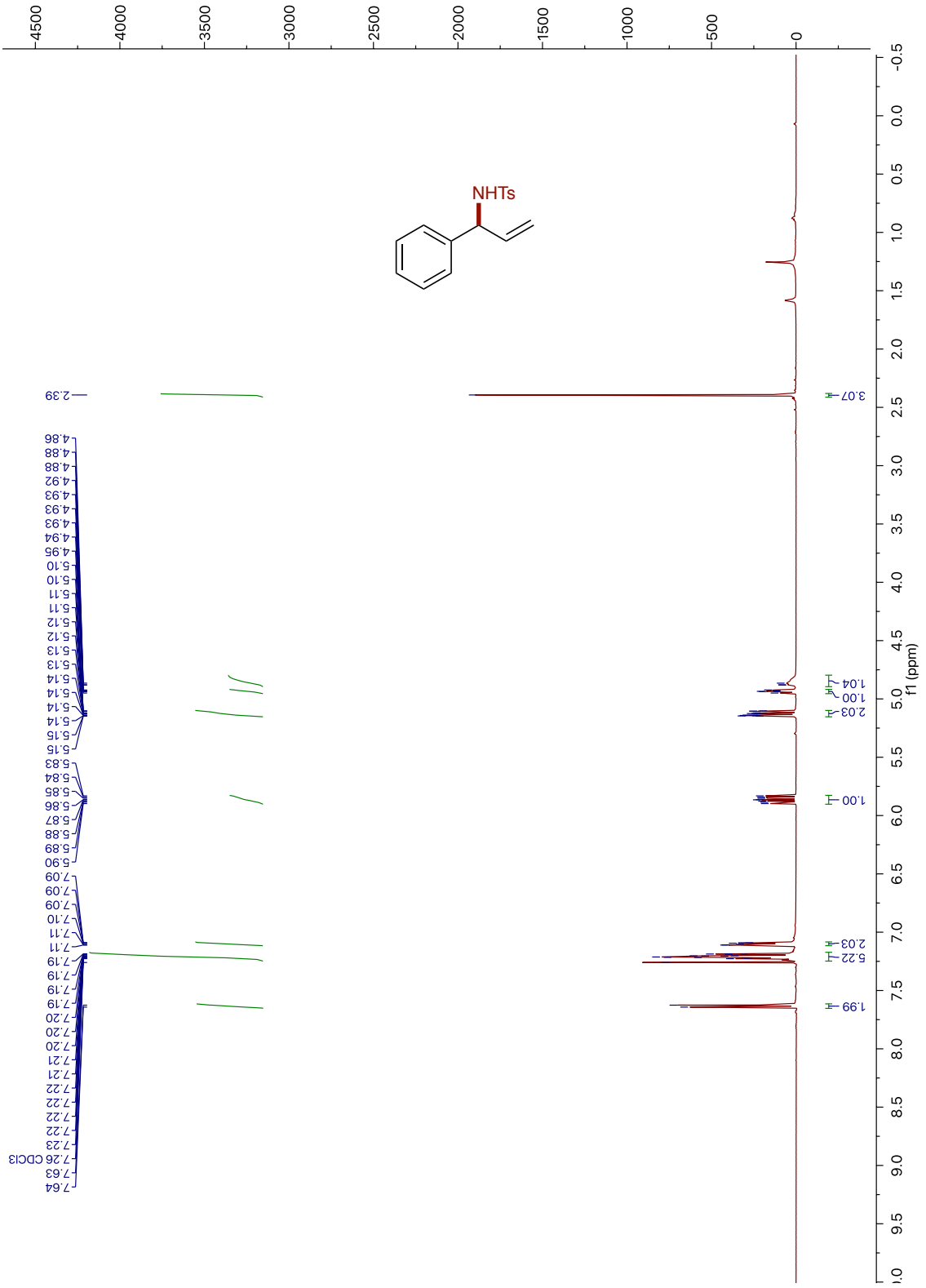

^{1}H NMR ($CDCl_3$, 400 MHz) **4-14**

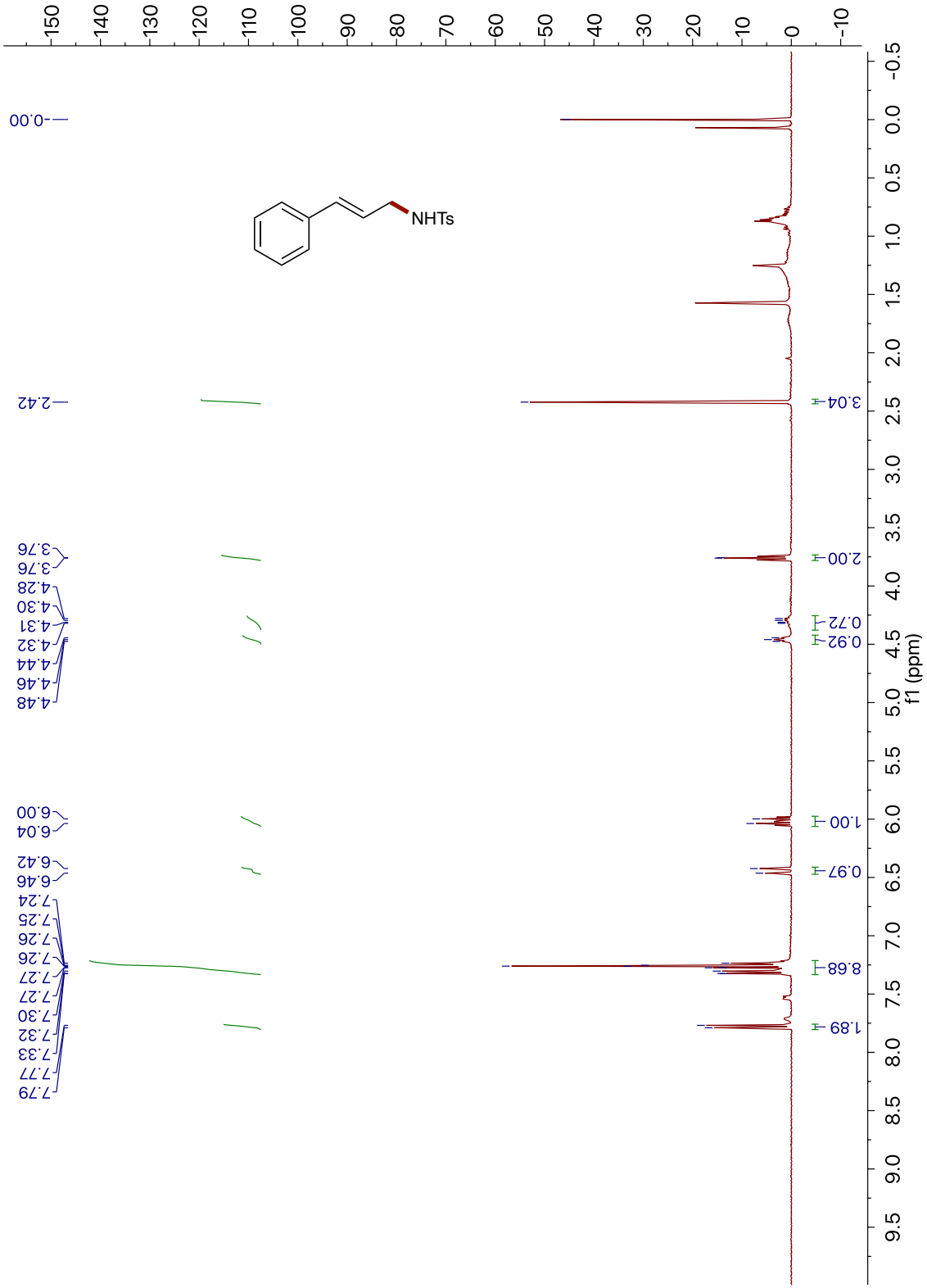

^{1}H NMR (400 MHz, $CDCl_3$) **4-23**

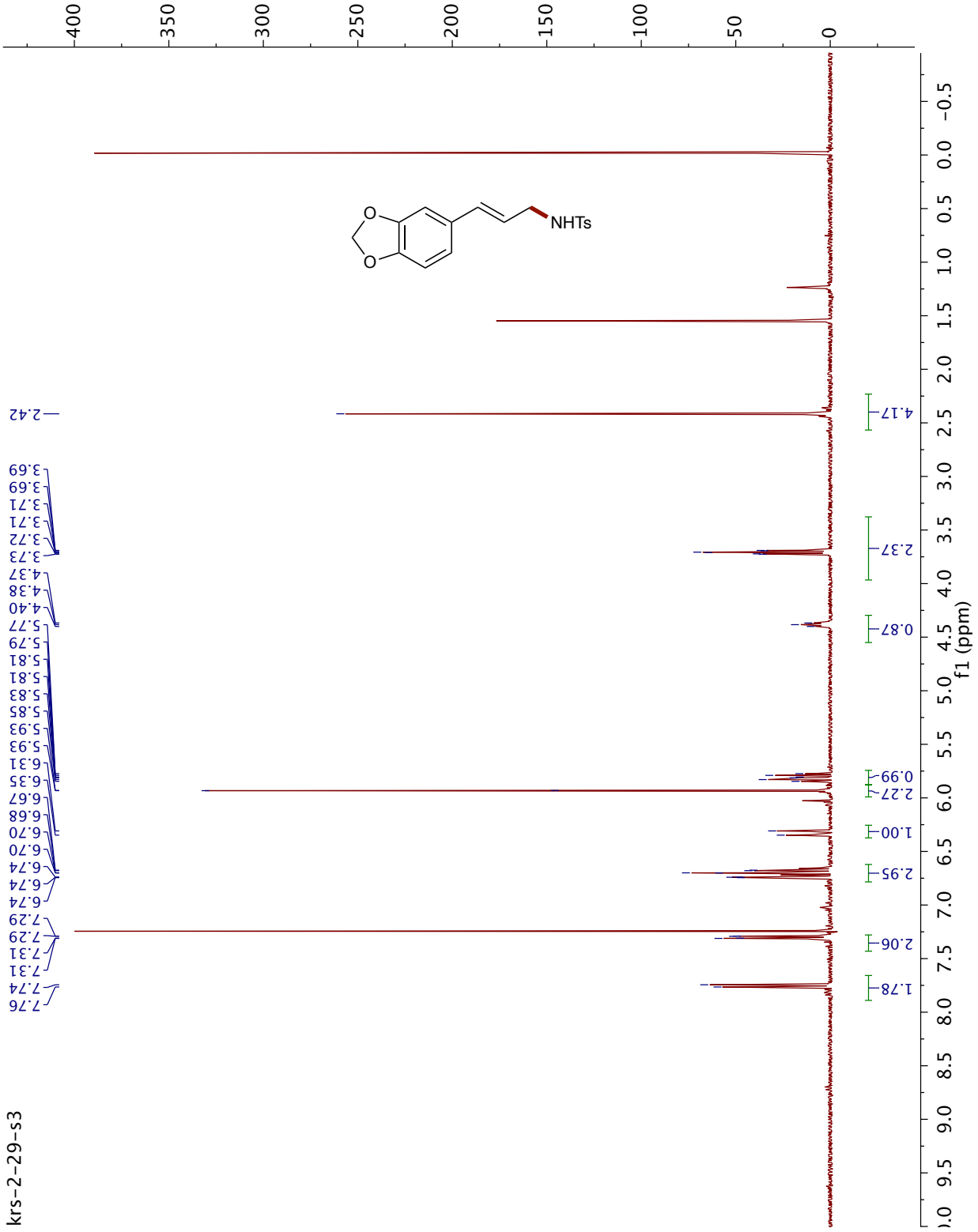

^{13}C NMR (126 MHz, $CDCl_3$) **4-23**

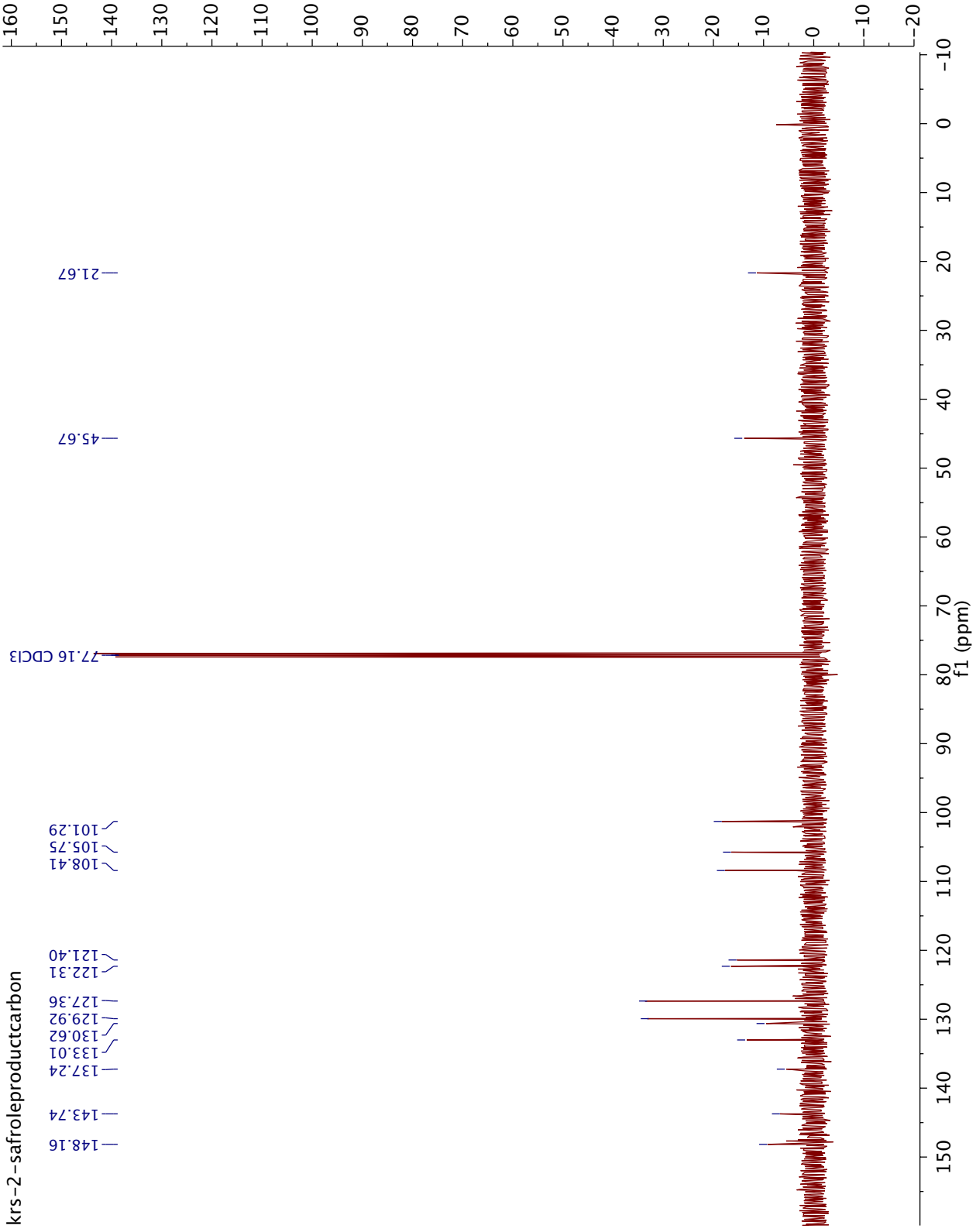

^{1}H NMR ($CDCl_3$, 500 MHz) **4-26**

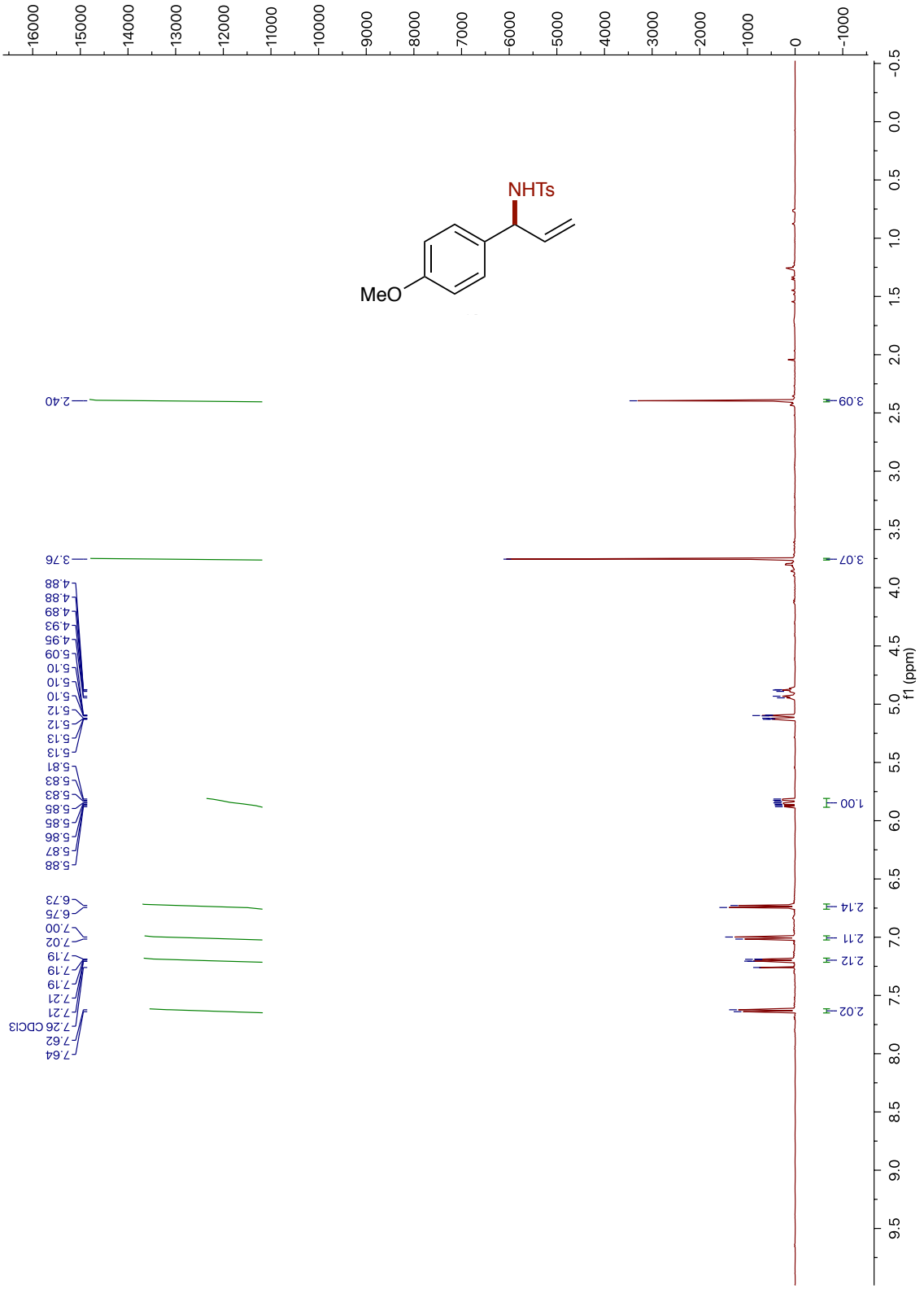

^{1}H NMR ($CDCl_3$, 600 MHz) **4-27**

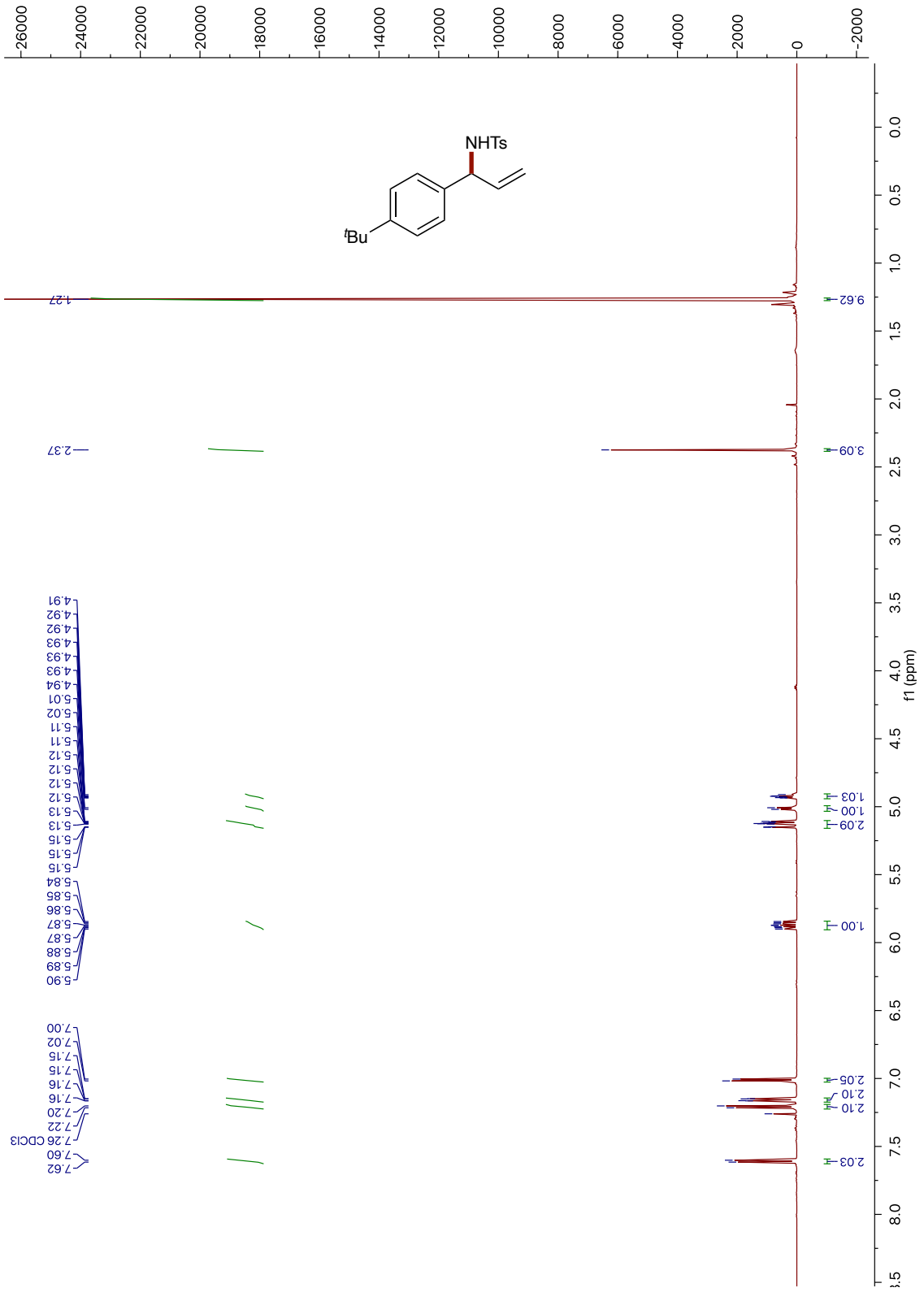

^{13}C NMR ($CDCl_3$, 151 MHz)

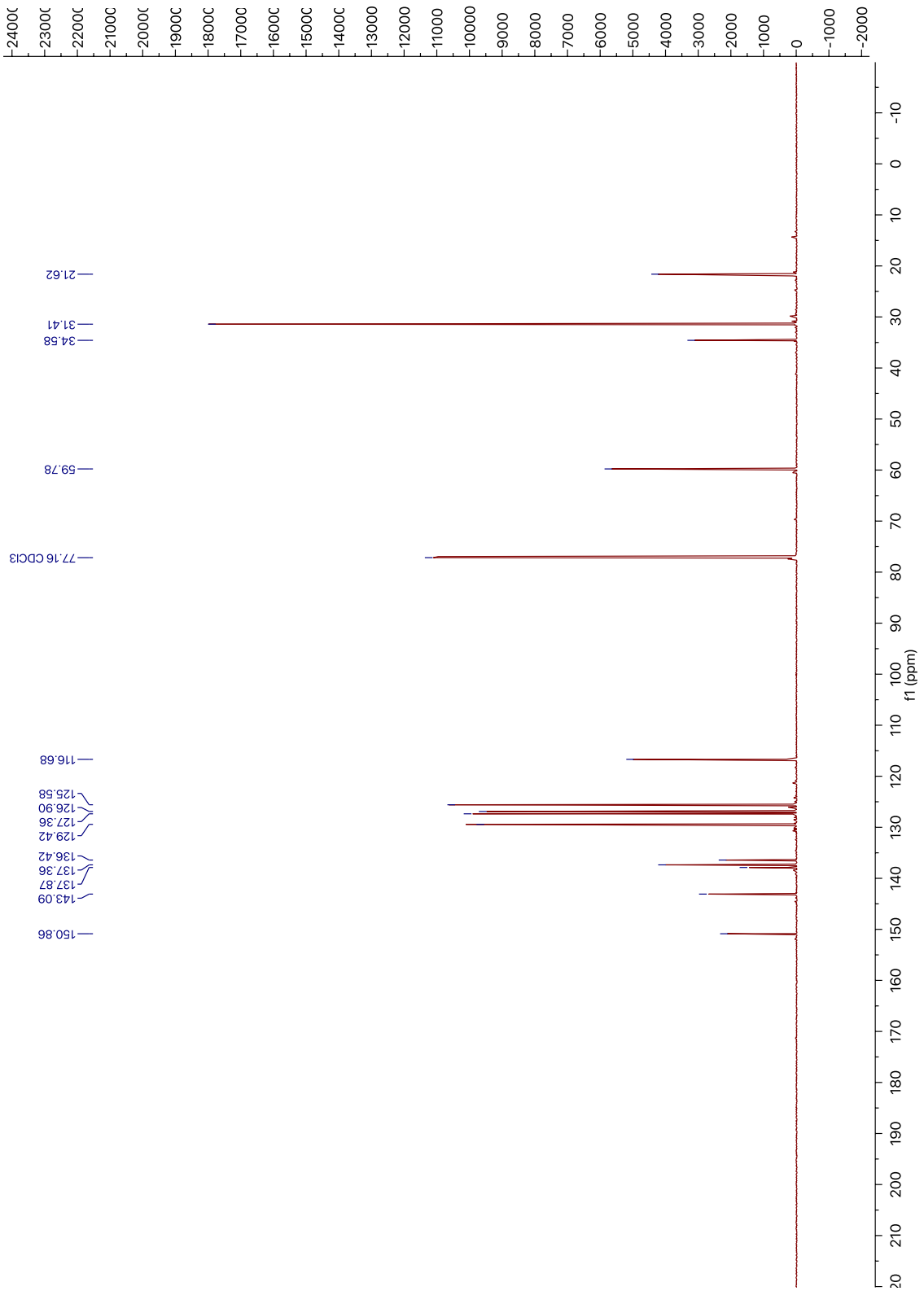

^{1}H NMR ($CDCl_3$, 600 MHz) **4-28**

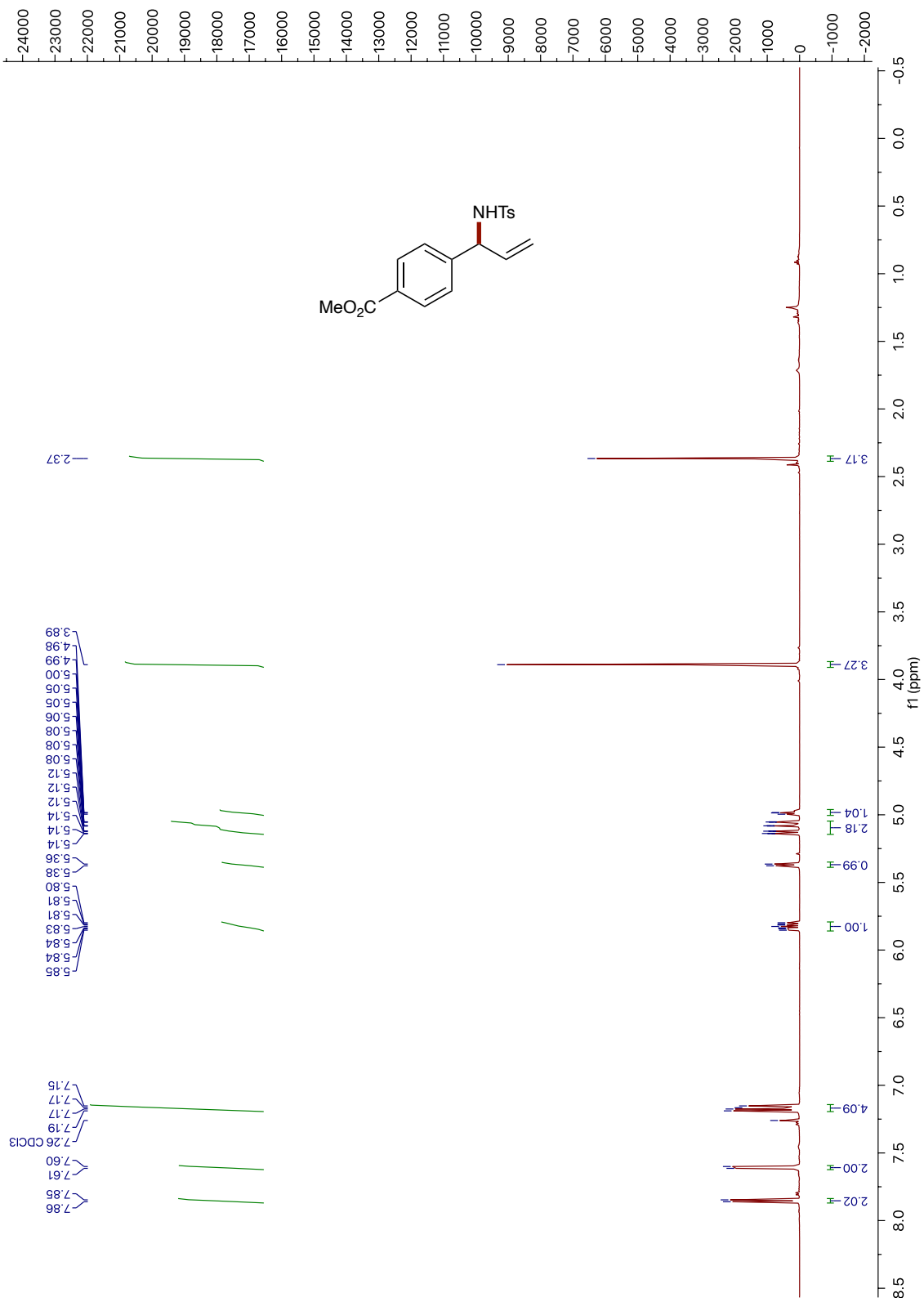

^{13}C NMR ($CDCl_3$, 151 MHz)

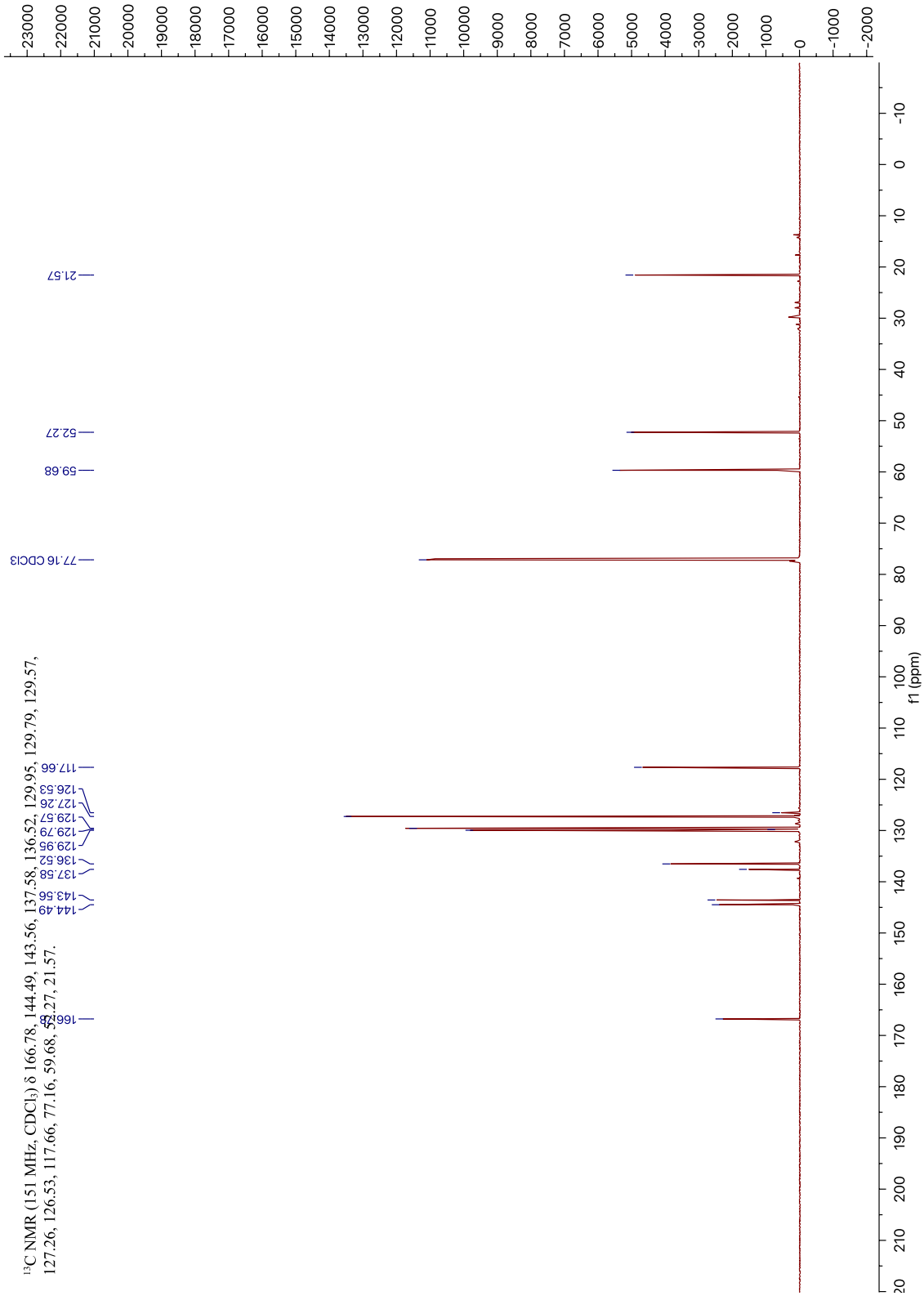

^{1}H NMR ($CDCl_3$, 600 MHz) **4-29**

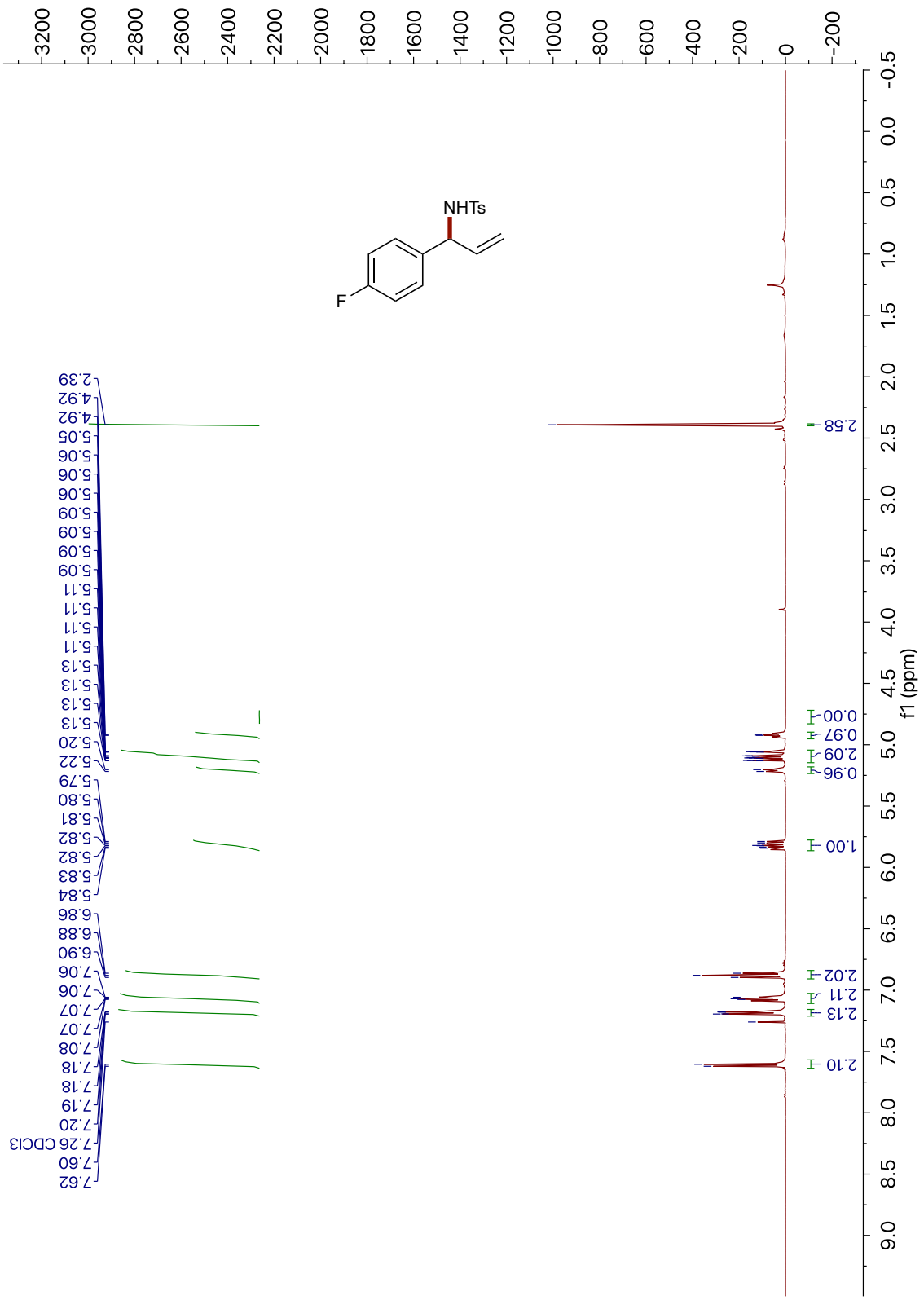

^{13}C NMR ($CDCl_3$, 151 MHz)

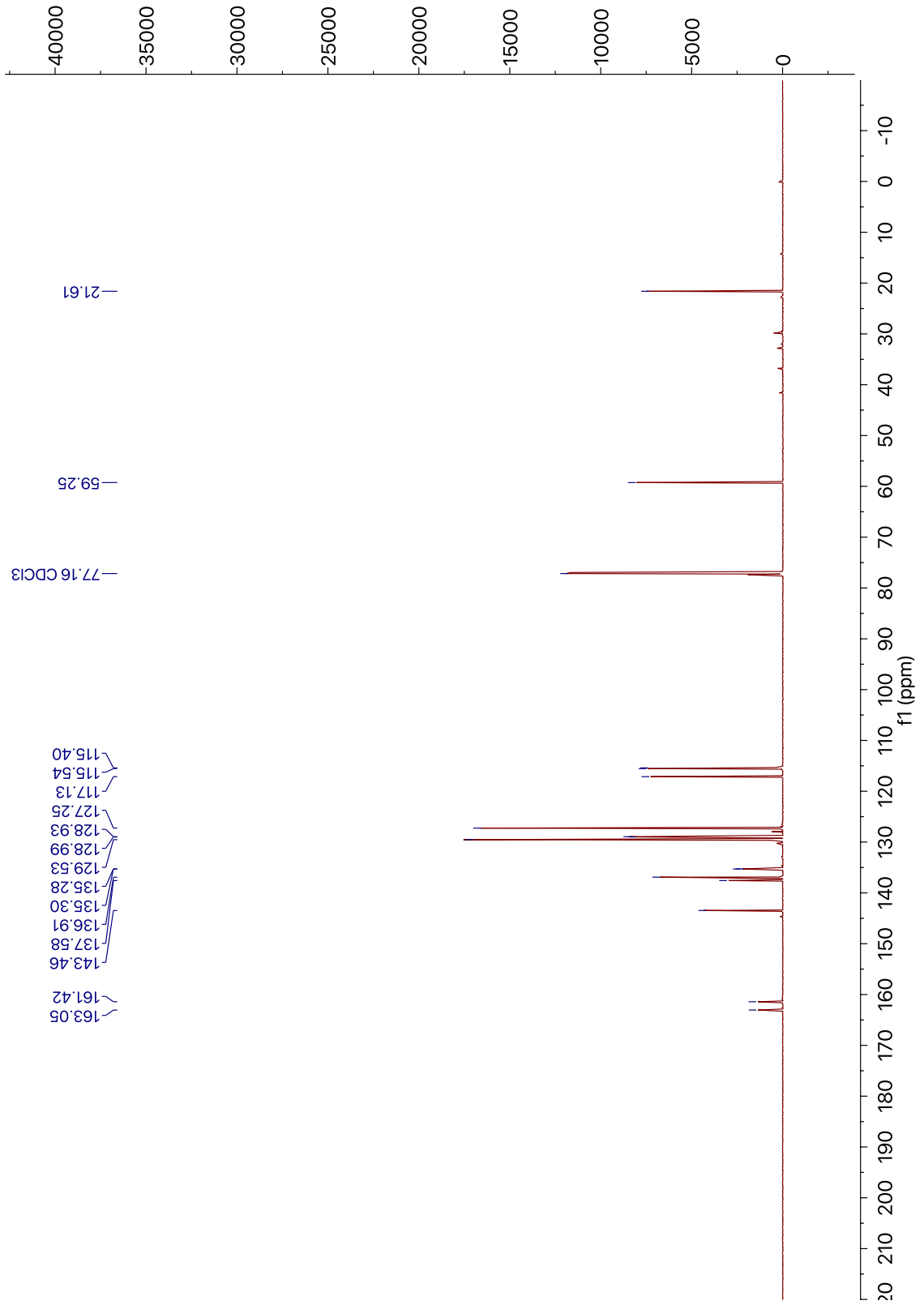

^{1}H NMR ($CDCl_3$, 500 MHz) **4-30**

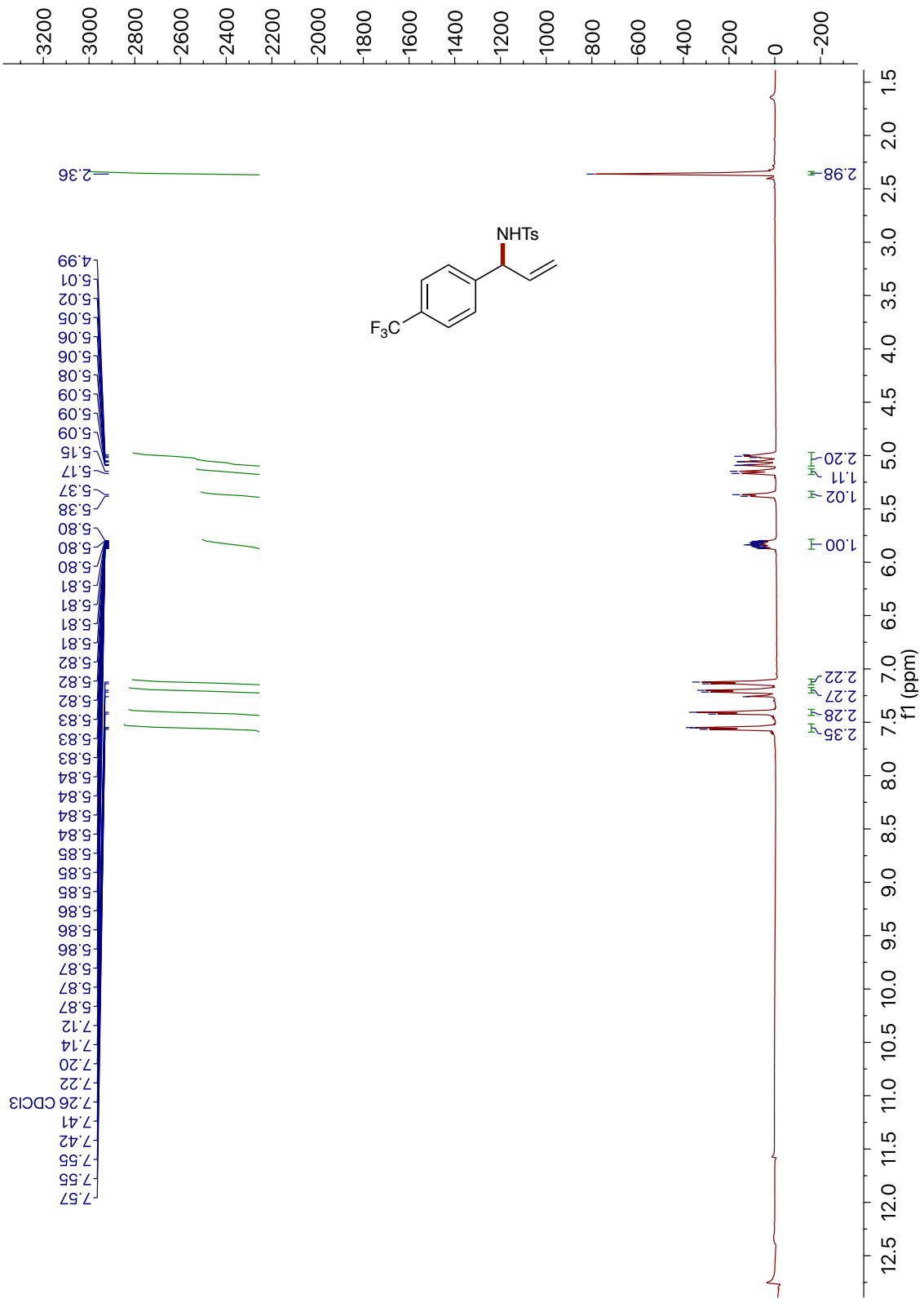

^{13}C NMR ($CDCl_3$, 126 MHz)

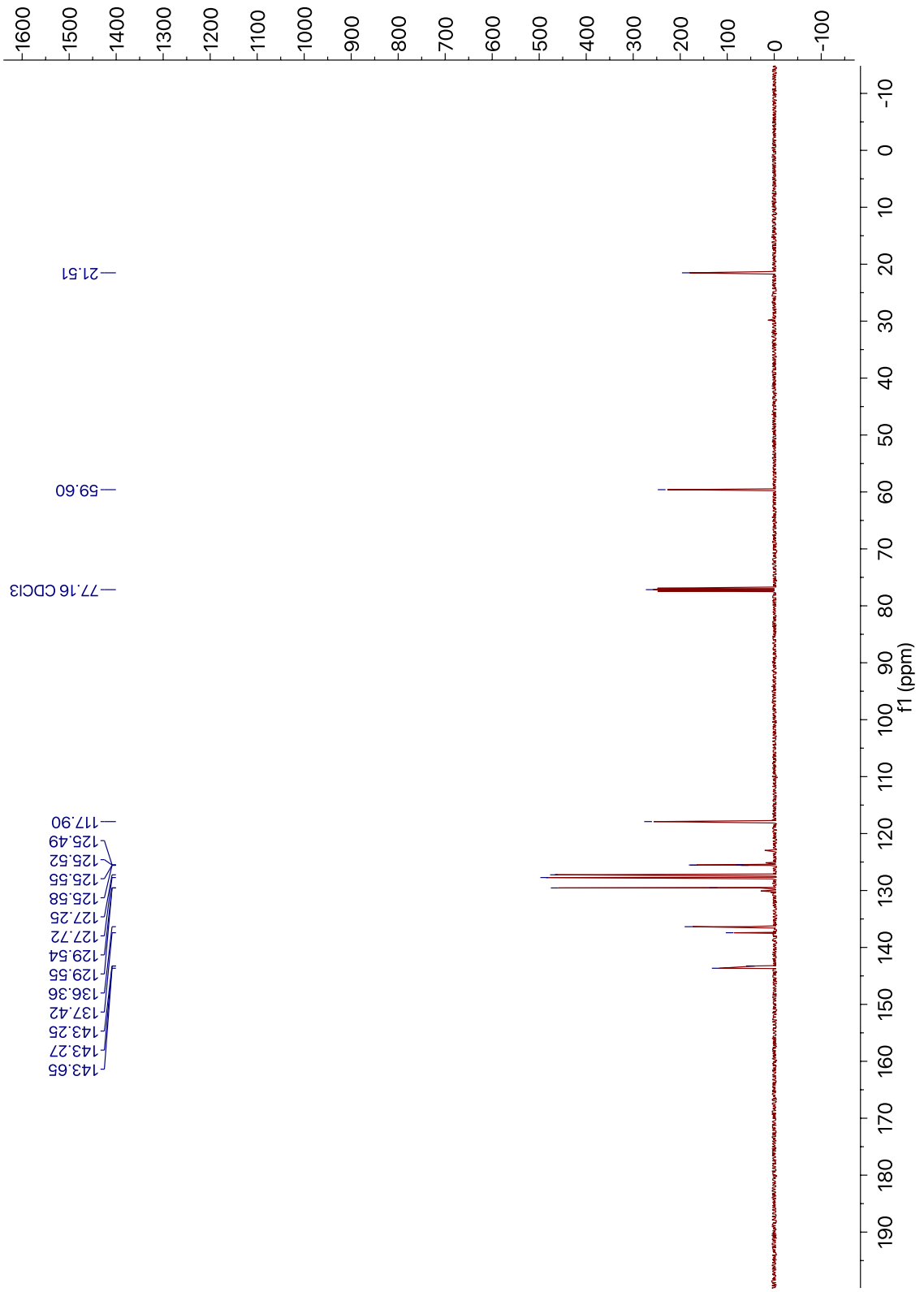

^{1}H NMR ($CDCl_3$, 500 MHz) **4-31**

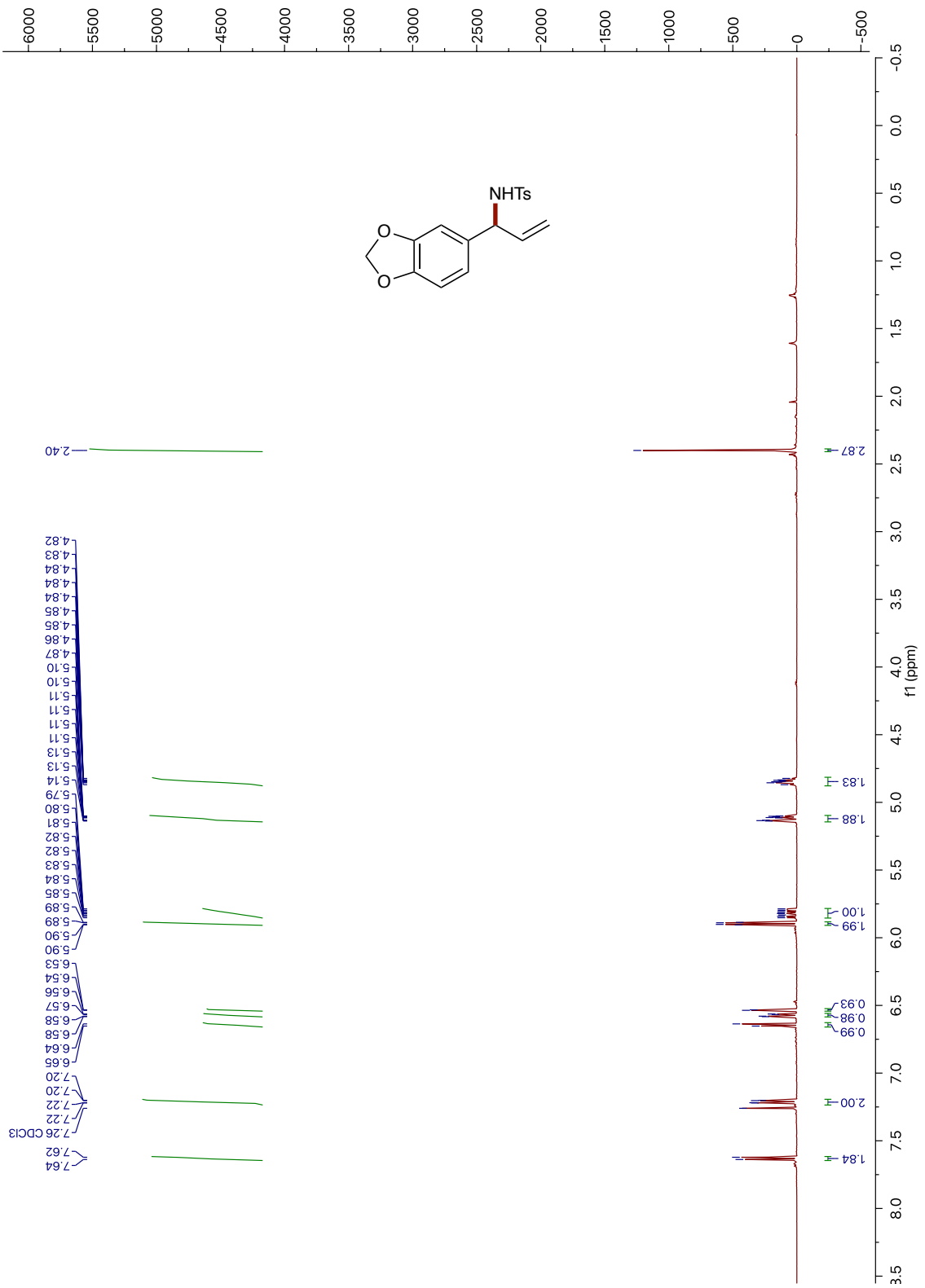

^{13}C NMR ($CDCl_3$, 151 MHz)

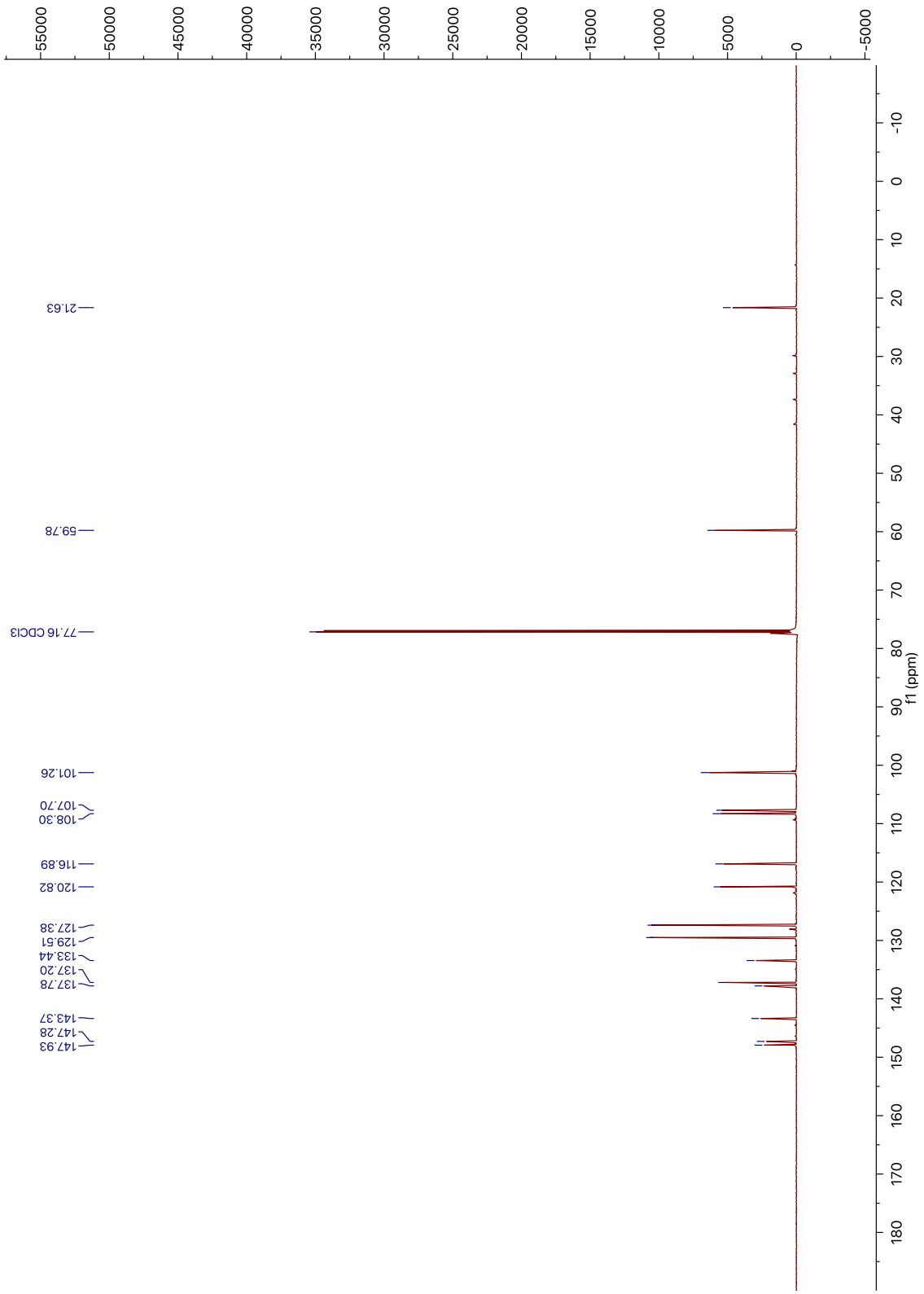

^{1}H NMR ($CDCl_3$, 600 MHz) **4-32**

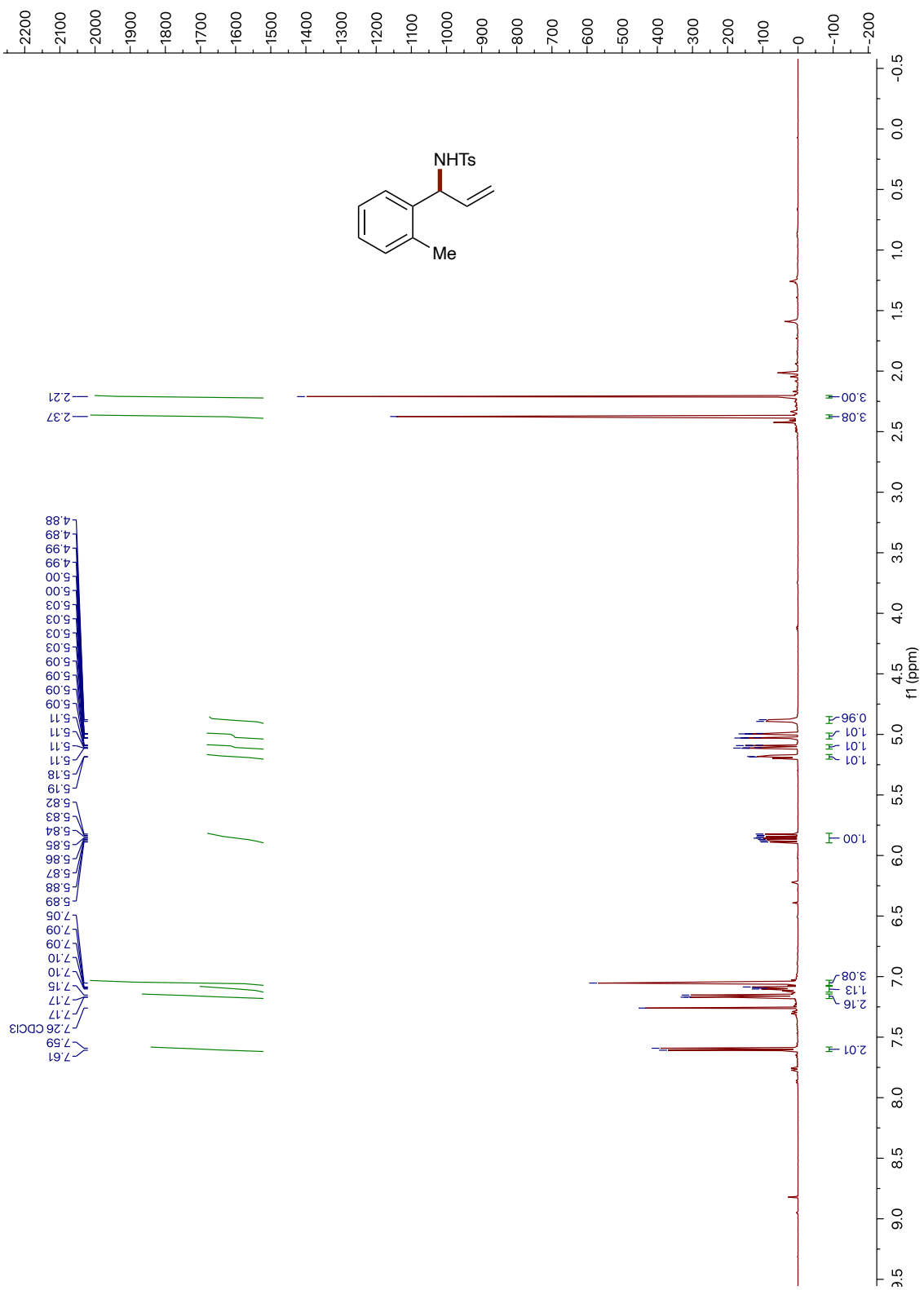

^{13}C NMR ($CDCl_3$, 126 MHz)

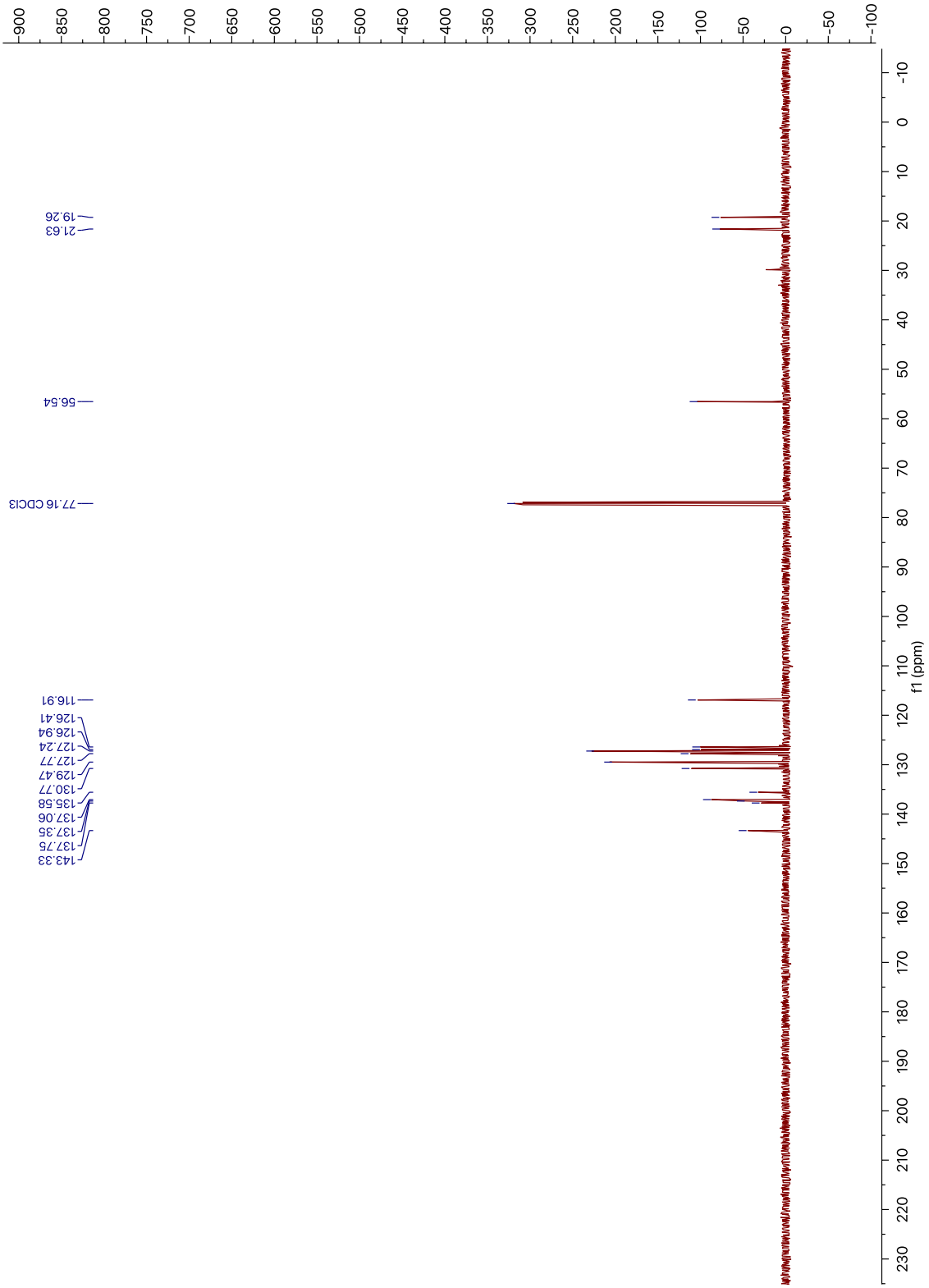

^{1}H NMR ($CDCl_3$, 400 MHz) **4-33**

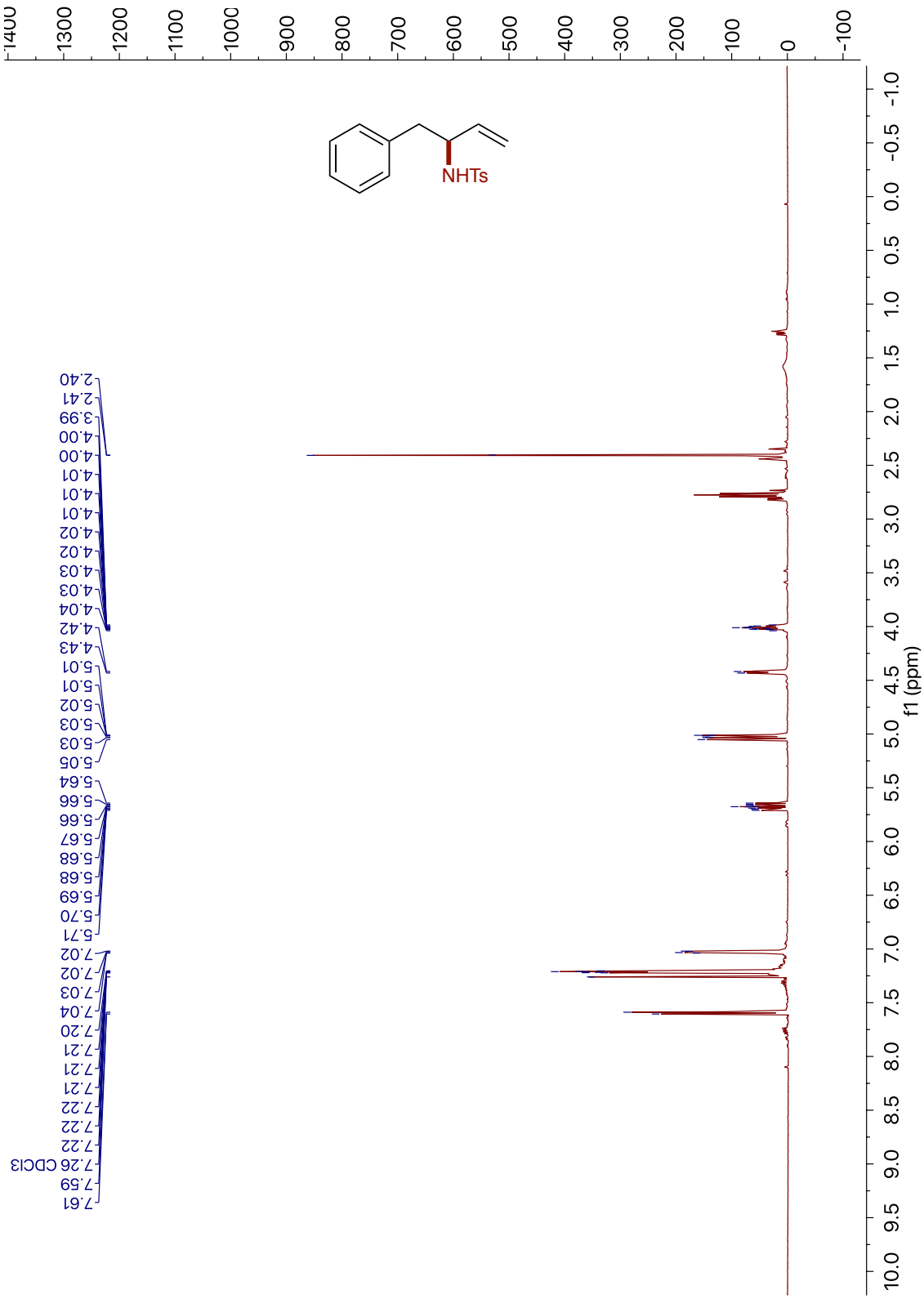

^{1}H NMR ($CDCl_3$, 400 MHz) **4-34**

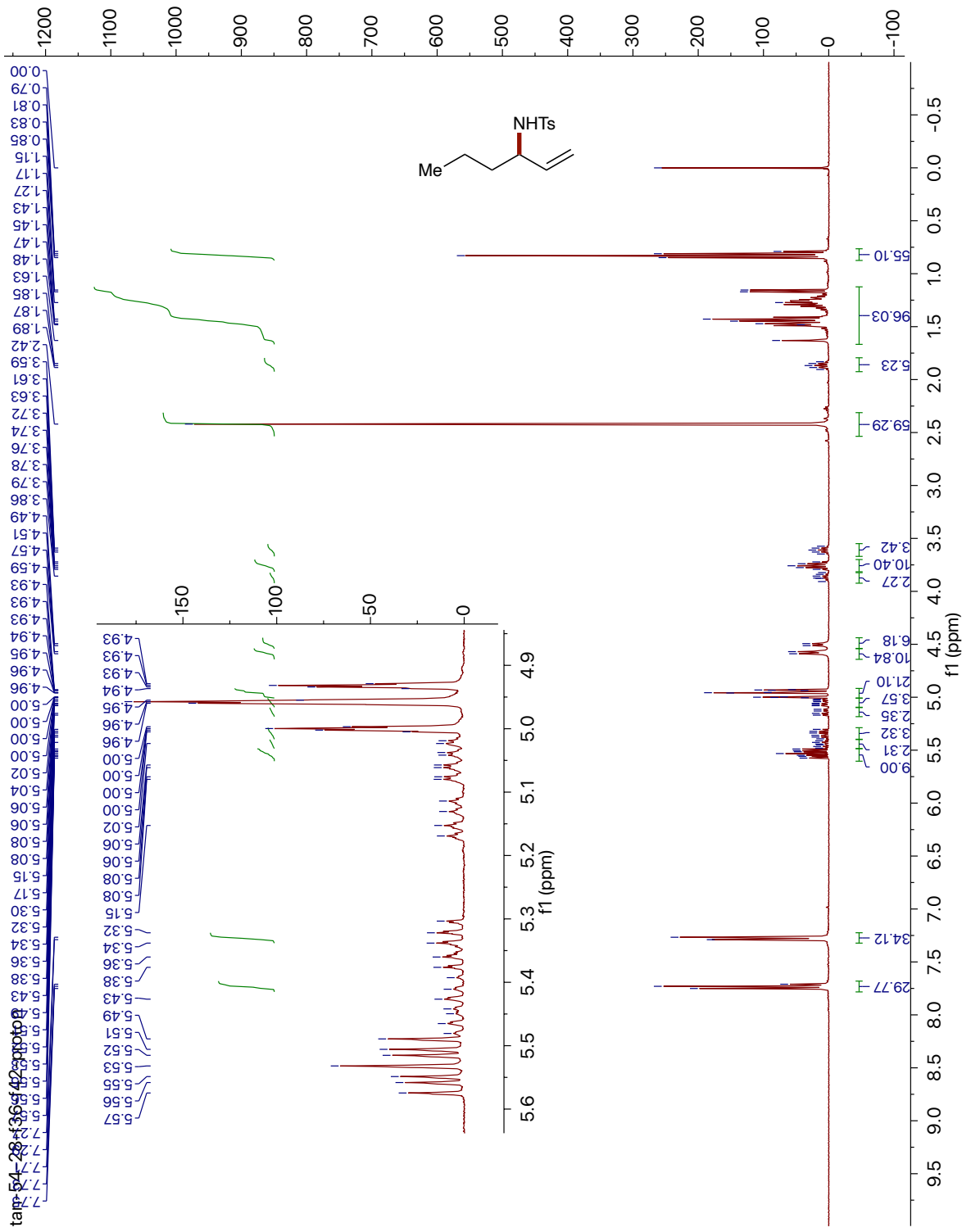

^{1}H NMR ($CDCl_3$, 500 MHz) **4-35**

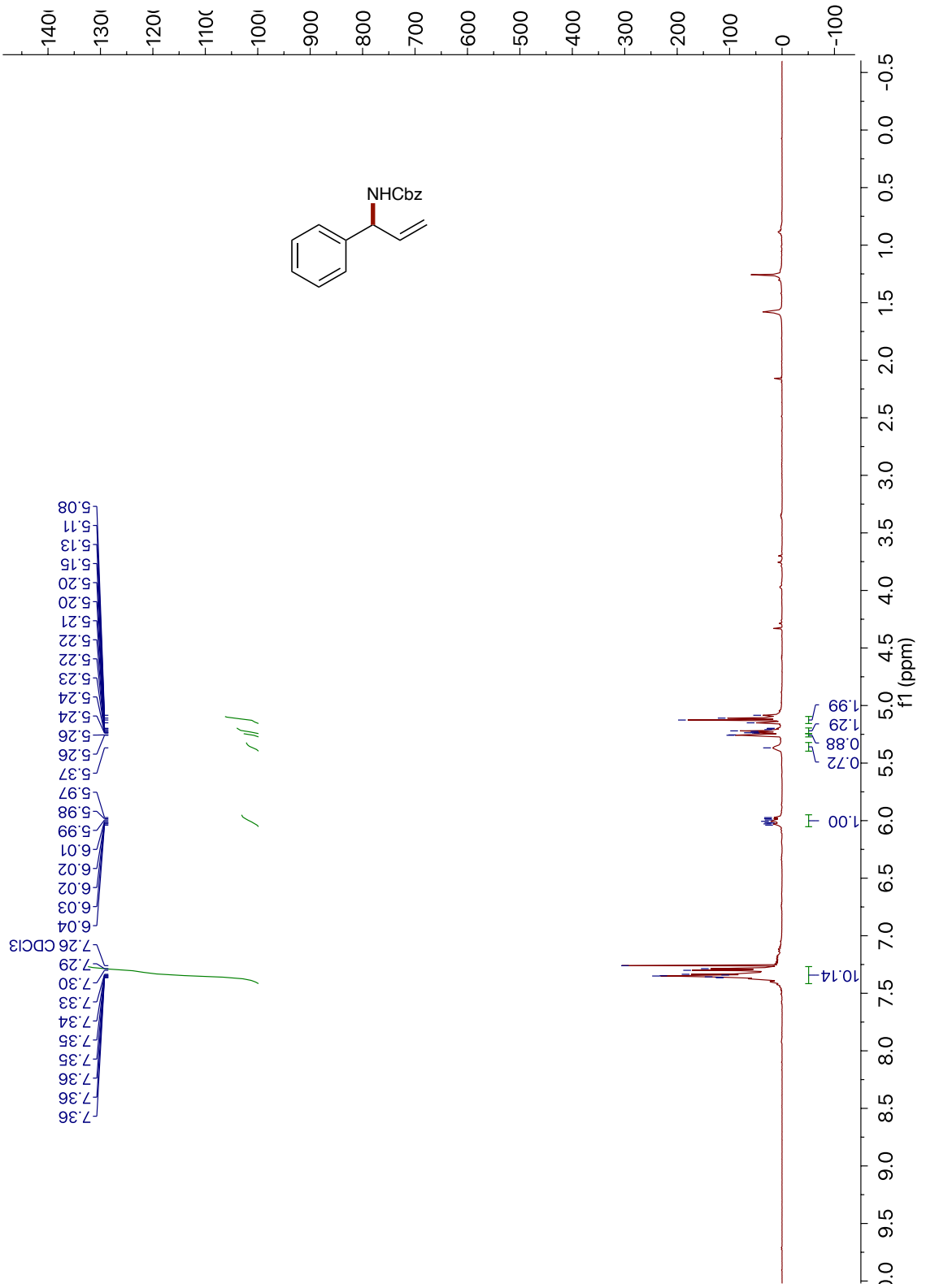

^{1}H NMR ($CDCl_3$, 500 MHz) **4-36**

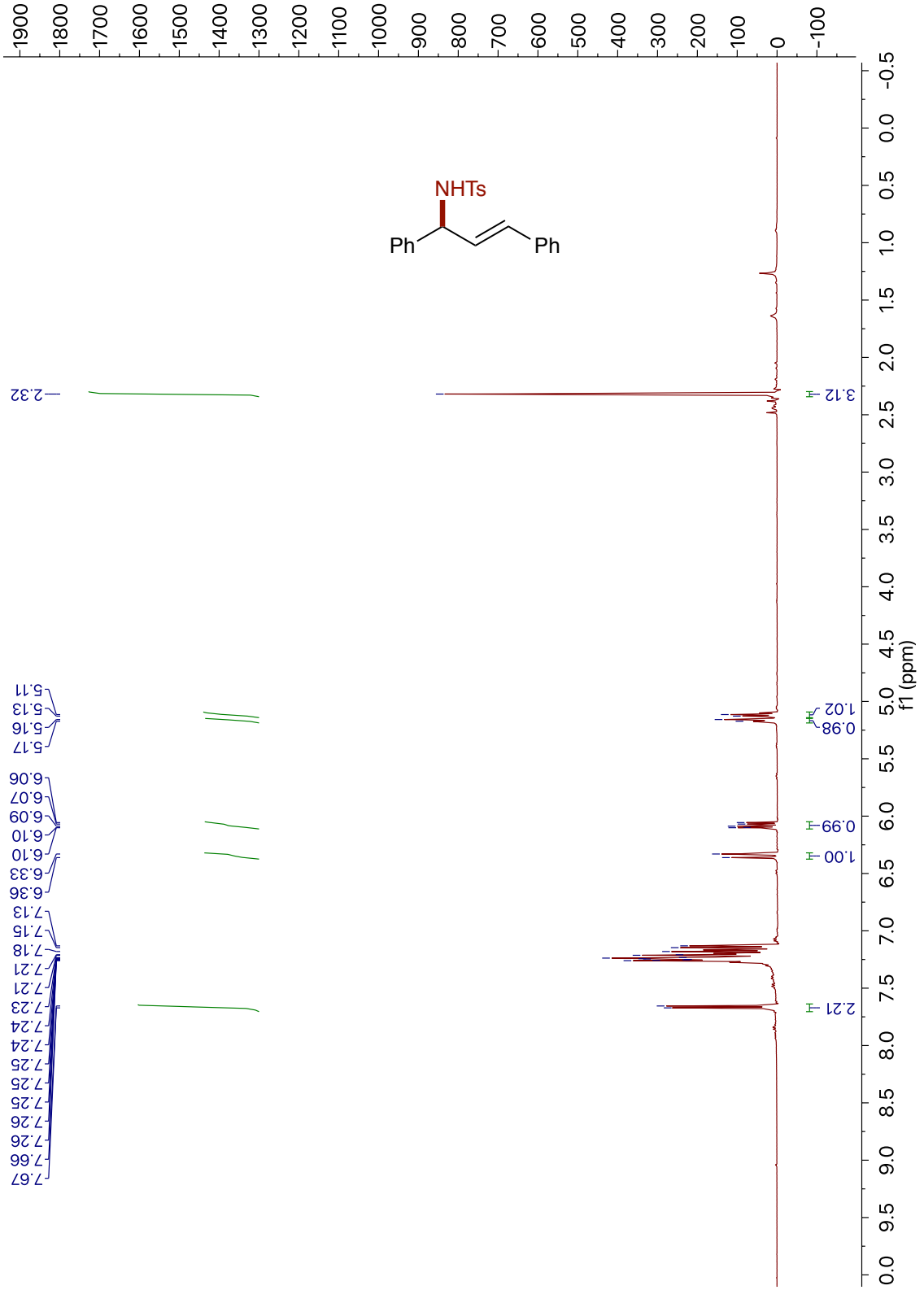

^{1}H NMR ($CDCl_3$, 600 MHz) **4-37**

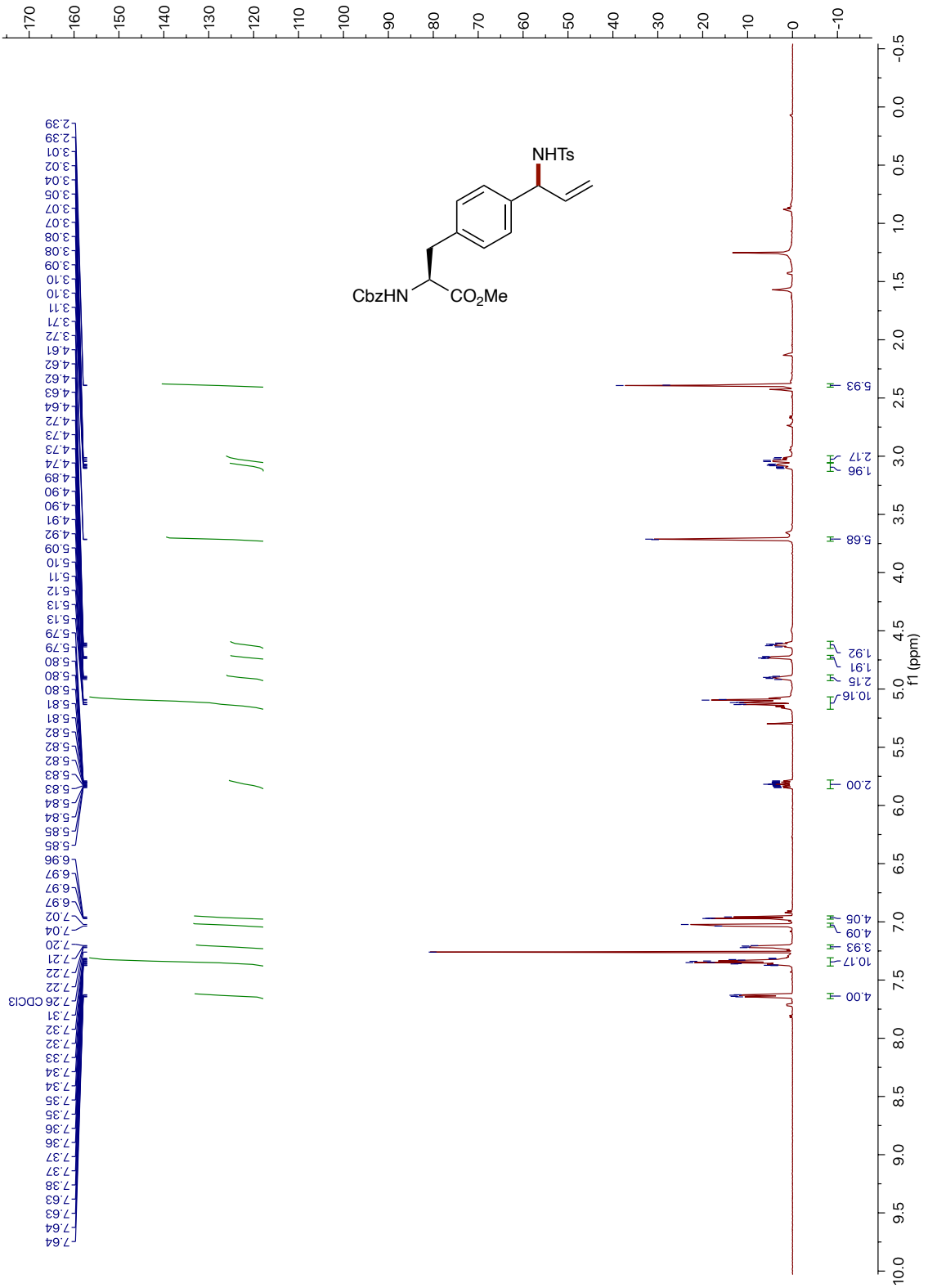

^{13}C NMR ($CDCl_3$, 151 MHz)

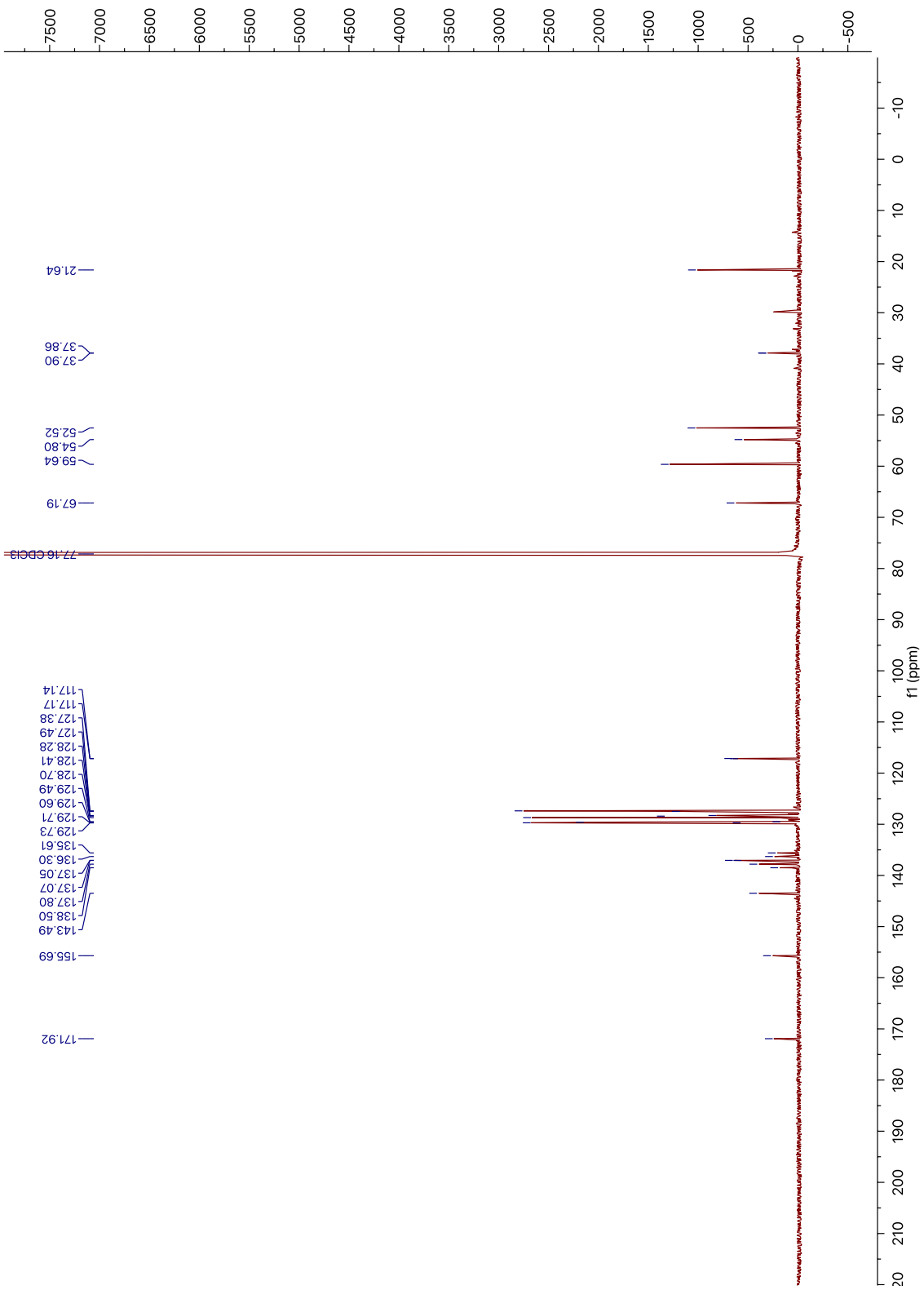

^{1}H NMR ($CDCl_3$, 500 MHz) **4-38**

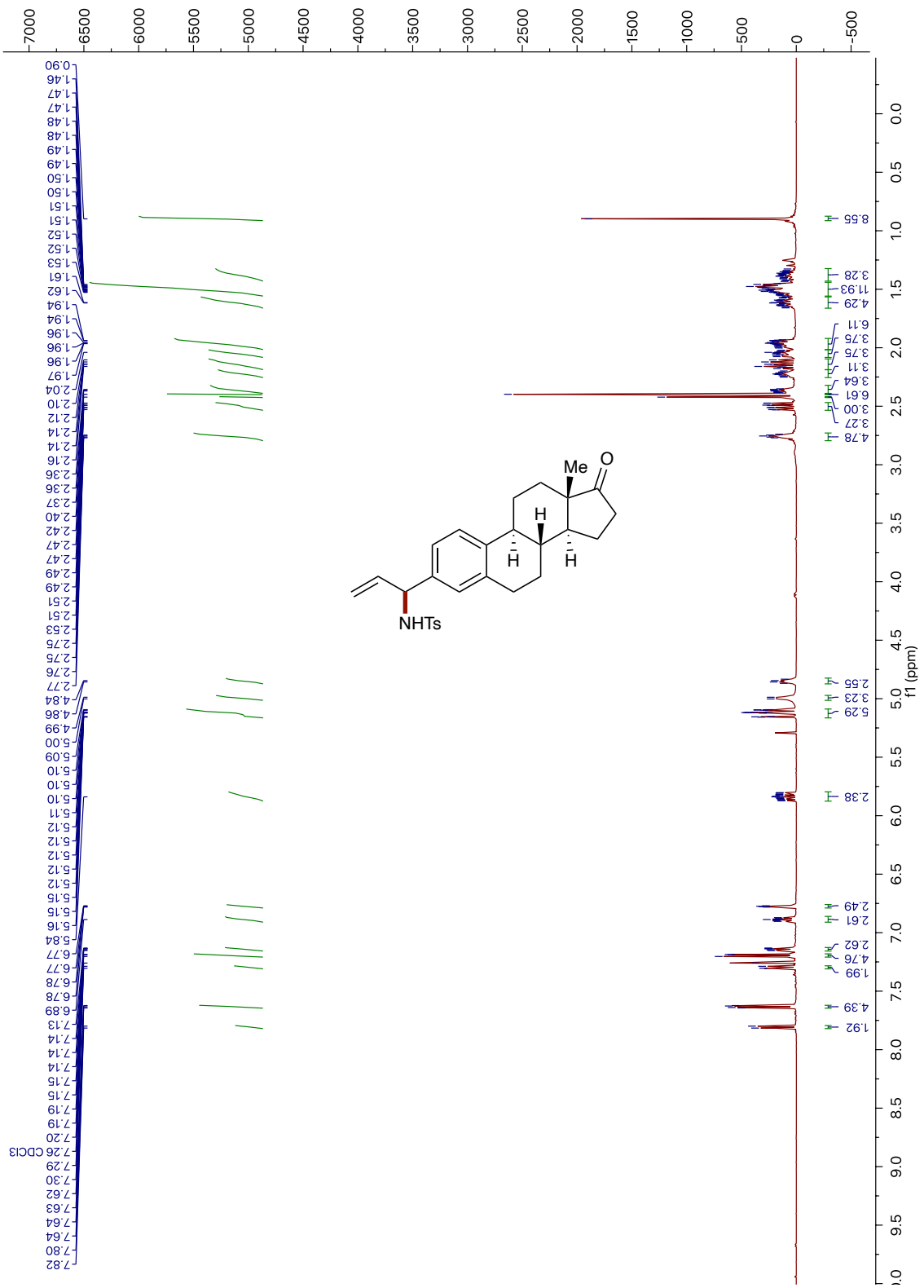

^{13}C NMR ($CDCl_3$, 126 MHz)

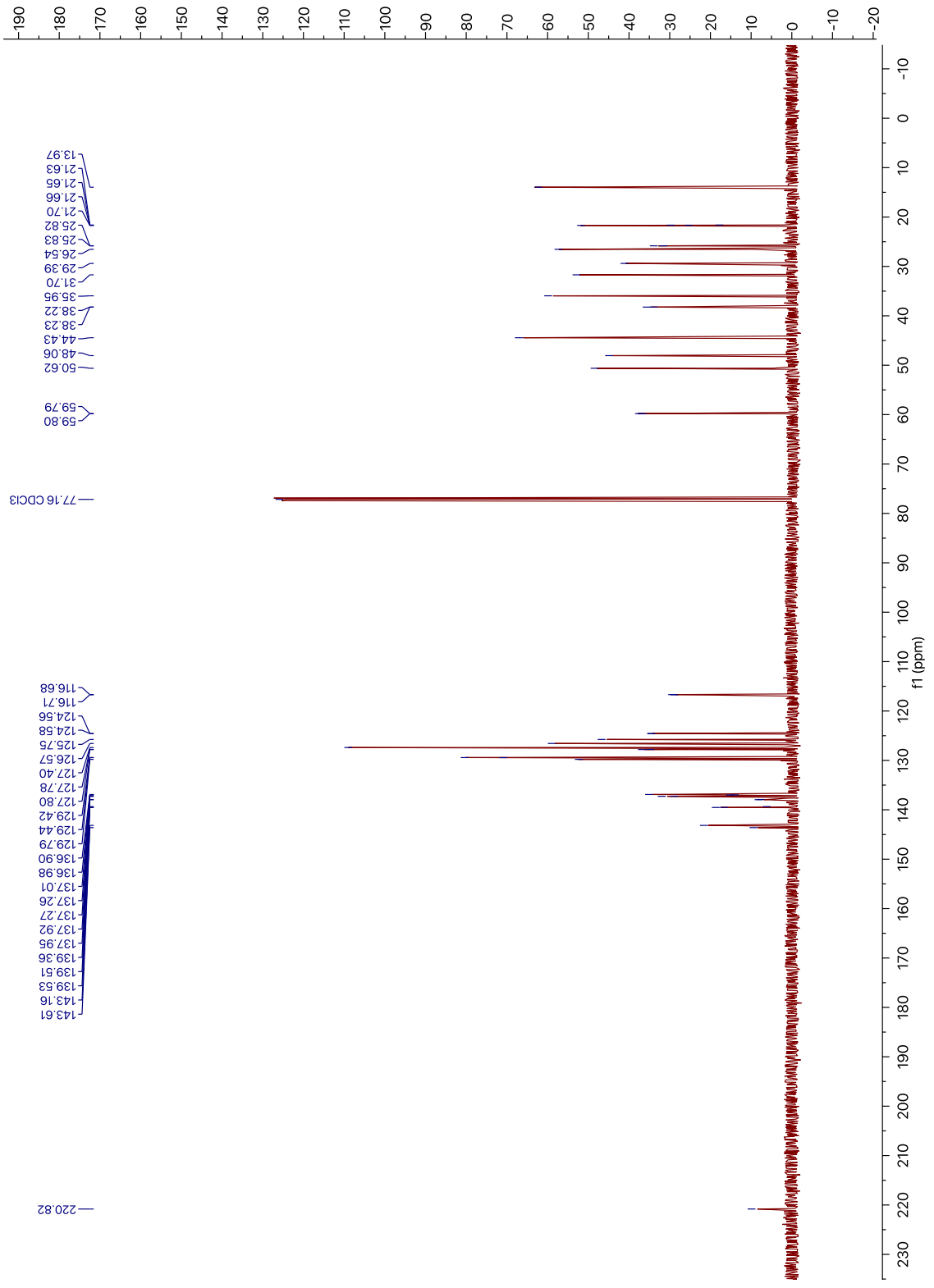

^{1}H NMR ($CDCl_3$, 500 MHz) **4-44**

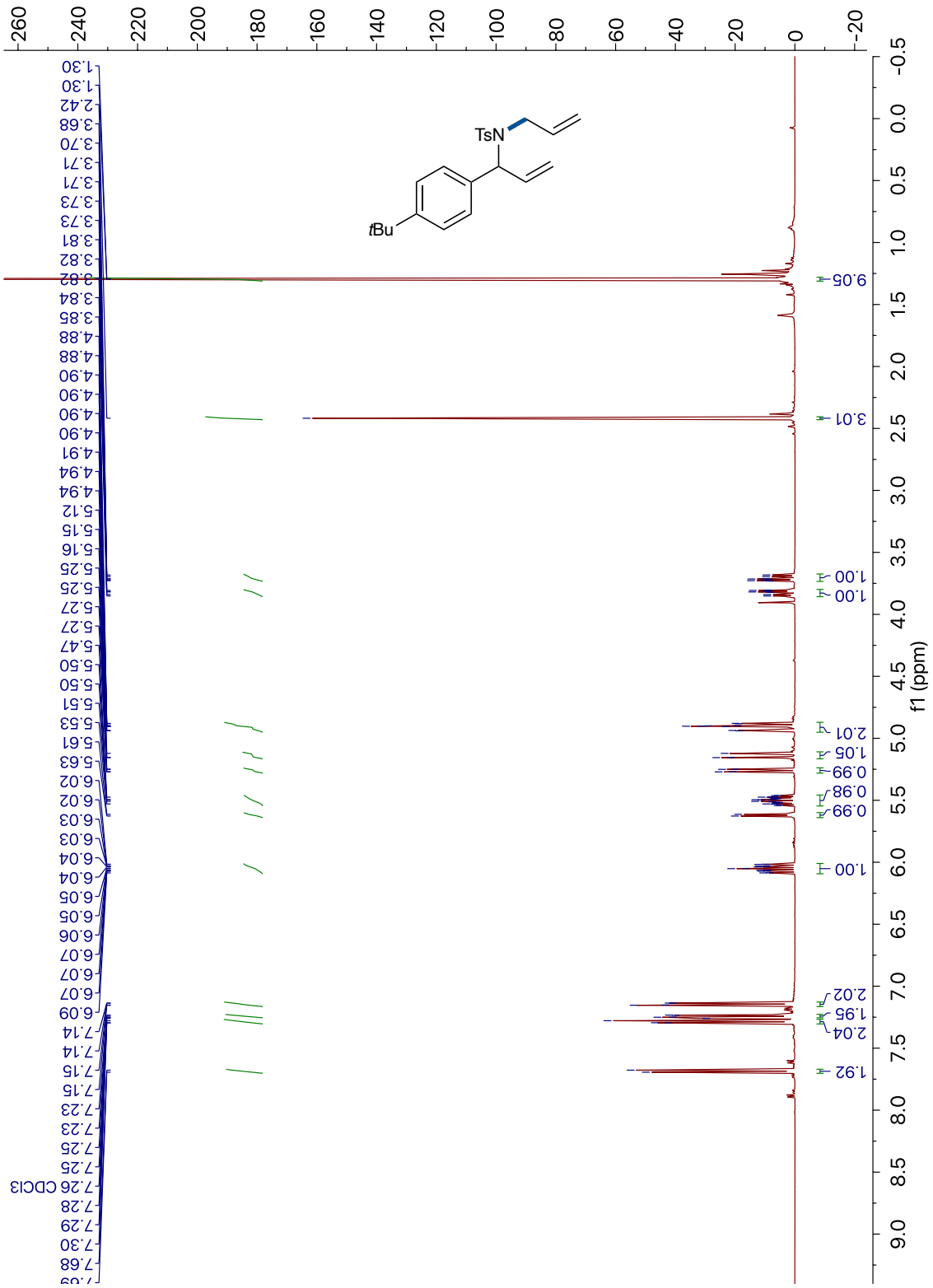

^{13}C NMR ($CDCl_3$, 126 MHz)

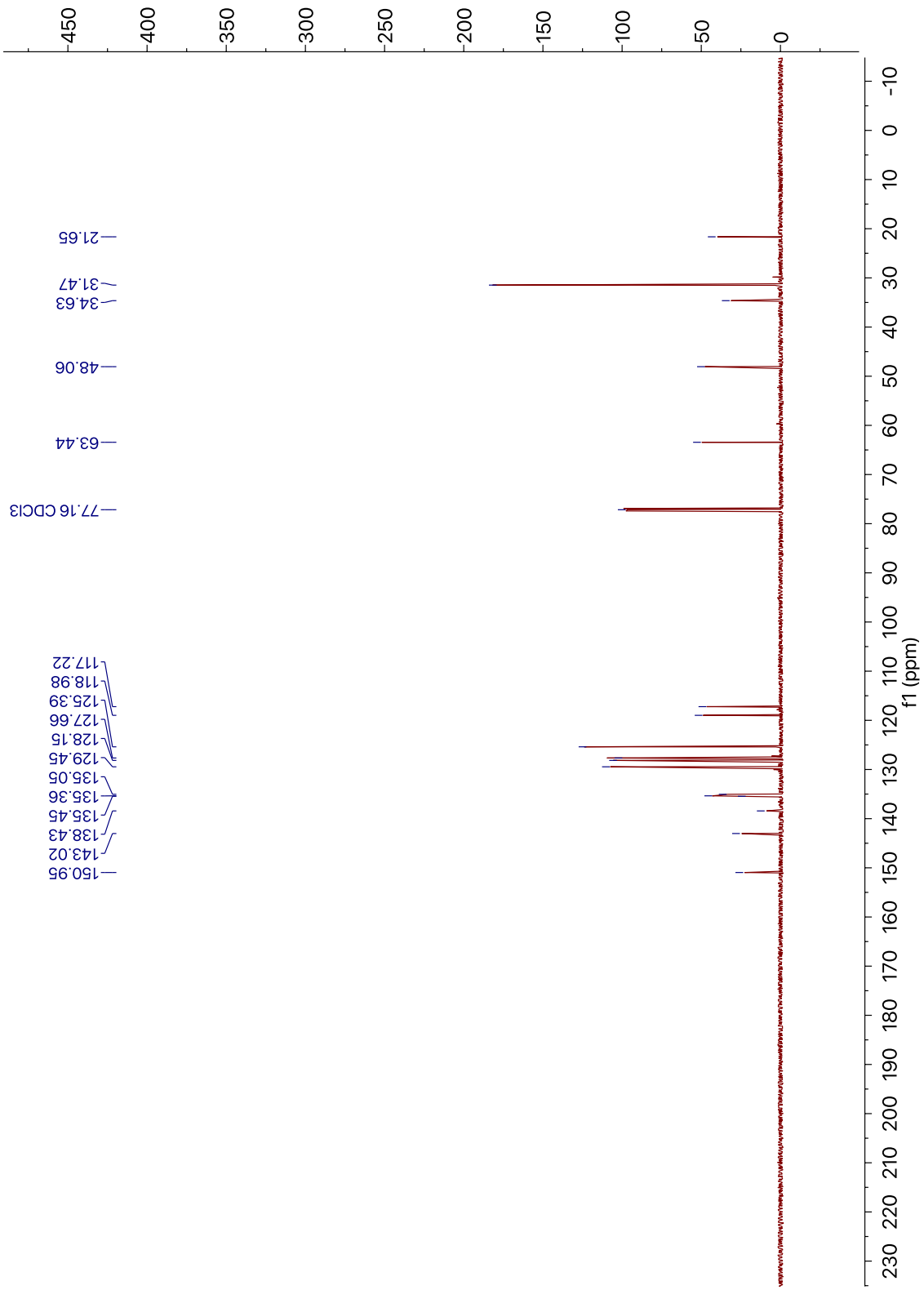

^{1}H NMR ($CDCl_3$, 600 MHz) **4-45**

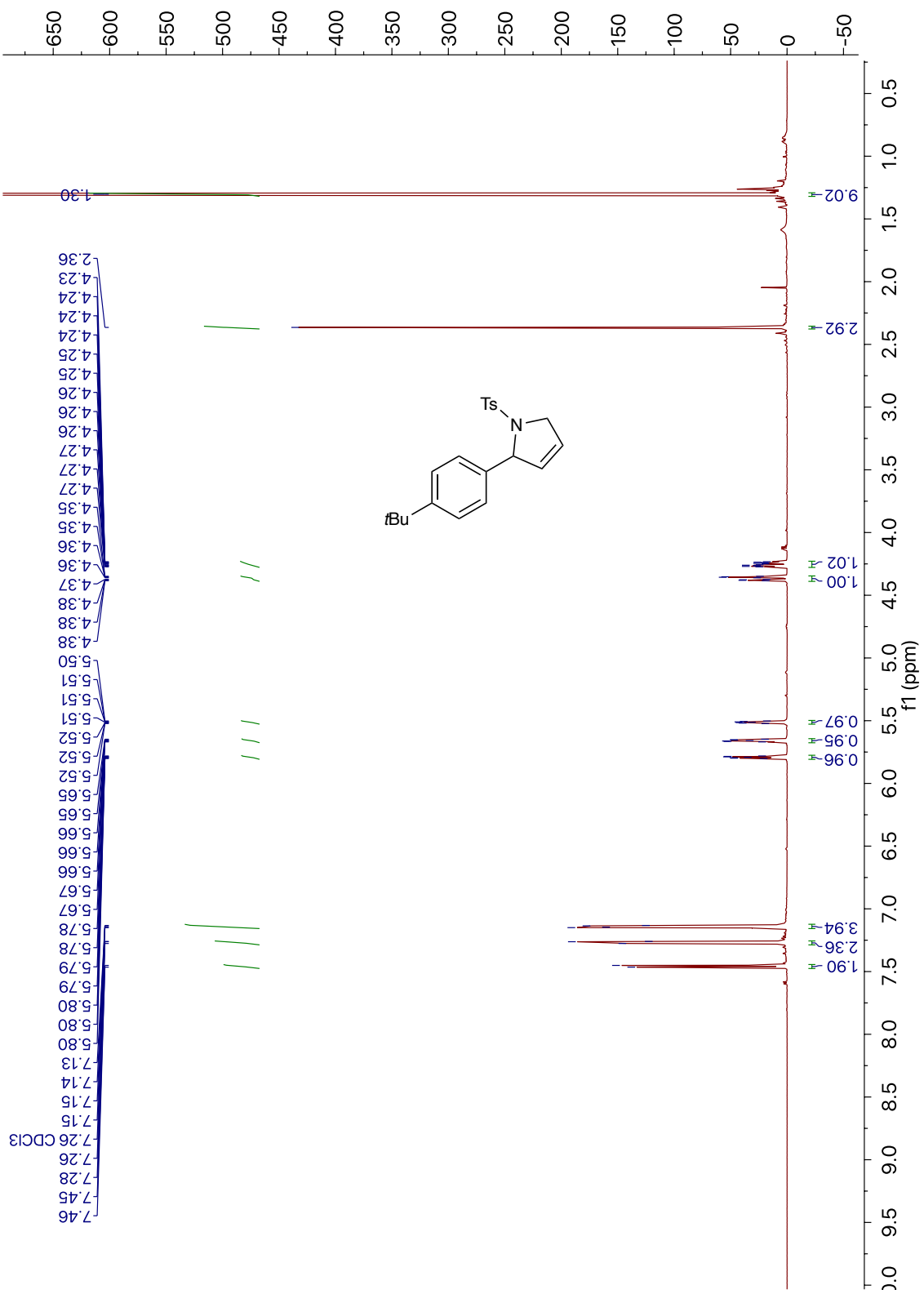

^{13}C NMR ($CDCl_3$, 126 MHz)

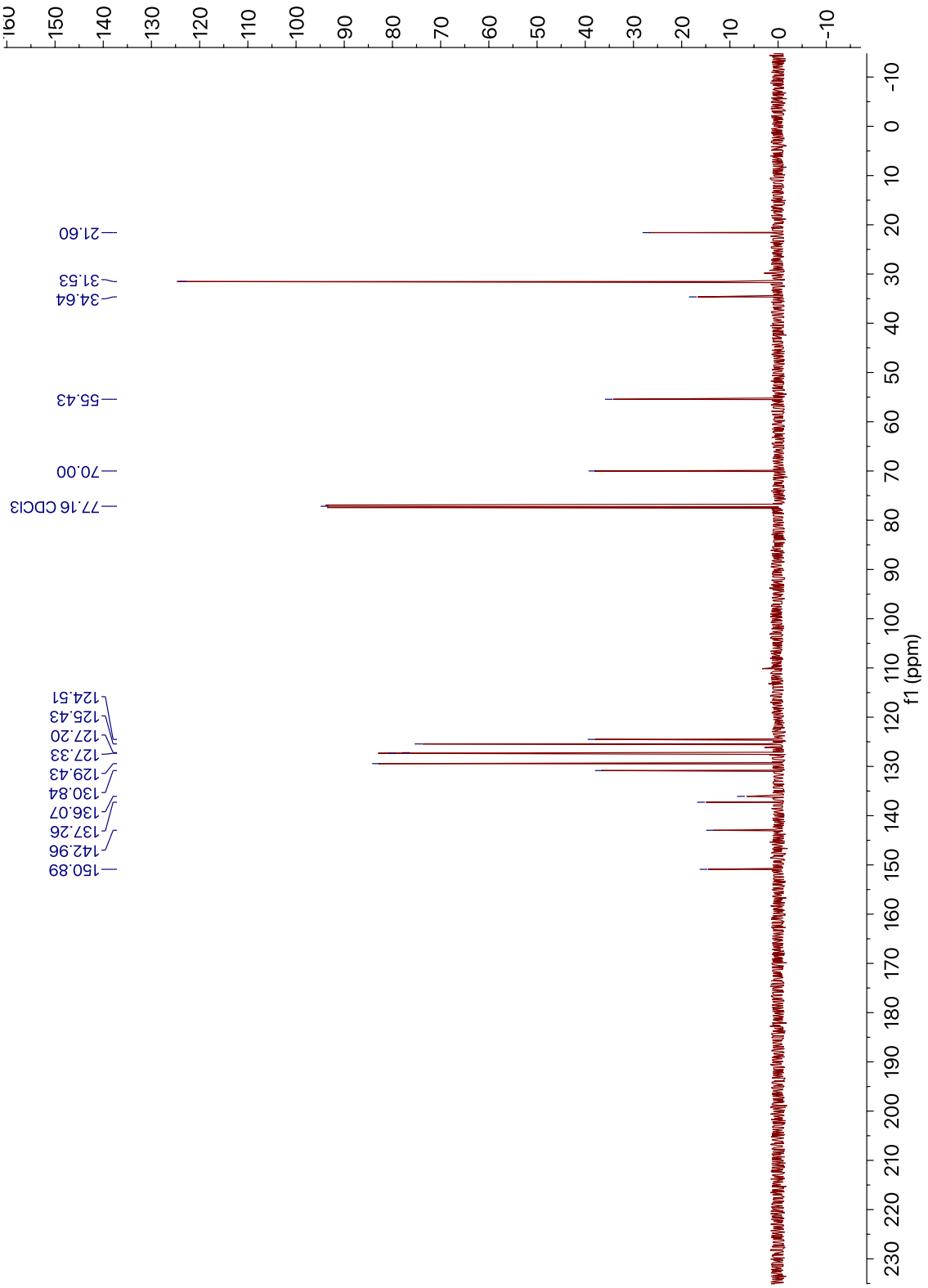

^{1}H NMR ($CDCl_3$, 400 MHz) **4-46**

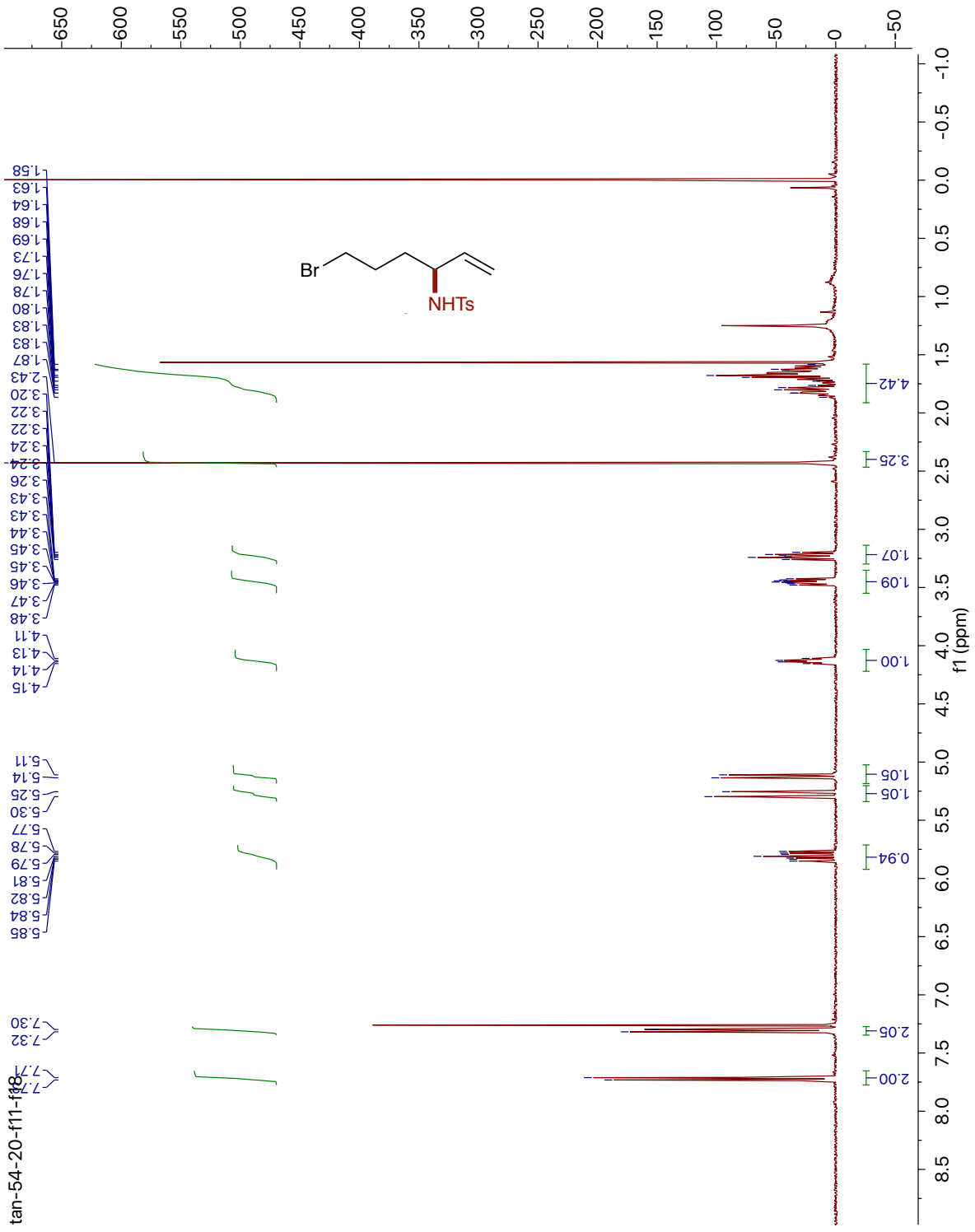

^{13}C NMR ($CDCl_3$, 151

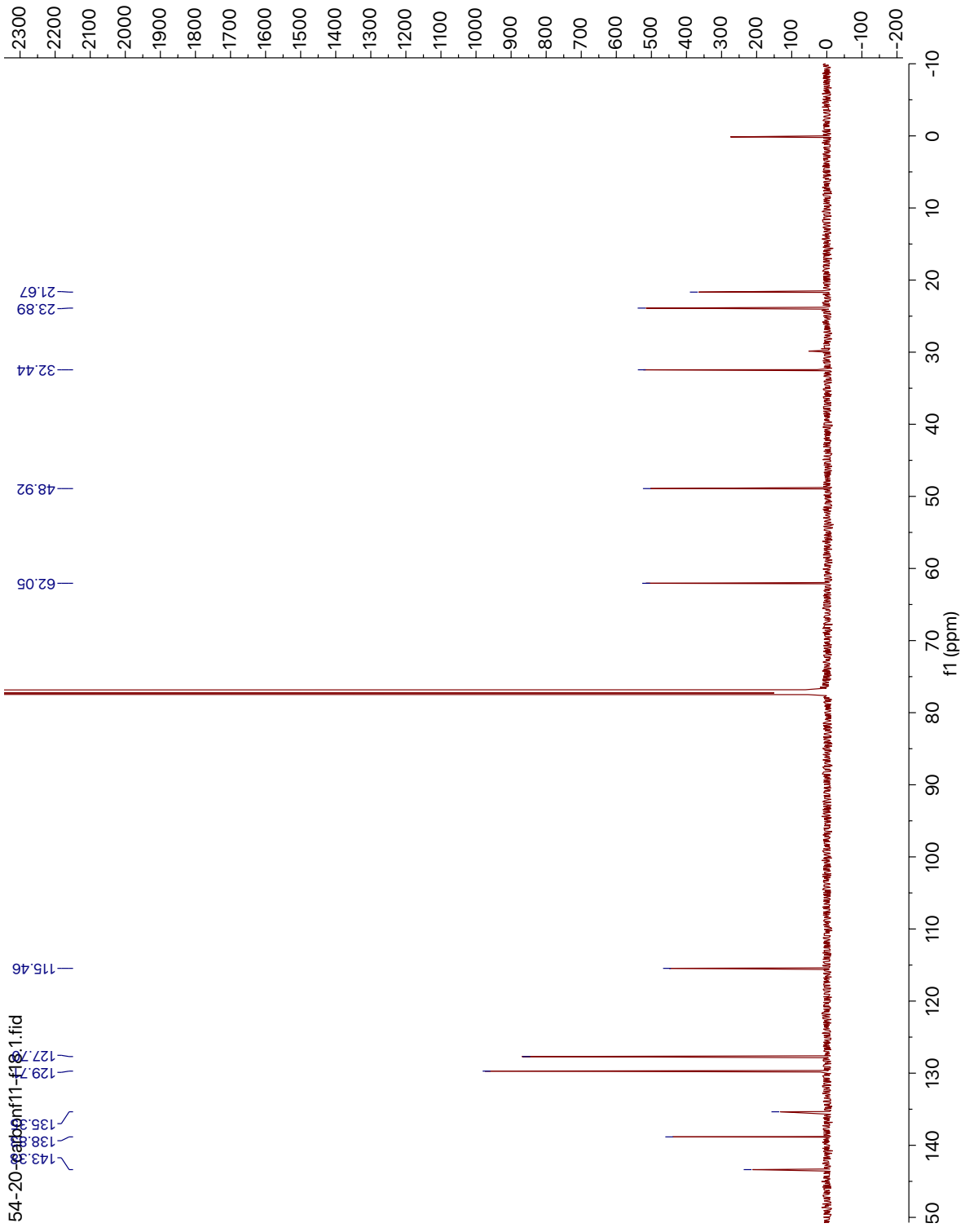

^{1}H NMR ($CDCl_3$, 400 MHz) **4-47**

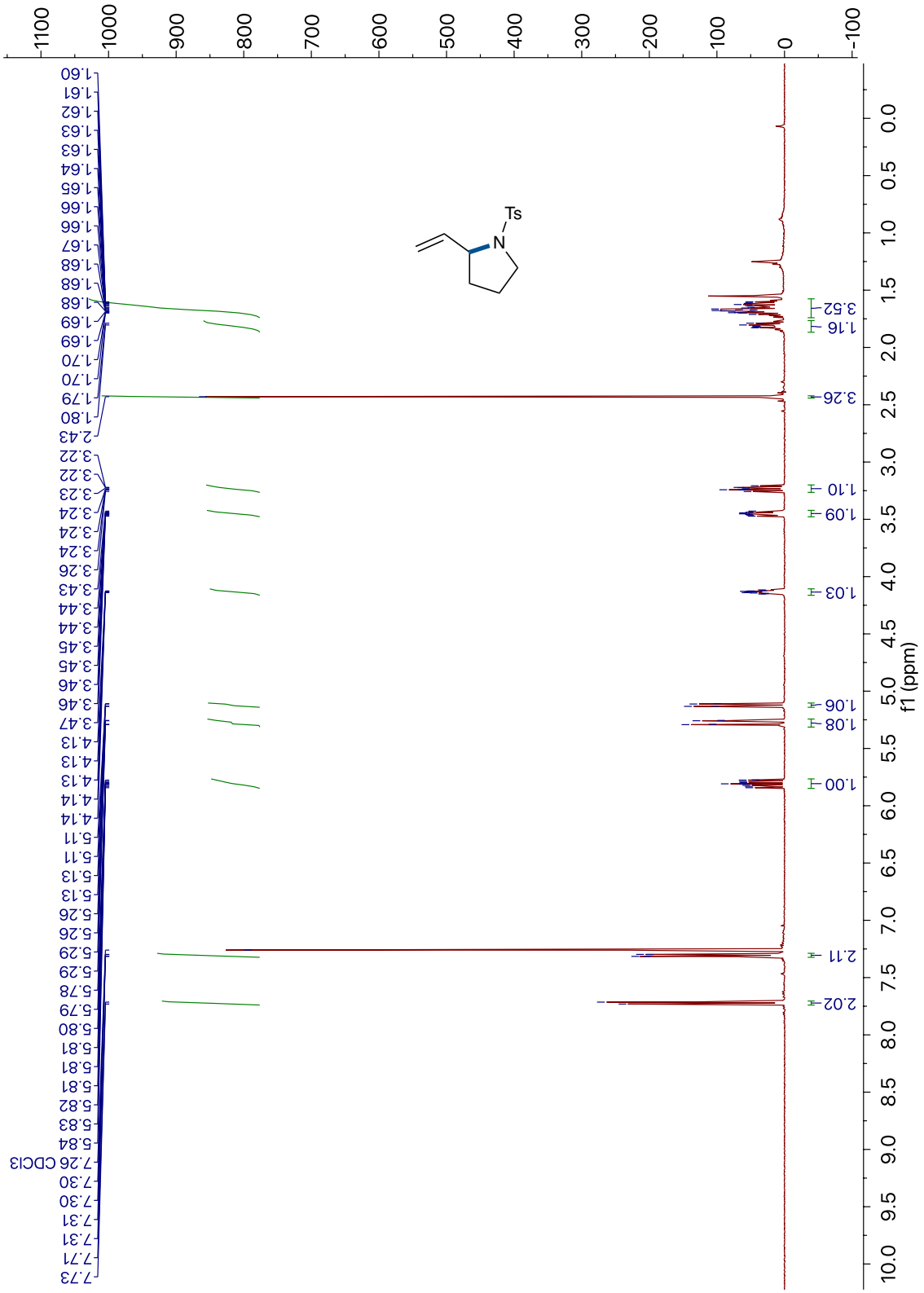

V. References

1. Harris, R. J.; Park, J.; Nelson, T. A. F.; Iqbal, N.; Salgueiro, D. C.; Bacsa, J.; Macbeth, C. E.; Baik, M.-H.; Blakey, S. B., The Mechanism of Rhodium-Catalyzed Allylic C–H Amination. *J. Am. Chem. Soc.* **2020,** *142*, 5842-5851.

2. Nelson, T. A. F.; Blakey, S. B., Intermolecular Allylic C−H Etherification of Internal Olefins. *Angew. Chem. Int. Ed.* **2018,** *57*, 14911-14915.

3. Burman, J. S.; Blakey, S. B., Regioselective Intermolecular Allylic C−H Amination of Disubstituted Olefins via Rhodium/π-Allyl Intermediates. *Angew. Chem. Int. Ed.* **2017,** *56*, 13666-13669.

4. Lerchen, A.; Knecht, T.; Koy, M.; Ernst, J. B.; Bergander, K.; Daniliuc, C. G.; Glorius, F., Non-Directed Cross-Dehydrogenative (Hetero)arylation of Allylic C(sp^3)−H bonds enabled by C−H Activation. *Angew. Chem. Int. Ed.* **2018,** *57*, 15248-15252.

5. Vásquez-Céspedes, S.; Wang, X.; Glorius, F., Plausible Rh(V) Intermediates in Catalytic C–H Activation Reactions. *ACS Catal.* **2018,** *8*, 242-257.

6. Van Vliet, K. M.; De Bruin, B., Dioxazolones: Stable Substrates for the Catalytic Transfer of Acyl Nitrenes. *ACS Catal.* **2020,** *10*, 4751-4769.

7. Park, J.; Chang, S., Comparative Catalytic Activity of Group 9 [Cp*M^{III}] Complexes: Cobalt-Catalyzed C–H Amidation of Arenes with Dioxazolones as Amidating Reagents. *Angew. Chem. Int. Ed.* **2015,** *54*, 14103-14107.

8. Burman, J. S.; Harris, R. J.; Farr, C. M. B.; Bacsa, J.; Blakey, S. B., Rh(III) and Ir(III)Cp* Complexes Provide Complementary Regioselectivity Profiles in Intermolecular Allylic C–H Amidation Reactions. *ACS Catal.* **2019,** *9*, 5474-5479.

9. Lei, H.; Rovis, T., Ir-Catalyzed Intermolecular Branch-Selective Allylic C–H Amidation of Unactivated Terminal Olefins. *J. Am. Chem. Soc.* **2019,** *141*, 2268-2273.

10. Knecht, T.; Mondal, S.; Ye, J. H.; Das, M.; Glorius, F., Intermolecular, Branch-Selective, and Redox-Neutral Cp*Ir^{III} -Catalyzed Allylic C–H Amidation. *Angew. Chem. Int. Ed.* **2019,** *58*, 7117-7121.

11. Mahesh, S.; Tang, K.-C.; Raj, M., Amide Bond Activation of Biological Molecules. *Molecules* **2018,** *23*, 2615.

12. Nishimura, S.; Wiley, J.; Sons; Knovel, *Handbook of Heterogeneous Catalytic Hydrogenation for Organic Synthesis*. Wiley: 2001.

13. Scriven, E. F. V.; Turnbull, K., Azides: their preparation and synthetic uses. *Chem. Rev.* **1988,** *88*, 297-368.

14. Ji, S.; Gortler, L. B.; Waring, A.; Battisti, A. J.; Bank, S.; Closson, W. D.; Wriede, P. A., Cleavage of sulfonamides with sodium naphthalene. *J. Am. Chem. Soc.* **1967,** *89*, 5311-5312.

15. Kazerouni, A. M.; Nelson, T. A. F.; Chen, S. W.; Sharp, K. R.; Blakey, S. B., Regioselective Cp*Ir(III)-Catalyzed Allylic C–H Sulfamidation of Allylbenzene Derivatives. *J. Org. Chem.* **2019,** *84*, 13179-13185.

16. Farr, C. M. B.; Kazerouni, A. M.; Park, B.; Poff, C. D.; Won, J.; Sharp, K. R.; Baik, M.-H.; Blakey, S. B., Designing a Planar Chiral Rhodium Indenyl Catalyst for Regio- and Enantioselective Allylic C–H Amidation. *J. Am. Chem. Soc.* **2020,** *142*, 13996-14004.

17. Lei, H.; Rovis, T., A site-selective amination catalyst discriminates between nearly identical C–H bonds of unsymmetrical disubstituted alkenes. *Nat. Chem.* **2020,** *12*, 725-731.

18. Chen, C.; Jin, S.; Zhang, Z.; Wei, B.; Wang, H.; Zhang, K.; Lv, H.; Dong, X.-Q.; Zhang, X., Rhodium/Yanphos-Catalyzed Asymmetric Interrupted Intramolecular

Hydroaminomethylation of trans -1,2-Disubstituted Alkenes. *J. Am. Chem. Soc.* **2016,** *138*, 9017-9020.

19. Grenet, E.; Waser, J., Iridium- and Rhodium-Catalyzed Directed C–H Heteroarylation of Benzaldehydes with Benziodoxolone Hypervalent Iodine Reagents. *Org. Lett.* **2018,** *20*, 1473-1476.

20. Liu, W.; Ali, S. Z.; Ammann, S. E.; White, M. C., Asymmetric Allylic C–H Alkylation via Palladium(II)/cis-ArSOX Catalysis. *J. Am. Chem. Soc.* **2018,** *140*, 10658-10662.

21. Ma, R.; White, M. C., C–H to C–N Cross-Coupling of Sulfonamides with Olefins. *J. Am. Chem. Soc.* **2018,** *140*, 3202-3205.

22. Aguila, M. J. B.; Badiei, Y. M.; Warren, T. H., Mechanistic Insights into C–H Amination via Dicopper Nitrenes. *J. Am. Chem. Soc.* **2013,** *135*, 9399-9406.

23. Prediger, P.; Barbosa, L. F.; Génisson, Y.; Correia, C. R. D., Substrate-Directable Heck Reactions with Arenediazonium Salts. The Regio- and Stereoselective Arylation of Allylamine Derivatives and Applications in the Synthesis of Naftifine and Abamines. *J. Org. Chem.* **2011,** *76*, 7737-7749.

24. Liang, Y.; Zhao, X., Enantioselective Construction of Chiral Sulfides via Catalytic Electrophilic Azidothiolation and Oxythiolation of N-Allyl Sulfonamides. *ACS Catal.* **2019,** *9*, 6896-6902.

25. Busacca, C. A.; Dong, Y., A facile synthesis of 4-aryl-2,3-dihydropyrroles. *Tetrahedron Lett.* **1996,** *37*, 3947-3950.

26. He, J.; Jia, Z.; Tan, H.; Luo, X.; Qiu, D.; Shi, J.; Xu, H.; Li, Y., Arene Trifunctionalization with Highly Fused Ring Systems through a Domino Aryne Nucleophilic and Diels–Alder Cascade. *Angew. Chem. Int. Ed.* **2019,** *58*, 18513-18518.

27. Li, Y.-G.; Li, L.; Yang, M.-Y.; He, G.; Kantchev, E. A. B., A Bulky Disulfoxide Ligand for Pd-Catalyzed Oxidative Allylic C–H Amination with 2,2,2-Trichloroethyl Tosyl Carbamate. *J. Org. Chem.* **2017,** *82*, 4907-4917.

28. Trillo, P.; Baeza, A.; Nájera, C., Fluorinated Alcohols As Promoters for the Metal-Free Direct Substitution Reaction of Allylic Alcohols with Nitrogenated, Silylated, and Carbon Nucleophiles. *J. Org. Chem.* **2012,** *77*, 7344-7354.

29. Bhanu Prasad, B. A.; Bisai, A.; Singh, V. K., 2-Aryl-N-tosylazetidines as Formal 1,4-Dipoles for [4 + 2] Cycloaddition Reactions with Nitriles: An Easy Access to the Tetrahydropyrimidine Derivatives. *Org. Lett.* **2004,** *6*, 4829-4831.

30. Xing, D.; Yang, D., Gold(I)-Catalyzed Highly Regio- and Stereoselective Decarboxylative Amination of Allylic N-Tosylcarbamates via Base-Induced Aza-Claisen Rearrangement in Water. *Org. Lett.* **2010,** *12*, 1068-1071.

31. Fukumoto, Y.; Okazaki, N.; Chatani, N., A New Class of Redox Isomerization of N-Alkylpropargylamines into N-Alkylideneallylamines Catalyzed by a $ReBr(CO)_5$/Amine N-oxide System. *Org. Lett.* **2019,** *21*, 1760-1765.

32. Mahy, J. P.; Bedi, G.; Battioni, P.; Mansuy, D., Allylic amination of alkenes by tosyliminoiodobenzene: manganese porphyrins as suitable catalysts. *Tetrahedron Lett.* **1988,** *29*, 1927-1930.

33. Donohoe, T. J.; Race, N. J.; Bower, J. F.; Callens, C. K. A., Substituted Pyrroles via Olefin Cross-Metathesis. *Org. Lett.* **2010,** *12*, 4094-4097.

34. Cochet, T.; Bellosta, V.; Roche, D.; Ortholand, J.-Y.; Greiner, A.; Cossy, J., Rhodium(III)-catalyzed allylic C–H bond amination. Synthesis of cyclic amines from ω-unsaturated N-sulfonylamines. *Chem. Commun.* **2012,** *48*, 10745-10747.

Chapter 5: Reactivity of Group (IX)Cp*-π-allyl Complexes as Putative Intermediates in Allylic C–H Arylation and Alkylation Reactions

I. Introduction

I.1. Allylic C–H Arylation Reactions

So far, the work described in this dissertation has focused on allylic C–H functionalization reactions to provide C–O and C–N bonds. One might argue that C–C bond forming reactions are the most important in organic chemistry.[1, 2] For this reason, our group turned our focus towards understanding and developing novel allylic C–C bond forming reactions. While our group was focusing on allylic C–H etherification and amination reactions, three allylic C–H arylation reactions were disclosed by the Glorius and Li groups which were proposed to proceed via a RhCp*-π-allyl intermediate.[3-5]

In 2018, the Glorius group developed an allylic C–H heteroarylation reaction proposed to proceed through a π-allyl complex (Figure 5-1**A**).[3] While much of this work was performed with thiophene nucleophiles, indoles, benzofurans, and electron-rich arenes (**5-2**) were also shown to provide product (**5-3**) in good yield with a variety of olefin coupling-partners (**5-1**). This reaction is consistent with the mechanism discussed in Chapter 3, forming the C–C bond via a Lewis-acid catalyzed allylic substitution of a transient allylic acetate. As was described in Chapter 3, this mechanistic paradigm precludes the development of an enantioselective method controlled via the metal-catalyst.[6] Furthermore, this arylation protocol is limited to electron-rich arene coupling partners, and so, a general arylation could not be developed based on this reactivity.

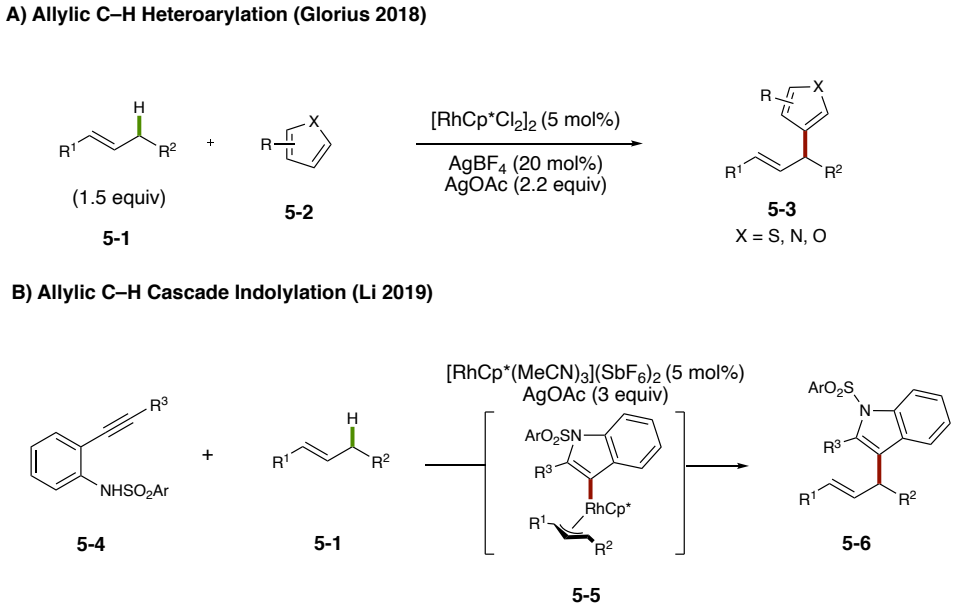

Figure 5-1. Recent Advances in Group(IX)Cp*-Catalyzed Allylic C–H Heteroarylation Reactions

Interestingly, in 2019 Li and co-workers developed a cascade indolylation reaction to form allylic indole products (**Figure 5-1B**).[5] In this example, rhodium-indole complex **5-5** is proposed to be formed through a nucleophilic cyclization of alkyne **5-4**. Subsequent π-allyl complex formation and reductive elimination is proposed to form allylic indole **5-6**. The authors first hypothesized that this reaction proceeded in two distinct steps to first form an indole via the cyclization followed by protodemetalation to form the free indole which would act as the nucleophile much like the heteroarylation developed by Glorius *et. al.*[3] However, experimental evidence suggested otherwise. Utilizing the corresponding free indole in a control experiment provided no product (**5-6**), supporting the presence of intermediate **5-5** for reactivity. Mechanistic experiments support the intermediacy of a π-allyl complex, as well

as irreversible C–H cleavage. While complex **5-5** was supported to be an intermediate in this reaction, more mechanistic studies would have to be performed to provide a complete picture.

Likewise, a general allylic C–H arylation reaction was developed by the Glorius group that same year (**Figure 5-2**).[4] The authors discovered that arylboroxine reagents could be utilized as the coupling partner for a RhCp*-catalyzed allylic C–H arylation. The main concern for developing this reaction was outcompeting a Heck-type coupling and homodimerization (**5-9**) of the aryl boron reagent. Fortunately, homodimerization could be reduced if the rate of π-allyl complex formation occurred at a faster rate than transmetallation. While homodimerization was the only productive pathway observed when boronic acids were used, utilizing boroxine reagents (**5-7**) afforded the desired product in good yield after optimization (**5-8**). A variety of boroxines were tolerated in this reaction providing arylated product in good yield (**5-10, 5-11**). Furthermore, a wide variety of internal and terminal olefins could provide product in good yield. For terminal olefins, an intriguing trend in regioselectivity was observed. In the case of neutral terminal olefins, the branched product was favored (**5-12**). On the other hand, allylbenzene type olefins provided the linear product (**5-13**), likely due to the lower energy provided from conjugation of the olefin to the aryl group. This trend in reactivity has not been observed for the previous disclosures. As a general trend, the first-generation methods proceeding via a transient allylic acetate provide linear products but when oxidizing coupling agents were used, branched products were observed. These results suggested to us that this allylic arylation reaction may be proceeding through a new mechanism entirely than the two previously reported.

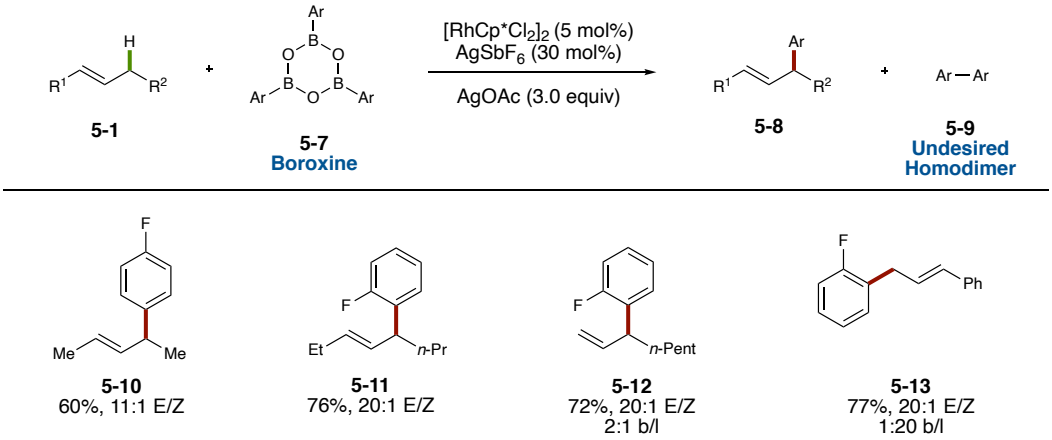

Figure 5-2. Selected Examples of Allylic C–H Arylation

I.2. Previous disclosed Allylic C–H Arylation Mechanistic Investigations

The authors performed mechanistic studies to provide further insight (**Figure 5-3**). Parallel kinetic analysis of the reactivity of **5-14** and **5-14^{D}** under standard reaction conditions revealed a primary kinetic isotope effect of 1.1. A KIE of 1.1 suggests that C–H cleavage is not the rate determining step (**Figure 5-3A**).[7] Furthermore, deuterium exchange studies were performed with a 1:1 mixture of **5-16** and deuterated **5-14^{D}**. The reaction was stopped after 1 h and the starting materials (**5-16, 5-14^{D}**) and the corresponding products (**5-17, 5-15^{D}**) were isolated and analyzed by crude ^{1}H NMR assay. No statistically significant deuterium exchange was observed, supporting irreversible C–H cleavage (**Figure 5-3B**). During the optimization of this reaction the authors found that $AgSbF_6$ lowered the observed yield of homodimer product **5-9**. Testing a short scope of silver and sodium salts and relative kinetic rates supports that the SbF_6^- counterion was responsible for lowering the formation of homodimer **5-9** and not Ag^+. Unfortunately, the authors performed no further experimental studies to parse out the full catalytic cycle.

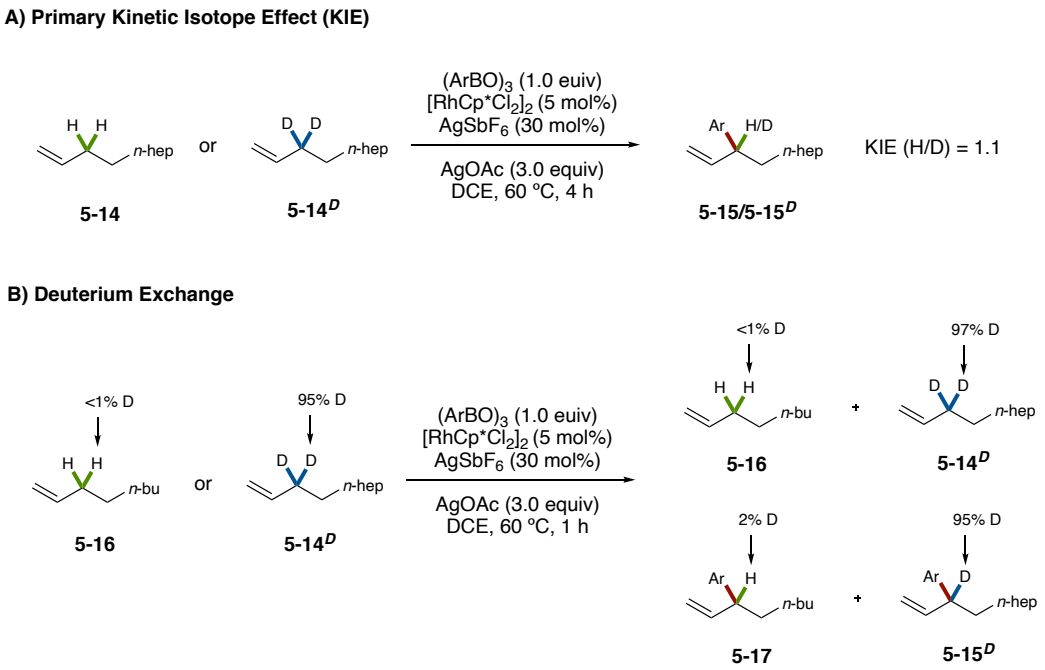

Figure 5-3. Mechanistic Investigations of Allylic C–H Arylation

While the mechanistic studies performed by Glorius did provide the necessary information to develop a general allylic C–H arylation reaction, our group desired to expand on this study. Furthermore, while arylation reactions are very useful, an allylic C–H alkylation reaction would greatly expand the overall utility of allylic C–H functionalization. Unfortunately, insufficient mechanistic studies were performed to confirm the catalytic cycle of the reaction, but the authors propose three steps (**Figure 5-4**). First, they propose activation of the allylic C–H bond to form π-allyl complex **5-18**, which, after transmetallation of the aryl boron reagent could form complex **5-19**. The authors then propose that reductive elimination of **5-19** could form product **5-8**. To test this hypothesis I set out to synthesize several group(IX)Cp*-π-allyl complexes with an aryl ligand to study the proposed direct reductive elimination. Likewise, the corresponding methyl MCp*-π-allyl complexes would

provide insight into the development of a novel allylic C–H alkylation reaction. While rhodium has been utilized for the allylic arylation reaction, we noted that the corresponding iridium complex may react in a complementary nature, and so set out to form the iridium complex counterparts.

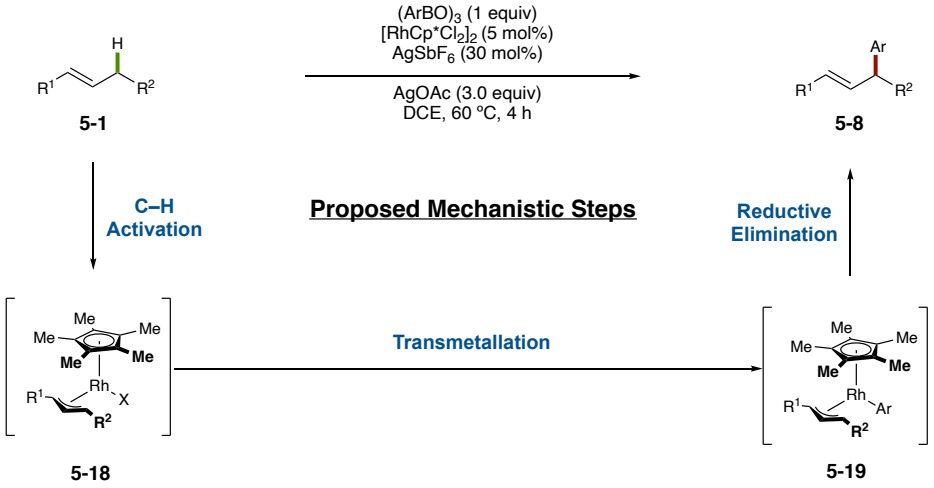

Figure 5-4. Proposed Catalytic Intermediates of the Allylic C–H Arylation Reaction by the Glorius Group

II. Results and Discussion:

II.1. Formation of MCp*-π-allyl Complexes with a Chloro Ligand

We proposed that the desired complexes could be formed from their chloro counterparts (Rh = **5-22**, Ir = **5-24**) with nucleophilic aryl and alkyl reagents. Fortunately, during our previous mechanistic investigation of the first-generation amination a reliable synthesis of MCp*-π-allyl complexes with a chloro ligand was developed.[6] Unfortunately, the average yield of complex formation was ~60%. It was determined that the reaction provided the complexes in high yields, but that the π-allyl complexes were decomposing on silica-gel

during purification. A combination of short flash column chromatography separation and crystallization was found to increase the yields observed to provide complexes **5-22** and **5-24** reliably (Figure 5-5). When $[RhCp^*(MeCN)_3][SbF_6]_2$ (1.0 equiv), 1,3-diphenylpropene (DPP, **5-21**), and CsOAc (1.0 equiv) were reacted in DCM at 40 °C for 15 h, followed by quenching with Et_4NCl, complex **5-22** was isolated in 81% yield as a dark red crystalline solid. We chose to use 1,3-diphenylpropene as the olefin precursor for a few practical reasons. This moiety would provide a means for visualization under UV light and would provide a symmetrical π-allyl complex for structural analysis. Furthermore, when the corresponding $[IrCp^*(MeCN)_3][SbF_6]_2$ was reacted under the same conditions for 19 h, followed by chloride quench, complex **5-24** was isolated in 95% yield as a bright yellow/orange solid.

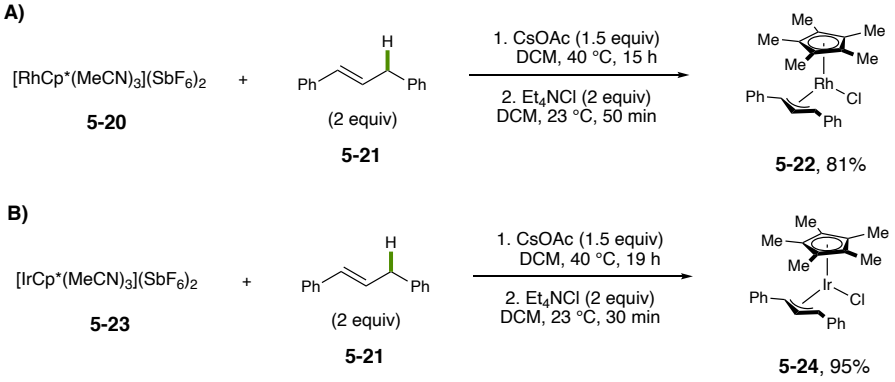

Figure 5-5. Formation Complexes 5-22 and 5-24 via C–H Activation

II.2. Formation of RhCp*-π-allyl Complexes with a Me or Ph Ligand

Now that complexes **5-22** and **5-24** could be accessed reliably, I turned my focus towards developing synthetic methods to form IrCp* and RhCp*-π-allyl complexes with a Me

or Ph ligand. Our first hypothesis was that organolithium reagents could provide the corresponding M-C bond without the need for other reactants. Fortunately, RhCp*(DPP)Cl (**5-22**) could be subjected to MeLi in THF at -78 °C for 25 min to afford RhCp*(DPP)Me (**5-25**) in 99% yield as a yellow/orange crystalline solid (**Figure 5-6A**). Furthermore, when complex **5-22** was reacted with 5 equiv of PhLi at -78 °C for 20 min and then at room temperature for 15 min, complex **5-26** could be formed in 91% yield as a yellow/orange solid (**Figure 5-6B**). We note that small quantities of biphenyl and the allylic aryl product were observed following this reaction.

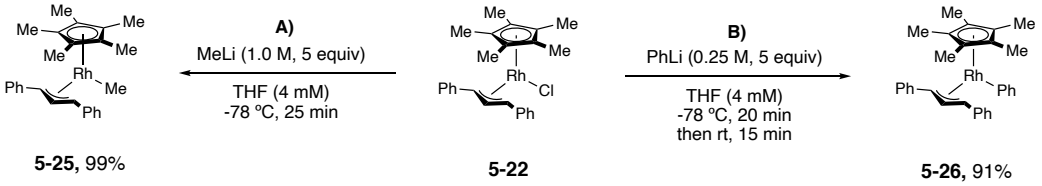

Figure 5-6. Formation of 5-25 and 5-26 from Complex 5-22

II.3. Formation of IrCp*-π-allyl Complexes with a Me or Ph Ligand

Unfortunately, the corresponding IrCp* complexes were only formed in trace yields following this standard method. In the case of IrCp*(DPP)Me (**5-31**), decomposition of the isolated product could be visually observed after exposure to air over extended periods of time. Fortunately, Bergman and co-workers had developed a method to form complex **5-28** from complex **5-27** using MeMgCl in Et_2O in a nitrogen-filled glovebox in 57% yield (**Figure 5-7A**).[8] We hypothesized that complex **5-31** could be synthesized using a similar method and purified in a nitrogen-filled glovebox to prevent decomposition. While the exact

conditions developed by Bergman did not provide IrCp*(DPP)Me (**5-31**) in good yield, reacting IrCp*(DPP)Cl (**5-24**) with MeLi in Et_2O/THF (8.5:1) in a nitrogen-filled glovebox followed by purification via a thin (2 mm) pad of silica in the glovebox afforded complex **5-31** in 67% yield as a light yellow crystalline solid (**Figure 5-7C**). Unfortunately, when this hybrid method was used to form the corresponding phenyl complex, only trace product was observed. In the same report discussed above, Bergman and co-workers also reported an unusual solvolysis of their complex **5-29** in benzene to afford the corresponding phenyl complex **5-30** in 55% yield (**Figure 5-7B**).[8] Fortunately, reacting IrCp*(DPP)Me (**5-31**) in benzene at 120 °C in a sealed tube for 4 days afforded IrCp*(DPP)Ph (**5-32**) in 87% yield as a light tan solid (**Figure 5-7D**).

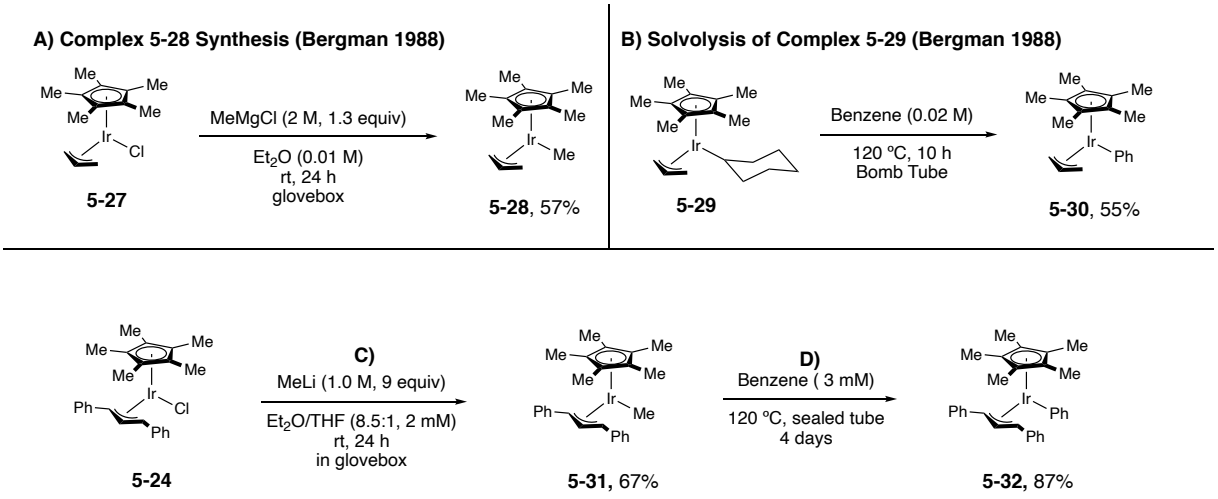

Figure 5-7. Literature Precedence and Formation of Complexes 5-31 and 5-32

II.4. Characterization of MCp*-π-allyl Complexes

Complexes **5-25, 5-26, 5-31,** and **5-32** were characterized via ^{1}H NMR, ^{13}C NMR, and single-crystal X-ray diffractometry (SC-XRD). ^{1}H NMR analysis of RhCp*(DPP)Me (**5-25**) showed a distinct triplet of doublets at δ = 5.26 ppm with coupling constants at J_{HH} = 9.9 Hz and J_{RhH} = 1.4 Hz, a doublet of doublets at δ = 3.15 ppm with coupling of J_{HH} = 10.0 Hz and J_{RhH} = 1.6 Hz, both corresponding to π-allylic protons. A doublet at δ = 0.26 ppm with hyperfine coupling of J_{RhH} = 2.5 Hz of the methyl group was also observed. Likewise, the ^{1}H NMR analysis of RhCp*(DPP)Ph (**5-26**), IrCp*(DPP)Me (**5-31**), and IrCp*(DPP)Ph (**5-32**) showed the corresponding distinct peaks with expected chemical shifts. In these cases, the hyperfine Rh-H or Ir-H coupling was not observed in the ^{1}H NMR, which we note has not always been observed for similar π-allyl complexes in the literature.[8] The rhodium and iridium coupling was observed in the ^{13}C NMR spectra of each complex. Analysis of the chemical shifts provided further insight into the electronic nature of each π-allyl complex. IrCp*(DPP)Me (**5-31**) was found to have the most electron-rich protons of the π-allyl moiety (5.06 ppm, 3.06 ppm). Rhodium complex **5-26** was determined to have the most electron-poor π-allyl moiety (5.52 ppm, 3.77 ppm). This general trend was IrCp*(DPP)Me (**5-31**) > RhCp*(DPP)Me (**5-25**) > IrCp*(DPP)Ph (**5-32**) > RhCp*(DPP)Ph (**5-26**) for the four complexes described above. While no large claims can be made from these observations, understanding the electronic nature of the complexes could provide insight into stoichiometric reactivity.

Table 5-1. Chemical Shifts and Coupling Constants for π-allyl Complexes

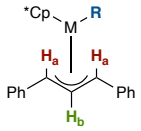

Complex	H_a (ppm)	H_b (ppm)	$J_{H/H}$ (Hz)	J_{HM} (Hz)	R (ppm)	J_{HM} (Hz)
RhCp*(DPP)Me [5-25]	5.26	3.15	9.9/10.0	1.6	0.26	2.5
RhCp*(DPP)Ph [5-26]	5.52	3.77	10.1/10.2	-	-	-
IrCp*(DPP)Me [5-31]	5.06	3.06	8.3	-	0.70	-
IrCp*(DPP)Ph [5-32]	5.42	3.67	8.7	-	-	-

II.5. Single-crystal X-Ray Diffractometry of MCp*-π-allyl Complexes

For each complex, diffraction quality crystals were obtained through slow evaporation of a concentrated DCM/hexanes solution (**5-31** under a nitrogen atmosphere). The solid-state molecular structures of the complexes (**5-25, 5-26, 5-31,** and **5-32**) were then determined by SC-XRD. RhCp*(DPP)Ph **5-26**, RhCp*(DPP)Me **5-25**, IrCp*(DPP)Ph **5-32**, and IrCp*(DPP)Me **5-31** are presented in **Table 5-2 A-E**. The M-C1 bond distances were varied amongst the complexes. Analysis of the π-allyl moiety revealed asymmetry and slight twisting from planarity of the phenyl rings of the diphenylpropene. RhCp*(DPP)Ph **5-26** has the shortest M–C1 bond distance (2.155 Å) when compared to complexes **5-25**, **5-31**, and **5-32** which favored ~2.20 Å bond distances. On the other hand, the M–C2 bond lengths were virtually identical for all four complexes at 2.11 Å. Likewise, the M–C3 bonds (~2.20 Å) were similar for the complexes, revealing a mostly symmetrical π-allyl group. This was not the case for RhCp*(DPP)Ph **5-26** whose M–C1 (2.156 Å) and M–C3 (2.203 Å) bonds were 0.048 Å different in length. As was expected, the M–Ph bond lengths were shorter than the corresponding M–Me bonds. Complexes **5-25** (2.111 Å) and **5-31** (2.124 Å) had lengths closer to 2.12 Å, while complexes **5-26** (2.060 Å) and **5-32** (2.066 Å) were ~2.06 Å. No large

claims can be made for the M–Me or M–Ph bond distances, but the short M–Ph bond lengths are consistent with the increase in s-orbital character. Likewise, the C2–M–R bond angles for the phenyl complexes were slightly larger (**5-26**, 106.05 °; **5-32**, 105.63 °) than for the methyl complexes (**5-25**, 103.84 °; **5-31**, 103.47°) likely because of the general steric differences between the two groups. One reason we chose to use 1,3-diphenylpropene as the olefin to form these complexes was because we believed the π-allyl complexes would be symmetric. While these complexes are generally symmetric, the phenyl rings of the diphenylpropene were observed to twist out of plane with the π-allyl moiety. Complexes **5-26** (1.6°, -0.5°) and **5-32** (-0.4°, 0.5°) had the lowest dihedral angles compared to complex **5-25** (-10.9°, -4.6°) and complex **5-31** (5.7 °, 12.4°). While these dihedral angles are observed in the solid-state structure, no broad claims can be made about the solution-phase structure. This structural information may provide insight into the stoichiometric reactivity of these complexes.

Table 5-2. Single-Crystal X-Ray Diffractometry Structures of π-allyl Complexes

A) Crystal Structure of Complex 5-25

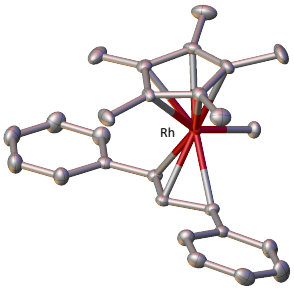

B) Representative Complex Labeled

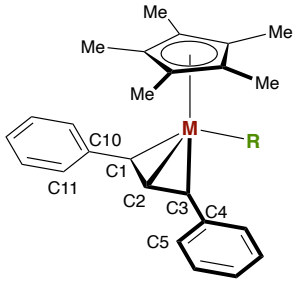

C) Crystal Structure of Complex 5-26

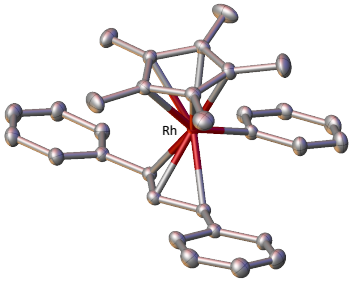

D) Crystal Structure of Complex 5-31

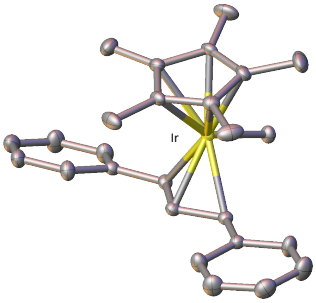

E) Crystal Structure of Complex 5-32

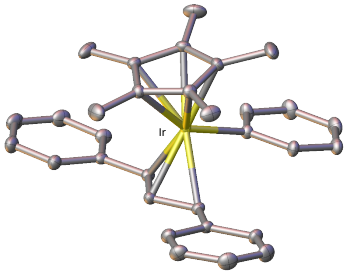

Entry	Complex	M–C1 (Å)	M–C2 (Å)	M–C3 (Å)	M–R (Å)	C2–M–R (°)	C2–C3–C4–C5 (°)	C2–C1–C10–C11(°)
1	RhCp*(DPP)Me	2.201	2.109	2.208	2.111	103.84	-10.9	-4.6
2	RhCp*(DPP)Ph	2.155	2.111	2.203	2.060	106.05	1.6	-0.5
3	IrCp*(DPP)Me	2.196	2.111	2.189	2.124	103.47	5.7	12.4
4	IrCp*(DPP)Ph	2.191	2.111	2.206	2.066	105.63	-0.4	0.5

II.6.Stoichiometric Reactivity of MCp*-π-allyl Complexes

With reliable methods to synthesize complexes **5-25**, **5-26**, **5-31**, and **5-32** and structural and electronic insight in hand, we set out to determine the reactive species via stoichiometric studies. As was described in Chapter 3, there were three possible mechanistic pathways the M(III)-π-allyl complexes could proceed to provide the reductive elimination product (**5-34**). The first of these is a M(III)/M(I) pathway. While our first-generation and

second-generation allylic C–H functionalization methods do not proceed through this mechanism, we did not rule this out as a possibility. Complexes **5-25**, **5-26**, **5-31**, and **5-32** were then dissolved in DCE and heated to 60 °C for 4 h and the crude ^{1}H NMR analyzed against an internal standard to observe any reactivity. In each case (**5-25** = 96%, **5-26** = 81%, **5-31** = 98%, **5-32** = 80%) the starting complexes were observed in significant yield and, more importantly, none of the reductive elimination products (**5-34**) were detected. Notably, the phenyl complexes **5-26** and **5-32** did decompose slightly at these elevated temperatures.

Table 5-3. Thermal Reactivity of Complexes 5-25, 5-26, 5-31, and 5-32

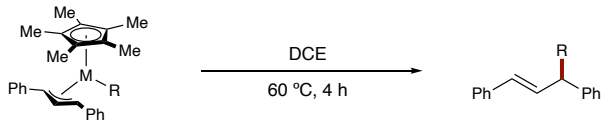

5-33 **5-34**

Entry	Complex	M	R	Complex **5-33**	**5-34**
1	**5-25**	Rh	Me	96%	-
2	**5-26**	Rh	Ph	81%	-
3	**5-31**	Ir	Me	98%	-
4	**5-32**	Ir	Ph	80%	-

Now that a M(III)/M(I) mechanistic pathway had been disproven, we hypothesized that an oxidatively induced reductive elimination may be occurring. This could be following a M(III)/M(IV)/M(II) catalytic cycle, like our first-generation report to form the C–C bond.[6] While less supported in the literature, a M(III)/M(V) mechanism could be occurring via a 2e$^-$ oxidation of the metal-center as well.[9] Luckily, both of these mechanisms could be tested by subjecting the π-allyl complexes to 1.0 equiv or 2.0 equiv of oxidant. Observation of >50%

yield of reductive elimination product with 1.0 equiv of oxidant would support the M(IV) mechanism while >50% with 2.0 equiv of oxidant suggests a M(V) intermediate.

Since complex **5-26** (RhCp*(DPP)Ph) is a proposed catalytic intermediate of the allylic C–H arylation disclosed by the Glorius group we hypothesized that corresponding allylic product would be observed via an oxidatively induced reductive elimination with a Ag(I) salt. Subjecting complex **5-26** to 1.0 equiv of $AgSbF_6$ at 60 °C in DCE resulted in consumption of starting material after 1 h and 70% yield of product **5-35** (**Figure 5-8**). To confirm a Rh(IV) oxidation, complex **5-26** was also subjected to 2.0 equiv of $AgSbF_6$ for 1 h in DCE resulting in 44% yield of product **5-35** and no recovered starting material. These two experiments support the allylic C–H arylation protocol disclosed by the Glorius group proceeds via reductive elimination of **5-35** from a Rh(IV)-π-allyl complex corresponding to **5-26.**

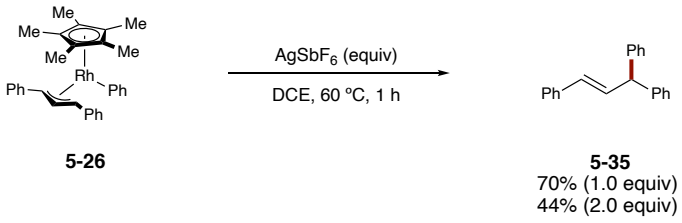

Figure 5-8. Stoichiometric Oxidation of 5-26 Supports Rh(IV) Reductive Elimination

We proposed that a corresponding alkylation reaction may proceed via complex **5-25.** For this reason, we subjected RhCp*(DPP)Me (**5-25**) to 1.0 equiv and 2.5 equiv of $AgSbF_6$ in DCE at 60 °C for 4 h with consumption of starting material observed for both reactions (**Figure 5-9**). Unfortunately, none of the expected product **5-36** was observed, but a complex

mixture of organic products was obtained. In-depth analysis of the crude ^{1}H NMR assay did reveal that an allylic product (**5-37**) was formed (1.0 equiv = 10%, 2.5 equiv = 23%). While not expected the formation of diphenylpropene dimer **5-37** is reasonable. Theoretically, **5-25** could transition to an η^1-allyl species followed by transmetallation with another **5-25** complex, but this is unclear. Regrettably, these results suggest that a rhodium-catalyzed allylic C–H alkylation proceeding through direct reductive elimination is unlikely to be developed at this time.

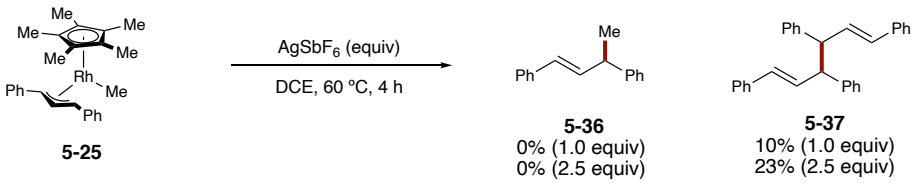

Figure 5-9. Stoichiometric Oxidation of Complex 5-25

Unexpectedly, no desired product **5-34** was detected when IrCp*(DPP)Me (**5-31**) or IrCp*(DPP)Ph (**5-32**) were oxidized with 1.0 or 2.5 equiv of $AgSbF_6$ for 4 h in DCE at 60 °C (**Table 5-4**). For all cases, none of the starting material complex was observed. In-depth analysis of the crude ^{1}H NMR assay for the reaction of complex **5-31** with $AgSbF_6$ revealed a complex mixture of products. Similarly, when complex **5-32** was reacted with $AgSbF_6$, several unidentified products were observed. While we had hoped to see productive reactivity of these complexes to form allylic products (**5-34**), this observation does provide useful information for future development. For reasons that are unclear at this time, the

iridium complexes are not reactive like their rhodium counterparts to produce allylic products.

Table 5-4. Oxidation of Complexes 5-31 and 5-32

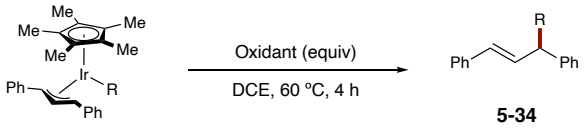

5-34

Entry	Complex	$AgSbF_6$ (equiv)	R	Recovered Complex	5-34
1	5-31	1.0	Me	-	-
2	5-31	2.5	Me	-	-
3	5-32	1.0	Ph	-	-
4	5-32	2.5	Ph	-	-

We were intrigued by the specific reactivity of RhCp*(DPP)Ph (**5-26**) and desired to understand the reactivity of this complex further. While heating complex **5-26** to 60 °C did not induce reductive elimination, we hypothesized that given enough energy this could be induced thermally. Complex **5-26** was then heated to 120 °C in DCE for 5 days in a sealed tube until no starting material could be observed by TLC analysis. Examination of the crude ^{1}H NMR spectrum resulted in the observation of **5-35** in 21% yield and **5-38** in 22% yield when compared to the internal standard. Compound **5-35** is likely formed from thermally induced reductive elimination of the Rh(III) complex **5-26**. Thermal isomerization of **5-35** to place the olefin in conjugation with the aryl groups explains the observation of **5-38** in such high yield. While not catalytically relevant, the thermal induced reductive elimination of **5-35** and **5-38** from complex **5-26** is an intriguing result.

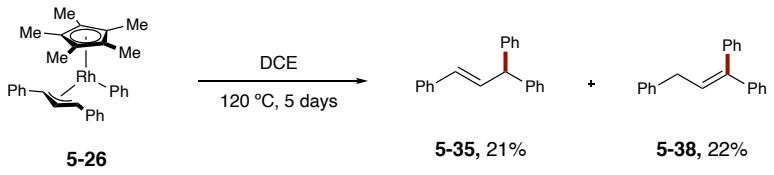

5-26 **5-35,** 21% **5-38,** 22%

Figure 5-10. Thermally Induced Reductive Elimination of Complex 5-26

II.7. Cyclic Voltammetry Studies

Since we had seen such fascinating results from the oxidation of complexes **5-25**, **5-26**, **5-31**, and **5-32**; we performed cyclic voltammetry analysis to further characterize the oxidation potentials of the complexes. Cyclic voltammetry of complex **5-25**, **5-31**, and **5-32** revealed two irreversible oxidation events which we tentatively assign to the M(III)/M(IV) and M(IV)/M(V) oxidation potentials. The two events for complex **5-25** were observed at 0.19 V and 0.91 V against Fc/Fc^{+}. The corresponding peaks for the analysis of complex **5-31** were found to be at 0.23 V and 0.85 V, while complex **5-32** had three events at 0.35 V, 0.60 V and 0.99 V. On the other hand, when complex **5-26** was analyzed via cyclic voltammetry only one oxidation event was observed at 0.33 V (**Figure 5-11,** V vs. Fc). We can tentatively assign this couple to a Rh(III)/Rh(IV) oxidation event due to our stoichiometric oxidation results. This event was isolated and scan-rate dependence studies were performed. As is expected with a chemical event coupled with an electrochemical event, the peaks showed a linear increase in current as the rate was increased. The lack of a second oxidation peak is likely due to a significant rearrangement of the complex after oxidation, which is not observed for

complexes **5-25**, **5-31**, and **5-32**. This may be why no direct reductive elimination of the corresponding C–C bond was observed from the stoichiometric oxidation of these complexes. We note that complex **5-26** was more electron-poor, asymmetric, and chemically active than the three other complexes confirming the distinct nature of this complex.

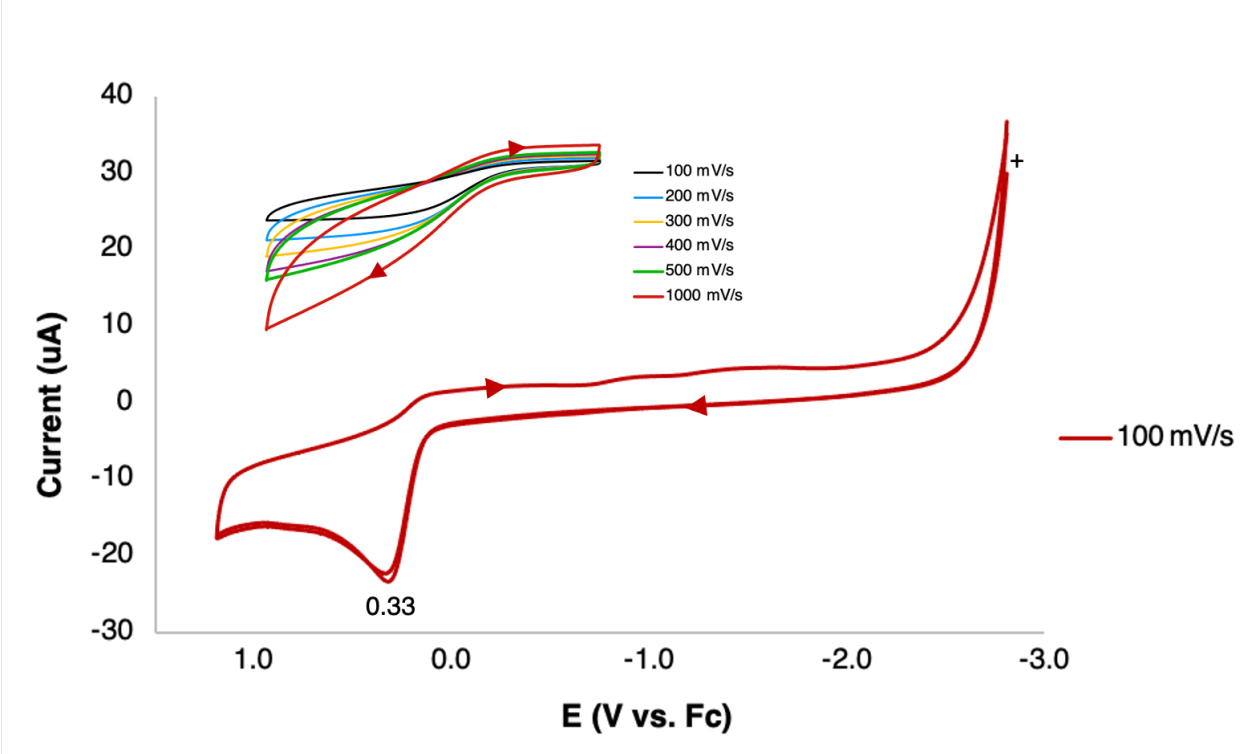

Figure 5-11. Cyclic Voltammogram of Complex 5-26 (Cyclic voltammogram recorded at room temperature in DCM (0.001 M in 0.10 M n-Bu_4NPF_6 vs. Fc/Fc^+)

II.8.<u>New Proposed Catalytic Cycle</u>

We can now propose a catalytic cycle for the allylic C–H arylation previously developed by the Glorius group. Activation of $[RhCp^*Cl_2]_2$ (**5-39**) via $AgSbF_6$ as the halide scavenger forms intermediate Rh(III)Cp* complex **5-40**. As has been discussed earlier, olefin (**5-21**) and acetate coordination followed by C–H activation results in Rh(III)Cp*-π-allyl

complex **5-42** with an open coordination site. The previous mechanistic work by Glorius suggests that this is not the rate-determining step. Transmetallation, followed by a 1e$^-$ oxidation affords Rh(IV)Cp* complex **5-26^{IV}** which we have shown reductively eliminates **5-35**. Ligand exchange and a second 1e$^-$ oxidation completes the catalytic cycle to form complex **5-40**. If π-allyl complex formation does not occur before transmetallation, dimer **5-9** is observed as an unproductive side-product via a separate catalytic cycle.

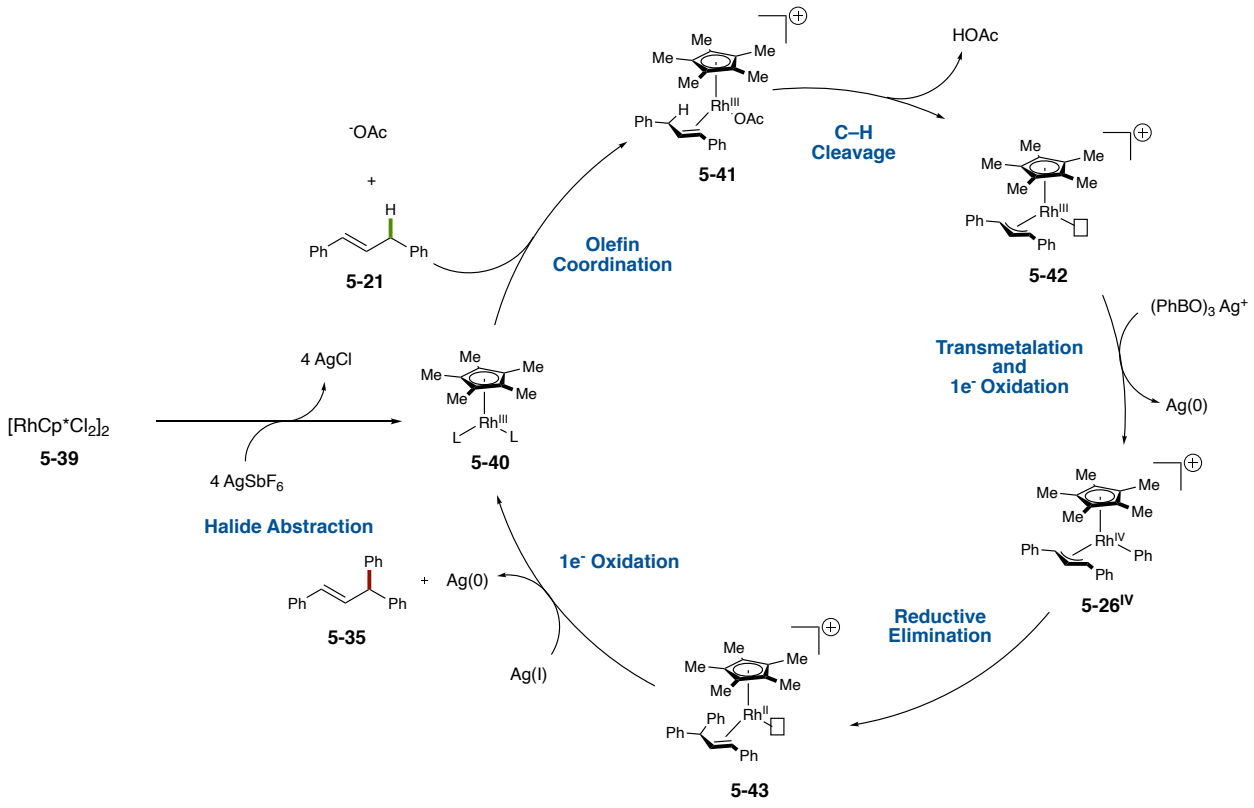

Figure 5-12. Proposed Catalytic Cycle for RhCp*-catalyzed Allylic C–H Arylation

III. Conclusion

In conclusion, we have reported the synthesis, characterization, and stoichiometric reactivity of four novel RhCp* and IrCp* π-allyl complexes with Ph or Me ligands. We confirm that direct reductive elimination is not observed thermally for any complex at 60 °C, refuting a M(III)/M(I) mechanism. Oxidation of each complex revealed that RhCp*(DPP)Ph (**5-26**) is the intermediate in a previously disclosed arylation reaction and proceeds through a Rh(III)/Rh(IV)/Rh(II) catalytic cycle. Unfortunately, RhCp*(DPP)Me **5-25**, IrCp*(DPP)Ph **5-32**, IrCp*(DPP)Me **5-31** did not afford any desired reductive elimination product under any conditions. Surprisingly when complex **5-25** was subjected to a silver(I) oxidant a diphenylpropene dimer (**5-37**) was observed in modest yield. These results suggest that an allylic C–H alkylation reaction resulting from direct reductive elimination from a MCp* metal center cannot be envisioned at this time. Furthermore, IrCp*-π-allyl Ph or Me π-allyl complexes (**5-32, 5-31**) are not stoichiometrically reactive and are, therefore, likely not catalytically active. We have confirmed a novel mechanistic paradigm that may be leveraged to afford enantioenriched products using a chiral-catalyst system. Additionally, our group has recently developed rhodium and iridium indenyl catalysts that provide excellent enantioinduction for the previously disclosed allylic C–H amidation reaction utilizing dioxazolone amidating reagents (see Chapter 4).[10] The confirmation that the previously disclosed allylic arylation reaction proceeds through direct reductive elimination suggests that an enantioselective method could be developed, possibly using these indenyl catalysts.

IV. Experimental Procedures:

IV.1. General Information:

All reactions were carried out under nitrogen atmospheres with anhydrous solvents in oven- or flame-dried glassware using standard Schlenk technique, unless otherwise stated. Anhydrous dichloromethane (DCM), diethyl ether (Et_2O), tetrahydrofuran (THF), and hexanes were obtained by passage through activated alumina using a *Glass Contours* solvent purification system. 1,2-dichloroethane (DCE) was distilled over CaH_2 and stored over activated molecular sieves in a Schlenk flask with a nitrogen atmosphere. Solvents used in a nitrogen filled glovebox were further stored over 3Å molecular sieves in standard screw-cap containers. All other reagents were obtained from commercial suppliers and used as received unless otherwise stated. $[RhCp^*(MeCN)_3][SbF_6]_2$, $[IrCp^*(MeCN)_3][SbF_6]_2$,[11] and 1,3-diphenyl-1-propene[12] were synthesized according to previously reported methods. Analytical thin layer chromatography (TLC) was performed on precoated glass backed Silicycle SiliaPure® 0.25 mm silica gel 60 plates and visualized with UV light, ethanolic *p*-anisaldehyde, or aqueous Hanessian's Stain. Flash column chromatography was performed using Silicycle SiliaFlash® F60 silica gel (40-63 μm). Preparatory TLC was performed on precoated glass backed Silicycle SiliaPure® 1.0 mm silica gel 60 plates. ^1H and ^{13}C nuclear magnetic resonance (NMR) spectra were recorded on a Varian Inova 600 spectrometer (600 MHz ^1H, 151 MHz ^{13}C), a Bruker 600 spectrometer (600 MHz ^1H, 151 MHz ^{13}C), a Varian Inova 500 spectrometer (500 MHz ^1H, 126 MHz ^{13}C), and a Varian Inova 400 spectrometer (400 MHz ^1H, 100 MHz ^{13}C) at room temperature in $CDCl_3$ with TMS (0.00 ppm for ^1H) or internal $CHCl_3$ as the reference (7.26 ppm for ^1H, 77.16 ppm for ^{13}C), unless otherwise stated.

Chemical shifts (δ values) were reported in parts per million (ppm) and coupling constants (*J* values) in Hz. Multiplicity is indicated using the following abbreviations: s = singlet, d = doublet, t = triplet, q = quartet, qn = quintet, hep = heptet, m = multiplet, b = broad signal. Infrared (IR) spectra were recorded using a Thermo Electron Corporation Nicolet 380 FT-IR spectrometer equipped with a diamond tip as a thin film. High resolution mass spectra (HRMS) were obtained using a Thermo Electron Corporation Finigan LTQFTMS (at the Mass Spectrometry Facility, Emory University). All cyclic voltammetry experiments were conducted in DCM with 0.10 M tetrabutylammonium hexafluorophosphate (electrochemical grade Sigma-Aldrich) as the supporting electrolyte in a three-S4 component cell consisting of a Pt-wire auxiliary electrode, a non-aqueous reference electrode ($Ag/AgNO_3$), and a glassy-carbon working electrode in a nitrogen-filled glove box using a CH Instruments (Austin, TX) Model 660C potentiostat. X-ray diffraction studies were carried out in the X-ray Crystallography Laboratory at Emory University on a Rigaku XtaLAB Synergy diffractometer. We acknowledge the use of shared instrumentation provided by grants from the NIH and the NSF.

IV.2. Synthesis of Complexes:

Synthesis of RhCp*(DPP)Cl (5-22):

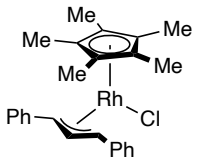

In a 100 mL three-neck round bottom flask with a reflux condenser equipped with a stir bar was added $[RhCp^*(MeCN)_3](SbF_6)_2$ (507 mg, 0.6 mmol, 1 equiv) and CsOAc (117.3 mg, 0.61 mmol, 1 equiv). The apparatus was then sealed, and the atmosphere exchanged by alternating vacuum and nitrogen 3x. Following this exchange, 30 mL of DCM was added via syringe and needle followed by addition of 1,3-diphenylpropene via microsyringe with density assumed to be 1.0 g/mL (250 µL, 1.29 mmol, 2.1 equiv). The reaction was then set to reflux and stirred for 15 hours and 22 min. The reaction was then removed from heat and allowed to cool to room temperature. In a 20 mL scintillation vial was weighed Et_4NCl (222.0 mg, 1.34 mmol, 2.2 equiv) was then dissolved in 2.6 mL DCM. The resulting Et_4NCl solution was then added to the reaction mixture and stirred for 50 min. The reaction mixture was then opened to air and filtered over celite in a syringe filter with DCM as the eluent. The resulting red/orange solution was concentrated under reduced pressure to afford a deep red residue. Purification via flash silica gel chromatography (0% Hexanes to 100% EtOAc) and crystallization from hexanes/DCM afforded complex **5-22** as a burgundy crystalline solid (231.5 mg, 0.49 mmol, 81%).

^{1}H NMR (400 MHz, $CDCl_3$) δ 7.43 (dd, J = 8.2, 1.2 Hz, 4H), 7.36 (t, J = 7.7 Hz, 4H), 7.25 – 7.17 (m, 2H), 5.44 (td, J = 11.1, 2.1 Hz, 1H), 4.96 (d, J = 11.1 Hz, 2H), 1.08 (s, 11H).

^{13}C NMR (151 MHz, $CDCl_3$) δ 139.64, 129.11, 126.42, 98.01, 97.97, 83.72, 83.68, 74.88, 74.83, 7.78.

IR (thin film, cm^{-1}): 3062.07, 3022.50, 2917.26, 1596.33, 1486.85, 1460.01, 1450.49, 1380.15, 1156.80, 1026.83, 761.70, 693.34.

HRMS (APCI): calculated $C_{25}H_{28}ClRh$ $[M+]^+$ 466.0929, found 466.0922

Synthesis of IrCp*(DPP)Cl (5-24)

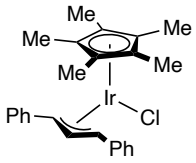

In a 50 mL three-neck round bottom flask with a reflux condenser equipped with a stir bar was added $[IrCp^*(MeCN)_3](SbF_6)_2$ (526.3 mg, 0.57 mmol, 1 equiv) and CsOAc (133.2mg, 0.69 mmol, 1.2 equiv). The apparatus was then sealed, and the atmosphere exchanged by alternating vacuum and nitrogen 3x. Following this exchange, 18 mL of DCM was added via syringe and needle followed by addition of 1,3-diphenylpropene via microsyringe with density assumed to be 1.0 g/mL (200 µL, 1.03 mmol, 1.8 equiv). The reaction was then set to reflux and stirred for 19 hours. The reaction was then removed from heat and allowed to cool to room temperature. In a 20 mL scintillation vial was weighed Et_4NCl (177.6 mg, 1.07 mmol, 1.9 equiv) was then dissolved in 2 mL DCM. The resulting Et_4NCl solution was then added to the reaction mixture and stirred for 50 min. The reaction mixture was then opened to air and filtered over celite in a syringe filter with DCM as the eluent. The resulting yellow/orange solution was concentrated under reduced pressure to afford a yellow residue. Purification via flash silica gel chromatography (0% Hexanes to 100% EtOAc) afforded complex **5-24** as a yellow crystalline solid (302.8 mg, 0.54 mmol, 95%).

^{1}H NMR (400 MHz, $CDCl_3$) δ 7.51 – 7.27 (m, 8H), 7.17 (t, *J* = 7.0 Hz, 4H), 5.74 (t, *J* = 9.7 Hz, 1H), 4.71 (d, *J* = 9.7 Hz, 2H), 1.14 (s, 15H).

^{13}C NMR (151 MHz, $CDCl_3$) δ 140.82, 128.85, 128.84, 125.93, 125.63, 92.61, 73.00, 61.63, 7.39.

IR (thin film, cm^{-1}): 3059.32, 2981.03, 3026.02, 2916.85, 1597.72, 1529.42, 1485.01, 1453.92, 1381.73, 1248.53, 1072.12, 1028.81, 912.72, 760.43, 731.62, 695.73, 658.80, 587.77, 532.25

HRMS (APCI): calculated $C_{25}H_{28}ClIr$ $[M+]^+$ 554.1480, found 554.1474

Synthesis of RhCp*(DPP)Me (5-25)

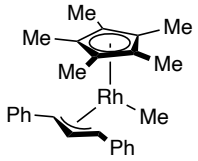

In a 15 mL oven dried vial equipped with a stir bar was weighed RhCp*(DPP)Cl **5-22** (20.1 mg, 0.04 mmol, 1 equiv). The vial was then sealed with a Teflon septa cap, and the atmosphere exchanged by alternating vacuum and nitrogen 3x. To the vial was added 10 mL of THF via syringe and needle. The vial was then submerged in a dry ice acetone bath (-78 °C) for 20 min. After this time, MeLi (1.0 M, 220 µL, 0.22 mmol, 5.5 equiv) was added via microsyringe and allowed to stir at -78 °C for 25 min. Following this time, the reaction was opened to air and quenched with 100 mL of deionized water and extracted with Et_2O (3 x 50 mL). the resulting ether solution was then washed with 100 mL of deionized water which was extracted with Et_2O (3 x 50 mL). the organic layers were combined and dried over anhydrous sodium sulfate, filtered, and concentrated under reduced pressure to afford a yellow/orange residue. Flash column chromatography (0% hexanes to 100% Et_2O) afforded complex **5-25** as a bright yellow/orange solid (19.1 mg, 0.04 mmol, 99% yield).

^{1}H NMR (600 MHz, $CDCl_3$): δ 7.30 – 7.23 (m, 4H), 7.19 (d, *J* = 8.0 Hz, 4H), 7.08 (td, *J* = 7.3, 1.2 Hz, 2H), 5.26 (t, *J* = 9.9 Hz, 1H), 3.15 (dt, *J* = 10.0, 1.6 Hz, 2H), 1.12 (s, 15H), 0.26 (dd, *J* = 2.5, 1.0 Hz, 3H).

^{13}C NMR (126 MHz, $CDCl_3$): δ 142.50, 128.70, 125.54, 124.48, 96.75 (d, *J* = 5.0 Hz), 75.77 (d, *J* = 2.5 Hz) , 63.82 (d, *J* = 12.5 Hz), 7.72, 7.71, 5.62 (d, *J* = 30.0 Hz).

IR (thin film, cm^{-1}): 3023.43, 2907.40, 2870.12, 2361.28, 2335.88, 1596.78, 1520.35, 1485.11, 1456.93, 1380.18, 1246.58, 1185.10, 1153.63, 1071.17, 1027.51, 947.07, 755.32, 692.37, 529.72

HRMS (NSI): calculated $C_{26}H_{31}Rh$ $[M+]^+$ 445.1475, found 446.1470

Synthesis of RhCp*(DPP)Ph (5-26)

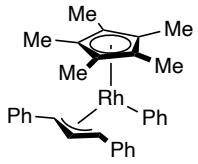

In a 15 mL oven dried vial equipped with a stir bar was weighed RhCp*(DPP)Cl **5-24** (22.5 mg, 0.048 mmol, 1 equiv). The vial was then sealed with a Teflon septa cap, and the atmosphere exchanged by alternating vacuum and nitrogen 3x. To the vial was added 10 mL of THF via syringe and needle. The vial was then submerged in a dry ice acetone bath (-78 °C) for 20 min. After this time, PhLi (0.25 M, 860 µL, 0.22 mmol, 5.5 equiv) was added via microsyringe and allowed to stir at -78 °C for 20 min. The reaction was then allowed to warm to room temperature and 2 mL of THF added to dissolve solids. After 20 min the reaction was opened to air and quenched with 100 mL of deionized water and extracted with Et_2O (3 x 50 mL). the resulting ether solution was then washed with 100 mL of deionized water

which was extracted with Et_2O (3 x 50 mL). the organic layers were combined and dried over anhydrous sodium sulfate, filtered, and concentrated under reduced pressure to afford a yellow/orange residue. Flash column chromatography in a pipette column in hexanes afforded complex **5-26** as a bright yellow/orange solid (19.8 mg, 0.039 mmol, 91% yield).

^{1}H NMR (600 MHz, $CDCl_3$): δ 7.58 (d, *J* = 7.5 Hz, 2H), 7.42 (d, *J* = 7.6 Hz, 4H), 7.35 (t, *J* = 7.7 Hz, 4H), 7.18 (t, *J* = 7.3 Hz, 2H), 7.08 (2, *J* = 7.4 Hz, 1H), 6.96 (t, *J* = 7.2 Hz, 1H), 5.52 (t, *J* = 10.1 Hz, 1H), 3.77 (d, *J* = 10.2 Hz, 2H), 1.09 (s, 15H).

^{13}C NMR (151 MHz, $CDCl_3$): δ 167.25 (d, *J* = 37.9 Hz), 141.76, 141.47, 128.93, 127.26, 125.41, 125.07, 122.07, 97.92 (d, *J* = 4.7 Hz), 78.93 (d, *J* = 5.5 Hz), 65.15 (d, *J* = 11.4 Hz), 8.30.

IR (thin film, cm^{-1}): 2965.55, 2879.27, 2361.40, 2252.45, 1671.76, 1472.69, 1385.92, 1108.74, 1034.10, 921.34, 878.01, 832.18, 738.69, 556.44

HRMS (NSI): calculated $C_{31}H_{34}RhNa$ $[M+H+Na]^+$ 532.1613 , found 532.2137

Synthesis of IrCp*(DPP)Me (5-31)

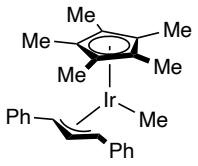

In a 20 mL oven dried vial equipped with a stir bar was weighed IrCp*(DPP)Cl **5-24** (31.2 mg, 0.058 mmol, 1 equiv) in a glove box. To the vial was added 17 mL of Et_2O and 2 mL of THF followed by MeLi (1.0 M, 700 µL, 0.7 mmol, 12 equiv). The vial was then sealed with a Teflon coated cap and allowed to stir at room temperature for 25 h. The vial was then opened, and the resulting orange solution filtered through ~2.5 inches of alumina in a pipette

filter with Et_2O as the eluent. The resulting solution was concentrated under reduced pressure to afford a yellow residue. The resulting residue was dissolved in minimal hexanes and then filtered through ~ 2mm of silica gel in a pipette filter (~8 mL, 2 fractions). The first fraction was concentrated under reduced pressure to afford **5-31** as a light yellow crystalline solid (20.2 mg, 0.038 mmol , 67%)

^{1}H NMR (400 MHz, $CDCl_3$): δ 7.26 – 7.19 (m, 4H), 7.17 (dd, *J* = 8.1, 1.3 Hz, 4H), 7.13 – 7.01 (m, 2H), 5.06 (t, *J* = 8.3 Hz, 1H), 3.06 (d, *J* = 8.3 Hz, 2H), 1.16 (s, 15H), 0.70 (s, 3H).

^{13}C NMR (150 MHz, $CDCl_3$): δ 144.06, 128.58, 125.21, 123.96, 92.23, 63.55, 50.84, 7.29, -12.27.

IR (thin film, cm^{-1}): 3021.76, 2914.82, 2875.16, 2809.90, 1597.79, 1502.36, 1479.63, 1468.33, 1461.07, 1494.18, 1452.93, 1380.51, 1028.36, 758.55, 693.73, 540.59

HRMS (APCI): calculated $C_{26}H_{31}Ir$ $[M+]^+$ 534.2026, found 534.2016

Synthesis of IrCp*(DPP)Ph (5-32)

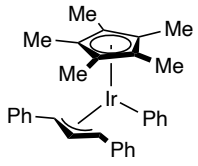

In a 7 mL side arm, sealed-tube charged with a stir bar was added IrCp*DPPMe **5-24** (6.4 mg, 0.012 mmol, 1 equiv) in a nitrogen filled glove box. 4 mL of benzene (dri-solv) was added to the sealed-tube to dissolve **5-24**. The screw valve was then attached and closed, followed by insertion of a septa on the side-arm. The tube was then removed from the glovebox and placed in a 120 °C metal heating block for 92 h (5 days). After this time the valve was opened to the side-arm and the solvent removed under reduced pressure to afford

a tan residue. The residue was dissolved in a small amount of DCM and purified via preparatory scale thin layer chromatography (hexanes, 2 passes, R_f = 0.1) afforded **5-32** as a light tan solid (5.6 mg, 0.01 mmol, 87%).

^{1}H NMR (600 MHz, $CDCl_3$): δ 7.54 (d, *J* = 7.7 Hz, 2H), 7.40 (d, *J* = 7.7 Hz, 4H), 7.32 (t, *J* = 7.6 Hz, 4H), 7.16 (t, *J* = 7.2 Hz, 2H), 7.04 (t, *J* = 7.4 Hz, 2H), 6.93 (t, *J* = 7.2 Hz, 1H), 5.41 (t, *J* = 8.7 Hz, 1H), 3.67 (d, *J* = 8.7 Hz, 2H), 1.12 (s, 15H).

^{13}C NMR (151 MHz, $CDCl_3$): δ 144.77, 143.24, 143.00, 128.84, 127.61, 125.00, 124.52, 122.02, 93.57, 67.87, 51.54, 7.95.

IR (thin film, cm^{-1}): 3045.61, 2921.98, 2851.88, 2360.87, 2336.89, 1598.15, 1152.70, 1031.29, 963.62, 758.80, 736.36, 692.74, 668.11, 538.57

HRMS (NSI): calculated $C_{31}H_{33}Ir$ $[M-H]^-$ 596.2196, found 596.2183

IV.3. Subjection of Complexes to Heat:

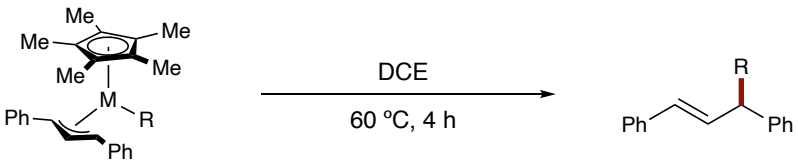

RhCp*DPPMe (5-25):

To a 4 mL oven-dried vial in a nitrogen filled glovebox was added RhCp*(DPP)Me **5-25** (1.5 mg, 3.3 μmol, 1 equiv) followed by 500 μL of DCE. The vial was capped with a Teflon lined pressure cap and placed in a 60 °C heating block. After 4 h the reaction was cooled to room temperature. To the resulting mixture was added 1.0 equiv of a 1,4-dinitrobenzene stock solution (DCM) and then filtered through a short celite plug with DCM as the eluent.

The resulting solution was concentrated under reduced pressure to afford a brown residue. The resulting brown residue was dissolved in ~500 μL of $CDCl_3$ for ^1H NMR analysis. (^1H NMR, 500 MHz, 32 scans, 5 s relation delay). The crude ^1H NMR assay revealed only starting **5-25** in 96% yield against the internal standard.

RhCp*DPPPh (5-26):

In a 4 mL oven-dried vial was weighed RhCp*(DPP)Ph **5-26** (4.8 mg) which was dissolved in 1.2 mL DCE. To a 4 mL oven-dried vial in a nitrogen filled glovebox was added 500 μL of the RhCp*(DPP)Ph solution **5-26** (2.0 mg, 3.9 μmol, 1 equiv). The vial was capped with a Teflon lined pressure cap and placed in a 60 °C heating block. After 4 h the reaction was cooled to room temperature. To the resulting mixture was added 1.0 equiv of a 1,4-dinitrobenzene stock solution (DCM) and then filtered through a short celite plug with DCM as the eluent. The resulting solution was concentrated under reduced pressure to afford a brown residue. The resulting brown residue was dissolved in ~500 μL of $CDCl_3$ for ^1H NMR analysis. (^1H NMR, 500 MHz, 32 scans, 5 s relation delay). The crude ^1H NMR assay revealed only starting **5-26** in 81% yield against the internal standard.

IrCp*DPPMe (5-31):

To a 4 mL oven-dried vial in a nitrogen filled glovebox was added IrCp*(DPP)Me **5-31** (2.9 mg, 5.4 μmol, 1 equiv) followed by 500 μL of DCE. The vial was capped with a Teflon lined pressure cap and placed in a 60 °C heating block. After 4 h the reaction was cooled to room temperature. To the resulting mixture was added 1.0 equiv of a 1,4-dinitrobenzene stock solution (DCM) and then filtered through a short celite plug with DCM as the eluent.

The resulting solution was concentrated under reduced pressure to afford a brown residue. The resulting brown residue was dissolved in ~500 μL of $CDCl_3$ for ^1H NMR analysis. (^1H NMR, 500 MHz, 32 scans, 5 s relation delay). The crude ^1H NMR assay revealed only starting **5-31** in 98% yield against the internal standard.

IrCp*DPPPh (5-32)

To a 4 mL oven-dried vial in a nitrogen filled glovebox was added IrCp*(DPP)Ph **5-32** (1.5 mg, 2.8 μmol, 1 equiv) followed by 500 μL of DCE. The vial was capped with a Teflon lined pressure cap and placed in a 60 °C heating block. After 4 h the reaction was cooled to room temperature. To the resulting mixture was added 1.0 equiv of a 1,4-dinitrobenzene stock solution (DCM) and then filtered through a short celite plug with DCM as the eluent. The resulting solution was concentrated under reduced pressure to afford a brown residue. The resulting brown residue was dissolved in ~500 μL of $CDCl_3$ for ^1H NMR analysis. (^1H NMR, 500 MHz, 32 scans, 5 s relation delay). The crude ^1H NMR assay revealed only starting **5-32** in 80% yield against the internal standard.

IV.4. Reaction of Complexes with $AgSbF_6$

RhCp*(DPP)Ph (5-26)

1.0 equiv:

In a 4 mL oven-dried vial in a nitrogen filled glovebox was weighed 2.1 mg of RhCp*(DPP)Ph **5-26** followed by addition of 525 μL of DCE to afford stock solution A. In a second 4 mL vial was added 2.8 mg of $AgSbF_6$ followed by addition of 500 μL DCE to afford stock solution B. In a third 4 mL vial was added 250 μL of stock solution A [RhCp*(DPP)Ph

(1.0 mg, 1.97 μmol, 1 equiv)], 125 μL of stock solution B [$AgSbF_6$ (0.7 mg, 2.0 μmol, 1.0 equiv)],and 125 mL of DCE (complete volume 500 μL). This third vial was sealed with a Teflon lined pressure cap and placed in a 60 °C heating block for 1 h. The reaction was then cooled to room temperature and to the resulting mixture was added 1.0 equiv of a 1,4-dinitrobenzene stock solution (DCM) and then filtered through a short celite plug with DCM as the eluent. The resulting solution was concentrated under reduced pressure to afford a brown residue. The resulting brown residue was dissolved in ~500 μL of $CDCl_3$ for ^1H NMR analysis. (^1H NMR, 500 MHz, 32 scans, 5 s relation delay). The crude ^1H NMR assay revealed product **5-35** in 70% yield against the internal standard. ^1H NMR matched those previously reported in the literature. [13]

^1H NMR (400 MHz, $CDCl_3$): δ 4.89 (d, *J*= 7.5, 1H), 6.34 (d, *J* =15.9, 1H), 6.67 (dd, *J* =15.9, 7.5, 1H), 7.16-7.39 (m, 15H)

2.0 equiv:

In a 4 mL oven-dried vial in a nitrogen filled glovebox was weighed 2.1 mg of RhCp*(DPP)Ph **5-26** followed by addition of 525 μL of DCE to afford stock solution A. In a second 4 mL vial was added 2.8 mg of $AgSbF_6$ followed by addition of 500 μL DCE to afford stock solution B. In a third 4 mL vial was added 250 μL of stock solution A [RhCp*(DPP)Ph (1.0 mg, 1.97 μmol, 1 equiv)] and 250 μL of stock solution B [$AgSbF_6$ (1.4 mg, 4.0 μmol, 2.0 equiv)] (complete volume 500 μL). This third vial was sealed with a Teflon lined pressure cap and placed in a 60 °C heating block for 1 h. The reaction was then cooled to room temperature and to the resulting mixture was added 1.0 equiv of a 1,4-dinitrobenzene stock solution (DCM) and then filtered through a short celite plug with DCM as the eluent. The resulting solution was

concentrated under reduced pressure to afford a brown residue. The resulting brown residue was dissolved in ~500 μL of $CDCl_3$ for ^1H NMR analysis. (^1H NMR, 500 MHz, 32 scans, 5 s relation delay). The crude ^1H NMR assay revealed product **5-35** in 44% yield against the internal standard.

RhCp*(DPP)Me (5-25)

1 equiv:

In a 4 mL oven-dried vial in a nitrogen filled glovebox was weighed 2.5 mg of RhCp*(DPP)Me **5-25** (5.6 μmol, 1 equiv) followed by addition of 500 μL of DCE to afford stock solution A. In a second 4 mL vial charged with a stir bar was added $AgSbF_6$ (1.3 mg, 3.8 μmol, 1 equiv) followed by addition of 500 μL of stock solution A. This second vial was sealed with a Teflon lined pressure cap and placed in a 60 °C heating block for 4 h. The reaction was then cooled to room temperature and to the resulting mixture was added 1.0 equiv of a 1,4-dinitrobenzene stock solution (DCM) and then filtered through a short celite plug with DCM as the eluent. The resulting solution was concentrated under reduced pressure to afford a brown residue. The resulting brown residue was dissolved in ~500 μL of $CDCl_3$ for ^1H NMR analysis. (^1H NMR, 500 MHz, 32 scans, 5 s relation delay). The crude ^1H NMR assay revealed product **5-37** in 10% yield against the internal standard.

2 equiv:

In a 4 mL oven-dried vial in a nitrogen filled glovebox was weighed 2.0 mg of RhCp*(DPP)Me **5-25** (4.5 μmol, 1 equiv) followed by addition of 500 μL of DCE to afford stock solution A. In a second 4 mL vial charged with a stir bar was added $AgSbF_6$ (4.0 mg, 11

μmol, 2 equiv) followed by addition of 500 μL of stock solution A. This second vial was sealed with a Teflon lined pressure cap and placed in a 60 °C heating block for 4 h. The reaction was then cooled to room temperature and to the resulting mixture was added 1.0 equiv of a 1,4-dinitrobenzene stock solution (DCM) and then filtered through a short celite plug with DCM as the eluent. The resulting solution was concentrated under reduced pressure to afford a brown residue. The resulting brown residue was dissolved in ~500 μL of $CDCl_3$ for ^1H NMR analysis. (^1H NMR, 500 MHz, 32 scans, 5 s relation delay). The crude ^1H NMR assay revealed product **5-37** in 23% yield against the internal standard.[15]

^1H NMR (400 MHz, CDCl3) δ 7.33-7.07 (m, 20H), 6.57-6.51 (m, 1H), 6.40 (d, J = 15.8 Hz, 1H), 6.34-6.28 (m, 1H), 6.20 (d, J = 15.8 Hz, 1H), 3.92-3.85 (m, 2H)

IrCp*(DPP)Ph (5-32)

1 equiv:

In a 4 mL oven-dried vial in a nitrogen filled glovebox was weighed 4.3 mg of IrCp*(DPP)Ph followed by 1 mL of DCE to afford stock solution A. In a second 4 mL vial charged with a stir bar was added $AgSbF_6$ (1.5 mg, 4.3 μmol, 1 equiv) followed by addition of 500 μL of stock solution A (**5-32**, 2.15 mg, 4.0 μmol, 1 equiv). This second vial was sealed with a Teflon lined pressure cap and placed in a 60 °C heating block for 4 h. The reaction was then cooled to room temperature and to the resulting mixture was added 1.0 equiv of a 1,4-dinitrobenzene stock solution (DCM) and then filtered through a short celite plug with DCM as the eluent. The resulting solution was concentrated under reduced pressure to afford a brown residue. The resulting brown residue was dissolved in ~500 μL of $CDCl_3$ for ^1H NMR

analysis. (^{1}H NMR, 500 MHz, 32 scans, 5 s relation delay). The crude ^{1}H NMR assay revealed no starting material or distinct products.

2.5 equiv:

In a 4 mL oven-dried vial in a nitrogen filled glovebox was weighed 4.3 mg of IrCp*(DPP)Ph **5-32** followed by 1 mL of DCE to afford stock solution A. In a second 4 mL vial charged with a stir bar was added $AgSbF_6$ (3.6 mg, 10.4 μmol, 1 equiv) followed by addition of 500 μL of stock solution A (**5-32**, 2.15 mg, 4.0 μmol, 2.5 equiv). This second vial was sealed with a Teflon lined pressure cap and placed in a 60 °C heating block for 4 h. The reaction was then cooled to room temperature and to the resulting mixture was added 1.0 equiv of a 1,4-dinitrobenzene stock solution (DCM) and then filtered through a short celite plug with DCM as the eluent. The resulting solution was concentrated under reduced pressure to afford a brown residue. The resulting brown residue was dissolved in ~500 μL of $CDCl_3$ for ^{1}H NMR analysis. (^{1}H NMR, 500 MHz, 32 scans, 5 s relation delay). The crude ^{1}H NMR assay revealed no starting material or distinct products.

IrCp*(DPP)Me (5-31)

1 equiv:

In a 4 mL oven-dried vial in a nitrogen filled glovebox was weighed 2.3 mg of IrCp*(DPP)Me **5-31** followed by 0.5 mL of DCE to afford stock solution A. In a second 4 mL vial charged with a stir bar was added $AgSbF_6$ (1.7 mg, 4.8 μmol, 1 equiv) followed by addition of 500 μL of stock solution A (**5-31**, 2.3 mg, 4.3 μmol, 1 equiv). This second vial was sealed with a Teflon lined pressure cap and placed in a 60 °C heating block for 4 h. The

reaction was then cooled to room temperature and to the resulting mixture was added 1.0 equiv of a 1,4-dinitrobenzene stock solution (DCM) and then filtered through a short celite plug with DCM as the eluent. The resulting solution was concentrated under reduced pressure to afford a brown residue. The resulting brown residue was dissolved in ~500 μL of $CDCl_3$ for ^1H NMR analysis. (^1H NMR, 500 MHz, 32 scans, 5 s relation delay). The crude ^1H NMR assay revealed no starting material or distinct products.

2.5 equiv:

In a 4 mL oven-dried vial in a nitrogen filled glovebox was weighed 2.0 mg of IrCp*(DPP)Me **5-31** followed by 0.5 mL of DCE to afford stock solution A. In a second 4 mL vial charged with a stir bar was added $AgSbF_6$ (3.2 mg, 9.0 μmol, 2.5 equiv) followed by addition of 500 μL of stock solution A (**5-31**, 2.0 mg, 3.7 μmol, 1 equiv). This second vial was sealed with a Teflon lined pressure cap and placed in a 60 °C heating block for 4 h. The reaction was then cooled to room temperature and to the resulting mixture was added 1.0 equiv of a 1,4-dinitrobenzene stock solution (DCM) and then filtered through a short celite plug with DCM as the eluent. The resulting solution was concentrated under reduced pressure to afford a brown residue. The resulting brown residue was dissolved in ~500 μL of $CDCl_3$ for ^1H NMR analysis. (^1H NMR, 500 MHz, 32 scans, 5 s relation delay). The crude ^1H NMR assay revealed no starting material or distinct products.

Thermolysis of RhCp*(DPP)Ph (5-26)

In a 7 mL side-arm sealed tube equipped with stir bar was weighed RhCp*(DPP)Ph **5-26** (2.6 mg, 5.1 μmol, 1 equiv) followed by addition on 1.0 mL DCE. The valve was tightened

and closed followed by addition of a septa to the sidearm. The sealed tube was then removed from the glovebox and placed in a 120 °C heating block for 5 days. The valve was then opened to the side-arm and 1 equiv of 1,4-dintrobenzene solution added as an internal standard. The resulting mixture was concentrated under reduced pressure resulting in a brown residue. The resulting residue was dissolved in 600 μL $CDCl_3$ and injected into an NMR with septa under nitrogen for ^1H NMR analysis (^1H NMR, 500 MHz, 32 scans, 5 s relation delay). Analysis of the crude ^1H NMR assay revealed 21% of **5-35** and 22% of **5-38**. ^1H NMR matched those previously reported in the literature.[14]

IV.5. Cyclic Voltammetry General Procedure:

All cyclic voltammetry experiments were conducted in DCM with 0.10 M tetrabutylammonium hexafluorophosphate (electrochemical grade Sigma-Aldrich) as the supporting electrolyte in a three-S4 component cell consisting of a Pt-wire auxiliary electrode, a non-aqueous reference electrode ($Ag/AgNO_3$), and a glassy-carbon working electrode in a nitrogen-filled glove box using a CH Instruments (Austin, TX) Model 660C potentiostat. All data was analyzed utilizing Fc/Fc^+ as the standard set to 0.0 V.

Complex 5-25 (RhCp*(DPP)Me)

In a 4 mL oven dried vial was weighed RhCp*(DPP)Me **5-25** (4.4 mg, 9.9 μmol). This resulting solid was dissolved and rinsed into the cell with 10 mL of a 0.10 M tetrabutylammonium hexafluorophosphate (DCM) solution (0.99 mM of **5-25**).

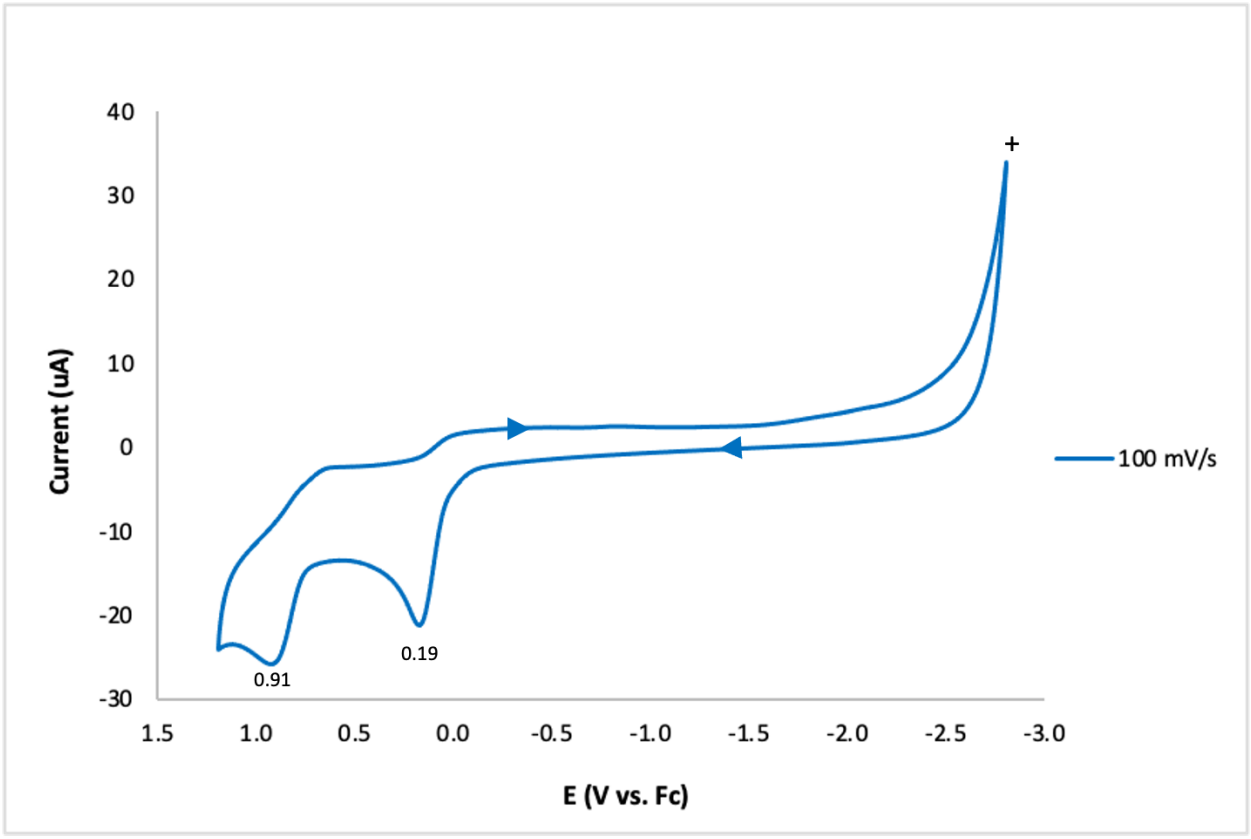

Figure 5-13. Full scan width of cyclic voltammogram 1.2 V to -2.8 V at 100 mV/s showing two quasireversible couples for Rh(III/IV) at ~0.19 V and Rh(IV/V) at ~0.91 V in DCM of 5-25.

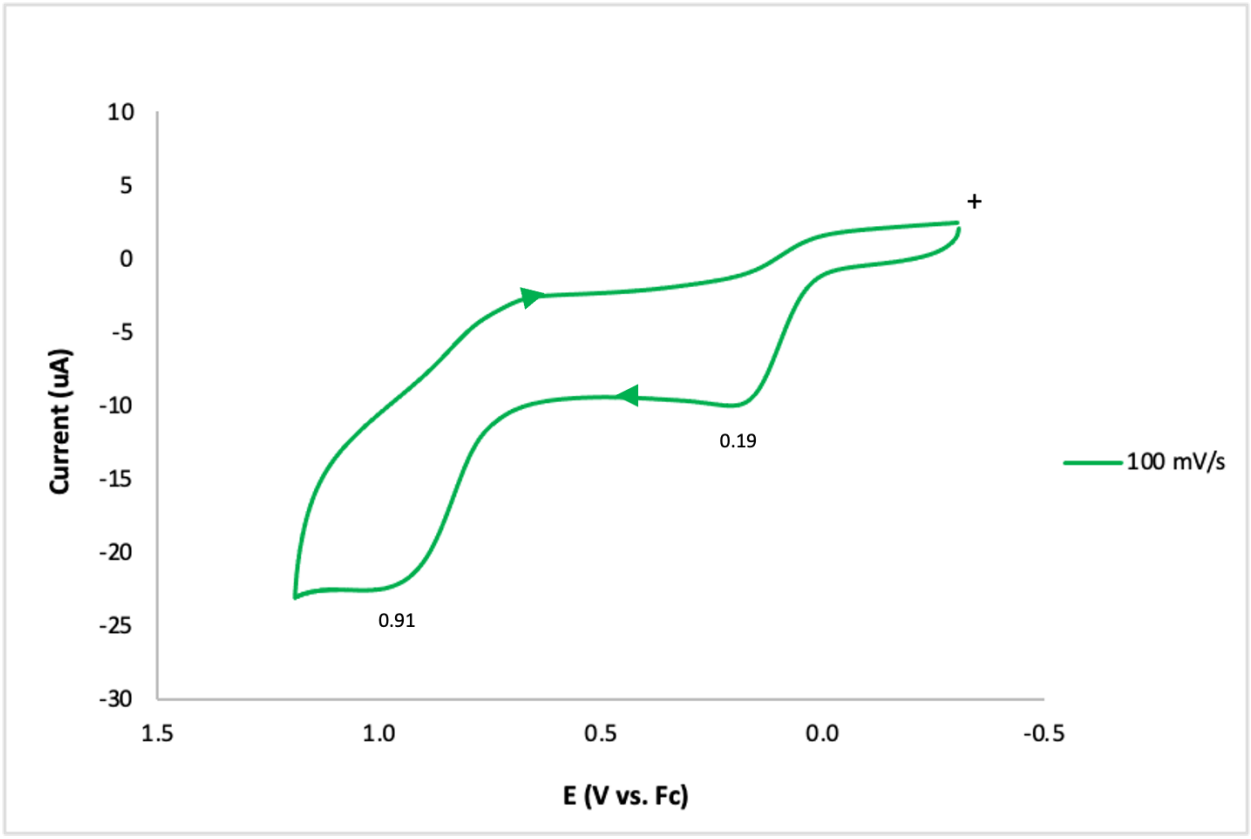

Figure 5-14. Scan width of cyclic voltammogram 1.2 V to -0.3 V at 100 mV/s showing two quasireversible couples for Rh(III/IV) at ~0.19 V and Rh(IV/V) at ~0.91 V in DCM of 5-25.

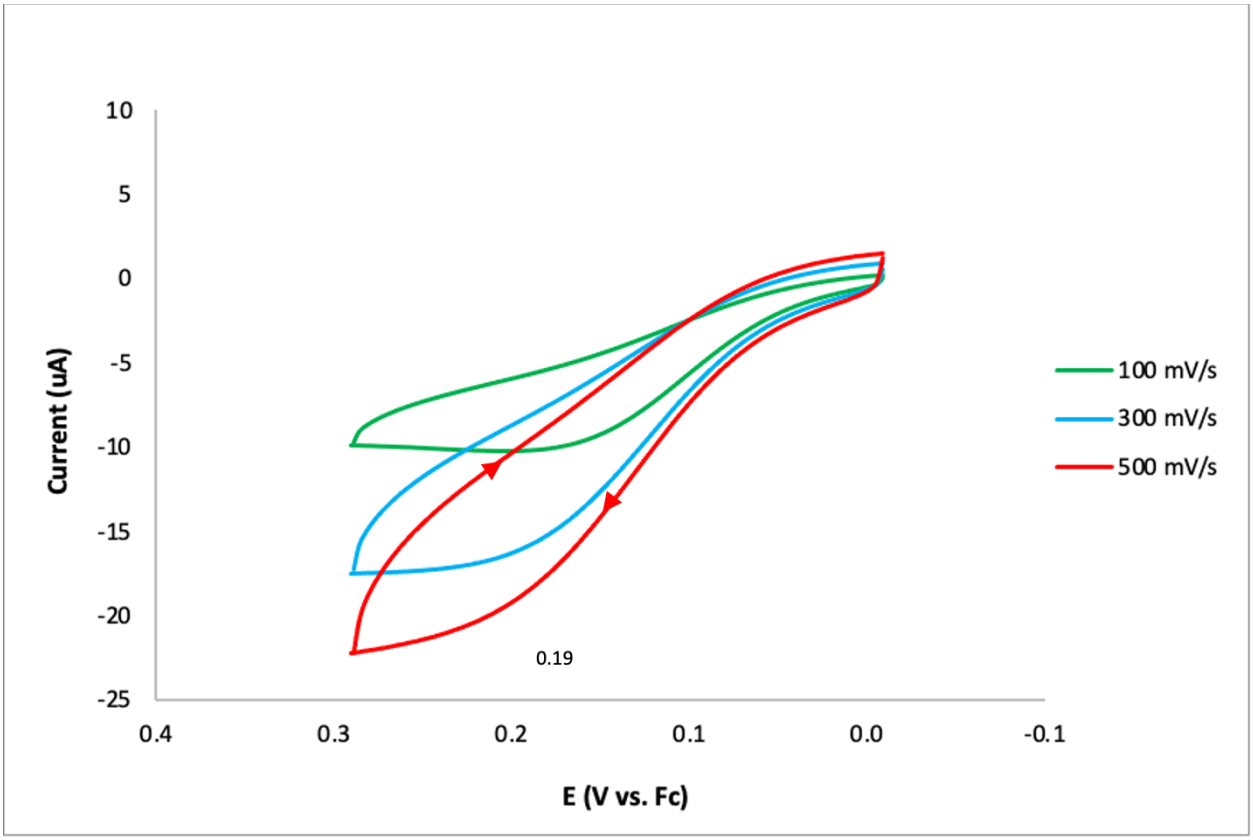

Figure 5-15. Scan width of cyclic voltammogram 0.3V to 0 V at 100 mV/s, 300 mV/s, and 500 mV/s showing one quasireversible couples for Rh(III/IV) at ~0.19 V of 5-25.

Complex 5-26 RhCp*(DPP)Ph:

In a 4 mL oven dried vial was weighed RhCp*(DPP)Ph **5-26** (5.3 mg, 10.4 μmol). This resulting solid was dissolved and rinsed into the cell with 10 mL of a 0.10 M tetrabutylammonium hexafluorophosphate (DCM) solution (1.0 mM of **5-26**).

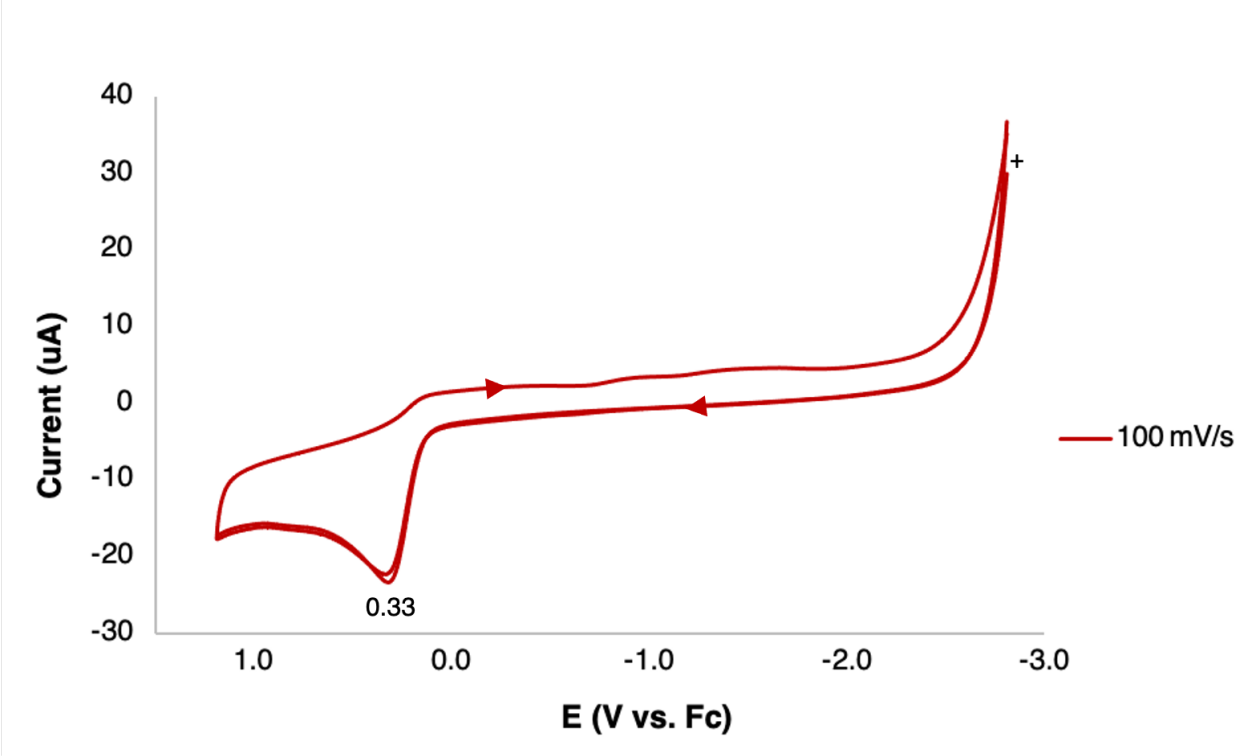

Figure 5-16 .Full scan width of cyclic voltammogram 1.2 V to -2.8 V at 100 mV/s showing one quasireversible couples for Rh(III/IV) at ~0.33 V in DCM of 5-26.

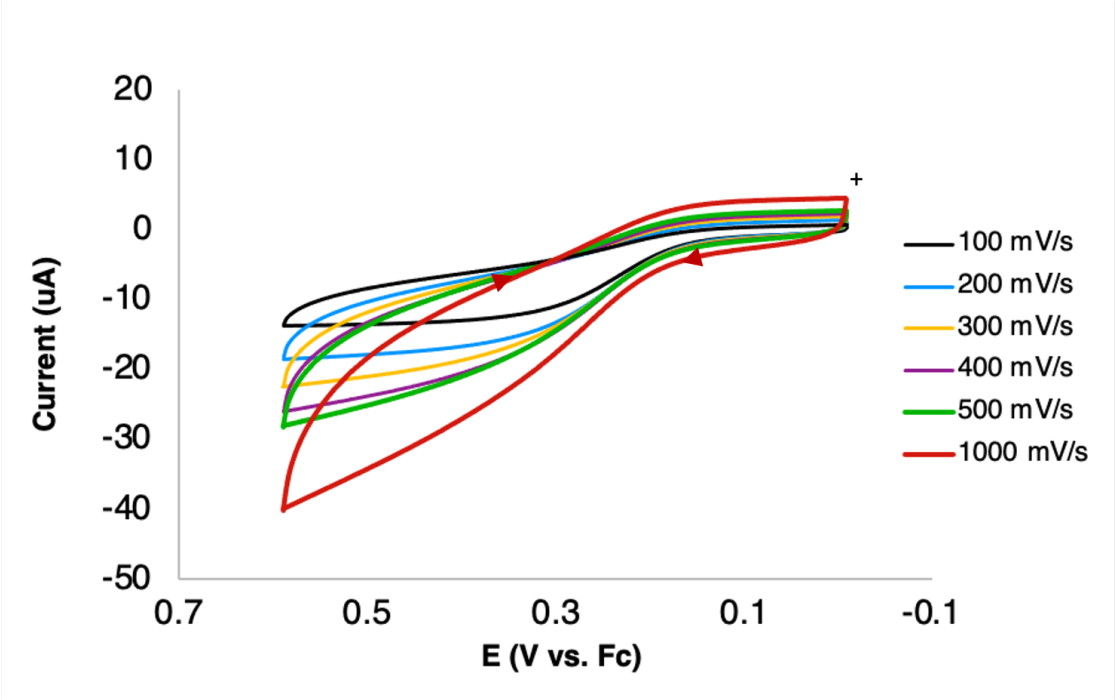

Figure 5-17. Scan width of cyclic voltammogram of proposed Rh(III/IV) couple 0.6 V to 0 V at 100 mV/s, 200 mV/s, 300 mV/s, 400 mV/s, 500 mV/s, 1000 mV/s in DCM 0f 5-26.

Complex 5-31 IrCp*(DPP)Me:

In a 4 mL oven dried vial was weighed IrCp*(DPP)Me **5-31** (6.2 mg, 11.6 μmol). This resulting solid was dissolved and rinsed into the cell with 10 mL of a 0.10 M tetrabutylammonium hexafluorophosphate (DCM) solution (1.2 mM of **5-31**).

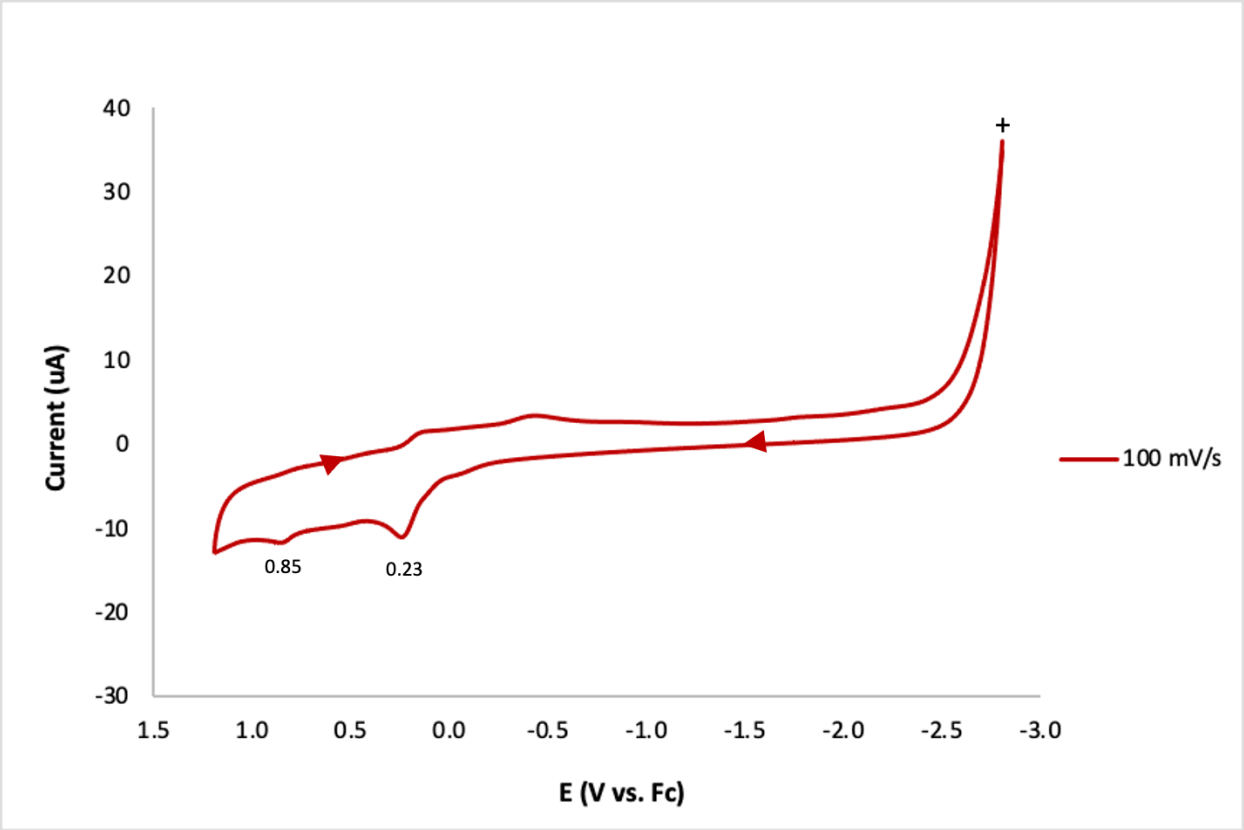

Figure 5-18. Full scan width of cyclic voltammogram 1.2 V to -2.8 V at 100 mV/s showing two quasireversible couples for Ir(III/IV) at ~0.23 V and Ir(IV/V) at ~0.85 V in DCM of 5-31.

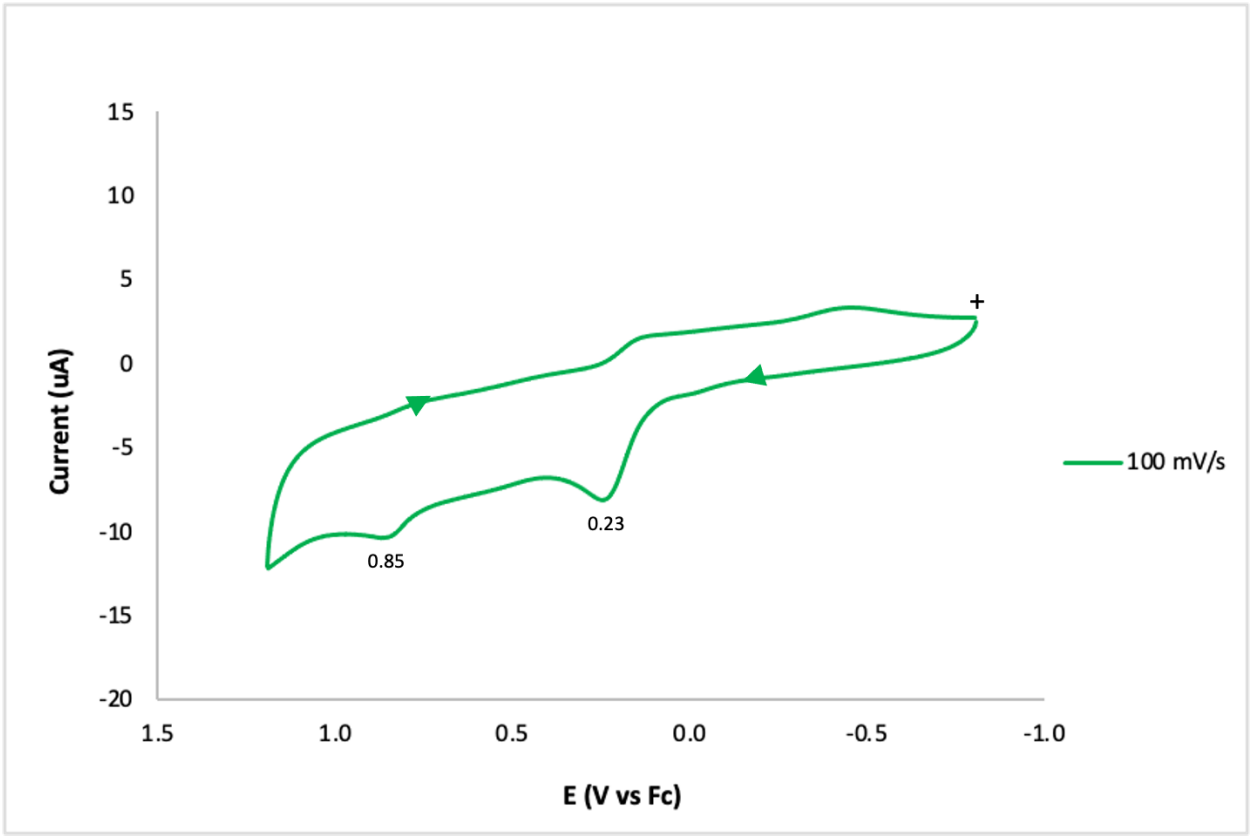

Figure 5-19. Scan width of cyclic voltammogram 1.2 V to -1.0 V at 100 mV/s showing two quasireversible couples for Ir(III/IV) at ~0.23 V and Ir(IV/V) at ~0.85 V in DCM of 5-31.

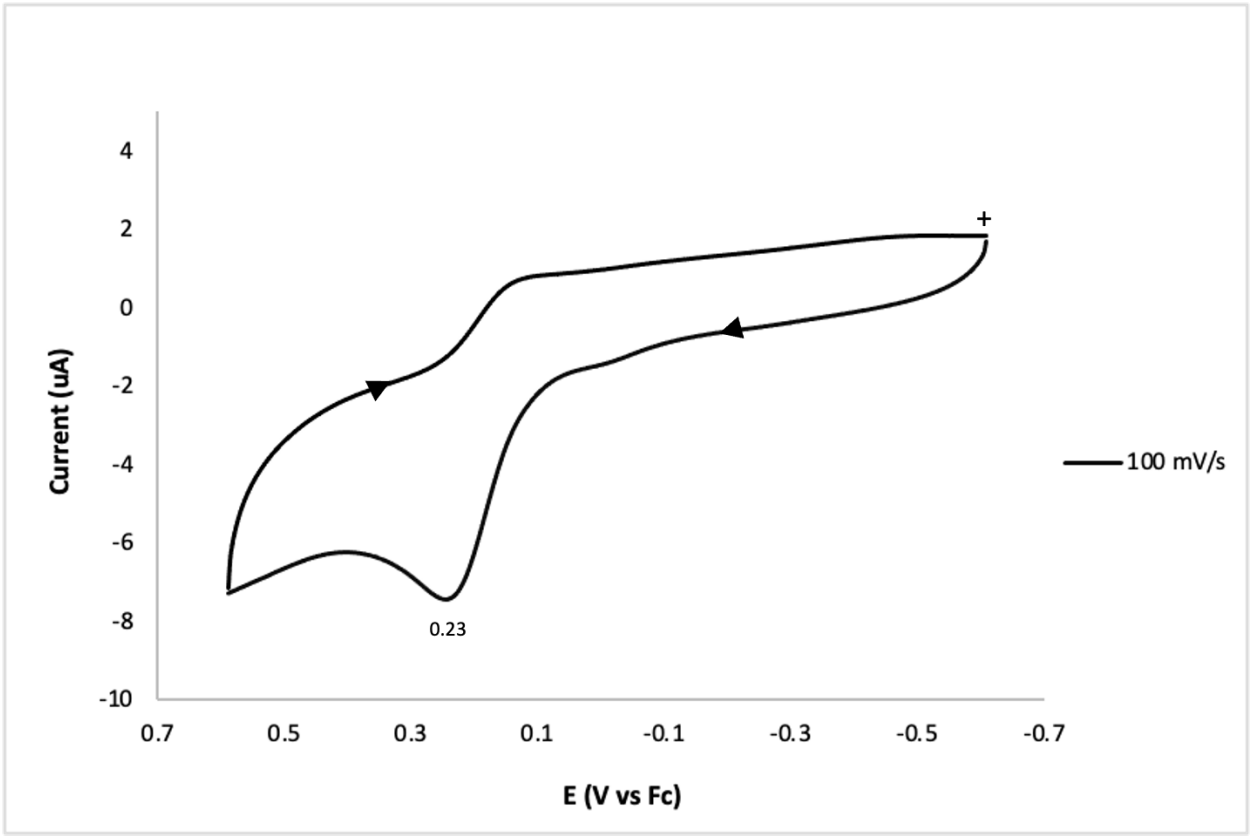

Figure 5-20. Scan width of cyclic voltammogram 1.2 V to -1.0 V at 100 mV/s showing one quasireversible couples for Ir(III/IV) at ~0.23 V in DCM of 5-31

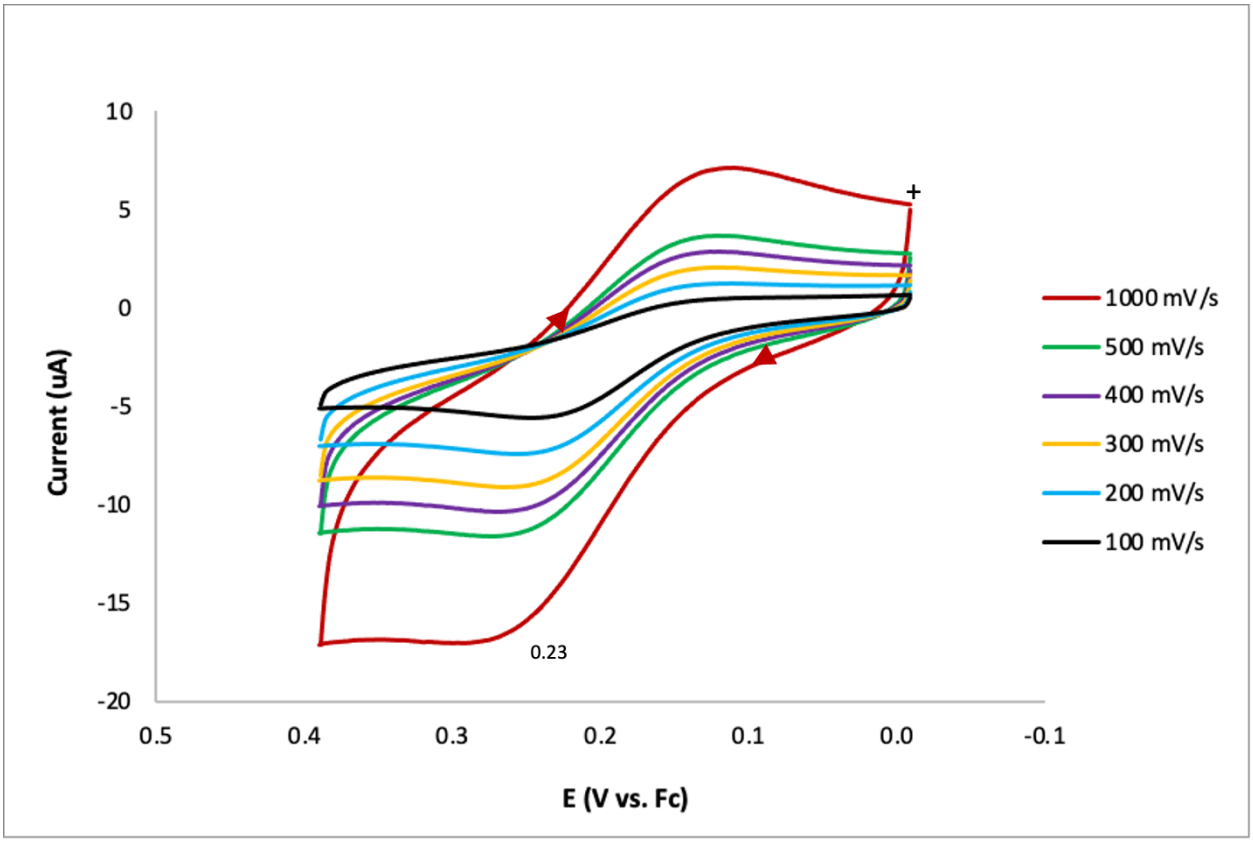

Figure 5-21. Scan width of cyclic voltammogram 0.4 V to 0.0 V at 100 mV/s, 200 mV/s, 300 mV/s, 400 mV/s, 500 mV/s, 1000 mV/ showing one quasireversible couples for Ir(III/IV) at ~0.23 V in DCM of 5-31.

Complex 5-32 IrCp*(DPP)Ph:

In a 4 mL oven dried vial was weighed IrCp*(DPP)Ph **5-32** (5.0 mg, 9.4 μmol). This resulting solid was dissolved and rinsed into the cell with 10 mL of a 0.10 M tetrabutylammonium hexafluorophosphate (DCM) solution (0.94 mM of **5-32**).

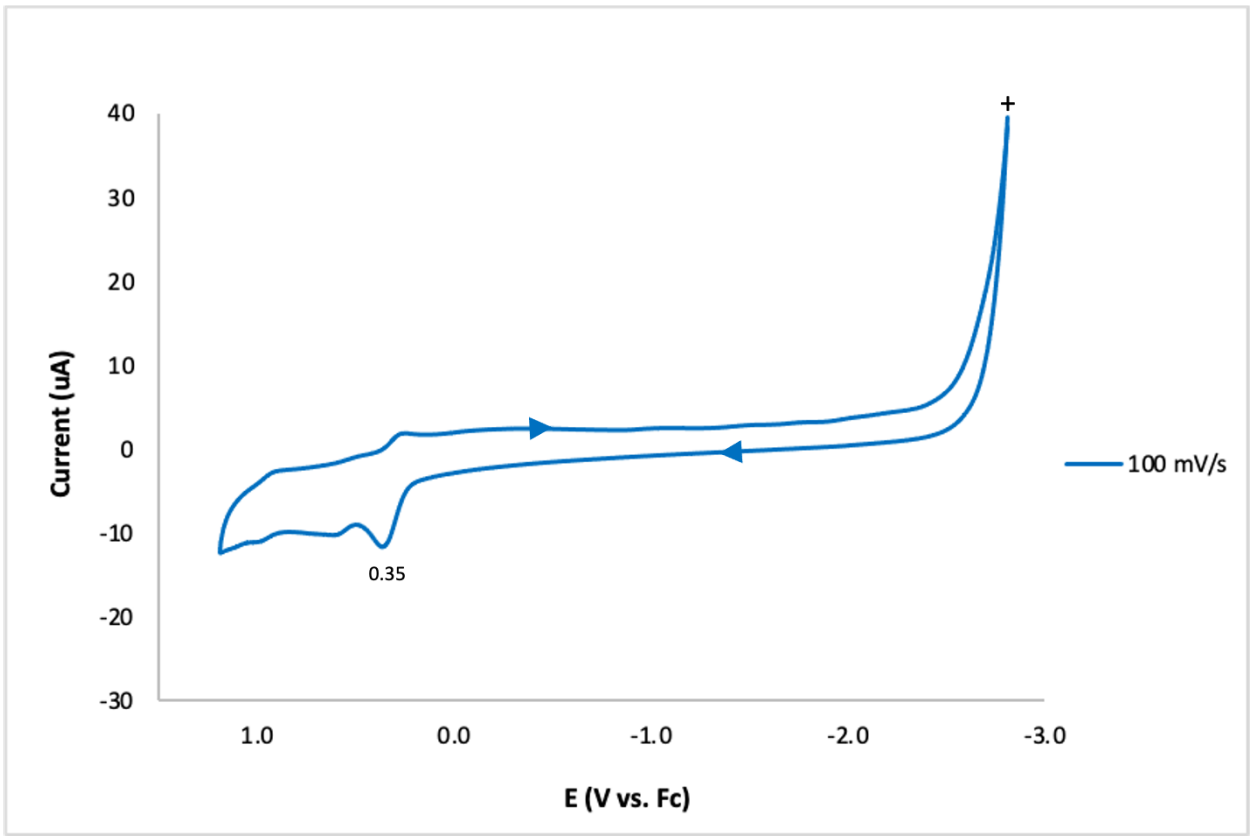

Figure 5-22. Full scan width of cyclic voltammogram 1.2 V to -2.8 V at 100 mV/s showing one quasireversible couple at ~0.35 V in DCM of 5-32.

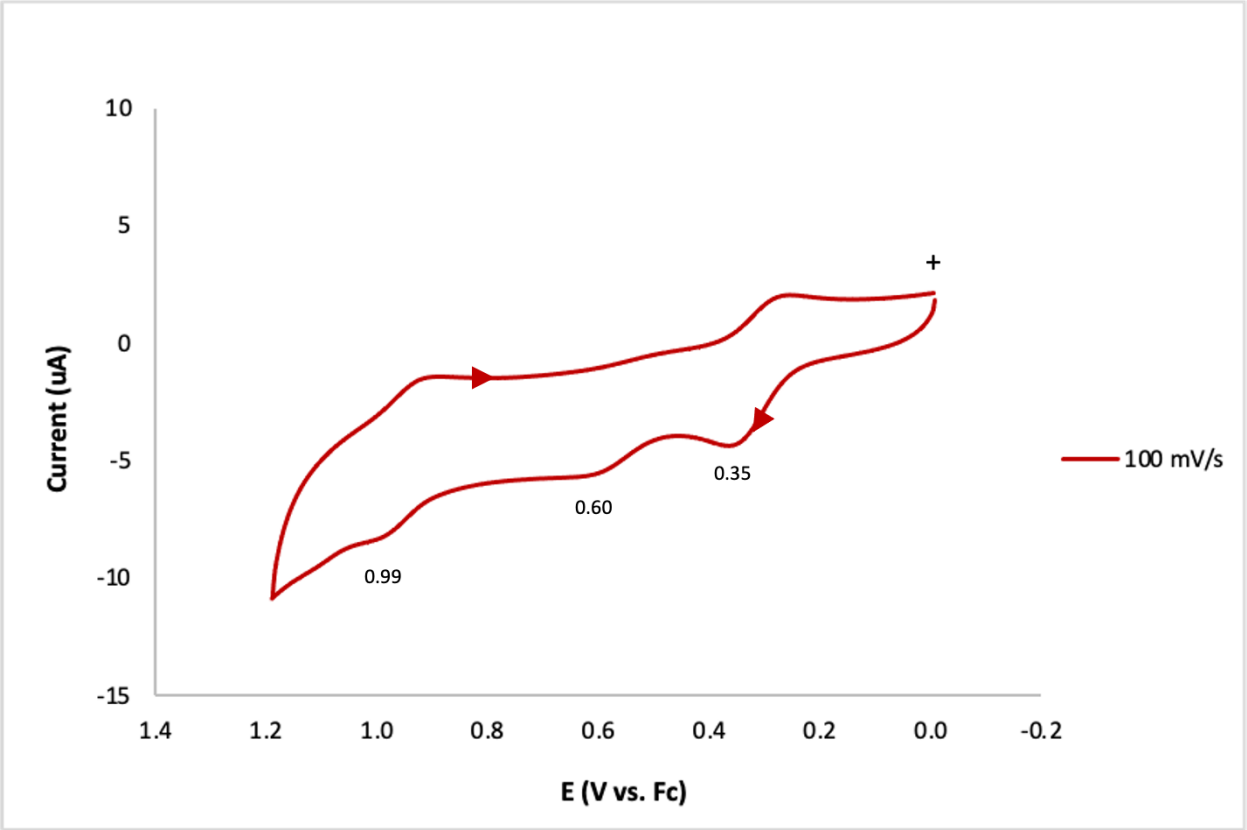

Figure 5-23.Scan width of cyclic voltammogram 1.2 V to 0.0 V at 100 mV/s showing three quasireversible couples at ~0.35 V, ~0.60 V, ~0.99 V in DCM.

IV.6. Crystallography:

Complex 5-25 RhCp*(DPP)Me:

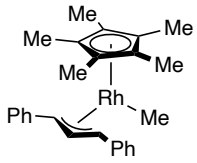

5-25

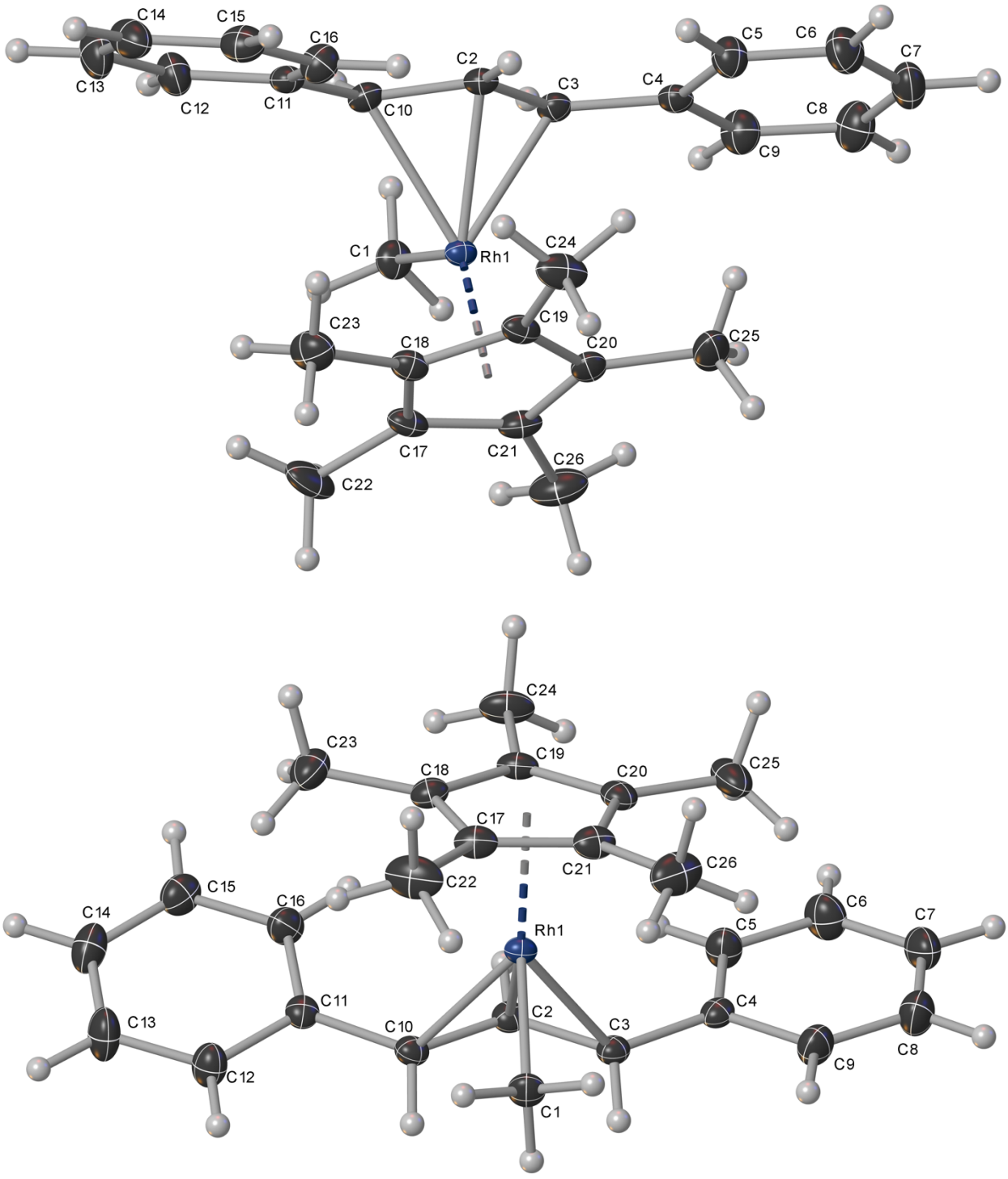

Crystal data for 5-25: $C_{26}H_{31}Rh$, Formula weight M = 446.42, orange prism, 0.44 x 0.352 x 0.146 mm^3, orthorhombic, space group *Pbca* (No. 61), a = 14.13714(16), b = 16.9303(2), c =

17.6178(2) Å, V = 4216.75(9) Å^3, Z = 8, D_c = 1.406 g cm^{-3}, F_{000} = 1856, XtaLAB Synergy-S Diffractometer, MoKα radiation, λ = 0.71073 Å, T = 99.97(10) K, $2\theta_{max}$ = 66.3°, 106458 reflections collected, 8037 unique (R_{int} = 0.0682). Final $GooF$ = 1.149, $R1$ = 0.0349, $wR2$ = 0.0824, R indices based on 7237 reflections with $I > 2\sigma(I)$ (refinement on F^2), 245 parameters, 389 restraints. Lp and absorption corrections applied, μ = 0.817 mm^{-1}.

Crystal data and structure refinement for 5-25.

Identification code	5-25	
Empirical formula	$C_{26}H_{31}Rh$	
Formula weight	446.42	
Temperature (K)	99.97(10)	
Wavelength (Å)	0.71073	
Crystal system	orthorhombic	
Space group	*Pbca*	
Unit cell dimensions (Å, °)	a = 14.13714(16)	α = 90
	b = 16.9303(2)	β = 90
	c = 17.6178(2)	γ = 90
Volume (Å)	4216.75(9)	
Z	8	
Calculated density (g cm^{-3})	1.406	
Absorption coefficient (mm^{-1})	0.817	
F_{000}	1856	
Crystal size (mm^3)	0.44 × 0.352 × 0.146	
θ range for data collection (°)	2.204 to 33.142	
Miller index ranges	$-21 \le h \le 21$, $-26 \le k \le 26$, $-27 \le l \le 27$	
Reflections collected	106458	

Independent reflections	8037 [R_{int} = 0.0682]
Completeness to θ_{max} (%)	1.000
Max. and min. transmission	0.369 and 1.000
Refinement method	Full-matrix least-squares on F^2
Data / restraints / parameters	8037 / 389 / 245
Goodness-of-fit on F^2	1.149
Final R indices [$I > 2\sigma(I)$]	$R1$ = 0.0349, $wR2$ = 0.0824
R indices (all data)	$R1$ = 0.0389, $wR2$ = 0.0838
Extinction coefficient	0.00024(8)
Largest diff. peak and hole (e Å^{-3})	1.170 and -1.641

Table 5-5. Atomic coordinates of 5-25

Atomic coordinates (x 10^4) and equivalent isotropic displacement parameters (Å^{2}x 10^3) for 5-25. U(eq) is defined as one third of the trace of the orthogonalized U^{ij} tensor.

	x	y	z	U(eq)
Rh(1)	6524(1)	7030(1)	6488(1)	13(1)
C(2)	5546(1)	6090(1)	6456(1)	16(1)
C(3)	5397(1)	6471(1)	7162(1)	16(1)
C(4)	5580(1)	6082(1)	7897(1)	17(1)
C(19)	7939(1)	6390(1)	6478(1)	18(1)
C(1)	5665(1)	8049(1)	6496(1)	20(1)
C(10)	5407(1)	6510(1)	5768(1)	17(1)
C(17)	7774(1)	7705(1)	6137(1)	20(1)
C(20)	7853(1)	6843(1)	7161(1)	19(1)
C(21)	7749(1)	7654(1)	6958(1)	21(1)

C(11)	5620(1)	6159(1)	5022(1)	17(1)
C(18)	7907(1)	6926(1)	5846(1)	18(1)
C(12)	5290(2)	6534(1)	4368(1)	25(1)
C(16)	6114(1)	5447(1)	4930(1)	23(1)
C(5)	5850(2)	5291(1)	7972(1)	23(1)
C(15)	6272(2)	5128(1)	4215(1)	25(1)
C(23)	8036(1)	6713(1)	5027(1)	29(1)
C(7)	5893(2)	5412(2)	9340(1)	30(1)
C(14)	5939(2)	5509(1)	3572(1)	28(1)
C(24)	8122(1)	5519(1)	6437(1)	28(1)
C(9)	5462(2)	6522(1)	8559(1)	26(1)
C(6)	6001(2)	4962(1)	8686(1)	30(1)
C(8)	5621(2)	6199(1)	9271(1)	32(1)
C(13)	5441(2)	6213(1)	3650(1)	32(1)
C(22)	7756(1)	8453(1)	5680(1)	34(1)
C(25)	7884(1)	6524(1)	7951(1)	32(1)
C(26)	7739(1)	8340(1)	7495(1)	35(1)

Table 5-6. Bond lengths [Å] and angles [°] for 5-25.

Rh(1)-C(2)	2.1091(16)
Rh(1)-C(3)	2.2013(17)
Rh(1)-C(19)	2.2743(17)
Rh(1)-C(1)	2.1113(17)
Rh(1)-C(10)	2.2087(17)
Rh(1)-C(17)	2.1927(18)
Rh(1)-C(20)	2.2431(18)
Rh(1)-C(21)	2.1910(18)
Rh(1)-C(18)	2.2652(18)
C(2)-C(3)	1.418(2)
C(2)-C(10)	1.418(2)
C(2)-H(2)	0.9691(14)
C(3)-C(4)	1.475(2)
C(3)-H(3)	0.9686(14)
C(4)-C(5)	1.399(3)
C(4)-C(9)	1.394(3)
C(19)-C(20)	1.431(3)
C(19)-C(18)	1.436(3)
C(19)-C(24)	1.499(3)
C(1)-H(1A)	0.9840(16)
C(1)-H(1B)	0.9851(16)
C(1)-H(1C)	0.9828(16)
C(10)-C(11)	1.473(2)
C(10)-H(10)	0.9688(14)
C(17)-C(21)	1.449(3)
C(17)-C(18)	1.428(3)

C(17)-C(22)	1.500(3)
C(20)-C(21)	1.426(3)
C(20)-C(25)	1.495(3)
C(21)-C(26)	1.500(3)
C(11)-C(12)	1.395(3)
C(11)-C(16)	1.403(3)
C(18)-C(23)	1.498(3)
C(12)-C(13)	1.393(3)
C(12)-H(12)	0.9695(19)
C(16)-C(15)	1.388(3)
C(16)-H(16)	0.9726(18)
C(5)-C(6)	1.394(3)
C(5)-H(5)	0.9693(18)
C(15)-C(14)	1.386(3)
C(15)-H(15)	0.9713(19)
C(23)-H(23A)	0.9850(18)
C(23)-H(23B)	0.9845(18)
C(23)-H(23C)	0.9824(17)
C(7)-C(6)	1.390(3)
C(7)-C(8)	1.392(3)
C(7)-H(7)	0.9689(18)
C(14)-C(13)	1.391(3)
C(14)-H(14)	0.9696(18)
C(24)-H(24A)	0.9855(18)
C(24)-H(24B)	0.9842(16)
C(24)-H(24C)	0.9842(17)
C(9)-C(8)	1.387(3)
C(9)-H(9)	0.9691(19)

C(6)-H(6)	0.9711(19)
C(8)-H(8)	0.9717(19)
C(13)-H(13)	0.9683(19)
C(22)-H(22A)	0.9836(18)
C(22)-H(22B)	0.9822(17)
C(22)-H(22C)	0.9859(19)
C(25)-H(25A)	0.9877(19)
C(25)-H(25B)	0.9870(18)
C(25)-H(25C)	0.9808(17)
C(26)-H(26A)	0.9873(18)
C(26)-H(26B)	0.9868(19)
C(26)-H(26C)	0.9824(17)

C(2)-Rh(1)-C(3)	38.33(6)
C(2)-Rh(1)-C(19)	102.59(6)
C(2)-Rh(1)-C(1)	103.84(6)
C(2)-Rh(1)-C(10)	38.26(7)
C(2)-Rh(1)-C(17)	156.08(7)
C(2)-Rh(1)-C(20)	117.19(7)
C(2)-Rh(1)-C(21)	153.16(7)
C(2)-Rh(1)-C(18)	119.62(6)
C(3)-Rh(1)-C(19)	115.86(6)
C(3)-Rh(1)-C(10)	67.74(7)
C(3)-Rh(1)-C(20)	105.07(6)
C(3)-Rh(1)-C(18)	149.40(6)
C(1)-Rh(1)-C(3)	86.04(6)
C(1)-Rh(1)-C(19)	153.57(6)
C(1)-Rh(1)-C(10)	85.31(6)

C(1)-Rh(1)-C(17)	92.25(6)
C(1)-Rh(1)-C(20)	126.42(7)
C(1)-Rh(1)-C(21)	93.34(7)
C(1)-Rh(1)-C(18)	124.32(6)
C(10)-Rh(1)-C(19)	115.78(6)
C(10)-Rh(1)-C(20)	147.76(6)
C(10)-Rh(1)-C(18)	107.44(7)
C(17)-Rh(1)-C(3)	163.57(7)
C(17)-Rh(1)-C(19)	62.47(7)
C(17)-Rh(1)-C(10)	128.46(7)
C(17)-Rh(1)-C(20)	63.15(7)
C(17)-Rh(1)-C(18)	37.32(7)
C(20)-Rh(1)-C(19)	36.93(7)
C(20)-Rh(1)-C(18)	61.98(7)
C(21)-Rh(1)-C(3)	125.11(7)
C(21)-Rh(1)-C(19)	62.43(7)
C(21)-Rh(1)-C(10)	167.02(7)
C(21)-Rh(1)-C(17)	38.61(8)
C(21)-Rh(1)-C(20)	37.50(7)
C(21)-Rh(1)-C(18)	62.87(7)
C(18)-Rh(1)-C(19)	36.88(7)
Rh(1)-C(2)-H(2)	114.69(12)
C(3)-C(2)-Rh(1)	74.36(10)
C(3)-C(2)-C(10)	120.14(14)
C(3)-C(2)-H(2)	120.61(17)
C(10)-C(2)-Rh(1)	74.68(10)
C(10)-C(2)-H(2)	118.65(16)
Rh(1)-C(3)-H(3)	102.46(12)

C(2)-C(3)-Rh(1)	67.31(9)
C(2)-C(3)-C(4)	122.83(14)
C(2)-C(3)-H(3)	118.18(16)
C(4)-C(3)-Rh(1)	122.62(11)
C(4)-C(3)-H(3)	113.61(16)
C(5)-C(4)-C(3)	123.85(16)
C(9)-C(4)-C(3)	118.38(16)
C(9)-C(4)-C(5)	117.76(17)
C(20)-C(19)-Rh(1)	70.35(10)
C(20)-C(19)-C(18)	108.13(15)
C(20)-C(19)-C(24)	125.58(17)
C(18)-C(19)-Rh(1)	71.21(10)
C(18)-C(19)-C(24)	126.07(17)
C(24)-C(19)-Rh(1)	128.31(12)
Rh(1)-C(1)-H(1A)	112.96(12)
Rh(1)-C(1)-H(1B)	107.96(12)
Rh(1)-C(1)-H(1C)	114.67(12)
H(1A)-C(1)-H(1B)	106.84(15)
H(1A)-C(1)-H(1C)	107.05(15)
H(1B)-C(1)-H(1C)	106.94(15)
Rh(1)-C(10)-H(10)	105.77(12)
C(2)-C(10)-Rh(1)	67.06(9)
C(2)-C(10)-C(11)	122.19(14)
C(2)-C(10)-H(10)	116.80(16)
C(11)-C(10)-Rh(1)	121.81(11)
C(11)-C(10)-H(10)	114.07(16)
C(21)-C(17)-Rh(1)	70.63(10)
C(21)-C(17)-C(22)	125.86(17)

C(18)-C(17)-Rh(1)	74.10(10)
C(18)-C(17)-C(21)	107.79(16)
C(18)-C(17)-C(22)	126.10(18)
C(22)-C(17)-Rh(1)	125.29(13)
C(19)-C(20)-Rh(1)	72.72(10)
C(19)-C(20)-C(25)	125.98(17)
C(21)-C(20)-Rh(1)	69.27(10)
C(21)-C(20)-C(19)	108.26(16)
C(21)-C(20)-C(25)	125.75(18)
C(25)-C(20)-Rh(1)	124.66(12)
C(17)-C(21)-Rh(1)	70.76(10)
C(17)-C(21)-C(26)	125.74(17)
C(20)-C(21)-Rh(1)	73.24(10)
C(20)-C(21)-C(17)	107.79(16)
C(20)-C(21)-C(26)	126.07(18)
C(26)-C(21)-Rh(1)	127.22(13)
C(12)-C(11)-C(10)	118.99(16)
C(12)-C(11)-C(16)	117.59(17)
C(16)-C(11)-C(10)	123.39(16)
C(19)-C(18)-Rh(1)	71.90(10)
C(19)-C(18)-C(23)	126.25(16)
C(17)-C(18)-Rh(1)	68.58(10)
C(17)-C(18)-C(19)	108.01(17)
C(17)-C(18)-C(23)	125.69(17)
C(23)-C(18)-Rh(1)	127.17(12)
C(11)-C(12)-H(12)	119.92(19)
C(13)-C(12)-C(11)	121.32(18)
C(13)-C(12)-H(12)	118.8(2)

C(11)-C(16)-H(16)	119.48(18)
C(15)-C(16)-C(11)	121.24(17)
C(15)-C(16)-H(16)	119.27(19)
C(4)-C(5)-H(5)	120.48(19)
C(6)-C(5)-C(4)	120.68(17)
C(6)-C(5)-H(5)	118.81(19)
C(16)-C(15)-H(15)	117.5(2)
C(14)-C(15)-C(16)	120.36(17)
C(14)-C(15)-H(15)	122.1(2)
C(18)-C(23)-H(23A)	112.99(17)
C(18)-C(23)-H(23B)	111.66(16)
C(18)-C(23)-H(23C)	111.01(17)
H(23A)-C(23)-H(23B)	106.84(18)
H(23A)-C(23)-H(23C)	107.00(17)
H(23B)-C(23)-H(23C)	107.02(17)
C(6)-C(7)-C(8)	118.90(17)
C(6)-C(7)-H(7)	120.9(2)
C(8)-C(7)-H(7)	120.2(2)
C(15)-C(14)-C(13)	119.35(17)
C(15)-C(14)-H(14)	121.9(2)
C(13)-C(14)-H(14)	118.6(2)
C(19)-C(24)-H(24A)	112.21(16)
C(19)-C(24)-H(24B)	112.28(16)
C(19)-C(24)-H(24C)	111.50(16)
H(24A)-C(24)-H(24B)	106.81(17)
H(24A)-C(24)-H(24C)	106.77(16)
H(24B)-C(24)-H(24C)	106.91(16)
C(4)-C(9)-H(9)	115.64(19)

C(8)-C(9)-C(4)	121.76(18)
C(8)-C(9)-H(9)	122.6(2)
C(5)-C(6)-H(6)	119.7(2)
C(7)-C(6)-C(5)	120.78(18)
C(7)-C(6)-H(6)	119.5(2)
C(7)-C(8)-H(8)	120.0(2)
C(9)-C(8)-C(7)	120.10(18)
C(9)-C(8)-H(8)	119.9(2)
C(12)-C(13)-H(13)	122.8(2)
C(14)-C(13)-C(12)	120.13(18)
C(14)-C(13)-H(13)	117.0(2)
C(17)-C(22)-H(22A)	109.98(17)
C(17)-C(22)-H(22B)	111.89(17)
C(17)-C(22)-H(22C)	113.70(17)
H(22A)-C(22)-H(22B)	107.16(17)
H(22A)-C(22)-H(22C)	106.82(17)
H(22B)-C(22)-H(22C)	106.95(18)
C(20)-C(25)-H(25A)	112.51(17)
C(20)-C(25)-H(25B)	111.85(17)
C(20)-C(25)-H(25C)	111.87(16)
H(25A)-C(25)-H(25B)	106.42(17)
H(25A)-C(25)-H(25C)	106.89(18)
H(25B)-C(25)-H(25C)	106.91(18)
C(21)-C(26)-H(26A)	112.80(18)
C(21)-C(26)-H(26B)	113.48(17)
C(21)-C(26)-H(26C)	109.90(17)
H(26A)-C(26)-H(26B)	106.52(17)
H(26A)-C(26)-H(26C)	106.86(17)

H(26B)-C(26)-H(26C) 106.88(18)

Table 5-7. Anisotropic displacement parameters for 5-25

Anisotropic displacement parameters ($Å^2 x\ 10^3$) for 5-25. The anisotropic displacement factor exponent takes the form: $-2\pi^2[\ h^2\ a^{*2}U^{11} + ... + 2\ h\ k\ a^*\ b^*\ U^{12}\ ]$

	U^{11}	U^{22}	U^{33}	U^{23}	U^{13}	U^{12}
Rh(1)	12(1)	10(1)	17(1)	0(1)	0(1)	0(1)
C(2)	14(1)	16(1)	19(1)	-1(1)	0(1)	-3(1)
C(3)	13(1)	18(1)	18(1)	-1(1)	0(1)	-1(1)
C(4)	13(1)	18(1)	19(1)	-1(1)	2(1)	-2(1)
C(19)	12(1)	14(1)	28(1)	3(1)	0(1)	1(1)
C(1)	22(1)	16(1)	23(1)	0(1)	0(1)	5(1)
C(10)	14(1)	18(1)	19(1)	-2(1)	-2(1)	-1(1)
C(17)	16(1)	13(1)	30(1)	3(1)	1(1)	-3(1)
C(20)	12(1)	24(1)	22(1)	2(1)	-2(1)	-2(1)
C(21)	16(1)	18(1)	30(1)	-6(1)	-1(1)	-3(1)
C(11)	15(1)	17(1)	18(1)	-1(1)	0(1)	-4(1)
C(18)	14(1)	17(1)	23(1)	0(1)	3(1)	-1(1)
C(12)	33(1)	22(1)	20(1)	2(1)	2(1)	0(1)
C(16)	24(1)	22(1)	22(1)	-4(1)	-1(1)	2(1)
C(5)	28(1)	20(1)	22(1)	0(1)	0(1)	2(1)
C(15)	26(1)	23(1)	27(1)	-7(1)	2(1)	-3(1)
C(23)	25(1)	35(1)	26(1)	-4(1)	6(1)	-3(1)
C(7)	29(1)	39(1)	21(1)	8(1)	1(1)	1(1)
C(14)	36(1)	29(1)	21(1)	-5(1)	6(1)	-9(1)
C(24)	20(1)	15(1)	49(1)	2(1)	0(1)	3(1)
C(9)	30(1)	26(1)	22(1)	-3(1)	2(1)	4(1)
C(6)	37(1)	25(1)	28(1)	6(1)	-2(1)	2(1)

C(8)	36(1)	38(1)	21(1)	-4(1)	2(1)	5(1)
C(13)	48(1)	32(1)	17(1)	2(1)	1(1)	0(1)
C(22)	29(1)	20(1)	52(2)	16(1)	1(1)	-4(1)
C(25)	19(1)	49(1)	27(1)	11(1)	-4(1)	-5(1)
C(26)	28(1)	32(1)	44(1)	-18(1)	0(1)	-5(1)

Table 5-8. Hydrogen coordinates (x 10^4) and isotropic displacement parameters ($Å^2$x 10^3)for 5-25.

	x	y	z	U(eq)
H(2)	5828	5569	6434	0
H(3)	4924	6884	7188	0
H(10)	4899	6893	5759	0
H(5)	5917	4959	7527	0
H(14)	6068	5314	3066	0
H(7)	5995	5183	9837	0
H(16)	6348	5169	5375	0
H(12)	4940	7025	4409	0
H(15)	6642	4645	4186	0
H(9)	5253	7063	8488	0
H(8)	5538	6522	9722	0
H(13)	5228	6467	3189	0
H(6)	6149	4403	8730	0
H(26A)	7404	8804	7288	0
H(26B)	7439	8219	7988	0
H(22A)	7331	8840	5919	0
H(24A)	7905	5288	5954	0
H(24B)	8799	5392	6484	0
H(26C)	8390	8509	7605	0
H(25A)	7556	6869	8319	0
H(24C)	7792	5234	6845	0

H(22B)	8384	8698	5648	0
H(22C)	7531	8379	5155	0
H(23A)	7809	6178	4905	0
H(25B)	7579	6001	7988	0
H(23B)	7695	7080	4690	0
H(23C)	8707	6735	4882	0
H(25C)	8536	6461	8134	0
H(1A)	5751	8382	6043	0
H(1B)	5847	8372	6937	0
H(1C)	4983	7945	6542	0

Table 5-9. Torsion angles [°] for 5-25.

Rh(1)-C(2)-C(3)-C(4)	-115.19(15)
Rh(1)-C(2)-C(10)-C(11)	114.20(15)
Rh(1)-C(3)-C(4)-C(5)	-87.0(2)
Rh(1)-C(3)-C(4)-C(9)	94.04(18)
Rh(1)-C(19)-C(20)-C(21)	-60.46(12)
Rh(1)-C(19)-C(20)-C(25)	120.67(17)
Rh(1)-C(19)-C(18)-C(17)	59.32(12)
Rh(1)-C(19)-C(18)-C(23)	-123.27(18)
Rh(1)-C(10)-C(11)-C(12)	-111.80(17)
Rh(1)-C(10)-C(11)-C(16)	70.4(2)
Rh(1)-C(17)-C(21)-C(20)	64.35(13)
Rh(1)-C(17)-C(21)-C(26)	-122.56(18)
Rh(1)-C(17)-C(18)-C(19)	-61.42(12)
Rh(1)-C(17)-C(18)-C(23)	121.16(17)
Rh(1)-C(20)-C(21)-C(17)	-62.73(13)
Rh(1)-C(20)-C(21)-C(26)	124.21(18)
C(2)-C(3)-C(4)-C(5)	-4.6(3)
C(2)-C(3)-C(4)-C(9)	176.45(18)
C(2)-C(10)-C(11)-C(12)	166.91(18)
C(2)-C(10)-C(11)-C(16)	-10.9(3)
C(3)-C(2)-C(10)-Rh(1)	61.16(14)
C(3)-C(2)-C(10)-C(11)	175.36(16)
C(3)-C(4)-C(5)-C(6)	-179.36(19)
C(3)-C(4)-C(9)-C(8)	-179.9(2)
C(4)-C(5)-C(6)-C(7)	-0.4(4)
C(4)-C(9)-C(8)-C(7)	-0.9(4)

C(19)-C(20)-C(21)-Rh(1)	62.65(12)
C(19)-C(20)-C(21)-C(17)	-0.1(2)
C(19)-C(20)-C(21)-C(26)	-173.14(16)
C(10)-C(2)-C(3)-Rh(1)	-61.32(14)
C(10)-C(2)-C(3)-C(4)	-176.51(16)
C(10)-C(11)-C(12)-C(13)	-177.6(2)
C(10)-C(11)-C(16)-C(15)	177.98(18)
C(20)-C(19)-C(18)-Rh(1)	-60.99(12)
C(20)-C(19)-C(18)-C(17)	-1.7(2)
C(20)-C(19)-C(18)-C(23)	175.74(16)
C(21)-C(17)-C(18)-Rh(1)	63.03(12)
C(21)-C(17)-C(18)-C(19)	1.6(2)
C(21)-C(17)-C(18)-C(23)	-175.82(16)
C(11)-C(12)-C(13)-C(14)	-0.7(4)
C(11)-C(16)-C(15)-C(14)	-0.2(3)
C(18)-C(19)-C(20)-Rh(1)	61.53(12)
C(18)-C(19)-C(20)-C(21)	1.1(2)
C(18)-C(19)-C(20)-C(25)	-177.80(16)
C(18)-C(17)-C(21)-Rh(1)	-65.30(13)
C(18)-C(17)-C(21)-C(20)	-0.9(2)
C(18)-C(17)-C(21)-C(26)	172.14(16)
C(12)-C(11)-C(16)-C(15)	0.2(3)
C(16)-C(11)-C(12)-C(13)	0.3(3)
C(16)-C(15)-C(14)-C(13)	-0.3(3)
C(5)-C(4)-C(9)-C(8)	1.1(3)
C(15)-C(14)-C(13)-C(12)	0.7(4)
C(24)-C(19)-C(20)-Rh(1)	-123.64(17)
C(24)-C(19)-C(20)-C(21)	175.90(16)

C(24)-C(19)-C(20)-C(25)	-3.0(3)
C(24)-C(19)-C(18)-Rh(1)	124.22(17)
C(24)-C(19)-C(18)-C(17)	-176.46(16)
C(24)-C(19)-C(18)-C(23)	0.9(3)
C(9)-C(4)-C(5)-C(6)	-0.4(3)
C(6)-C(7)-C(8)-C(9)	0.0(4)
C(8)-C(7)-C(6)-C(5)	0.6(4)
C(22)-C(17)-C(21)-Rh(1)	120.10(18)
C(22)-C(17)-C(21)-C(20)	-175.54(16)
C(22)-C(17)-C(21)-C(26)	-2.5(3)
C(22)-C(17)-C(18)-Rh(1)	-122.40(18)
C(22)-C(17)-C(18)-C(19)	176.19(17)
C(22)-C(17)-C(18)-C(23)	-1.2(3)
C(25)-C(20)-C(21)-Rh(1)	-118.47(17)
C(25)-C(20)-C(21)-C(17)	178.79(16)
C(25)-C(20)-C(21)-C(26)	5.7(3)

Complex 5-26 RhCp*(DPP)Ph:

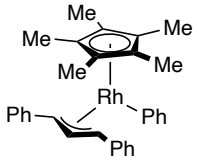

5-26

EMORY UNIVERSITY | X-ray Crystallography Center

Submitted by: **Taylor Farmer**

Blakey Research Group, Emory University

Solved by: **Elaine Liu, John Bacsa**

Sample ID: **tan5524**

Crystal Data and Experimental

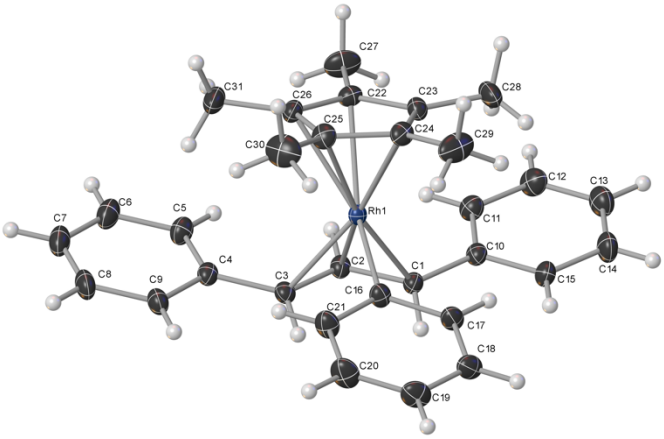

Experimental. Single orange prism-shaped crystals of **5-26** were chosen from the sample as supplied. A suitable crystal 0.20×0.13×0.09 mm^3 was selected and mounted on a loop with paratone oil on an XtaLAB Synergy, Dualflex, HyPix diffractometer. The crystal was kept at a steady T = 99.96(14) K during data collection. The structure was solved with the **ShelXT** (Sheldrick, 2015) structure solution program using the Intrinsic Phasing solution method and by using **Olex2** (Dolomanov et al., 2009) as the graphical interface. The model was refined with version 2018/3 of **ShelXL** (Sheldrick, 2015) using Least Squares minimisation.

Crystal Data. $C_{31}H_{33}Rh$, M_r = 508.48, orthorhombic, $Pna2_1$ (No. 33), a = 17.4414(3) Å, b = 19.1462(3) Å, c = 7.27239(14) Å, $\alpha = \beta = \gamma = 90^\circ$, V = 2428.51(7) Å^3, T = 99.96(14) K, Z = 4, Z' = 1, μ(MoK$_\alpha$) = 0.719 mm^{-1}, 49029 reflections measured, 15454 unique (R_{int} = 0.0460) which were used in all calculations. The final wR_2 was 0.1012 (all data) and R_1 was 0.0432 (I > 2σ(I)).

Compound	**5-26**
Formula	$C_{31}H_{33}Rh$
$D_{calc.}$/ g cm^{-3}	1.391
μ/mm^{-1}	0.719
Formula Weight	508.48
Colour	orange
Shape	prism
Size/mm^3	0.20×0.13×0.09
T/K	99.96(14)
Crystal System	orthorhombic
Flack Parameter	-0.019(17)
Hooft Parameter	-0.006(11)
Space Group	$Pna2_1$
a/Å	17.4414(3)
b/Å	19.1462(3)
c/Å	7.27239(14)
α/°	90
β/°	90
γ/°	90
V/Å^3	2428.51(7)
Z	4
Z'	1
Wavelength/Å	0.71073
Radiation type	MoK_α
Θ_{min}/°	1.579

Θ_{max}/°	41.127
Measured Refl.	49029
Independent Refl.	15454
Reflections with I >2(I)	12792
R_{int}	0.0460
Parameters	16
Restraints	4
Largest Peak	1.525
Deepest Hole	-1.641
GooF	1.044
wR_2 (all data)	0.1012
wR_2	0.0969
R_1 (all data)	0.0558
R_1	0.0432

Structure Quality Indicators

Reflections: d min (Mo) 0.54 | I/σ 20.9 | Rint 4.60% | complete 100% (IUCr) 99%

Refinement: Shift 0.001 | Max Peak 1.5 | Min Peak -1.6 | GooF 1.044 | Flack -.019(17)

A orange prism-shaped crystal with dimensions 0.20×0.13×0.09 mm^3 was mounted on a loop with paratone oil. Data were collected using an XtaLAB Synergy, Dualflex, HyPix diffractometer equipped with an Oxford Cryosystems low-temperature device operating at T = 99.96(14) K.

Data were measured using ω scans using MoK_α radiation. The total number of runs and images was based on the strategy calculation from the program **CrysAlisPro** (Rigaku, V1.171.40.50a, 2019). The maximum resolution that was achieved was Θ = 41.127° (0.54 Å).

The diffraction pattern was indexed. The total number of runs and images was based on the strategy calculation from the program **CrysAlisPro** (Rigaku, V1.171.40.50a, 2019) and the unit cell was refined using **CrysAlisPro** (Rigaku, V1.171.40.50a, 2019) on 24724 reflections, 50% of the observed reflections.

Data reduction, scaling and absorption corrections were performed using **CrysAlisPro** (Rigaku, V1.171.40.50a, 2019). The final completeness is 99.90 % out to 41.127° in Θ. A numerical absorption correction based on Gaussian integration over a multifaceted crystal model was performed using **CrysAlisPro** (Rigaku, V1.171.40.37a, 2019). An empirical absorption correction using spherical harmonics as implemented in SCALE3 ABSPACK in **CrysAlisPro** (Rigaku, V1.171.40.37a, 2019) was also applied. The absorption coefficient μ of this material is 0.719 mm^{-1} at this wavelength (λ = 0.711Å) and the minimum and maximum transmissions are 0.852 and 1.000.

The structure was solved and the space group $Pna2_1$ (# 33) determined by the **ShelXT** (Sheldrick, 2015) structure solution program using Intrinsic Phasing and refined by Least Squares using version 2018/3 of **ShelXL** (Sheldrick, 2015). All non-hydrogen atoms were refined anisotropically. Most hydrogen atom positions were calculated geometrically and refined using the riding model, but some hydrogen atoms were refined freely.

There is a single molecule in the asymmetric unit, which is represented by the reported sum formula. In

other words: Z is 4 and Z' is 1.

The Flack parameter was refined to -0.019(17). Determination of absolute structure using Bayesian statistics on Bijvoet differences using the Olex2 results in -0.006(11).

Images of the Crystal on the Diffractometer

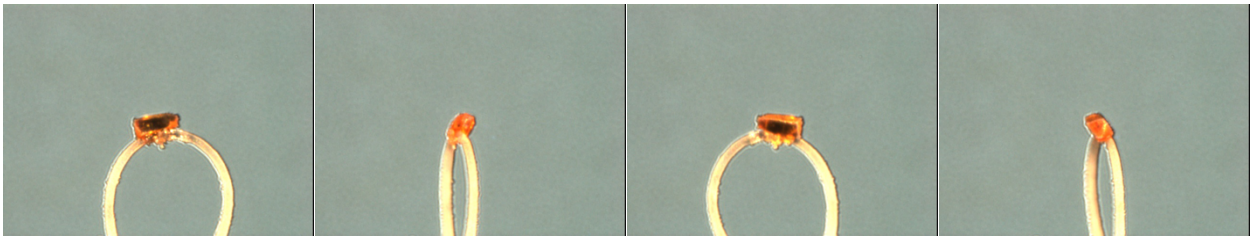

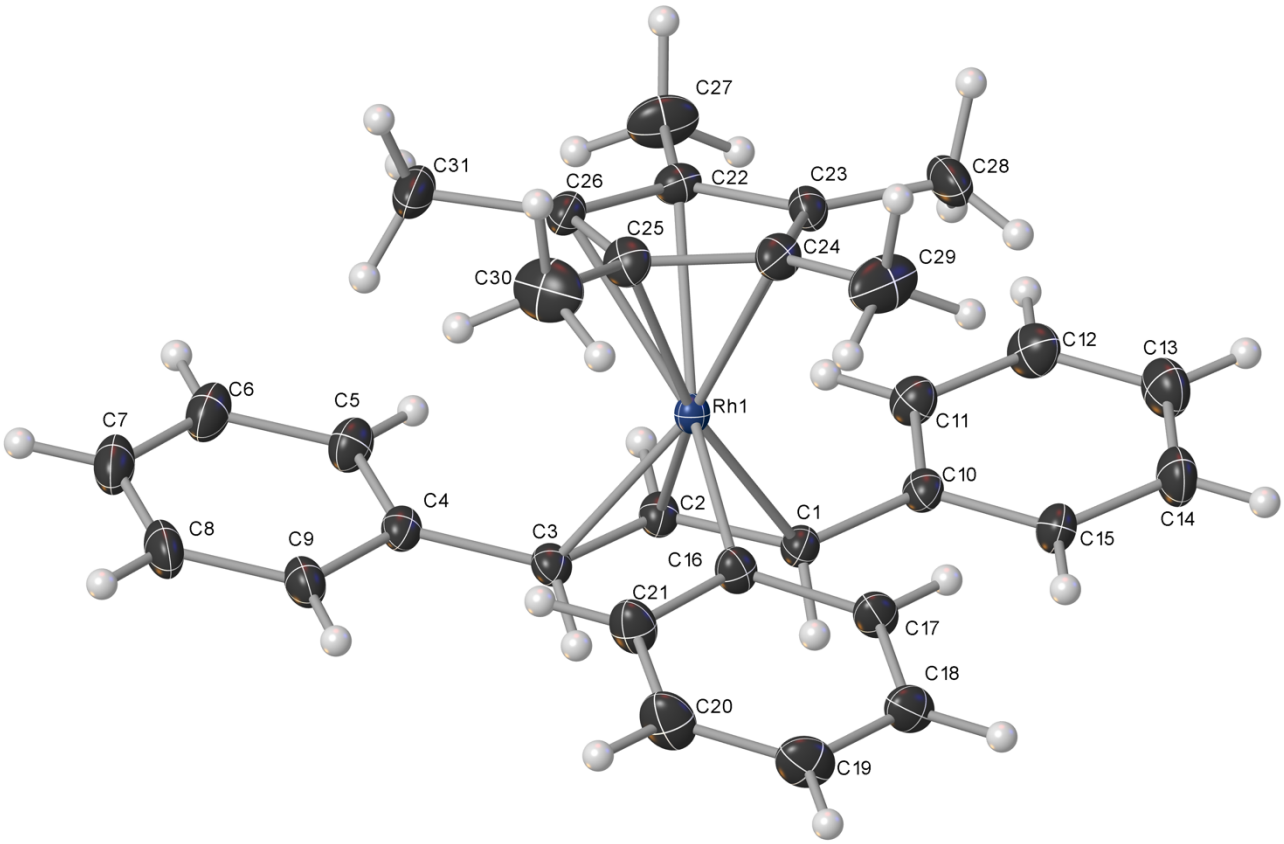
C27
C31
C26
C22
C23
C28
C25
C24
C29
C30
C12
C13
C6
C5
C7
Rh1
C11
C10
C4
C2
C1
C14
C8
C9
C3
C16
C15
C21
C17
C18
C20
C19

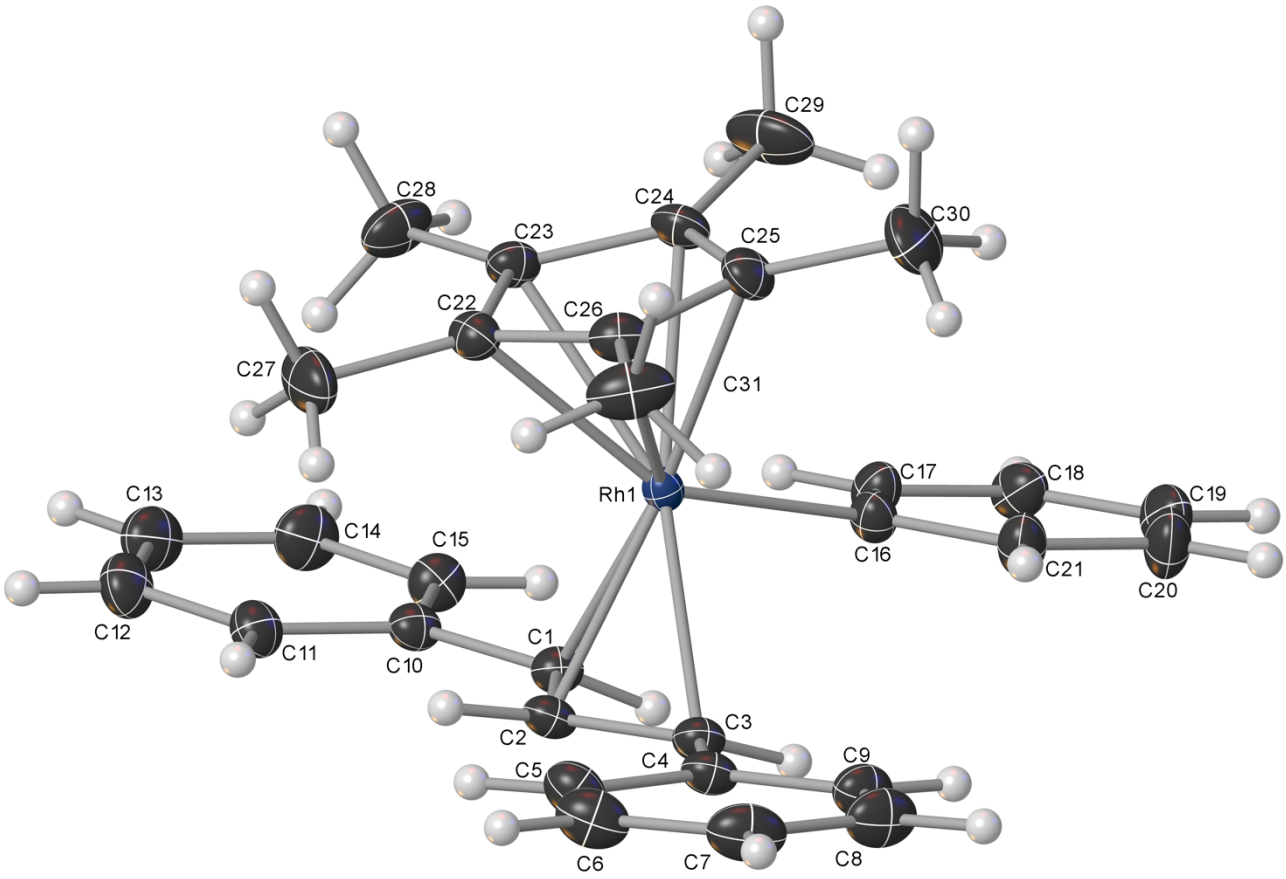

Data Plots: Diffraction Data

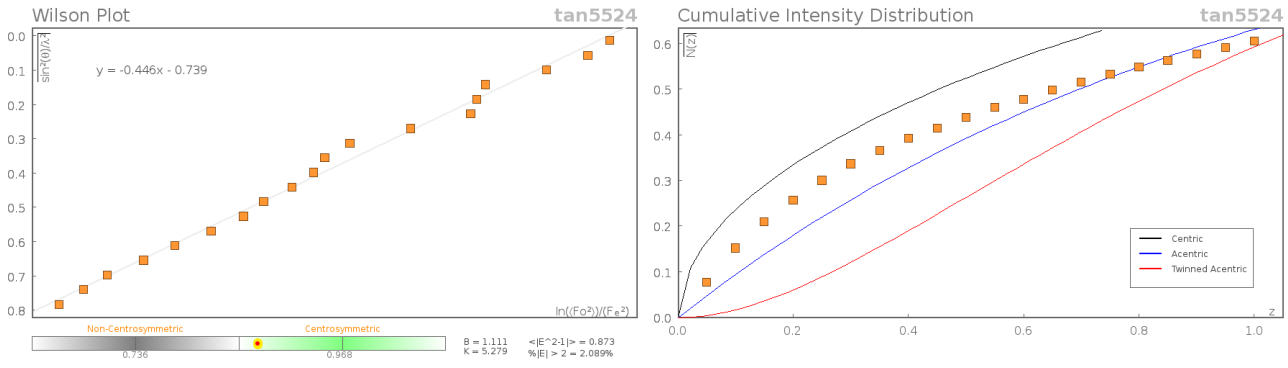

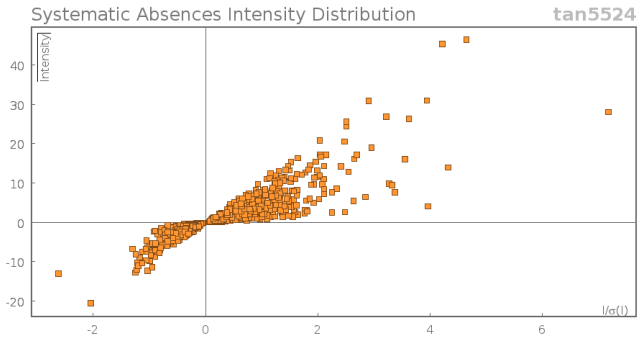

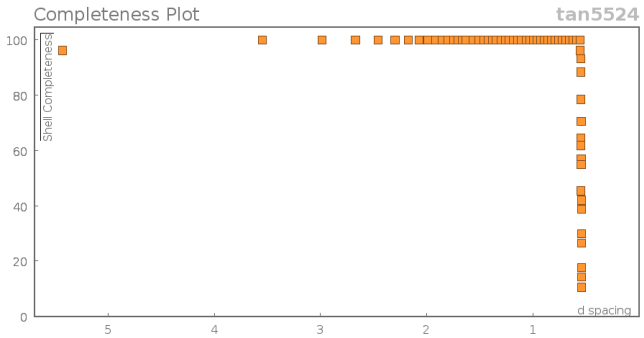

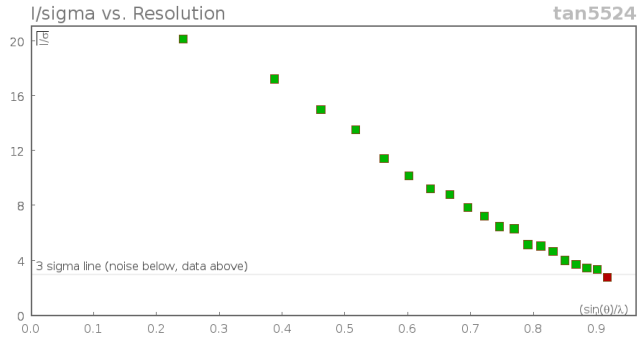

Data Plots: Refinement and Data

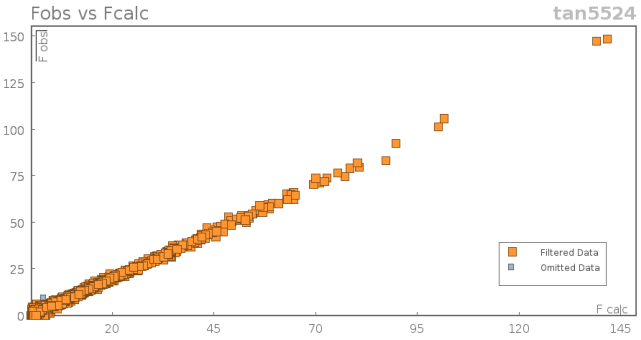

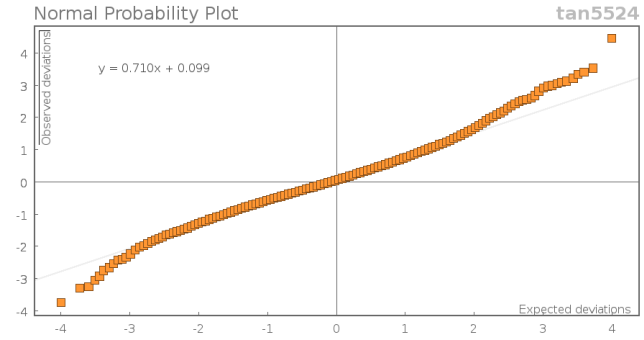

Reflection Statistics

Total reflections (after filtering)	50231	Unique reflections	15454
Completeness	0.959	Mean I/σ	14.94
hkl_{max} collected	(31, 34, 13)	hkl_{min} collected	(-31, -28, -13)
hkl_{max} used	(31, 34, 13)	hkl_{min} used	(0, 0, -13)

Lim d_{max} collected	100.0	Lim d_{min} collected	0.36
d_{max} used	12.89	d_{min} used	0.54
Friedel pairs	9908	Friedel pairs merged	0
Inconsistent equivalents	1	R_{int}	0.046
R_{sigma}	0.0478	Intensity transformed	0
Omitted reflections	0	Omitted by user (OMIT hkl)	3
Multiplicity	(23640, 7753, 2660, 622, 111, 8, 2)	Maximum multiplicity	14
Removed systematic absences	1199	Filtered off (Shel/OMIT)	0

Images of the Crystal on the Diffractometer

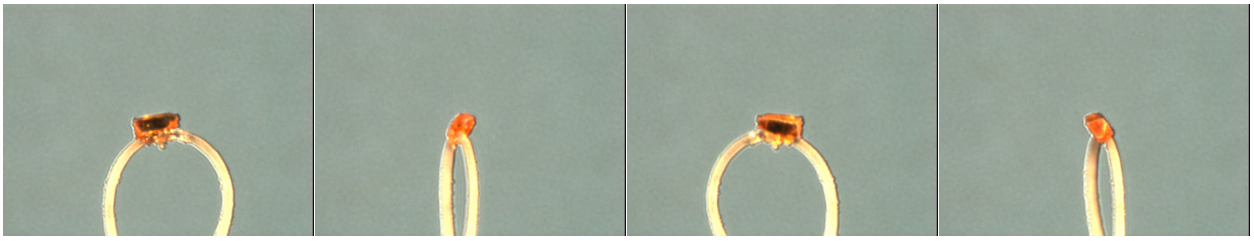

Table 5-10. Fractional Atomic Coordinates (×10⁴) and Equivalent Isotropic Displacement Parameters (Å²×10³) for 5-26.

Fractional Atomic Coordinates (×10⁴) and Equivalent Isotropic Displacement Parameters (Å²×10³) for **5-26**.

U_{eq} is defined as 1/3 of the trace of the orthogonalised U_{ij}.

Atom	x	y	z	U_{eq}
Rh1	4289.7	2137.8	4702.09	14
C4	3023.61	1118.01	2991.09	18
C3	3577.3	1676.3	2514.5	18
C26	3860.4	1689.71	7419.4	20
C12	3341.2	4672.1	3935.4	27

Atom	x	y	z	U_{eq}
C6	1803.9	697.4	4171	29
C5	2294.89	1248.21	3712.9	24
C16	5226.1	1836.1	3168.6	19
C1	4034.69	2876.8	2439	17
C17	5783.81	2329.8	2608.4	21
C21	5385.89	1133.91	2802.2	25
C7	2033	8.2	3886.4	30
C20	6076	930.9	1949.61	30
C9	3236.01	423.2	2686	23
C10	3993.01	3630.81	2831.8	18
C29	5873.4	2402.5	7113.61	38
C15	4626.29	4047.09	2433	22
C2	3425.49	2400	2791.19	17
C25	4665.89	1585.81	7196.49	21
C31	3274.8	1132.31	7677.6	33
C28	4553.7	3550.5	7344.28	30
C13	3985.4	5074.6	3559.3	30
C24	5022.9	2270.3	7126.6	20
C14	4624.29	4763.39	2807.29	28
C18	6458.81	2127.9	1750.1	24
C11	3342.8	3957.3	3582.81	22
C27	2961.09	2774.49	7731.6	33
C30	5065.09	899.8	7321.8	37
C22	3714.29	2428.29	7410.2	19
C8	2753.4	-123.41	3147.3	29
C23	4436.2	2782.3	7262.8	19

Atom	x	y	z	U_{eq}
C19	6608.91	1424.29	1426.4	28

Table 5-11. Anisotropic Displacement Parameters (×10⁴) 5-26.

Anisotropic Displacement Parameters (×10⁴) **5-26**. The anisotropic displacement factor exponent takes the form: $-2\pi^2[h^2a^{*2} \times U_{11} + \ldots + 2hka^* \times b^* \times U_{12}]$

Atom	U_{11}	U_{22}	U_{33}	U_{23}	U_{13}	U_{12}
Rh1	12	13	16	0	0	0
C4	18	19	18	2	0	0
C3	18	18	17	0	0	0
C26	21	21	18	3	0	0
C12	31	20	29	4	1	5
C6	25	30	31	7	0	0
C5	18	25	28	5	0	0
C16	14	19	23	0	0	0
C1	19	17	17	1	0	0
C17	17	23	24	0	4	0
C21	21	20	32	0	2	2
C7	33	27	30	6	0	0
C20	24	27	39	0	4	6
C9	27	17	24	0	0	0
C10	21	16	17	3	0	0
C29	17	69	30	5	0	0
C15	24	18	24	3	2	0
C2	17	18	18	3	0	0
C25	24	18	22	5	0	3

Atom	U_{11}	U_{22}	U_{33}	U_{23}	U_{13}	U_{12}
C31	39	36	23	5	0	0
C28	47	18	24	0	0	0
C13	36	19	34	1	0	0
C24	15	26	20	2	0	0
C14	33	17	34	2	0	0
C18	16	30	25	0	2	0
C11	23	20	24	3	0	2
C27	22	47	30	1	5	12
C30	47	27	37	6	0	17
C22	18	23	17	1	1	1
C8	38	18	31	1	0	0
C23	21	16	19	0	0	0
C19	18	35	31	0	5	4

Table 5-12. Bond Lengths in Å for **5-26**.

Bond Lengths in Å for **5-26**.

Atom	Atom	Length/Å
Rh1	C3	2.20355(2)
Rh1	C26	2.28075(3)
Rh1	C16	2.06027(2)
Rh1	C1	2.21549(3)
Rh1	C2	2.110728(19)
Rh1	C25	2.19958(3)

Atom	Atom	Length/Å
Rh1	C24	2.19283(3)
Rh1	C22	2.27931(4)
Rh1	C23	2.24853(3)
C4	C3	1.481661(16)
C4	C5	1.397521(14)
C4	C9	1.39862(2)
C3	C2	1.42495(3)
C26	C25	1.428137(15)
C26	C31	1.48909(2)
C26	C22	1.436895(19)
C12	C13	1.38965(2)
C12	C11	1.39238(2)
C6	C5	1.398738(17)
C6	C7	1.39418(2)
C16	C17	1.416208(18)
C16	C21	1.39863(2)
C1	C10	1.47343(3)
C1	C2	1.424053(18)
C17	C18	1.38747(3)
C21	C20	1.408646(14)
C7	C8	1.38965(2)
C20	C19	1.378786(18)
C9	C8	1.384309(17)
C10	C15	1.39261(2)
C10	C11	1.405389(14)
C29	C24	1.50487(3)

Atom	Atom	Length/Å
C15	C14	1.39820(3)
C25	C24	1.45183(3)
C25	C30	1.489364(18)
C28	C23	1.48621(3)
C13	C14	1.376876(9)
C24	C23	1.420523(18)
C18	C19	1.392374(19)
C27	C22	1.48988(2)
C22	C23	1.43395(2)

Table 5-13. Bond Angles in ° for **5-26**.

Bond Angles in ° for **5-26**.

Atom	Atom	Atom	Angle/°
C3	Rh1	C26	106.833(2)
C3	Rh1	C1	66.831(1)
C3	Rh1	C22	118.255(1)
C3	Rh1	C23	151.9
C16	Rh1	C3	86.776(1)
C16	Rh1	C26	128.6
C16	Rh1	C1	86.336(1)
C16	Rh1	C2	106.045(2)
C16	Rh1	C25	94.315(1)
C16	Rh1	C24	90.309(1)

Atom	Atom	Atom	Angle/°
C16	Rh1	C22	152.3
C16	Rh1	C23	120.803(1)
C1	Rh1	C26	144.9
C1	Rh1	C22	113.431(1)
C1	Rh1	C23	106.713(1)
C2	Rh1	C3	38.497(1)
C2	Rh1	C26	115.181(1)
C2	Rh1	C1	38.340(1)
C2	Rh1	C25	150.491(1)
C2	Rh1	C24	156.683(1)
C2	Rh1	C22	101.328(1)
C2	Rh1	C23	119.730(1)
C25	Rh1	C3	124.817(1)
C25	Rh1	C26	37.120(1)
C25	Rh1	C1	168.3
C25	Rh1	C22	62.354(1)
C25	Rh1	C23	63.048(1)
C24	Rh1	C3	162.9
C24	Rh1	C26	62.502(1)
C24	Rh1	C1	129.830(1)
C24	Rh1	C25	38.602(1)
C24	Rh1	C22	62.211(1)
C24	Rh1	C23	37.3
C22	Rh1	C26	36.734(1)
C23	Rh1	C26	61.715(1)
C23	Rh1	C22	36.919(1)

Atom	Atom	Atom	Angle/°
C5	C4	C3	123.501(1)
C5	C4	C9	118.043(1)
C9	C4	C3	118.453(2)
C4	C3	Rh1	119.204(1)
C2	C3	Rh1	67.2
C2	C3	C4	123.186(1)
C25	C26	Rh1	68.4
C25	C26	C31	126.101(1)
C25	C26	C22	108.120(1)
C31	C26	Rh1	127.159(1)
C22	C26	Rh1	71.578(1)
C22	C26	C31	125.752(1)
C13	C12	C11	120.477(2)
C7	C6	C5	120.183(1)
C4	C5	C6	120.782(1)
C17	C16	Rh1	120.867(1)
C21	C16	Rh1	122.046(1)
C21	C16	C17	116.737(1)
C10	C1	Rh1	119.446(1)
C2	C1	Rh1	66.845(1)
C2	C1	C10	123.807(1)
C18	C17	C16	121.753(2)
C16	C21	C20	121.290(1)
C8	C7	C6	119.2
C19	C20	C21	120.559(1)
C8	C9	C4	121.303(1)

Atom	Atom	Atom	Angle/°
C15	C10	C1	118.766(1)
C15	C10	C11	117.800(1)
C11	C10	C1	123.4
C10	C15	C14	121.255(1)
C3	C2	Rh1	74.277(1)
C1	C2	Rh1	74.815(1)
C1	C2	C3	117.343(1)
C26	C25	Rh1	74.5
C26	C25	C24	107.466(1)
C26	C25	C30	125.2
C24	C25	Rh1	70.448(1)
C24	C25	C30	126.705(1)
C30	C25	Rh1	127.853(1)
C14	C13	C12	119.508(2)
C29	C24	Rh1	126.104(1)
C25	C24	Rh1	70.950(1)
C25	C24	C29	125.1
C23	C24	Rh1	73.489(1)
C23	C24	C29	126.474(1)
C23	C24	C25	108.152(1)
C13	C14	C15	120.252(1)
C17	C18	C19	120.3
C12	C11	C10	120.688(1)
C26	C22	Rh1	71.687(1)
C26	C22	C27	126.404(1)
C27	C22	Rh1	129.2

Atom	Atom	Atom	Angle/°
C23	C22	Rh1	70.374(1)
C23	C22	C26	108.047(1)
C23	C22	C27	125.146(1)
C9	C8	C7	120.426(1)
C28	C23	Rh1	126.284(1)
C24	C23	Rh1	69.231(1)
C24	C23	C28	125.901(1)
C24	C23	C22	108.153(1)
C22	C23	Rh1	72.707(1)
C22	C23	C28	125.865(1)
C20	C19	C18	119.306(1)

Table 5-14. Hydrogen Fractional Atomic Coordinates (×10⁴) and Equivalent Isotropic Displacement Parameters (Å²×10³) for 5-26.

Hydrogen Fractional Atomic Coordinates (×10⁴) and Equivalent Isotropic Displacement Parameters (Å²×10³) for **5-26**. U_{eq} is defined as 1/3 of the trace of the orthogonalised U_{ij}.

Atom	x	y	z	U_{eq}
H12	2905.86	4881.67	4426.15	32
H6	1323.3	791.18	4666.8	34
H5	2134.51	1706.5	3890.76	28
H17	5695.24	2801.9	2821.51	25
H21	5029.57	794.38	3127.82	29
H7	1707.54	-359.14	4187.66	36
H20	6172.99	460.09	1737.83	36
H9	3710.85	326.51	2162.9	28
H29A	6125.53	2040.43	6429.3	58
H29B	6062.34	2405.06	8353.44	58
H29C	5974.9	2846.34	6549.8	58
H15	5058.77	3844.79	1907.74	27
H31A	2773.09	1338.27	7704.07	49
H31B	3368.44	893.59	8816.52	49
H31C	3305.35	805.71	6678.67	49
H28A	5038.43	3666.21	6798.15	45
H28B	4548.84	3700.73	8603.65	45
H28C	4149.73	3780.77	6683.69	45
H13	3985	5550.63	3813.66	35
H14	5056.14	5030.66	2547.31	34

Atom	x	y	z	U_{eq}
H18	6812.82	2464.25	1389.13	29
H11	2909.08	3693.17	3847.03	27
H27A	2952.54	3217.49	7113.64	49
H27B	2888.05	2844.81	9026.82	49
H27C	2557.36	2484.22	7261.43	49
H30A	4742.62	541.29	6818.23	56
H30B	5173.76	796.09	8586.74	56
H30C	5536.19	919.84	6641.19	56
H8	2912.32	-581.66	2961.37	35
H19	7063.84	1288.56	863.19	34
H1	4405(18)	2730(20)	1480(40)	19(5)
H3	4006(15)	1560(20)	1670(40)	19(5)
H2	2971(14)	2566(19)	3480(50)	19(5)

Citations for 5-26

CrysAlisPro Software System, Rigaku Oxford Diffraction, (2019).

O.V. Dolomanov and L.J. Bourhis and R.J. Gildea and J.A.K. Howard and H. Puschmann, Olex2: A complete structure solution, refinement and analysis program, *J. Appl. Cryst.*, (2009), **42**, 339-341.

Sheldrick, G.M., Crystal structure refinement with ShelXL, *Acta Cryst.*, (2015), **C27**, 3-8.

Sheldrick, G.M., ShelXT-Integrated space-group and crystal-structure determination, *Acta Cryst.*, (2015), **A71**, 3-8.

==========

Complex 5-31 IrCp*(DPP)Me:

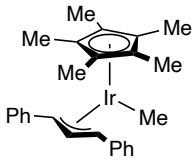

IrMe_1

Submitted by: **Taylor Farmer**

Blakey lab, Emory University

R_1=2.79%

Crystal Data and Experimental

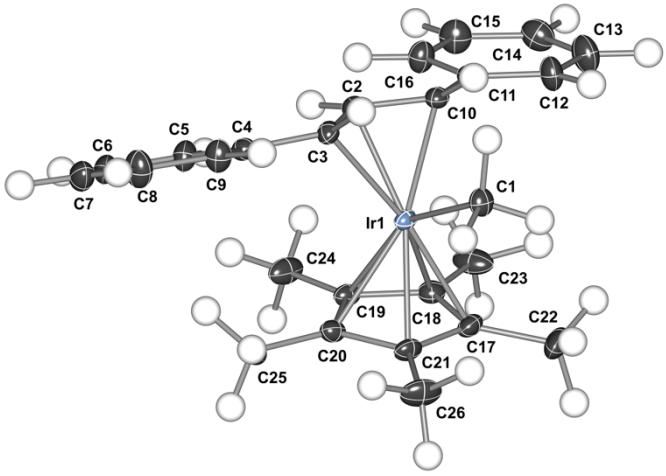

Experimental. Single light-yellow plate crystals of **5-31** were grown from hexanes by slow evaporation. A suitable crystal with dimensions 0.30 × 0.26 × 0.12 mm^3 was selected and mounted on a loop with paratone on a XtaLAB Synergy, Dualflex, HyPix diffractometer. The crystal was kept at a steady T = 100(1) K during data collection. The structure was solved with the ShelXT (Sheldrick, 2015) solution program using dual methods and by using Olex2 (Dolomanov et al., 2009) as the graphical interface. The model was refined with olex2.refine 1.3-dev (Bourhis et al., 2015) using full matrix least squares minimisation on $\boldsymbol{F^2}$.

Crystal Data. $C_{26}H_{31}Ir$, M_r = 535.752, orthorhombic, *Pbca* (No. 61), a = 14.17025(16) Å, b = 16.87891(16) Å, c = 17.6194(2) Å, $\alpha = \beta = \gamma = 90°$, V = 4214.18(8) Å^3, T = 104(6) K, Z = 8, Z' = 1, μ(Mo K$_\alpha$) = 6.344 mm^{-1}, 111552 reflections measured, 13190 unique (R_{int} = 0.0495) which were used in all calculations. The final wR_2 was 0.0512 (all data) and R_1 was 0.0279 (I≥2 σ(I)).

Compound	**5-31**
Formula	$C_{26}H_{31}Ir$
$D_{calc.}$/ g cm^{-3}	1.689
μ/mm^{-1}	6.344
Formula Weight	535.752
Colour	light yellow
Shape	plate
Size/mm^3	0.30×0.26×0.12
T/K	100(1)
Crystal System	orthorhombic
Space Group	*Pbca*
a/Å	14.17025(16)
b/Å	16.87891(16)
c/Å	17.6194(2)
α/°	90
β/°	90
γ/°	90
V/Å^3	4214.18(8)
Z	8
Z'	1
Wavelength/Å	0.71073
Radiation type	Mo K$_\alpha$
Θ_{min}/°	2.20
Θ_{max}/°	40.25
Measured Refl's.	111552

Indep't Refl's	13190
Refl's I≥2 σ(I)	10334
R_{int}	0.0495
Parameters	530
Restraints	423
Largest Peak	3.5392
Deepest Hole	-3.2353
GooF	1.0209
wR_2 (all data)	0.0512
wR_2	0.0475
R_1 (all data)	0.0440
R_1	0.0279

Structure Quality Indicators

Reflections:	d min (Mo) 0.62	I/σ(I) 41.7	Rint 4.71%	complete 100% (IUCr) 100%
Refinement:	Shift 0.000	Max Peak 3.5	Min Peak -3.2	GooF 1.021

A light-yellow plate-shaped crystal with dimensions 0.30 × 0.26 × 0.12 mm^3 was mounted on a loop with paratone. Data were collected using a XtaLAB Synergy, Dualflex, HyPix diffractometer equipped with an Oxford Cryosystems low-temperature device operating at T = 100(1) K.

Data were measured using ω scans using Mo K_α radiation. The diffraction pattern was indexed and the total number of runs and images was based on the strategy calculation from the program CrysAlisPro (Rigaku, V1.171.40.84a, 2020). The maximum resolution that was achieved was Θ = 40.25° (0.62 Å).

The unit cell was refined using CrysAlisPro (Rigaku, V1.171.40.84a, 2020) on 19290 reflections, 17% of the observed reflections.

Data reduction, scaling and absorption corrections were performed using CrysAlisPro (Rigaku, V1.171.40.84a, 2020). The final completeness is 100.00 % out to 40.25° in Θ. A numerical absorption correction based on Gaussian integration over a multifaceted crystal model was performed using CrysAlisPro 1.171.40.71a (Rigaku Oxford Diffraction, 2020). An empirical absorption correction using spherical harmonics, implemented in SCALE3 ABSPACK scaling algorithm was also used. The absorption coefficient μ of this material is 6.344 mm^{-1} at this wavelength (λ = 0.71073Å) and the minimum and maximum transmissions are 0.229 and 1.000.

The structure was solved and the space group *Pbca* (# 61) determined by the ShelXT (Sheldrick, 2015) structure solution program using dual methods and refined by full matrix least squares minimisation on F^2 using version of olex2.refine 1.3-dev (Bourhis et al., 2015). All atoms as well as hydrogen atoms were refined anisotropically with Hirshfeld scattering factors.

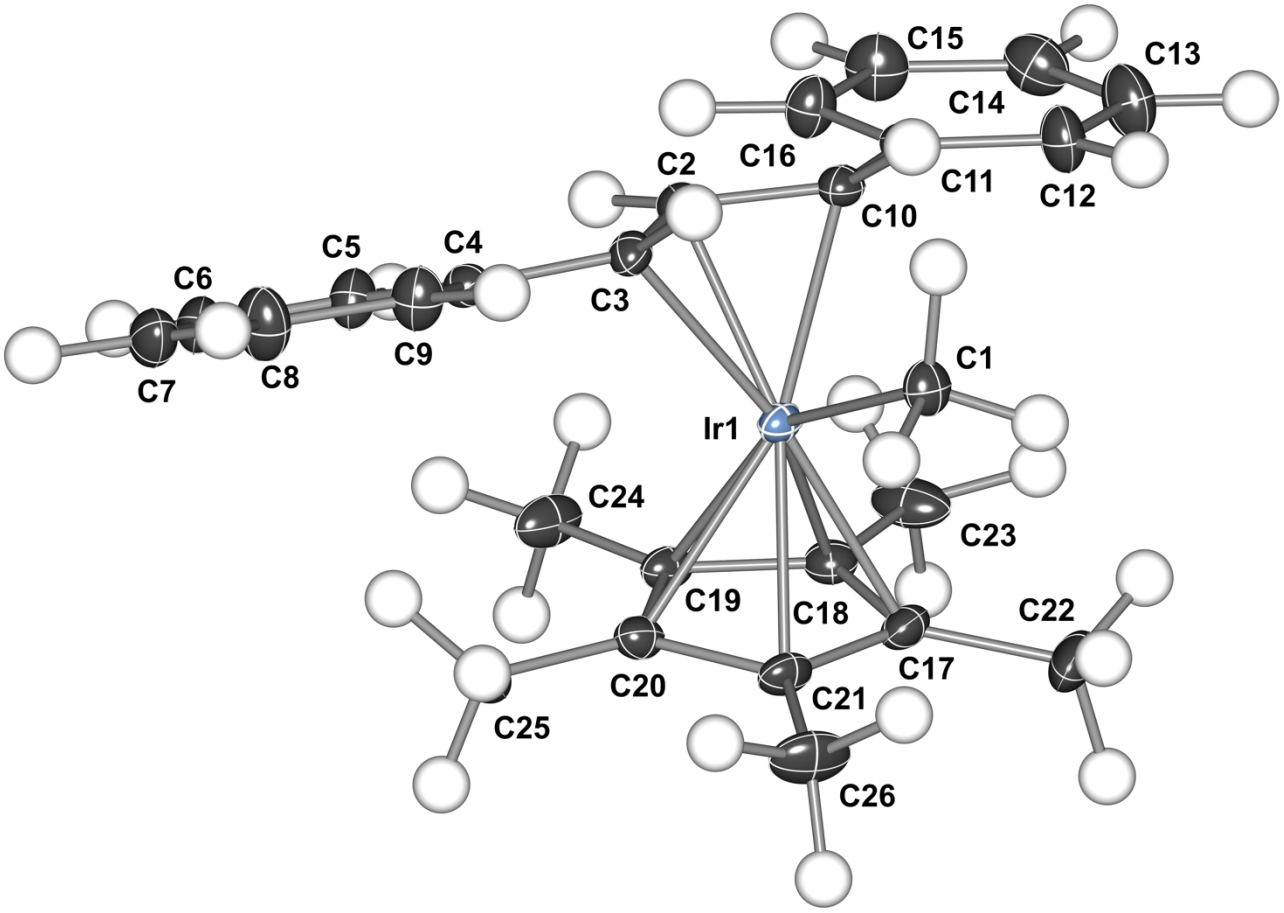

Figure 5-24: Thermal ellipsoid representation of the asymmetric unit.

_refine_special_details: Refinement using NoSpherA2, an implementation of NOn-SPHERical Atom-form-factors in Olex2.Please cite:F. Kleemiss, H. Puschmann, O. Dolomanov, S.Grabowsky - to be published - 2020NoSpherA2 implementation of HAR makes use of tailor-made aspherical atomic form factors calculatedon-the-fly from a Hirshfeld-partitioned electron density (ED) - not fromspherical-atom form factors.The ED is calculated from a gaussian basis set single determinant SCFwavefunction - either Hartree-Fock or DFT using selected funtionals - for a fragment of the crystal.This fregment can be embedded in an electrostatic crystal field by employing cluster charges.The following options were used: SOFTWARE: ORCA PARTITIONING: NoSpherA2 INT ACCURACY: Normal METHOD: B3LYP BASIS SET: x2c-TZVP CHARGE: 0 MULTIPLICITY: 1 RELATIVISTIC: DKH2 DATE: 2020-10-16_16-58-51

Data Plots: Diffraction Data

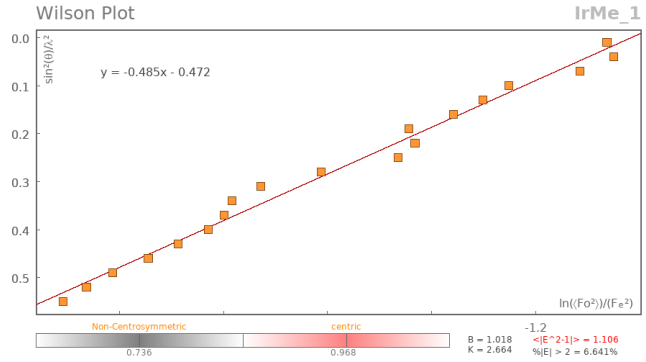

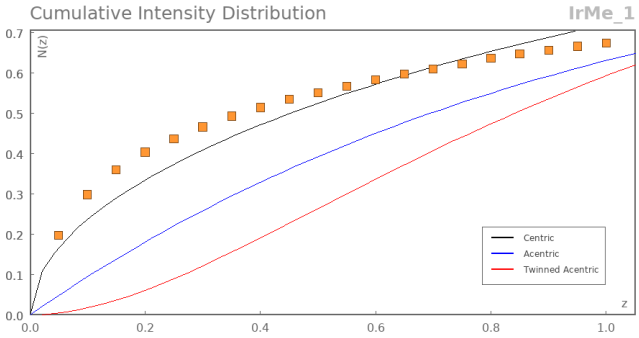

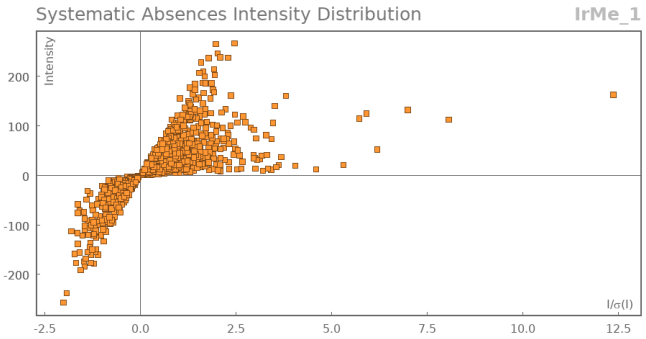

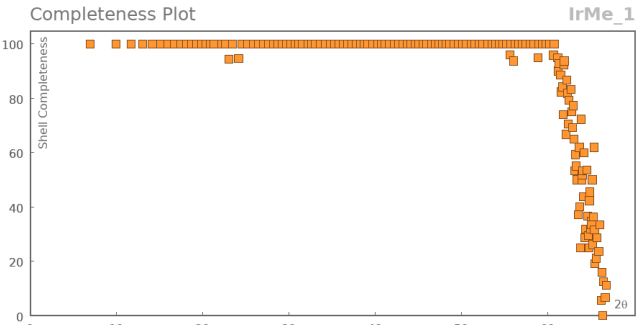

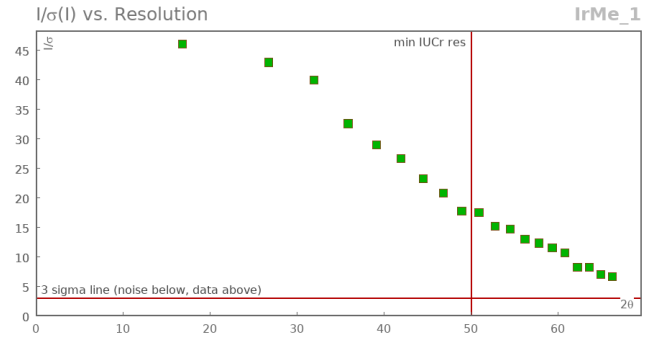

Data Plots: Refinement and Data

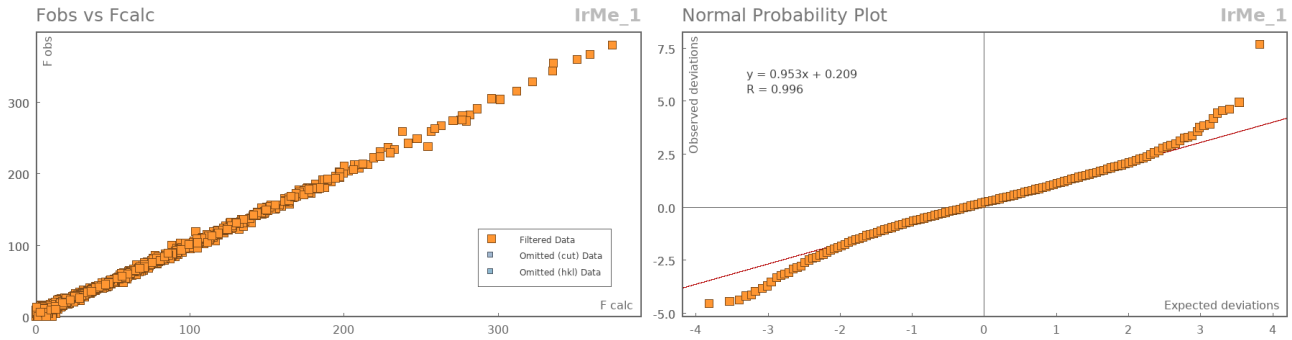

Reflection Statistics

Total reflections (after filtering)	38597	Unique reflections	7331
Completeness	0.893	Mean I/σ	21.73
hkl_{max} collected	(21, 24, 20)	hkl_{min} collected	(-20, -17, -26)
hkl_{max} used	(21, 24, 26)	hkl_{min} used	(0, 0, 0)
Lim d_{max} collected	20.0	Lim d_{min} collected	0.62
d_{max} used	16.88	d_{min} used	0.65
Friedel pairs	6057	Friedel pairs merged	1
Inconsistent equivalents	0	R_{int}	0.0411
R_{sigma}	0.0327	Intensity transformed	0
Omitted reflections	0	Omitted by user (OMIT hkl)	0
Multiplicity	(19904, 6751, 1222, 291, 59, 11)	Maximum multiplicity	18
Removed systematic absences	2075	Filtered off (Shel/OMIT)	0

Images of the Crystal on the Diffractometer

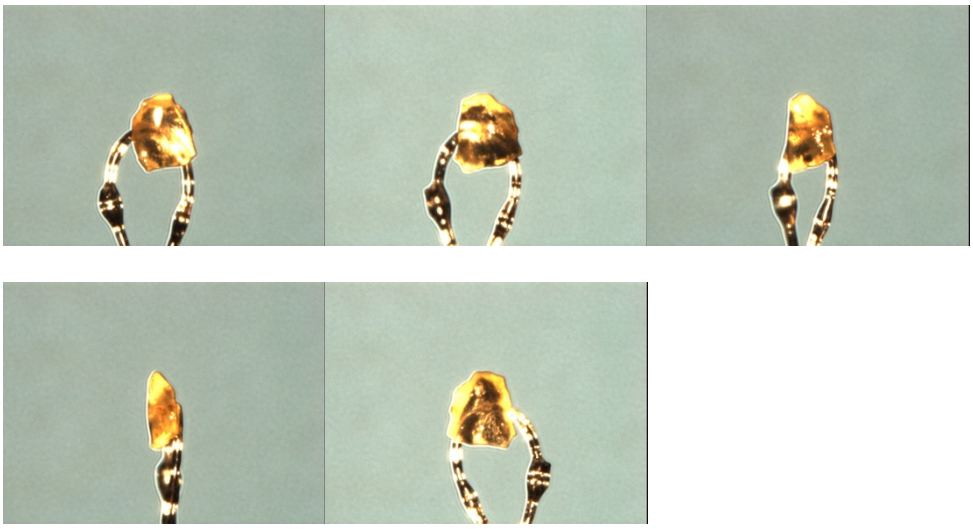

Table 5-15: Fractional Atomic Coordinates (×10⁴) and Equivalent Isotropic Displacement Parameters (Å²×10³) for **5-31**. U_{eq} is defined as 1/3 of the trace of the orthogonalised U_{ij}.

Atom	x	y	z	U_{eq}
Ir1	3471.03(10)	2974.83(8)	3476.71(8)	13.96(6)
C20	2098.2(12)	3072.1(10)	4118.9(11)	18.6(3)
C3	4585.3(12)	3481.6(10)	4193.6(10)	16.7(3)
C11	4412.6(12)	3910.2(10)	2066.7(10)	17.1(3)
C21	2228.4(13)	2289.7(10)	3818.8(12)	19.7(3)
C19	2056.5(12)	3616.9(9)	3495.9(11)	18.2(3)
C25	1965.6(16)	3272.6(14)	4939.3(13)	28.3(4)
C23	2113.9(15)	3503.5(16)	2016.0(13)	31.8(5)
C14	4101.4(16)	4580.0(14)	624.1(13)	30.0(4)
C5	3875.5(15)	4548.2(12)	5035.7(12)	23.5(3)
C1	4344.3(14)	1952.4(10)	3465.9(11)	20.1(3)
C8	4575.5(19)	3794.1(13)	6318.6(12)	32.2(5)

Atom	x	y	z	U_{eq}
C17	2256.1(13)	2353.7(10)	2994.4(11)	19.9(3)
C26	2245.5(17)	1536.2(12)	4264.1(17)	33.0(5)
C15	4010.8(17)	5038.9(13)	1275.6(13)	29.9(4)
C4	4376.8(12)	3838.8(10)	4942.7(10)	17.3(3)
C6	3720.0(15)	4871.9(12)	5749.4(12)	25.6(4)
C7	4067.6(17)	4496.8(13)	6396.4(12)	27.7(4)
C2	4446.3(11)	3919.7(10)	3508.7(10)	17.1(3)
C12	4514.7(16)	3462.4(12)	1404.7(11)	26.0(4)
C9	4722.3(16)	3472.0(12)	5598.2(11)	25.4(4)
C10	4595.0(12)	3520.2(10)	2803.1(10)	17.0(3)
C18	2151.1(12)	3174.6(11)	2804.4(11)	19.0(3)
C24	1867.3(15)	4486.7(11)	3542.6(15)	28.6(4)
C22	2261.9(17)	1672.3(14)	2453.8(16)	33.8(5)
C16	4163.8(16)	4707.7(11)	1990.4(12)	24.3(4)
C13	4352.0(18)	3788.3(14)	694.9(13)	32.1(5)

Table 5-16: Anisotropic Displacement Parameters ($\times 10^4$) for **5-31**. The anisotropic displacement factor exponent takes the form: $-2\pi^2[h^2a^{*2} \times U_{11} + ... + 2hka^* \times b^* \times U_{12}]$

Atom	U_{11}	U_{22}	U_{33}	U_{23}	U_{13}	U_{12}
Ir1	12.77(8)	10.77(8)	18.33(9)	-0.03(5)	-0.48(6)	-0.61(6)
C20	16.5(7)	15.7(7)	23.6(8)	-0.7(5)	2.7(5)	0.6(5)
C3	15.1(6)	17.8(6)	17.3(7)	-0.3(5)	-2.1(5)	-2.8(5)
H3	32(8)	38(8)	18(10)	19(4)	0(6)	-1(6)

Atom	U_{11}	U_{22}	U_{33}	U_{23}	U_{13}	U_{12}
C11	16.2(7)	17.7(6)	17.3(7)	-1.3(5)	1.4(5)	0.2(5)
C21	18.5(7)	12.0(6)	28.6(8)	-2.7(5)	0.9(6)	1.7(5)
C19	15.3(6)	12.3(6)	27.0(8)	0.5(4)	0.7(6)	1.5(5)
C25	25.3(9)	34.4(10)	25.2(9)	-2.7(8)	6.8(7)	-4.8(7)
H25a	80(20)	80(20)	46(17)	32(10)	-4(9)	8(8)
H25b	80(20)	45(6)	70(20)	-22(6)	15(14)	-19(6)
H25c	30(4)	120(30)	70(20)	-7(5)	21(4)	-15(16)
C23	18.4(9)	49.9(14)	27.1(10)	-5.0(8)	-5.0(7)	12.7(9)
H23a	90(30)	70(8)	70(20)	-43(7)	-12(15)	20(8)
H23b	60(20)	72(18)	31(14)	22(10)	-3(8)	10(7)
H23c	27(4)	110(30)	90(20)	-6(6)	-26(4)	21(16)
C14	30.9(10)	35.4(10)	23.8(9)	1.7(7)	0.9(7)	6.3(7)
H14	80(30)	40(17)	25(5)	7(15)	-4(7)	8(4)
C5	27.0(9)	21.5(8)	22.1(8)	3.3(6)	-2.1(6)	-4.6(6)
H5	80(30)	80(20)	30(11)	44(15)	-4(7)	9(7)
C1	23.5(7)	15.5(6)	21.4(7)	4.0(5)	0.0(7)	0.1(6)
H1a	25(3)	50(20)	80(30)	-2(3)	6(3)	-4(15)
H1b	100(30)	54(18)	43(10)	0(14)	16(10)	25(6)
H1c	90(30)	28(14)	30(10)	-5(11)	-13(9)	-7(5)
C8	48.1(13)	29.0(9)	19.5(8)	2.5(8)	1.6(8)	1.4(6)
H8	120(40)	80(30)	29(12)	39(18)	-10(9)	10(8)
C17	17.8(7)	16.2(7)	25.8(8)	-3.5(5)	-1.7(6)	-3.3(5)
C26	29.3(10)	19.0(8)	50.7(14)	-3.7(7)	0.3(10)	14.2(8)
H26a	62(17)	39(14)	90(30)	17(7)	23(10)	16(10)
H26b	90(30)	70(20)	59(5)	2(15)	-21(5)	3(5)
H26c	35(5)	47(18)	110(30)	-15(4)	-10(7)	43(14)

Atom	U_{11}	U_{22}	U_{33}	U_{23}	U_{13}	U_{12}
C15	38.7(11)	25.7(9)	25.4(9)	2.7(8)	-1.5(7)	6.3(6)
H15	140(20)	35(3)	16(3)	33(4)	-3(2)	4.1(12)
C4	16.9(7)	17.0(6)	17.8(7)	-2.4(5)	-1.0(5)	-0.4(5)
C6	29.8(9)	22.7(8)	24.2(8)	-2.6(7)	2.7(6)	-7.4(6)
H6	180(40)	64(12)	21(19)	75(11)	-1(17)	-9(9)
C7	35.8(10)	26.9(9)	20.4(9)	-6.3(7)	4.0(7)	-4.2(6)
H7	70(30)	49(18)	23(5)	9(15)	2(6)	-11(4)
C2	16.2(6)	17.2(6)	18.1(7)	-2.3(5)	-0.4(5)	-1.1(5)
H2	43(18)	22(4)	28(16)	9(4)	15(12)	5(6)
C12	35.5(10)	25.6(8)	17.0(8)	4.6(7)	1.9(6)	-2.9(6)
H12	170(30)	38(4)	27(3)	45(5)	-16(2)	-8.5(12)
C9	35.6(10)	21.0(8)	19.5(8)	2.3(7)	-0.7(6)	1.9(6)
H9	110(30)	44(9)	50(20)	43(8)	-12(15)	-7(9)
C10	13.7(6)	17.6(6)	19.7(7)	-0.9(5)	0.3(5)	-1.0(5)
H10	32(8)	38(8)	18(10)	19(4)	0(6)	-1(6)
C18	15.0(7)	20.6(7)	21.6(7)	-0.7(5)	-1.5(5)	1.7(5)
C24	20.6(8)	14.6(7)	50.7(14)	2.4(6)	-0.7(9)	0.8(7)
H24a	70(20)	30(16)	64(9)	7(12)	-23(7)	-8(6)
H24b	50(20)	41(17)	79(16)	1(10)	21(8)	19(8)
H24c	22(3)	40(18)	90(30)	8(2)	-4(3)	-6(14)
C22	29.6(11)	29.7(10)	42.0(13)	-4.5(8)	-0.9(9)	-18.8(9)
H22a	70(20)	70(20)	49(7)	-16(13)	14(6)	-15(6)
H22b	80(20)	45(13)	80(20)	15(8)	-26(12)	-16(8)
H22c	39(6)	80(20)	70(20)	-23(5)	-7(6)	-17(15)
C16	33.0(10)	18.1(7)	21.9(8)	1.7(6)	-2.1(7)	0.9(6)
H16	170(30)	38(4)	27(3)	45(5)	-16(2)	-8.5(12)

Atom	U_{11}	U_{22}	U_{33}	U_{23}	U_{13}	U_{12}
C13	41.3(12)	36.5(11)	18.7(8)	7.2(8)	1.6(8)	-1.0(7)
H13	140(20)	35(3)	16(3)	33(4)	-3(2)	4.1(12)

Table 5-17: Bond Lengths in Å for **5-31**.

Atom	Atom	Length/Å
Ir1	C20	2.2564(17)
Ir1	C3	2.1955(17)
Ir1	C21	2.1911(17)
Ir1	C19	2.2789(16)
Ir1	C1	2.1236(17)
Ir1	C17	2.1876(17)
Ir1	C2	2.1110(16)
Ir1	C10	2.1892(17)
Ir1	C18	2.2395(18)
C20	C21	1.435(2)
C20	C19	1.433(3)
C20	C25	1.496(3)
C3	C4	1.481(2)
C3	C2	1.429(2)
C11	C12	1.397(3)
C11	C10	1.478(2)
C11	C16	1.398(3)
C21	C17	1.457(3)

Atom	Atom	Length/Å
C21	C26	1.495(3)
C19	C18	1.435(3)
C19	C24	1.495(2)
C23	C18	1.497(3)
C14	C15	1.391(3)
C14	C13	1.388(3)
C5	C4	1.402(3)
C5	C6	1.389(3)
C8	C7	1.394(3)
C8	C9	1.396(3)
C17	C18	1.433(2)
C17	C22	1.493(3)
C15	C16	1.395(3)
C4	C9	1.399(3)
C6	C7	1.394(3)
C2	C10	1.430(2)
C12	C13	1.386(3)

Table 5-18: Bond Angles in ° for **5-31**.

Atom	Atom	Atom	Angle/°
C3	Ir1	C20	107.65(7)
C21	Ir1	C20	37.60(6)
C21	Ir1	C3	128.71(7)

Atom	Atom	Atom	Angle/°
C19	Ir1	C20	36.84(6)
C19	Ir1	C3	116.02(6)
C19	Ir1	C21	62.62(6)
C1	Ir1	C20	124.47(7)
C1	Ir1	C3	84.42(7)
C1	Ir1	C21	92.40(7)
C1	Ir1	C19	154.04(7)
C17	Ir1	C20	63.33(7)
C17	Ir1	C3	167.48(7)
C17	Ir1	C21	38.87(7)
C17	Ir1	C19	62.71(6)
C17	Ir1	C1	93.76(7)
C2	Ir1	C20	119.74(6)
C2	Ir1	C3	38.69(7)
C2	Ir1	C21	156.56(7)
C2	Ir1	C19	102.48(6)
C2	Ir1	C1	103.46(7)
C2	Ir1	C17	152.58(7)
C10	Ir1	C20	150.28(6)
C10	Ir1	C3	67.97(6)
C10	Ir1	C21	162.88(7)
C10	Ir1	C19	116.61(6)
C10	Ir1	C1	85.01(7)
C10	Ir1	C17	124.30(7)
C10	Ir1	C2	38.79(6)
C18	Ir1	C20	62.24(7)

Atom	Atom	Atom	Angle/°
C18	Ir1	C3	147.81(6)
C18	Ir1	C21	63.50(7)
C18	Ir1	C19	37.03(7)
C18	Ir1	C1	127.17(7)
C18	Ir1	C17	37.76(7)
C18	Ir1	C2	116.56(7)
C18	Ir1	C10	104.92(7)
C21	C20	Ir1	68.73(10)
C19	C20	Ir1	72.44(10)
C19	C20	C21	108.28(16)
C25	C20	Ir1	127.53(14)
C25	C20	C21	125.48(17)
C25	C20	C19	126.13(17)
C4	C3	Ir1	121.87(12)
C2	C3	Ir1	67.45(9)
C2	C3	C4	120.97(15)
C10	C11	C12	118.28(16)
C16	C11	C12	117.82(17)
C16	C11	C10	123.88(16)
C20	C21	Ir1	73.67(10)
C17	C21	Ir1	70.43(10)
C17	C21	C20	107.62(15)
C26	C21	Ir1	125.48(14)
C26	C21	C20	126.3(2)
C26	C21	C17	125.87(19)
C20	C19	Ir1	70.73(10)

Atom	Atom	Atom	Angle/°
C18	C19	Ir1	69.99(10)
C18	C19	C20	108.22(14)
C24	C19	Ir1	128.73(12)
C24	C19	C20	126.54(19)
C24	C19	C18	125.06(18)
C13	C14	C15	119.0(2)
C6	C5	C4	121.48(19)
C9	C8	C7	119.8(2)
C21	C17	Ir1	70.70(10)
C18	C17	Ir1	73.09(10)
C18	C17	C21	107.56(16)
C22	C17	Ir1	127.77(14)
C22	C17	C21	125.38(18)
C22	C17	C18	126.6(2)
C16	C15	C14	120.5(2)
C5	C4	C3	123.58(16)
C9	C4	C3	119.07(16)
C9	C4	C5	117.31(17)
C7	C6	C5	120.39(19)
C6	C7	C8	119.24(19)
C3	C2	Ir1	73.85(10)
C10	C2	Ir1	73.56(10)
C10	C2	C3	118.04(15)
C13	C12	C11	121.42(19)
C4	C9	C8	121.74(19)
C11	C10	Ir1	122.42(12)

Atom	Atom	Atom	Angle/˚
C2	C10	Ir1	67.65(9)
C2	C10	C11	121.85(15)
C19	C18	Ir1	72.98(10)
C23	C18	Ir1	125.18(13)
C23	C18	C19	126.26(18)
C17	C18	Ir1	69.16(10)
C17	C18	C19	108.32(16)
C17	C18	C23	125.39(19)
C15	C16	C11	120.80(19)
C12	C13	C14	120.4(2)

Table 5-19: Torsion Angles in ˚ for **5-31**.

Atom	Atom	Atom	Atom	Angle/˚
Ir1	C20	C21	C17	-62.66(11)
Ir1	C20	C21	C26	122.36(13)
Ir1	C20	C19	C18	60.22(10)
Ir1	C20	C19	C24	-124.46(11)
Ir1	C3	C4	C5	-68.75(16)
Ir1	C3	C4	C9	113.64(15)
Ir1	C3	C2	C10	-60.80(11)
Ir1	C21	C20	C19	61.99(11)
Ir1	C21	C20	C25	-

Atom	Atom	Atom	Atom	Angle/°
				121.69(12)
Ir1	C21	C17	C18	-64.27(11)
Ir1	C21	C17	C22	123.18(12)
Ir1	C19	C20	C21	-59.65(11)
Ir1	C19	C20	C25	124.06(12)
Ir1	C19	C18	C23	-121.51(12)
Ir1	C19	C18	C17	60.44(11)
Ir1	C17	C21	C20	64.79(10)
Ir1	C17	C21	C26	-120.21(12)
Ir1	C17	C18	C19	-62.87(10)
Ir1	C17	C18	C23	119.06(12)
Ir1	C2	C3	C4	-114.69(9)
Ir1	C2	C10	C11	115.28(9)
Ir1	C10	C11	C12	-93.58(16)
Ir1	C10	C11	C16	87.93(16)
Ir1	C10	C2	C3	60.95(11)
Ir1	C18	C19	C20	-60.68(10)
Ir1	C18	C19	C24	123.91(11)
Ir1	C18	C17	C21	62.70(11)
Ir1	C18	C17	C22	-124.86(13)
C20	C21	C17	C18	0.52(16)
C20	C21	C17	C22	-172.03(15)

Atom	Atom	Atom	Atom	Angle/°
C20	C19	C18	C23	177.81(14)
C20	C19	C18	C17	-0.24(16)
C3	C4	C5	C6	-178.17(19)
C3	C4	C9	C8	177.89(19)
C3	C2	C10	C11	176.23(14)
C11	C12	C13	C14	1.4(3)
C11	C16	C15	C14	0.1(3)
C21	C17	C18	C19	-0.17(16)
C21	C17	C18	C23	-178.24(15)
C19	C18	C17	C22	172.26(15)
C23	C18	C17	C22	-5.8(2)
C5	C4	C9	C8	0.1(2)
C5	C6	C7	C8	0.2(3)

Table 5-20: Hydrogen Fractional Atomic Coordinates (×10^4) and Equivalent Isotropic Displacement Parameters (Å^2×10^3) for **5-31**. U_{eq} is defined as 1/3 of the trace of the orthogonalised U_{ij}.

Atom	x	y	z	U_{eq}
H3	5160(20)	3031(16)	4226(15)	30(5)
H25a	2340(30)	2890(20)	5310(20)	68(11)
H25b	2200(30)	3860(20)	5090(20)	63(10)
H25c	1260(20)	3270(30)	5120(20)	72(11)

Atom	x	y	z	U_{eq}
H23a	2450(30)	4070(20)	1970(20)	79(11)
H23b	2470(30)	3090(20)	1580(18)	53(10)
H23c	1420(20)	3530(30)	1820(20)	76(11)
H14	3990(30)	4834(17)	64(16)	47(9)
H5	3590(30)	4830(20)	4524(18)	63(11)
H1a	5110(20)	2066(18)	3410(20)	51(9)
H1b	4200(30)	1610(20)	3950(19)	67(11)
H1c	4180(30)	1580(17)	3011(17)	50(9)
H8	4880(30)	3500(20)	6856(19)	75(14)
H26a	2750(30)	1103(19)	4070(20)	65(10)
H26b	2470(30)	1630(20)	4830(20)	76(11)
H26c	1570(20)	1260(20)	4300(20)	64(10)
H15	3790(30)	5674(19)	1238(17)	64(8)
H6	3370(30)	5430(20)	5805(19)	87(16)
H7	3970(30)	4748(19)	6959(16)	48(9)
H2	4130(20)	4500(16)	3534(15)	31(7)
H12	4740(30)	2865(9)	1416(17)	77(10)
H9	5080(30)	2926(12)	5541(18)	66(11)
H10	5140(20)	3070(16)	2781(14)	30(5)
H24a	2130(30)	4747(18)	4070(20)	55(9)
H24b	2230(30)	4814(19)	3110(20)	58(9)
H24c	1110(20)	4621(19)	3500(20)	50(9)
H22a	2580(30)	1830(20)	1910(20)	61(10)
H22b	2670(30)	1180(20)	2710(20)	68(11)
H22c	1550(20)	1440(20)	2320(20)	61(10)
H16	4090(30)	5071(18)	2486(17)	77(10)

Atom	x	y	z	U_{eq}
H13	4430(30)	3437(14)	203(9)	64(8)

Table 5-21: Selected Bond Lengths in Å for **5-31**.

Atom	Atom	Length/Å
C3	H3	1.11(3)
C25	H25a	1.06(3)
C25	H25b	1.08(3)
C25	H25c	1.05(3)
C23	H23a	1.07(4)
C23	H23b	1.16(3)
C23	H23c	1.04(3)
C14	H14	1.09(3)
C5	H5	1.10(3)
C1	H1a	1.10(3)
C1	H1b	1.05(3)
C1	H1c	1.05(3)
C8	H8	1.15(3)
C26	H26a	1.08(3)
C26	H26b	1.06(4)
C26	H26c	1.06(3)
C15	H15	1.12(3)
C6	H6	1.07(3)
C7	H7	1.09(3)

Atom	Atom	Length/Å
C2	H2	1.08(3)
C12	H12	1.056(3)
C9	H9	1.056(3)
C10	H10	1.09(3)
C24	H24a	1.10(3)
C24	H24b	1.07(3)
C24	H24c	1.10(3)
C22	H22a	1.10(4)
C22	H22b	1.10(3)
C22	H22c	1.11(3)
C16	H16	1.07(3)
C13	H13	1.056(3)

Table 5-22: Selected Bond Angles in ° for **5-31**.

Atom	Atom	Atom	Angle/°
H3	C3	Ir1	106.6(15)
C4	C3	H3	112.2(14)
C2	C3	H3	119.8(14)
H25a	C25	C20	113.4(19)
H25b	C25	C20	113.8(19)
H25b	C25	H25a	105(3)
H25c	C25	C20	114(2)
H25c	C25	H25a	107(3)

Atom	Atom	Atom	Angle/°
H25c	C25	H25b	103(3)
H23b	C23	H23a	107(3)
H23c	C23	H23a	111(3)
H23c	C23	H23b	102(3)
C18	C23	H23a	113(2)
C18	C23	H23b	112.1(16)
C18	C23	H23c	111(2)
C15	C14	H14	121.1(16)
C13	C14	H14	119.9(16)
C4	C5	H5	117.8(18)
C6	C5	H5	120.7(17)
H1a	C1	Ir1	115.5(16)
H1b	C1	Ir1	109(2)
H1b	C1	H1a	111(3)
H1c	C1	Ir1	111.3(18)
H1c	C1	H1a	105(3)
H1c	C1	H1b	104(3)
C7	C8	H8	118.4(19)
C9	C8	H8	121.8(19)
H26a	C26	C21	115.0(18)
H26b	C26	C21	112(2)
H26b	C26	H26a	102(3)
H26c	C26	C21	113.0(17)
H26c	C26	H26a	108(3)
H26c	C26	H26b	106(3)
H15	C15	C14	120.7(16)

Atom	Atom	Atom	Angle/°
C16	C15	H15	118.7(16)
H6	C6	C5	120.1(18)
C7	C6	H6	119.3(18)
H7	C7	C8	119.1(17)
H7	C7	C6	121.6(17)
H2	C2	Ir1	114.4(16)
H2	C2	C3	119.5(14)
C10	C2	H2	121.7(14)
H12	C12	C11	122.1(16)
C13	C12	H12	116.4(16)
H9	C9	C8	119.9(18)
H9	C9	C4	118.3(18)
H10	C10	Ir1	104.2(15)
H10	C10	C11	113.8(14)
H10	C10	C2	117.8(14)
H24a	C24	C19	112.4(16)
H24b	C24	C19	112.4(18)
H24b	C24	H24a	104(3)
H24c	C24	C19	112.0(17)
H24c	C24	H24a	107(3)
H24c	C24	H24b	109(3)
H22a	C22	C17	112.5(18)
H22b	C22	C17	108.7(18)
H22b	C22	H22a	109(3)
H22c	C22	C17	113.6(19)
H22c	C22	H22a	106(3)

Atom	Atom	Atom	Angle/°
H22c	C22	H22b	107(3)
H16	C16	C11	119.8(16)
H16	C16	C15	119.4(16)
H13	C13	C14	119.6(15)
H13	C13	C12	120.0(15)

Citations for Complex 5-31

CrysAlisPro (ROD), Rigaku Oxford Diffraction, Poland.

CrysAlisPro Software System, Rigaku Oxford Diffraction, (2020).

L.J. Bourhis and O.V. Dolomanov and R.J. Gildea and J.A.K. Howard and H. Puschmann, The Anatomy of a Comprehensive Constrained, Restrained, Refinement Program for the Modern Computing Environment - Olex2 Disected, *Acta Cryst. A*, (2015), **A71**, 59-71.

O.V. Dolomanov and L.J. Bourhis and R.J. Gildea and J.A.K. Howard and H. Puschmann, Olex2: A complete structure solution, refinement and analysis program, *J. Appl. Cryst.*, (2009), **42**, 339-341.

Complex 5-32 IrCp*(DPP)Ph:

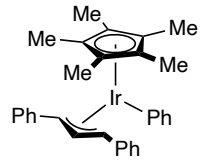

Structure Tables

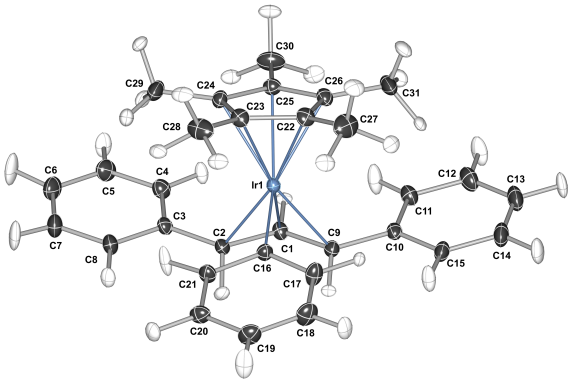

Complex 5-32 was crystallized by slow evaportaion of hexanes DCM solution. The data for tan-55-90-ircpdpppph were collected from a shock-cooled single crystal at 101 K on a XtaLAB Synergy, Dualflex, HyPix four-circle diffractometer with a micro-focus sealed X-ray tube using graphite as monochromator and a HyPix detector. The diffractometer was equipped with a low temperature device and used MoK_α radiation (λ = 0.71073 Å). All data were integrated and a absorption correction using SCALE3 ABSPACK was applied.[1,2] The structure were solved by dual methods and refined by full-matrix least-squares methods against F^2 [3,4] All non-hydrogen atoms were refined with anisotropic displacement parameters.

The hydrogen atoms were refined isotropically on calculated positions using a riding model with their U_{iso} values constrained to 1.5 times the U_{eq} of their pivot atoms for terminal sp^3 carbon atoms and 1.2 times for all other carbon atoms. Crystallographic data (including structure factors) for the structures reported in this paper have been deposited with the Cambridge Crystallographic Data Centre.[5] CCDC contain the supplementary crystallographic data for this paper. Copies of the data can be obtained free of charge from the Cambridge Crystallographic Data Centre via www.ccdc.cam.ac.uk/structures. This report and the CIF file were generated using FinalCif.[6]

Crystal data and structure refinement for 5-32

CCDC number	
Empirical formula	$C_{31}H_{33}Ir$
Formula weight	597.82
Temperature [K]	101
Crystal system	?
Space group (number)	?
a [Å]	17.4633(1)
b [Å]	19.1923(2)
c [Å]	7.2836(1)
α [Å]	90
β [Å]	90
γ [Å]	90
Volume [Å^3]	2441.18(4)
Z	4
ρ_{calc} [g/cm^3]	1.627
μ [mm^{-1}]	5.485
F(000)	1184
Crystal size [mm^3]	0.326×0.257×0.146
Crystal colour	light yellow
Crystal shape	prism

Radiation	MoK_α (λ=0.71073 Å)	Data / Restraints / Parameters	12393/514/612
2Θ range [°]	3.16 to 76.30 (0.58 Å)	Goodness-of-fit on F^2	1.028
Index ranges	-29 ≤ h ≤ 29 -32 ≤ k ≤ 32 -12 ≤ l ≤ 12	Final R indexes [$I \geq 2\sigma(I)$]	R_1 = 0.0190 wR_2 = 0.0355
Reflections collected	78781	Final R indexes [all data]	R_1 = 0.0233 wR_2 = 0.0361
Independent reflections	12393 R_{int} = 0.0452 R_{sigma} = ?	Largest peak/hole [eÅ^3]	1.53/-1.57
Completeness to θ = 25.24°	100.0 %	Flack X parameter	0.040(5)

Atomic coordinates and U_{eq} [Å^2] for Complex 5-32

Atom	***x***	***y***	***z***	U_{eq}
Ir1	0.57149(1)	0.78602(1)	0.50011(2)	0.0108(1)
C1	0.65722(9)	0.75992(9)	0.6925(3)	0.0150(4)
C2	0.59539(10)	0.71271(8)	0.7263(3)	0.0143(4)
C3	0.59990(9)	0.63719(8)	0.6884(3)	0.0150(4)
C4	0.66469(10)	0.60432(9)	0.6148(3)	0.0187(4)
C5	0.66530(12)	0.53291(9)	0.5801(3)	0.0229(5)
C6	0.60091(13)	0.49251(9)	0.6174(3)	0.0252(5)
C7	0.53630(11)	0.52391(9)	0.6921(3)	0.0232(5)
C8	0.53620(10)	0.59518(9)	0.7284(3)	0.0182(4)
C9	0.64147(10)	0.83253(8)	0.7176(3)	0.0145(4)
C10	0.69714(9)	0.88811(8)	0.6727(3)	0.0149(4)
C11	0.77000(10)	0.87528(9)	0.6005(3)	0.0194(4)
C12	0.81945(11)	0.93003(11)	0.5565(3)	0.0253(5)
C13	0.79701(12)	0.99886(10)	0.5834(3)	0.0272(5)
C14	0.72499(13)	1.01242(10)	0.6573(3)	0.0256(5)
C15	0.67605(11)	0.95797(9)	0.7028(3)	0.0193(4)
C16	0.47775(9)	0.81633(8)	0.6537(3)	0.0144(4)
C17	0.46151(10)	0.88643(9)	0.6914(3)	0.0210(5)
C18	0.39336(11)	0.90719(10)	0.7762(3)	0.0245(5)
C19	0.33942(10)	0.85796(11)	0.8293(3)	0.0231(5)
C20	0.35412(10)	0.78817(10)	0.7961(3)	0.0193(4)
C21	0.42180(12)	0.76779(12)	0.7087(4)	0.0167(5)
C22	0.53359(10)	0.84065(9)	0.2514(3)	0.0175(4)
C23	0.49814(10)	0.77248(9)	0.2585(3)	0.0167(4)

C24	0.55722(11)	0.72121(8)	0.2450(3)	0.0156(4)
C25	0.62949(9)	0.75683(9)	0.2302(3)	0.0157(4)
C26	0.61452(11)	0.83045(9)	0.2317(3)	0.0165(4)
C27	0.49298(15)	0.90906(11)	0.2374(4)	0.0299(6)
C28	0.41378(14)	0.75814(18)	0.2570(5)	0.0281(7)
C29	0.54563(13)	0.64430(10)	0.2373(3)	0.0244(5)
C30	0.70500(12)	0.72279(12)	0.1984(4)	0.0269(6)
C31	0.67233(13)	0.88695(11)	0.2050(3)	0.0269(6)
H1	0.7105(14)	0.7412(13)	0.624(4)	0.023(6)
H2	0.5553(16)	0.7302(15)	0.847(5)	0.032(6)
H4	0.7160(14)	0.6332(12)	0.581(4)	0.040(7)
H5	0.7174(14)	0.5070(11)	0.534(7)	0.051(11)
H6	0.6050(18)	0.4381(13)	0.577(6)	0.079(17)
H7	0.487(2)	0.4939(17)	0.709(7)	0.067(14)
H8	0.4851(15)	0.6147(14)	0.800(5)	0.039(8)
H9	0.5992(14)	0.8475(13)	0.823(4)	0.019(5)
H11	0.7874(16)	0.8240(13)	0.574(6)	0.071(14)
H12	0.8770(14)	0.9180(13)	0.500(9)	0.067(11)
H13	0.8367(15)	1.0409(12)	0.548(5)	0.053(11)
H14	0.7075(18)	1.0664(13)	0.682(5)	0.057(11)
H15	0.6180(16)	0.9666(13)	0.756(5)	0.053(11)
H17	0.5028(14)	0.9261(13)	0.652(4)	0.026(6)
H18	0.3864(17)	0.9587(13)	0.800(5)	0.049(8)
H19	0.2861(17)	0.8742(15)	0.889(6)	0.069(11)
H20	0.3114(16)	0.7466(14)	0.842(5)	0.045(8)
H21	0.4360(18)	0.7079(13)	0.695(7)	0.063(14)

H27A	0.4351(16)	0.9085(15)	0.324(4)	0.037(5)
H27B	0.5316(17)	0.9512(14)	0.300(4)	0.035(5)
H27C	0.4819(18)	0.9234(15)	0.109(5)	0.044(5)
H28A	0.4001(19)	0.7106(15)	0.334(5)	0.033(4)
H28B	0.3822(17)	0.7945(15)	0.330(5)	0.037(4)
H28C	0.3836(16)	0.7467(18)	0.137(5)	0.041(5)
H29A	0.5903(18)	0.6092(14)	0.296(5)	0.036(5)
H29B	0.4924(18)	0.6304(14)	0.299(5)	0.038(5)
H29C	0.5381(18)	0.6259(13)	0.093(4)	0.037(5)
H30A	0.7578(17)	0.7557(17)	0.254(5)	0.043(5)
H30B	0.7093(16)	0.6705(15)	0.266(4)	0.035(5)
H30C	0.7190(17)	0.7141(13)	0.053(4)	0.041(5)
H31A	0.6697(17)	0.9292(14)	0.310(4)	0.033(5)
H31B	0.7310(18)	0.8746(16)	0.216(5)	0.044(5)
H31C	0.6655(18)	0.9075(16)	0.082(4)	0.046(4)

U_{eq} is defined as 1/3 of the trace of the orthogonalized U_{ij} tensor.

Bond lengths and angles for 5-32

Atom–Atom	**Length [Å]**
Ir1–C1	2.1110(19)
Ir1–C2	2.2064(19)
Ir1–C9	2.191(2)
Ir1–C16	2.0663(18)
Ir1–C22	2.195(2)
Ir1–C23	2.192(2)
Ir1–C24	2.250(2)
Ir1–C25	2.281(2)
Ir1–C26	2.261(2)
C1–C2	1.431(2)
C1–C9	1.432(2)
C2–C3	1.478(2)
C3–C4	1.402(2)
C3–C8	1.404(2)
C4–C5	1.394(2)

C5–C6	1.393(3)
C6–C7	1.390(3)
C7–C8	1.393(2)
C9–C10	1.480(2)
C10–C11	1.399(2)
C10–C15	1.408(2)
C11–C12	1.397(3)
C12–C13	1.392(3)
C13–C14	1.393(3)
C14–C15	1.390(3)
C16–C17	1.402(2)
C16–C21	1.408(3)
C17–C18	1.399(3)
C18–C19	1.389(3)
C19–C20	1.385(3)
C20–C21	1.398(3)
C22–C23	1.448(2)
C22–C26	1.434(3)
C22–C27	1.496(3)
C23–C24	1.429(2)
C23–C28	1.499(3)
C24–C25	1.439(2)
C24–C29	1.491(2)
C25–C26	1.437(2)
C25–C30	1.490(3)
C26–C31	1.494(3)

C1–H1	1.12(3)
C2–H2	1.17(3)
C4–H4	1.08(2)
C5–H5	1.09(3)
C6–H6	1.09(3)
C7–H7	1.04(3)
C8–H8	1.10(3)
C9–H9	1.10(3)
C11–H11	1.05(3)
C12–H12	1.11(3)
C13–H13	1.09(3)
C14–H14	1.10(3)
C15–H15	1.10(3)
C17–H17	1.09(3)
C18–H18	1.01(3)
C19–H19	1.07(3)
C20–H20	1.14(3)
C21–H21	1.18(3)
C27–H27A	1.19(3)
C27–H27B	1.15(3)
C27–H27C	0.99(4)
C28–H28A	1.10(3)
C28–H28B	1.04(3)
C28–H28C	1.04(3)
C29–H29A	1.12(3)
C29–H29B	1.07(3)

C29–H29C	1.12(3)
C30–H30A	1.19(3)
C30–H30B	1.12(3)
C30–H30C	1.10(3)
C31–H31A	1.12(3)
C31–H31B	1.06(3)
C31–H31C	0.99(3)
Atom–Atom–Atom	**Angle [°]**
C1–Ir1–C2	38.63(7)
C1–Ir1–C9	38.84(6)
C1–Ir1–C16	105.62(8)
C1–Ir1–C22	151.04(7)
C1–Ir1–C23	156.81(7)
C1–Ir1–C24	119.71(7)
C1–Ir1–C25	101.47(7)
C1–Ir1–C26	115.32(7)
C2–Ir1–C9	67.32(6)
C2–Ir1–C16	85.71(7)
C2–Ir1–C22	167.90(7)
C2–Ir1–C23	129.37(7)
C2–Ir1–C24	106.56(7)
C2–Ir1–C25	113.75(7)
C2–Ir1–C26	145.40(7)
C9–Ir1–C16	86.32(7)
C9–Ir1–C22	124.77(6)

C9–Ir1–C23	162.70(6)
C9–Ir1–C24	152.15(7)
C9–Ir1–C25	118.39(7)
C9–Ir1–C26	106.63(7)
C16–Ir1–C22	94.22(7)
C16–Ir1–C23	90.29(7)
C16–Ir1–C24	121.00(7)
C16–Ir1–C25	152.55(7)
C16–Ir1–C26	128.70(7)
C22–Ir1–C23	38.55(7)
C22–Ir1–C24	63.20(7)
C22–Ir1–C25	62.62(7)
C22–Ir1–C26	37.50(7)
C23–Ir1–C24	37.51(7)
C23–Ir1–C25	62.52(7)
C23–Ir1–C26	62.93(7)
C24–Ir1–C25	37.03(6)
C24–Ir1–C26	62.05(7)
C25–Ir1–C26	36.88(6)
Ir1–C1–C2	74.29(11)
Ir1–C1–C9	73.60(11)
C2–C1–C9	116.70(15)
Ir1–C2–C1	67.08(11)
Ir1–C2–C3	119.75(15)
C1–C2–C3	123.28(16)
C2–C3–C4	123.77(15)

C2–C3–C8	118.83(15)
C4–C3–C8	117.40(15)
C3–C4–C5	121.20(17)
C4–C5–C6	120.40(18)
C5–C6–C7	119.37(16)
C6–C7–C8	120.06(17)
C3–C8–C7	121.55(17)
Ir1–C9–C1	67.57(11)
Ir1–C9–C10	120.02(15)
C1–C9–C10	123.16(15)
C9–C10–C11	123.63(15)
C9–C10–C15	118.70(15)
C11–C10–C15	117.66(15)
C10–C11–C12	121.07(16)
C11–C12–C13	120.49(18)
C12–C13–C14	119.08(18)
C13–C14–C15	120.46(18)
C10–C15–C14	121.20(18)
Ir1–C16–C17	122.44(13)
Ir1–C16–C21	121.16(14)
C17–C16–C21	116.02(17)
C16–C17–C18	122.13(16)
C17–C18–C19	120.41(18)
C18–C19–C20	118.91(17)
C19–C20–C21	120.44(18)
C16–C21–C20	122.1(2)

Ir1–C22–C23	70.61(11)
Ir1–C22–C26	73.75(12)
Ir1–C22–C27	128.20(17)
C23–C22–C26	107.55(15)
C23–C22–C27	126.35(17)
C26–C22–C27	125.47(17)
Ir1–C23–C22	70.84(11)
Ir1–C23–C24	73.44(12)
Ir1–C23–C28	127.01(19)
C22–C23–C24	108.12(15)
C22–C23–C28	125.86(19)
C24–C23–C28	125.64(19)
Ir1–C24–C23	69.05(11)
Ir1–C24–C25	72.67(11)
Ir1–C24–C29	126.40(15)
C23–C24–C25	108.13(14)
C23–C24–C29	125.89(17)
C25–C24–C29	125.90(17)
Ir1–C25–C24	70.29(11)
Ir1–C25–C26	70.80(12)
Ir1–C25–C30	129.40(16)
C24–C25–C26	107.87(14)
C24–C25–C30	125.42(16)
C26–C25–C30	126.40(16)
Ir1–C26–C22	68.74(12)
Ir1–C26–C25	72.32(12)

Ir1–C26–C31	127.64(15)
C22–C26–C25	108.32(15)
C22–C26–C31	125.44(16)
C25–C26–C31	126.13(17)
Ir1–C1–H1	111.8(15)
C2–C1–H1	120.2(13)
C9–C1–H1	122.1(13)
Ir1–C2–H2	105.3(15)
C1–C2–H2	113.5(14)
C3–C2–H2	116.9(14)
C3–C4–H4	121.7(13)
C5–C4–H4	117.1(13)
C4–C5–H5	120.7(12)
C6–C5–H5	118.7(12)
C5–C6–H6	115.4(17)
C7–C6–H6	125.1(17)
C6–C7–H7	119(2)
C8–C7–H7	121(2)
C3–C8–H8	123.1(14)
C7–C8–H8	115.2(14)
Ir1–C9–H9	103.7(14)
C1–C9–H9	118.1(13)
C10–C9–H9	113.9(13)
C10–C11–H11	119.9(16)
C12–C11–H11	119.0(16)
C11–C12–H12	119.2(13)

C13–C12–H12	120.3(13)
C12–C13–H13	119.2(13)
C14–C13–H13	121.7(14)
C13–C14–H14	119.5(17)
C15–C14–H14	120.0(17)
C10–C15–H15	116.1(13)
C14–C15–H15	122.6(13)
C16–C17–H17	119.1(13)
C18–C17–H17	118.8(13)
C17–C18–H18	117.2(17)
C19–C18–H18	122.4(18)
C18–C19–H19	120.2(15)
C20–C19–H19	120.8(15)
C19–C20–H20	120.2(15)
C21–C20–H20	119.3(15)
C16–C21–H21	118.3(17)
C20–C21–H21	119.3(18)
C22–C27–H27A	111.0(14)
C22–C27–H27B	108.2(14)
C22–C27–H27C	113.6(18)
H27A–C27–H27B	107(2)
H27A–C27–H27C	110(2)
H27B–C27–H27C	107(2)
C23–C28–H28A	111.3(18)
C23–C28–H28B	113.3(17)
C23–C28–H28C	122.8(17)

H28A–C28–H28B	101(2)
H28A–C28–H28C	98(3)
H28B–C28–H28C	108(3)
C24–C29–H29A	119.2(15)
C24–C29–H29B	110.5(15)
C24–C29–H29C	111.4(13)
H29A–C29–H29B	107(2)
H29A–C29–H29C	105(2)
H29B–C29–H29C	102(2)
C25–C30–H30A	113.6(15)
C25–C30–H30B	112.6(14)

C25–C30–H30C	114.4(15)
H30A–C30–H30B	106(2)
H30A–C30–H30C	104(2)
H30B–C30–H30C	106(2)
C26–C31–H31A	114.2(15)
C26–C31–H31B	118.9(17)
C26–C31–H31C	109.1(18)
H31A–C31–H31B	99(2)
H31A–C31–H31C	109(2)
H31B–C31–H31C	106(3)

Torsion angles for 5-32

Atom–Atom–Atom–Atom	**Torsion Angle [°]**
C2–Ir1–C1–C9	-124.70(16)
C9–Ir1–C1–C2	124.70(16)
C16–Ir1–C1–C2	61.68(11)
C16–Ir1–C1–C9	-63.02(12)
C22–Ir1–C1–C2	-166.80(13)
C22–Ir1–C1–C9	68.50(19)
C23–Ir1–C1–C2	-70.1(2)
C23–Ir1–C1–C9	165.21(16)
C24–Ir1–C1–C2	-79.15(12)
C24–Ir1–C1–C9	156.15(11)
C25–Ir1–C1–C2	-113.86(11)
C25–Ir1–C1–C9	121.44(11)

C26–Ir1–C1–C2	-150.06(10)
C26–Ir1–C1–C9	85.24(12)
C1–Ir1–C2–C3	-116.40(18)
C9–Ir1–C2–C1	-33.97(11)
C9–Ir1–C2–C3	-150.37(15)
C16–Ir1–C2–C1	-121.77(11)
C16–Ir1–C2–C3	121.83(14)
C23–Ir1–C2–C1	151.38(11)
C23–Ir1–C2–C3	34.99(17)
C24–Ir1–C2–C1	117.13(11)
C24–Ir1–C2–C3	0.73(15)
C25–Ir1–C2–C1	78.31(12)
C25–Ir1–C2–C3	-38.09(15)
C26–Ir1–C2–C1	52.60(17)

C26–Ir1–C2–C3	-63.79(18)
C1–Ir1–C9–C10	116.42(18)
C2–Ir1–C9–C1	33.80(11)
C2–Ir1–C9–C10	150.22(15)
C16–Ir1–C9–C1	120.68(11)
C16–Ir1–C9–C10	-122.90(13)
C22–Ir1–C9–C1	-146.74(11)
C22–Ir1–C9–C10	-30.32(16)
C24–Ir1–C9–C1	-48.74(19)
C24–Ir1–C9–C10	67.68(19)
C25–Ir1–C9–C1	-71.89(12)
C25–Ir1–C9–C10	44.53(14)
C26–Ir1–C9–C1	-109.93(11)
C26–Ir1–C9–C10	6.49(14)
C1–Ir1–C16–C17	96.84(17)
C1–Ir1–C16–C21	-90.48(19)
C2–Ir1–C16–C17	130.28(17)
C2–Ir1–C16–C21	-57.04(19)
C9–Ir1–C16–C17	62.78(17)
C9–Ir1–C16–C21	-124.54(19)
C22–Ir1–C16–C17	-61.85(17)
C22–Ir1–C16–C21	110.83(19)
C23–Ir1–C16–C17	-100.24(17)
C23–Ir1–C16–C21	72.44(19)
C24–Ir1–C16–C17	-122.96(16)
C24–Ir1–C16–C21	49.7(2)

C25–Ir1–C16–C17	-92.7(2)
C25–Ir1–C16–C21	80.0(2)
C26–Ir1–C16–C17	-45.6(2)
C26–Ir1–C16–C21	127.06(18)
C1–Ir1–C22–C23	141.13(14)
C1–Ir1–C22–C26	25.3(2)
C1–Ir1–C22–C27	-97.4(2)
C9–Ir1–C22–C23	-173.61(10)
C9–Ir1–C22–C26	70.58(13)
C9–Ir1–C22–C27	-52.1(2)
C16–Ir1–C22–C23	-85.17(11)
C16–Ir1–C22–C26	159.02(11)
C16–Ir1–C22–C27	36.34(18)
C23–Ir1–C22–C26	-115.82(15)
C23–Ir1–C22–C27	121.5(2)
C24–Ir1–C22–C23	37.61(11)
C24–Ir1–C22–C26	-78.21(11)
C24–Ir1–C22–C27	159.1(2)
C25–Ir1–C22–C23	79.40(11)
C25–Ir1–C22–C26	-36.42(10)
C25–Ir1–C22–C27	-159.09(19)
C26–Ir1–C22–C23	115.82(15)
C26–Ir1–C22–C27	-122.7(2)
C1–Ir1–C23–C22	-129.51(17)
C1–Ir1–C23–C24	-13.0(2)
C1–Ir1–C23–C28	109.5(2)

C2–Ir1–C23–C22	-178.91(10)
C2–Ir1–C23–C24	-62.38(14)
C2–Ir1–C23–C28	60.1(2)
C16–Ir1–C23–C22	96.40(11)
C16–Ir1–C23–C24	-147.06(11)
C16–Ir1–C23–C28	-24.6(2)
C22–Ir1–C23–C24	116.53(15)
C22–Ir1–C23–C28	-121.0(2)
C24–Ir1–C23–C22	-116.53(15)
C24–Ir1–C23–C28	122.5(2)
C25–Ir1–C23–C22	-79.68(11)
C25–Ir1–C23–C24	36.86(10)
C25–Ir1–C23–C28	159.4(2)
C26–Ir1–C23–C22	-37.99(10)
C26–Ir1–C23–C24	78.55(11)
C26–Ir1–C23–C28	-159.0(2)
C1–Ir1–C24–C23	174.16(10)
C1–Ir1–C24–C25	-67.91(12)
C1–Ir1–C24–C29	54.31(19)
C2–Ir1–C24–C23	134.39(11)
C2–Ir1–C24–C25	-107.68(11)
C2–Ir1–C24–C29	14.55(18)
C9–Ir1–C24–C23	-152.97(13)
C9–Ir1–C24–C25	-35.04(19)
C9–Ir1–C24–C29	87.2(2)
C16–Ir1–C24–C23	39.37(13)

C16–Ir1–C24–C25	157.30(10)
C16–Ir1–C24–C29	-80.48(18)
C22–Ir1–C24–C23	-38.66(10)
C22–Ir1–C24–C25	79.28(11)
C22–Ir1–C24–C29	-158.50(19)
C23–Ir1–C24–C25	117.94(15)
C23–Ir1–C24–C29	-119.8(2)
C25–Ir1–C24–C23	-117.94(15)
C25–Ir1–C24–C29	122.2(2)
C26–Ir1–C24–C23	-81.09(11)
C26–Ir1–C24–C25	36.85(10)
C26–Ir1–C24–C29	159.07(19)
C1–Ir1–C25–C24	124.79(10)
C1–Ir1–C25–C26	-117.18(11)
C1–Ir1–C25–C30	4.64(18)
C2–Ir1–C25–C24	86.20(11)
C2–Ir1–C25–C26	-155.77(10)
C2–Ir1–C25–C30	-33.96(18)
C9–Ir1–C25–C24	162.25(10)
C9–Ir1–C25–C26	-79.72(12)
C9–Ir1–C25–C30	42.09(19)
C16–Ir1–C25–C24	-45.85(18)
C16–Ir1–C25–C26	72.18(17)
C16–Ir1–C25–C30	-166.01(15)
C22–Ir1–C25–C24	-81.00(11)
C22–Ir1–C25–C26	37.03(11)

C22–Ir1–C25–C30	158.85(19)
C23–Ir1–C25–C24	-37.33(10)
C23–Ir1–C25–C26	80.70(11)
C23–Ir1–C25–C30	-157.48(19)
C24–Ir1–C25–C26	118.03(15)
C24–Ir1–C25–C30	-120.2(2)
C26–Ir1–C25–C24	-118.03(15)
C26–Ir1–C25–C30	121.8(2)
C1–Ir1–C26–C22	-166.76(10)
C1–Ir1–C26–C25	74.69(12)
C1–Ir1–C26–C31	-47.71(18)
C2–Ir1–C26–C22	159.96(12)
C2–Ir1–C26–C25	41.41(17)
C2–Ir1–C26–C31	-81.0(2)
C9–Ir1–C26–C22	-126.05(11)
C9–Ir1–C26–C25	115.39(10)
C9–Ir1–C26–C31	-7.00(18)
C16–Ir1–C26–C22	-27.23(14)
C16–Ir1–C26–C25	-145.79(10)
C16–Ir1–C26–C31	91.82(18)
C22–Ir1–C26–C25	-118.55(15)
C22–Ir1–C26–C31	119.1(2)
C23–Ir1–C26–C22	39.06(10)
C23–Ir1–C26–C25	-79.50(11)
C23–Ir1–C26–C31	158.11(19)
C24–Ir1–C26–C22	81.55(11)

C24–Ir1–C26–C25	-37.00(10)
C24–Ir1–C26–C31	-159.39(19)
C25–Ir1–C26–C22	118.55(15)
C25–Ir1–C26–C31	-122.4(2)
Ir1–C1–C2–C3	111.5(2)
C9–C1–C2–Ir1	61.98(17)
C9–C1–C2–C3	173.5(2)
Ir1–C1–C9–C10	-112.1(2)
C2–C1–C9–Ir1	-62.36(17)
C2–C1–C9–C10	-174.5(2)
Ir1–C2–C3–C4	80.3(2)
Ir1–C2–C3–C8	-100.0(2)
C1–C2–C3–C4	-0.4(3)
C1–C2–C3–C8	179.3(2)
C2–C3–C4–C5	-179.3(2)
C8–C3–C4–C5	1.0(3)
C2–C3–C8–C7	178.6(2)
C4–C3–C8–C7	-1.7(3)
C3–C4–C5–C6	0.3(3)
C4–C5–C6–C7	-0.9(3)
C5–C6–C7–C8	0.2(3)
C6–C7–C8–C3	1.1(3)
Ir1–C9–C10–C11	-81.0(2)
Ir1–C9–C10–C15	98.7(2)
C1–C9–C10–C11	0.5(3)
C1–C9–C10–C15	-179.9(2)

C9–C10–C11–C12	178.4(2)
C15–C10–C11–C12	-1.2(3)
C9–C10–C15–C14	-177.8(2)
C11–C10–C15–C14	1.9(3)
C10–C11–C12–C13	-0.2(3)
C11–C12–C13–C14	0.9(3)
C12–C13–C14–C15	-0.3(3)
C13–C14–C15–C10	-1.1(3)
Ir1–C16–C17–C18	172.15(16)
C21–C16–C17–C18	-0.9(3)
Ir1–C16–C21–C20	-173.27(18)
C17–C16–C21–C20	-0.1(4)
C16–C17–C18–C19	1.1(3)
C17–C18–C19–C20	-0.3(3)
C18–C19–C20–C21	-0.7(3)
C19–C20–C21–C16	0.9(4)
Ir1–C22–C23–C24	-64.46(15)
Ir1–C22–C23–C28	122.4(3)
C26–C22–C23–Ir1	65.02(15)
C26–C22–C23–C24	0.6(2)
C26–C22–C23–C28	-172.6(2)
C27–C22–C23–Ir1	-123.7(2)
C27–C22–C23–C24	171.8(2)
C27–C22–C23–C28	-1.4(4)
Ir1–C22–C26–C25	61.83(15)
Ir1–C22–C26–C31	-121.8(2)

C23–C22–C26–Ir1	-62.94(15)
C23–C22–C26–C25	-1.1(2)
C23–C22–C26–C31	175.2(2)
C27–C22–C26–Ir1	125.7(2)
C27–C22–C26–C25	-172.5(2)
C27–C22–C26–C31	3.9(4)
Ir1–C23–C24–C25	-62.55(15)
Ir1–C23–C24–C29	120.5(2)
C22–C23–C24–Ir1	62.77(15)
C22–C23–C24–C25	0.2(2)
C22–C23–C24–C29	-176.7(2)
C28–C23–C24–Ir1	-124.0(3)
C28–C23–C24–C25	173.4(2)
C28–C23–C24–C29	-3.5(4)
Ir1–C24–C25–C26	-61.15(15)
Ir1–C24–C25–C30	124.9(2)
C23–C24–C25–Ir1	60.25(15)
C23–C24–C25–C26	-0.9(2)
C23–C24–C25–C30	-174.8(2)
C29–C24–C25–Ir1	-122.8(2)
C29–C24–C25–C26	176.1(2)
C29–C24–C25–C30	2.1(4)
Ir1–C25–C26–C22	-59.58(15)
Ir1–C25–C26–C31	124.1(2)
C24–C25–C26–Ir1	60.83(15)
C24–C25–C26–C22	1.3(2)

C24–C25–C26–C31	-175.1(2)
C30–C25–C26–Ir1	-125.3(2)
C30–C25–C26–C22	175.1(2)
C30–C25–C26–C31	-1.2(4)

References for Complex 32

[5] C. R. Groom, I. J. Bruno, M. P. Lightfoot, S. C. Ward, *Acta Cryst.* **2016**, *B72*, 171–179, doi:10.1107/S2052520616003954.

[6] D. Kratzert, *FinalCif*, *V64*, https://www.xs3.uni-freiburg.de/research/finalcif.

IV.7. Spectra of Complexes

Complex **5-22** (^{1}H NMR 400 MHz)

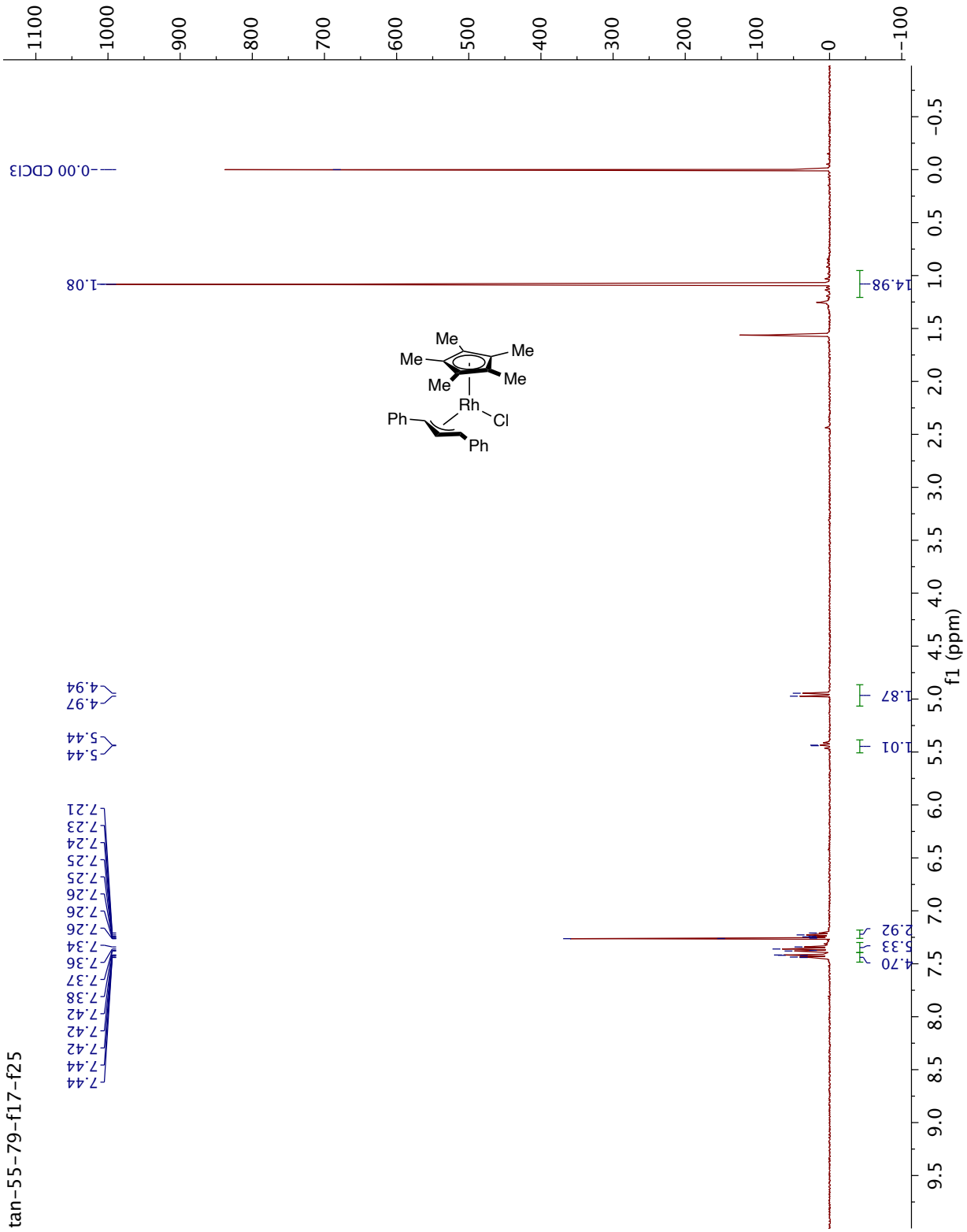

Complex **5-22** (^{13}C NMR 150 MHz)

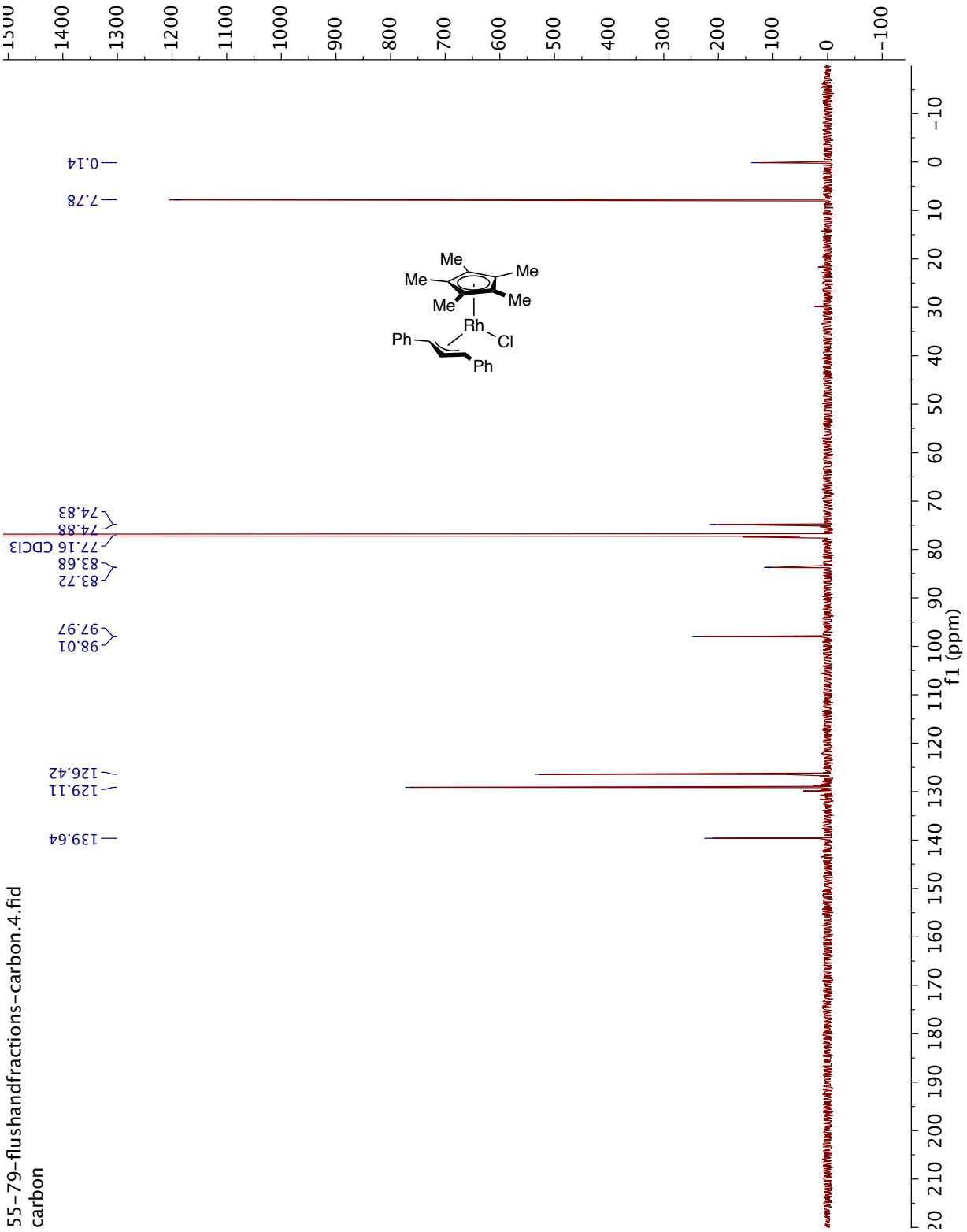

Complex **5-24** (^{1}H NMR 400 MHz)

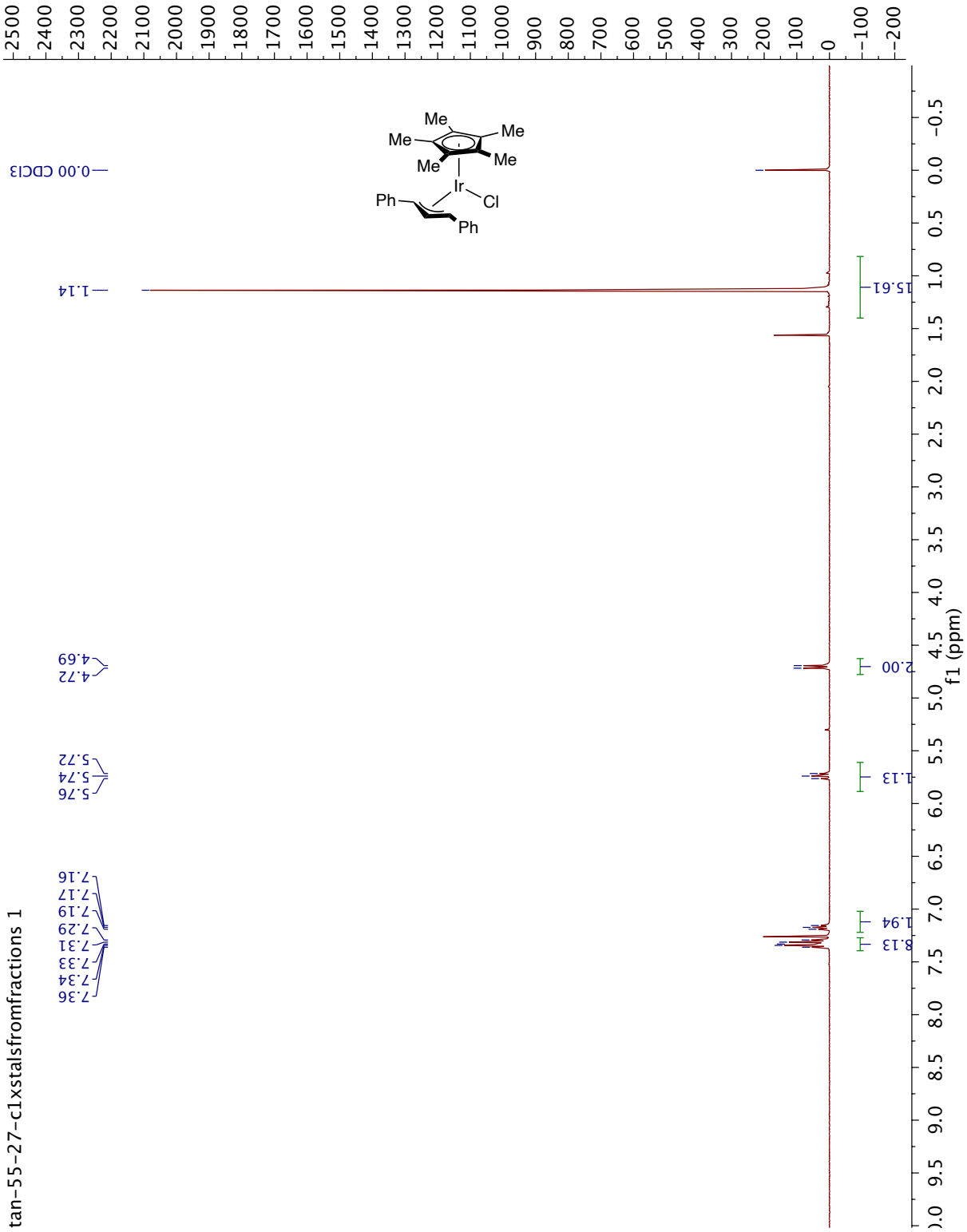

Complex **5-24** (^{13}C NMR 150 MHz)

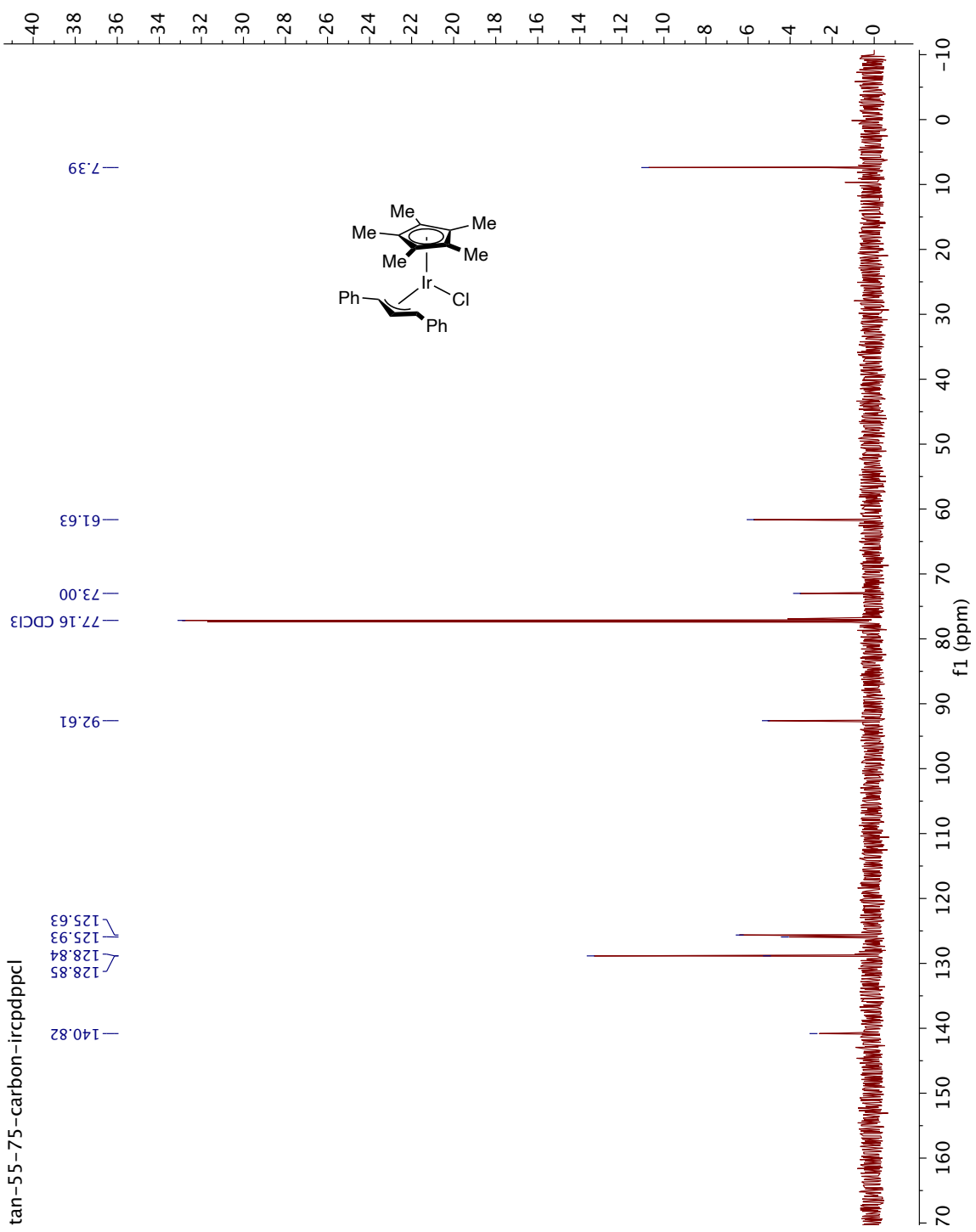

Complex **5-25** (^{1}H NMR 600 MHz)

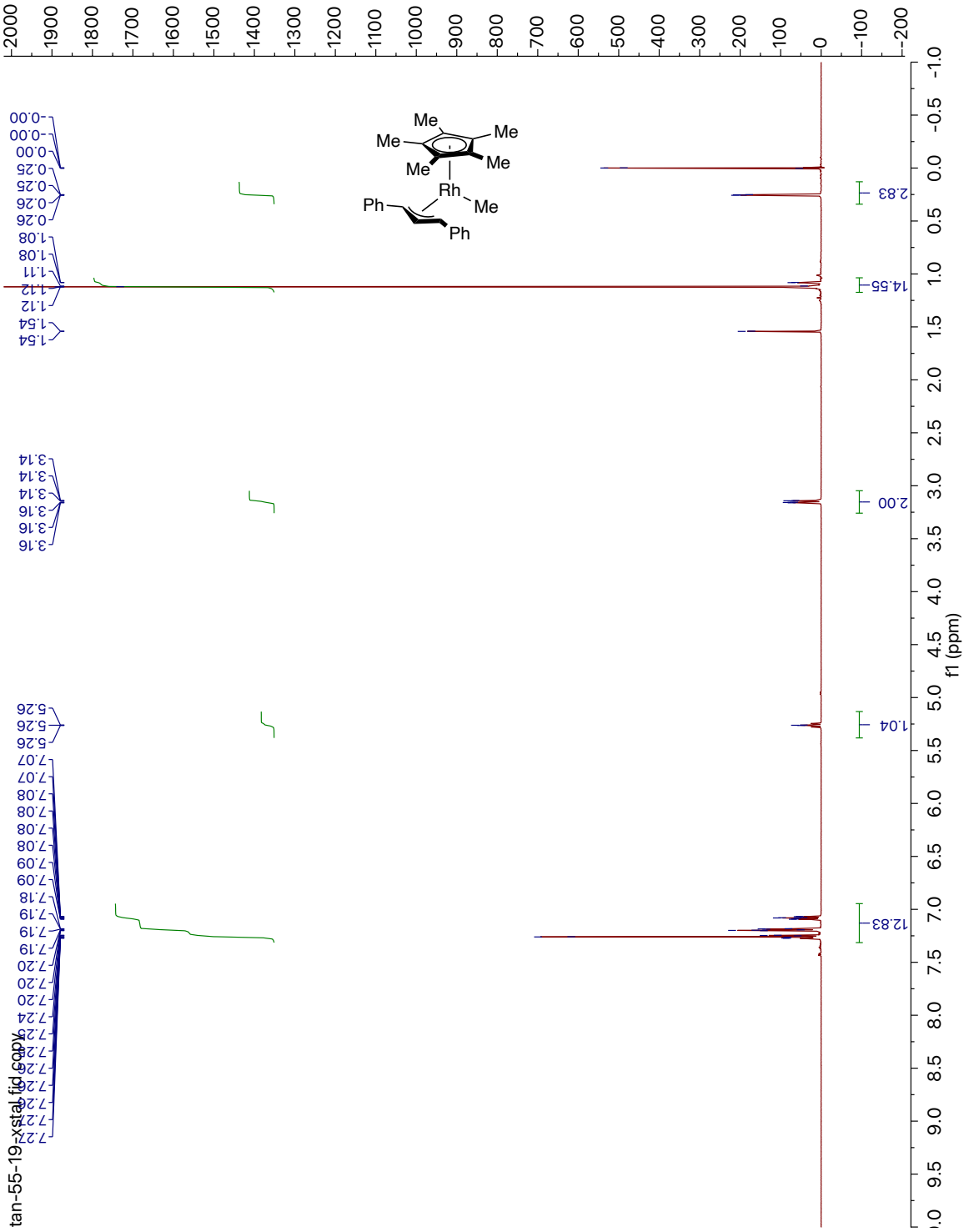

Complex **5-25** (^{13}C NMR 125 MHz)

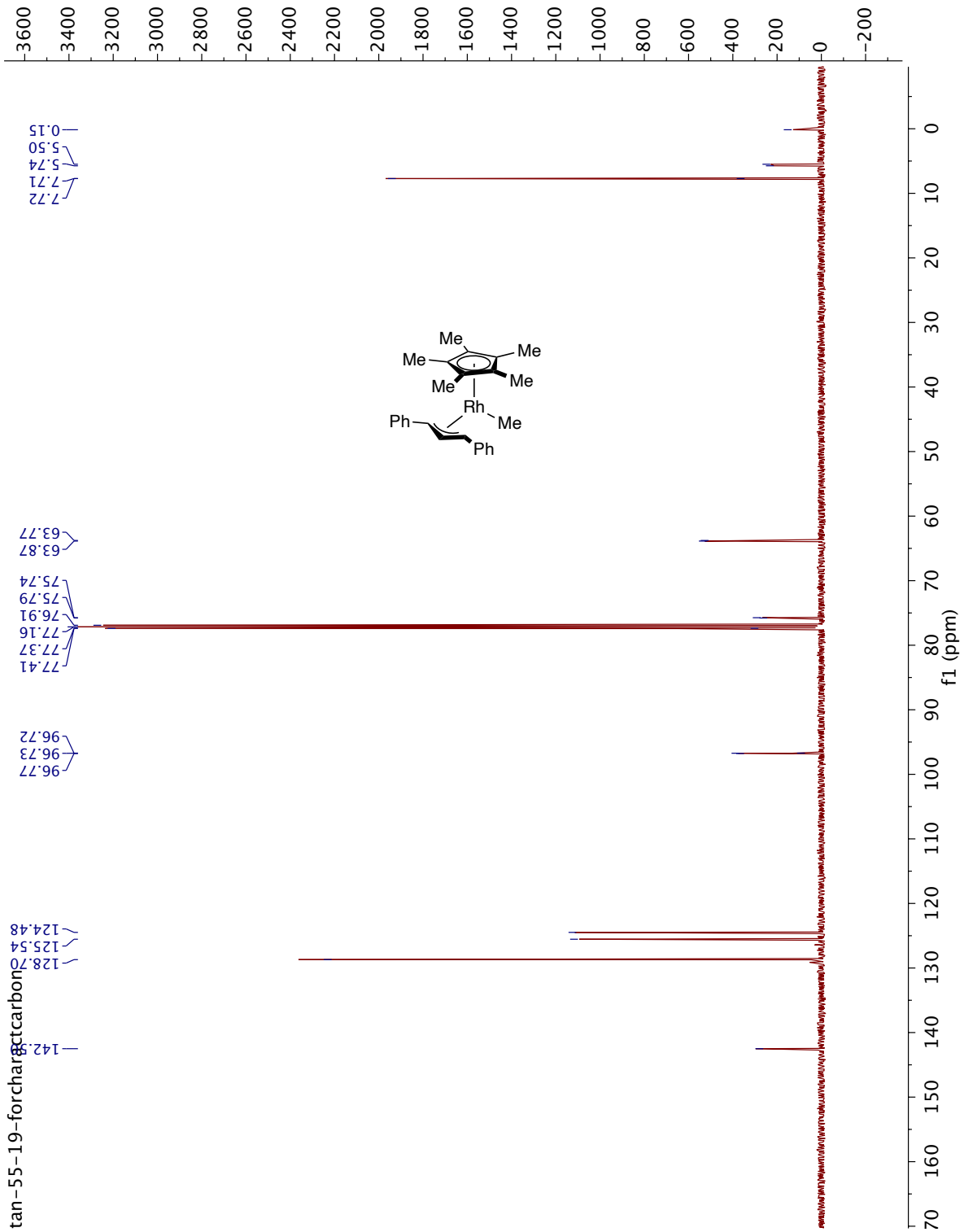

Complex **5-26** (^{1}H NMR 600 MHz)

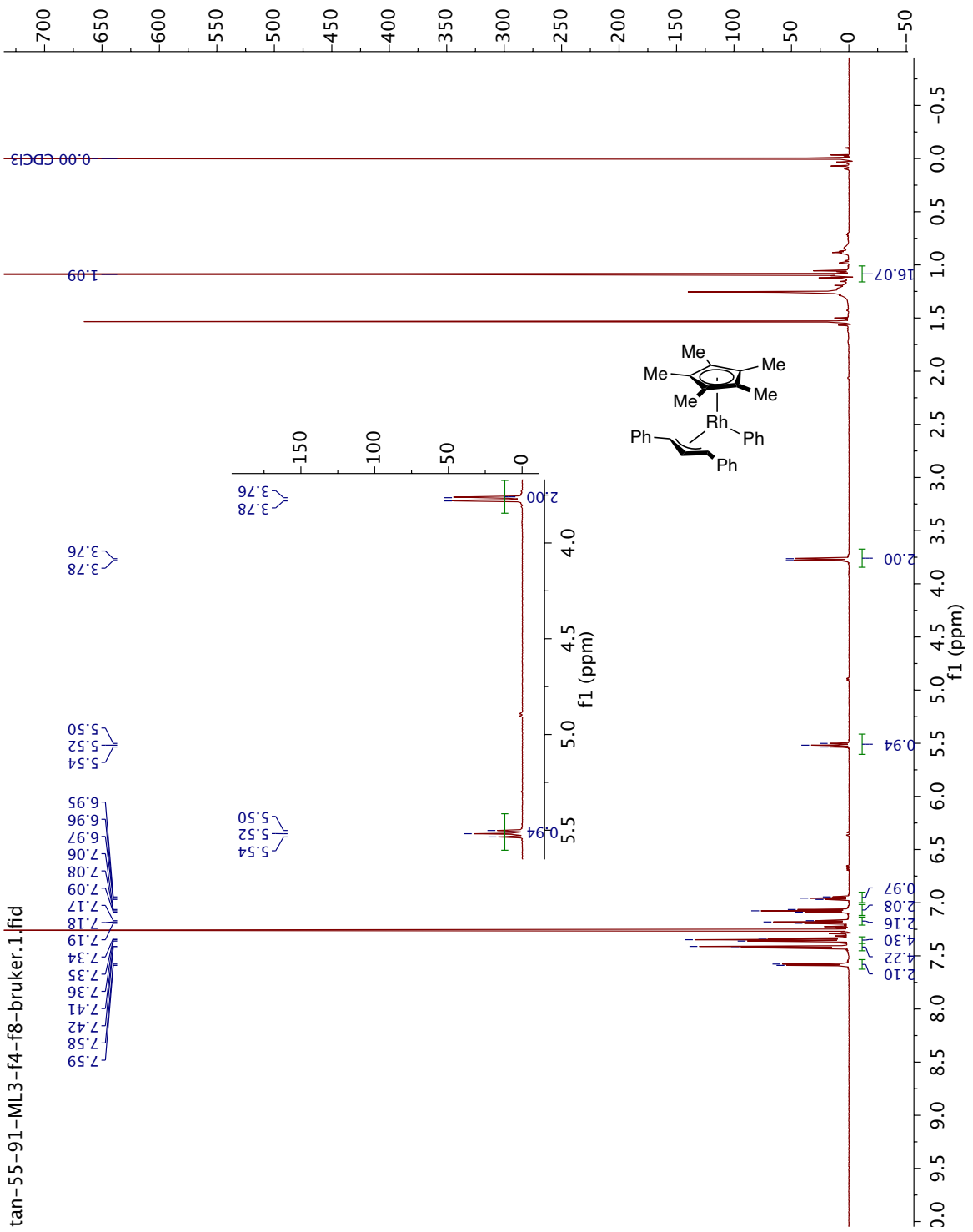

Complex **5-26** (^{13}C NMR 150 MHz)

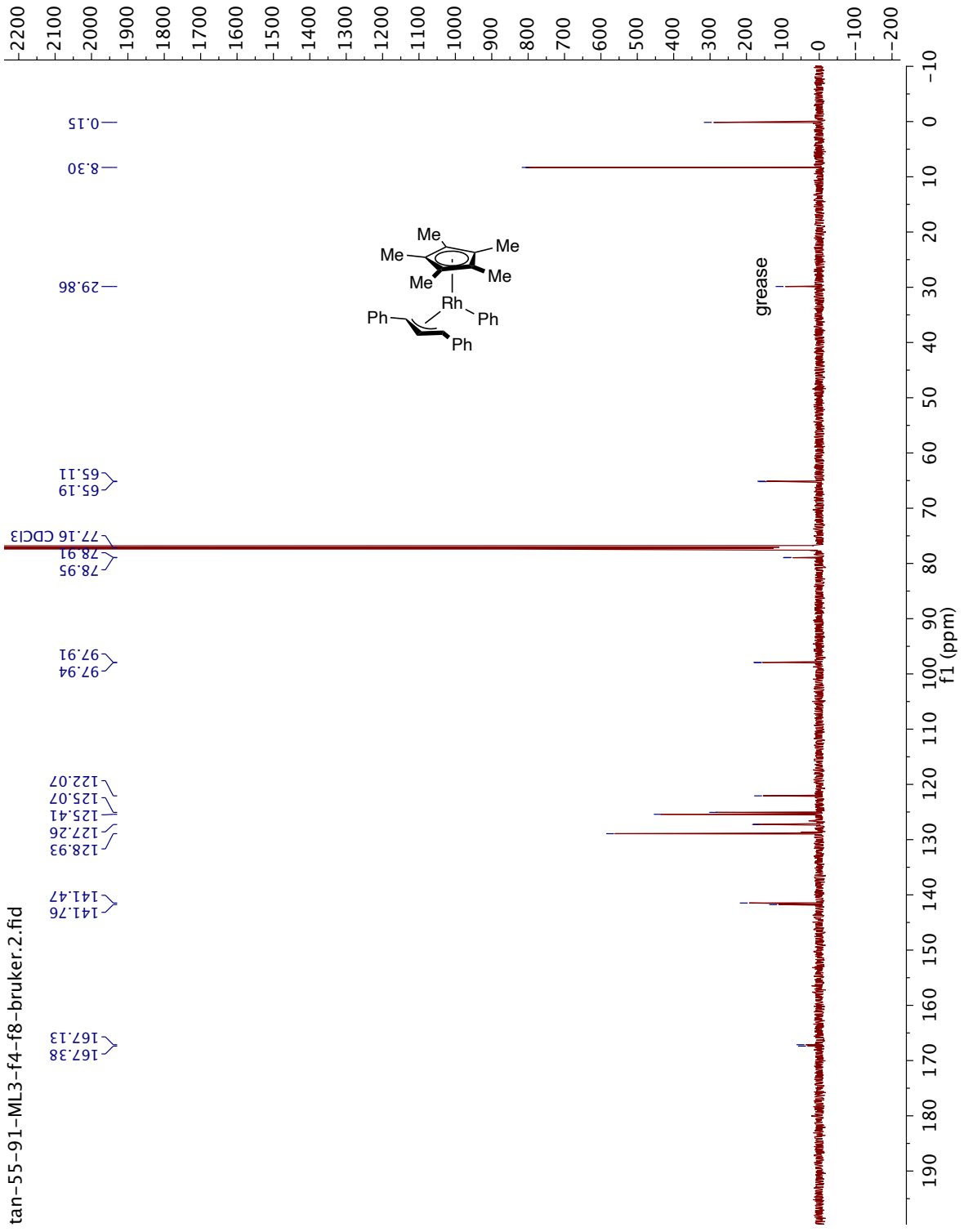

Complex **5-31** (^{1}H NMR 400 MHz)

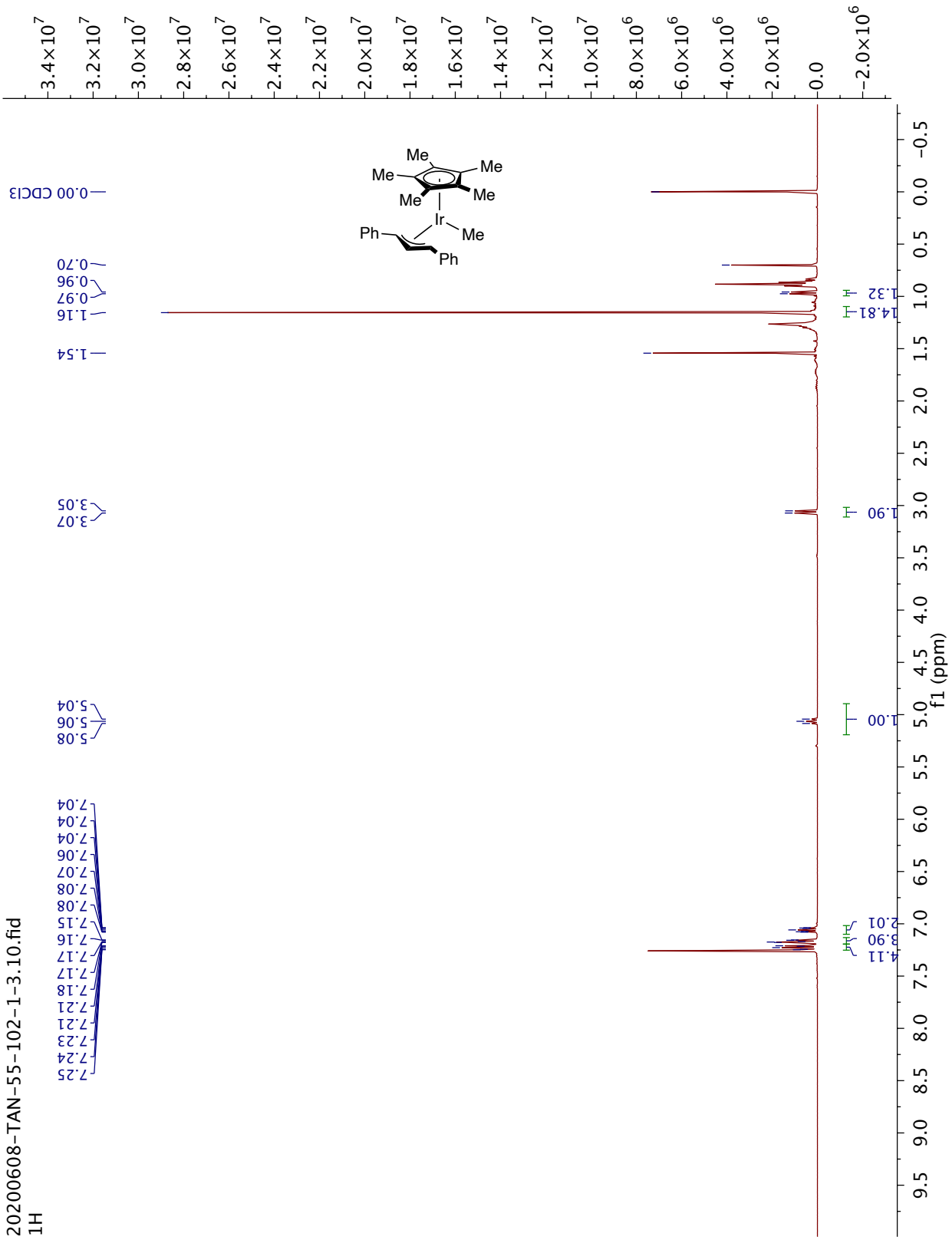

Complex **5-31** (^{13}C NMR 150 MHz)

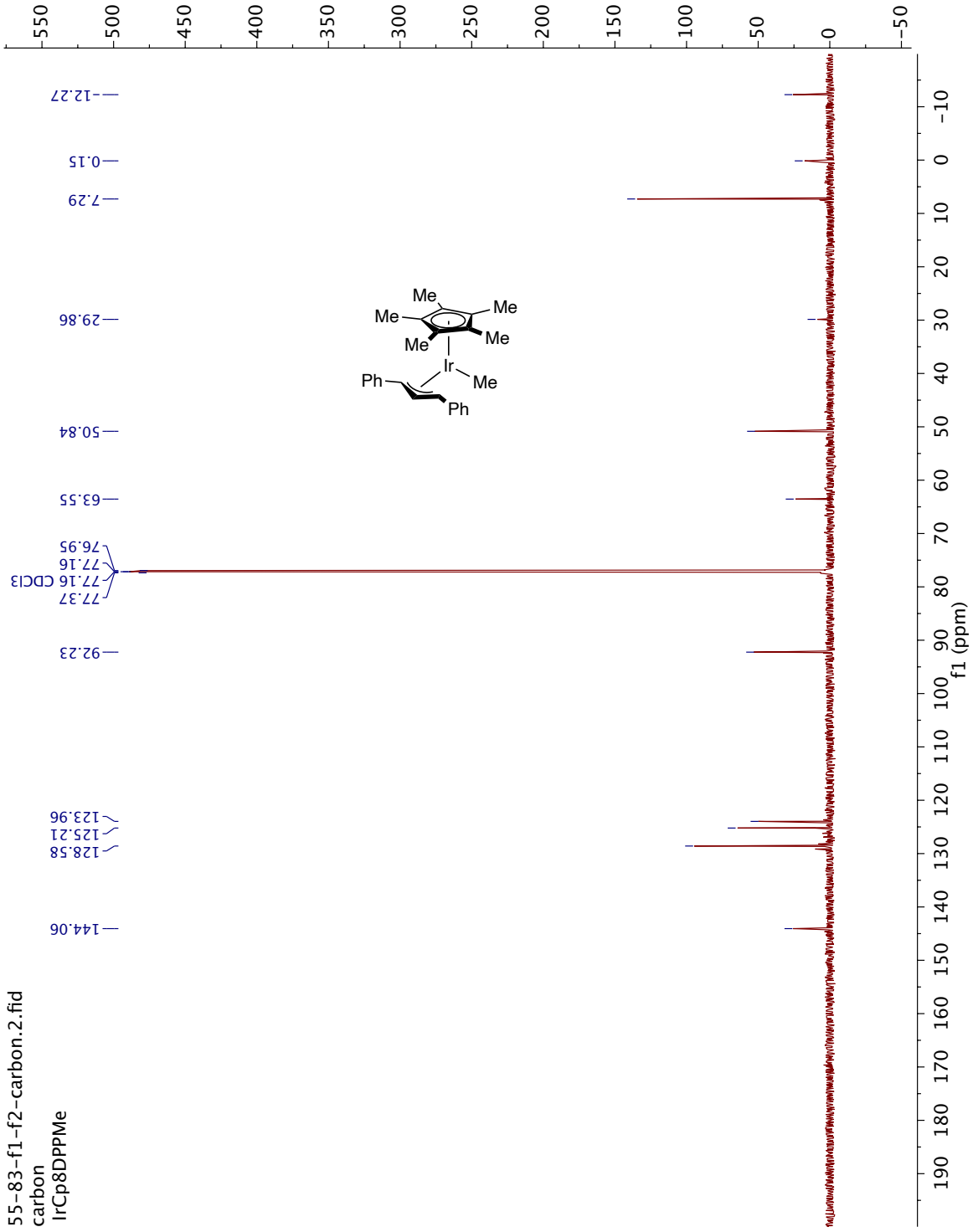

Complex **5-32** (^{1}H NMR 600 MHz)

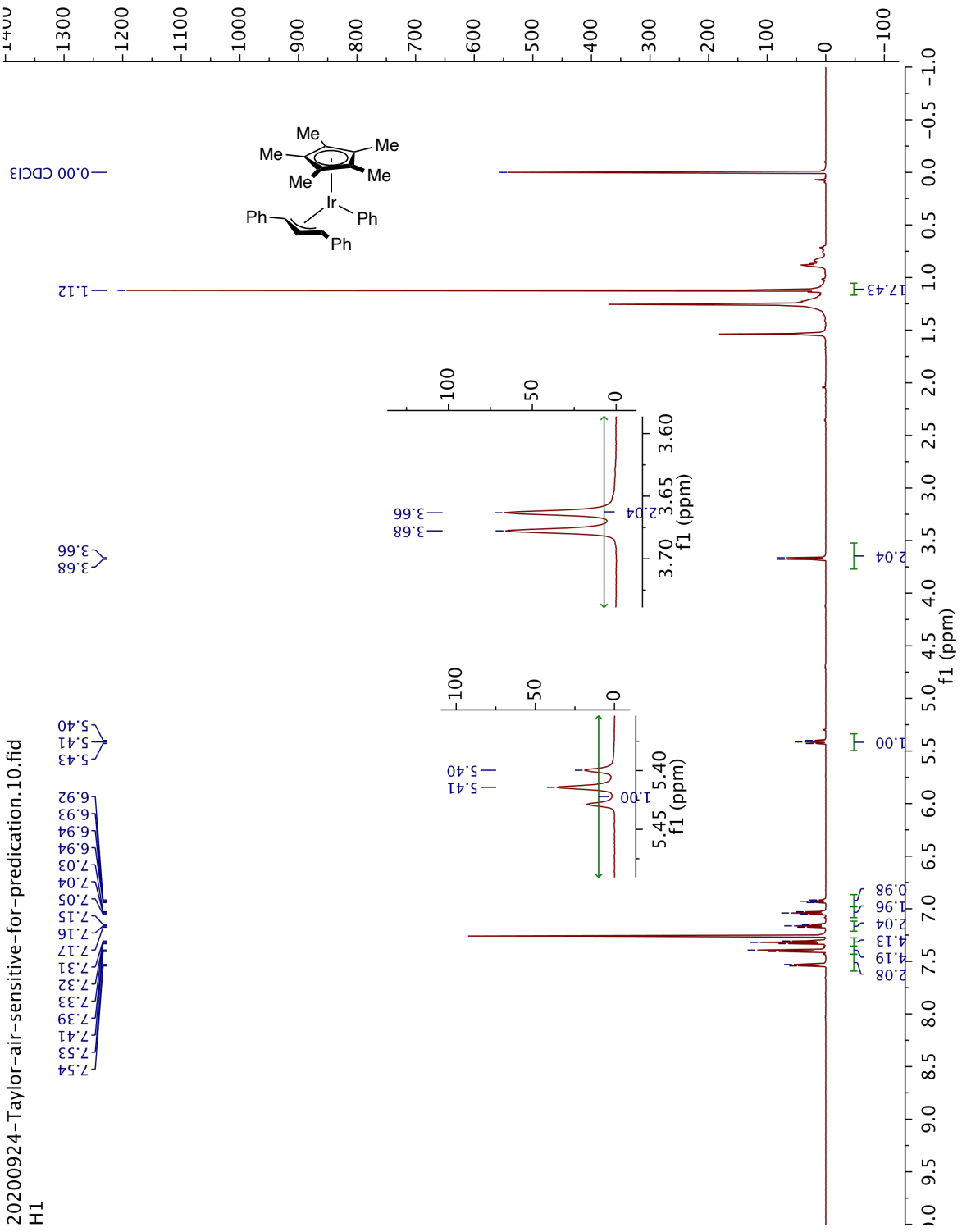

Complex **5-32** (^{13}C NMR 150 MHz)

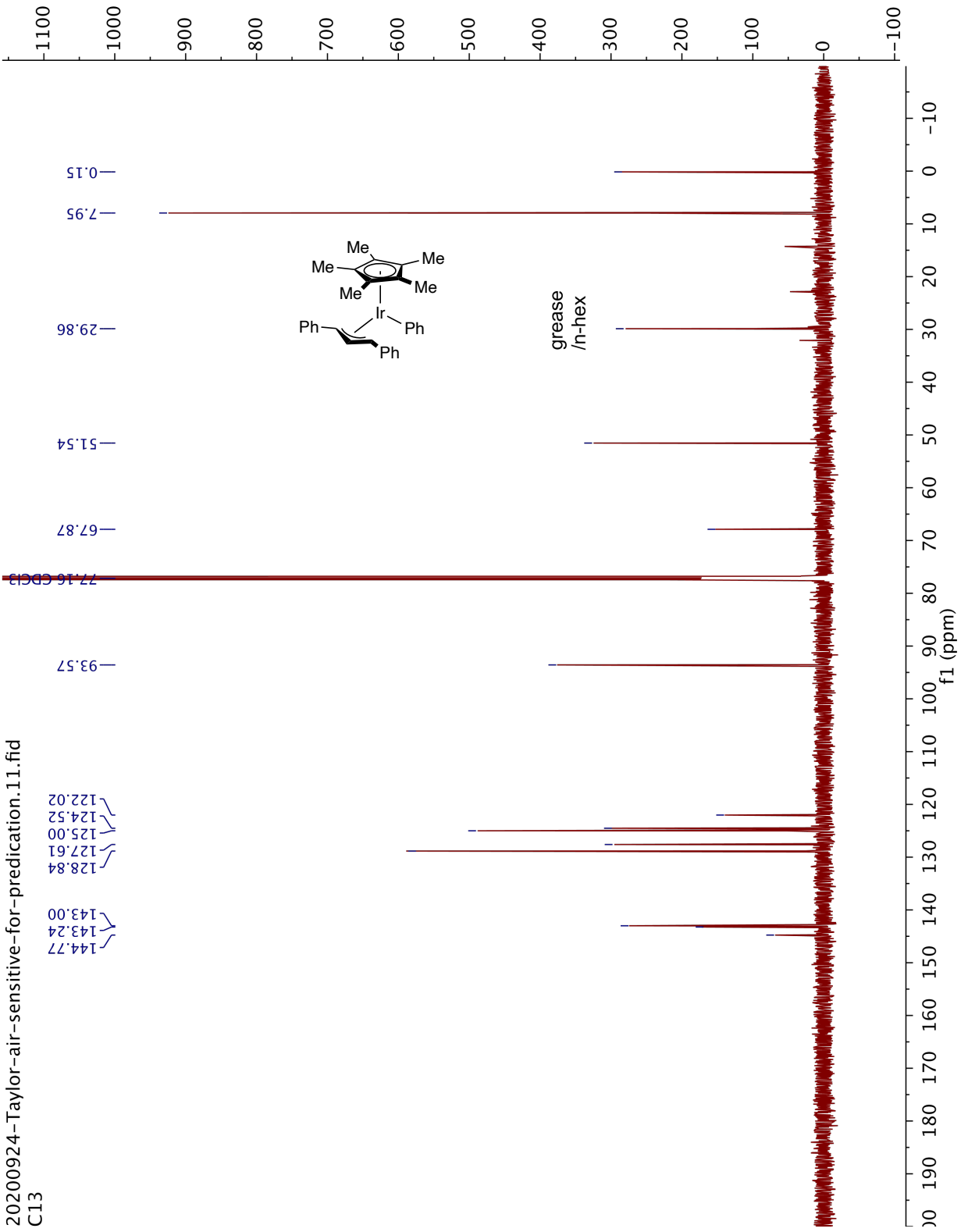

V. References

1. Quasdorf, K. W.; Overman, L. E., Catalytic enantioselective synthesis of quaternary carbon stereocentres. *Nature* **2014,** *516*, 181-191.

2. Sultan, S.; Shah, B. A., Carbon-carbon and Carbon-heteroatom Bond Formation Reactions using Unsaturated Carbon Compounds. *Chem. Rec.* **2018**, *19,* 644-660

3. Lerchen, A.; Knecht, T.; Koy, M.; Ernst, J. B.; Bergander, K.; Daniliuc, C. G.; Glorius, F., Non-Directed Cross-Dehydrogenative (Hetero)arylation of Allylic C(sp^3)–H bonds enabled by C–H Activation. *Angew. Chem. Int. Ed.* **2018,** *57*, 15248-15252.

4. Knecht, T.; Pinkert, T.; Dalton, T.; Lerchen, A.; Glorius, F., Cp*Rh^{III}-Catalyzed Allyl–Aryl Coupling of Olefins and Arylboron Reagents Enabled by C(sp^3)–H Activation. *ACS Catal.* **2019,** *9*, 1253-1257.

5. Sun, J.; Wang, K.; Wang, P.; Zheng, G.; Li, X., Rhodium(III)-Catalyzed Oxidative Allylic C–H Indolylation via Nucleophilic Cyclization. *Org. Lett.* **2019,** *21*, 4662-4666.

6. Harris, R. J.; Park, J.; Nelson, T. A. F.; Iqbal, N.; Salgueiro, D. C.; Bacsa, J.; Macbeth, C. E.; Baik, M.-H.; Blakey, S. B., The Mechanism of Rhodium-Catalyzed Allylic C–H Amination. *J. Am. Chem. Soc.* **2020,** *142*, 5842-5851.

7. Simmons, E. M.; Hartwig, J. F., On the Interpretation of Deuterium Kinetic Isotope Effects in C–H Bond Functionalizations by Transition-Metal Complexes. *Angew. Chem. Int. Ed.* **2012,** *51*, 3066-3072.

8. McGhee, W. D.; Bergman, R. G., Synthesis of an (η^3-allyl)(hydrido)iridium complex and its reactions with arenes and alkanes. Sequential intermolecular carbon-hydrogen oxidative addition and hydride-to-alkene migratory insertion reactions. *J. Am. Chem. Soc.* **1988,** *110*, 4246-4262.

9. Kim, J.; Shin, K.; Jin, S.; Kim, D.; Chang, S., Oxidatively Induced Reductive Elimination: Exploring the Scope and Catalyst Systems with Ir, Rh, and Ru Complexes. *J. Am. Chem. Soc.* **2019,** *141*, 4137-4146.

10. Farr, C. M. B.; Kazerouni, A. M.; Park, B.; Poff, C. D.; Won, J.; Sharp, K. R.; Baik, M.-H.; Blakey, S. B., Designing a Planar Chiral Rhodium Indenyl Catalyst for Regio- and Enantioselective Allylic C–H Amidation. *J. Am. Chem. Soc.* **2020,** *142*, 13996-14004.

11. Barday, M.; Janot, C.; Halcovitch, N. R.; Muir, J.; Aïssa, C., Cross-Coupling of α-Carbonyl Sulfoxonium Ylides with C–H Bonds. *Angew. Chem. Int. Ed.* **2017,** *56*, 13117-13121.

12. Yuan, Q.; Yao, K.; Liu, D.; Zhang, W., Iridium-catalyzed allyl–allyl cross-coupling of allylic carbonates with (E)-1,3-diarylpropenes. *Chem. Commun.* **2015,** *51*, 11834-11836.

13. Correia, R.; Deshong, P., Palladium-Catalyzed Arylation of Allylic Benzoates Using Hypervalent Siloxane Derivatives. *J. Org. Chem.* **2001,** *66*, 7159-7165.

14. Liwosz, T. W.; Chemler, S. R., Copper-Catalyzed Oxidative Heck Reactions between Alkyltrifluoroborates and Vinyl Arenes. *Org. Lett.* **2013,** *15*, 3034-3037.

15. Sakuramoto, T.; Donaka, Y.; Tobisu, M.; Moriuchi, T., Oxovanadium(v)-catalyzed deoxygenative homocoupling reaction of alcohols. *New J. Chem.* **2019,** *43,* 17571-17576